frontiers
RESEARCH TOPICS

EXTRASYNAPTIC NEUROTRANSMISSION AS A WAY OF MODULATING MULTIPLE NEURONAL FUNCTIONS

Topic Editors
Francisco F. De-Miguel and Kjell Fuxe

frontiers in PHYSIOLOGY

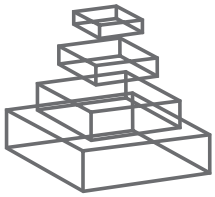

frontiers

Cover image provided by Ibbl sarl, Lausanne CH

ISSN 1664-8714
ISBN 978-2-88919-109-3
DOI 10.3389/978-2-88919-109-3

ABOUT FRONTIERS

Frontiers is more than just an open-access publisher of scholarly articles: it is a pioneering approach to the world of academia, radically improving the way scholarly research is managed. The grand vision of Frontiers is a world where all people have an equal opportunity to seek, share and generate knowledge. Frontiers provides immediate and permanent online open access to all its publications, but this alone is not enough to realize our grand goals.

FRONTIERS JOURNAL SERIES

The Frontiers Journal Series is a multi-tier and interdisciplinary set of open-access, online journals, promising a paradigm shift from the current review, selection and dissemination processes in academic publishing.
All Frontiers journals are driven by researchers for researchers; therefore, they constitute a service to the scholarly community. At the same time, the Frontiers Journal Series operates on a revolutionary invention, the tiered publishing system, initially addressing specific communities of scholars, and gradually climbing up to broader public understanding, thus serving the interests of the lay society, too.

DEDICATION TO QUALITY

Each Frontiers article is a landmark of the highest quality, thanks to genuinely collaborative interactions between authors and review editors, who include some of the world's best academicians. Research must be certified by peers before entering a stream of knowledge that may eventually reach the public - and shape society; therefore, Frontiers only applies the most rigorous and unbiased reviews.
Frontiers revolutionizes research publishing by freely delivering the most outstanding research, evaluated with no bias from both the academic and social point of view.
By applying the most advanced information technologies, Frontiers is catapulting scholarly publishing into a new generation.

WHAT ARE FRONTIERS RESEARCH TOPICS?

Frontiers Research Topics are very popular trademarks of the Frontiers Journals Series: they are collections of at least ten articles, all centered on a particular subject. With their unique mix of varied contributions from Original Research to Review Articles, Frontiers Research Topics unify the most influential researchers, the latest key findings and historical advances in a hot research area!
Find out more on how to host your own Frontiers Research Topic or contribute to one as an author by contacting the Frontiers Editorial Office: researchtopics@frontiersin.org

EXTRASYNAPTIC NEUROTRANSMISSION AS A WAY OF MODULATING MULTIPLE NEURONAL FUNCTIONS

Topic Editors:
Francisco F. De-Miguel, Universidad Nacional Autonoma de Mexico, Mexico
Kjell Fuxe, Karolinska Institutet, Sweden

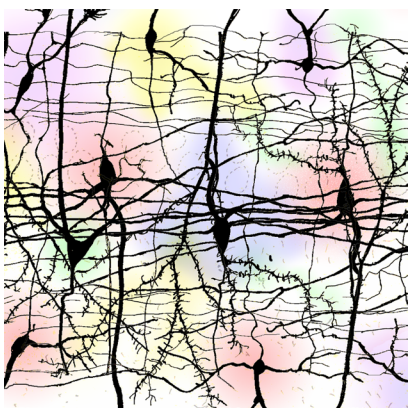

By releasing substances from the cell bodies, dendrites and axons, neurons produce hues in the nervous system functions. The image shows a neural network representing with colors transmitters being released from the somata and dendrites and diffusing around them, thus representing the two main aspects of this Special Issue: the mechanisms of extrasynaptic release and the functions of these molecules by acting through volume transmission. The image was prepared by F.F. De-Miguel, based on a modified original drawing by Santiago Ramón y Cajal, gently provided by the Cajal Legacy, at the Instituto Cajal (CSIC). Madrid, and adds to it what Cajal could have not seen in his studies.

Extrasynaptic transmission is a unifying term for a wide variety of cellular processes, in which outside of synaptic terminals transmitter substances activate extrasynaptic receptors. Whereas "synaptic transmission" immediately refers to a process occurring at nerve terminals in which the arrival of a presynaptic impulse evokes exocytosis followed by a postsynaptic response within a millisecond time scale, extrasynaptic transmission has a wide diversity of ultrastructural and therefore mechanistic associated phenomena. In comparison to synaptic, extrasynaptic exocytosis may last for seconds or even minutes, thus expanding the timing of neuronal signaling. Extrasynaptic transmission has now been demonstrated in central and peripheral neurons of vertebrates and invertebrates, and involves many different types of transmitter substances than include low molecular weight transmitters (acetilcholine, GABA, glutamate, ATP, and biogenic amines) and peptides (substance P, vasopressin and others). It may occur when transmitters leak out from the synaptic cleft and activate extrasynaptic receptors in neighboring neurons or glial cells, or when axonal varicosities, dendrites or the somata release transmitters in the absence of postsynaptic counterparts.

The release mechanisms also vary from one neuron type to another and from one neuronal compartment to another. In some cases, clear vesicles are apposed to the resting plasma membrane, as in presynaptic terminals. In other cases, transmitters are packed onto dense core vesicles that rest at a distance from the release sites. In between, there are multiple morphological combinations that point to complementary mechanisms in different compartments of the same neuron and some times, even in the same compartment. For example, serotonergic varicosities may combine clear and dense core vesicles in stereotyped arrays.

This diversity adds complexity to the nervous system and raises many questions that are waiting for answers. Extrasynaptic transmission may be the main source of transmitter molecules causing volume transmission, however this still lacks direct demonstration. From the physiological point of view, one may ask how does the neuronal firing pattern evokes synaptic or extrasynaptic transmitter release or what are the physiological effects of these modes of transmission. From the behavioral point of view it becomes interesting to explore how circuits and therefore behaviors are modulated. Some neurological disfunctions may also be related to deficiencies in extrasynaptic transmission, however, again, direct studies are still lacking. Developmental and evolutionary biologists may also find the topic inspiring.

Extrasynaptic transmission not only expands our view about how the nervous system works, but also requires a change in the way we plan our research. New technological and computational tools are now being applied to analyze intracellular and extracellular transmitter mobilizations or long term changes of neuronal circuits. New definitions and mechanisms may become visible. In the meanwhile, this seems to be a good moment for a first common effort to analyze and discuss extrasynaptic transmission in different systems and from different perspectives.

Table of Contents

frontiers in
PHYSIOLOGY

EDITORIAL
published: 15 February 2012
doi: 10.3389/fphys.2012.00016

Extrasynaptic neurotransmission as a way of modulating neuronal functions

Francisco F. De-Miguel[1]* and Kjell Fuxe[2]

[1] *Instituto de Fisiología Celular-Neurociencias, Universidad Nacional Autónoma de México, Circuito Exterior, Ciudad Universitaria, Mexico City, México*
[2] *Division of Cellular and Molecular Neuroscience, Department of Neuroscience, Karolinska Institutet, Stockholm, Sweden*
**Correspondence: ffernand@ifc.unam.mx*

Extrasynaptic neurotransmission allows neuronal communication at variable distances, based on the release and diffusion of chemical substances from the soma, axon, or dendrites of neurons, or after transmitter leak-out from the synaptic cleft (De-Miguel and Trueta, 2005; Fuxe et al., 2007). Extrasynaptic neurotransmission modulates the input–output relationships of whole circuits by changing the electrical properties of neuronal populations, their chemical and electrical connectivities and also by activating the transport and release of transmitters by glial cells. The term synaptic transmission immediately refers to a confined process in which the arrival of an impulse at a presynaptic ending evokes a rapid burst of exocytosis that triggers an electrical reaction in the postsynaptic cell, within millisecond time and micrometer distance scales. By contrast, extrasynaptic exocytosis involves diverse ultrastructural and mechanistic principles that, when active, expand the timing and volume possibilities of nerve cell communication (Trueta et al., 2003, 2004; De-Miguel and Trueta, 2005; Agnati et al., 2010). Extrasynaptic sites release transmitters into the extracellular fluid in the absence of identifiable postsynaptic counterparts, producing the activation mainly of extrasynaptic receptors in neighboring neurons and/or glial cells. Although extrasynaptic exocytosis is triggered by electrical activity, it may start after a lag (asynchronous transmission) and may continue for seconds or even minutes once the depolarization has ended, thus expanding the timing of neuronal signaling.

Extrasynaptic exocytosis exists in central and peripheral neurons of vertebrates and invertebrates and involves many different types of substances including low molecular weight transmitters, such as acetylcholine, GABA, glutamate, ATP, and biogenic amines, and peptides such as substance P, vasopressin, oxytocin, beta-endorphin, and also proteins (De-Miguel and Trueta, 2005). Diffusible modulators such as nitric oxide (Joca et al., 2007) and endocannabinoids (Yuan and Burrell, 2010) produced by postsynaptic targets also act on neighboring groups of neurons and glial cells.

The intracellular mechanisms of extrasynaptic exocytosis vary from one neuronal compartment to another in the same neuron and also from one neuron type to another (De-Miguel and Trueta, 2005). For example, in axonal varicosities, clear vesicles may be apposed to the resting plasma membrane as in canonical presynaptic active zones or may rest at a certain distance from the plasma membrane, but these endings lack morphologically-defined postsynaptic counterparts, therefore being asynaptic and sources of extrasynaptic release. Transmitters and/or peptides may also be packed onto axonal and somatic dense core vesicles, most of which rest at a distance from the plasma membrane and in response to electrical activity move towards it and fuse, as in excitable endocrine cells. A single neuron may use several of these exocytosis mechanisms in separate compartments and it is also common that more than one mechanism may coexist in the same compartment. For example, while the soma of leech serotonergic Retzius neurons releases serotonin exclusively from dense core vesicles (Trueta et al., 2003), synaptic clear vesicles in serotonergic neurons of leech or mammals are surrounded by serotonin-containing dense core vesicles that release their contents extrasynaptically (De-Miguel and Trueta, 2005). Electrical stimulation of serotonergic leech or mammalian neurons increases the serotonin concentration in the extracellular fluid microns away from the release sites, and serotonin release modulates the activity of neurons (Perrier and Cotel, 2008) and in addition inhibits the electrical activity of serotonergic neurons (Cercós et al., 2009). Increasing evidence shows that in response to extrasynaptic exocytosis, glial cells may take up and afterwards release transmitters, and by doing so may modulate neuronal activity.

Extrasynaptic transmission represents a subtype of volume (diffuse) transmission, namely the short-distance transmission of signaling molecules (*inter alia* transmitters, neuropeptides, and diffusible modulators) taking place in the extracellular fluid of local circuits (Fuxe and Agnati, 1991a,b; Descarries and Mechawar, 2000; Fuxe et al., 2007, 2010). Even the classical synaptic transmitter glutamate can be released to reach the extracellular fluid and activate extrasynaptic glutamate receptors located close to active glutamate synapses, as shown in brain slices, leading to increases in astroglial glutamate release (Del Arco et al., 2003). Glutamate as an astroglial derived volume transmission signal can then contribute to metabolic and trophic adjustments in the neuron-astrocytic unit in response to the activity of the glutamate synapses. Volume transmission also includes long distance diffusion in the extracellular fluid and the cerebrospinal fluid mainly mediated via neuropeptides like beta-endorphin and their fragments as well as proteins like, e.g., prolactin and Interleukin 1beta released from neurons and/or from glial cells (Agnati et al., 1986).

This diversity of mechanisms and their effects adds complexity to the nervous system and raises many questions that still wait for answers. From the physiological point of view, one may ask how the neuronal firing pattern determines whether to evoke synaptic and/or extrasynaptic exocytosis in a given neuron; how activation of different synaptic inputs induces release from different release compartments, and by doing so affect different targets (Velazquez-Ulloa et al., 2003). From the behavioral point of view it becomes highly interesting to explore how the timing of circuits and therefore behaviors are modulated by extrasynaptic transmission. Some psychiatric and neurological dysfunctions, such as depression may be related to deficiencies in extrasynaptic transmission (Fuxe et al., 1991). A new research field is exploring whether antidepressant drugs used to reduce the symptoms of depression and/or of post-traumatic stress syndrome exert their effects by increasing the extracellular fluid levels of transmitters

such as serotonin and thus volume transmission and by doing that restore the activity of distinct 5-HT receptor subtypes (Jansson et al., 2002), and in parallel activate neurogenesis, thus favoring mood elevation on one hand and the recovery of damaged brain areas on the other. This may occur at least in part through activating neurogenesis. Developmental and evolutionary biologists may also find the topic inspiring for future research, since some of the exocytosis mechanisms involved in extrasynaptic transmission evolved before chemical synapses. For a similar reason, one may expect that during development, the extracellular levels of transmitters, modulators, and peptides may contribute to axonal pathfinding and electrogenesis before massive synaptogenesis takes place.

Extrasynaptic transmission expands our view about how the nervous system works and also imposes new challenges to the way we plan our research. New technological developments are focused on imaging transmitters (Kaushalya et al., 2008a,b) and new computational tools are being developed to analyze transmitter mobilizations or long-term changes of neuronal circuit activity. New definitions and mechanisms may become visible. Meanwhile, this is a good moment for a first common effort to analyze and discuss extrasynaptic transmission in different systems and from different perspectives. We hope the readers of this issue will find the articles included of significant interest and helpful clarifying the field of extrasynaptic transmission.

REFERENCES

Agnati, L. F., Fuxe, K., Zoli, M., Ozini, I., Toffano, G., and Ferraguti, F. (1986). A correlation analysis of the regional distribution of central enkephalin and beta-endorphin immunoreactive terminals and of opiate receptors in adult and old male rats. Evidence for the existence of two main types of communication in the central nervous system: the volume transmission and the wiring transmission. *Acta Physiol. Scand.* 128, 201–207.

Agnati, L. F., Guidolin, D., Guescini, M., Genedani, S., and Fuxe, K. (2010). Understanding wiring and volume transmission. *Brain Res. Rev.* 64, 137–159.

Cercós, M., De-Miguel, F. F., and Trueta, C. (2009). Real-time measurements of synaptic autoinhibition produced by serotonin release in cultured leech neurons. *J. Neurophysiol.* 102, 1075–1085.

De-Miguel, F. F., and Trueta, C. (2005). Synaptic and extrasynaptic secretion of serotonin. *Cell. Mol. Neurobiol.* 25, 297–312.

Del Arco, A., Segovia, G., Fuxe, K., and Mora, F. (2003). Changes in dialysate concentrations of glutamate and GABA in the brain: an index of volume transmission mediated actions? *J. Neurochem.* 85, 23–33.

Descarries, L., and Mechawar, N. (2000). Ultrastructural evidence for diffuse transmission by monoamine and acetylcholine neurons of the central nervous system. *Prog. Brain Res.* 125, 27–47.

Fuxe, K., and Agnati, L. F. (eds). (1991b). *Volume Transmission in the Brain: Novel Mechanisms for Neural Transmission*. New York: Raven Press.

Fuxe, K., and Agnati, L. F. (1991a). "Wo principle modes of electrochemical communication in the brain: volume versus wiring transmission," in *Volume Transmission in the Brain: Novel Mechanisms of Neuronal Transmission*, eds K. Fuxe and L. F. Agnati (New York: Raven Press), 1–9.

Fuxe, K., Dahlstrom, A., Hoistad, M., Marcellino, D., Jansson, A., Rivera, A., Diaz-Cabiale, Z., Jacobsen, K., Tinner-Staines, B., Hagman, B., Leo, G., Staines, W., Guidolin, D., Kehr, J., Genedani, S., Belluardo, N., and Agnati, L. F. (2007). From the Golgi–Cajal mapping to the transmitter-based characterization of the neuronal networks leading to two modes of brain communication: wiring and volume transmission. *Brain Res. Rev.* 55, 17–54.

Fuxe, K., Dahlström, A. B., Jonsson, G., Marcellino, D., Guescini, M., Dam, M., Manger, P., and Agnati, L. (2010). The discovery of central monoamine neurons gave volume transmission to the wired brain. *Prog. Neurobiol.* 90, 82–100.

Fuxe, K., Hedlund, P., von Euler, G., Lundgren, K., Martire, M., Ögren, S. O., Eneroth, P., and Agnati, L. F. (1991). "Galanin/5-HT interactions in the rat central nervous system. Relevance for depression," in *Galanin. A New Multifunctional Peptide in the Neuroendocrine System, Wenner-Gren Int Series Vol 58,* eds T. Hökfelt, T. Bartfai, D. Jacobowitz, and D. Ottoson (London: Macmillan Press), 221–235.

Jansson, A., Descarries, L., Cornea-Hebert, V., Riad, M., Verge, D., Bancila, M., Agnati, L. F., Fuxe, K. (2002). "Transmitter-receptor mismatches in central dopamine serotonin and neuropeptide systems," in *The Neuronal Environment: Brain Homeostasis in Health and Disease*, ed. W. Walz (Totowa, NJ: Humana Press), 83–107.

Jansson, A., Lippoldt, A., Mazel, T., Bartfai, T., Ogren, S. O., Sykova, E., Agnati, L. F., and Fuxe, K. (2000). Long distance signalling in volume transmission. Focus on clearance mechanisms. *Prog. Brain Res.* 125, 399–413.

Joca, S. R., Guimarães, F. S., and Del-Bel, E. (2007). Inhibition of nitric oxide synthase increases synaptophysin mRNA expression in the hippocampal formation of rats. *Neurosci. Lett.* 421, 72–76.

Kaushalya, S. K., Nag, S., Ghosh, H., Arumugam, S., and Maiti, S. (2008a). A high-resolution large area serotonin map of a live rat brain section. *Neuroreport* 19, 717–721.

Kaushalya, S. K., Desai, R., Arumugam, S., Ghosh, H., Balaji, J., and Maiti, S. (2008b). Three-photon microscopy shows that somatic release can be a quantitatively significant component of serotonergic neurotransmission in the mammalian brain. *J. Neurosci. Res.* 86, 3469–3480.

Perrier, J. F., and Cotel, F. (2008). Serotonin differentially modulates the intrinsic properties of spinal motoneurons from the adult turtle. *J. Physiol. (Lond.)* 586, 1233–1238.

Trueta, C., Mendez, B., and De-Miguel, F. F. (2003). Somatic exocytosis of serotonin mediated by L-type calcium channels in cultured leech neurones. *J. Physiol. (Lond.)* 547, 405–416.

Trueta, C., Sanchez-Armass, S., Morales, M. A., and De-Miguel, F. F. (2004). Calcium-induced calcium release contributes to somatic secretion of serotonin in leech Retzius neurons. *J. Neurobiol.* 61, 309–316.

Velazquez-Ulloa, N., Blackshaw, S. E., Szczupak, L., Trueta, C., Garcia, E., and De-Miguel, F. F. (2003). Convergence of mechanosensory inputs onto neuromodulatory serotonergic neurons in the leech. *J. Neurobiol.* 54, 604–617.

Yuan, S., and Burrell, B. D. (2010). Endocannabinoid-dependent LTD in a nociceptive synapse requires activation of a presynaptic TRPV-like receptor. *J. Neurophysiol.* 104, 2766–2777.

Received: 22 December 2011; accepted: 24 January 2012; published online: 15 February 2012.

Citation: De-Miguel FF and Fuxe K (2012) Extrasynaptic neurotransmission as a way of modulating neuronal functions. Front. Physio. ***3****:16. doi: 10.3389/fphys.2012.00016*

This article was submitted to Frontiers in Membrane Physiology and Biophysics, a specialty of Frontiers in Physiology.

frontiers in
PHYSIOLOGY

REVIEW ARTICLE
published: 04 September 2012
doi: 10.3389/fphys.2012.00319

Extrasynaptic exocytosis and its mechanisms: a source of molecules mediating volume transmission in the nervous system

Citlali Trueta*[1] *and* ***Francisco F. De-Miguel*[2]**

[1] *Departamento de Neurofisiología, Instituto Nacional de Psiquiatría Ramón de la Fuente Muñiz, México, D.F., México*
[2] *Instituto de Fisiología Celular, Universidad Nacional Autónoma de México, México, D.F., México*

Edited by:
Kjell Fuxe, Karolinska Institutet, Sweden

Reviewed by:
Kjell Fuxe, Karolinska Institutet, Sweden
A. Del Arco, Universidad Complutense de Madrid, Spain

****Correspondence:***
Citlali Trueta, Departamento de Neurofisiología, Instituto Nacional de Psiquiatría Ramón de la Fuente Muñiz, Calzada México-Xochimilco 101, Tlalpan 14370, México, D.F., México.
e-mail: ctrueta@imp.edu.mx

We review the evidence of exocytosis from extrasynaptic sites in the soma, dendrites, and axonal varicosities of central and peripheral neurons of vertebrates and invertebrates, with emphasis on somatic exocytosis, and how it contributes to signaling in the nervous system. The finding of secretory vesicles in extrasynaptic sites of neurons, the presence of signaling molecules (namely transmitters or peptides) in the extracellular space outside synaptic clefts, and the mismatch between exocytosis sites and the location of receptors for these molecules in neurons and glial cells, have long suggested that in addition to synaptic communication, transmitters are released, and act extrasynaptically. The catalog of these molecules includes low molecular weight transmitters such as monoamines, acetylcholine, glutamate, gama-aminobutiric acid (GABA), adenosine-5-triphosphate (ATP), and a list of peptides including substance P, brain-derived neurotrophic factor (BDNF), and oxytocin. By comparing the mechanisms of extrasynaptic exocytosis of different signaling molecules by various neuron types we show that it is a widespread mechanism for communication in the nervous system that uses certain common mechanisms, which are different from those of synaptic exocytosis but similar to those of exocytosis from excitable endocrine cells. Somatic exocytosis has been measured directly in different neuron types. It starts after high-frequency electrical activity or long experimental depolarizations and may continue for several minutes after the end of stimulation. Activation of L-type calcium channels, calcium release from intracellular stores and vesicle transport towards the plasma membrane couple excitation and exocytosis from small clear or large dense core vesicles in release sites lacking postsynaptic counterparts. The presence of synaptic and extrasynaptic exocytosis endows individual neurons with a wide variety of time- and space-dependent communication possibilities. Extrasynaptic exocytosis may be the major source of signaling molecules producing volume transmission and by doing so may be part of a long duration signaling mode in the nervous system.

Keywords: exocytosis, extrasynaptic, serotonin, somatic exocytosis, volume transmission, mechanisms of extrasynaptic exocytosis

INTRODUCTION

Communication in the nervous system is classically known to occur at synapses, where a neurotransmitter released from the presynaptic active zone reaches the postsynaptic membrane and produces a local synaptic potential. The millisecond time scale of these responses allows neuronal circuits to produce rapid behavioral responses, from relatively simple ones, like an avoidance reaction to a warm surface, to others requiring incredible amounts of computation in extremely short periods of time, such as playing tennis at high speed, in which the location of the ball, its speed, trajectory, force, and direction must be calculated in less than a second to hit the ball back and send it to the right place. However, the nervous system also possesses the parallel capacity of changing its responses for very long periods of time, lasting from seconds to days. For example, mood states may change the quality of the tennis player performance by modulating the input–output relationships of the brain. Events lasting for seconds or less may change the responses of our brain circuits for hours or longer. How does this happen?

The discovery of extrasynaptic receptors by Miledi (1960), was followed by observations by Dun and Minota (1982) of peripheral neuronal responses that could be attributed to somatic exocytosis of signaling molecules upon electrical stimulation. In addition, the discovery of extracellular concentrations of monoamines at a distance from synaptic endings, and the mismatch between peptide exocytosis sites and receptors, led Fuxe and colleagues to propose volume transmission as a way of communication in the nervous system, parallel to that of hard-wired circuits (Agnati et al., 1986a,b; Fuxe et al., 2012; see also Fuxe et al., in this issue). The presence of extrasynaptic receptors for acetylcholine,

glutamate, and gama-aminobutiric acid (GABA) in vertebrate (for review see Vizi et al., 2010) and invertebrate (see for example, Sargent et al., 1977) neurons and the detection of these transmitters in the extracellular fluid in concentrations capable of activating their receptors suggest that the "classical" low molecular weight neurotransmitters previously thought to act exclusively on synapses, also participate in extrasynaptic communication. In fact, several functions for extrasynaptic communication through these transmitters have been demonstrated in different areas of the central nervous system.

However the source of these molecules in the extracellular space was not clear, and while it was initially thought that it was caused by transmitter spillover from synaptic release sites, the amount of transmitter released from presynaptic endings and their local degradation or uptake makes it difficult to expect that these molecules have a synaptic origin.

Morphological evidence as to the presence of small clear and large dense core vesicles in the soma, axonal varicosities, and dendrites and of dense core vesicles in the periphery of synapses in the absence of postsynaptic counterparts, suggested that transmitters and peptides could also be released extrasynaptically. In the past fifteen years a variety of studies applying diverse techniques have provided direct evidence that serotonin, dopamine, noradrenaline, adenosine-5-triphosphate (ATP), and peptides such as substance P, brain-derived neurotrophic factor (BDNF), or oxytocin, are released by exocytosis from extrasynaptic sites by central and peripheral neurons of invertebrates and vertebrates. These molecules activate mainly metabotropic receptors that exert indirect and therefore slower effects than those of synaptic transmitters acting on ionotropic receptors. This already is sufficient to expand the timing of neuronal communication, and in addition to the diffusion and permanence of transmitter molecules in the extracellular space, explains the long time course of modulation mediated by volume transmission. Acetylcholine, glutamate and GABA have now been added to the list of transmitters acting extrasynaptically.

Extrasynaptic release of low molecular weight transmitters occurs through different mechanisms, including exocytosis, the reversal of transporter proteins, release through pores or diffusion through the plasma membrane. In this review we will focus on extrasynaptic exocytosis of different signaling molecules and its mechanisms. We will start this review with the evidence for extrasynaptic exocytosis of serotonin for two reasons. The first is that many of the mechanisms underlying its exocytosis from the soma have now been studied with detail and thus, it serves as a reference point for the search for general principles. The second is that many of its extrasynaptic effects have been demonstrated experimentally.

SEROTONIN

5-hydroxytriptamine (5-HT), also known as serotonin because of the first function described for it, is a monoamine involved in the regulation of multiple functions including sleep, circadian rhythms, digestion, hormone secretion, learning, and the generation of central rhythmic locomotory, respiratory, masticatory and pyloric patterns (McCall and Aghajanian, 1979; Prosser et al., 1990; Raleigh et al., 1991; Jacobs and Azmitia, 1992; Jacobs and Fornal, 1993; White et al., 1996; Weiger, 1997; Hull et al., 1999; Kravitz, 2000; Richards et al., 2003; Cruz-Bermúdez and Marder, 2007). Alterations in the serotonergic system in humans lead to psychiatric disorders such as depression, anxiety, feeding, or sleep disorders or schizophrenia (Charney, 1998; Arango et al., 2002; Brieden et al., 2002; Durant et al., 2010).

MORPHOLOGY OF SEROTONERGIC SYSTEMS IN RELATION TO EXTRASYNAPTIC EXOCYTOSIS

A striking but conserved characteristic of serotonergic systems is that relatively small numbers of neurons accomplish multiple functions. While the serotonergic system in a leech intermediate ganglion is composed by a network of three pairs plus one single neuron (out of 400 total neurons), in mammals there are only between 9000 (in rodents) and 90,000 (in humans; Underwood et al., 1999) serotonergic neurons (accounting to a proportion of 1:1,000,000 of the total neurons in the human brain), whose somata are located in the raphe brainstem nuclei, (Dahlström and Fuxe, 1964; Jacobs and Azmitia, 1992).

Serotonergic projections in vertebrates and invertebrates branch profusely and have complex innervations to virtually all areas of the central nervous system, sometimes forming synapses, while others forming varicosities that contain clear and/or dense core vesicles but lacking postsynaptic counterparts (Descarries and Mechawar, 2000; reviewed by Bunin and Wightman, 1999). Serotonergic axons innervating the ventral horns of the spinal cord (Kiehn et al., 1992; Alvarez et al., 1998) or the substantia nigra reticulata (Moukhles et al., 1997) establish mostly synaptic contacts with well-defined target neurons; however in dorsal horns of the spinal cord (Ridet et al., 1993) and in the nucleus accumbens (Van Bockstaele and Pickel, 1993), nearly 60% of the 5-HT terminals do not form synapses. Axons originating in different mammalian nuclei and projecting to the same brain area may have different connection patterns. For example, in the hippocampus, varicosities of fibers arriving from the median raphe form direct synapses with interneurons (Freund and Buzsáki, 1996; Varga et al., 2009), whereas fibers originating in the dorsal raphe form varicosities but rarely synapses (Kosofsky and Molliver, 1987). Recurrent axon collaterals ending in the dorsal raphe contain both synaptic and non-synaptic endings (Chazal and Ralston, 1987).

The dendrites of serotonergic neurons in the dorsal raphe nucleus also contain serotonin in small clear and large dense-core vesicles (Kapadia et al., 1985; Liposits et al., 1985; Chazal and Ralston, 1987). These vesicles can be densely packed in clusters, some of which are located at dendro-dendritic synapses with serotonergic or other types of neurons. Other vesicles are not associated with the characteristic presynaptic active zone specializations, and thus seem to be suitable for extrasynaptic exocytosis. In the somata of serotonergic neurons of leech and rat, visualized by electron microscopy (Coggeshall, 1972; Trueta et al., 2004, 2012) or 3-photon microscopy (Kaushalya et al., 2008a) serotonin accumulates in multivesicular structures, which in leech Retzius neurons have been clearly identified as clusters of dense core vesicles (Trueta et al., 2012). In fact, the amount of serotonin in the somatic area of raphe neurons is quantitatively comparable to that

in brain areas with dense serotonergic innervation (Kaushalya et al., 2008b).

All this morphological evidence suggests that serotonin is not only released from presynaptic terminals, but also from extrasynaptic sites in axons, dendrites, and somata.

INDIRECT EVIDENCE OF EXTRASYNAPTIC SEROTONIN EXOCYTOSIS

Morphological evidences of extrasynaptic exocytosis sites agree with serotonin measurements in the extracellular fluid. The serotonin concentration and, more importantly, its dynamic changes in response to stimulation, have been monitored by fast-scan cyclic voltammetry in several areas of the central nervous system of vertebrates and invertebrates. Since the size of carbon fiber electrodes used for voltammetry is much bigger than the synaptic clefts, it is generally accepted that these measurements reflect the serotonin concentration in extrasynaptic sites. Extracellular serotonin has been measured by amperometry in the neuropile of the *Aplysia* central nervous system (Marinesco and Carew, 2002), where it modulates synaptic plasticity and simple learning (Marinesco et al., 2006). In mammalian central nervous systems, extrasynaptic serotonin has been detected both in regions with primarily synaptic connections, and in regions where exocytosis seems to be extrasynaptic. In the substantia nigra reticulata (Bunin and Wightman, 1998) or the spinal cord (Hentall et al., 2006), which have serotonergic synaptic terminals, 5-HT has been readily detected in response to single stimulation pulses. In these regions the amount of serotonin molecules released following single impulses is smaller than the amount of receptors and transporters, but its detection is not affected by reuptake inhibitors or receptor antagonists, suggesting that although exocytosis occurs mainly from synaptic terminals, transporters are localized extrasynaptically, thus allowing serotonin spillover (Bunin and Wightman, 1998). On the other hand, extracellular serotonin has also been measured in brain regions such as the dorsal raphe or the hippocampus, which lack synaptic contacts, thus supporting that release occurs also from extrasynaptic sites. Microdialysis studies showed physiological changes in the extracellular levels of serotonin in response to pharmacological or behavioral modulation (Brazell et al., 1985; Sharp et al., 1989; Wright et al., 1992; Pudovkina et al., 2003; Mansari et al., 2007), and voltammetry studies have measured increases in extracellular serotonin upon electrical stimulation (Bunin and Wightman, 1998; Swanson et al., 2005).

The presence of extrasynaptic 5-HT receptors in the central nervous system further supports the possibility of serotonin acting through paracrine or volume transmission (Bunin and Wightman, 1999). 5-HT1A receptors are located exclusively in the somata and dendrites of serotonergic neurons in the dorsal raphe (Kia et al., 1996; Riad et al., 2000), and in non-serotonergic neurons in the hippocampus, suggesting that they modulate neuronal firing of serotonergic and non-serotonergic neurons. On the other hand, 5-HT1B receptors are preferentially associated with preterminal axons in the globus pallidus and the substantia nigra, where they could modulate axonal impulse conduction (Riad et al., 2000). In addition, direct evidence of the extrasynaptic localization of functional 5-HT transporters along axons has been provided by immunohystochemistry in the cingulated cortex, cingulum bundle, medial forebrain bundle, corpus callosum, and dorsal raphe (Zhou et al., 1998). The extrasynaptic serotonin concentrations, as measured by voltammetry, match the affinities of the predominant receptors in each brain region (Bunin and Wightman, 1998), further supporting that serotonin acts through volume transmission.

DIRECT EVIDENCE AND MECHANISMS OF SOMATIC SEROTONIN EXOCYTOSIS

Direct evidence of physiological somatic exocytosis of serotonin first came from Retzius neurons of the leech central nervous system (Trueta et al., 2003). The soma of these neurons contains "astronomical quantities" of large (100 nm) dense-core vesicles containing serotonin (Coggeshall, 1972). Retzius neurons have the advantage that they can be studied in the ganglion or in culture, since in spite of being adult, they can be isolated individually and maintained in culture for weeks, where they keep their electrical properties, continue to synthesize and release quantal packages of serotonin both from the soma or from synapses with another Retzius neuron or with pressure-sensory neurons (for review see Fernández-de-Miguel and Drapeau, 1995). These synapses were the first established in culture (Fuchs et al., 1981) and have been useful to study on one hand, the steps in the formation of synapses. For example, the formation of serotonergic synapses produces retrograde and anterograde effects on calcium currents and reduces neurite extension by postsynaptic neurons (Cooper et al., 1992; Fernandez-De-Miguel et al., 1992). On the other hand this preparation has allowed studying the fine mechanisms of serotonin exocytosis. In these synapses clear synaptic vesicles are surrounded by electrodense vesicles, and both types of vesicles contain serotonin (Kuffler et al., 1987; Bruns and Jahn, 1995). Serotonin exocytosis from clear and dense core vesicles is quantal (Henderson et al., 1983; Bruns and Jahn, 1995) and calcium dependent (Dietzel et al., 1986), although serotonin release from clear vesicles occurs in response to single action potentials, whereas exocytosis from electrodense vesicles occurs upon subsequent stimulation (Bruns and Jahn, 1995; see **Figure 1**). Released serotonin reduces the amplitude of action potentials arriving at the serotonergic terminals, thus producing a presynaptic autoinhibition (Cercós et al., 2009). Altogether, these studies have provided most of our current knowledge about the fine mechanisms of serotonin release from synapses (Nicholls and Kuffler, 1990; Zimmermann, 1993).

Retzius neurons have also provided substantial evidence about the mechanisms of somatic exocytosis of serotonin (De-Miguel and Trueta, 2005; **Figure 1**). This information is proving useful to explain processes that also apply to other cell types releasing different signaling molecules, as will be seen below.

Addition of ionomycin to the soma of isolated Retzius neurons evokes quantal serotonin exocytosis from dense core vesicles, as demonstrated by amperometric recordings (Bruns et al., 2000). That somatic serotonin exocytosis is physiological was demonstrated by our own studies combining electrophysiology, fluorescence imaging, and electron microscopy in neurons in the ganglion and in culture. Somatic dense core vesicles at rest are located in two pools: one around the nucleus and another in more peripheral areas of the cytoplasm, although distant from the

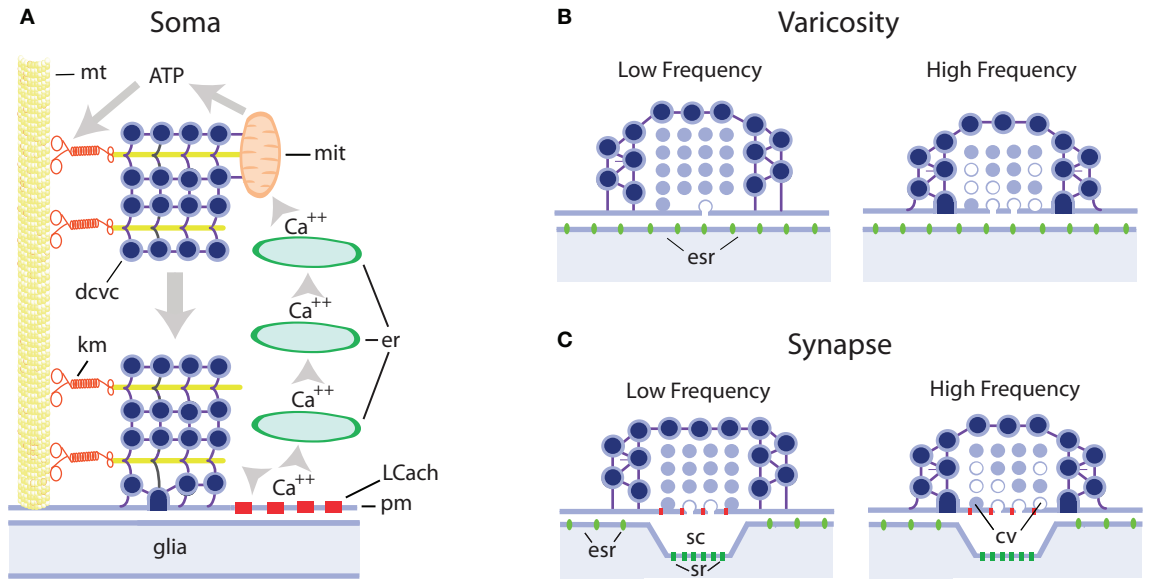

FIGURE 1 | Schematic representation of extrasynaptic and synaptic exocytosis from clear and dense core vesicles in different regions of serotonergic neurons. (A) Mechanism of long-lasting somatic secretion from dense core vesicles in leech Retzius neurons. Electrical stimulation of neurons with trains of 10–20 Hz produces transmembrane calcium entry through L type channels (LCach). This calcium in turn activates calcium-induced calcium release from progressively more internal endoplasmic reticulum stores (er). Calcium waves propagate to internal regions of the soma and activate ATP synthesis by the mithocondria (mit). The ATP increase activates kinesin motors (km) that transport dense core vesicle clusters (dcvc) along microtubule rails (mt) towards the plasma membrane (pm), with which they fuse. This exocytosis lasts for minutes after the end of the train of electrical activity. Serotonin is released onto glial cells. **(B)** Hypothetical model of serotonin release from axonal varicosities containing clear and/or dense core vesicles. Both vesicle types may contain serotonin, as in serotonergic raphe neurons, and at rest lay at nanometer distances from the plasma membrane. In these cases exocytosis occurs in the absence of a postsynaptic counterpart and serotonin activates extrasynaptic receptors (esr). It is expected that with this configuration single impulses or low frequency trains do not evoke significant amounts of exocytosis although they contribute to approaching vesicles toward the plasma membrane, thus increasing the probability of release upon subsequent impulses. At high frequencies, both vesicle pools increase their fusion probability. The vesicles with white centers represent those during or after exocytosis **(C)** Synaptic and extrasynaptic exocytosis from synaptic bouttons. Clear vesicles at presynaptic endings are apposed to the plasma membrane and single impulses evoke exocytosis with mechanisms similar to those in neuromuscular junction. Dense core vesicles surrounding clear vesicles have low release probability and subsequent impulses increase the probability of exocytosis. At high frequencies, the clear vesicle pool enters the facilitation/depression dynamics, whereas the dense core vesicle pool increases its release probability. While clear vesicle contents are released onto the synaptic cleft and affect mostly synaptic receptors (sr), dense core vesicles release their contents extrasynaptically and serotonin activates extrasynaptic receptors (esr). For additional details and references see the text.

plasma membrane (Rude et al., 1969; Trueta et al., 2004, 2012). Electrical stimulation with trains of 10 impulses at 10 or 20 Hz, but not at a low 1 Hz frequency, induces exocytosis for several minutes. The kinetics of somatic serotonin exocytosis in Retzius neurons have been studied by the gradual incorporation of fluorescent dye FM1-43 (Trueta et al., 2003), which binds to the vesicles as they fuse with the plasma membrane, thus increasing the fluorescence of the dye (Kilic et al., 2001). Exocytosis usually starts tens of seconds after stimulation and lasts for several minutes. The interpretation for this slow kinetics is the involvement of active transport of vesicle clusters from distant intracellular regions to the plasma membrane using microtubules as rails (Trueta et al., 2012; De-Miguel et al., in press). Electrical stimulation activates L-type calcium channels (Trueta et al., 2003), and at high stimulation frequencies, this calcium activates calcium-induced calcium release from intracellular stores (Trueta et al., 2004). It is possible to suppose that calcium arriving at the mitochondria activates ATP synthesis and this in turn activates kinesin-mediated transport of vesicles (**Figure 1**). An open question is how exocytosis is sustained for such long periods of time. After exocytosis, dense core, and small clear vesicles, the later formed in response to endocytosis, are incorporated into multivesicular bodies that travel back to the perinuclear zone, where they apparently release their contents, some of which are re-used in the formation of new vesicles (Trueta et al., 2012, in this issue).

Each Retzius neuron produces 100–120 FM1-43 fluorescent spots upon a train of ten impulses at 20 Hz (Trueta et al., 2003), each spot corresponding to a release site in which 100–1000 vesicles fuse (De-Miguel et al., in press). Therefore, tens of thousands of somatic vesicles may fuse in response to a 20 Hz train lasting 0.5 s, with each vesicle containing 67,000 molecules of serotonin (Bruns and Jahn, 1995). An equivalent amount of serotonin is secreted by the other Retzius neuron in the ganglion, since both respond in parallel upon the activation of common synaptic inputs (Velázquez-Ulloa et al., 2003). Although several questions still remain open, it is not surprising that a neuron pair is capable of producing the multiple modulatory effects of serotonin seen in the leech (Willard, 1981; Kristan and Nusbaum, 1982; Burrell et al., 2002; Crisp and Mesce, 2006; Calviño and Szczupak, 2008; Bisson and Torre, 2011).

It is noteworthy that somatic serotonin is released onto glial cells wrapping the somata of Retzius neurons (Trueta et al., 2012). Therefore, not only exocytosis occurs from regions with an apparent absence of well-defined presynaptic structures, but the immediate target is non neuronal. How does serotonin reach its neuronal targets through glial cells is not yet known; however studies on peripheral ATP-releasing somata (Zhang et al., 2007; see below) have provided interesting evidence about this (see below).

A similar slow kinetics of somatic exocytosis of serotonin has been demonstrated in dissociated rat dorsal raphe neurons, by measuring serotonin fluorescence with multi-photon microscopy. Serotonin in the soma of these neurons is contained in perinuclear vesicle clusters and is released upon depolarization with high potassium (Kaushalya et al., 2008a) or glutamate receptor activation (Colgan et al., 2009). The amount of serotonin released from the soma is comparable to that released in areas with a high density of serotonergic processes, suggesting that somatic exocytosis plays a major role in the overall serotonergic transmission (Kaushalya et al., 2008b). Somatic serotonin exocytosis upon stimulation is maintained by continuous vesicular packaging by the vesicular monoamine transporter located in the nucleus and cytoplasm. Serotonin packaged during stimulation is released preferentialy, while that packaged at rest is held in a reserve pool (Colgan et al., 2009).

The frequency dependence of somatic secretion correlates with the responses of 5-HT autoreceptors in raphe nucleus neurons, used as an indirect measure of serotonin release (O'Connor and Kruk, 1991). This frequency dependence and the latency of exocytosis can be explained in terms of a highly regulated secretion process that requires the active transport of vesicles toward the plasma membrane in response to electrical stimulation and, as result of this, high energy expenses (De-Miguel et al., in press). On the other hand a question yet to be answered is how calcium-dependent exocytosis is sustained long after electrical stimulation has ended, since vesicular transport seems to be the major source of delay between stimulation and secretion.

REGULATION OF SOMATODENDRITIC SEROTONIN EXOCYTOSIS

Somatodendritic serotonin release is regulated by multiple factors, including different synaptic inputs onto serotonergic neurons (Velázquez-Ulloa et al., 2003) and by serotonin itself (see below). In raphe neurons glutamate stimulates somato-dendritic serotonin exocytosis (de Kock et al., 2006; Colgan et al., 2009), and dendritic calcium influx through NMDA receptors evokes exocytosis in the absence of action potentials (de Kock et al., 2006). In contrast, noradrenaline and GABA inhibit serotonin release by activating α-2 and GABA-A receptors, respectively (Kalsner and Abdali, 2001; de Kock et al., 2006).

Somatodendritic serotonin release activates 5-HT2A and 5-TH2C receptors in GABAergic neurons that innervate the dorsal raphe (Liu et al., 2000), thus increasing the frequency of GABAergic inputs onto 5-HT neurons (de Kock et al., 2006), and producing a negative feedback loop within the nucleus. In addition, serotonin released from the somatodendritic compartments activates 5-HT1A, 5-HT1B, and 5-HT1D autoreceptors, which in turn inhibit serotonin exocytosis (Davidson and Stamford, 1995) through the activation of calcium/calmodulin protein kinase II and protein kinase A (Liu et al., 2005).

PHYSIOLOGICAL FUNCTIONS OF EXTRASYNAPTIC SEROTONIN RELEASE

Important roles for the extracellular elevations of serotonin, presumably from extrasynaptic exocytosis, have been shown in food-related behaviors in *C. elegans* (Harris et al., 2011; Jafari et al., 2011) and leech (Lent and Dickinson, 1984; Lent, 1985; Groome et al., 1993). Serotonin in leeches regulates sensitization of the whole body-shortening reflex by potentiating excitability and modulating the electrical coupling between S-cells (Moss et al., 2005), and induces social behavior (Burrell and Sahley, 2005; see Bisson et al., 2012, in this issue). Circulating serotonin in lobsters determines their social dominance by affecting from sensory inputs to motor outputs of behavioral circuits (Kravitz, 2000), and manipulation of serotonergic transmission in flies modulates fighting and aggression (Alekseyenko et al., 2010), although it has not been determined if these effects operate through synaptic or extrasynaptic mechanisms. Extrasynaptic serotonin may also modulate mood and social behavior in mammals. In fact, the effects of many antidepressant drugs seem to be mostly extrasynaptic (Kiss, 2008). Thus, understanding the regulation of extrasynaptic release of serotonin should lead to improvements in the treatment of depression and other psychiatric disorders.

DOPAMINE

From mandibulate fish to mammals (Reiner, 2009), basal ganglia contain the somata of dopaminergic neurons clustered in two main areas: the substantia nigra and the ventral tegmental area (Dahlström and Fuxe, 1964). Substantia nigra neurons project to the striatum of the basal ganglia, forming the nigrostriatal pathway; neurons in the ventral tegmental area project to the nucleus accumbens, amygdala, and prefrontal cortex, forming the mesolimbic and mesocortical systems. The arcuate nucleus and hypothalamus also contain dopaminergic neurons, which project to the median eminence forming the tuberoinfundibular system; dopaminergic neurons in the dorsal raphe nucleus project to the prefrontal cortex (Yoshida et al., 1989).

Dopamine acts exclusively through G-protein-coupled receptors that usually modulate cyclic AMP production (for review, see Romanelli et al., 2010). The D1 family, which includes D1 and D5 receptors, increases the levels of cyclic AMP, whereas activation of D2-like (including D3 and D4) receptors inhibits adenylate cyclase, and thereby decreases the cAMP levels. D1 receptors are located at extrasynaptic sites in dendritic spines in the cerebral cortex of primates (Smiley et al., 1992), while D2 receptors are located both in synaptic terminals and in preterminal axons in the striatum (Sesack et al., 1994). D2 receptors are also located in the somatodendritic area of dopaminergic neurons in the substantia nigra (Sesack et al., 1994), where they produce autoinhibitory effects (see below). The high affinity of D2 receptors suggests that they participate in dopaminergic volume transmission *in vivo* (Marcellino et al., 2011). Dopamine mediates fear and anxiety responses in the amygdala where dopamine release by synaptic terminals produces disinhibition of fear responses, leading to anxious behavior. Extrasynaptic dopamine on the other hand,

contributes to reducing the anxiety levels under no danger conditions, by activating GABAergic neurons that inhibit anxiety responses (for review, see Pérez de la Mora et al., 2008).

EXTRASYNAPTIC DOPAMINE EXOCYTOSIS

As in the serotonergic system, small numbers of dopaminergic neurons give rise to hundreds of thousands of varicosities that diffusely innervate large target areas (reviewed by Descarries and Mechawar, 2000). Dopaminergic varicosities may contain small clear or large dense-cored vesicles but they lack postsynaptic specializations in the cortex (Séguéla et al., 1988; Papadopoulos et al., 1989; Smiley et al., 1992; Smiley and Goldman-Rakic, 1993; Erickson et al., 2000), striatum (Descarries et al., 1996), and spinal cord (Ridet et al., 1993), suggesting that these structures display extrasynaptic exocytosis.

The somata and dendrites of dopaminergic neurons in the substantia nigra and the ventral tegmental area also release dopamine (Björklund and Lindvall, 1975; Geffen et al., 1976; Cheramy et al., 1981; Jaffe et al., 1998), as first shown by H^3-incubated nigral slices (Geffen et al., 1976), and by push-pull cannula *in vivo* in anaesthetized rats (Nieoullon et al., 1977). More recently, extracellular dopamine increases were detected upon electrical stimulation by use of fast scan cyclic voltammetry in slices containing the substantia nigra or the ventral tegmental area (Rice et al., 1997; Chen and Rice, 2001; Chen et al., 2006; Ford et al., 2010), suggesting that dopamine had been released from the somata and dendrites, presumably through exocytosis (Fortin et al., 2006; Witkovsky et al., 2009). As with varicose axonal endings, the evidence for pre- or postsynaptic specializations in the midbrain DA neurons is limited (Wilson et al., 1977; Groves and Linder, 1983), suggesting that dopamine exocytosis from these compartments is extrasynaptic.

Direct records of dopamine somatic exocytosis have been obtained using carbon fiber amperometry from giant dopaminergic neurons of the pond snail *Planorbis corneus*. These neurons produce bursts of quantal release from two vesicle populations (Chen et al., 1996; Anderson et al., 1999). Amperometric currents recorded from neurons in the pars compacta of the substantia nigra demonstrated quantal release in response to glutamate or high potassium application (Jaffe et al., 1998). This evidence has been complemented by the amperometric demonstration that dopamine is released in the retina from the soma of amacrine cells, depending on electrical activity and calcium entry though L-type channels (Puopolo et al., 2001).

MECHANISMS OF EXTRASYNAPTIC EXOCYTOSIS OF DOPAMINE

That dopamine extrasynaptic release occurs through exocytosis in nigral dopaminergic neurons was supported by its blockade by botulinum toxins (Fortin et al., 2006). However, its mechanisms differ from those of presynaptic terminals in several respects. First, the presynaptic proteins synaptotagmin 1, syntaxin1, synaptic vesicle proteins 2a and 2b, synaptophysin, and synaptobrevin 1 (VAMP 1) are absent from these neurons (Witkovsky et al., 2009). Similar striking results have been obtained from hypothalamic neurons (reviewed by Tobin et al., 2012, in this issue). Second and similar to serotonergic somatic secretion (Trueta et al., 2004), dopamine release in the substantia nigra has a significant contribution of calcium release from intracellular stores (Patel et al., 2009). Third, the time course of evoked increases in extracellular dopamine in guinea pig slices is ten-fold slower in somatodendritic areas in the substantia nigra, than in the synaptic striatal areas (Chen and Rice, 2001). Additional differences have been found in dopaminergic neurons of guinea pig substantia nigra, which has a much lower calcium dependence, with a maximum at 1.5 mM extracellular concentration (Chen and Rice, 2001; Chen et al., 2011), showing high calcium affinity but low cooperativity, while release in the striatum requires concentrations above 1.5 mM and has low affinity and high cooperativity (Chen et al., 2011). While synaptic dopamine release from the striatum is reduced by blockers of N, P/Q, T, or R calcium channels, release in the substantia nigra is insensitive to all these blockers, although it depends on the activation of voltage-gated calcium channels in the substantia nigra of rat (Jaffe et al., 1998) and guinea pig (Patel et al., 2009). These last differences could be a particularity of guinea pig dopaminergic neurons since in mouse brain slices the calcium-dependence and time course of release are similar in the substantia nigra, the ventral tegment, and striatum (Ford et al., 2010).

REGULATION OF SOMATODENDRITIC DOPAMINE RELEASE IN THE SUBSTANTIA NIGRA

Activation of the serotonergic innervation to the substantia nigra increases somatodendritic dopamine release. In contrast, synaptic dopamine release from the projections of these same neurons to the striatum is not affected by serotonin, suggesting that the serotonergic regulation of somatic release is independent of impulse generation (Cobb and Abercrombie, 2003). Both axonal and somatodendritic release of dopamine are auto-inhibited by dopamine through D2 receptors (Cobb and Abercrombie, 2003).

EXTRASYNAPTIC EXOCYTOSIS OF DOPAMINE IN THE RETINA

Dopamine in the retina is produced by a group of amacrine cells that send fine processes toward photoreceptors, bipolar, and horizontal cells (Dacey, 1990; Kolb et al., 1990; Marshak, 2001). However, most of these processes do not make morphologically defined synapses (Bjelke et al., 1996), and although certain amacrine cells receive dopaminergic synaptic inputs (Kolb et al., 1990), the vast majority of retinal cells respond to dopamine that reaches them through volume transmission (Bjelke et al., 1996; Witkovsky, 2004). Dopaminergic amacrine cells release dopamine by exocytosis from the cell body (Puopolo et al., 2001) depending on the cell's electrical activity. This exocytosis is mediated by calcium entry though L-type channels, modulated by glutamate and GABA and auto-inhibited by dopamine through D2 receptors (Puopolo et al., 2001), with this last effect being similar to its autoinhibitory effects in the substantia nigra and striatum (Cobb and Abercrombie, 2003).

In the retina, 50% of the released dopamine escapes transporter uptake by dopaminergic neurons and therefore the dopamine concentration in the extracellular fluid reaches 100–1000 nM concentrations (Witkovsky et al., 1993), high enough to activate dopamine receptors in the different retinal neuronal types (Cohen et al., 1992; Muresan and Besharse, 1993; Nguyen-Legros et al., 1997), in Muller glial cells (Biedermann et al., 1995)

and in the pigment epithelium (Versaux-Botteri et al., 1997). Cells that are more distant from dopaminergic amacrine cells have the most sensitive receptors, thus being compatible with volume transmission actions (Witkovsky, 2004).

Retinal dopamine effects that may be attributed to extrasynaptic exocytosis have long been known in the retina. Electrical coupling of horizontal cells allow the flow of light responses of a particular spot to the surrounding cells (Naka and Rushton, 1967; Kaneko, 1971), thus enlarging the horizontal cell's receptive fields at the expense of space resolution. Dopamine reduces the horizontal cell coupling, thus narrowing their receptive fields (Piccolino et al., 1984; Teranishi et al., 1984) and increases the coupling between cone and rod photoreceptors, thus allowing the rod pathway to convey red chromatic information (Krizaj et al., 1998). Dopamine also activates calcium-dependent chloride channels in rods, thus reducing their synaptic transmission onto horizontal and bipolar cells and decreasing the rod pathway output. On the other hand, dopamine increases the cone output by exerting opposite effects on red cones (Stella and Thoreson, 2000; Thoreson et al., 2002). By modulating synaptic transmission from photoreceptors to horizontal and bipolar cells, dopamine changes the balance between rod and cone inputs to second order cells in the retina. Since the production of dopamine in the retina varies with a circadian rhythm, it produces an oscillation between rod and cone dominance depending on the time of the day (Wang and Mangel, 1996; Manglapus et al., 1999).

NORADRENALINE

Noradrenaline in the central nervous system modulates alertness, arousal, reward (Aston-Jones and Cohen, 2005), stress (Valentino and Van Bockstaele, 2008), and sensory information processing (Svensson, 1987). Most noradrenergic neurons have their somata in the locus coeruleus, a pontine nucleus near the fourth ventricle in the brainstem, and they innervate large areas of the nervous system, including the cortex, hippocampus, amygdala, hypothalamus, striatum, thalamus, and spinal cord (Swanson and Hartman, 1975). Like in serotonergic and dopaminergic neurons, axonal projections of noradrenergic neurons have varicose nerve endings, most of which lack synaptic contacts, but seem suitable for extrasynaptic exocytosis. Nearly all noradrenergic varicosities in the cerebral cortex are non-synaptic (Descarries et al., 1977; Aoki et al., 1998), as are more than 60% of those in the hippocampus (Hökfelt, 1968; Umbriaco et al., 1995) and in the dorsal horns of the spinal cord (Ridet et al., 1993).

Noradrenaline acts on metabotropic receptors, many of which are extrasynaptic. In monkey prefrontal cortex, immunocytochemical electron microscopy has revealed that α2A receptors are mostly localized at preterminal axons, dendritic shafts, and astrocytic processes, all lacking morphologically identifiable synaptic junctions (Aoki et al., 1998). α2A receptors are also located in extrasynaptic sites of dendrites in the central nucleus of the amygdala (Glass et al., 2002) and the tractus solitarius (Glass et al., 2001). β2 adrenergic receptors are also located in extrasynaptic dendritic and preterminal axonal sites in the spinal cord (Mizukami, 2004). Moreover, the presence of dopamine-β-hydroxylase (the noradrenaline synthesizing enzyme) in the soma and dendrites in the locus coeruleus, and the measurement of extracellular noradrenaline by microdialysis correlating with neuronal activity within the nucleus (Reviewed by Singewald and Philippu, 1998; Berridge and Abercrombie, 1999), have suggested that noradrenaline can be released from somatodendritic compartments of locus coeruleus neurons.

Carbon fiber amperometry and capacitance measurements of noradrenaline somatic exocytosis from locus coeruleus neurons (Huang et al., 2007) have demonstrated that, as for serotonergic and dopaminergic neurons, somatic exocytosis occurs from dense core vesicles, can be elicited by depolarization or impulse trains, requires calcium entry and depends on the stimulation frequency. In addition, the >100 ms latency of evoked exocytosis suggests that it also requires vesicle mobilization from internal regions to the plasma membrane.

Noradrenaline somatic exocytosis in the locus coeruleus is stimulated by NMDA and by the hormone hypocretin, which potentiates the NMDA-mediated exocytosis through the activation of protein kinase C (Chen et al., 2008). Somatic exocytosis of noradrenaline autoinhibits noradrenergic neurons through the activation of α2a adrenoreceptors, which produces a potassium-dependent hyperpolarization and decreases their firing rate (Williams et al., 1985). This in turn decreases noradrenaline release both in the locus coeruleus (Pudovkina et al., 2001; Fernández-Pastor et al., 2005; Huang et al., 2007) and in the brain projections of these neurons (Fernández-Pastor and Meana, 2002). The frequency-dependence of somatic noradrenaline exocytosis suggests that stress-induced hyperactivity of locus coeruleus neurons autoinhibits these neurons and prevents possible damaging effects of extracellular noradrenaline excess in epilepsy, stress disorders, or disorders in the sleep/arousal cycles (Reviewed by Huang et al., 2012).

ACETYLCHOLINE

Acetylcholine in the brain mediates sophisticated central aspects of behavioral control, including wakefulness and somnolence the readiness of the forebrain for input processing and essential aspects of attentional information processing (Yu and Dayan, 2002; Sarter et al., 2006; Parikh et al., 2007). The whole cerebral cortex and the hippocampus are innervated by cholinergic neurons originating in the nucleus basalis of Meynert, the substantia innominata, and the horizontal limb of the diagonal band. Cholinergic neurons in the tegmental area innervate the thalamus and midbrain dopaminergic areas, while neurons originating in the medial habenular nucleus form the habenulo-interpeduncular tract, and neurons in the striatum innervate this area and the ofactory tubercle.

In contrast to monoaminergic neurons that contain clear and dense core vesicles, cholinergic neurons in the cerebral cortex, hippocampus, and striatum have axonal varicosities bearing only small clear vesicles (Descarries and Mechawar, 2000). However, like in serotonergic and dopaminergic systems, some of these structures are synaptic (Smiley et al., 1997; Turrini et al., 2001) but most are not (Umbriaco et al., 1994; Kása et al., 1995; Descarries et al., 1997; Descarries and Mechawar, 2000), suggesting that extrasynaptic exocytosis also takes place in the cholinergic system. In support of this morphological evidence,

acetylcholine has been measured in the extracellular space by microdialysis in the striatum and the cortex (Fadel et al., 1996; Vinson and Justice, 1997; Johnson et al., 2012) showing level variations during different arousal states (reviewed by Sarter et al., 2009).

Most cholinergic receptors in the central nervous system are metabotropic and thus mediate slow indirect responses characteristic of volume transmission, although central extrasynaptic locations also contain ionotropic nicotinic receptors (reviewed by Vizi et al., 2010). Metabotropic muscarinic M1 and M2 receptors, with high affinity, are located in cortical non-cholinergic synapses (Mrzljak et al., 1993), suggesting that acetylcholine diffuses to reach these heterosynaptic receptors.

Immunolabeling or α-bungarotoxin binding in electron microscopy sections demonstrate nicotinic receptors in extrasynaptic sites or in pre- or post-synaptic terminals of GABAergic or glutamatergic synapses in the ventral tegmental area (Jones and Wonnacott, 2004), the hippocampus (Vizi and Kiss, 1998; Fabian-Fine et al., 2001), and the chick ciliary ganglion (Jacob and Berg, 1983), where they modulate the release of transmitters and their postsynaptic effects (Lendvai and Vizi, 2008). The dendrites of bipolar, amacrine, and ganglion cells in the goldfish retina also have nicotinic acetylcholine receptors in non-synaptic sites (Zucker and Yazulla, 1982). In addition, nicotinic receptors are expressed by microglial cells (Shytle et al., 2004) and astrocytes (Gahring et al., 2004), further supporting the possibility that acetylcholine diffuses through the extracellular fluid and regulates neuronal and glial cell activity. The presence of extrasynaptic nicotinic receptors suggests that they produce faster volume transmission responses than those mediated by metabotropic receptors for biogenic amines (for a detailed review, see Lendvai and Vizi, 2008).

Acetylcholine was one of the first transmitters found to be released from neuronal somata. Calcium-dependent acetylcholine somatic release in response to depolarization with high potassium or to antidromic electrical stimulation of ciliary nerves was found in denervated parasympathetic ganglia incubated with [^{3}H]-choline (Johnson and Pilar, 1980). In the habenullointerpeduncular tract, optical stimulation of cholinergic neurons expressing ChanelRhodopsin-2 induces co-release of glutamate and acetylcholine from the same terminals. Brief stimulation pulses induce glutamate release which acts as a direct transmitter; tetanic stimulation induces acetylcholine release, which produces slow inward currents in the interpeduncular nucleus cells, mediated by nicotinic receptors. The slow time course of these currents suggests that acetylcholine acts through volume transmission (Ren et al., 2011).

In autonomic ganglia synapses, the level of acetylcholinesterase activity is lower than that in the neuromuscular junction (Hartzell et al., 1977) and this could allow acetylcholine synaptic spillover. However, at synapses with a high concentration of cholinesterase, such as in the neuromuscular junction, the degradation of acetylcholine after dissociation from its receptors is so efficient, that a single molecule cannot activate a second receptor (Kuffler and Yoshikami, 1975). Thus, the evidence that acetylcholine acts by volume transmission in the brain could be an indication that this transmitter is released also from extrasynaptic sites, where it does not encounter acetylcholinesterase immediately.

Acetylcholine exocytosis from the axon, dendrites, and soma was demonstrated by use of outside-out patches of embryonic muscle membrane as detectors of release from *Xenopus* dissociated spinal neurons (Sun and Poo, 1987). Somatic exocytosis in this preparation requires prolonged suprathreshold stimulation and is dependent on the extracellular calcium concentration, supporting that vesicles need to move toward the plasma membrane. Activity- and calcium-dependent exocytosis from neurite varicosities has been demonstrated by a similar technique in magnocellular neurons dissociated from the rat basal forebrain, where exocytosis is autoinhibited by acetylcholine acting though muscarinic receptors (Allen and Brown, 1996).

GLUTAMATE

Extrasynaptic glutamate accumulates from extrasynaptic vesicular exocytosis, synaptic spillover and non-vesicular release through reversal of transporters. In neuropathic rats, the down regulation of glial glutamate transporters leads to spillover from peripheral sensory to spinal horn synapses, producing an increased NMDA receptor activation that in turn results in pathological pain (Nie and Weng, 2010). Evidence suggests that glutamate spillover and activation of extrasynaptic receptors occurs when large glutamate amounts are released from synaptic endings. For example, in the cerebellar molecular layer interneurons, activation of small numbers of parallel fibers by short stimuli produces only AMPA receptor-dependent excitatory postsynaptic currents, but synaptic facilitation or activation of large numbers of fibers adds a slow NMDA receptor-mediated current that may have an extrasynaptic origin (Clark and Cull-Candy, 2002; Ikonomu et al., 2012 in this issue).

Extrasynaptic glutamate is co-released with ATP through calcium-dependent vesicular exocytosis from olfactory bulb axons (Rieger et al., 2007; Thyssen et al., 2010) in response to action potentials. Both transmitters mediate axonal-glial communication through activation of mGluR1 and P2Y1 receptors respectively (Rieger et al., 2007). These transmitters also activate calcium signals in white matter astrocytes, which in turn release ATP, thus spreading the calcium signals to neighboring glial cells (Hamilton et al., 2008).

Astrocytes in culture and in slice preparations also release glutamate by several mechanisms (Parpura et al., 1994; Bezzi et al., 1998; reviewed by Malarkey and Parpura, 2008) including calcium-dependent vesicular exocytosis, as demonstrated by use of total internal reflection fluorescence (TIRF) microscopy (Bezzi et al., 2004), amperometry of dopamine as a surrogate transmitter for glutamate (Chen et al., 2005), or measurements of membrane capacitance (Zhang et al., 2004). Exocytosis in astrocytes occurs from small clear vesicles, which fuse with the membrane using the SNARE protein complex. Calcium release from IP3- and ryanodine-sensitive stores has a crucial contribution to this astrocytic glutamate exocytosis (Hua et al., 2004). Although glutamate release sites in astrocytes are unknown, this source of extrasynaptic glutamate can produce calcium elevations in neighboring neurons (Bezzi et al., 1998).

GABA

GABA is the main inhibitory synaptic transmitter in the nervous system. However, the presence of extrasynaptic GABA receptors in addition to the occurrence of slow and diffuse effects of GABAergic neurons, and the tonic inhibition of neurons in different areas of the central nervous system, suggest that GABA acts also through volume transmission.

Extrasynaptic GABA-A receptors are present in several areas of the nervous system (Somogyi et al., 1989; for review see Mody, 2001; Kullmann et al., 2005). In cerebellar granule cells, the number of extrasynaptic GABA-A receptors is higher than that of synaptic receptors (Nusser et al., 1995). Moreover, GABA-A receptors containing the delta subunit are exclusive of extrasynaptic sites in these cells (Nusser et al., 1998) and in hippocampal dentate gyrus granule cells (Wei et al., 2003). It is noteworthy that these receptors have a 50-fold higher affinity for GABA than other GABA-A receptors, and do not desensitize upon the prolonged presence of agonists (Saxena and Macdonald, 1994), thus being suitable to mediate tonic extrasynaptic inhibition. Extrasynaptic GABA-Aδ receptors in the suprachiasmatic nucleus modulate circadian phase shifts (McElroy et al., 2009). GABAρ receptors in the neostriatum and the hippocampus are perisynaptic and extrasynaptic (Rosas-Arellano et al., 2011a,b).

In agreement with the presence of extrasynaptic receptors, extracellular GABA, as measured by microdialysis, is present in the extracellular space of rat hippocampus (Lerma et al., 1986; de Groote and Linthorst, 2007), striatum (Kennedy et al., 2002), and nucleus accumbens (Xi et al., 2003), and extrasynaptic or paracrine effects of GABA occur in the cortex (Zhu et al., 2008; Oláh et al., 2009; Vélez-Fort et al., 2010), cerebellum, and hipocampppus, where stress increases the extracellular GABA levels (de Groote and Linthorst, 2007). The excitability of cerebellar granule cells is reduced by GABA in the extracellular fluid, through the activation of a tonic inhibitory current (Kaneda et al., 1995; Nusser et al., 1998; for review see Farrant and Nusser, 2005). A similar tonic GABAergic inhibition exists in dentate gyrus granule cells, thalamocortical relay neurons of the ventral basal complex (Porcello et al., 2003), CA1 pyramidal neurons (Bai et al., 2001), inhibitory interneurons in the CA1 region of the hippocampus (Semyanov et al., 2003), neurons of the medial geniculate body of the auditory thalamus (Richardson et al., 2011), neurons in the avian nucleus laminaris (Tang et al., 2011), and in the neuromuscular junction of crustaceans (Parnas et al., 1975). In the avian nucleus laminaris, this GABA-A receptor-mediated tonic inhibition improves coincidence detection by sharpening excitatory postsynaptic potentials and reducing spike probability, thus improving the localization of sound by birds (Tang et al., 2011).

In the cerebellum, the extrasynaptic GABA producing this tonic inhibition during development is released by exocytosis from Golgi cells (Tia et al., 1996). During cerebellar development, GABA is located in all regions of Golgi cells and the vesicular GABA transporter accumulates in axon varicosities and growth cones, suggesting that GABA is released from these structures (Takayama and Inoue, 2004). In the adult, however, extrasynaptic GABA apparently comes both from vesicular (Brickley et al., 2003) and non-vesicular release (Rossi et al., 2003) and it is not clear if release occurs from extrasynaptic sites or if GABA increases upon synaptic spillover. In the hippocampus, tonic (extrasynaptic) and phasic (synaptic) inhibition change in a correlated manner, suggesting that the source of GABA is the same for both effects and that tonic inhibition could have a synaptic spillover origin (Glykys and Mody, 2007).

Extrasynaptic GABA release has been demonstrated in cortical neurogliaform interneurons (Oláh et al., 2009), which form dense axonal arborizations with varicosities that establish very few synapses, as shown by 3D reconstructions obtained from serial electron micrographs. Despite the low incidence of synaptic contacts, stimulation of these interneurons causes slow inhibitory potentials in most of their surrounding cells, suggesting that transmission takes place through GABA diffusion. In addition, stimulation of neurogliaform cells decreases the synaptic responses of other cells in the circuit only if applied at least 120 ms before stimulation of a presynaptic neuron, indicating a volume effect.

Direct evidence of extrasynaptic vesicular co-release of GABA and dopamine comes from the soma of dissociated amacrine retinal cells. Somatic GABA exocytosis is calcium-dependent and produces autocrine miniature-like currents, with variable latencies after stimulation (Hirasawa et al., 2009), suggesting again the fusion of vesicles arriving from different distances to the plasma membrane, as in somatic exocytosis of other signaling molecules (Trueta et al., 2004; Huang et al., 2007; Xia et al., 2009).

ATP

ATP in neurons is a multifunctional nucleoside, used as energetic "currency" and as a signaling molecule. Extracellular ATP activates ionotropic and metabotropic purinergic P2 receptors, some of which, like P2Y receptors, are extrasynaptic in hippocampal and glial cells (Rodrigues et al., 2005; Hussl and Boehm, 2006). Metabotropic P2 receptors (P2Y, P2U, and P2T) activate phospholipase C through $G_{q/11}$ proteins, or inhibit adenyl cyclase through G_i proteins. On the other hand, synaptic ionotropic receptors (P2X and P2Z) allow the transmembrane flux of cations. It is noteworthy that ATP leaks out from neurons through pannexin hemichannles, a way of non synaptic release (Li et al., 2011).

Dorsal root ganglia neurons release ATP by exocytosis from the soma, as shown by the opening of P2X2-EGFP receptors in membrane patches used as biosensors (Zhang et al., 2007). Somatic release is quantal and after stimulation, electron micrographs show photoconverted fluorescent dye FM1-43 inside clear vesicles. ATP exocytosis depends on calcium entry through L-type calcium channels and increasing the stimulation frequency increases the amount of exocytosis and reduces its latency to a minimum of several seconds. Interestingly, somatic ATP exocytosis evokes an increase in the intracellular calcium concentration in the satellite glial cells enwrapping the neurons, which respond by releasing the tumor necrosis factor TNFα. This peptide in turn potentiates the neuronal responses to ATP and their excitability, thus triggering a bi-directional neuron-glia communication (Zhang et al., 2007).

Extrasynaptic sites in axons of olfactory bulb and optic nerve neurons co-release ATP and glutamate (Rieger et al., 2007;

Hamilton et al., 2008). Astrocytes in the optic nerve become activated by either transmitter, and respond to them by releasing more ATP, which in turn triggers a calcium wave that spreads to neighboring glial cells (Hamilton et al., 2008). The co-release of ATP and glutamate in olfactory bulb axons is calcium-dependent and occurs through vesicular exocytosis, as shown by its elimination in the presence of bafilomycin A1 and botulinum A toxins (Rieger et al., 2007) Calcium signals produced in the ensheathing glial cells by ATP and glutamate mediate neurovascular coupling, resulting in constriction of adjacent blood vessels (Thyssen et al., 2010).

PEPTIDES

There is now a wide catalog of peptides released by neurons that modulate neuronal activity or act as hormones when secreted to the circulatory system. Peptide transmitters are released by exocytosis from dense core vesicles in the soma, axons, dendrites, and perisynaptic sites in a variety of neurons upon high frequency electrical activity.

Peptide exocytosis from presynaptic active zones or from postsynaptic dendrites modulates the synaptic function in a localized manner. By contrast, when released from extrasynaptic locations, for example the soma or axons, peptides diffuse away, and act through volume transmission (Agnati et al., 1986a,b). Somatic exocytosis from dense core vesicles has been demonstrated by electron microscopy, through the formation of omega figures in sympathetic or hypothalamic neurons (Zaidi and Matthews, 1997, 1999; see Tobin et al., 2012 in this issue). Somatic exocytosis of substance P was also demonstrated in dissociated dorsal root ganglia neurons by capacitance increases in response to high potassium depolarization, and confirmed by single-cell immunoblot assays (Huang and Neher, 1996). In these neurons somatic exocytosis has a calcium-dependence 10 times lower than that of presynaptic exocytosis, but similar to that for dense core vesicle fusion in neuroendocrine cells, which requires more homogeneous calcium levels to promote vesicle transport, but lower calcium concentration for their fusion (Augustine and Neher, 1992; Becherer et al., 2003).

Ultrastructural studies in the trigeminal subnucleus caudalis of rats showed exocytosis of large dense core vesicles in extrasynaptic locations at axon terminals and dendrites containing substance P (Zhu et al., 1986). The immunofluorescence levels of this peptide correlate with the number of extrasynaptic dense core vesicles undergoing exocytosis counted in electron micrographs after lessoning the whisker area, suggesting that substance P exocytosis mediates neuronal responses to lesions.

The soma of neurons in the supraoptic nucleus releases oxytocin by exocytosis, as shown by omega figures in electron microscopy studies (Morris and Pow, 1991) and by capacitance increases after stimulation (Soldo et al., 2004). Exocytosis depends on the magnitude and duration of the depolarization or on action potential firing at frequencies higher than 13 Hz. Physiological electrical activity patterns, such as those recorded during the milk ejection reflex, stimulate this exocytosis. Notably, oxytocin activates its own somatodendritic exocytosis through activation of G protein-coupled receptors that in turn trigger calcium release from intracellular stores (Lambert et al., 1994), thus producing self-sustained and long lasting exocytosis (Ludwig and Leng, 2006). Somatic exocytosis of oxytocin from these neurons is also induced by NMDA receptor activation (de Kock et al., 2004) and this stimulation is upregulated during lactation. It is also noteworthy that extrasynaptic ATP in this nucleus facilitates glutamate release (Vavra et al., 2011) and by doing so potentiates oxytocin somatic exocytosis. In turn, oxytocin released in this way inhibits GABA release from presynaptic terminals contacting oxytocinergic neurons, thus removing inhibition and providing a positive feedback for release.

Somatic exocytosis from dense core vesicles has also been directly shown in cultured hippocampal neurons using fluorescent propeptide cargo and TIRF microscopy. Exocytosis events were triggered by calcium entry with long time constants of 16 s and showed rapid fusion-pore openings and closures (kiss and run), associated with limited cargo secretion (Xia et al., 2009). These long latencies in exocytosis from dense core vesicles are also characteristic of somatic exocytosis of other transmitters, as shown in previous sections.

Hypothalamic neurons secreting gonadotropin releasing hormone (GnRH) in a pulsatile way, take up the fluorescent dye FM1-43 by endocytosis in the soma, dendrites, and axon in response to electrical activity. GnRH and vesicle-associated membrane protein (VAMP) co-localize in double immunocytochemistry images, confirming somatic vesicular hormone release, which might contribute to synchronizing electrical activity among GnRH neurons (Fuenzalida et al., 2011).

Neurotrophins such as nerve growth factor (NGF) and BDNF are also released by exocytosis from dense core vesicles in different areas of the nervous system and regulate neuronal survival (Levi-Montalcini and Hamburger, 1953) and synaptic plasticity (for review see Lu et al., 2005). Although neurotrophin secretion *in situ* has been studied by measuring the bulk secretion in the extracellular medium, NGF release occurs from the soma and dendrites of cultured hippocampal neurons (Blöchl and Thoenen, 1996). Neurotrophin release requires stimulation in bursts of high frequency impulses (Balkowiec and Katz, 2000; Lever et al., 2001) and calcium release from intracellular stores following transmembrane calcium entry through voltage-gated channels (reviewed by Lessmann et al., 2003).

Neurons in the mesencephalic trigeminal nucleus display somatic exocytosis from small clear vesicles (Zhang et al., 2012) with a calcium and electrical activity dependence. However, it is not clear what molecules these neurons release.

CONCLUDING REMARKS

Increasing evidence is firmly establishing that different signaling molecules are released by exocytosis from extrasynaptic sites in different types of central and peripheral neurons of vertebrates and invertebrates. The mechanisms of extrasynaptic exocytosis are significantly different from those of exocytosis from synaptic terminals (see **Figure 1**), and share similarities with the mechanisms of exocytosis from excitable endocrine cells. While central synaptic terminals usually release small amounts of quanta of neurotransmitters, enough to produce local hard-wired responses, the large amounts of molecules necessary for volume

Table 1 | Mechanisms for extrasynaptic exocytosis in different cell types.

Signaling molecule	Subcellular compartment	Preparation	Vesicle type	Resting distance from vesicles to plasma membrane	Trans-membrane calcium channel type triggering exocytosis	Intracellular calcium sources	Latency to beginning of exocytosis	Duration of exocytosis	Exocytosis-triggering stimuli	Recording techniques and references
Serotonin	Soma	Leech Retzius neurons	Large dense core	>600 nm	L-type	Ryanodine-sensitive	Seconds to minutes	2–10 min (after 0.5 s train)	Long depolarizations, trains at 10 or 20 Hz	Amperometry (Bruns et al., 2000); FM1-43; Electron microscopy (Trueta et al., 2003, 2012).
	Soma	Rat raphe neurons	NA	NA	NA	NA	NA	Minutes	Long depolarizations	3-photon microscopy (Kaushalya et al., 2008a)
Dopamine	Soma	Giant snail dopaminergic neurons	Large dense core	NA	NA	NA	NA	Seconds	Long depolarizations	Amperometry (Chen et al., 1996)
	Soma	Neurons in substantia nigra slices	NA	NA	NA	Ryanodine- and IP3-sensitive	Seconds	NA	Long depolarizations, application of glutamate or serotonin	Amperometry (Jaffe et al., 1998)
	Soma	Retinal amacrine cells	Small clear and large dense core	NA	L-type	NA	NA	Seconds	Long depolarizations; trains at 20 Hz	Amperometry (Puopolo et al., 2001)
Noradrenaline	Soma	Locus coeruleus slices	Large dense core	~200 nm	NA	NA	>100 ms Avg = 1,870 ms	Seconds	Long depolarizations; trains at >20 Hz frequencies; NMDA or hypocretin application	Amperommetry and capacitance records (Huang et al., 2007)
Acetylcholine	Soma and neurites	Xenopus cultured spinal cord neurons	small clear	NA	NA	NA	1–40 ms (1–5 ms for burst events)	2–17 ms	Long depolarizations; trains at 30 Hz	Sniffer patches as sensors (Sun and Poo, 1987)

(Continued)

Table 1 | Continued

Signaling molecule	Subcellular compartment	Preparation	Vesicle type	Resting distance from vesicles to plasma membrane	Trans-membrane calcium channel type triggering exocytosis	Intracellular calcium sources	Latency to beginning of exocytosis	Duration of exocytosis	Exocytosis-triggering stimuli	Recording techniques and references
Glutamate	Soma	Astrocytes in brain slices	small clear	NA	NA	Ryanodine and IP3-sensitive	NA	Seconds	Calcium oscillations; ionomicin application; caged calcium photolysis	Total internal refraction fluorescence microscopy (Bezzi et al., 2004), capacitance measurements (Zhang et al., 2004); amperometry (Chen et al., 2005)
	Axon	Olfactory bulb	NA	NA	NA	NA	NA	NA	Trains at 20 Hz	Calcium signals in ensheating glial cells in response to stimulation of olfactory nerve axons (Rieger et al., 2007)
GABA	Soma and dendrites	Cortical slices	small clear	NA	NA	NA	NA	NA	Single action potentials	Electrophysiological records from cortical neurons upon stimulation of neurogliaform cells (Oláh et al., 2009).
	Soma	Retinal amacrine cells	NA	NA	L-type, R-type	NA	7–960 ms	Seconds	1-s depolarizations	Miniature-like currents in retinal amacrine cells (Hirasawa et al., 2009)
ATP	Soma	Dorsal root ganglia neurons	small clear	500 nm	L-type	NA	Seconds	2–5 min	Trains at >20Hz	Sniffer patches expressing P2X2 as sensors and capacitance measurements (Zhang et al., 2007).
	Axon	Olfactory bulb		NA	NA	Cyclopiazonic acid-sensitive intracellular stores	NA	NA	Trains at 20 Hz	Calcium signals in ensheating glial cells; exocytosis blocking toxins (Rieger et al., 2007)
Oxytocin	Soma and dendrites	Supraoptic nucleus neurons	Large dense core	NA	High voltage-activated	Thapsigargin-sensisitve intracellular stores	NA	Seconds	Trains at >13 Hz; Glutamate or Oxytocin application	Omega figures in electronmicrographs (Morris and Pow, 1991). Capacitance measurements (Soldo et al., 2004)

Only direct evidence of extrasynaptic exocytosis is summarized. References are provided in parenthesis. The cases where information is not available are indicated by NA.

transmission may be reached by exocytosis from extrasynaptic locations in the cell body, axons, and dendrites.

Studies of exocytosis in the neuronal soma, which allows direct electrophysiological, amperometric and optical recordings of exocytosis and calcium concentrations, which can be correlated with ultrastructural analysis, have shown that somatic exocytosis occurs from small clear vesicles or large dense core vesicles. The volume of dense core vesicles allows them to pack about 15 times more transmitter than small clear vesicles and therefore to produce larger extracellular transmitter increases upon exocytosis of single quanta. In most extrasynaptic exocytosis sites vesicles rest at distances from the plasma membrane ranging from nanometers in varicosities to several microns in the somata. The need for vesicle transport (or diffusion) as an intermediate step in the excitation-secretion coupling confers long latencies and time courses to exocytosis. In addition, the requirement of high stimulation frequencies is explained by the need of intracellular calcium waves produced by transmembrane calcium flow through L-type calcium channels, which are resistant to inactivation and therefore efficient for calcium injection under subsequent depolarizations, followed by the activation of calcium release from intracellular stores. These intracellular changes in calcium concentration are required for exocytosis, but in leech serotonergic neurons also seem to trigger the active vesicle transport toward the plasma membrane by using cytoskeletal-coupled molecular motors. The known mechanisms involved in extrasynaptic exocytosis in different preparations discussed in this review have been summarized in **Table 1**.

The different frequency-dependence of synaptic and extrasynaptic exocytosis allows neurons to select from which compartments transmitter will be released. This possibility makes of these neurons multifunctional units in terms of their transmission possibilities, by contributing to fast transmission in hard wired circuits, and slow transmission through volume communication. This capability is of particular relevance for monoaminergic and cholinergic systems, which are composed of small numbers of neurons clustered in specific nuclei that send projections to large brain areas, and modulate a wide variety of functions. In addition, the auto-inhibitory mechanisms of transmitters, along with the multiple steps that couple excitation with exocytosis make of extrasynaptic exocytosis a highly regulated process.

Another feature of extrasynaptic exocytosis is that transmitters may be released directly onto glial cells, which seem to act as mediators for communication with other neurons and with other cells such as those in blood vessels. Therefore extrasynaptic exocytosis of transmitter molecules allows a wide variety of modulatory and integrative properties in the nervous system, from the local modulation of synaptic function to a wide modulation of whole brain areas.

ACKNOWLEDGMENTS

This work was funded by CONACYT 43703 and TWAS 03-263 RG/BIO/LA grants to Citlali Trueta and by DGAPA-UNAM IN211511-23 and CONACYT 130031 grants to Francisco F. De-Miguel.

REFERENCES

Agnati, L. F., Fuxe, K., Zoli, M., Ozini, I., Toffano, G., and Ferraguti, F. (1986a). A correlation analysis of the regional distribution of central enkephalin and β-endorphin immunoreactive terminals and of opiate receptors in adult and old male rats. Evidence for the existence of two main types of communication in the central nervous system: the volume transmission and the wiring transmission. *Acta. Physiol. Scand.* 128, 201–207.

Agnati, L. F., Fuxe, K., Zoli, M., Pich, E. M., Benfenati, F., Zini, I., and Goldstein, M. (1986b). Aspects on the information handling by the central nervous system: focus on cotransmission in the aged rat brain. *Prog. Brain Res.* 68, 291–301.

Alekseyenko, O. V., Lee, C., and Kravitz, E. A. (2010). Targeted manipulation of serotonergic neurotransmission affects the escalation of aggression in adult male *Drosophila melanogaster*. *PLoS ONE* 5, e10806. doi: 10.1371/journal.pone.0010806

Allen, T. G., and Brown, D. A. (1996). Detection and modulation of acetylcholine release from neurites of rat basal forebrain cells in culture. *J. Physiol.* 492, 453–466.

Alvarez, F. J., Pearson, J. C., Harrington, D., Dewey, D., Torbeck, L., and Fyffe, R. E. (1998). Distribution of 5-hydroxytryptamine-immunoreactive boutons on alpha-motoneurons in the lumbar spinal cord of adult cats. *J. Comp. Neurol.* 393, 69–83.

Anderson, B. B., Chen, G., Gutman, D. A., and Ewing, A. G. (1999). Demonstration of two distributions of vesicle radius in the dopamine neuron of *Planorbis corneus* from electrochemical data. *J. Neurosci. Methods* 88, 153–161.

Aoki, C., Venkatesan, C., Go, C. G., Forman, R., and Kurose, H. (1998). Cellular and subcellular sites for noradrenergic action in the monkey dorsolateral prefrontal cortex as revealed by the immunocytochemical localization of noradrenergic receptors and axons. *Cereb. Cortex* 8, 269–277.

Arango, V., Underwood, M. D., and Mann, J. J. (2002). Serotonin brain circuits involved in major depression and suicide. *Prog. Brain Res.* 136, 443–453.

Aston-Jones, G., and Cohen, J. D. (2005). An integrative theory of locus coeruleus-norepinephrine function: adaptive gain and optimal performance. *Annu. Rev. Neurosci.* 28, 403–450.

Augustine, G. J., and Neher, E. (1992). Calcium requirements for secretion in bovine chromaffin cells. *J. Physiol. (Lond.)* 450, 247–271.

Bai, D., Zhu, G., Pennefather, P., Jackson, M. F., MacDonald, J. F., and Orser, B. A. (2001). Distinct functional and pharmacological properties of tonic and quantal inhibitory postsynaptic currents mediated by gamma-aminobutyric acid(A) receptors in hippocampal neurons. *Mol. Pharmacol.* 59, 814–824.

Balkowiec, A., and Katz, D. M. (2000). Activity-dependent release of endogenous brain-derived neurotrophic factor from primary sensory neurons detected by ELISA *in situ*. *J. Neurosci.* 20, 7417–7423.

Becherer, U., Moser, T., Stühmer, W., and Oheim, M. (2003). Calcium regulates exocytosis at the level of single vesicles. *Nat. Neurosci.* 6, 846–853.

Berridge, C. W., and Abercrombie, E. D. (1999). Relationship between locus coeruleus discharge rates and rates of norepinephrine release within neocortex as assessed by *in vivo* microdialysis. *Neuroscience* 93, 1263–1270.

Bezzi, P., Carmignoto, G., Pasti, L., Vesce, S., Rossi, D., Rizzini, B. L., Pozzan, T., and Volterra, A. (1998). Prostaglandins stimulate calcium-dependent glutamate release in astrocytes. *Nature* 391, 281–285.

Bezzi, P., Gundersen, V., Galbete, J. L., Seifert, G., Steinhäuser, C., Pilati, E., and Volterra, A. (2004). Astrocytes contain a vesicular compartment that is competent for regulated exocytosis of glutamate. *Nat. Neurosci.* 7, 613–620.

Biedermann, B., Fröhlich, E., Grosche, J., Wagner, H. J., and Reichenbach, A. (1995). Mammalian Müller (glial) cells express functional D2 dopamine receptors. *Neuroreport* 6, 609–612.

Bisson, G., Bianconi, G., and Torre, V. (2012). The dynamics of group formation among leeches. *Front. Physiol.* 3, 133. doi: 10.3389/fphys.2012.00133

Bisson, G., and Torre, V. (2011). Statistical characterization of social interactions and collective behavior in medicinal leeches. *J. Neurophysiol.* 106, 78–90.

Bjelke, B., Goldstein, M., Tinner, B., Andersson, C., Sesack, S. R.,

Steinbusch, H. W., Lew, J. Y., He, X., Watson, S., Tengroth, B., and Fuxe, K. (1996). Dopaminergic transmission in the rat retina: evidence for volume transmission. *J. Chem. Neuroanat.* 12, 37–50.

Björklund, A., and Lindvall, O. (1975). Dopamine in dendrites of substantia nigra neurons: suggestions for a role in dendritic terminals. *Brain Res.* 83, 531–537.

Blöchl, A., and Thoenen, H. (1996). Localization of cellular storage compartments and sites of constitutive and activity-dependent release of nerve growth factor (NGF) in primary cultures of hippocampal neurons. *Mol. Cell. Neurosci.* 7, 173–190.

Brazell, M. P., Marsden, C. A., Nisbet, A. P., and Routledge, C. (1985). The 5-HT1 receptor agonist RU-24969 decreases 5-hydroxytryptamine (5-HT) release and metabolism in the rat frontal cortex *in vitro* and *in vivo*. *Br. J. Pharmacol.* 86, 209–216.

Brickley, S. G., Cull-Candy, S. G., and Farrant, M. (2003). Vesicular release of GABA contributes to both phasic and tonic inhibition of granule cells in the mature cerebellum of mice. *J. Physiol.* 547P, C30.

Brieden, T., Ujeyl, M., and Naber, D. (2002). Psychopharmacological treatment of aggression in schizophrenic patients. *Pharmacopsychiatry* 35, 83–89.

Bruns, D., Riedel, D., Klingauf, J., and Jahn, R. (2000). Quantal release of serotonin. *Neuron* 28, 205–220.

Bruns, D., and Jahn, R. (1995). Real-time measurement of transmitter release from single synaptic vesicles. *Nature* 377, 62–65.

Bunin, M. A., and Wightman, R. M. (1998). Quantitative evaluation of 5-hydroxytryptamine (serotonin) neuronal release and uptake: an investigation of extrasynaptic transmission. *J. Neurosci* 18, 4854–4860.

Bunin, M. A., and Wightman, R. M. (1999). Paracrine neurotransmission in the CNS: involvement of 5-HT. *Trends Neurosci.* 22, 377–382.

Burrell, B. D., Sahley, C. L., and Muller, K. J. (2002). Differential effects of serotonin enhance activity of an electrically coupled neural network. *J. Neurophysiol.* 87, 2889–2895.

Burrell, B. D., and Sahley, C. L. (2005). Serotonin mediates learning-induced potentiation of excitability. *J. Neurophysiol.* 94, 4002–4010.

Calviño, M. A., and Szczupak, L. (2008). Spatial-specific action of serotonin within the leech mid-body ganglion. *J. Comp. Physiol. A Neuroethol. Sens. Neural. Behav. Physiol.* 194, 523–531.

Cercós, M. G., De-Miguel, F. F., and Trueta, C. (2009). Real-time measurements of synaptic autoinhibition produced by serotonin release in cultured leech neurons. *J. Neurophysiol.* 102, 1075–1085.

Charney, D. S. (1998). Monoamine dysfunction and the pathophysiology and treatment of depression. *J. Clin. Psychiatry* 59, 11–14.

Chazal, G., and Ralston, H. J. 3rd. (1987). Serotonin-containing structures in the nucleus raphe dorsalis of the cat: an ultrastructural analysis of dendrites, presynaptic dendrites, and axon terminals. *J. Comp. Neurol.* 259, 317–329.

Chen, B. T., Moran, K. A., Avshalumov, M. V., and Rice, M. E. (2006). Limited regulation of somatodendritic dopamine release by voltage-sensitive Ca channels contrasted with strong regulation of axonal dopamine release. *J. Neurochem.* 96, 645–655.

Chen, B. T., Patel, J. C., Moran, K. A., and Rice, M. E. (2011). Differential calcium dependence of axonal versus somatodendritic dopamine release, with characteristics of both in the ventral tegmental area. *Front. Syst. Neurosci.* 5, 39. doi: 10.3389/fnsys.2011.00039.

Chen, B. T., and Rice, M. E. (2001). Novel Ca^{2+} dependence and time course of somatodendritic dopamine release: substantia nigra versus striatum. *J. Neurosci.* 21, 7841–7847.

Chen, G., Gutman, D. A., Zerby, S. E., and Ewing, A. G. (1996). Electrochemical monitoring of bursting exocytotic events from the giant dopamine neuron of *Planorbis corneus*. *Brain Res.* 733, 119–124.

Chen, X., Wang, L., Zhou, Y., Zheng, L.-H., and Zhou, Z. (2005). "Kiss-and-run" glutamate secretion in cultured and freshly isolated rat hippocampal astrocytes. *J. Neurosci.* 25, 9236–9243.

Chen, X.-W., Mu, Y., Huang, H.-P., Guo, N., Zhang, B., Fan, S.-Y., Xiong, J.-X., Wang, S.-R., Xiong, W., Huang, W., Liu, T., Zheng, L-H., Zhang, C. X., Li, L-H., Yu, Z-P., Hu, Z-A., and Zhou, Z. (2008). Hypocretin-1 potentiates NMDA receptor-mediated somatodendritic secretion from locus ceruleus neurons. *J. Neurosci.* 28, 3202–3208.

Cheramy, A., Leviel, V., and Glowinski, J. (1981). Dendritic release of dopamine in the substantia nigra. *Nature* 289, 537–542.

Clark, B. A., and Cull-Candy, S. G. (2002). Activity-dependent recruitment of extrasynaptic NMDA receptor activation at an AMPA receptor-only synapse. *J. Neurosci.* 22, 4428–4436.

Cobb, W. S., and Abercrombie, E. D. (2003). Differential regulation of somatodendritic and nerve terminal dopamine release by serotonergic innervation of substantia nigra. *J. Neurochem.* 84, 576–584.

Coggeshall, R. E. (1972). Autoradiographic and chemical localization of 5-hydroxytryptamine in identified neurons in the leech. *Anat. Rec.* 172, 489–498.

Cohen, A. I., Todd, R. D., Harmon, S., and O'Malley, K. L. (1992). Photoreceptors of mouse retinas possess D4 receptors coupled to adenylate cyclase. *PNAS* 89, 12093–12097.

Colgan, L. A., Putzier, I., and Levitan, E. S. (2009). Activity-dependent vesicular monoamine transporter-mediated depletion of the nucleus supports somatic release by serotonin neurons. *J. Neurosci.* 29, 15878–15887.

Cooper, R. L., Fernández-de-Miguel, F., Adams, W. B., and Nicholls, J. G. (1992). Anterograde and retrograde effects of synapse formation on calcium currents and neurite outgrowth in cultured leech neurons. *Proc. Biol. Sci.* 249, 217–222.

Crisp, K. M., and Mesce, K. A. (2006). Beyond the central pattern generator: amine modulation of decision-making neural pathways descending from the brain of the medicinal leech. *J. Exp. Biol.* 209, 1746–1756.

Cruz-Bermúdez, N. D., and Marder, E. (2007). Multiple modulators act on the cardiac ganglion of the crab, cancer borealis. *J. Exp. Biol.* 210, 2873–2884.

Dacey, D. M. (1990). The dopaminergic amacrine cell. *J. Comp. Neurol.* 301, 461–489.

Dahlström, A., and Fuxe, K. (1964). Localization of monoamines in the lower brain stem. *Experientia* 20, 389–399.

Davidson, C., and Stamford, J. A. (1995). Evidence that 5-hydroxytryptamine release in rat dorsal raphé nucleus is controlled by 5-HT1A, 5-HT1B and 5-HT1D autoreceptors. *Br. J. Pharmacol.* 114, 1107–1109.

de Groote, L., and Linthorst, A. C. E. (2007). Exposure to novelty and forced swimming evoke stressor-dependent changes in extracellular GABA in the rat hippocampus. *Neuroscience* 148, 794–805.

de Kock, C. P. J., Burnashev, N., Lodder, J. C., Mansvelder, H. D., and Brussaard, A. B. (2004). NMDA receptors induce somatodendritic secretion in hypothalamic neurones of lactating female rats. *J. Physiol. (Lond.)* 561, 53–64.

de Kock, C. P. J., Cornelisse, L. N., Burnashev, N., Lodder, J. C., Timmerman, A. J., Couey, J. J., Mansvelder, H. D., and Brussaard, A. B. (2006). NMDA receptors trigger neurosecretion of 5-HT within dorsal raphe nucleus of the rat in the absence of action potential firing. *J. Physiol. (Lond.)* 577, 891–905.

De-Miguel, F. F., and Trueta, C. (2005). Synaptic and extrasynaptic secretion of serotonin. *Cell. Mol. Neurobiol.* 25, 297–312.

Descarries, L., Gisiger, V., and Steriade, M. (1997). Diffuse transmission by acetylcholine in the CNS. *Prog. Neurobiol.* 53, 603–625.

Descarries, L., Watkins, K. C., Garcia, S., Bosler, O., and Doucet, G. (1996). Dual character, asynaptic and synaptic, of the dopamine innervation in adult rat neostriatum: a quantitative autoradiographic and immunocytochemical analysis. *J. Comp. Neurol.* 375, 167–186.

Descarries, L., Watkins, K. C., and Lapierre, Y. (1977). Noradrenergic axon terminals in the cerebral cortex of rat. III. Topometric ultrastructural analysis. *Brain Res.* 133, 197–222.

Descarries, L., and Mechawar, N. (2000). Ultrastructural evidence for diffuse transmission by monoamine and acetylcholine neurons of the central nervous system. *Prog. Brain Res.* 125, 27–47.

Dietzel, I. D., Drapeau, P., and Nicholls, J. G. (1986). Voltage dependence of 5-hydroxytryptamine release at a synapse between identified leech neurones in culture. *J. Physiol. (Lond.)* 372, 191–205.

Dun, N. J., and Minota, S. (1982). Post-tetanic depolarization in sympathetic neurones of the guinea-pig. *J. Physiol. (Lond.)* 323, 325–337.

Durant, C., Christmas, D., and Nutt, D. (2010). The pharmacology of anxiety. *Curr. Top. Behav. Neurosci.* 2, 303–330.

Erickson, S. L., Sesack, S. R., and Lewis, D. A. (2000). Dopamine innervation of monkey entorhinal cortex: postsynaptic targets of tyrosine hydroxylase-immunoreactive terminals. *Synapse* 36, 47–56.

Fabian-Fine, R., Skehel, P., Errington, M. L., Davies, H. A., Sher, E., Stewart, M. G., and Fine, A. (2001). Ultrastructural distribution of the A7 nicotinic acetylcholine receptor subunit in rat hippocampus. *J. Neurosci.* 21, 7993–8003.

Fadel, J., Moore, H., Sarter, M., and Bruno, J. P. (1996). Trans-synaptic

stimulation of cortical acetylcholine release after partial 192 IgG-saporin-induced loss of cortical cholinergic afferents. *J. Neurosci.* 16, 6592–6600.

Farrant, M., and Nusser, Z. (2005). Variations on an inhibitory theme: phasic and tonic activation of GABA(A) receptors. *Nat. Rev. Neurosci.* 6, 215–229.

Fernandez-De-Miguel, F., Cooper, R. L., and Adams, W. B. (1992). Synaptogenesis and calcium current distribution in cultured leech neurons. *Proc. R. Soc. B Biol. Sci.* 247, 215–221.

Fernández-Pastor, B., Mateo, Y., Gómez-Urquijo, S., and Javier Meana, J. (2005). Characterization of noradrenaline release in the locus coeruleus of freely moving awake rats by *in vivo* microdialysis. *Psychopharmacology (Berl.)* 180, 570–579.

Fernández-Pastor, B., and Meana, J. J. (2002). *In vivo* tonic modulation of the noradrenaline release in the rat cortex by locus coeruleus somatodendritic alpha(2)-adrenoceptors. *Eur. J. Pharmacol.* 442, 225–229.

Fernández-de-Miguel, F., and Drapeau, P. (1995). Synapse formation and function: insights from identified leech neurons in culture. *J. Neurobiol.* 27, 367–379.

Ford, C. P., Gantz, S. C., Phillips, P. E. M., and Williams, J. T. (2010). Control of extracellular dopamine at dendrite and axon terminals. *J. Neurosci.* 30, 6975–6983.

Fortin, G. D., Desrosiers, C. C., Yamaguchi, N., and Trudeau, L.-E. (2006). Basal somatodendritic dopamine release requires snare proteins. *J. Neurochem.* 96, 1740–1749.

Freund, T. F., and Buzsáki, G. (1996). Interneurons of the hippocampus. *Hippocampus* 6, 347–470.

Fuchs, P. A., Nicholls, J. G., and Ready, D. F. (1981). Membrane properties and selective connexions of identified leech neurones in culture. *J. Physiol. (Lond.)* 316, 203–223.

Fuenzalida, L. C., Keen, K. L., and Terasawa, E. (2011). Colocalization of FM1-43, Bassoon, and GnRH-1, GnRH-1 release from cell bodies and their neuroprocesses. *Endocrinology* 152, 4310–4321.

Fuxe, K., Borroto-Escuela, D. O., Romero-Fernandez, W., Ciruela, F., Manger, P., Leo, G., Díaz-Cabiale, Z., and Agnati, L. F. (2012). On the role of volume transmission and receptor-receptor interactions in social behaviour: Focus on central catecholamine and oxytocin neurons. *Brain Res.* Available at: http://www.ncbi.nlm.nih.gov/pubmed/22373652

Gahring, L. C., Persiyanov, K., Dunn, D., Weiss, R., Meyer, E. L., and Rogers, S. W. (2004). Mouse strain-specific nicotinic acetylcholine receptor expression by inhibitory interneurons and astrocytes in the dorsal hippocampus. *J. Comp. Neurol.* 468, 334–346.

Geffen, L. B., Jessell, T. M., Cuello, A. C., and Iversen, L. L. (1976). Release of dopamine from dendrites in rat substantia nigra. *Nature* 260, 258–260.

Glass, M. J., Colago, E. E. O., and Pickel, V. M. (2002). Alpha-2A-adrenergic receptors are present on neurons in the central nucleus of the amygdala that project to the dorsal vagal complex in the rat. *Synapse* 46, 258–268.

Glass, M. J., Huang, J., Aicher, S. A., Milner, T. A., and Pickel, V. M. (2001). Subcellular localization of alpha-2A-adrenergic receptors in the rat medial nucleus tractus solitarius: regional targeting and relationship with catecholamine neurons. *J. Comp. Neurol.* 433, 193–207.

Glykys, J., and Mody, I. (2007). The main source of ambient GABA responsible for tonic inhibition in the mouse hippocampus. *J. Physiol.* 582, 1163–1178.

Groome, J. R., Clark, M., and Lent, C. M. (1993). The behavioural state of satiation in the leech is regulated by body distension and mimicked by serotonin depletion. *J. Exp. Biol.* 182, 265–270.

Groves, P. M., and Linder, J. C. (1983). Dendro-dendritic synapses in substantia nigra: descriptions based on analysis of serial sections. *Exp. Brain Res.* 49, 209–217.

Hamilton, N., Vayro, S., Kirchhoff, F., Verkhratsky, A., Robbins, J., Gorecki, D. C., and Butt, A. M. (2008). Mechanisms of ATP- and glutamate-mediated calcium signaling in white matter astrocytes. *Glia* 56, 734–749.

Harris, G., Korchnak, A., Summers, P., Hapiak, V., Law, W. J., Stein, A. M., Komuniecki, P., and Komuniecki, R. (2011). Dissecting the serotonergic food signal stimulating sensory-mediated aversive behavior in *C. elegans*. *PLoS ONE* 6, e21897. doi: 10.1371/journal.pone.0021897

Hartzell, H. C., Kuffler, S. W., Stickgold, R., and Yoshikami, D. (1977). Synaptic excitation and inhibition resulting from direct action of acetylcholine on two types of chemoreceptors on individual amphibian parasympathetic neurones. *J. Physiol.* 271, 817–846.

Henderson, L. P., Kuffler, D. P., Nicholls, J., and Zhang, R. (1983). Structural and functional analysis of synaptic transmission between identified leech neurones in culture. *J. Physiol. (Lond.)* 340, 347–358.

Hentall, I. D., Pinzon, A., and Noga, B. R. (2006). Spatial and temporal patterns of serotonin release in the rat's lumbar spinal cord following electrical stimulation of the nucleus raphe magnus. *Neuroscience* 142, 893–903.

Hirasawa, H., Puopolo, M., and Raviola, E. (2009). Extrasynaptic release of GABA by retinal dopaminergic neurons. *J. Neurophysiol.* 102, 146–158.

Hua, X., Malarkey, E. B., Sunjara, V., Rosenwald, S. E., Li, W.-H., and Parpura, V. (2004). C(a2+)-dependent glutamate release involves two classes of endoplasmic reticulum Ca(2+) stores in astrocytes. *J. Neurosci. Res.* 76, 86–97.

Huang, H.-P., Wang, S.-R., Yao, W., Zhang, C., Zhou, Y., Chen, X.-W., Zhang, B., Xiong, W., Wang, L.-Y., Zheng, L.-H., Landry, M., Höckfelt, T., Xu, Z. Q., and Zhou, Z. (2007). Long latency of evoked quantal transmitter release from somata of locus coeruleus neurons in rat pontine slices. *Proc. Natl. Acad. Sci.* 104, 1401–1406.

Huang, H.-P., Zhu, F.-P., Chen, X.-W., Xu, Z.-Q. D., Zhang, C. X., and Zhou, Z. (2012). Physiology of quantal norepinephrine release from somatodendritic sites of neurons in locus coeruleus. *Front. Mol. Neurosci.* 5. Available at: http://www.frontiersin.org/Molecular_Neuroscience/10.3389/fnmol.2012.00029/abstract

Huang, L. Y., and Neher, E. (1996). Ca(2+)-dependent exocytosis in the somata of dorsal root ganglion neurons. *Neuron* 17, 135–145.

Hull, E. M., Lorrain, D. S., Du, J., Matuszewich, L., Lumley, L. A., Putnam, S. K., and Moses, J. (1999). Hormone-neurotransmitter interactions in the control of sexual behavior. *Behav. Brain Res.* 105, 105–116.

Hussl, S., and Boehm, S. (2006). Functions of neuronal P2Y receptors. *Pflugers Arch.* 452, 538–551.

Hökfelt, T. (1968). *In vitro* studies on central and peripheral monoamine neurons at the ultrastructural level. *Z. Zellforsch. Mikrosk. Anat.* 91, 1–74.

Ikonomu, K. D., Short, S. M., Rich, M. T., and Antic, S. D. (2012). Extrasynaptic glutamate receptor activation as cellular bases for dynamic range compression in pyramidal neurons. *Front. Membr. Physiol.* 3.

Jacob, M. H., and Berg, D. K. (1983). The ultrastructural localization of alpha-bungarotoxin binding sites in relation to synapses on chick ciliary ganglion neurons. *J. Neurosci.* 3, 260–271.

Jacobs, B. L., and Azmitia, E. C. (1992). Structure and function of the brain serotonin system. *Physiol. Rev.* 72, 165–229.

Jacobs, B. L., and Fornal, C. A. (1993). 5-HT and motor control: a hypothesis. *Trends Neurosci.* 16, 346–352.

Jafari, G., Xie, Y., Kullyev, A., Liang, B., and Sze, J. Y. (2011). Regulation of extrasynaptic 5-HT by serotonin reuptake transporter function in 5-HT-absorbing neurons underscores adaptation behavior in *Caenorhabditis elegans*. *J. Neurosci.* 31, 8948–8957.

Jaffe, E. H., Marty, A., Schulte, A., and Chow, R. H. (1998). Extrasynaptic vesicular transmitter release from the somata of substantia nigra neurons in rat midbrain slices. *J. Neurosci* 18, 3548–3553.

Johnson, D. A., and Pilar, G. (1980). The release of acetylcholine from post-ganglionic cell bodies in response to depolarization. *J. Physiol. (Lond.)* 299, 605–619.

Johnson, D. E., Drummond, E., Grimwood, S., Sawant-Basak, A., Miller, E., Tseng, E., McDowell, L. L., Vanase-Frawley, M. A., Fisher, K. E., Rubitski, D. M., Stutzman-Engwall, K. J., Nelson, R. T., Horner, W. E., Gorczyca, R. R., Hajos, M., and Siok, C. J. (2012). The 5-HT4 agonists prucalopride and PRX-03140 increase acetylcholine and histamine levels in the rat prefrontal cortex as well as the power of stimulated hippocampal theta oscillations. *J. Pharmacol. Exp. Ther.* Available at: http://jpet.aspetjournals.org.laneproxy.stanford.edu/content/early/2012/03/09/jpet.112.192351

Jones, I. W., and Wonnacott, S. (2004). Precise localization of alpha7 nicotinic acetylcholine receptors on glutamatergic axon terminals in the rat ventral tegmental area. *J. Neurosci.* 24, 11244–11252.

Kalsner, S., and Abdali, S. A. (2001). Rate-independent inhibition by norepinephrine of 5-HT release from the somadendritic region of serotonergic neurons. *Brain Res. Bull.* 55, 761–765.

Kaneda, M., Farrant, M., and Cull-Candy, S. G. (1995). Whole-cell and

single-channel currents activated by GABA and glycine in granule cells of the rat cerebellum. *J. Physiol. (Lond.)* 485, 419–435.

Kaneko, A. (1971). Electrical connexions between horizontal cells in the dogfish retina. *J. Physiol. (Lond.)* 213, 95–105.

Kapadia, S. E., de Lanerolle, N. C., and LaMotte, C. C. (1985). Immunocytochemical and electron microscopic study of serotonin neuronal organization in the dorsal raphe nucleus of the monkey. *Neuroscience* 15, 729–746.

Kasa, P., Hlavati, I., Dobo, E., Wolff, A., Joo, F., and Wolff, J. (1995). Synaptic and non-synaptic cholinergic innervation of the various types of neurons in the main olfactory bulb of adult rat: immunocytochemistry of choline acetyltransferase. *Neuroscience* 67, 667–677.

Kaushalya, S. K., Desai, R., Arumugam, S., Ghosh, H., Balaji, J., and Maiti, S. (2008a). Three-photon microscopy shows that somatic release can be a quantitatively significant component of serotonergic neurotransmission in the mammalian brain. *J. Neurosci. Res* 86, 3469–3480.

Kaushalya, S. K., Nag, S., Ghosh, H., Arumugam, S., and Maiti, S. (2008b). A high-resolution large area serotonin map of a live rat brain section. *Neuroreport* 19, 717–721.

Kennedy, R. T., Thompson, J. E., and Vickroy, T. W. (2002). *In vivo* monitoring of amino acids by direct sampling of brain extracellular fluid at ultralow flow rates and capillary electrophoresis. *J. Neurosci. Methods* 114, 39–49.

Kia, H. K., Miquel, M. C., Brisorgueil, M. J., Daval, G., Riad, M., El Mestikawy, S., Hamon, M., and Vergé, D. (1996). Immunocytochemical localization of serotonin1A receptors in the rat central nervous system. *J. Comp. Neurol.* 365, 289–305.

Kiehn, O., Rostrup, E., and Møller, M. (1992). Monoaminergic systems in the brainstem and spinal cord of the turtle Pseudemys scripta elegans as revealed by antibodies against serotonin and tyrosine hydroxylase. *J. Comp. Neurol.* 325, 527–547.

Kilic, G., Angleson, J. K., Cochilla, A. J., Nussinovitch, I., and Betz, W. J. (2001). Sustained stimulation of exocytosis triggers continuous membrane retrieval in rat pituitary somatotrophs. *J. Physiol. (Lond.)* 532, 771–783.

Kiss, J. P. (2008). Theory of active antidepressants: a nonsynaptic approach to the treatment of depression. *Neurochem. Int.* 52, 34–39.

Kolb, H., Cuenca, N., Wang, H. H., and Dekorver, L. (1990). The synaptic organization of the dopaminergic amacrine cell in the cat retina. *J. Neurocytol.* 19, 343–366.

Kosofsky, B. E., and Molliver, M. E. (1987). The serotoninergic innervation of cerebral cortex: different classes of axon terminals arise from dorsal and median raphe nuclei. *Synapse* 1, 153–168.

Kravitz, E. A. (2000). Serotonin and aggression: insights gained from a lobster model system and speculations on the role of amine neurons in a complex behavior. *J. Comp. Physiol. A* 186, 221–238.

Kristan, W. B., Jr, and Nusbaum, M. P. (1982). The dual role of serotonin in leech swimming. *J. Physiol. (Paris)* 78, 743–747.

Krizaj, D., Gábriel, R., Owen, W. G., and Witkovsky, P. (1998). Dopamine D2 receptor-mediated modulation of rod-cone coupling in the Xenopus retina. *J. Comp. Neurol.* 398, 529–538.

Kuffler, D. P., Nicholls, J., and Drapeau, P. (1987). Transmitter localization and vesicle turnover at a serotoninergic synapse between identified leech neurons in culture. *J. Comp. Neurol.* 256, 516–526.

Kuffler, S. W., and Yoshikami, D. (1975). The distribution of acetylcholine sensitivity at the post-synaptic membrane of vertebrate skeletal twitch muscles: iontophoretic mapping in the micron range. *J. Physiol. (Lond.)* 244, 703–730.

Kullmann, D. M., Ruiz, A., Rusakov, D. M., Scott, R., Semyanov, A., and Walker, M. C. (2005). Presynaptic, extrasynaptic and axonal GABAA receptors in the CNS: where and why? *Prog. Biophys. Mol. Biol.* 87, 33–46.

Lambert, R. C., Dayanithi, G., Moos, F. C., and Richard, P. (1994). A rise in the intracellular Ca^{2+} concentration of isolated rat supraoptic cells in response to oxytocin. *J. Physiol. (Lond.)* 478, 275–287.

Lendvai, B., and Vizi, E. S. (2008). Nonsynaptic chemical transmission through nicotinic acetylcholine receptors. *Physiol. Rev.* 88, 333–349.

Lent, C. M. (1985). Serotonergic modulation of the feeding behavior of the medicinal leech. *Brain Res. Bull.* 14, 643–655.

Lent, C. M., and Dickinson, M. H. (1984). Serotonin integrates the feeding behavior of the medicinal leech. *J. Comp. Physiol. A* 154, 457–471.

Lerma, J., Herranz, A. S., Herreras, O., Abraira, V., and Martín del Río, R. (1986). *In vivo* determination of extracellular concentration of amino acids in the rat hippocampus. A method based on brain dialysis and computerized analysis. *Brain Res.* 384, 145–155.

Lessmann, V., Gottmann, K., and Malcangio, M. (2003). Neurotrophin secretion: current facts and future prospects. *Prog. Neurobiol.* 69, 341–374.

Lever, I. J., Bradbury, E. J., Cunningham, J. R., Adelson, D. W., Jones, M. G., McMahon, S. B., Marvizón, J. C., and Malcangio, M. (2001). Brain-derived neurotrophic factor is released in the dorsal horn by distinctive patterns of afferent fiber stimulation. *J. Neurosci.* 21, 4469–4477.

Levi-Montalcini, R., and Hamburger, V. (1953). A diffusible agent of mouse sarcoma, producing hyperplasia of sympathetic-ganglia and hyperneurotization of viscera in the chick embryo. *J. Exp. Zool.* 123, 233–287.

Li, A., Banerjee, J., Leung, C. T., Peterson-Yantorno, K., Stamer, W. D., and Civan, M. M. (2011). Mechanisms of ATP release, the enabling step in purinergic dynamics. *Cell. Physiol. Biochem.* 28, 1135–1144.

Liposits, Z., Görcs, T., and Trombitás, K. (1985). Ultrastructural analysis of central serotoninergic neurons immunolabeled by silver-gold-intensified diaminobenzidine chromogen. Completion of immunocytochemistry with X-ray microanalysis. *J. Histochem. Cytochem.* 33, 604–610.

Liu, R., Jolas, T., and Aghajanian, G. (2000). Serotonin 5-HT(2) receptors activate local GABA inhibitory inputs to serotonergic neurons of the dorsal raphe nucleus. *Brain Res.* 873, 34–45.

Liu, R.-J., Lambe, E. K., and Aghajanian, G. K. (2005). Somatodendritic autoreceptor regulation of serotonergic neurons: dependence on L-tryptophan and tryptophan hydroxylase-activating kinases. *Eur. J. Neurosci.* 21, 945–958.

Lu, B., Pang, P. T., and Woo, N. H. (2005). The yin and yang of neurotrophin action. *Nat. Rev. Neurosci.* 6, 603–614.

Ludwig, M., and Leng, G. (2006). Dendritic peptide release and peptide-dependent behaviours. *Nat. Rev. Neurosci.* 7, 126–136.

Malarkey, E. B., and Parpura, V. (2008). Mechanisms of glutamate release from astrocytes. *Neurochem. Int.* 52, 142–154.

Manglapus, M. K., Iuvone, P. M., Underwood, H., Pierce, M. E., and Barlow, R. B. (1999). Dopamine mediates circadian rhythms of rod–cone dominance in the Japanese quail retina. *J. Neurosci.* 19, 4132–4141.

Mansari, M. E., Wiborg, O., Mnie-Filali, O., Benturquia, N., Sánchez, C., and Haddjeri, N. (2007). Allosteric modulation of the effect of escitalopram, paroxetine and fluoxetine: *in-vitro* and *in-vivo* studies. *Int. J. Neuropsychopharmacol.* 10, 31–40.

Marcellino, D., Kehr, J., Agnati, L. F., and Fuxe, K. (2011). Increased affinity of dopamine for D(2) -like versus D(1) -like receptors. Relevance for volume transmission in interpreting PET findings. *Synapse*. Available at: http://www.ncbi.nlm.nih.gov/pubmed/22034017

Marinesco, S., Wickremasinghe, N., and Carew, T. J. (2006). Regulation of behavioral and synaptic plasticity by serotonin release within local modulatory fields in the CNS of Aplysia. *J. Neurosci.* 26, 12682–12693.

Marinesco, S., and Carew, T. J. (2002). Serotonin release evoked by tail nerve stimulation in the CNS of aplysia: characterization and relationship to heterosynaptic plasticity. *J. Neurosci.* 22, 2299–2312.

Marshak, D. W. (2001). Synaptic inputs to dopaminergic neurons in mammalian retinas. *Prog. Brain Res.* 131, 83–91.

McCall, R. B., and Aghajanian, G. K. (1979). Serotonergic facilitation of facial motoneuron excitation. *Brain Res.* 169, 11–27.

McElroy, B., Zakaria, A., Glass, J. D., and Prosser, R. A. (2009). Ethanol modulates mammalian circadian clock phase resetting through extrasynaptic GABA receptor activation. *Neuroscience* 164, 842–848.

Miledi, R. (1960). Junctional and extrajunctional acetylcholine receptors in skeletal muscle fibres. *J. Physiol.* 151, 24–30.

Mizukami, T. (2004). Immunocytochemical localization of beta2-adrenergic receptors in the rat spinal cord and their spatial relationships to tyrosine hydroxylase-immunoreactive terminals. *Kurume Med. J.* 51, 175–183.

Mody, I. (2001). Distinguishing between GABA(A) receptors responsible for tonic and phasic conductances. *Neurochem. Res.* 26, 907–913.

Morris, J. F., and Pow, D. V. (1991). Widespread release of peptides in

the central nervous system: quantitation of tannic acid-captured exocytoses. *Anat. Rec.* 231, 437–445.

Moss, B. L., Fuller, A. D., Sahley, C. L., and Burrell, B. D. (2005). Serotonin modulates axo-axonal coupling between neurons critical for learning in the leech. *J. Neurophysiol.* 94, 2575–2589.

Moukhles, H., Bosler, O., Bolam, J. P., Vallée, A., Umbriaco, D., Geffard, M., and Doucet, G. (1997). Quantitative and morphometric data indicate precise cellular interactions between serotonin terminals and postsynaptic targets in rat substantia nigra. *Neuroscience* 76, 1159–1171.

Mrzljak, L., Levey, A. I., and Goldman-Rakic, P. S. (1993). Association of m1 and m2 muscarinic receptor proteins with asymmetric synapses in the primate cerebral cortex: morphological evidence for cholinergic modulation of excitatory neurotransmission. *Proc. Natl. Acad. Sci. U.S.A.* 90, 5194–5198.

Muresan, Z., and Besharse, J. C. (1993). D2-like dopamine receptors in amphibian retina: localization with fluorescent ligands. *J. Comp. Neurol.* 331, 149–160.

Naka, K. I., and Rushton, W. A. H. (1967). The generation and spread of S-potentials in fish (Cyprinidae). *J. Physiol.* 192, 437–461.

Nguyen-Legros, J., Simon, A., Caillé, I., and Bloch, B. (1997). Immunocytochemical localization of dopamine D1 receptors in the retina of mammals. *Vis. Neurosci.* 14, 545–551.

Nicholls, J. G., and Kuffler, D. P. (1990). Quantal release of serotonin from presynaptic nerve terminals. *Neurochem. Int.* 17, 157–163.

Nie, H., and Weng, H.-R. (2010). Impaired glial glutamate uptake induces extrasynaptic glutamate spillover in the spinal sensory synapses of neuropathic rats. *J. Neurophysiol.* 103, 2570–2580.

Nieoullon, A., Cheramy, A., and Glowinski, J. (1977). An adaptation of the push-pull cannula method to study the *in vivo* release of (3H)dopamine synthesized from (3H)tyrosine in the cat caudate nucleus: effects of various physical and pharmacological treatments. *J. Neurochem.* 28, 819–828.

Nusser, Z., Roberts, J. D., Baude, A., Richards, J. G., and Somogyi, P. (1995). Relative densities of synaptic and extrasynaptic GABAA receptors on cerebellar granule cells as determined by a quantitative immunogold method. *J. Neurosci.* 15, 2948–2960.

Nusser, Z., Sieghart, W., and Somogyi, P. (1998). Segregation of different GABAA receptors to synaptic and extrasynaptic membranes of cerebellar granule cells. *J. Neurosci.* 18, 1693–1703.

Oláh, S., Füle, M., Komlósi, G., Varga, C., Báldi, R., Barzó, P., and Tamás, G. (2009). Regulation of cortical microcircuits by unitary GABA-mediated volume transmission. *Nature* 461, 1278–1281.

O'Connor, J. J., and Kruk, Z. L. (1991). Frequency dependence of 5-HT autoreceptor function in rat dorsal raphe and suprachiasmatic nuclei studied using fast cyclic voltammetry. *Brain Res.* 568, 123–130.

Papadopoulos, G. C., Parnavelas, J. G., and Buijs, R. M. (1989). Light and electron microscopic immunocytochemical analysis of the dopamine innervation of the rat visual cortex. *J. Neurocytol.* 18, 303–310.

Parikh, V., Kozak, R., Martinez, V., and Sarter, M. (2007). Prefrontal acetylcholine release controls cue detection on multiple timescales. *Neuron* 56, 141–154.

Parnas, I., Rahamimoff, R., and Sarney, (1975). Tonic release of transmitter at the neuromuscular junction of the crab. *J. Physiol. (Lond.)* 250, 275–286.

Parpura, V., Basarsky, T. A., Liu, F., Jeftinija, K., Jeftinija, S., and Haydon, P. G. (1994). Glutamate-mediated astrocyte-neuron signalling. *Nature* 369, 744–747.

Patel, J. C., Witkovsky, P., Avshalumov, M. V., and Rice, M. E. (2009). Mobilization of calcium from intracellular stores facilitates somatodendritic dopamine release. *J. Neurosci.* 29, 6568–6579.

Piccolino, M., Neyton, J., and Gerschenfeld, H. M. (1984). Decrease of gap junction permeability induced by dopamine and cyclic adenosine 3′:5′-monophosphate in horizontal cells of turtle retina. *J. Neurosci.* 4, 2477–2488.

Porcello, D. M., Huntsman, M. M., Mihalek, R. M., Homanics, G. E., and Huguenard, J. R. (2003). Intact synaptic GABAergic inhibition and altered neurosteroid modulation of thalamic relay neurons in mice lacking delta subunit. *J. Neurophysiol.* 89, 1378–1386.

Prosser, R. A., Miller, J. D., and Heller, H. C. (1990). A serotonin agonist phase-shifts the circadian clock in the suprachiasmatic nuclei *in vitro*. *Brain Res.* 534, 336–339.

Pudovkina, O. L., Cremers, T. I. F. H., and Westerink, B. H. C. (2003). Regulation of the release of serotonin in the dorsal raphe nucleus by alpha1 and alpha2 adrenoceptors. *Synapse* 50, 77–82.

Pudovkina, O. L., Kawahara, Y., de Vries, J., and Westerink, B. H. (2001). The release of noradrenaline in the locus coeruleus and prefrontal cortex studied with dual-probe microdialysis. *Brain Res.* 906, 38–45.

Puopolo, M., Hochstetler, S. E., Gustincich, S., Wightman, R. M., and Raviola, E. (2001). Extrasynaptic release of dopamine in a retinal neuron: activity dependence and transmitter modulation. *Neuron* 30, 211–225.

Pérez de la Mora, M., Jacobsen, K. X., Crespo-Ramírez, M., Flores-Gracia, C., and Fuxe, K. (2008). Wiring and volume transmission in rat amygdala. Implications for fear and anxiety. *Neurochem. Res.* 33, 1618–1633.

Raleigh, M. J., McGuire, M. T., Brammer, G. L., Pollack, D. B., and Yuwiler, A. (1991). Serotonergic mechanisms promote dominance acquisition in adult male vervet monkeys. *Brain Res.* 559, 181–190.

Reiner, A. (2009). "You cannot have a vertebrate brain without a basal ganglia," in *The Basal Ganglia IX*, eds H. J. Groenewegen, P. Voorn, H. W. Berendse, A. B. Mulder, and A. R. Cools (New York, NY: Springer), 3–24. Available at: http://www.springerlink.com/index/10.1007/978-1-4419-0340-2_1

Ren, J., Qin, C., Hu, F., Tan, J., Qiu, L., Zhao, S., Feng, G., and Luo, M. (2011). Habenula "cholinergic" neurons corelease glutamate and acetylcholine and activate postsynaptic neurons via distinct transmission modes. *Neuron* 69, 445–452.

Riad, M., Garcia, S., Watkins, K. C., Jodoin, N., Doucet, E., Langlois, X., el Mestikawy, S., Hamon, M., and Descarries, L. (2000). Somatodendritic localization of 5-HT1A and preterminal axonal localization of 5-HT1B serotonin receptors in adult rat brain. *J. Comp. Neurol.* 417, 181–194.

Rice, M. E., Cragg, S. J., and Greenfield, S. A. (1997). Characteristics of electrically evoked somatodendritic dopamine release in substantia nigra and ventral tegmental area *in vitro*. *J. Neurophysiol.* 77, 853–862.

Richards, K. S., Simon, D. J., Pulver, S. R., Beltz, B. S., and Marder, E. (2003). Serotonin in the developing stomatogastric system of the lobster, *Homarus americanus*. *J. Neurobiol.* 54, 380–392.

Richardson, B. D., Ling, L. L., Uteshev, V. V., and Caspary, D. M. (2011). Extrasynaptic GABAA receptors and tonic inhibition in rat auditory thalamus. *PLoS ONE* 6, e16508. doi: 10.1371/journal.pone.0016508

Ridet, J. L., Rajaofetra, N., Teilhac, J. R., Geffard, M., and Privat, A. (1993). Evidence for nonsynaptic serotonergic and noradrenergic innervation of the rat dorsal horn and possible involvement of neuron-glia interactions. *Neuroscience* 52, 143–157.

Rieger, A., Deitmer, J. W., and Lohr, C. (2007). Axon-glia communication evokes calcium signaling in olfactory ensheathing cells of the developing olfactory bulb. *Glia* 55, 352–359.

Rodrigues, R. J., Almeida, T., Richardson, P. J., Oliveira, C. R., and Cunha, R. A. (2005). Dual presynaptic control by ATP of glutamate release via facilitatory P2X1, P2X2/3, and P2X3 and inhibitory P2Y1, P2Y2, and/or P2Y4 receptors in the rat hippocampus. *J. Neurosci.* 25, 6286–6295.

Romanelli, R. J., Williams, J. T., and Neve, K. A. (2010). "Dopamine receptor signaling: intracellular pathways to behavior," in *The Dopamine Receptors* (New York, NY: Springer), 137–173.

Rosas-Arellano, A., Machuca-Parra, A. I., Reyes-Haro, D., Miledi, R., and Martínez-Torres, A. (2011a). Expression of GABAρ receptors in the neostriatum: localization in aspiny, medium spiny neurons and GFAP-positive cells. *J. Neurochem*. Available at: http://www.ncbi.nlm.nih.gov/pubmed/22168837

Rosas-Arellano, A., Parodi, J., Machuca-Parra, A. I., Sánchez-Gutiérrez, A., Inestrosa, N. C., Miledi, R., and Martínez-Torres, A. (2011b). The GABA(A)ρ receptors in hippocampal spontaneous activity and their distribution in hippocampus, amygdala and visual cortex. *Neurosci. Lett.* 500, 20–25.

Rossi, D. J., Hamann, M., and Attwell, D. (2003). Multiple modes of GABAergic inhibition of rat cerebellar granule cells. *J. Physiol.* 548, 97–110.

Rude, S., Coggeshall, E., and Van Orden, L. S. (1969). Chemical and ultrastructural identification of 5-hydroxytryptamine in an identified neuron. *J. Cell Biol.*3, 832–854.

Sargent, P. B., Yau, K. W., and Nicholls, J. G. (1977). Extrasynaptic receptors on cell bodies of neurons in central nervous system of the leech. *J. Neurophysiol.* 40, 446–452.

Sarter, M., Gehring, W. J., and Kozak, R. (2006). More attention must be paid: the neurobiology of attentional effort. *Brain Res. Rev.* 51, 145–160.

Sarter, M., Parikh, V., and Howe, W. M. (2009). Phasic acetylcholine release and the volume transmission hypothesis: time to move on. *Nat. Rev. Neurosci.* 10, 383–390.

Saxena, N. C., and Macdonald, R. L. (1994). Assembly of GABAA receptor subunits: role of the delta subunit. *J. Neurosci.* 14, 7077–7086.

Semyanov, A., Walker, M. C., and Kullmann, D. M. (2003). GABA uptake regulates cortical excitability via cell type-specific tonic inhibition. *Nat. Neurosci.* 6, 484–490.

Sesack, S. R., Aoki, C., and Pickel, V. M. (1994). Ultrastructural localization of D2 receptor-like immunoreactivity in midbrain dopamine neurons and their striatal targets. *J. Neurosci.* 14, 88–106.

Sharp, T., Bramwell, S. R., Clark, D., and Grahame-Smith, D. G. (1989). *In vivo* measurement of extracellular 5-hydroxytryptamine in hippocampus of the anaesthetized rat using microdialysis: changes in relation to 5-hydroxytryptaminergic neuronal activity. *J. Neurochem.* 53, 234–240.

Shytle, R. D., Mori, T., Townsend, K., Vendrame, M., Sun, N., Zeng, J., Ehrhart, J., Silver, A. A., Sanberg, P. R., and Tan, J. (2004). Cholinergic modulation of microglial activation by alpha 7 nicotinic receptors. *J. Neurochem.* 89, 337–343.

Singewald, N., and Philippu, A. (1998). Release of neurotransmitters in the locus coeruleus. *Prog. Neurobiol.* 56, 237–267.

Smiley, J. F., Morrell, F., and Mesulam, M. M. (1997). Cholinergic synapses in human cerebral cortex: an ultrastructural study in serial sections. *Exp. Neurol.* 144, 361–368.

Smiley, J. F., Williams, S. M., Szigeti, K., and Goldman-Rakic, P. S. (1992). Light and electron microscopic characterization of dopamine-immunoreactive axons in human cerebral cortex. *J. Comp. Neurol.* 321, 325–335.

Smiley, J. F., and Goldman-Rakic, P. S. (1993). Heterogeneous targets of dopamine synapses in monkey prefrontal cortex demonstrated by serial section electron microscopy: a laminar analysis using the silver-enhanced diaminobenzidine sulfide (SEDS) immunolabeling technique. *Cereb. Cortex* 3, 223–238.

Soldo, B. L., Giovannucci, D. R., Stuenkel, E. L., and Moises, H. C. (2004). Ca^{2+} and frequency dependence of exocytosis in isolated somata of magnocellular supraoptic neurones of the rat hypothalamus. *J. Physiol.* 555, 699–711.

Somogyi, P., Takagi, H., Richards, J. G., and Mohler, H. (1989). Subcellular localization of benzodiazepine/GABAA receptors in the cerebellum of rat, cat, and monkey using monoclonal antibodies. *J. Neurosci.* 9, 2197–2209.

Stella, S. L., Jr., and Thoreson, W. B. (2000). Differential modulation of rod and cone calcium currents in tiger salamander retina by D2 dopamine receptors and cAMP. *Eur. J. Neurosci.* 12, 3537–3548.

Sun, Y. A., and Poo, M. M. (1987). Evoked release of acetylcholine from the growing embryonic neuron. *Proc. Natl. Acad. Sci. U.S.A.* 84, 2540–2544.

Svensson, T. H. (1987). Peripheral, autonomic regulation of locus coeruleus noradrenergic neurons in brain: putative implications for psychiatry and psychopharmacology. *Psychopharmacology (Berl.)* 92, 1–7.

Swanson, C. J., Blackburn, T. P., Zhang, X., Zheng, K., Xu, Z.-Q. D., Hökfelt, T., Wolinsky, T. D., Konkel, M. J., Chen, H., Zhong, H., et al. (2005). Anxiolytic- and antidepressant-like profiles of the galanin-3 receptor (Gal3) antagonists SNAP 37889 and SNAP 398299. *Proc. Natl. Acad. Sci. U.S.A.* 102, 17489–17494.

Swanson, L. W., and Hartman, B. K. (1975). The central adrenergic system. An immunofluorescence study of the location of cell bodies and their efferent connections in the rat utilizing dopamine-beta-hydroxylase as a marker. *J. Comp. Neurol.* 163, 467–505.

Séguéla, P., Watkins, K. C., and Descarries, L. (1988). Ultrastructural features of dopamine axon terminals in the anteromedial and the suprarhinal cortex of adult rat. *Brain Res.* 442, 11–22.

Takayama, C., and Inoue, Y. (2004). Extrasynaptic localization of GABA in the developing mouse cerebellum. *Neurosci. Res.* 50, 447–458.

Tang, Z.-Q., Hoang Dinh, E., Shi, W., and Lu, Y. (2011). Ambient GABA-activated tonic inhibition sharpens auditory coincidence detection via a depolarizing shunting mechanism. *J. Neurosci.* 31, 6121–6131.

Teranishi, T., Negishi, K., and Kato, S. (1984). Regulatory effect of dopamine on spatial properties of horizontal cells in carp retina. *J. Neurosci.* 4, 1271–1280.

Thoreson, W. B., Stella, S. L., Bryson, E. J., Clements, J., and Witkovsky, P. (2002). D2-like dopamine receptors promote interactions between calcium and chloride channels that diminish rod synaptic transfer in the salamander retina. *Vis. Neurosci.* 19. Available at: http://www.journals.cambridge.org/abstract_S0952523802192017

Thyssen, A., Hirnet, D., Wolburg, H., Schmalzing, G., Deitmer, J. W., and Lohr, C. (2010). Ectopic vesicular neurotransmitter release along sensory axons mediates neurovascular coupling via glial calcium signaling. *Proc. Natl. Acad. Sci. U.S.A.* 107, 15258–15263.

Tia, S., Wang, J. F., Kotchabhakdi, N., and Vicini, S. (1996). Developmental changes of inhibitory synaptic currents in cerebellar granule neurons: role of GABA(A) receptor alpha 6 subunit. *J. Neurosci.* 16, 3630–3640.

Tobin, V., Leng, G., and Ludwig, M. (2012). The involvement of actin, calcium channels and exocytosis proteins in somato-dendritic oxytocin and vasopressin release. *Front. Membr. Physiol.* 3.

Trueta, C., Kuffler, D. P., and De-Miguel, F. F. (2012). Cycling of dense core vesicles involved in somatic exocytosis of serotonin by leech neurons. *Front. Physiol.* 3. Available at: http://www.frontiersin.org/Membrane_Physiology_and_Biophysics/10.3389/fphys.2012.00175/abstract

Trueta, C., Méndez, B., and De-Miguel, F. F. (2003). Somatic exocytosis of serotonin mediated by L-type calcium channels in cultured leech neurones. *J. Physiol. (Lond.)* 547, 405–416.

Trueta, C., Sánchez-Armass, S., Morales, M. A., and De-Miguel, F. F. (2004). Calcium-induced calcium release contributes to somatic secretion of serotonin in leech retzius neurons. *J. Neurobiol.* 61, 309–316.

Turrini, P., Casu, M. A., Wong, T. P., De Koninck, Y., Ribeiro-da-Silva, A., and Cuello, A. C. (2001). Cholinergic nerve terminals establish classical synapses in the rat cerebral cortex: synaptic pattern and age-related atrophy. *Neuroscience* 105, 277–285.

Umbriaco, D., Garcia, S., Beaulieu, C., and Descarries, L. (1995). Relational features of acetylcholine, noradrenaline, serotonin and GABA axon terminals in the stratum radiatum of adult rat hippocampus (CA1). *Hippocampus* 5, 605–620.

Umbriaco, D., Watkins, K. C., Descarries, L., Cozzari, C., and Hartman, B. K. (1994). Ultrastructural and morphometric features of the acetylcholine innervation in adult rat parietal cortex: an electron microscopic study in serial sections. *J. Comp. Neurol.* 348, 351–373.

Underwood, M. D., Khaibulina, A. A., Ellis, S. P., Moran, A., Rice, P. M., Mann, J. J., and Arango, V. (1999). Morphometry of the dorsal raphe nucleus serotonergic neurons in suicide victims. *Biol. Psychiatry* 46, 473–483.

Valentino, R. J., and Van Bockstaele, E. (2008). Convergent regulation of locus coeruleus activity as an adaptive response to stress. *Eur. J. Pharmacol.* 583, 194–203.

Van Bockstaele, E. J., and Pickel, V. M. (1993). Ultrastructure of serotonin-immunoreactive terminals in the core and shell of the rat nucleus accumbens: cellular substrates for interactions with catecholamine afferents. *J. Comp. Neurol.* 334, 603–617.

Varga, V., Losonczy, A., Zemelman, B. V., Borhegyi, Z., Nyiri, G., Domonkos, A., Hangya, B., Holderith, N., Magee, J. C., and Freund, T. F. (2009). Fast synaptic subcortical control of hippocampal circuits. *Science* 326, 449–453.

Vavra, V., Bhattacharya, A., and Zemkova, H. (2011). Facilitation of glutamate and GABA release by P2X receptor activation in supraoptic neurons from freshly isolated rat brain slices. *Neuroscience* 188, 1–12.

Velázquez-Ulloa, N., Blackshaw, S. E., Szczupak, L., Trueta, C., García, E., and De-Miguel, F. F. (2003). Convergence of mechanosensory inputs onto neuromodulatory serotonergic neurons in the leech. *J. Neurobiol.* 54, 604–617.

Versaux-Botteri, C., Gibert, J. M., Nguyen-Legros, J., and Vernier, P. (1997). Molecular identification of a dopamine D1b receptor in bovine retinal pigment epithelium. *Neurosci. Lett.* 237, 9–12.

Vinson, P. N., and Justice, J. B., Jr, (1997). Effect of neostigmine on concentration and extraction fraction of acetylcholine using quantitative microdialysis. *J. Neurosci. Methods* 73, 61–67.

Vizi, E. S., Fekete, A., Karoly, R., and Mike, A. (2010). Non-synaptic receptors and transporters involved in brain functions and targets of drug treatment. *Br. J. Pharmacol.* 160, 785–809.

Vizi, E. S., and Kiss, J. P. (1998). Neurochemistry and pharmacology of the major hippocampal transmitter systems: synaptic and nonsynaptic interactions. *Hippocampus* 8, 566–607.

Vélez-Fort, M., Maldonado, P. P., Butt, A. M., Audinat, E., and Angulo, M. C. (2010). Postnatal switch from synaptic to extrasynaptic transmission between interneurons and NG2 cells. *J. Neurosci.* 30, 6921–6929.

Wang, Y., and Mangel, S. C. (1996). A circadian clock regulates rod and cone input to fish retinal cone horizontal cells. *PNAS* 93, 4655–4660.

Wei, W., Zhang, N., Peng, Z., Houser, C. R., and Mody, I. (2003). Perisynaptic localization of delta subunit-containing GABA(A) receptors and their activation by GABA spillover in the mouse dentate gyrus. *J. Neurosci.* 23, 10650–10661.

Weiger, W. A. (1997). Serotonergic modulation of behaviour: a phylogenetic overview. *Biol. Rev. Camb. Philos. Soc.* 72, 61–95.

White, S. R., Fung, S. J., Jackson, D. A., and Imel, K. M. (1996). Serotonin, norepinephrine and associated neuropeptides: effects on somatic motoneuron excitability. *Prog. Brain Res.* 107, 183–199.

Willard, A. L. (1981). Effects of serotonin on the generation of the motor program for swimming by the medicinal leech. *J. Neurosci.* 1, 936–944.

Williams, J. T., Henderson, G., and North, R. A. (1985). Characterization of alpha 2-adrenoceptors which increase potassium conductance in rat locus coeruleus neurones. *Neuroscience* 14, 95–101.

Wilson, C. J., Groves, P. M., and Fifková, E. (1977). Monoaminergic synapses, including dendro-dendritic synapses in the rat substantia nigra. *Exp. Brain Res.* 30, 161–174.

Witkovsky, P. (2004). Dopamine and retinal function. *Doc. Ophthalmol.* 108, 17–40.

Witkovsky, P., Nicholson, C., Rice, M. E., Bohmaker, K., and Meller, E. (1993). Extracellular dopamine concentration in the retina of the clawed frog, Xenopus laevis. *Proc. Natl. Acad. Sci. U.S.A.* 90, 5667–5671.

Witkovsky, P., Patel, J. C., Lee, C. R., and Rice, M. E. (2009). Immunocytochemical identification of proteins involved in dopamine release from the somatodendritic compartment of nigral dopaminergic neurons. *Neuroscience* 164, 488–496.

Wright, I. K., Upton, N., and Marsden, C. A. (1992). Effect of established and putative anxiolytics on extracellular 5-HT and 5-HIAA in the ventral hippocampus of rats during behaviour on the elevated X-maze. *Psychopharmacology (Berl.)* 109, 338–346.

Xi, Z.-X., Ramamoorthy, S., Shen, H., Lake, R., Samuvel, D. J., and Kalivas, P. W. (2003). GABA transmission in the nucleus accumbens is altered after withdrawal from repeated cocaine. *J. Neurosci.* 23, 3498–3505.

Xia, X., Lessmann, V., and Martin, T. F. J. (2009). Imaging of evoked dense-core-vesicle exocytosis in hippocampal neurons reveals long latencies and kiss-and-run fusion events. *J. Cell. Sci.* 122, 75–82.

Yoshida, M., Shirouzu, M., Tanaka, M., Semba, K., and Fibiger, H. C. (1989). Dopaminergic neurons in the nucleus raphe dorsalis innervate the prefrontal cortex in the rat: a combined retrograde tracing and immunohistochemical study using anti-dopamine serum. *Brain Res.* 496, 373–376.

Yu, A. J., and Dayan, P. (2002). Acetylcholine in cortical inference. *Neural Netw.* 15, 719–730.

Zaidi, Z. F., and Matthews, M. R. (1997). Exocytotic release from neuronal cell bodies, dendrites and nerve terminals in sympathetic ganglia of the rat, and its differential regulation. *Neuroscience* 80, 861–891.

Zaidi, Z. F., and Matthews, M. R. (1999). Stimulant-induced exocytosis from neuronal somata, dendrites, and newly formed synaptic nerve terminals in chronically decentralized sympathetic ganglia of the rat. *J. Comp. Neurol.* 415, 121–143.

Zhang, B., Zhang, X.-Y., Luo, P.-F., Huang, W., Zhu, F.-P., Liu, T., Du, Y.-R., Wu, Q.-H., Lü, J., Xiu, Y., Liu, L. N., Huang, H. P., Guo, S., Zheng, H., Zhang, C. X., and Zhou, Z. (2012). Action potential-triggered somatic exocytosis in mesencephalic trigeminal nucleus neurons in rat brain slices. *J. Physiol. (Lond.)* 590, 753–762.

Zhang, Q., Pangrsic, T., Kreft, M., Krzan, M., Li, N., Sul, J.-Y., Halassa, M., Van Bockstaele, E., Zorec, R., and Haydon, P. G. (2004). Fusion-related release of glutamate from astrocytes. *J. Biol. Chem.* 279, 12724–12733.

Zhang, X., Chen, Y., Wang, C., and Huang, L.-Y. M. (2007). Neuronal somatic ATP release triggers neuron-satellite glial cell communication in dorsal root ganglia. *Proc. Natl. Acad. Sci. U.S.A.* 104, 9864–9869.

Zhou, F. C., Tao-Cheng, J. H., Segu, L., Patel, T., and Wang, Y. (1998). Serotonin transporters are located on the axons beyond the synaptic junctions: anatomical and functional evidence. *Brain Res.* 805, 241–254.

Zhu, G., Okada, M., Yoshida, S., Ueno, S., Mori, F., Takahara, T., Saito, R., Miura, Y., Kishi, A., Tomiyama, M., Satoshi, K. A., Kojima, T., Fukuma, G., Wakabayashi, K., Hase, K., Ohno, H., Kijima, H., Takano, Y., Mitsudome, A., Kaneko, S., and Hirose, S. (2008). Rats harboring S284L Chrna4 mutation show attenuation of synaptic and extrasynaptic GABAergic transmission and exhibit the nocturnal frontal lobe epilepsy phenotype. *J. Neurosci.* 28, 12465–12476.

Zhu, P. C., Thureson-Klein, A., and Klein, R. L. (1986). Exocytosis from large dense cored vesicles outside the active synaptic zones of terminals within the trigeminal subnucleus caudalis: a possible mechanism for neuropeptide release. *Neuroscience* 19, 43–54.

Zimmermann, H. (1993). *Synaptic Transmission. Cellular and Molecular Basis*. Stuttgart-New York: Georg Thieme Verlag, Oxford University Press.

Zucker, C., and Yazulla, S. (1982). Localization of synaptic and non-synaptic nicotinic-acetylcholine receptors in the goldfish retina. *J. Comp. Neurol.* 204, 188–195.

Conflict of Interest Statement: This research was conducted in the absence of any commercial or financial relationships that could be construed as a potential conflict of interest.

Received: 18 April 2012; paper pending published: 02 May 2012; accepted: 21 July 2012; published online: 04 September 2012.

*Citation: Trueta C and De-Miguel FF (2012) Extrasynaptic exocytosis and its mechanisms: a source of molecules mediating volume transmission in the nervous system. Front. Physio. **3**:319. doi: 10.3389/fphys.2012.00319*

This article was submitted to Frontiers in Membrane Physiology and Biophysics, a specialty of Frontiers in Physiology.

frontiers in
PHYSIOLOGY

REVIEW ARTICLE
published: 04 June 2012
doi: 10.3389/fphys.2012.00136

Extrasynaptic neurotransmission in the modulation of brain function. Focus on the striatal neuronal–glial networks

Kjell Fuxe[1]*, Dasiel O. Borroto-Escuela[1], Wilber Romero-Fernandez[1], Zaida Diaz-Cabiale[2], Alicia Rivera[3], Luca Ferraro[4], Sergio Tanganelli[4], Alexander O. Tarakanov[5], Pere Garriga[6], José Angel Narváez[2], Francisco Ciruela[7], Michele Guescini[8] and Luigi F. Agnati[9]

[1] *Department of Neuroscience, Karolinska Institutet, Stockholm, Sweden*
[2] *Department of Physiology, School of Medicine, University of Málaga, Málaga, Spain*
[3] *Department of Cell Biology, Faculty of Sciences, University of Málaga, Málaga, Spain*
[4] *Pharmacology Section, Department of Clinical and Experimental Medicine, University of Ferrara, Ferrara, Italy*
[5] *Russian Academy of Sciences, St. Petersburg Institute for Informatics and Automation, Saint Petersburg, Russia*
[6] *Departament d´Enginyeria Química, Centre de Biotecnologia Molecular, Universitat Politècnica de Catalunya, Barcelona, Spain*
[7] *Unitat de Farmacologia, Departament Patologia i Terapèutica Experimental, Universitat de Barcelona, Barcelona, Spain*
[8] *Department of Biomolecular Sciences, University of Urbino "CarloBo," Urbino, Italy*
[9] *IRCCS Lido, Venice, Italy*

Edited by:
Francisco Fernandez De-Miguel, Universidad Nacional Autonoma de Mexico, Mexico

Reviewed by:
Francisco Fernandez De-Miguel, Universidad Nacional Autonoma de Mexico, Mexico
Teresa Giraldez, University Hospital NS Candelaria, Spain

****Correspondence:***
Kjell Fuxe, Department of Neuroscience, Karolinska Institutet, Retzius väg 8, 17177 Stockholm, Sweden.
e-mail: kjell.fuxe@ki.se

Extrasynaptic neurotransmission is an important short distance form of volume transmission (VT) and describes the extracellular diffusion of transmitters and modulators after synaptic spillover or extrasynaptic release in the local circuit regions binding to and activating mainly extrasynaptic neuronal and glial receptors in the neuroglial networks of the brain. Receptor-receptor interactions in G protein-coupled receptor (GPCR) heteromers play a major role, on dendritic spines and nerve terminals including glutamate synapses, in the integrative processes of the extrasynaptic signaling. Heteromeric complexes between GPCR and ion-channel receptors play a special role in the integration of the synaptic and extrasynaptic signals. Changes in extracellular concentrations of the classical synaptic neurotransmitters glutamate and GABA found with microdialysis is likely an expression of the activity of the neuron-astrocyte unit of the brain and can be used as an index of VT-mediated actions of these two neurotransmitters in the brain. Thus, the activity of neurons may be functionally linked to the activity of astrocytes, which may release glutamate and GABA to the extracellular space where extrasynaptic glutamate and GABA receptors do exist. Wiring transmission (WT) and VT are fundamental properties of all neurons of the CNS but the balance between WT and VT varies from one nerve cell population to the other. The focus is on the striatal cellular networks, and the WT and VT and their integration via receptor heteromers are described in the GABA projection neurons, the glutamate, dopamine, 5-hydroxytryptamine (5-HT) and histamine striatal afferents, the cholinergic interneurons, and different types of GABA interneurons. In addition, the role in these networks of VT signaling of the energy-dependent modulator adenosine and of endocannabinoids mainly formed in the striatal projection neurons will be underlined to understand the communication in the striatal cellular networks.

Keywords: extrasynaptic, neurotransmission, receptor–receptor interactions, volume transmission, G protein coupled receptors, striatal networks, heteromers, wiring transission

INTRODUCTION

The discovery of the central dopamine (DA), noradrenaline (NA), and 5-hydroxytryptamine (5-HT) pathways was made in 1963–1965 with the Falck-Hillarp technique (Falck et al., 1962) and represented my thesis work (see Fuxe, 1965; Fuxe et al., 2007a). These monoamine brainstem systems were unique in having ascending monosynaptic connections with the tel- and diencephalon including the cerebral cortex giving rise to global networks all over the tel- and diencephalon with collaterals forming terminal networks in the lower brainstem. They also produced descending connections to the spinal cord innervating its entire gray matter at all rostro-caudal levels. The locus coeruleus built up of NA cell bodies could even send out both ascending and descending NA projections as well as NA projections to the cerebellum resulting in a global modulation of the entire central nervous system (CNS) from a single nerve cell nucleus through the vast NA nerve terminal plexa formed. This unique architecture of the central monoamine neurons gave thoughts on if in fact these neurons communicated via synaptic transmission.

In 1969–1970 we observed the appearance of extraneuronal diffuse (catecholamine) fluorescence around midbrain DA nerve cell bodies after amphetamine, a catecholamine releasing drug,

in reserpine-nialamide-L-dopa treated rats (Fuxe and Ungerstedt, 1970a). In parallel, a similar diffuse extraneuronal 5-HT fluorescence was found among the 5-HT cell bodies of the dorsal raphe nucleus after 5-HT uptake blockade with chlorimipramine in reserpine and nialamide pretreated rats (Fuxe et al., 1970b). We did not, in the beginning, understand these observations but we asked the question if they reflected a communication different from the synaptic one. We also observed that microinjected DA in the striatum could diffuse (Ungerstedt et al., 1969). This observation was confirmed in 1992 with DA immunohistochemistry (Agnati et al., 1992).

Such observations and the existence of global monoamine terminal networks together with several other observations in the literature, especially the demonstration of non-junctional monoamine varicosities by Descarries et al. (1975) led Agnati et al. (1986) to propose the concept of volume transmission (VT). The major observation in this paper was the failure to see a correlation between the regional distribution of central encephalin and beta-endorphin immunoreactive terminal networks and of central opioid receptors. The existence of two main modes of intercellular communication in the CNS was proposed and called wiring transmission (WT; prototype: synaptic transmission) and VT (Agnati et al., 1986). The major criterion for this classification was the different characteristics of the communication channel with physical boundaries well delimited in the case of WT (axons and their synapses; gap junctions) (Froes et al., 1999; Ozog et al., 2002; Bennett et al., 2003; Duan et al., 2004; Schools et al., 2006) but not in the case of VT (the extracellular fluid (ECF) filled tortuous channels of the extracellular space (ECS) and the cerebrospinal fluid (CSF) filled ventricular space and sub-arachnoidal space). Of special importance for us was the demonstration of relative transmitter-receptor mismatches in the opioid peptide systems (Agnati et al., 1986; Fuxe et al., 1988c). In parallel, Descarries et al. (1991) developed his concept of diffuse transmission based on the existence of non-junctional monoamine varicosities which is in line with our concept of VT.

VOLUME TRANSMISSION

Volume transmission is defined as "A widespread mode of intercellular communication that occurs in the ECF and in the CSF of the CNS with VT signals moving from source to target cells via energy gradients leading to diffusion and convection." The communication channels are diffuse; there exists a reserved or private communication mainly mediated via high affinity G protein-coupled receptors (GPCRs); the safety of communication is low as a result of the diffusion process and the connectivity of the diffusion channels is dynamic from open to closed (see Fuxe and Agnati, 1991b; Agnati et al., 2000, 2006; Chen et al., 2002a; Fuxe et al., 2005, 2007a). There may exist three subtypes of VT: extrasynaptic fast VT (100 msec-sec), the long-distance slow VT (sec-hour), and the roamer type of VT-mediated via microvesicles (Agnati et al., 2010a; Fuxe et al., 2010a). Two modes of microvesicle release exist namely the exocytosis of internal luminal vesicles formed in the multivesicular bodies (exosomes) and the direct budding of small vesicles from the plasma membrane (shedding vesicles). Exosomes represent a subclass of such membrane vesicles which are released by cells upon fusion of the multivesicular bodies with the plasma membrane (Guescini et al., 2012).

Migration (diffusion and flow) of VT signals (transmitters, modulators, trophic factors, ions, etc.) takes place via concentration gradients, temperature gradients, and pressure waves.

Wiring transmission, the prototype being synaptic transmission is characterized by private channels (axons) and a private or reserved communication mainly mediated by ion-channel receptors and operates with high speed (msecs); the safety is high and the connectivity static and/or dynamic. One subtype of WT is the gap junction the communication of which has no privacy but can be described as having a broadcasting character.

The overall evidence indicates that *vast majority of neurons possess the fundamental property of operating via both WT and VT but the balance between them varies from one nerve cell population to the other and with the dynamic state of the neuron.* In contrast, glial cells and endothelial cells operate exclusively via VT. The source of the neuronal VT signal is mainly from nerve terminal networks but also from soma and dendrites.

The ECS is characterized by three parameters (see Nicholson and Sykova, 1998). Volume fraction is the relative size of the ECS compared to total brain tissue volume. Tortuosity is the increase in path length that is imposed on a migrating molecule by cellular structures and extracellular matrix components. These two parameters are unit-less. Then, there is the clearance which is a constant that reflects the removal or disappearance of a compound from the ECS, and has the unit per second. Also a mathematical theory of diffusion in the brain with dual-probe microdialysis has been developed and the theory was able to fit the experimental data (Chen et al., 2002b; Hoistad et al., 2002). The diffusion of ^{3}H-mannitol using dual-probe microdialysis enabled a quantification of the classical diffusion parameters discussed above in the rat striatum.

EXTRASYNAPTIC TRANSMISSION (A SUBTYPE OF VT)

Extrasynaptic VT including perisynaptic transmission is linked to synaptic transmission and likely often takes place due to incomplete diffusion barriers (transmitter spillover or extrasynaptic release) with the synaptic transmitter reaching extrasynaptic domains of the pre and postsynaptic membrane of the synapse, the astroglia, and even adjacent synapses (Vizi, 1980; Vizi et al., 2004; Harvey and Svoboda, 2007). Other terminal varicosities fail to form synapses and are asynaptic and release the transmitter directly into the ECS. This subtype of VT operates at the local circuit level mainly through binding and activation of extrasynaptic high affinity GPCRs on neuronal and glial cells (Carmignoto, 2000) but also receptor tyrosine kinase, ion-channel receptors, and cytokine receptors are involved in linking together regulation of gene expression, firing and trophism, blood flow, and immune responses in the neuroglial networks of the CNS. In this integrative process, receptor–receptor interactions in different types of receptor heteromers play a major role (see Fuxe et al., 2007a; Borroto-Escuela et al., 2010, 2011; Fuxe et al., 2010a,b; Kenakin et al., 2010).

Extrasynaptic glutamate and GABA transmission

The classical synaptic transmitters glutamate and GABA can be measured extracellularly with microdialysis (see Ferraro et al., 1998) and reach receptors at surrounding astroglia, and at neighboring synapses, modulating the synaptic transmission

process and leading to astroglial release of glutamate being dependent on the efficacy of the glial and neuronal transporters of glutamate (see Del Arco et al., 2003; Fuxe et al., 2007b). Thus, the extrasynaptic transmission can be blocked by glial sheaths and extracellular matrix through their formation of diffusion barriers e.g., perineuronal nets and the astrocytic isolation may change over a short or long time-scale. The fate of escaping transmitters is determined not only by the transporters but also by inactivating enzymes. It seems clear that one and the same transmitter, like glutamate and GABA, can be released both as a synaptic signal and as an extrasynaptic signal producing a rapid form of VT.

As an extrasynaptic signal, glutamate can increase calcium mediated astroglial glutamate release via activation of astroglial metabotropic glutamate receptors which may involve both exocytosis and transporters (Del Arco et al., 2003). The increase of extracellular glutamate levels can be detected by microdialysis (Del Arco et al., 2003). In this way, metabolic and trophic adjustments can develop in the neuron-astrocytic unit upon activation of its glutamate synapses including increases in blood flow.

Recently, imaging of extrasynaptic glutamate VT has been accomplished by Okubo et al. (2010) during synaptic activity. The glutamate optical sensor (EOS) is a hybrid-type fluorescent indicator consisting of the glutamate-binding domain of the AMPAR subunit GluR2 and a fluorescent small molecule conjugated near the glutamate-binding pocket. EOS changes its fluorescence intensity upon binding of glutamate, for which it has both high affinity and high selectivity. The electron microscopy analysis indicated that labeled K716A-EOS was distributed throughout the extracellular surface of cells without any accumulation in the synaptic cleft, and that $>$ 97% of the indicator molecules were present extrasynaptically. They imaged the K716A-glutamate optical signal (EOS) fluorescence at various depths of the brain slice in response to parallel fiber stimulation. The magnitude and duration of the extrasynaptic dynamics were adequate for the activation of the extrasynaptic glutamate receptors and crosstalk between synapses was established (Okubo et al., 2010; Okubo and Iino, 2011).

Extrasynaptic 5-HT transmission

Double immunolabeling of 5-HT immunoreactivity (IR) in nerve terminals and 5-HT2A IR in apical dendritic shafts of pyramidal nerve cells of the cerebral cortex have demonstrated their relationships (Jansson et al., 2001). In the horizontal sections, the mean distance from a 5-HT2A-IR apical dendrite to the closest 5-HT-IR terminal-like varicosity was calculated to be 7.7 μm. Thus, these observations indicate the existence of an extrasynaptic 5-HT2A mediated VT in the cerebral cortex. The 5-HT terminal-extrasynaptic 5-HT receptor subtype relationships have been reviewed by Jansson et al. (2002). These observations are in line with the early work of Fuxe et al. (1970b) on 5-HT diffusion in the raphe dorsalis and of Descarries et al. (1975) on the existence of large numbers of non-junctional 5-HT terminal varicosities which vary from one region to the other (Descarries and Mechawar, 2000). De-Miguel and Trueta (2005) have also demonstrated extrasynaptic exocytosis of 5-HT involving multiple mechanisms including both clear vesicles and dense core vesicles. Somatic exocytosis of 5-HT in cultured leech neurons takes place exclusively from dense core vesicles (Trueta et al., 2003). It is of substantial interest that 5-HT released from cultured leech neurons produces inhibition of the firing of the 5-HT neurons through activation of 5-HT autoreceptors (Cercos et al., 2009).

Extrasynaptic DA transmission

Dopamine transmitter/D1 receptor mismatches have been observed by receptor autoradiography and dual immunolabeling of the pre and postjunctional structures of the ascending DA neurons (Fuxe et al., 1988a,b). Thus, release of DA is often observed not to be in strict contiguity with postsynaptic membranes, and a high incidence of non-junctional DA terminal varicosities is observed in the neostriatum (Descarries et al., 1996; Descarries and Mechawar, 2000). The ultrastructural analysis, based on transmitter and receptor immunocytochemistry, has repeatedly demonstrated short distance transmitter/receptor mismatches for the DA transmitter with the major part of the D1 and D2 receptor labeling being outside the DA synapses in the local striatal circuits, in which the DA synapses and/or non-junctional DA terminals are found (Dana et al., 1989; Levey et al., 1993; Sesack et al., 1994; Smiley et al., 1994; Hersch et al., 1995, 1997; Yung et al., 1995; Caille et al., 1996; for review see Jansson et al., 2002). The evidence therefore indicates that DA mainly acts as a VT transmitter being directly released into the ECF or reaching it via leaking DA synapses (Fuxe and Agnati, 1991a,b; Zoli and Agnati, 1996; Fuxe et al., 2007a). Rice and Cragg (2008) have modeled DA spillover after quantal release based on a large number of experimental data. In the updated DA synapse the DA release is unconstrained by the extrasynapic dopamine transporter (DAT), the diffusion process being too fast for the DAT which mainly increases clearance of DA and thus its half-life. A cloud of DA is formed and can reach the extrasynaptic DA receptors which are in majority. Thus, the primary mode of DA communication is VT. The effective radius for high affinity DA receptors is 7–8 μm which is compatible with extrasynaptic VT. This is the extrasynaptic short distance subtype of VT. The spheres obtained would encompass tens to thousands of synapses and the action of DA involves the activation of extrasynaptic receptors on terminals, dendrites, soma, and axons.

The D2 receptors are of special interest since the KiH (the dissociation constant of the high affinity state of the receptor) value for DA at [^{3}H] raclopride-labeled D2-like receptors in dorsal striatum was 12 nM (Marcellino et al., 2011), and this can help explain PET findings that amphetamine-induced increases in DA release can produce an up to 50% decrease of [^{11}C] raclopride binding in the dorsal striatum *in vivo* (Dewey et al., 1993; Laruelle, 2000; Seneca et al., 2006). These combined results give indications for the existence of striatal D2-like receptor-mediated extrasynaptic form of DA VT at the local circuit level *in vivo* in the human striatum (Marcellino et al., 2011). However, in Parkinson disease also a long-distance form of DA VT likely develops due to the development of DA receptor supersensitivity (Fuxe et al., 2003, 2010c). Thus, larger distances of diffusion of released DA can still maintain DA transmission since the supersensitive DA receptors are sensitive to very low concentrations of DA. Parkinson disease develops when too few DA terminal networks remain and distance from the DA release site to the vast majority of DA becomes too distant for DA receptor activation (Fuxe, 1979). At this stage l-DOPA

treatment and/or D2 receptor agonist treatment are introduced producing antiparkinson actions through activation of the supersensitive striatal DA (Fuxe et al., 2003, 2010c). Thus, this treatment substitutes for the loss of DA VT in Parkinson disease.

Extrasynaptic noradrenaline transmission

The low synaptic incidence of cortical NA nerve terminal plexa has been demonstrated in the rat and monkey being in the order of 7–18% (Seguela et al., 1990; Aoki et al., 1998), which is clearly lower than the synaptic incidence in cortical (56–92%) and neostriatal (30–40%) DA nerve terminal plexa in the rat (Descarries and Mechawar, 2000).

The relationships of NA nerve terminal to extrasynaptic adrenergic receptors have been established (Aoki et al., 1998). Dual immunolabeling of β-adrenergic receptors and CA nerve terminal networks in the cerebral cortex using electron microscopic immunocytochemistry have demonstrated membrane contacts between CA nerve terminals rich in vesicles and β-adrenergic IR astrocytes, giving evidence for neuroglia communication via VT (Aoki, 1992; Aoki and Pickel, 1992). It was of interest that these β-adrenergic receptor IR astrocytes also surrounded asymmetric axo-spinous synapses, where the astroglia β-adrenergic receptors may modulate e.g., glutamate spillover by modulating the activity of the glial glutamate transporters and/or the permeability of the astroglial gap junctions, and thus the sphere of astroglia activation (Aoki, 1992). In another study with similar techniques, Aoki et al. (1998) also demonstrated that prefrontal NA terminal networks can interact via VT with astroglia, dendritic shafts, and axon terminals through their α2-adrenergic receptors as well as via synaptic transmission through α2-adrenergic receptors located in postsynaptic membranes at spines of pyramidal cells.

A dysfunction of the locus coeruleus NA system together with meso-cortical DA system may contribute to attention deficit hyperactivity disorders (ADHD). High levels of D4 IR have been found in many cortical regions like motor, somatosensory, temporal association, and cingulate cortices with synaptic and extrasynaptic locations (Rivera et al., 2008). In addition, these receptors have a high affinity for NA (Newman-Tancredi et al., 1997), and the D4 IR is in fact more closely related to the widespread NA terminal plexa than the restricted DA terminal plexa (mainly limbic cortex).

It should therefore be considered that CAs may be released from the cortical NA nerve terminals and may, via extrasynaptic VT, reach and activate dopamine D4 receptors located on pyramidal and non-pyramidal nerve cells in many regions of the cerebral cortex (Rivera et al., 2008). Thus, methylphenidate drugs used in the treatment of ADHD are known to release DA and NA and may therefore act in part by restoring synaptic and extrasynaptic DA and NA transmission in the cerebral cortex (see Smiley et al., 1992; Smiley et al., 1997) involving not only classical D1, D2, and adrenergic receptors but also D4 receptors which may be activated also by extrasynaptic NA transmission (Rivera et al., 2008).

Extrasynaptic acetylcholine transmission

Widespread plexa of cholinergic nerve terminals exist in the CNS with high densities especially in the striatum and have, like the NA and 5-HT nerve terminal networks, been found to have a low synaptic incidence in the cerebral cortex and neostriatum and thus mainly operate via volume (diffuse) transmission (Descarries and Mechawar, 2000). This was in the beginning found to be surprising since acetylcholinesterase was believed to quickly degrade acetylcholine in the synaptic cleft. The explanation is that this effective degradation is performed by the A12 isoform of acetylcholinesterase while brain acetylcholinesterase mainly consists of the G4 isoform (Gisiger and Stephens, 1988) as discussed by Descarries et al. (1997). Thus, the extrasynaptic form of VT can develop but long distance VT is prevented by the brain acetylcholinesterase.

Extracellular monoamine and acetylcholine transmission and vesicular glutamate transporters

Large numbers of monoamine and acetylcholine neurons have been shown to contain a vesicular glutamate transporter (VGLUT; see El Mestikawy et al., 2011) which may have relevance for extrasynaptic monoamine and acetylcholine transmission. Thus, the VGLUT is mainly driven by the vesicular transmembrane potential component of the proton gradient which leads to more acidified vesicles. This allows the vesicular monoamine transporter (VMAT2) and vesicular acetylcholine transporters (VAChT) to accumulate higher amounts of monoamines and acetylcholine, respectively since these transporters are mainly dependent on the pH gradient over the vesicular membrane (El Mestikawy et al., 2011). Three types of VGLUT exist namely VGLUT1, VGLUT2, and VGLUT3 and are present in central monoamine and acetylcholine neurons besides GABA and glutamate neurons. This has led to discussions on whether glutamate can be co-transmitter in these neurons enabling glutamate co-release. It has been especially discussed if glutamate in DA neurons is linked to the formation of junctional DA terminals (synapses; Descarries et al., 2008). However, it appears to be largely a developmental feature since double labeling of tyrosine hydroxylase (TH) and VGLUT2 in DA terminals is hardly observed in adult rats. It is of substantial interest that a heterogeneity in DA, 5-HT and acetylcholine terminals may exist with regard to co-expression of VGLUTs and VMAT2 or VAChT (see El Mestikawy et al., 2011). In some of them it seems possible that there may exist synaptic vesicles containing both VMAT2 and VGLUT2 (DA varicosity), VMAT2 and VGLUT3 (5-HT varicosity), and VAChT and VGLUT3 (acetylcholine varicosity). In fact, evidence exists that the presence of VGLUT can lead to so-called vesicular synergy meaning increased accumulation of the primary transmitter (monoamine or acetylcholine; Gras et al., 2008; Amilhon et al., 2010; Hnasko et al., 2010). The molecular mechanism for vesicular synergy is likely that the VGLUT is driven by the vesicular transmembrane potential with the accumulation of glutamate (acid) leading to an acidification of the vesicle. In view of the fact that the VMAT2 and VAChT is dependent on a pH gradient over the vesicular membrane this will allow increased amounts of monoamines and acetylcholine to accumulate in the monoamine and acetylcholine vesicles (El Mestikawy et al., 2011). This is likely of relevance for the extrasynaptic monoamine and acetylcholine transmission since higher amounts of transmitter can be released into the ECF directly or via synaptic spillover from these varicosities and a larger volume can be reached with sufficient concentrations of monoamines and

acetylcholine to activate their extrasynaptic high affinity receptors. Increased quantal contents of vesicles of the primary transmitter with increased release has in fact been shown for VGLUT3 in 5-HT and acetylcholine neurons (Gras et al., 2008; Amilhon et al., 2010). Thus, an increase in extrasynaptic transmission is obtained. The VGLUT research will represent an exciting field for understanding VT in the CNS.

LONG DISTANCE VT

1. Long distance DA VT up to 30–50 μm may also exist in the striatum of the intact rat. Thus, we have observed substantial D1-TH terminal mismatches (in the maximal range of 30–50 μm) in the nucleus accumbens shell with D1 rich areas surrounded by highly dense DA nerve terminal plexa (Jansson et al., 1999). It may be that here the existence of energy gradients, especially temperature gradients created by the uncoupling protein 2 (UCP2) in the DA terminal regions, increase the migration of DA into the D1 rich and TH poor region (Rivera et al., 2006). UCP2 produces a disappearance of the H+ gradient in the mitochondria with generation of heat leading to a temperature gradient vs. the D1 receptor rich cellular network. This may lead to mass movement of the ECF (flow) carrying DA into the mismatch region which is more rapid than DA diffusion alone. It should be mentioned that DA can also be released into the portal blood vessels from the tuberoinfundibular DA neurons (Fuxe, 1963, 1964; Fuxe et al., 1967; MacLeod and Lehmeyer, 1974; Andersson et al., 1981) to activate the D2 receptors on the prolactin cells of the anterior pituitary. Thus, DA can act as a synaptic transmitter, VT transmitter, and as a hypothalamic hormone.
2. Long distance peptide VT and CSF VT

Peptide neurons likely operate via long distance VT with distances over 1 mm involving also flow in the CSF (Fuxe et al., 2010a). One of the best examples is CSF delivered beta-endorphin (2500 pmol in 5 μl) which could accumulate in nerve cell body subpopulations and their dendrites all over the paraventricular hypothalamus as seen 15 min after the CSF injection (Agnati et al., 1992; Bjelke and Fuxe, 1993). The likely mechanism is that beta-endorphin is internalized into discrete subependymal and periventricular nerve terminal plexa and then undergoes retrograde transport to the nerve cell bodies developing beta-endorphin IR. These results indicate that beta-endorphin CSF VT may exist which – via opioid receptors located on periventricular nerve terminal plexa – may become internalized and retrogradely transported to potentially modulate the gene expression and firing of such neurons (Agnati et al., 1992). Striatally microinjected beta-endorphin can also reach the CSF as an intact peptide as shown with mass-spectrometry (Hoistad et al., 2005). So, beta-endorphin may not only employ long distance diffusion in the ECF but also CSF mediated VT as a complementary communication pathway, to also reach and activate distant opioid receptors. These results are in line with the work of Duggan's group on beta-endorphin based on antibody microprobes (MacMillan et al., 1998). They observed that beta-endorphin IR could be detected in CSF and remote brain areas lacking beta-endorphin IR terminals, like the cerebral cortex, 60–90 min after the initial stimulation of the arcuate nucleus where the beta-endorphin cell bodies are located.

These results taken together give strong indications that beta-endorphin could migrate for long distances in the ECF and CSF after its release from beta-endorphin IR nerve terminal networks.

These results are also of relevance for understanding cotransmission in monoamine neurons often containing neuropeptides (see book by Hökfelt et al., 1986). The release of neuropeptides may allow the monoamine neurons to send VT signals to cellular networks further away from the monoamine terminals. Peptides and proteins may have a high stability and/or act via active peptide fragments which make long distance VT possible involving also CSF VT (Fuxe et al., 2010a and see above). The temporal code of VT related to dynamic changes in release of transmitters is likely to exist especially at short distances, while with long distances of diffusion/convection observed with peptides/proteins the dynamic changes in VT modulating the wired networks may be less pronounced. However, it seems likely that peptide release may be exceptionally enhanced with burst firing based on the work of Lundberg (1991) indicating that long-distance peptides/protein VT can be markedly increased under specific physiological conditions.

In the case of monoamine/peptide co-storing neurons it thus seems likely that the co-released monoamines and peptides from the same nerve terminal networks only interact via receptor-receptor interactions in the range of short diffusion distances. At long distances the migrating peptides/proteins probably along preferential VT channels (paravascular ECF channels or ECF channels along myelinated fiber bundles) instead activate receptors which interact with receptors stimulated by transmitters belonging to other types of neurons.

UNDERSTANDING THE ROLE OF EXTRASYNAPTIC AND LONG DISTANCE VT IN THE FUNCTIONAL MODULES (NEURONAL NETWORKS) OF THE CNS GIVING RISE TO THE NEURONAL CIRCUITS

The neuronal–astroglial networks form functional modules which give rise to several outputs/efferents that is several types of axon bundles forming fiber tracts that influence in various ways other functional modules linked to it. The resulting activity changes in these functional modules will, by forming dynamic brain circuits, have an impact on brain function e.g., behavioral changes. A major role of the VT signals is to modulate the WT, especially the synaptic transmission, in the neuronal networks forming the functional modules. In this way, via changes in VT, it becomes possible for the same neuronal network to change the balance of activity in its different projection neurons to other functional modules (neuronal networks) and thus in their brain circuits and in brain function. The mechanism involved is likely the ability of the diffusing VT signals in ECF to upregulate and/or downregulate synaptic transmission in different parts of the neuronal network via activation of e.g., monoamine, acetylcholine, and/or peptide receptors mainly located in the local circuits of the neuronal–astroglial network. Both neuronal extrasynaptic and long distance VT signaling can be involved and the architecture of the diverse high affinity receptor distributions on the neurons and glia will determine the outcome on the balance of activity in the different types of projection neurons from the functional module. These neuronal VT

signals can be released from terminal networks within the functional module with nerve cell bodies located outside the functional module or from interneurons within the module. Also the projection neurons of the module can mainly via recurrent collaterals give rise to VT signals. There also exists soma-dendritic extrasynaptic exocytosis of VT signals within the neurons of the module contributing *inter alia* to the activation and regulation of the high affinity soma-dendritic autoreceptors at this level (see De-Miguel and Trueta, 2005). Finally, VT signals arise also from the glial cells of the module like adenosine (Ferre and Fuxe, 2000) and kynurenic acid (Schwarcz and Pellicciari, 2002) from the astroglia. The major molecular mechanism appears to be the modulation of synaptic receptors through activation of extrasynaptic receptors by VT signals which modulate the synaptic receptors via allosteric receptor–receptor interactions in receptor heteromers built up of synaptic and extrasynaptic receptors (Agnati et al., 2010a; Fuxe et al., 2010a). The formation of receptor heteromers by synaptic ion-channel receptors like NMDA and GABA receptors and GPCRs have been demonstrated by Fang Liu and colleagues (see Liu et al., 2000; Lee et al., 2002; Liu et al., 2006). In addition, also VT signals can interact and integrate their signaling via GPCR–GPCR interactions in heteromers e.g., A2A-D2 heteromers at the extrasynaptic level (Fuxe et al., 1998, 2010b).

EXTRASYNAPTIC AND LONG DISTANCE VOLUME TRANSMISSION IN THE NEURONAL–ASTROGLIAL NETWORKS OF THE MATRIX OF THE DORSAL STRIATUM

Projection neurons

The analysis of this striatal network gives a beautiful example of the interplay of synaptic transmission and VT in the regulation of the neuronal–astroglial networks of the CNS. Around 95% of the nerve cells represent projection neurons, the so-called GABAergic medium spiny neurons (MSN). There exist mainly two subtypes: The enkephalin containing striato-pallidal GABA neurons (indirect pathway; external globus pallidus) and the dynorphin and substance P containing striato-entopeduncular (internal globus pallidus) and striato-nigral GABA neurons (direct pathway). The MSN GABA neurons give rise to axon collaterals which may have a significant feedback effect with a reduction of the overall activity in the striatal matrix through GABA synapses (Tepper et al., 2008).

Opioid peptides. The axon collaterals of the striato-pallidal GABA neurons forming junctional and non-junctional varicosities likely release enkephalins into ECF extrasynaptically or via synaptic spillover (Agnati et al., 1986; Fuxe et al., 1988c), to activate mu and delta opioid receptors located on terminals (mainly delta opioid receptors) and dendrites (mainly mu opioid receptors) of the striatal local circuits including the DA nerve terminals (Eghbali et al., 1987; Arvidsson et al., 1995). Enkephalin immunoreactive terminals in double immunolabeling experiments are closely associated with these two types of opioid receptors and therefore the enkephalin transmission likely mainly involves extrasynaptic VT (Arvidsson et al., 1995). It is of substantial interest that D1-mu-opioid receptor heteromers have been demonstrated in cellular models (Juhasz et al., 2008) and morphine induced locomotion requires D1 receptor activation (Hnasko et al., 2005). In view of the fact that the vast majority of the D1 receptors exist in the striato-entopeduncular/nigral GABA neurons (direct pathway) lacking D2 receptors one important function of the released enkephalins from the axon collaterals, and possibly dendrites of the striato-pallidal GABA neurons, may be to diffuse to and enhance signaling in the D1-mu-opioid receptor heteromer located in the dendrites of the direct pathway increasing its activity. D1 and mu opioid receptors are also co-located in the striatum (Juhasz et al., 2008). Thus, the extrasynaptic enkephalin signaling of the striato-pallidal GABA neurons causing motor inhibition may *inter alia* facilitate cross-modulation of the adjacent neurons of the direct pathway which increases motor initiation. In this way the unbalance of activity in the two main efferent pathways will be reduced and assisting in counteracting excessive motor inhibition. There may exist also D4-mu opioid receptor heteromers in the striatum especially in the striatal islands (striosomes) where the D4 and mu opioid receptors are enriched and co-located (Gago et al., 2007; Fuxe et al., 2008c; Rivera et al., 2008) with D4 activation markedly antagonizing morphine induced transcription factor expression in the striatum (Gago et al., 2011).

In contrast, the dynorphin immunoreactive terminals of the direct pathway are in proximity with the dendritic kappa opioid receptors (Elde et al., 1995) likely representing a kappa opioid receptor-mediated extrasynaptic dynorphin transmission. It can be speculated that this partially represents a reciprocal regulation by the direct pathway of the indirect pathway, the striato-pallidal GABA neurons which are enriched in D2 receptors and may possess kappa opioid receptors. It seems likely that these dynorphin immunoreactive terminals also may contain substance P immunoreactivity (Bolam et al., 1983) and also operate via extrasynaptic substance P transmission. There does also exist a DA D1-D2 receptor heteromer signaling pathway in dynorphin/enkephalin MSN but they have a low incidence in the caudate putamen (Perreault et al., 2010; Hasbi et al., 2011).

Neurotensin peptides. The striatal NT tissue IR and mRNA levels are increased by antipsychotic drugs through their D2 receptor blocking actions (see Frey et al., 1986; Augood et al., 1991). These results indicated that the acute administration of D2 DA receptor antagonists increased NT levels in the striatum and nuc. accumbens, and that antipsychotic drugs (clozapine, fluperlapine) showing a relative lack of extrapyramidal side effects may be characterized by a failure to maintain increased NT levels in the basal ganglia upon long-term treatment in contrast to chronic haloperidol, chlorpromazine, and sulpiride (Frey et al., 1986). Instead, the D1 receptor antagonist 23390 acutely reduced the striatal NT tissue levels (Frey et al., 1986). The signs of increased NT storage and synthesis in the striatum – at least after long-term treatment with haloperidol – have been found to be associated with reduced NT IR efflux into the ECF in the ventral striatum (Gruber et al., 2002). The NT mRNA signals as studied with *in situ* hybridization are normally sparsely distributed (Schiffmann and Vanderhaeghen, 1993) and markedly increased by D2 antagonist treatment in the MSN representing the projection neurons (Augood et al., 1991). Thus, NT peptides may be synthesized and released from the D2 enriched striato-pallidal and D1 enriched striato-nigral GABA neurons to activate NTS1 receptors through extrasynaptic transmission. Antagonistic NTS1-D2 receptor–receptor interaction in

putative NTS1-D2 heteromers have been repeatedly demonstrated in the striatum (Agnati et al., 1983a; Von Euler and Fuxe, 1987; von Euler, 1991; Li et al., 1994b; Diaz-Cabiale et al., 2002) located on the striatal DA terminals (NTS1-D2 autoreceptor interactions, Tanganelli et al. (1989)) and at the postjunctional level (Fuxe et al., 1992, 1995; Tanganelli et al., 1994; Li et al., 1995a) as indicated from microdialysis studies. A major achievement by Ferraro et al. (1995, 2011, 2012) has also been the discovery that NT peptides – via facilitatory NTS1-NMDA receptor-receptor interactions – can enhance the synaptic glutamate transmission. In this way, extrasynaptic and synaptic signals can become integrated as previously shown by Liu and colleagues through demonstration of D5-GABAA, D1-NMDA, and D2-NMDA heteromer formation and their receptor-receptor interactions (Liu et al., 2000; Lee et al., 2002, 2005). Specifically, the NT peptides when released can enhance the glutamate synaptic signaling onto the striato-pallidal GABA neurons through the enhancing NTS1-NMDA receptor–receptor interaction (Tanganelli et al., 2012). This increased activation of the striato-pallidal GBA neurons is further strengthened by the antagonistic D2-NTS1 receptor–receptor interactions at the postjunctional level of the DA transmission reducing D2 signaling and its inhibitory action on the striato-pallidal GABA neurons (Tanganelli et al., 2012). The antagonistic NTS1-D2 autoreceptor interaction at the DA terminal level in contrast will increase DA release which via diffusion can increase D1 receptor signaling in the direct pathway since antagonistic D1-NTS1 receptor–receptor interactions do not exist. The net result of the NT extrasynaptic signaling will therefore be an increase in the activity of the striato-pallidal GABA neurons. This leads to increased motor inhibition balanced by increased activity of the direct pathway mediating motor initiation via increasing D1 receptor activity in the striato-entopeduncular-nigral GABA pathway.

It seems that cholecystokinin (CCK) peptides from glutamate synapses and NT peptides from MSN have similar functional and neurochemical actions by reducing and signaling of the D2 protomers in putative CCK2-D2 and NTS1-D2 heteromers, respectively but with the difference that NTS1 may also form heteromers with NMDA receptors. In line with these observations, threshold doses of CCK and NT peptides have been found to produce synergistic effects on D2 receptor affinity and DA release as seen in microdialysis studies (Tanganelli et al., 1993).

Afferents

Cortico-striatal and thalamo-striatal glutamate synapses. These glutamate synapses have a major impact on the firing of the striatal projection neurons and the striatal interneurons (Bennett and Bolam, 1994; Surmeier et al., 2007; Tepper et al., 2007; Gerfen and Surmeier, 2011). It is of interest that CCK immunoreactivity exists in the cortico-striatal glutamate neurons (Morino et al., 1994). CCK peptides may therefore be released from these glutamate synapses via spillover or extrasynaptic release to modulate the activity of the striatal local circuits via extrasynaptic transmission. In view of the demonstration of antagonistic CCK2-D2 receptor–receptor interactions in putative CCK2-D2 heteromers (Fuxe et al., 1981, 1983; Agnati et al., 1983b; Li et al., 1995b; Dasgupta et al., 1996) in the striato-pallidal GABA neurons (postjunctional CCK2 receptors) and on the striatal DA afferents (Tanganelli et al., 1990, 2001) one role of the CCK peptides released upon firing of the cortico-striatal neurons may be to enhance glutamate signaling on the D1 enriched direct pathway versus the D2 enriched striato-pallidal GABA pathways eliciting motor inhibition. The existence of striatal nerve cells coexpressing CCK2 and D2 receptor mRNAs have in fact been demonstrated (Hansson et al., 1998). Thus, CCK2 activation by the diffusing CCK peptides in the local circuit will increase DA release by inhibiting the signaling over the D2 autoreceptor and the postjunctional D2 but not D1 signaling will be reduced. This will result in increased D1 signaling in the D1 enriched direct pathway favoring motor initiation.

It is of substantial interest that DA D1 receptors are involved in the modulation of DA D2 receptors induced by CCK receptor subtypes in rat neostriatal membranes (Li et al., 1994a), in view of the recent demonstration of DA D1–D2 heteromers by George and O'Dowd (2007) operating via a calcium signaling pathway. They have now been shown to exist in DA D1 expressing neurons especially in nuc accumbens (20–30%) and in the globus pallidus (59%; Hasbi et al., 2011). Our findings in 1994 (Li et al., 1994a), which demanded the coexistence of D1 and D2 receptors in the same striatal neurons, indicated that CCK-8 can reduce or increase the affinity of DA D2 receptors in rat neostriatal membrane preparations depending on the activity at the D1 receptors which when activated caused the CCK-8 to increase the affinity of the D2 receptors instead of reducing it. Thus, D1 receptors exert a switching role in the modulation of D2 receptors by CCK receptors. Our hypothesis is that the molecular basis for this phenomenon is the existence of CCK2-D1-D2 trimeric heteromers or trimeric receptor mosaics in which the allosteric receptor-receptor interaction between CCK2-D2 receptors becomes markedly altered through the activation of the D1 receptor. In view of the fact that CCK2 receptor activation does not alter the binding characteristics of the D1 receptors it may be that the receptor mosaic has a triangular geometry.

It should be noticed that antipsychotic drugs, after subchronic treatment, increase the CCK octapeptide tissue levels in striatum and the meso-limbic system and remain increased even 4 weeks after cessation of treatment (Frey, 1983). Thus, the blockade of the D2 receptors results in a sustained increase in the expression of CCK peptides which if leading to increased release may reduce the affinity of the D2 receptors which may assist in the maintenance of antipsychotic actions (see Fuxe et al., 2009).

DA, 5-HT and histamine afferents. The highly dense DA nerve terminal plexa in the dorsal striatal cellular network originate from the substantia nigra in the ventral midbrain (see Anden et al., 1964; Fuxe et al., 1970b,c, 2007a), the moderately dense 5-HT nerve terminal plexa from the midbrain raphe (Anden et al., 1965, 1966; see Fuxe et al., 1970b,c, 2007a) and the histamine nerve terminal plexa from the tubero-mammillary nucleus in the hypothalamus (Haas and Panula, 2003). These three terminal networks originating from the brainstem mainly operate via extrasynaptic transmission to modulate the dorsal striatal cellular networks using various subtypes of dopamine (D1–D5), 5-HT (Di Matteo et al., 2008) and histamine (mainly H2–H3) receptors with extrasynaptic receptors in dominance, see special issue on the basal ganglia (Fuxe et al., 2008a). These receptors are located both on projection

neurons and interneurons as well as on the afferent nerve terminal networks. The DA and 5-HT signals can in part become integrated via the existence of D2-5-HT2A heteromers (Borroto-Escuela et al., 2010; Lukasiewicz et al., 2010; Albizu et al., 2011) mainly located in the striato-pallidal GABA neurons. We found that the 5-HT2AR-mediated phospholipase C (PLC) activation was synergistically enhanced by the concomitant activation of the D2LR and costimulation of D2LR and 5-HT2AR within the heteromer led to inhibition of the D2LR functioning, thus suggesting the existence of a 5-HT2AR-mediated D2LR trans-inhibition phenomenon (Borroto-Escuela et al., 2010). Furthermore, 5-HT2AR expression is required to obtain the complete blockade of the D2R antagonist haloperidol on the MK-801-induced increase in locomotion (Albizu et al., 2011).

The DA and histamine signals can instead become integrated by the existence of DA D1-histamine H3 receptor heteromers giving a selective link to MAPK signaling in the striato-entopeduncular-nigral GABA neurons forming the direct striatal pathway (Moreno et al., 2010).

Through these different types of brainstem afferents, the sensory-motor regulation of the dorsal striatum can obtain information from a motor system favoring movements (the nigral DA system), from an emotional system favoring an elevation of mood (midbrain raphe 5-HT system), and from a sleep-wakefulness system favoring arousal (the tubero-mammillary histamine system).

Interneurons

Cholinergic interneurons. The large aspiny cholinergic interneurons represent 1–3% if the striatal neurons and give rise to highly dense nerve terminal plexus all over the cellular networks of the striatum and possess a slow firing tonic in nature (for recent reviews see Pisani et al., 2007; Oldenburg and Ding, 2011). This plexus mainly operates via extrasynaptic transmission (Descarries and Mechawar, 2000) and modulates the transmission of the medium spiny GABA projection neurons, the different types of striatal interneurons and the striatal afferents mainly via five subtypes of muscarinic receptors (M1–M5) but also via nicotinic receptors (**Figure 1**). The striatal M1 receptors are mainly present in the two major projection neurons, the D2 enriched striato-pallidal GABA neurons and the D1 enriched striato-entopeduncular-nigral GABA neurons (direct pathway). It is mainly coupled to Gq/11 and signal by increasing intracellular Ca levels and PLC and protein kinase C (PKC) activities. In contrast, M4 is predominantly expressed in the direct pathway and coupled to Gi/o reducing calcium channel activity and activity in the AC-PKA-CREB intracellular pathway. M1 excites the MSN and enhance their spiking by modulating potassium and Cav channels and M4 differentially shapes these actions in the striato-nigral GABA pathways by inhibiting the Cav channels (see Oldenburg and Ding, 2011). In addition, M2 and M3 receptor activation on glutamate synapses modulates the glutamate release in an inhibitory way also reducing the M1 induced excitatory effects on MSN. M4 receptors together with M2 receptor, which is linked to Gi/o as well, are also located on the cholinergic interneurons where they function as inhibitory autoreceptors.

The role of endocannabinoids. It is of substantial interest that another type of extrasynaptic transmission mediated by endocannabinoids is involved in mediating the actions of M1 mediated transmission of the cholinergic interneurons. Thus, long-term synaptic depression in MSN is modulated by cholinergic interneurons (Wang et al., 2006). M1 mediated actions at dendritic spines of MSN leads to reduced activity of Cav1.3 channels which brings down the formation and subsequent migration of endocannabinoids potentially located in microvesicles (Agnati et al., 2010a) with reduced activation *inter alia* of the extrasynaptic CB1 receptors on the glutamate terminals. In this way the synaptic glutamate excitatory transmission is increased. However, DA extrasynaptic transmission via D2 mediated inhibitory control of the cholinergic interneurons will restore the activation of the retrograde endocannabinoid signaling and LTD. The mGluR1/5 mediated extrasynaptic transmission of glutamate also plays an important role for LTD development since this receptor – through Gq/11 coupling leading to increased IP3 levels – will increase intracellular Ca levels followed by activation of PLC and DAG lipase, and increased formation of endocannabinoids and reduction of excitatory glutamate transmission.

The complexity of the M1 mediated cholinergic actions on formation of endocannabinoids, however, should be noticed since at inhibitory GABA synapses located on the shafts of MSN the M1 receptor activation leads to an increase in formation of endocannabinoid 2-arachidonoylglycerol (2-AG) with increased CB1 receptor activity at the GABA synapses and suppression of synaptic GABA transmission (Narushima et al., 2007). The reason is likely that in these microdomains the M1 excitatory coupling to PLC and DAG lipase dominates and here also M1 likely acts synergistically with mGluR1/5 to enhance 2-AG formation and thus the retrograde inhibitory signaling on the GABA synapses (see Uchigashima et al., 2007). It should be underlined that CB1 receptors also exist in the striato-pallidal GABA neurons and in the striato-entopeduncular-nigral GABA neurons (Martin et al., 2008) and endocannabinoids can therefore exert direct actions on these neurons reducing *inter alia* D2 signaling in the striato-pallidal GABA neurons through participation in CB1-D2 heteromers and CB1-D2-A2A trimers (Fuxe et al., 2008b; Marcellino et al., 2008). This may be part of an inhibitory feedback since D2 receptor activation leads to an increased formation of anandamide (see Piomelli, 2003).

Recently muscarinic acetylcholine receptor homo- and heterodimerization has been observed in live cells (Goin and Nathanson, 2006). The existence of high affinity M1–M2, M2–M3, and M1–M3 mAChR heterodimers could be demonstrated and an increased agonist induced downregulation of M3 developed when present as a protomer in M2–M3 heteromers. Based on these findings it will be of interest if in fact M2–M3 heteromers exist in the striatal glutamate terminals where they are collocated. We are presently studying to which extent striatal DA and cholinergic transmission can become integrated through the formation of different types of heteromers of DA and muscarinic receptors, especially D1-M4 (**Figure 1**), D2-M1, and D2-M4 heteromers. Such discoveries would open up new possibilities for treatment of Parkinson disease and improve the use of muscarinic receptor antagonists in the treatment of this disease based on an increased activity of

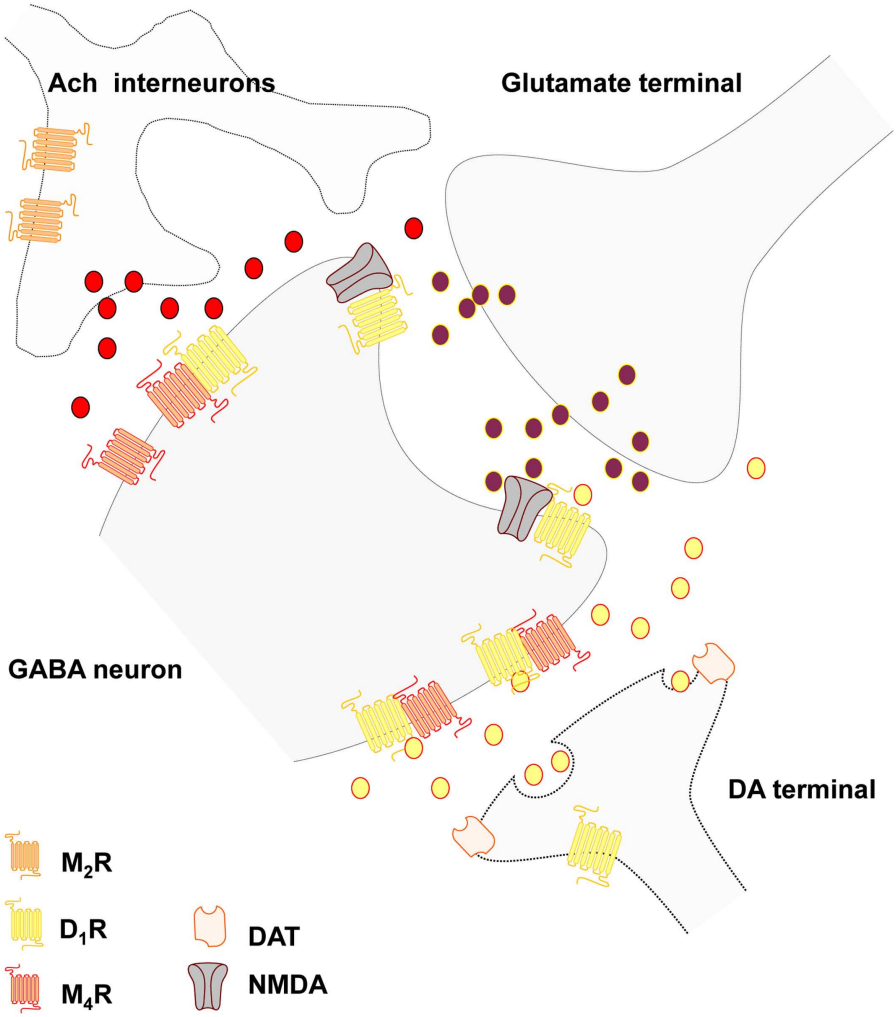

FIGURE 1 | Schematic representation of the postulated D1-M4 receptor heteromers in the local striatal circuits of the striato-entopenduncular-nigral GABA neurons. The D_1-M_4 receptor heteromers probably mainly exist in an extrasynaptic location on the dendritic spines and on the dendritic shafts of these neurons where inputs from striatal dopamine and cholinergic transmission can become integrated through the formation of this heteromers. The D_1-NMDA receptor mosaics in the glutamate synapses are also indicated. Thus, dopamine may diffuse into glutamate synapse to modulate NMDA signaling unless D_1 exclusively binds to extrajunctional NMDA receptors.

the cholinergic neurons related to a reduced activation of the D2 receptors located on these neurons (Pisani et al., 2007). It has been proposed that the adaptive changes taking place in PD involves an increase in the formation of RGS4, a regulator of G protein signaling which reduces the coupling of the M4 autoreceptor to the Cav2 calcium channels and to the potassium cannels leading to overactivity of these interneurons (Ding et al., 2006; Pisani et al., 2007). A new hypothesis may be that the disruption of the M4 autoreceptor function may be caused by dysfunction of a D2-M4 heteromer located on the striatal interneurons due to the abnormal reduction of D2 signaling in the D2 protomer in Parkinson disease.

The reason that anticholinergic drugs like scopolamine can block catalepsy induced by both D2 and D1 receptor antagonists was in 1988 explained within the frame of the hypothesis of different striatal efferent pathways one being D2 enriched and the other D1 enriched (Ogren and Fuxe, 1988). The mechanism may be the preferential enrichment of inhibitory M4 receptors in the striato-entopeduncular-nigral GABA neurons vs. the striato-pallidal GABA neurons both of which are enriched in excitatory M1 receptors (see above). The results from the overall pharmacological analysis of the catalepsy obtained, including the use of benzodiazepine antagonists (Ogren and Fuxe, 1988), could be explained on the basis of a circuitry involving D2 regulated striato-pallidal GABA pathways and a D1 regulated circuitry involving D1 regulated nigro-thalamic GABA pathways. DA release and diffusion in the zona reticulata of the substantia nigra may take place from dendrites of nigral DA nerve cells via extrasynaptic transmission reaching *inter alia* D1 receptors on the striato-nigral GABA terminals enhancing the release of GABA with increased inhibition of the nigro-thalamic GABA pathway setting free the excitatory thalamo-cortical system from the motor thalamus (Ogren and Fuxe, 1988).

GABA interneurons. The calcium binding protein parvalbumin positive aspiny GABAergic interneurons exist mainly in two classes: the fast spiking interneurons and the low threshold spike (LTS) interneurons (Kawaguchi, 1995; Tepper et al., 2008). They are driven by cortico-striatal glutamate synapses and project to the MSN and mediate powerful feed-forward inhibition of the MSN via GABAergic synapses. These are striatal interneurons where synaptic high speed GABA transmission dominates and can profoundly bring down spiking in the MSN and controlling its timing.

Other striatal GABAergic interneurons instead coexpress also somatostatin, neuropeptide Y (NPY), and neuronal nitric oxide synthase (NOS) and likely operate via both synaptic (GABA) and VT (somatostatin, NPY, and NOS; see **Figure 2**).

They are evenly dispersed all over the striatum with widespread collaterals and are neurophysiologically characterized as LTS neurons with persistent depolarization (Kawaguchi, 1995). They receive cortical glutamate inputs and likely mediate feed-forward modulation of the striatal networks. Somatostatin and NPY peptides may modulate the activity of the neuronal and glial cell populations via extrasynaptic and long distance VT through their striatal receptor subtypes (**Figure 2**). Rocheville et al. (2000) have also demonstrated that somatostatin receptor 5 (SSTR5) can form heteromers with D2 receptors which are formed after agonist activation (Rocheville et al., 2000). Thus, again receptor-receptor interaction in heteromers can play a role in the integration of signals in the neuronal and glial networks of the brain (Agnati et al., 2010b; Fuxe et al., 2010a,b). Heteromers between NPY Y1 and alpha2 receptors have also been indicated (Fuxe et al., 2008c).

Also nitric oxide (NO) is formed in these NOS positive cells and diffuse into adjacent nerve, glial, and endothelial cells via VT (Fuxe et al., 2010a; **Figure 2**). Most of them likely express soluble guanylate cyclase which indicates that they are likely targets for NO produced by the NOS positive GABA interneurons (see Kawaguchi, 1995). This communication upon activation by glutamate synapses of these neurons modulates transmitter release and increases blood flow according to the pattern of cortico-striatal glutamate projection activation of these neurons. This is likely linked to the activation of discrete populations of striatal projection neurons. In this way the assemblies of activated glutamate projection neurons can perform their tasks in cellular networks that adapt to this task to achieve an optimal sensory-motor function.

Adenosine as a VT signal in the striatal cellular networks. Adenosine is an endogenous nucleoside mostly formed as a degradation product of adenosine triphosphate (ATP) and to a lesser degree from S-adenosyl-L-homocysteine (SAH) metabolism and present in all cells of the striatal cellular networks and in the ECS (Ferre and Fuxe, 2000; Ciruela et al., 2011). Upon adenosine generation in neuronal and glial cells, it can be intracellularly phosphorylated to form AMP, react with L-homocysteine to form SAH or be eliminated out of the cells by means of ubiquitous

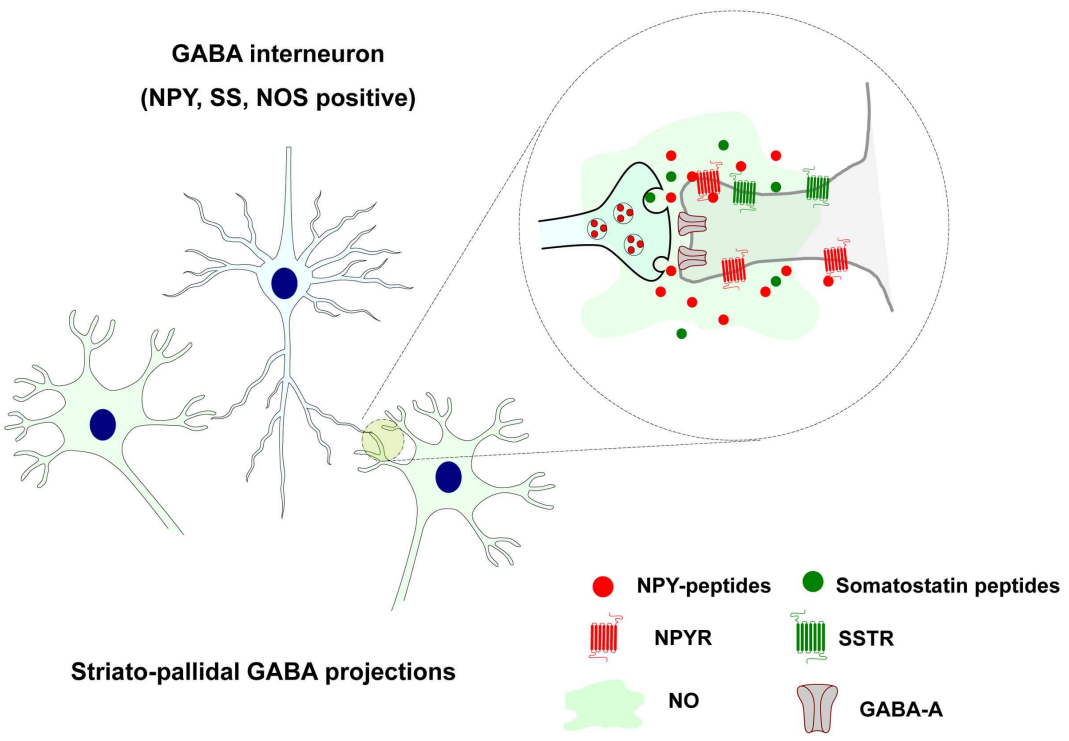

FIGURE 2 | Extrasynaptic and long distance volume transmission in the positive somatostatin, neuropeptide Y, and neuronal nitric oxide synthase striatal GABAergic interneurons. Somatostatin and NPY peptides may via extrasynaptic and long distance VT through their striatal receptor subtypes modulate the activity of the neuronal and glial cell populations. Also nitric oxide (NO) is formed in these NOS positive cells and diffuse into adjacent nerve, glial, and endothelial cells via VT.

nitrobenzylthioinosine-sensitive equilibrative nucleoside transporters (ENTs; Cunha, 2005). In the cellular networks, extracellular adenosine can also derive from ATP released from nerve and glial cells including release from glutamate terminals together with glutamate. Intra- and extra-cellular adenosine can be deaminated to form inosine by the action of intra and ecto-adenosine deaminase, respectively. In the nervous system the extracellular concentration of adenosine raises as a function of the neuronal activity, it acts as an energy-dependent neuromodulator through combined presynaptic and postsynaptic actions through VT (**Figure 3**; Ferre and Fuxe, 2000; Sebastiao and Ribeiro, 2000; Fredholm et al., 2005; Ciruela et al., 2011). Therefore, extracellular adenosine regulates several functions in the brain, including neuronal viability, neuronal membrane potential, propagation of action potentials, astrocytic functions, microglia reactivity, primary metabolism in both neurons and astrocytes, and blood flow (Ferre and Fuxe, 2000; Fredholm et al., 2005; Ciruela et al., 2011).

The most abundant and homogeneously distributed adenosine receptor in the brain is the extrasynaptic inhibitory A1R, which is functionally coupled to members of the pertussis toxin-sensitive family of G proteins (Gi/o) and whose activation regulates the activity of membrane and intracellular proteins such as adenylate cyclase, Ca2+ channels, K+ channels, and phospholipase C. In contrast, the extrasynaptic A2AR is expressed at high levels in only a few regions of the brain, namely the dorsal striatum, the olfactory tubercle, and the nucleus accumbens. The A2AR is mostly coupled to Gs in the peripheral systems but mediates its effects predominantly through activation of Golf in the striatum (see Ciruela et al., 2011).

It is of substantial interest that adenosine receptor can form heteromers with extrasynaptic DA receptors and glutamate receptors to modulate striatal cellular networks (Fuxe et al., 1998; Ciruela et al., 2011). A1R has been found to heteromerize with the dopamine D1 receptor (D1R), this phenomenon being essential

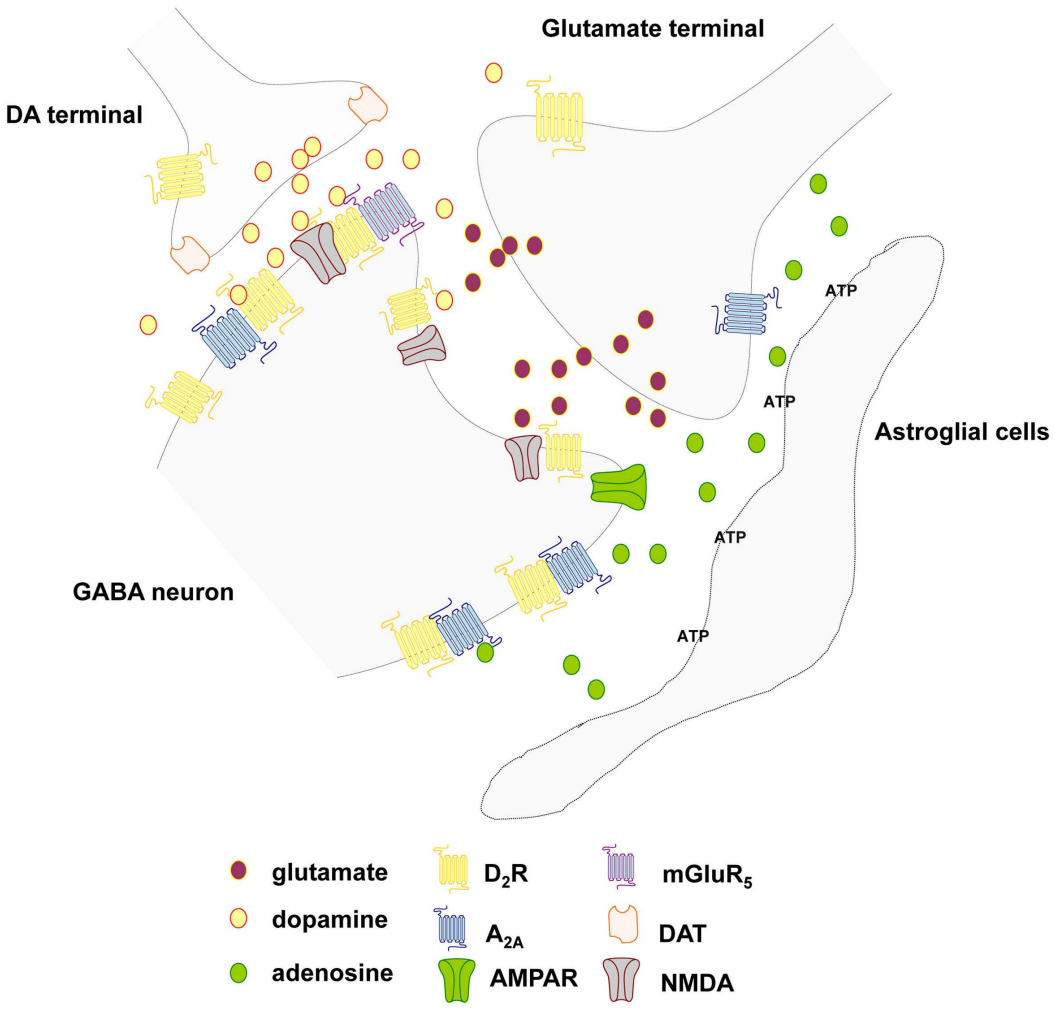

FIGURE 3 | Schematic representation of the extrasynaptic transmission in the local circuits around the striatal glutamate synapse of the striato-pallidal GABA neurons. Focus on the glutamate, adenosine, and dopamine signal and the postulated A_{2A}-D_2, A_{2A}-D_2-mGluR5, and D_2-NMDA receptor heteromers. Different cell types (microglia, astrocytes) can release both adenosine triphosphate (ATP) and adenosine. In the nervous system the extracellular concentration of adenosine raises as a function of the neuronal activity and acts as an energy-dependent neuromodulator through combined presynaptic and postsynaptic actions through VT.

for differential desensitization mechanisms and for receptor trafficking (Torvinen et al., 2002). It also contributes to reduce EEG and behavioral arousal (Fuxe et al., 2007b). The heterodimer composed by the A1R and the metabotropic glutamate type 1α (mGlu1α) receptor seems to play a key role in preventing glutamate excitotoxicity (Ciruela et al., 2001).

The A2AR possesses the ability to heteromerize with the DA D2 receptor (D2R; **Figure 3**; Hillion et al., 2002; Canals et al., 2003). The latter receptor–receptor interaction underlies the molecular mechanism behind the antagonistic adenosine-dopamine interactions that regulate the function of the GABAergic enkephalinergic striato-pallidal GABA neurons and reduces behavioral arousal (Fuxe et al., 2007b). Finally, the A2AR also heteromerizes with the metabotropic glutamate type 5 (mGlu5) receptor, and in this case, a synergistic functional interaction has been demonstrated at both biochemical and behavioral levels (Ferre et al., 2002). They also synergize to bring down D2 receptor function in A2A-D2-mGluR5 receptor mosaics located in the perisynaptic regions of the glutamate synapses representing integrative heteromers for extracellular adenosine, dopamine and glutamate signals (Cabello et al., 2009; Ciruela et al., 2011) as early indicated in studies on receptor-receptor interactions (see Popoli et al., 2001; Fuxe et al., 2003). These extrasynaptic trimeric heteromers may represent centers for integration of VT signals. In the integration of the synaptic and extrasynaptic signals of the striatal networks the heteromeric complexes between GPCRs and ion-channel receptors in the synaptic regions play a special role *inter alia* D1-NMDA and D2-NMDA and D5-GABAA heteromers (Liu et al., 2000, 2006; Lee et al., 2002).

CONCLUSIONS

Evidence is accumulating that extrasynaptic and long distance VT plays a major role in communication within the neuronal–glial networks of the brain as exemplified here within the striatal cellular networks. The integration of synaptic with extrasynaptic and long distance VT signals may take place to a substantial degree via the formation of receptor heteromers between ion-channel receptors and GPCRs in the plasma membrane of synaptic regions. The integration among VT signals may to a substantial degree occur via GPCR heteromers including higher order heteromers in dendrites, axon terminals, and soma including extrasynaptic regions. This opens up a new way of understanding communication in the CNS.

ACKNOWLEDGMENTS

This work was supported by grants from the Swedish Research Council (04X-715), Hjärnfonden, Torsten, and Ragnar Söderberg, Telethon TV3's La Marató Foundation 2009 and M.M. Wallenberg Foundation to Kjell Fuxe, Karolinska Institutets Forskningsstiftelser 2010 and 2011 to Dasiel O. Borroto-Escuela, and also by grants SAF2008-01462 and Consolider-Ingenio CSD2008-00005 from Ministerio de Ciencia e Innovación and ICREA Academia-2010 from the Catalan Institution for Research and Advanced Studies to Francisco Ciruela, and Telethon TV3's La Marató Foundation 2009 and grant SAF2008-04943-C02-02 to Pere Garriga. Alexander O. Tarakanov has not received any support for this work.

REFERENCES

Agnati, L. F., Bjelke, B., and Fuxe, K. (1992). Volume transmission in the brain. *Am. Sci.* 80, 362–373.

Agnati, L. F., Fuxe, K., Benfenati, F., and Battistini, N. (1983a). Neurotensin in vitro markedly reduces the affinity in subcortical limbic 3H-N-propylnorapomorphine binding sites. *Acta Physiol. Scand.* 119, 459–461.

Agnati, L. F., Fuxe, K., Benfenati, F., Celani, M. F., Battistini, N., Mutt, V., Cavicchioli, L., Galli, G., and Hokfelt, T. (1983b). Differential modulation by CCK-8 and CCK-4 of [3H]spiperone binding sites linked to dopamine and 5-hydroxytryptamine receptors in the brain of the rat. *Neurosci. Lett.* 35, 179–183.

Agnati, L. F., Fuxe, K., Nicholson, C., and Sykova, E. (2000). *Volume Transmission Revisited, in Progress in Brain Research*, Vol. 125 (Amsterdam: Elsevier), 1–447.

Agnati, L. F., Fuxe, K., Zoli, M., Ozini, I., Toffano, G., and Ferraguti, F. (1986). A correlation analysis of the regional distribution of central enkephalin and beta-endorphin immunoreactive terminals and of opiate receptors in adult and old male rats. Evidence for the existence of two main types of communication in the central nervous system: the volume transmission and the wiring transmission. *Acta Physiol. Scand.* 128, 201–207.

Agnati, L. F., Guidolin, D., Guescini, M., Genedani, S., and Fuxe, K. (2010a). Understanding wiring and volume transmission. *Brain Res. Rev.* 64, 137–159.

Agnati, L. F., Guidolin, D., Leo, G., Carone, C., Genedani, S., and Fuxe, K. (2010b). Receptor-receptor interactions: a novel concept in brain integration. *Prog. Neurobiol.* 90, 157–175.

Agnati, L. F., Leo, G., Zanardi, A., Genedani, S., Rivera, A., Fuxe, K., and Guidolin, D. (2006). Volume transmission and wiring transmission from cellular to molecular networks: history and perspectives. *Acta Physiol. (Oxf.)* 187, 329–344.

Albizu, L., Holloway, T., Gonzalez-Maeso, J., and Sealfon, S. C. (2011). Functional crosstalk and heteromerization of serotonin 5-HT2A and dopamine D2 receptors. *Neuropharmacology* 61, 770–777.

Amilhon, B., Lepicard, E., Renoir, T., Mongeau, R., Popa, D., Poirel, O., Miot, S., Gras, C., Gardier, A. M., Gallego, J., Hamon, M., Lanfumey, L., Gasnier, B., Giros, B., and El Mestikawy, S. (2010). VGLUT3 (vesicular glutamate transporter type 3) contribution to the regulation of serotonergic transmission and anxiety. *J. Neurosci.* 30, 2198–2210.

Anden, N. E., Carlsson, A., Dahlstroem, A., Fuxe, K., Hillarp, N. A., and Larsson, K. (1964). Demonstration and mapping out of nigro-neostriatal dopamine neurons. *Life Sci.* 3, 523–530.

Anden, N. E., Dahlstrom, A., Fuxe, K., and Larsson, K. (1965). Mapping out of catecholamine and 5-hydroxytryptamine neurons innervating the telencephalon and diencephalon. *Life Sci.* 4, 1275–1279.

Anden, N. E., Fuxe, K., and Larsson, K. (1966). Effect of large mesencephalic-diencephalic lesions on the noradrenalin, dopamine and 5-hydroxytryptamine neurons of the central nervous system. *Experientia* 22, 842–843.

Andersson, K., Fuxe, K., Eneroth, P., Nyberg, F., and Roos, P. (1981). Rat prolactin and hypothalamic catecholamine nerve terminal systems. Evidence for rapid and discrete increases in dopamine and noradrenaline turnover in the hypophysectomized male rat. *Eur. J. Pharmacol.* 76, 261–265.

Aoki, C. (1992). Beta-adrenergic receptors: astrocytic localization in the adult visual cortex and their relation to catecholamine axon terminals as revealed by electron microscopic immunocytochemistry. *J. Neurosci.* 12, 781–792.

Aoki, C., and Pickel, V. M. (1992). C-terminal tail of beta-adrenergic receptors: immunocytochemical localization within astrocytes and their relation to catecholaminergic neurons in N. tractus solitarii and area postrema. *Brain Res.* 571, 35–49.

Aoki, C., Venkatesan, C., Go, C. G., Forman, R., and Kurose, H. (1998). Cellular and subcellular sites for noradrenergic action in the monkey dorsolateral prefrontal cortex as revealed by the immunocytochemical localization of noradrenergic receptors and axons. *Cereb. Cortex* 8, 269–277.

Arvidsson, U., Riedl, M., Chakrabarti, S., Lee, J. H., Nakano, A. H., Dado, R. J., Loh, H. H., Law, P. Y., Wessendorf, M. W., and Elde, R. (1995). Distribution and targeting

of a mu-opioid receptor (MOR1) in brain and spinal cord. *J. Neurosci.* 15, 3328–3341.

Augood, S. J., Kiyama, H., Faull, R. L., and Emson, P. C. (1991). Differential effects of acute dopaminergic D1 and D2 receptor antagonists on proneurotensin mRNA expression in rat striatum. *Brain Res. Mol. Brain Res.* 9, 341–346.

Bennett, B. D., and Bolam, J. P. (1994). Synaptic input and output of parvalbumin-immunoreactive neurons in the neostriatum of the rat. *Neuroscience* 62, 707–719.

Bennett, M. V., Contreras, J. E., Bukauskas, F. F., and Saez, J. C. (2003). New roles for astrocytes: gap junction hemichannels have something to communicate. *Trends Neurosci.* 26, 610–617.

Bjelke, B., and Fuxe, K. (1993). Intraventricular beta-endorphin accumulates in DARPP-32 immunoreactive tanycytes. *Neuroreport* 5, 265–268.

Bolam, J. P., Somogyi, P., Takagi, H., Fodor, I., and Smith, A. D. (1983). Localization of substance P-like immunoreactivity in neurons and nerve terminals in the neostriatum of the rat: a correlated light and electron microscopic study. *J. Neurocytol.* 12, 325–344.

Borroto-Escuela, D. O., Romero-Fernandez, W., Tarakanov, A. O., Marcellino, D., Ciruela, F., Agnati, L. F., and Fuxe, K. (2010). Dopamine D2 and 5-hydroxytryptamine 5-HT(A) receptors assemble into functionally interacting heteromers. *Biochem. Biophys. Res. Commun.* 401, 605–610.

Borroto-Escuela, D. O., Tarakanov, A. O., Guidolin, D., Ciruela, F., Agnati, L. F., and Fuxe, K. (2011). Moonlighting characteristics of G protein-coupled receptors: focus on receptor heteromers and relevance for neurodegeneration. *IUBMB Life* 63, 463–472.

Cabello, N., Gandia, J., Bertarelli, D. C., Watanabe, M., Lluis, C., Franco, R., Ferre, S., Lujan, R., and Ciruela, F. (2009). Metabotropic glutamate type 5, dopamine D2 and adenosine A2a receptors form higher-order oligomers in living cells. *J. Neurochem.* 109, 1497–1507.

Caille, I., Dumartin, B., and Bloch, B. (1996). Ultrastructural localization of D1 dopamine receptor immunoreactivity in rat striatonigral neurons and its relation with dopaminergic innervation. *Brain Res.* 730, 17–31.

Canals, M., Marcellino, D., Fanelli, F., Ciruela, F., De Benedetti, P., Goldberg, S. R., Neve, K., Fuxe, K., Agnati, L. F., Woods, A. S., Ferre, S., Lluis, C., Bouvier, M., and Franco, R. (2003). Adenosine A2A-dopamine D2 receptor-receptor heteromerization: qualitative and quantitative assessment by fluorescence and bioluminescence energy transfer. *J. Biol. Chem.* 278, 46741–46749.

Carmignoto, G. (2000). Reciprocal communication systems between astrocytes and neurones. *Prog. Neurobiol.* 62, 561–581.

Cercos, M. G., De-Miguel, F. F., and Trueta, C. (2009). Real-time measurements of synaptic autoinhibition produced by serotonin release in cultured leech neurons. *J. Neurophysiol.* 102, 1075–1085.

Chen, K. C., Hoistad, M., Kehr, J., Fuxe, K., and Nicholson, C. (2002a). Quantitative dual-probe microdialysis: mathematical model and analysis. *J. Neurochem.* 81, 94–107.

Chen, K. C., Hoistad, M., Kehr, J., Fuxe, K., and Nicholson, C. (2002b). Theory relating in vitro and in vivo microdialysis with one or two probes. *J. Neurochem.* 81, 108–121.

Ciruela, F., Escriche, M., Burgueno, J., Angulo, E., Casado, V., Soloviev, M. M., Canela, E. I., Mallol, J., Chan, W. Y., Lluis, C., Mcilhinney, R. A., and Franco, R. (2001). Metabotropic glutamate 1alpha and adenosine A1 receptors assemble into functionally interacting complexes. *J. Biol. Chem.* 276, 18345–18351.

Ciruela, F., Gomez-Soler, M., Guidolin, D., Borroto-Escuela, D. O., Agnati, L. F., Fuxe, K., and Fernandez-Duenas, V. (2011). Adenosine receptor containing oligomers: their role in the control of dopamine and glutamate neurotransmission in the brain. *Biochim. Biophys. Acta* 1808, 1245–1255.

Cunha, R. A. (2005). Neuroprotection by adenosine in the brain: from A(1) receptor activation to A (2A) receptor blockade. *Purinergic Signal.* 1, 111–134.

Dana, C., Vial, M., Leonard, K., Beauregard, A., Kitabgi, P., Vincent, J. P., Rostene, W., and Beaudet, A. (1989). Electron microscopic localization of neurotensin binding sites in the midbrain tegmentum of the rat. I. Ventral tegmental area and the interfascicular nucleus. *J. Neurosci.* 9, 2247–2257.

Dasgupta, S., Li, X. M., Jansson, A., Finnman, U. B., Matsui, T., Rinken, A., Arenas, E., Agnati, L. F., and Fuxe, K. (1996). Regulation of dopamine D2 receptor affinity by cholecystokinin octapeptide in fibroblast cells cotransfected with human CCKB and D2L receptor cDNAs. *Brain Res. Mol. Brain Res.* 36, 292–299.

Del Arco, A., Segovia, G., Fuxe, K., and Mora, F. (2003). Changes in dialysate concentrations of glutamate and GABA in the brain: an index of volume transmission mediated actions? *J. Neurochem.* 85, 23–33.

De-Miguel, F. F., and Trueta, C. (2005). Synaptic and extrasynaptic secretion of serotonin. *Cell. Mol. Neurobiol.* 25, 297–312.

Descarries, L., Beaudet, A., and Watkins, K. C. (1975). Serotonin nerve terminals in adult rat neocortex. *Brain Res.* 100, 563–588.

Descarries, L., Berube-Carriere, N., Riad, M., Bo, G. D., Mendez, J. A., and Trudeau, L. E. (2008). Glutamate in dopamine neurons: synaptic versus diffuse transmission. *Brain Res. Rev.* 58, 290–302.

Descarries, L., Gisiger, V., and Steriade, M. (1997). Diffuse transmission by acetylcholine in the CNS. *Prog. Neurobiol.* 53, 603–625.

Descarries, L., and Mechawar, N. (2000). Ultrastructural evidence for diffuse transmission by monoamine and acetylcholine neurons of the central nervous system. *Prog. Brain Res.* 125, 27–47.

Descarries, L., Seguela, P., and Watkins, K. C. (1991). "Nonjunctional relationship of monoamine axon terminals in the cerebral cortex of adult rat," in *Volume Transmission in the Brain, Novel Mechanisms for Neural Transmission*, eds K. Fuxe and L. F. Agnati (New York: Raven Press), 53–62.

Descarries, L., Watkins, K. C., Garcia, S., Bosler, O., and Doucet, G. (1996). Dual character, asynaptic and synaptic, of the dopamine innervation in adult rat neostriatum: a quantitative autoradiographic and immunocytochemical analysis. *J. Comp. Neurol.* 375, 167–186.

Dewey, S. L., Smith, G. S., Logan, J., Brodie, J. D., Fowler, J. S., and Wolf, A. P. (1993). Striatal binding of the PET ligand 11C-raclopride is altered by drugs that modify synaptic dopamine levels. *Synapse* 13, 350–356.

Di Matteo, V., Di Giovanni, G., Pierucci, M., and Esposito, E. (2008). Serotonin control of central dopaminergic function: focus on in vivo microdialysis studies. *Prog. Brain Res.* 172, 7–44.

Diaz-Cabiale, Z., Fuxe, K., Narvaez, J. A., Finetti, S., Antonelli, T., Tanganelli, S., and Ferraro, L. (2002). Neurotensin-induced modulation of dopamine D2 receptors and their function in rat striatum: counteraction by a NTR1-like receptor antagonist. *Neuroreport* 13, 763–766.

Ding, J., Guzman, J. N., Tkatch, T., Chen, S., Goldberg, J. A., Ebert, P. J., Levitt, P., Wilson, C. J., Hamm, H. E., and Surmeier, D. J. (2006). RGS4-dependent attenuation of M4 autoreceptor function in striatal cholinergic interneurons following dopamine depletion. *Nat. Neurosci.* 9, 832–842.

Duan, L., Yuan, H., Su, C. J., Liu, Y. Y., and Rao, Z. R. (2004). Ultrastructure of junction areas between neurons and astrocytes in rat supraoptic nuclei. *World J. Gastroenterol.* 10, 117–121.

Eghbali, M., Santoro, C., Paredes, W., Gardner, E. L., and Zukin, R. S. (1987). Visualization of multiple opioid-receptor types in rat striatum after specific mesencephalic lesions. *Proc. Natl. Acad. Sci. U.S.A.* 84, 6582–6586.

El Mestikawy, S., Wallen-Mackenzie, A., Fortin, G. M., Descarries, L., and Trudeau, L. E. (2011). From glutamate co-release to vesicular synergy: vesicular glutamate transporters. *Nat. Rev. Neurosci.* 12, 204–216.

Elde, R., Arvidsson, U., Riedl, M., Vulchanova, L., Lee, J. H., Dado, R., Nakano, A., Chakrabarti, S., Zhang, X., Loh, H. H., Law, P. Y., Hökfelt, T., and Wessendorf, M. (1995). Distribution of neuropeptide receptors. New views of peptidergic neurotransmission made possible by antibodies to opioid receptors. *Ann. N. Y. Acad. Sci.* 757, 390–404.

Falck, B., Hillarp, N. A., Thieme, G., and Torp, A. (1962). Fluorescence of catechol amines and related compounds condensed with formaldehyde. *In J. Histochem. Cytochem.* 10, 348–354.

Ferraro, L., Antonelli, T., O'Connor, W. T., Tanganelli, S., Rambert, F. A., and Fuxe, K. (1998). The effects of modafinil on striatal, pallidal and nigral GABA and glutamate release in the conscious rat: evidence for a preferential inhibition of striatopallidal GABA transmission. *Neurosci. Lett.* 253, 135–138.

Ferraro, L., Beggiato, S., Tomasini, M. C., Fuxe, K., Tanganelli, S., and Antonelli, T. (2011). Neurotensin regulates cortical glutamate transmission by modulating N-methyl-D-aspartate receptor functional activity: an in vivo microdialysis study. *J. Neurosci. Res.* 89, 1618–1626.

Ferraro, L., O'Connor, W. T., Beggiato, S., Tomasini, M. C., Fuxe, K., Tanganelli, S., and Antonelli, T. (2012). Striatal NTS(1), dopamine D(2) and NMDA receptor regulation of pallidal GABA and glutamate release - a dual-probe microdialysis study in the intranigral 6-hydroxydopamine unilaterally lesioned rat. *Eur. J. Neurosci.* 35, 207–220.

Ferraro, L., Tanganelli, S., O'Connor, W. T., Bianchi, C., Ungerstedt, U., and Fuxe, K. (1995). Neurotensin increases endogenous glutamate release in the neostriatum of the awake rat. *Synapse* 20, 362–364.

Ferre, S., and Fuxe, K. (2000). Adenosine as a volume transmission signal. A feedback detector of neuronal activation. *Prog. Brain Res.* 125, 353–361.

Ferre, S., Karcz-Kubicha, M., Hope, B. T., Popoli, P., Burgueno, J., Gutierrez, M. A., Casado, V., Fuxe, K., Goldberg, S. R., Lluis, C., Franco, R., and Ciruela, F. (2002). Synergistic interaction between adenosine A2A and glutamate mGlu5 receptors: implications for striatal neuronal function. *Proc. Natl. Acad. Sci. U.S.A.* 99, 11940–11945.

Fredholm, B. B., Chen, J. F., Cunha, R. A., Svenningsson, P., and Vaugeois, J. M. (2005). Adenosine and brain function. *Int. Rev. Neurobiol.* 63, 191–270.

Frey, P. (1983). Cholecystokinin octapeptide levels in rat brain are changed after subchronic neuroleptic treatment. *Eur. J. Pharmacol.* 95, 87–92.

Frey, P., Fuxe, K., Eneroth, P., and Agnati, L. F. (1986). Effects of acute and long-term treatment with neuroleptics on regional telencephalic neurotensin levels in the male rat. *Neurochem. Int.* 8, 429–434.

Froes, M. M., Correia, A. H., Garcia-Abreu, J., Spray, D. C., Campos De Carvalho, A. C., and Neto, M. V. (1999). Gap-junctional coupling between neurons and astrocytes in primary central nervous system cultures. *Proc. Natl. Acad. Sci. U.S.A.* 96, 7541–7546.

Fuxe, K. (1963). Cellular localization of monoamines in the median eminence and in the infundibular stem of some mammals. *Acta Physiol. Scand.* 58, 383–384.

Fuxe, K. (1964). Cellular localization of monoamines in the median eminence and the infundibular stem of some mammals. *Z. Zellforsch. Mikrosk. Anat.* 61, 710–724.

Fuxe, K. (1965). *Evidence for the Existence of Monoamine Neurons in the Central Nervous System.* Uppsala: Almqvist and Wiksells Boktryckeri.

Fuxe, K. (1979). Dopamine receptor agonists in brain research and as therapeutic agents. *Trends Neurosci.* 2, 1–4.

Fuxe, K., and Agnati, L. F. (eds). (1991b). *Volume Transmission in the Brain, Novel Mechanisms for Neural Transmission.* New York: Raven Press.

Fuxe, K., and Agnati, L. F. (1991a). "Two principle modes of electrochemical communication in the brain: volume versus wiring transmission," in *Volume Transmission in the Brain: Novel Mechanisms of Neuronal Transmission*, eds K. Fuxe and L. F. Agnati (New York: Raven Press), 1–9.

Fuxe, K., Agnati, L. F., Benfenati, F., Celani, M., Zini, I., Zoli, M., and Mutt, V. (1983). Evidence for the existence of receptor-receptor interactions in the central nervous system. Studies on the regulation of monoamine receptors by neuropeptides. *J. Neural Transm. Suppl.* 18, 165–179.

Fuxe, K., Agnati, L. F., Benfenati, F., Cimmino, M., Algeri, S., Hokfelt, T., and Mutt, V. (1981). Modulation by cholecystokinins of 3H-spiroperidol binding in rat striatum: evidence for increased affinity and reduction in the number of binding sites. *Acta Physiol. Scand.* 113, 567–569.

Fuxe, K., Hokfelt, T., Jonsson, G., and Ungerstedt, U. (1970b). "Fluorescence microscopy in neuroanatomy," in *Contemporary Research Methods in Neuroanatomy*, eds W. J. H. Narura and S. O. E. Ebbesson (Berlin: Springer-Verlag), 275–314.

Fuxe, K., Hokfelt, T., and Ungerstedt, U. (1970c). Morphological and functional aspects of central monoamine neurons. *Int. Rev. Neurobiol.* 13, 93–126.

Fuxe, K., Agnati, L. F., Cintra, A., Andersson, K., Eneroth, P., Harfstrand, A., Zoli, M., and Goldstein, M. (1988a). Studies on central D1 receptors role in volume transmission, neuroendrocrine regulation and release of noradrenaline. *Adv. Exp. Med. Biol.* 235, 83–119.

Fuxe, K., Cintra, A., Agnati, L. F., Harfstrand, A., and Goldstein, M. (1988b). Studies on the relationship of tyrosine hydroxylase, dopamine and cyclic amp-regulated phosphoprotein-32 immunoreactive neuronal structures and d1 receptor antagonist binding sites in various brain regions of the male rat-mismatches indicate a role of d1 receptors in volume transmission. *Neurochem. Int.* 13, 179–197.

Fuxe, K., Agnati, L. F., Zoli, M., Cintra, A., Härfstrand, A., von Euler, G., Grimaldi, R., Kalia, M., and Eneroth, P. (1988c). "The opioid peptide sytems: their organization and role in volume transmission and neuroendocrine regulation," in *Regulatory Roles of Opioid Peptides,* eds P. Illes and C. Farsang (Weinheim: VCH), 33–68.

Fuxe, K., Agnati, L. F., Jacobsen, K., Hillion, J., Canals, M., Torvinen, M., Tinner-Staines, B., Staines, W., Rosin, D., Terasmaa, A., Popoli, P., Leo, G., Vergoni, V., Lluis, C., Ciruela, F., Franco, R., and Ferre, S. (2003). Receptor heteromerization in adenosine A2A receptor signaling: relevance for striatal function and Parkinson's disease. *Neurology* 61, S19–S23.

Fuxe, K., Agnati, L. F., and Mora, F. (2008a). The basal ganglia. *Brain Res. Rev.* 58, 1–482.

Fuxe, K., Marcellino, D., Guidolin, D., Woods, A. S., and Agnati, L. F. (2008b). Heterodimers and receptor mosaics of different types of G-protein-coupled receptors. *Physiology (Bethesda)* 23, 322–332.

Fuxe, K., Marcellino, D., Rivera, A., Diaz-Cabiale, Z., Filip, M., Gago, B., Roberts, D. C., Langel, U., Genedani, S., Ferraro, L., De La Calle, A., Narvaez, J., Tanganelli, S., Woods, A., and Agnati, L. F. (2008c). Receptor-receptor interactions within receptor mosaics. Impact on neuropsychopharmacology. *Brain Res. Rev.* 58, 415–452.

Fuxe, K., Dahlstrom, A., Hoistad, M., Marcellino, D., Jansson, A., Rivera, A., Diaz-Cabiale, Z., Jacobsen, K., Tinner-Staines, B., Hagman, B., Leo, G., Staines, W., Guidolin, D., Kehr, J., Genedani, S., Belluardo, N., and Agnati, L. F. (2007a). From the Golgi-Cajal mapping to the transmitter-based characterization of the neuronal networks leading to two modes of brain communication: wiring and volume transmission. *Brain Res. Rev.* 55, 17–54.

Fuxe, K., Ferre, S., Genedani, S., Franco, R., and Agnati, L. F. (2007b). Adenosine receptor-dopamine receptor interactions in the basal ganglia and their relevance for brain function. *Physiol. Behav.* 92, 210–217.

Fuxe, K., Dahlstrom, A. B., Jonsson, G., Marcellino, D., Guescini, M., Dam, M., Manger, P., and Agnati, L. (2010a). The discovery of central monoamine neurons gave volume transmission to the wired brain. *Prog. Neurobiol.* 90, 82–100.

Fuxe, K., Marcellino, D., Borroto-Escuela, D. O., Frankowska, M., Ferraro, L., Guidolin, D., Ciruela, F., and Agnati, L. F. (2010b). The changing world of G protein-coupled receptors: from monomers to dimers and receptor mosaics with allosteric receptor-receptor interactions. *J. Recept. Signal Transduct. Res.* 30, 272–283.

Fuxe, K., Marcellino, D., Borroto-Escuela, D. O., Guescini, M., Fernandez-Duenas, V., Tanganelli, S., Rivera, A., Ciruela, F., and Agnati, L. F. (2010c). Adenosine-dopamine interactions in the pathophysiology and treatment of CNS disorders. *CNS Neurosci. Ther.* 16, e18–e42.

Fuxe, K., Ferre, S., Zoli, M., and Agnati, L. F. (1998). Integrated events in central dopamine transmission as analyzed at multiple levels. Evidence for intramembrane adenosine A2A/dopamine D2 and adenosine A1/dopamine D1 receptor interactions in the basal ganglia. *Brain Res. Brain Res. Rev.* 26, 258–273.

Fuxe, K., Hokfelt, T., and Nilsson, O. (1967). Activity changes in the tubero-infundibular dopamine neurons of the rat during various states of the reproductive cycle. *Life Sci.* 6, 2057–2061.

Fuxe, K., Li, X. M., Tanganelli, S., Hedlund, P., O'Connor, W. T., Ferraro, L., Ungerstedt, U., and Agnati, L. F. (1995). Receptor-receptor interactions and their relevance for receptor diversity. Focus on neuropeptide/dopamine interactions. *Ann. N. Y. Acad. Sci.* 757, 365–376.

Fuxe, K., Marcellino, D., Woods, A. S., Giuseppina, L., Antonelli, T., Ferraro, L., Tanganelli, S., and Agnati, L. F. (2009). Integrated signaling in heterodimers and receptor mosaics of different types of GPCRs of the forebrain: relevance for schizophrenia. *J. Neural Transm.* 116, 923–939.

Fuxe, K., Rivera, A., Jacobsen, K. X., Hoistad, M., Leo, G., Horvath, T. L., Staines, W., De La Calle, A., and Agnati, L. F. (2005). Dynamics of volume transmission in the brain. Focus on catecholamine and opioid peptide communication and the role of uncoupling protein 2. *J. Neural Transm.* 112, 65–76.

Fuxe, K., and Ungerstedt, U. (1970a). "Histochemical, biochemical, and functional studies on central monoamine neurons after acute and chronic amphetamine administration," in *Amphetamines and Related Compounds*, eds E. Costa and S. Garattini (New York: Raven Press), 257–288.

Fuxe, K., Von Euler, G., Agnati, L. F., Merlo Pich, E., O'Connor, W. T., Tanganelli, S., Li, X. M., Tinner, B., Cintra, A., Carani, C., and Benfenati, F. (1992). Intramembrane interactions

between neurotensin receptors and dopamine D2 receptors as a major mechanism for the neuroleptic-like action of neurotensin. *Ann. N. Y. Acad. Sci.* 668, 186–204.

Gago, B., Fuxe, K., Agnati, L., Penafiel, A., De La Calle, A., and Rivera, A. (2007). Dopamine D(4) receptor activation decreases the expression of mu-opioid receptors in the rat striatum. *J. Comp. Neurol.* 502, 358–366.

Gago, B., Suarez-Boomgaard, D., Fuxe, K., Brene, S., Reina-Sanchez, M. D., Rodriguez-Perez, L. M., Agnati, L. F., De La Calle, A., and Rivera, A. (2011). Effect of acute and continuous morphine treatment on transcription factor expression in subregions of the rat caudate putamen. Marked modulation by D4 receptor activation. *Brain Res.* 1407, 47–61.

George, S. R., and O'Dowd, B. F. (2007). A novel dopamine receptor signaling unit in brain: heterooligomers of D1 and D2 dopamine receptors. *ScientificWorldJournal* 7, 58–63.

Gerfen, C. R., and Surmeier, D. J. (2011). Modulation of striatal projection systems by dopamine. *Annu. Rev. Neurosci.* 34, 441–466.

Gisiger, V., and Stephens, H. R. (1988). Localization of the pool of G4 acetylcholinesterase characterizing fast muscles and its alteration in murine muscular dystrophy. *J. Neurosci. Res.* 19, 62–78.

Goin, J. C., and Nathanson, N. M. (2006). Quantitative analysis of muscarinic acetylcholine receptor homo- and heterodimerization in live cells: regulation of receptor down-regulation by heterodimerization. *J. Biol. Chem.* 281, 5416–5425.

Gras, C., Amilhon, B., Lepicard, E. M., Poirel, O., Vinatier, J., Herbin, M., Dumas, S., Tzavara, E. T., Wade, M. R., Nomikos, G. G., Hanoun, N., Saurini, F., Kemel, M. L., Gasnier, B., Giros, B., and El Mestikawy, S. (2008). The vesicular glutamate transporter VGLUT3 synergizes striatal acetylcholine tone. *Nat. Neurosci.* 11, 292–300.

Gruber, S. H., Nomikos, G. G., and Mathe, A. A. (2002). Effects of haloperidol and risperidone on neurotensin levels in brain regions and neurotensin efflux in the ventral striatum of the rat. *Neuropsychopharmacology* 26, 595–604.

Guescini, M., Leo, G., Genedani, S., Carone, C., Pederzoli, F., Ciruela, F., Guidolin, D., Stocchi, V., Mantuano, M., Borroto-Escuela, D. O., Fuxe, K., and Agnati, L. F. (2012). Microvesicle and tunneling nanotube mediated intercellular transfer of g-protein coupled receptors in cell cultures. *Exp. Cell Res.* 318, 603–613.

Haas, H., and Panula, P. (2003). The role of histamine and the tuberomamillary nucleus in the nervous system. *Nat. Rev. Neurosci.* 4, 121–130.

Hansson, A. C., Andersson, A., Tinner, B., Cui, X., Sommer, W., and Fuxe, K. (1998). Existence of striatal nerve cells coexpressing CCK(B) and D2 receptor mRNAs. *Neuroreport* 9, 2035–2038.

Harvey, C. D., and Svoboda, K. (2007). Locally dynamic synaptic learning rules in pyramidal neuron dendrites. *Nature* 450, 1195–1200.

Hasbi, A., O'Dowd, B. F., and George, S. R. (2011). Dopamine D1-D2 receptor heteromer signaling pathway in the brain: emerging physiological relevance. *Mol. Brain* 4, 26.

Hersch, S. M., Ciliax, B. J., Gutekunst, C. A., Rees, H. D., Heilman, C. J., Yung, K. K., Bolam, J. P., Ince, E., Yi, H., and Levey, A. I. (1995). Electron microscopic analysis of D1 and D2 dopamine receptor proteins in the dorsal striatum and their synaptic relationships with motor corticostriatal afferents. *J. Neurosci.* 15, 5222–5237.

Hersch, S. M., Yi, H., Heilman, C. J., Edwards, R. H., and Levey, A. I. (1997). Subcellular localization and molecular topology of the dopamine transporter in the striatum and substantia nigra. *J. Comp. Neurol.* 388, 211–227.

Hillion, J., Canals, M., Torvinen, M., Casado, V., Scott, R., Terasmaa, A., Hansson, A., Watson, S., Olah, M. E., Mallol, J., Canela, E. I., Zoli, M., Agnati, L. F., Ibanez, C. F., Lluis, C., Franco, R., Ferre, S., and Fuxe, K. (2002). Coaggregation, cointernalization, and codesensitization of adenosine A2A receptors and dopamine D2 receptors. *J. Biol. Chem.* 277, 18091–18097.

Hnasko, T. S., Chuhma, N., Zhang, H., Goh, G. Y., Sulzer, D., Palmiter, R. D., Rayport, S., and Edwards, R. H. (2010). Vesicular glutamate transport promotes dopamine storage and glutamate corelease in vivo. *Neuron* 65, 643–656.

Hnasko, T. S., Sotak, B. N., and Palmiter, R. D. (2005). Morphine reward in dopamine-deficient mice. *Nature* 438, 854–857.

Hoistad, M., Chen, K. C., Nicholson, C., Fuxe, K., and Kehr, J. (2002). Quantitative dual-probe microdialysis: evaluation of [3H]mannitol diffusion in agar and rat striatum. *J. Neurochem.* 81, 80–93.

Hoistad, M., Samskog, J., Jacobsen, K. X., Olsson, A., Hansson, H. A., Brodin, E., and Fuxe, K. (2005). Detection of beta-endorphin in the cerebrospinal fluid after intrastriatal microinjection into the rat brain. *Brain Res.* 1041, 167–180.

Hökfelt, T., Fuxe, K., and Pernow, B. (1986). *Coexistence of Neuronal Messengers: A New Principle in Chemical Transmission, in Progress in Brain Research*, Vol. 68 (New York: Elsevier), 1–403.

Jansson, A., Descarries, L., Cornea-Hebert, V., Riad, M., Verge, D., Bancila, M., Agnati, L. F., and Fuxe, K. (2002). "Transmitter-receptor mistaches in central dopamine serotonin and neuropeptide systems," in *The Neuronal Environment: Brain Homeostasis in Health and Disease*, ed. W. Walz (Totowa, NJ: Humana Press), 83–107.

Jansson, A., Goldstein, M., Tinner, B., Zoli, M., Meador-Woodruff, J. H., Lew, J. Y., Levey, A. I., Watson, S., Agnati, L. F., and Fuxe, K. (1999). On the distribution patterns of D1, D2, tyrosine hydroxylase and dopamine transporter immunoreactivities in the ventral striatum of the rat. *Neuroscience* 89, 473–489.

Jansson, A., Tinner, B., Bancila, M., Verge, D., Steinbusch, H. W., Agnati, L. F., and Fuxe, K. (2001). Relationships of 5-hydroxytryptamine immunoreactive terminal-like varicosities to 5-hydroxytryptamine-2A receptor-immunoreactive neuronal processes in the rat forebrain. *J. Chem. Neuroanat.* 22, 185–203.

Juhasz, J. R., Hasbi, A., Rashid, A. J., So, C. H., George, S. R., and O'Dowd, B. F. (2008). Mu-opioid receptor heterooligomer formation with the dopamine D1 receptor as directly visualized in living cells. *Eur. J. Pharmacol.* 581, 235–243.

Kawaguchi, Y. (1995). Physiological subgroups of nonpyramidal cells with specific morphological characteristics in layer II/III of rat frontal cortex. *J. Neurosci.* 15, 2638–2655.

Kenakin, T., Agnati, L. F., Caron, M., Fredholm, B., Guidoli, D., Kobilka, B., Lefkowitz, R. W., Lohse, M., Woods, A., and Fuxe, K. (2010). International Workshop at the Nobel Forum, Karolinska Institutet on G protein-coupled receptors: finding the words to describe monomers, oligomers, and their molecular mechanisms and defining their meaning. Can a consensus be reached? *J. Recept. Signal Transduct. Res.* 30, 284–286.

Laruelle, M. (2000). Imaging synaptic neurotransmission with in vivo binding competition techniques: a critical review. *J. Cereb. Blood Flow Metab.* 20, 423–451.

Lee, F. J., Wang, Y. T., and Liu, F. (2005). Direct receptor cross-talk can mediate the modulation of excitatory and inhibitory neurotransmission by dopamine. *J. Mol. Neurosci.* 26, 245–252.

Lee, F. J., Xue, S., Pei, L., Vukusic, B., Chery, N., Wang, Y., Wang, Y. T., Niznik, H. B., Yu, X. M., and Liu, F. (2002). Dual regulation of NMDA receptor functions by direct protein-protein interactions with the dopamine D1 receptor. *Cell* 111, 219–230.

Levey, A. I., Hersch, S. M., Rye, D. B., Sunahara, R. K., Niznik, H. B., Kitt, C. A., Price, D. L., Maggio, R., Brann, M. R., and Ciliax, B. J. (1993). Localization of D1 and D2 dopamine receptors in brain with subtype-specific antibodies. *Proc. Natl. Acad. Sci. U.S.A.* 90, 8861–8865.

Li, X. M., Ferraro, L., Tanganelli, S., O'Connor, W. T., Hasselrot, U., Ungerstedt, U., and Fuxe, K. (1995a). Neurotensin peptides antagonistically regulate postsynaptic dopamine D2 receptors in rat nucleus accumbens: a receptor binding and microdialysis study. *J. Neural Transm. Gen. Sect.* 102, 125–137.

Li, X. M., Hedlund, P. B., and Fuxe, K. (1995b). Cholecystokinin octapeptide in vitro and ex vivo strongly modulates striatal dopamine D2 receptors in rat forebrain sections. *Eur. J. Neurosci.* 7, 962–971.

Li, X. M., Hedlund, P. B., Agnati, L. F., and Fuxe, K. (1994a). Dopamine D1 receptors are involved in the modulation of D2 receptors induced by cholecystokinin receptor subtypes in rat neostriatal membranes. *Brain Res.* 650, 289–298.

Li, X. M., Hedlund, P. B., and Fuxe, K. (1994b). Strong effects of NT/NN peptides on DA D2 receptors in rat neostriatal sections. *Neuroreport* 5, 1621–1624.

Liu, F., Wan, Q., Pristupa, Z. B., Yu, X. M., Wang, Y. T., and Niznik, H. B. (2000). Direct protein-protein coupling enables cross-talk between dopamine D5 and gamma-aminobutyric acid A receptors. *Nature* 403, 274–280.

Liu, X. Y., Chu, X. P., Mao, L. M., Wang, M., Lan, H. X., Li, M. H., Zhang, G. C., Parelkar, N. K., Fibuch, E. E., Haines, M., Neve, K. A., Liu, F., Xiong, Z. G., and Wang, J. Q. (2006). Modulation of D2R-NR2B interactions in response to cocaine. *Neuron* 52, 897–909.

Lukasiewicz, S., Polit, A., Kedracka-Krok, S., Wedzony, K., Mackowiak, M., and Dziedzicka-Wasylewska, M. (2010). Hetero-dimerization of serotonin 5-HT(2A) and dopamine D(2) receptors. *Biochim. Biophys. Acta* 1803, 1347–1358.

Lundberg, J. (1991). "Volume transmission by coreleased peptides in the autonomic nervous system," in *Volume Transmission in the Brain*, eds K. Fuxe and L. Agnati (Stockholm: Raven Press), 425–432.

MacLeod, R. M., and Lehmeyer, J. E. (1974). Studies on the mechanism of the dopamine-mediated inhibition of prolactin secretion. *Endocrinology* 94, 1077–1085.

MacMillan, S. J., Mark, M. A., and Duggan, A. W. (1998). The release of beta-endorphin and the neuropeptide-receptor mismatch in the brain. *Brain Res.* 794, 127–136.

Marcellino, D., Carriba, P., Filip, M., Borgkvist, A., Frankowska, M., Bellido, I., Tanganelli, S., Muller, C. E., Fisone, G., Lluis, C., Agnati, L. F., Franco, R., and Fuxe, K. (2008). Antagonistic cannabinoid CB1/dopamine D2 receptor interactions in striatal CB1/D2 heteromers. A combined neurochemical and behavioral analysis. *Neuropharmacology* 54, 815–823.

Marcellino, D., Kehr, J., Agnati, L. F., and Fuxe, K. (2011). Increased affinity of dopamine for D(2) -like versus D(1) -like receptors. Relevance for volume transmission in interpreting PET findings. *Synapse*. doi: 10.1002/syn.21501. [Epub ahead of print].

Martin, A. B., Fernandez-Espejo, E., Ferrer, B., Gorriti, M. A., Bilbao, A., Navarro, M., Rodriguez De Fonseca, F., and Moratalla, R. (2008). Expression and function of CB1 receptor in the rat striatum: localization and effects on D1 and D2 dopamine receptor-mediated motor behaviors. *Neuropsychopharmacology* 33, 1667–1679.

Moreno, E., Hoffmann, H., Gonzalez-Sepulveda, M., Navarro, G., Casado, V., Cortes, A., Mallol, J., Vignes, M., Mccormick, P. J., Canela, E. I., Lluis, C., Moratalla, R., Ferre, S., Ortiz, J., and Franco, R. (2010). Dopamine D1-histamine H3 receptor heteromers provide a selective link to MAPK signaling in GABAergic neurons of the direct striatal pathway. *J. Biol. Chem.* 286, 5846–5854.

Morino, P., Herrera-Marschitz, M., Castel, M. N., Ungerstedt, U., Varro, A., Dockray, G., and Hokfelt, T. (1994). Cholecystokinin in cortico-striatal neurons in the rat: immunohistochemical studies at the light and electron microscopical level. *Eur. J. Neurosci.* 6, 681–692.

Narushima, M., Uchigashima, M., Fukaya, M., Matsui, M., Manabe, T., Hashimoto, K., Watanabe, M., and Kano, M. (2007). Tonic enhancement of endocannabinoid-mediated retrograde suppression of inhibition by cholinergic interneuron activity in the striatum. *J. Neurosci.* 27, 496–506.

Newman-Tancredi, A., Audinot-Bouchez, V., Gobert, A., and Millan, M. J. (1997). Noradrenaline and adrenaline are high affinity agonists at dopamine D4 receptors. *Eur. J. Pharmacol.* 319, 379–383.

Nicholson, C., and Sykova, E. (1998). Extracellular space structure revealed by diffusion analysis. *Trends Neurosci.* 21, 207–215.

Ogren, S. O., and Fuxe, K. (1988). D1- and D2-receptor antagonists induce catalepsy via different efferent striatal pathways [corrected]. *Neurosci. Lett.* 85, 333–338.

Okubo, Y., and Iino, M. (2011). Visualization of glutamate as a volume transmitter. *J. Physiol. (Lond.)* 589, 481–488.

Okubo, Y., Sekiya, H., Namiki, S., Sakamoto, H., Iinuma, S., Yamasaki, M., Watanabe, M., Hirose, K., and Iino, M. (2010). Imaging extrasynaptic glutamate dynamics in the brain. *Proc. Natl. Acad. Sci. U.S.A.* 107, 6526–6531.

Oldenburg, I. A., and Ding, J. B. (2011). Cholinergic modulation of synaptic integration and dendritic excitability in the striatum. *Curr. Opin. Neurobiol.* 21, 425–432.

Ozog, M. A., Siushansian, R., and Naus, C. C. (2002). Blocked gap junctional coupling increases glutamate-induced neurotoxicity in neuron-astrocyte co-cultures. *J. Neuropathol. Exp. Neurol.* 61, 132–141.

Perreault, M. L., Hasbi, A., Alijaniaram, M., Fan, T., Varghese, G., Fletcher, P. J., Seeman, P., O'Dowd, B. F., and George, S. R. (2010). The dopamine D1-D2 receptor heteromer localizes in dynorphin/enkephalin neurons: increased high affinity state following amphetamine and in schizophrenia. *J. Biol. Chem.* 285, 36625–36634.

Piomelli, D. (2003). The molecular logic of endocannabinoid signalling. *Nat. Rev. Neurosci.* 4, 873–884.

Pisani, A., Bernardi, G., Ding, J., and Surmeier, D. J. (2007). Re-emergence of striatal cholinergic interneurons in movement disorders. *Trends Neurosci.* 30, 545–553.

Popoli, P., Pezzola, A., Torvinen, M., Reggio, R., Pintor, A., Scarchilli, L., Fuxe, K., and Ferre, S. (2001). The selective mGlu(5) receptor agonist CHPG inhibits quinpirole-induced turning in 6-hydroxydopamine-lesioned rats and modulates the binding characteristics of dopamine D(2) receptors in the rat striatum: interactions with adenosine A(2a) receptors. *Neuropsychopharmacology* 25, 505–513.

Rice, M. E., and Cragg, S. J. (2008). Dopamine spillover after quantal release: rethinking dopamine transmission in the nigrostriatal pathway. *Brain Res. Rev.* 58, 303–313.

Rivera, A., Agnati, L. F., Horvath, T. L., Valderrama, J. J., De La Calle, A., and Fuxe, K. (2006). Uncoupling protein 2/3 immunoreactivity and the ascending dopaminergic and noradrenergic neuronal systems: relevance for volume transmission. *Neuroscience* 137, 1447–1461.

Rivera, A., Penafiel, A., Megias, M., Agnati, L. F., Lopez-Tellez, J. F., Gago, B., Gutierrez, A., De La Calle, A., and Fuxe, K. (2008). Cellular localization and distribution of dopamine D(4) receptors in the rat cerebral cortex and their relationship with the cortical dopaminergic and noradrenergic nerve terminal networks. *Neuroscience* 155, 997–1010.

Rocheville, M., Lange, D. C., Kumar, U., Patel, S. C., Patel, R. C., and Patel, Y. C. (2000). Receptors for dopamine and somatostatin: formation of hetero-oligomers with enhanced functional activity. *Science* 288, 154–157.

Schiffmann, S. N., and Vanderhaeghen, J. J. (1993). Adenosine A2 receptors regulate the gene expression of striatopallidal and striatonigral neurons. *J. Neurosci.* 13, 1080–1087.

Schools, G. P., Zhou, M., and Kimelberg, H. K. (2006). Development of gap junctions in hippocampal astrocytes: evidence that whole cell electrophysiological phenotype is an intrinsic property of the individual cell. *J. Neurophysiol.* 96, 1383–1392.

Schwarcz, R., and Pellicciari, R. (2002). Manipulation of brain kynurenines: glial targets, neuronal effects, and clinical opportunities. *J. Pharmacol. Exp. Ther.* 303, 1–10.

Sebastiao, A. M., and Ribeiro, J. A. (2000). Fine-tuning neuromodulation by adenosine. *Trends Pharmacol. Sci.* 21, 341–346.

Seguela, P., Watkins, K. C., Geffard, M., and Descarries, L. (1990). Noradrenaline axon terminals in adult rat neocortex: an immunocytochemical analysis in serial thin sections. *Neuroscience* 35, 249–264.

Seneca, N., Finnema, S. J., Farde, L., Gulyas, B., Wikstrom, H. V., Halldin, C., and Innis, R. B. (2006). Effect of amphetamine on dopamine D2 receptor binding in nonhuman primate brain: a comparison of the agonist radioligand [11C]MNPA and antagonist [11C]raclopride. *Synapse* 59, 260–269.

Sesack, S. R., Aoki, C., and Pickel, V. M. (1994). Ultrastructural localization of D2 receptor-like immunoreactivity in midbrain dopamine neurons and their striatal targets. *J. Neurosci.* 14, 88–106.

Smiley, J. F., Levey, A. I., Ciliax, B. J., and Goldman-Rakic, P. S. (1994). D1 dopamine receptor immunoreactivity in human and monkey cerebral cortex: predominant and extrasynaptic localization in dendritic spines. *Proc. Natl. Acad. Sci. U.S.A.* 91, 5720–5724.

Smiley, J. F., Morrell, F., and Mesulam, M. M. (1997). Cholinergic synapses in human cerebral cortex: an ultrastructural study in serial sections. *Exp. Neurol.* 144, 361–368.

Smiley, J. F., Williams, S. M., Szigeti, K., and Goldman-Rakic, P. S. (1992). Light and electron microscopic characterization of dopamine-immunoreactive axons in human cerebral cortex. *J. Comp. Neurol.* 321, 325–335.

Surmeier, D. J., Ding, J., Day, M., Wang, Z., and Shen, W. (2007). D1 and D2 dopamine-receptor modulation of striatal glutamatergic signaling in striatal medium spiny neurons. *Trends Neurosci.* 30, 228–235.

Tanganelli, S., Antonelli, T., Tomasini, M. C., Beggiato, S., Fuxe, K., and Ferraro, L. (2012). Relevance of dopamine D(2)/neurotensin NTS1 and NMDA/neurotensin NTS1 receptor interaction in psychiatric and neurodegenerative disorders. *Curr. Med. Chem.* 19, 304–316.

Tanganelli, S., Fuxe, K., Antonelli, T., O'Connor, W. T., and Ferraro, L. (2001). Cholecystokinin/dopamine/GABA interactions in the nucleus accumbens: biochemical and functional correlates. *Peptides* 22, 1229–1234.

Tanganelli, S., Fuxe, K., Von Euler, G., Eneroth, P., Agnati, L. F., and Ungerstedt, U. (1990). Changes in pituitary-adrenal activity affect the apomorphine- and cholecystokinin-8-induced changes in striatal

dopamine release using microdialysis. *J. Neural Transm. Gen. Sect.* 81, 183–194.

Tanganelli, S., Li, X. M., Ferraro, L., Von Euler, G., O'Connor, W. T., Bianchi, C., Beani, L., and Fuxe, K. (1993). Neurotensin and cholecystokinin octapeptide control synergistically dopamine release and dopamine D2 receptor affinity in rat neostriatum. *Eur. J. Pharmacol.* 230, 159–166.

Tanganelli, S., O'Connor, W. T., Ferraro, L., Bianchi, C., Beani, L., Ungerstedt, U., and Fuxe, K. (1994). Facilitation of GABA release by neurotensin is associated with a reduction of dopamine release in rat nucleus accumbens. *Neuroscience* 60, 649–657.

Tanganelli, S., Von Euler, G., Fuxe, K., Agnati, L. F., and Ungerstedt, U. (1989). Neurotensin counteracts apomorphine-induced inhibition of dopamine release as studied by microdialysis in rat neostriatum. *Brain Res.* 502, 319–324.

Tepper, J. M., Abercrombie, E. D., and Bolam, J. P. (2007). Basal ganglia macrocircuits. *Prog. Brain Res.* 160, 3–7.

Tepper, J. M., Wilson, C. J., and Koos, T. (2008). Feedforward and feedback inhibition in neostriatal GABAergic spiny neurons. *Brain Res. Rev.* 58, 272–281.

Torvinen, M., Gines, S., Hillion, J., Latini, S., Canals, M., Ciruela, F., Bordoni, F., Staines, W., Pedata, F., Agnati, L. F., Lluis, C., Franco, R., Ferre, S., and Fuxe, K. (2002). Interactions among adenosine deaminase, adenosine A(1) receptors and dopamine D(1) receptors in stably cotransfected fibroblast cells and neurons. *Neuroscience* 113, 709–719.

Trueta, C., Mendez, B., and De-Miguel, F. F. (2003). Somatic exocytosis of serotonin mediated by L-type calcium channels in cultured leech neurones. *J. Physiol. (Lond.)* 547, 405–416.

Uchigashima, M., Narushima, M., Fukaya, M., Katona, I., Kano, M., and Watanabe, M. (2007). Subcellular arrangement of molecules for 2-arachidonoyl-glycerol-mediated retrograde signaling and its physiological contribution to synaptic modulation in the striatum. *J. Neurosci.* 27, 3663–3676.

Ungerstedt, U., Butcher, L. L., Butcher, S. G., Anden, N. E., and Fuxe, K. (1969). Direct chemical stimulation of dopaminergic mechanisms in the neostriatum of the rat. *Brain Res.* 14, 461–471.

Vizi, E. S. (1980). Non-synaptic modulation of transmitter release: pharmacological implications. *Trends Pharmacol. Sci.* 1, 172–175.

Vizi, E. S., Kiss, J. P., and Lendvai, B. (2004). Nonsynaptic communication in the central nervous system. *Neurochem. Int.* 45, 443–451.

von Euler, G. (1991). Biochemical characterization of the intramembrane interaction between neurotensin and dopamine D2 receptors in the rat brain. *Brain Res.* 561, 93–98.

Von Euler, G., and Fuxe, K. (1987). Neurotensin reduces the affinity of D-2 dopamine receptors in rat striatal membranes. *Acta Physiol. Scand.* 131, 625–626.

Wang, Z., Kai, L., Day, M., Ronesi, J., Yin, H. H., Ding, J., Tkatch, T., Lovinger, D. M., and Surmeier, D. J. (2006). Dopaminergic control of corticostriatal long-term synaptic depression in medium spiny neurons is mediated by cholinergic interneurons. *Neuron* 50, 443–452.

Yung, K. K., Bolam, J. P., Smith, A. D., Hersch, S. M., Ciliax, B. J., and Levey, A. I. (1995). Immunocytochemical localization of D1 and D2 dopamine receptors in the basal ganglia of the rat: light and electron microscopy. *Neuroscience* 65, 709–730.

Zoli, M., and Agnati, L. F. (1996). Wiring and volume transmission in the central nervous system: the concept of closed and open synapses. *Prog. Neurobiol.* 49, 363–380.

Conflict of Interest Statement: The authors declare that the research was conducted in the absence of any commercial or financial relationships that could be construed as a potential conflict of interest.

Received: 24 March 2012; paper pending published: 12 April 2012; accepted: 23 April 2012; published online: 04 June 2012.

Citation: Fuxe K, Borroto-Escuela DO, Romero-Fernandez W, Diaz-Cabiale Z, Rivera A, Ferraro L, Tanganelli S, Tarakanov AO, Garriga P, Narváez JA, Ciruela F, Guescini M and Agnati LF (2012) Extrasynaptic neurotransmission in the modulation of brain function. Focus on the striatal neuronal–glial networks. Front. Physio. ***3****:136. doi: 10.3389/fphys.2012.00136*

This article was submitted to Frontiers in Membrane Physiology and Biophysics, a specialty of Frontiers in Physiology.

frontiers in
PHYSIOLOGY

MINI REVIEW ARTICLE
published: 12 July 2012
doi: 10.3389/fphys.2012.00261

The involvement of actin, calcium channels and exocytosis proteins in somato-dendritic oxytocin and vasopressin release

Vicky Tobin, Gareth Leng and Mike Ludwig*

Centre for Integrative Physiology, University of Edinburgh, Edinburgh, UK

Edited by:
Kjell Fuxe, Karolinska Institutet, Sweden

Reviewed by:
Francisco F. De-Miguel, Universidad Nacional Autonoma de Mexico, Mexico
Roger A. Bannister, University of Colorado Denver-Anschutz Medical Campus, USA

***Correspondence:**
Mike Ludwig, Centre for Integrative Physiology, University of Edinburgh, Hugh Robson Building, George Square, Edinburgh EH8 9XD, UK.
e-mail: mike.ludwig@ed.ac.uk

Hypothalamic magnocellular neurons release vasopressin and oxytocin not only from their axon terminals into the blood, but also from their somata and dendrites into the extracellular space of the brain, and this can be regulated independently. Differential release of neurotransmitters from different compartments of a single neuron requires subtle regulatory mechanisms. Somato-dendritic, but not axon terminal release can be modulated by changes in intracellular calcium concentration [(Ca^{2+})] by release of calcium from intracellular stores, resulting in priming of dendritic pools for activity-dependent release. This review focuses on our current understanding of the mechanisms of priming and the roles of actin remodeling, voltage-operated calcium channels (VOCCs) and SNARE proteins in the regulation somato-dendritic and axon terminal peptide release.

Keywords: exocytosis, hypothalamus, pituitary, vasopressin, oxytocin, neuropeptides

INTRODUCTION

Neurons have classically been considered to propagate information in one direction; synaptic inputs onto the dendrites or soma initiate action potentials which, after conduction to the axon terminal, transmit information to the postsynaptic neuron via a neurochemical signal that is confined to the pre- and postsynaptic area. However, neurochemicals can 'spillover' to have extra-synaptic actions, and in some cases can be released from dendrites. Peptides in particular have actions unlikely to be confined to synapses: they are packaged in large dense-cored vesicles (LDCVs), containing much more cargo than conventional synaptic vesicles; they have much higher affinities for their receptors than conventional neurotransmitters, half-lives much longer than conventional neurotransmitters, and in general are not conspicuously located at synapses but are present throughout the cell (Leng and Ludwig, 2008). More than 100 peptides are expressed and secreted by different neuronal populations throughout the brain, and many neuropeptides have profound effects on specific behaviors. These considerations imply that neuropeptides have organizational and activational roles that make them more akin to hormones than to classical neurotransmitters (Ludwig and Leng, 2006).

Among the best-established sites of dendritic release are the supraoptic (SON) and paraventricular nuclei (PVN) of the hypothalamus, where magnocellular neurons synthesize vasopressin and oxytocin. These peptides are packaged into LDCVs that are abundant in the soma and dendrites as well as in swellings and nerve endings in the neurohypophysis (**Figure 1**; Leng and Ludwig, 2008). These neurons are aggregated into relatively homogeneous nuclei, and the SON is particularly homogeneous, containing only magnocellular vasopressin and oxytocin neurons, so studies of dendritic release from the SON can be accomplished in the absence of contamination by axonal release of peptide.

Somato-dendritic release was first unequivocally confirmed in this system using tannic acid fixation and electron microscopy; this allowed the visualization of omega fusion profiles in the dendritic plasma membrane and the dense-cores from exocytosed vesicles in the extracellular space (Morris and Pow, 1991). These studies also showed that magnocellular neurons lack active zones – the specialized region of the presynaptic terminal at which exocytosis typically occurs (Pow and Morris, 1989; Morris and Pow, 1991). Indeed they showed that exocytosis could occur from any part of the neuron with the probability of release from any compartment determined simply by the number of vesicles that were close to the plasma membrane.

The blood-brain barrier is impermeable to oxytocin and vasopressin, and simultaneous measurement of peptide release within the blood and the brain has demonstrated that release from these compartments can be independently controlled (Ludwig and Leng, 2006). For example, in lactating rats, suckling evokes intermittent pulsatile secretion of oxytocin into the blood to mediate milk let-down, and this is the result of synchronous bursting discharge of the oxytocin neurons. However, suckling stimulates dendritic oxytocin release *before* peripheral secretion occurs, and this is essential for co-ordinating the bursting activity (Moos et al., 1989; Rossoni et al., 2008). By contrast, systemic osmotic stimulation activates vasopressin neurons and increases secretion of vasopressin from the pituitary, but dendritic vasopressin release is delayed, occurring after plasma concentrations of vasopressin have returned to baseline (Ludwig et al., 1994).

Over the last decade, *in vivo* and *in vitro* studies have revealed many aspects of the control of dendritic vasopressin and oxytocin

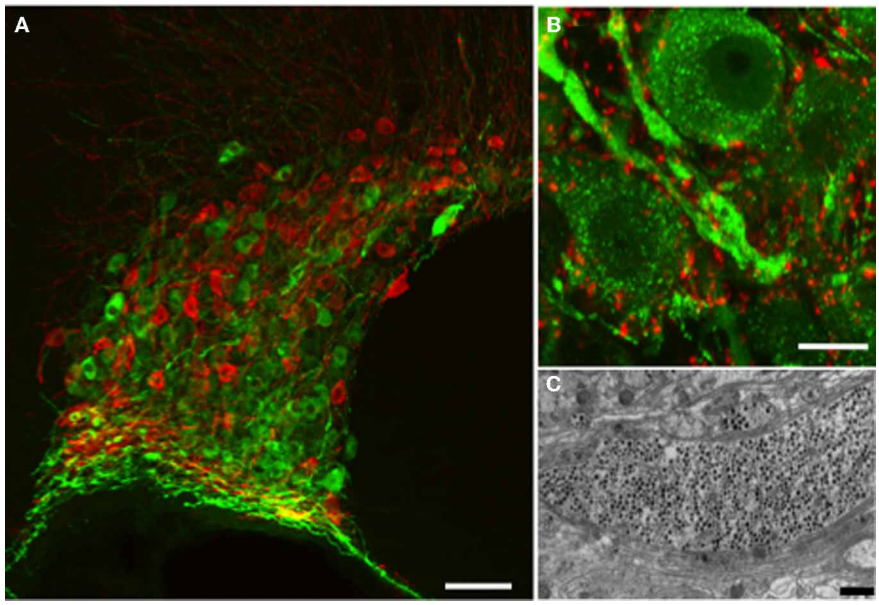

FIGURE 1 | Vasopressin and oxytocin are synthesized by a few thousand large (magnocellular) neurons (vasopressin cells are immunostained with fluo escent green and oxytocin cells with fluo escent red) whose cell bodies are located mainly in the supraoptic (A) and paraventricular (not shown) nuclei of the hypothalamus. (B) The vasopressin immunostaining is punctate and represents individual or aggregates of large dense-cored vesicles. In the dendrite thickenings the vesicles are particularly abundant. Strong punctuate staining of VAMP2 (red labeling) was seen around the vasopressin and oxytocin (not shown) somata and dendrites, however there was no co-localization with the peptide suggesting labeling of pre-synaptic terminals. **(C)** Large dense-core vesicles in an electron microscopic section of a dendrite appear as dark, round, membrane-bound organelles (black dots). Scale bars show **(A)** 100, **(B)** 10, and **(C)** 1 μm respectively.

release (Landgraf, 1995; Ludwig, 1998; Ludwig and Pittman, 2003; Landgraf and Neumann, 2004). Here we focus on the roles of actin remodeling, voltage operated calcium channels (VOCCs) and SNARE proteins in the regulation of somato-dendritic and axon terminal release.

AUTOREGULATION AND PRIMING

Exocytosis of oxytocin and vasopressin from the neurohypophysis results from calcium entry via voltage-gated channels following depolarization of the terminals by invading action potentials (Leng et al., 1999) (**Figure 2**). By contrast, some chemical signals, notably oxytocin itself, can elicit dendritic release without increasing the electrical activity of the neurons. In particular, activation of G-protein coupled receptors on the dendrites can elevate intracellular $[Ca^{2+}]$ enough to trigger exocytosis of LDCVs from the soma and dendrites (**Figure 2**). Oxytocin neurons express oxytocin receptors (Freund-Mercier et al., 1994), and activation of these receptors mobilises calcium from thapsigargin-sensitive intracellular stores, producing a rise in intracellular $[Ca^{2+}]$ that can trigger dendritic oxytocin release (Lambert et al., 1994). Thus, once triggered, dendritic oxytocin release can be self-sustaining and hence long-lasting (Ludwig and Leng, 2006). This self-sustaining nature of oxytocin release and its physiological role has been demonstrated in parturient rats. During parturition, oxytocin is released from the SON and this drives the pulsatile release of oxytocin into the periphery to cause uterine contractions and thus regulate pup delivery. Infusion of an oxytocin receptor antagonist into the SON during parturition significantly reduced SON oxytocin release, and delayed further pup delivery (Neumann et al., 1996).

As vasopressin neurons similarly express receptors for vasopressin, part of the function of dendritic release involves auto-regulation of neuronal activity, either by acting directly (Gouzenes et al., 1998), or indirectly, by regulating afferent inputs (Kombian et al., 1997, 2002; Curras-Collazo et al., 2003). For oxytocin neurons, this presynaptic action is partly mediated by oxytocin-induced production of endocannabinoids (Hirasawa et al., 2004), acting at CB1 receptors on presynaptic glutamatergic terminals. These effects act on different spatial and temporal scales, and one important consequence is the emergence of intense, synchronous bursting activity, the key phenomenon that underpins the milk-ejection reflex (Rossoni et al., 2008). For vasopressin cells, the autoregulatory effects are different, but are also complex, because vasopressin is inhibitory to active vasopressin cells but excitatory to inactive cells (Gouzenes et al., 1998). Thus, vasopressin release tends to reduce the heterogeneity of firing rates amongst vasopressin cells, and this may be an important load-sharing mechanism during sustained secretory demand, such as dehydration (Leng et al., 2008b).

How much dendritic release occurs in response to electrical activity depends on the extent to which the vesicle pools in the dendrites are available for release. In magnocellular neurons, increases in intracellular $[Ca^{2+}]$ induced by agents such as thapsigargin or cyclopiazonic acid, which block calcium re-uptake into intracellular calcium stores and hence result in

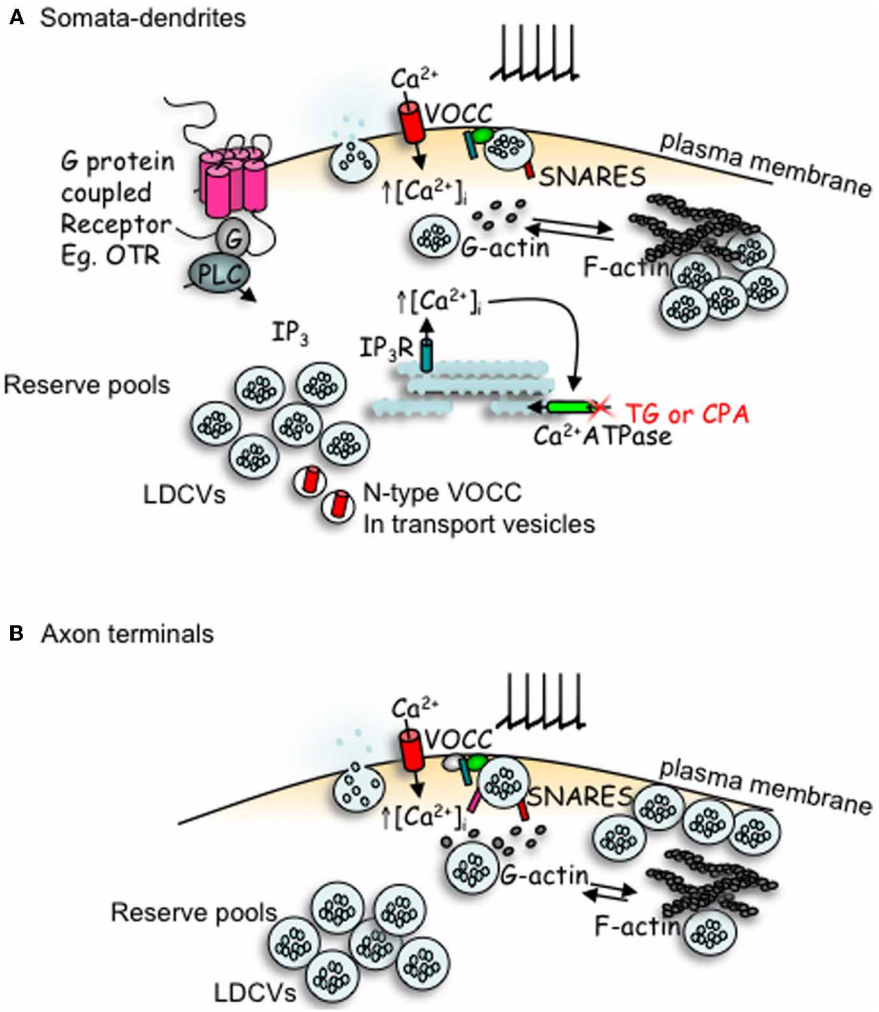

FIGURE 2 | Comparison of peptides release from somata-dendrites (A) and axon terminals (B) of magnocellular neurons. Depolarization induced calcium entry via voltage-operated calcium channels (VOCCs) stimulates peptide release from large dense-cored vesicles (LDCVs). In the somata-dendrites this requires the depolymerization of F-actin to G-actin. The stimulation of G-protein coupled receptors, such as the oxytocin receptor (OTR), stimulates the mobilization of calcium from intracellular stores and an increase in both the number of LDCVs and N-type channels at the plasma membrane which primes release for subsequent activity-dependent release. In contrast, release from axon terminal appears more simple; LDCV movement utilizes actin depolymerization, but release does not depend upon it. Although some members of the SNARE family are detectable by immunocytochemistry in both compartments, there appears to be a lack of VAMP, SNAP-25 and synaptotagmin-1 in the somata-dendrites, with their function perhaps being replaced by other SNARE proteins.

a large, transient increase in intracellular [Ca^{2+}], result in the preparation ("priming") of dendritic vesicle pools for subsequent activity-dependent release (Ludwig et al., 2002, 2005) (**Figure 2**). This priming is not a consequence of elevation of intracellular [Ca^{2+}] *per se*, as priming is detected well after the increase in intracellular [Ca^{2+}] has returned to baseline levels (Lambert et al., 1994), and as depolarization-induced increases in intracellular [Ca^{2+}] do not result in priming. Priming involves *preparing* a system for some anticipated trigger that will come at some uncertain time in the future; it involves making the secretory pool of the target cell available for rapid release in response to that future trigger. In particular, oxytocin binding to oxytocin neurons has been shown to prime dendritic oxytocin release (Ludwig et al., 2002).

Analogous priming occurs in some endocrine cells. In the anterior pituitary of oestrogen-primed female rats, luteinising hormone releasing hormone (LHRH) is capable of "self-priming" gonadotrophs, causing a potentiation of luteinising hormone release in response to successive challenges with LHRH. This priming is delayed and long-lasting, and involves translocation of LDCVs to docking sites at the plasma membrane (Thomas and Clarke, 1997; Leng et al., 2008a). Priming in magnocellular neurons similarly involves a recruitment of LDCVs from a reserve pool into a readily-releasable pool (Tobin et al., 2004), but also involves a recruitment of VOCCs (Tobin et al., 2011). Priming does not appear to require either *de novo* transcription or translation (Tobin and Ludwig, 2007a).

F-ACTIN

Because peptide release from magnocellular neurons is not restricted to any particular part of the plasma membrane (Morris and Pow, 1991), regulation depends on controlling the access of vesicles to the plasma membrane, and in endocrine cells this control is exerted by cytoskeletal elements (Morgan, 1995; Park and Loh, 2008). Many secretory cells possess a network of cortical polymerized actin (filamentous or F-actin) in the subplasmalemal space. Cortical F-actin is often described as a barrier, as it is thought to anchor the LDCVs and regulate their availability for docking at the plasma membrane (Goddette and Frieden, 1986; Vitale et al., 1995; Ehre et al., 2005). Consistent with this idea, F-actin undergoes fast, transient and reversible depolymerization during exocytosis from many cells (Cheek and Burgoyne, 1986; Nakata and Hirokawa, 1992; Trifaro et al., 2000) and areas of exocytosis have been shown to be void of F-actin (Goddette and Frieden, 1986; Nakata and Hirokawa, 1992). In general, release of neurotransmitters from axon terminals is increased after F-actin depolymerization (Morales et al., 2000; Sankaranarayanan et al., 2003). Similarly, in chromaffin cells, depolymerization of F-actin increases the translocation of vesicles to the plasma membrane (Vitale et al., 1995) and polymerization of actin inhibits exocytosis (Zhang et al., 1995). However, depolymerization of F-actin *inhibits* release from PC12 cells (Matter et al., 1989), HIT insulin-secreting cells (Li et al., 1994) and mast cells (Pendleton and Koffer, 2001). Thus, F-actin can also facilitate vesicle fusion for release, depending on the cell type or time course of measured response.

As well as a network throughout the cytoplasm, the cell bodies of magnocellular neurons possess a network of F-actin beneath the plasma membrane (Tobin and Ludwig, 2007b). Actin depolymerization can stimulate peptide release from both the dendritic and axonal compartments, consistent with the idea of cortical actin acting as a barrier for LDCVs to access release sites. Concomitant actin polymerization or depolymerization does not affect secretion from the axon terminals, but release from the dendrites is inhibited by actin polymerization and potentiated by actin depolymerization. Thus, depolarization-evoked release from the dendrites, unlike that from the axon terminals, *requires* actin depolymerization. It has previously been suggested that a cortical F-actin network might separate vesicles into a small readily releasable pool and a larger reserve pool (Trifaro et al., 2000).

The role of actin in regulating the availability of LDCVs for dendritic release is highlighted by the observation that actin depolymerization potentiates depolarization-evoked dendritic release, yet blocks thapsigargin-induced priming. In hippocampal neurons, F-actin polymerization potentiates thapsigargin-induced increases in intracellular $[Ca^{2+}]$ (Wang et al., 2002), so it seems unlikely that the block of priming is because of an effect on calcium mobilization.

F-actin might facilitate release either by providing "tracks" that permit the docking of vesicles at appropriate membrane sites, or by spatially constraining components of the exocytotic machinery. This suggests that activation of release involves a reorganization of F-actin which allows the vesicles access to the exocytotic sites and provides the structural support necessary for exocytosis. In the magnocellular system, it appears that F-actin remodeling regulates the availability of mature and readily-releasable vesicles in different parts of the cell, and thus may be involved in the differential control of release from different parts of the cell.

VOLTAGE OPERATED CALCIUM CHANNELS

Like axon terminal release, dendritic release of oxytocin and vasopressin depends on the entry of calcium into the cell (Neumann et al., 1993; Shibuya et al., 1998; de Kock et al., 2003) via VOCCs (Fisher and Bourque, 1996). Whereas terminal secretion is very sensitive to the frequency of action potentials, dendritic release is normally less tightly coupled to action potential events (Leng and Ludwig, 2008), but depolarization-induced dendritic release can be primed by a prior mobilization of intracellular calcium (Ludwig et al., 2002, 2005). This mechanism is absent from the axon terminals of magnocellular neurones, which lack thapsigargin-sensitive calcium stores. In some systems, neuronal synaptic release of neurotransmitters can be potentiated by a recruitment of VOCCs to the active zone, increasing calcium entry upon depolarization. Thus, one target for priming may be a change in the number and/or activity of VOCCs or an increased proximity of channels to docked vesicles (Becherer et al., 2003).

Magnocellular neurons express several types of VOCC (Foehring and Armstrong, 1996; Joux et al., 2001), but one subtype in particular, the N-type channels, appears to be particularly important for dendritic release. Although the current carried by N-type channels is comparatively minor in magnocellular somata compared to the other VOCC types or indeed the whole-cell calcium current (Joux et al., 2001; Tobin et al., 2011), release of oxytocin from SONs is most sensitive to blockade of N-type channels. This suggests that a change in the expression and/or activity of VOCCs might underlie priming, and indeed, thapsigargin treatment significantly increases the calcium current carried by N-type channels as a proportion of the whole-cell calcium current (Tobin et al., 2011).

As mentioned, priming does not require *de novo* transcription or translation, arguing against new channels or channel constituents being made. Therefore, the potential mechanisms are either that existing N-type channels at the plasma membrane carry more charge per channel, or that more N-type channels are inserted into the membrane. The latter is more likely, as there is no change in the voltage-dependent activity of the N-type channels after priming, and suggests that there is a "reserve pool" of channels (Tobin et al., 2011).

We observed a strong perinuclear immunocytochemical signal for N-type channels in both oxytocin and vasopressin somata. Differentiated neuroblastoma, neuronal and endocrine cell types all contain an intracellular pool of recruitable N-type channels which can be translocated to the plasma membrane (Passafaro et al., 1994, 1998; Sher et al., 1998). This suggests the presence of a channel reserve pool via which a neuron can increase the number of cell surface VOCCs, for example during synaptogenesis or, as in this case, to increase secretory responsiveness. In neuroendocrine bag cell neurons of *Aplysia californica*, actin-dependent translocation of VOCCs from the central region of a growth cone into the plasma membrane of the growth cone is an important part of the process of transformation into mature neurosecretory endings (Knox et al., 1992; Zhang et al., 2008). Recruitment of N-type

channels on peptide-containing LDCVs seems unlikely, as there is not a strong co-localization of the N-type channel and either oxytocin or vasopressin (Tobin et al., 2011). Thus, the priming signal stimulates the translocation of both peptide-containing LDCVs and N-type channels in parallel.

The particular involvement of one type of VOCC with a secretory response has previously been demonstrated with the involvement of L-type channels in somato-dendritic vasopressin release by pituitary adenylate cyclase activating polypeptide (PACAP) (Shibuya et al., 1998), R-type channels with the axon terminal release of oxytocin (Wang et al., 1999) and P/Q-type channels with vasopressin secretion (Wang et al., 1997). The requirement for somato-dendritic release of calcium entry through mainly L- and N-type channels has been shown for other transmitters, including dynorphin (Simmons et al., 1995), dopamine (Kim et al., 2009; Mendez et al., 2011) and serotonin (De-Miguel and Trueta, 2005).

As previously reviewed (Catterall, 2000; Felix, 2005) VOCC activity can be acutely modulated by events such as phosphorylation/de-phosphorylation or by interaction (via G-proteins) with other membrane receptors. These rapid modulatory events occur, and revert, within a time-scale of a few milliseconds to minutes. By contrast, gonadotrophs also show a steroid-dependent modulation of VOCCs which occurs over a much longer time-scale (24–36 h). Treating gonadotrophs with estradiol produces a time-dependent change in secretory responsiveness which mimics the pre-ovulatory luteinizing hormone surge. This treatment also stimulates a parallel change in the calcium current (Heyward and Clarke, 1995) that depends on the synthesis of new VOCCs and their insertion into the plasma membrane, and this change is a prerequisite for gonadotrophs to display the self-priming response to LHRH. Here, we suggest that a stimulus that produces an increased secretory responsiveness with an intermediate time scale (30–90 min) may cause magnocellular neurons to recruit N-type channels to the plasma membrane, allowing them to respond to a subsequent depolarization with a larger secretory response.

SNARE PROTEINS

The stimulated release of both LDCVs and synaptic vesicles involves the N-ethylmaleimide sensitive fusion protein attachment protein receptor (SNARE) complex, which allows the vesicle membrane to fuse with the plasma membrane. The roles in dendritic release of the protein members which comprise this complex have been reviewed recently (Ovsepian and Dolly, 2011). The basic configuration of this complex comprises a vesicle associated membrane protein-2 (VAMP2), syntaxin-1 and soluble N-ethylmaleimide attachment protein-25 (SNAP25) (or other members of the VAMP, syntaxin or SNAP families). Other proteins regulate the activity of these core proteins (e.g., munc18 regulating syntaxin-1), or act as calcium sensors (e.g., synaptotagmin-1). Some of these proteins, including VAMP-2, are targeted to exocytosis sites by being inserted into the coat of the vesicle, others, including RIM, bassoon and piccolo, are targeted to the pre-synaptic area and assembled into specialized zones of release by the cytomatrix proteins (tom Dieck et al., 1998; Fenster et al., 2000).

Despite their ability to release LDCVs, the magnocellular neuron dendrites showed a surprising lack of some of these core proteins. We (Tobin et al., 2012) and others (Deleuze et al., 2005) did not detect any immunocytochemical signal for VAMP-2 despite abundant signal surrounding these cells on pre-synaptic contacts (**Figure 1**). In fact, we did not detect co-localization of any VAMP family member with either peptide, as would be expected for a protein inserted into the vesicle coat. We also failed to detect SNAP-25, but did detect syntaxin-1 and munc-18. Although we detected all of these in the axon terminals, the resolution did not allow us to determine if the terminal VAMP-2 was associated with LDCVs. An earlier study using electron microscopy also failed to demonstrate an association between LDCVs and VAMP-2 in the terminals (Zhang et al., 2000).

Although they express VAMP-2 and SNAP-25, gonadotrophs lack an immunocytochemically-detectable signal for syntaxin-1 (Thomas et al., 1998). Knock-out of syntaxin 1A was not lethal in mice, and although synaptic plasticity was impaired, basic synaptic release appeared normal (Fujiwara et al., 2006). Although knock-out of either SNAP-25 or VAMP-2 in mice was lethal after birth, *in vitro* recordings from embryonic brains showed compromised but not ablated evoked synaptic release, as well as reduced spontaneous release. Significantly in all three cases, there was no compensatory expression of other SNARE proteins (Schoch et al., 2001; Washbourne et al., 2002). Perhaps there are more members or isoforms of the existing members to be identified, but for the time being somato-dendritic peptide release from these magnocellular neurons and anterior pituitary gonadotrophs appear to occur in the absence of the full complement of exocytotic machinery considered to be mandatory.

ACKNOWLEDGMENTS

Work was supported by a BBSRC grant.

REFERENCES

Becherer, U., Moser, T., Stuhmer, W., and Oheim, M. (2003). Calcium regulated exocytosis at the level of single vesicles. *Nat. Neurosci.* 6, 846–853.

Catterall, W. A. (2000). Structure and regulation of voltage-gated Ca^{2+} channels. *Annu. Rev. Cell Dev. Biol.* 16, 521–555.

Cheek, T. R., and Burgoyne, R. D. (1986). Nicotine-evoked disassembly of cortical actin filaments in adrenal chromaffin cells. *FEBS Lett.* 207, 110–114.

Curras-Collazo, M. C., Gillard, E. R., Jin, J., and Pandika, J. (2003). Vasopressin and oxytocin decrease excitatory amino acid release in adult rat supraoptic nucleus. *J. Neuroendocrinol.* 15, 182–190.

de Kock, C. P., Wierda, K. D., Bosman, L. W., Min, R., Koksma, J. J., Mansvelder, H. D., Verhage, M., and Brussaard, A. B. (2003). Somatodendritic secretion in oxytocin neurons is upregulated during the female reproductive cycle. *J. Neurosci.* 23, 2726–2734.

Deleuze, C., Alonso, G., Lefevre, I. A., Duvoid-Guillou, A., and Hussy, N. (2005). Extrasynaptic localization of glycine receptors in the rat supraoptic nucleus: further evidence for their involvement in glia-to-neuron communication. *Neuroscience* 133, 175–183.

De-Miguel, F. F., and Trueta, C. (2005). Synaptic and extrasynaptic secretion of serotonin. *Cell Mol. Neurobiol.* 25, 297–312.

Ehre, C., Rossi, A. H., Abdullah, L. H., De Pestel, K., Hill, S., Olsen, J. C., and Davis, C. W. (2005). Barrier role of actin filaments in regulated mucin secretion from airway goblet cells. *Am. J. Physiol. Cell Physiol.* 288, C46–C56.

Felix, R. (2005). Molecular regulation of voltage-gated Ca2+ channels. *J. Recept. Signal Transduct. Res.* 25, 57–71.

Fenster, S. D., Chung, W. J., Zhai, R., Cases-Langhoff, C., Voss, B., Garner, A. M., Kaempf, U., Kindler, S., Gundelfinger, E. D., and Garner, C. C. (2000). Piccolo, a presynaptic zinc finger protein structurally related to bassoon. *Neuron* 25, 203–214.

Fisher, T. E., and Bourque, C. W. (1996). Calcium-channel subtypes in the somata and axon terminals of magnocellular neurosecretory cells. *Trends Neurosci.* 19, 440–444.

Foehring, R. C., and Armstrong, W. E. (1996). Pharmacological dissection of high-voltage-activated Ca^{2+} current types in acutely dissociated rat supraoptic magnocellular neurons. *J. Neurophysiol.* 76, 977–983.

Freund-Mercier, M. J., Stoeckel, M. E., and Klein, M. J. (1994). Oxytocin receptors on oxytocin neurones: histoautoradiographic detection in the lactating rat. *J. Physiol.* 480, 155–161.

Fujiwara, T., Mishima, T., Kofuji, T., Chiba, T., Tanaka, K., Yamamoto, A., and Akagawa, K. (2006). Analysis of knock-out mice to determine the role of HPC-1/Synatxin 1A in expressing synaptic plasticity. *J. Neurosci.* 26, 5767–5776.

Goddette, D. W., and Frieden, C. (1986). Actin polymerization. The mechanism of action of cytochalasin D. *J. Biol. Chem.* 261, 15974–15980.

Gouzenes, L., Desarmenien, M. G., Hussy, N., Richard, P., and Moos, F. C. (1998). Vasopressin regularizes the phasic firing pattern of rat hypothalamic magnocellular vasopressin neurons. *J. Neurosci.* 18, 1879–1885.

Heyward, P. M., and Clarke, I. J. (1995). A transient effect of estrogen on calcium currents and electrophysiological responses to gonadotropin-releasing hormone in ovine gonadotropes. *Neuroendocrinology* 62, 543–552.

Hirasawa, M., Schwab, Y., Natah, S., Hillard, C. J., Mackie, K., Sharkey, K. A., and Pittman, Q. J. (2004). Dendritically released transmitters cooperate via autocrine and retrograde actions to inhibit afferent excitation in rat brain. *J. Physiol.* 559, 611–624.

Joux, N., Chevaleyre, V., Alonso, G., Boissin-Agasse, L., Moos, F. C., Desarmenien, M. G., and Hussy, N. (2001). High voltage-activated Ca^{2+} currents in rat supraoptic neurones: biophysical properties and expression of the various channel alpha1 subunits. *J. Neuroendocrinol.* 13, 638–649.

Kim, Y., Park, M. K., and Chung, S. (2009). Regulation of somatodendritic dopamine release by corticotropin-releasing factor via the inhibition of voltage-operated Ca^{2+} channels. *Neurosci. Lett.* 465, 31–35.

Knox, R. J., Quattrocki, E. A., Connor, J. A., and Kaczmarek, L. K. (1992). Recruitment of Ca^{2+} channels by protein kinase c during rapid formation of putative neuropeptide release sites in isolated aplysia neurons. *Neuron* 8, 883–889.

Kombian, S. B., Hirasawa, M., Mouginot, D., and Pittman, Q. J. (2002). Modulation of synaptic transmission by oxytocin and vasopressin in the supraoptic nucleus. *Prog. Brain Res.* 139, 235–246.

Kombian, S. B., Mouginot, D., and Pittman, Q. J. (1997). Dendritically released peptides act as retrograde modulators of afferent excitation in the supraoptic nucleus *in vitro*. *Neuron* 19, 903–912.

Lambert, R. C., Dayanithi, G., Moos, F. C., and Richard, P. (1994). A rise in the intracellular Ca^{2+} concentration of isolated rat supraoptic cells in response to oxytocin. *J. Physiol.* 478, 275–287.

Landgraf, R. (1995). Intracerebrally released vasopressin and oxytocin: measurement, mechanisms and behavioural consequences. *J. Neuroendocrinol.* 7, 243–253.

Landgraf, R., and Neumann, I. D. (2004). Neuropeptide release within the brain: a dynamic concept of multiple and variable modes of communication. *Front. Neuroendocrinol.* 25:150–176. doi: 10.1016/j.yfrne.2004.05.001

Leng, G., Brown, C. H., and Russell, J. A. (1999). Physiological pathways regulating the activity of magnocellular neurosecretory cells. *Prog. Neurobiol.* 57, 625–655.

Leng, G., Caquineau, C., and Ludwig, M. (2008a). Priming in oxytocin cells and in gonadotrophs. *Neurochem. Res.* 33, 668–677.

Leng, G., Brown, C., Sabatier, N., and Scott, V. (2008b). Population dynamics in vasopressin neurons. *Neuroendocrinology* 88, 160–172.

Leng, G., and Ludwig, M. (2008). Neurotransmitters and peptides: whispered secrets and public announcements. *J. Physiol.* 586, 5625–5632.

Li, G., Rungger-Brandle, E., Just, I., Jonas, J. C., Aktories, K., and Wollheim, C. B. (1994). Effect of disruption of actin filaments by clostridium botulinum c2 toxin on insulin secretion in hit-t15 cells and pancreatic islets. *Mol. Biol. Cell* 5, 1199–1213.

Ludwig, M. (1998). Dendritic release of vasopressin and oxytocin. *J. Neuroendocrinol.* 10, 881–895.

Ludwig, M., Bull, P. M., Tobin, V. A., Sabatier, N., Landgraf, R., Dayanithi, G., and Leng, G. (2005). Regulation of activity-dependent dendritic vasopressin release from rat supraoptic neurones. *J. Physiol.* 564, 515–522.

Ludwig, M., Horn, T., Callahan, M. F., Grosche, A., Morris, M., and Landgraf, R. (1994). Osmotic stimulation of the supraoptic nucleus: central and peripheral vasopressin release and blood pressure. *Am. J. Physiol.* 266, E351–E356.

Ludwig, M., and Leng, G. (2006). Dendritic peptide release and peptide-dependent behaviours. *Nat. Rev. Neurosci.* 7, 126–136.

Ludwig, M., and Pittman, Q. J. (2003). Talking back: dendritic neurotransmitter release. *Trends Neurosci.* 26, 255–261.

Ludwig, M., Sabatier, N., Bull, P. M., Landgraf, R., Dayanithi, G., and Leng, G. (2002). Intracellular calcium stores regulate activity-dependent neuropeptide release from dendrites. *Nature* 418, 85–89.

Matter, K., Dreyer, F., and Aktories, K. (1989). Actin involvement in exocytosis from pc12 cells: studies on the influence of botulinum c2 toxin on stimulated noradrenaline release. *J. Neurochem.* 52, 370–376.

Mendez, J. A., Bourque, M. J., Fasano, C., and Trudeua, L. E. (2011). Somatodendritic dopamine release requires synaptotagmin 4 and 7 and the participation of voltage-gated calcium channels. *J. Biol. Chem.* 286, 23928–23937.

Moos, F., Poulain, D. A., Rodriguez, F., Guerne, Y., Vincent, J. D., and Richard, P. (1989). Release of oxytocin within the supraoptic nucleus during the milk ejection reflex in rats. *Exp. Brain Res.* 76, 593–602.

Morales, M., Colicos, M. A., and Goda, Y. (2000). Actin-dependent regulation of neurotransmitter release at central synapses. *Neuron* 27, 539–550.

Morgan, A. (1995). Exocytosis. *Essays Biochem.* 30, 77–95.

Morris, J. F., and Pow, D. V. (1991). Widespread release of peptides in the central nervous system: quantitation of tannic acid-captured exocytoses. *Anat. Rec.* 231, 437–445.

Nakata, T., and Hirokawa, N. (1992). Organization of cortical cytoskeleton of cultured chromaffin cells and involvement in secretion as revealed by quick-freeze, deep-etching, and double-label immunoelectron microscopy. *J. Neurosci.* 12, 2186–2197.

Neumann, I., Douglas, A. J., Pittman, Q. J., Russell, J. A., and Landgraf, R. (1996). Oxytocin released within the supraoptic nucleus of the rat brain by positive feedback action is involved in parturition-related events. *J. Neuroendocrinol.* 8, 227–233.

Neumann, I., Russell, J. A., and Landgraf, R. (1993). Oxytocin and vasopressin release within the supraoptic and paraventricular nuclei of pregnant, parturient and lactating rats: a microdialysis study. *Neuroscience* 53, 65–75.

Ovsepian, S. V., and Dolly, J. O. (2011). Dendritic snares add a new twist to the old neuron theory. *Proc. Natl. Acad. Sci. U.S.A.* 108, 19113–19120.

Park, J. J., and Loh, Y. P. (2008). How peptide hormone vesicle are transported to the secretion site for exocytosis. *Mol. Endocrinol.* 22, 2583–2595.

Passafaro, M., Clementi, F., Pollo, A., Carbone, E., and Sher, E. (1994). Omega-conotoxin and cd2+stimulate the recruitment to the plasmamembrane of an intracellular pool of voltage-operated Ca^{2+} channels. *Neuron* 12, 317–326.

Passafaro, M., Taverna, E., Morlacchi, E., Rosa, P., Clementi, F., and Sher, E. (1998). Transient translocation of N-type calcium channels from secretory granules to the cell surface. *Ann. N.Y. Acad. Sci.* 841, 119–121.

Pendleton, A., and Koffer, A. (2001). Effects of latrunculin reveal requirements for the actin cytoskeleton during secretion from mast cells. *Cell Motil. Cytoskeleton* 48, 37–51.

Pow, D. V., and Morris, J. F. (1989). Dendrites of hypothalamic magnocellular neurons release neurohypophysial peptides by exocytosis. *Neuroscience* 32, 435–439.

Rossoni, E., Feng, J., Tirozzi, B., Brown, D., Leng, G., and Moos, F. (2008). Emergent synchronous bursting of oxytocin neuronal network. *PLoS Comput. Biol.* 18, 4:e1000123.

Sankaranarayanan, S., Atluri, P. P., and Ryan, T. A. (2003). Actin has a molecular scaffolding, not propulsive, role in presynaptic function. *Nat. Neurosci.* 6, 127–135.

Schoch, S., Deak, F., Konigstorfer, A., Mozhayeva, M., Sara, Y., Sudhof, T. C., and Kavalati, E. T. (2001). *Science* 294, 1117–1122.

Sher, E., Rosa, P., Francolini, M., Codignola, A., Morlacchi, E., Taverna, E., Giovannini, F.,

Brioschi, A., Clementi, F., McEnery, M. W., and Passafaro, M. (1998). Metabolism and trafficking of N-type voltage-operated calcium channels in neurosecretory cells. *J. Bioenerg. Biomembr.* 30, 399–407.

Shibuya, I., Noguchi, J., Tanaka, K., Harayama, N., Inoue, U., Kabashima, N., Ueta, Y., Hattori, Y., and Yamashita, H. (1998). Pacap increases the cytosolic Ca^{2+} concentration and stimulates somatodendritic vasopressin release in rat supraoptic neurons. *J. Neuroendocrinol.* 10, 31–42.

Simmons, M. L., Terman, G. W., Gibbs, S. M., and Chavkin, C. (1995). L-type calcium channels mediate dynorphin neuropeptide release from dendrites but not axons of hippocampal granule cells. *Neuron* 14, 1265–1272.

Thomas, S. G., and Clarke, I. J. (1997). The positive feedback action of estrogen mobilizes LH-containing, but not FSH-containing secretory granules in ovine gonadotropes. *Endocrinology* 138, 1347–1350.

Thomas, S. G., Takahashi, M., Neill, J. D., and Clarke, I. J. (1998). Components of the neuronal exocytotic machinery in the anterior pituitary of the ovariectomised ewe and the effects of oestrogen in gonadotropes as studied with confocal microscopy. *Neuroendocrinology* 67, 244–259.

Tobin, V., Schwab, Y., Lelos, N., Onaka, T., Pittman, Q. J., and Ludwig, M. (2012). Expression of exocytosis proteins in rat supraoptic nucleus neurones. *J. Neuroendocrinol.* 24, 629–641.

Tobin, V. A., Douglas, A. J., Leng, G., and Ludwig, M. (2011). The involvement of voltage-operated calcium channels in somato-dendritic oxytocin release. *PLoS ONE* 6:e25366. doi: 10.1371/journal.pone.0025366

Tobin, V. A., Hurst, G., Norrie, L., Dal Rio, F. P., Bull, P. M., and Ludwig, M. (2004). Thapsigargin-induced mobilization of dendritic dense-cored vesicles in rat supraoptic neurons. *Eur. J. Neurosci.* 19, 2909–2912.

Tobin, V. A., and Ludwig, M. (2007a). The actin filament and dendritic peptide release. *Biochem. Soc. Trans.* 35, 1243–1246.

Tobin, V. A., and Ludwig, M. (2007b). The role of the actin cytoskeleton in oxytocin and vasopressin release from rat supraoptic nucleus neurons. *J. Physiol.* 582, 1337–1348.

tom Dieck, S., Sanmarti-Vila, L., Langnaese, K., Richter, K., Kindler, S., Soyke, A., Wex, H., Smalla, K. H., Kampf, U., Franzer, J. T., Stumm, M., Garner, C. C., and Gundelfinger, E. D. (1998). Bassoon, a novel zinc-finger CAG/glutamine-repeat protein selectively localized at the active zone of presynaptic nerve terminals. *J. Cell Biol.* 142, 499–509.

Trifaro, J., Rose, S. D., Lejen, T., and Elzagallaai, A. (2000). Two pathways control chromaffin cell cortical f-actin dynamics during exocytosis. *Biochimie* 82, 339–352.

Vitale, M. L., Seward, E. P., and Trifaro, J. M. (1995). Chromaffin cell cortical actin network dynamics control the size of the release-ready vesicle pool and the initial rate of exocytosis. *Neuron* 14, 353–363.

Wang, G., Dayanithi, G., Kim, S., Hom, D., Nadasdi, L., Kristipati, R., Ramachandran, J., Stuenkel, E. L., Nordmann, J. J., Newcomb, R., and Lemos, J. R. (1997). Role of Q-type Ca^{2+} channels in vasopressin secretion from neurohypophysial terminals of the rat. *J. Physiol.* 502, 351–363.

Wang, G., Dayanithi, G., Newcomb, R., and Lemos, J. R. (1999). An R-type Ca^{2+} current in neurohypophysial terminals preferentially regulates oxytocin secretion. *J. Neurosci.* 19, 9235–9241.

Wang, Y., Mattson, M. P., and Furukawa, K. (2002). Endoplasmic reticulum calcium release is modulated by actin polymerization. *J. Neurochem.* 82, 945–952.

Washbourne, P., Thompson, P. M., Carta, M., Costa, E. T., Mathews, J. R., Lopez-Bendito, G., Molnar, Z., Becher, M. W., Valenzuela, C. F., Partridge, L. D., and Wilson, M. C. (2002). Genetic ablation of the t-SNARE SNAP-25 distinguishes mechanisms of neuroexocytosis. *Nat. Neurosci.* 5, 19–26.

Zhang, L., Rodriguez Del Castillo, A., and Trifaro, J. M. (1995). Histamine-evoked chromaffin cell scinderin redistribution, F-actin disassembly, and secretion: in the absence of cortical F-actin disassembly, an increase in intracellular Ca^{2+} fails to trigger exocytosis. *J. Neurochem.* 65, 1297–1308.

Zhang, L., Volknandt, W., Gundelfinger, E. D., and Zimmermann, H. (2000). A comparison of synaptic protein localization in hippocampal mossy fiber terminals and neurosecretory endings of the neurohypophysis using the cryo-immunogold technique. *J. Neurocytol.* 29, 19–30.

Zhang, Y., Helm, J. S., Senatore, A., Spafford, J. D., Kaczmarek, L. K., and Jonas, E. A. (2008). PKC-induced intracellular trafficking of Ca(V)2 precedes its rapid recruitment to the plasma membrane. *J. Neurosci.* 28, 2601–2612.

Conflict of Interest Statement: The authors declare that the research was conducted in the absence of any commercial or financial relationships that could be construed as a potential conflict of interest.

Received: 04 May 2012; paper pending published: 22 May 2012; accepted: 22 June 2012; published online: 12 July 2012.

Citation: Tobin V, Leng G and Ludwig M (2012) The involvement of actin, calcium channels and exocytosis proteins in somato-dendritic oxytocin and vasopressin release. Front. Physio. ***3****:261. doi: 10.3389/fphys.2012.00261*

This article was submitted to Frontiers in Membrane Physiology and Biophysics, a specialty of Frontiers in Physiology.

frontiers in
PHYSIOLOGY

MINI REVIEW ARTICLE
published: 09 July 2012
doi: 10.3389/fphys.2012.00259

Dendritic signaling in inhibitory interneurons: local tuning via group I metabotropic glutamate receptors

Olivier Camiré[1], Jean-Claude Lacaille[2] and Lisa Topolnik[1]*

[1] *Department of Biochemistry, Microbiology and Bioinformatics, Axis of Cellular and Molecular Neuroscience, CRIUSMQ, Université Laval, Québec, PQ, Canada*
[2] *Département de Physiologie and Groupe de Recherche sur le Système Nerveux Central, Université de Montréal, Montréal, PQ, Canada*

Edited by:
Francisco Fernandez De-Miguel, Universidad Nacional Autonoma de Mexico, Mexico

Reviewed by:
Harald Janovjak, Institute of Science and Technology Austria, Austria
Enrique Hernandez-Lemus, National Institute of Genomic Medicine, Mexico

***Correspondence:**
Lisa Topolnik, Department of Biochemistry, Microbiology and Bioinformatics, Axis of Cellular and Molecular Neuroscience, CRIUSMQ, Université Laval, 2601 Ch. De La Canardière, CRULRG, Québec, PQ, Canada G1J 2G3.
e-mail: lisa.topolnik@crulrg.ulaval.ca

Communication between neurons is achieved by rapid signal transduction via highly specialized structural elements known as synaptic contacts. In addition, numerous extrasynaptic mechanisms provide a flexible platform for the local regulation of synaptic signals. For example, peri- and extra-synaptic signaling through the group I metabotropic glutamate receptors (mGluRs) can be involved in the highly compartmentalized regulation of dendritic ion conductances, the induction of input-specific synaptic plasticity, and the local release of retrograde messengers. Therefore, extrasynaptic mechanisms appear to play a key role in the local tuning of dendritic computations. Here, we review recent findings on the role of group I mGluRs in the dendritic signaling of inhibitory interneurons. We propose that group I mGluRs provide a dual-mode signaling device that integrates different patterns of neural activity. By implementing distinct forms of intrinsic and synaptic regulation, group I mGluRs may be responsible for the local fine-tuning of dendritic function.

Keywords: GABAergic interneuron, dendrite, synapse, ion channel, plasticity, metabotropic glutamate receptor

INTRODUCTION

Over a century ago, Santiago Ramón y Cajal postulated the law of dynamic polarization, according to which dendrites represent the receiving apparatus of the neuron (Ramón y Cajal, 1891) that integrates the vast majority of synaptic inputs over time. Since then, dendrites have captured the imagination of many researchers. It is difficult not to marvel at the wide diversity and complexity of dendritic arbors, which resemble distinct kinds of trees in a forest. In addition to their morphological complexity, dendrites exhibit a highly complex functional organization. They are endowed with multiple active ion conductances, which control the integration and propagation of local and global dendritic signals in a highly dynamic manner. Two types of signals are generated in dendrites: electrical and chemical. Both can be compartmentalized within individual dendritic branches, providing a means for the synapse-specific integration and modification of incoming information (reviewed in Branco and Häusser, 2010). GABAergic inhibitory interneurons are well known for their heterogeneity at multiple levels, from structural and physiological properties to their corresponding functions in the network. Not surprisingly, interneuron dendrites also exhibit a highly heterogeneous and complex functional organization, which is determined largely by the cell type, the incoming input, and the patterns of ongoing activity. It has been established that an average hippocampal interneuron may receive up to 17,000 synaptic inputs (Gulyás et al., 1999). In addition, a large repertoire of extrasynaptic mechanisms respond to local changes in activity and allow the efficient control of synaptic integration and signal transduction. These mechanisms involve the activation of extrasynaptic glutamate, GABA, acetylcholine, and monoamine and peptide receptors, which can be located in the presynaptic terminals, dendrites, and astrocytes. The mechanisms underlying extrasynaptic signaling in interneurons and its functional role in the modulation of local circuit activity are currently under intensive investigation.

Here, we review recent work that supports the idea that the integrative properties of interneuron dendrites are controlled via activation of group I metabotropic glutamate receptors (mGluRs), which orchestrate a variety of local processes, including calcium signaling, modulation of specific ion conductances, and several forms of synaptic plasticity (Perez et al., 2001; Lapointe et al., 2003; Topolnik et al., 2006, 2009; Galván et al., 2008; Le Duigou and Kullmann, 2011). As local modulation of dendritic function is important for single neuron computations, defining the factors that control dendritic signaling in interneurons will be crucial to understanding interneuron computations. It is not our intention to discuss the important role of group I mGluRs in the regulation of network activity and in different disease states as these topics have been deeply explored in several recent reviews (Nistri et al., 2006; Bartos et al., 2007; Topolnik and Lacaille, 2009; Ribeiro et al., 2010).

INTEGRATIVE PROPERTIES OF INTERNEURON DENDRITES

As in most neurons, the synaptic inputs received by interneuron dendrites are transformed into electrical signals and conducted to the soma. The degree of the signal propagation and its impact on neuronal output are determined by the dendritic architecture and the passive and active properties of dendrites (Geiger et al., 1997; Emri et al., 2001; Nörenberg et al., 2010). In addition, the amplitude and temporal summation of excitatory postsynaptic potentials (EPSPs) are controlled via the activation of local ion

conductances, which are often distributed non-uniformly along the somatodendritic axis. For example, direct recordings from dendrites of dentate gyrus basket cells (BCs) and hippocampal *Cornu Ammonis* 1 (CA1) oriens–lacunosum-moleculare (O–LMs) interneurons revealed a relatively constant density of dendritic K^+ channels (Martina et al., 2000; Hu et al., 2010). The activation of these channels during synaptic depolarization can speed up the time course of EPSPs and, therefore, control the temporal summation of synaptic inputs and the time window for spike generation in interneurons (Fricker and Miles, 2000; Galarreta and Hestrin, 2001). Furthermore, distinct distribution of dendritic Na^+ channels in BCs vs O–LMs can also affect the amplification of sub-threshold synaptic inputs and spike initiation and propagation. For example, a steep distance-dependent decay of Na^+ channels is found in dendrites of BCs. Accordingly, Na^+ spikes can only be initiated in the BC axon but not in its dendrites (Hu et al., 2010). The situation is different however in O–LM interneurons. The estimated density of Na^+ channels in these cells is threefold larger than in pyramidal cell dendrites (Stuart and Sakmann, 1994; Martina et al., 2000). Accordingly, Na^+ spikes can be initiated in dendritic sites and can propagate over somatodendritic domain with a relatively constant amplitude and time course.

The propagation of an action potential into neuronal dendrites has a major impact on synaptic input integration and plasticity. These functions of the backpropagating action potential (bAP) are associated with significant depolarization and calcium (Ca^{2+}) entry resulting from the activation of voltage-gated Ca^{2+} mechanisms. The properties of bAP-evoked Ca^{2+} transients (bAP-CaTs) vary between types of neurons, depending on dendritic geometry, the properties and the availability of dendritic voltage-gated channels, the endogenous Ca^{2+}-binding capacity, and level of activity (Kaiser et al., 2001; Sabatini et al., 2002; Goldberg et al., 2003a; Aponte et al., 2008; Evstratova et al., 2011). However, in most GABAergic interneurons, bAP-CaTs are largely attenuated with distance from the soma (Kaiser et al., 2001; Goldberg et al., 2003a; Evstratova et al., 2011). What can be the factors responsible for such proximal compartmentalization of bAP-CaTs? First, as in most neurons, backpropagation of APs in interneurons is likely to be decremental because of dendritic geometry (Rall, 1964; Goldstein and Rall, 1974; Spruston et al., 1995). The complex dendritic profile of most interneurons, with extensive branching close to the soma, may affect the shape of bAPs and result in rapid branch-dependent bAP attenuation (Rall, 1964; Vetter et al., 2001). Second, the differential subcellular distribution of active conductances and their activity-dependent regulation via extrasynaptic mechanisms play an important role in AP backpropagation (Frick et al., 2004; Sjöström and Häusser, 2006; Hu et al., 2010). Because in most interneurons spike propagation is restricted within proximal dendritic branches, the spike-timing-dependent plasticity regulated by bAPs is likely to occur predominantly at proximal synapses. This raises an important question: what kind of associative signal may operate in distally located synapses of interneurons? One possibility is that local Ca^{2+} spikes can control cooperative plasticity in distal dendrites. Ca^{2+} regenerative events (e.g., Ca^{2+} spikes) have been well characterized in pyramidal neurons, where they require the activation of *N*-methyl-D-aspartate (NMDA) receptors, voltage-gated calcium channels (VGCCs), and Na^+ channels (Schiller et al., 1997; Larkum et al., 1999; Golding et al., 2002; Losonczy and Magee, 2006). However, the mechanisms underlying Ca^{2+} spike initiation in distal dendrites of interneurons remain unknown.

In summary, despite the lack of the detailed information regarding the subcellular distribution of distinct ion conductances in different types of interneurons, at least two conclusions can be drawn from the findings reported so far. First, the distribution of active ion conductances may vary among different types of interneurons. Second, dependent on the density of voltage-gated Na^+/Ca^{2+} vs K^+ conductances, two distinct modes of synaptic integration may operate in interneuron dendrites: compartmentalized (different in proximal vs distal sites or within different dendritic branches) or relatively uniform. Accordingly, distinct types of interneurons will be differentially recruited by the inputs innervating different dendritic regions. Local fine-tuning via extrasynaptic mechanisms may provide additional ways for compartmentalized regulation of synaptic integration. In the following sections we will present the evidence for a compartmentalized regulation of interneuron dendritic conductances and synapse-specific plasticity by group I mGluRs.

LOCAL BIOCHEMICAL SIGNALING VIA GROUP I mGluRs

Depending on the level of activity, synaptic inputs can initiate various local biochemical reactions via the activation of synaptic and extrasynaptic signaling mechanisms. In different types of neurons, mGluRs represent the major extrasynaptic signaling platform that couple synaptic activity to various second messengers, including inositol-1,4,5-triphosphate (IP_3), Ca^{2+}, and cyclic adenosine monophosphate (cAMP). Group I mGluRs include two receptor subtypes, mGluR1α and mGluR5, coupled both to the $G\alpha_{q/11}$ G-protein subunit and to activation of phospholipase C, IP_3 production, and intracellular Ca^{2+} release (Pin and Duvoisin, 1995; Hermans and Challiss, 2001). In addition, the coupling of group I mGluRs to alternative cascades, such as cAMP-dependent release of arachidonic acid, has been reported (Aramori and Nakanishi, 1992). Group I mGluRs also partake in G-protein-independent signaling via Src-family tyrosine kinases (Heuss et al., 1999; Gee and Lacaille, 2004; Topolnik et al., 2006). For example, in hippocampal CA1 oriens/alveus (O/A) interneurons, activation of mGluR1α triggers membrane depolarization and dendritic Ca^{2+} transients via a G-protein-independent mechanism involving the Src/extracellular signal-regulated kinase (ERK) cascade (**Figure 1**; Gee and Lacaille, 2004; Topolnik et al., 2006).

Many cell types coexpress mGluR1α and mGluR5, whereas others exhibit specific patterns of distribution of these receptors. In hippocampal CA1 area, mGluR1α is present in several distinct classes of interneurons with their somata located in strata pyramidale, radiatum, and lacunosum moleculare, whereas mGluR5 is expressed uniformly by many cell types (Baude et al., 1993; Lujan et al., 1996; Shigemoto et al., 1997; van Hooft et al., 2000; Ferraguti et al., 2004). However, mGluR1α and mGluR5 may populate distinct dendritic sites (Topolnik et al., 2006). Differential group I mGluR expression was also found in layer IV of the somatosensory cortex, in fast-spiking and regularly spiking interneurons (Sun et al., 2009). Furthermore, using immunogold localization, group I mGluRs have been shown to concentrate in perisynaptic areas

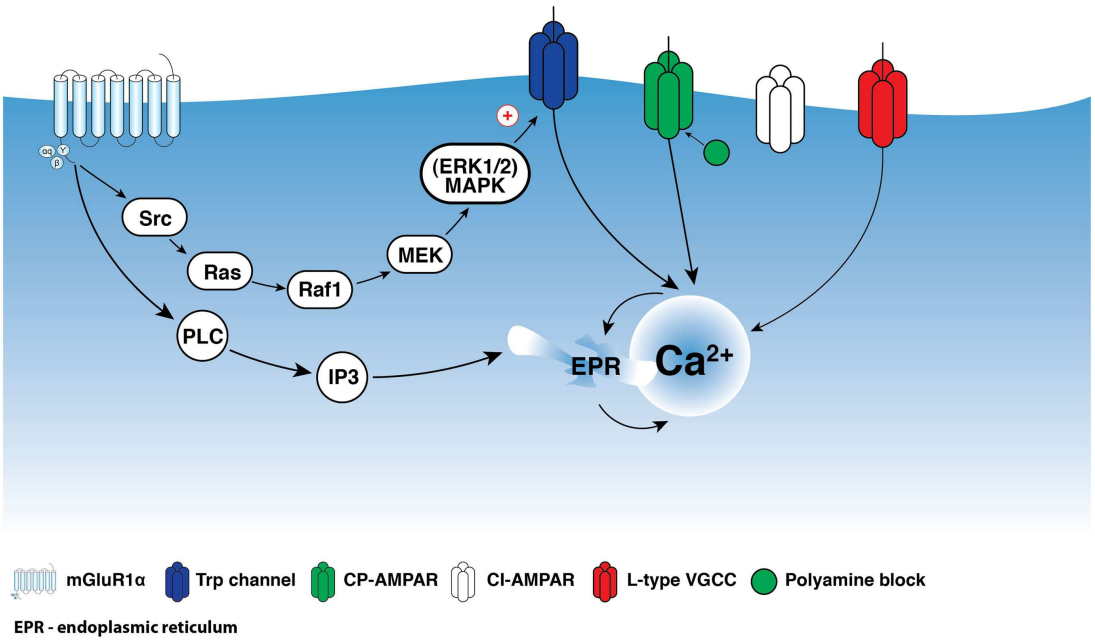

FIGURE 1 | Schematic representation of mGluR1α signaling in interneuron dendrites. Activation of mGluR1α is coupled to two parallel signaling pathways: one leading to Ca^{2+} entry via TRP channels and a second producing Ca^{2+} release from intracellular stores. Src/ERK-cascade appears to be involved in the regulation of Ca^{2+} entry via TRP channels, which together with intracellular release are necessary for the induction of Hebbian LTP. In addition, mGluR1α activation together with Ca^{2+} entry through CP-AMPARs appear to be involved in anti-Hebbian LTP induction.

(surrounding synaptically located ionotropic receptors) in Purkinje cells (Nusser et al., 1994), hippocampal neurons (Baude et al., 1993; Lujan et al., 1996), neurons of the dorsal horn of the spinal cord (Vidnyánszky et al., 1994), and neurons of the subthalamic nucleus (Kuwajima et al., 2004). The subcellular localization of these receptors is controlled by their direct interaction with Homer proteins (Brakeman et al., 1997).

The recruitment of group I mGluRs depends on both pre- and post-synaptic activity. In hippocampal interneurons, high-frequency repetitive synaptic stimulation is required to evoke responses mediated by group I mGluRs (Topolnik et al., 2005). It has been demonstrated that the inhibition of the activity of astrocytic glutamate transporters, i.e., increase of the availability of extrasynaptic glutamate, facilitates mGluR1α activation in hippocampal O/A interneurons (Huang et al., 2004). Interestingly, mGluR activation in interneurons is also achieved via synaptic stimulation paired with postsynaptic depolarization (Huang et al., 2004; Topolnik et al., 2005). Similar depolarization-dependent activation of mGluR-mediated responses has been shown in pyramidal neurons (Lüthi et al., 1997; Chuang et al., 2000; Rae et al., 2000; Rae and Irving, 2004). The mechanism responsible for the enhancement of mGluR responses through depolarization has yet to be identified in interneurons. The modulation of VGCCs or the activation of non-selective cation currents through the transient-receptor-potential (TRP) channels (Congar et al., 1997; Woodhall et al., 1999; Gee et al., 2003; Topolnik et al., 2006; Hartmann et al., 2008) may be associated with group I mGluR activation. In particular, some members of the canonical subfamily of TRP channels (TRPC1, TRPC4, TRPC5) show a similar voltage-dependence and high Ca^{2+} permeability and are likely to be activated by mGluR1α (Topolnik et al., 2005, 2006).

A hallmark of group I mGluR activation is an increase in intracellular Ca^{2+} concentration resulting from intracellular Ca^{2+} release and/or Ca^{2+} influx through VGCCs or store-operated channels (Pin and Duvoisin, 1995; Hermans and Challiss, 2001). Depending on the cell type and the receptor subtype being activated, group I mGluR-induced intracellular Ca^{2+} elevations may exhibit different temporal properties, varying from plateau-like transient Ca^{2+} rises to Ca^{2+} oscillations. Overall, these Ca^{2+} signals are kinetically slow and may last several seconds. An exemption to this rule is the activation of mGluR1α in O/A interneurons, where it is associated with a relatively fast Ca^{2+} response (Topolnik et al., 2005, 2006). Moreover, mGluR1α/mGluR5-mediated Ca^{2+} signals in these cells can be spatially restricted within individual dendritic branches and play distinct roles in local biochemical signaling (Topolnik et al., 2006). This is in contrast to pyramidal neurons, where group I mGluRs have been involved in the generation of traveling Ca^{2+} waves (Nakamura et al., 1999, 2002; Larkum et al., 2003; Hagenston et al., 2008).

Taken together, these data indicate that biochemical signaling via group I mGluRs is determined by the cell type, the receptor subtype distribution, the local interacting partners, and the conditions of the receptor activation. In interneurons, this signaling can be restricted within individual dendritic branches likely due to a local dendritic geometry and Ca^{2+} buffering. Therefore, in interneurons, group I mGluRs may be well positioned to control the immediate "voisinage" of activated synapses.

REGULATION OF DENDRITIC CONDUCTANCES VIA GROUP I mGluRs

The activation of group I mGluRs has a profound effect on the state of ion conductances and on the input–output relationship. The modulation of VGCCs and Na^+ and K^+ channels, or channels that mediate non-selective cation currents, has been associated with group I mGluR activation in different cell types including interneurons (Congar et al., 1997; Woodhall et al., 1999; Gee et al., 2003; Huang et al., 2004; Carlier et al., 2006; Ramsey et al., 2006; Topolnik et al., 2006; Hartmann et al., 2008). In O/A interneurons, L-type VGCCs were functionally linked with mGluR5 and played a critical role in regulating the coupling between dendritic APs and Ca^{2+} (Topolnik et al., 2009). bAP-evoked Ca^{2+} entry into dendrites was enhanced for at least 30 min after the activation of mGluR5, but not mGluR1α (**Figure 2**). This long-lasting increase in bAP Ca^{2+} signaling resulted from the potentiation of L-type VGCCs through Ca^{2+} release from ryanodine-sensitive stores and protein kinase C activation (**Figure 3**). Importantly, mGluR5 activation and bAP-CaTs potentiation were limited to ∼15 μm of dendritic length (**Figure 2D**), enabling local boosting of bAP Ca^{2+} signaling with a potential effect on the induction of Hebbian long-term potentiation (LTP). A similar form of mGluR – L-type VGCC interaction – exists in cerebellar granule cells (Chavis et al., 1996), which suggests that this mechanism is not limited to O/A interneurons. Such long-lasting potentiation of dendritic Ca^{2+} mechanisms is likely to have an effect on the activation of Ca^{2+}-dependent K^+ channels, with consequences for local input integration and spike generation. Furthermore, several non-specific cation channels or members of the family of TRP channels can be activated by mGluR1α in interneurons (**Figure 1**; Topolnik et al., 2005, 2006). In addition to their role in synaptic plasticity (see below), these channels provide a persistent membrane depolarization in an input-specific manner, thus shaping local synaptic conductances and controlling the input–output relationship (Egorov et al., 2002).

Together with the highly compartmentalized modulation of dendritic conductances within particular dendritic domains, group I mGluRs may provide global control of information flow via the generation of propagating activity. For example, in pyramidal neurons, mGluR activation is associated with generation of spreading Ca^{2+} waves or regenerative Ca^{2+} events that can control neuronal firing (Larkum et al., 2003; Hagenston et al., 2008). This form of supralinear mGluR signaling is important for overall control of synaptic integration and dendrite-to-soma signaling, but remains to be identified in interneurons.

GROUP I MGLURS AND SYNAPSE-SPECIFIC PLASTICITY

Because the activation of group I mGluRs is associated with an increase in intracellular Ca^{2+} concentration, the involvement of these receptors in synaptic plasticity has been studied extensively. Several forms of synapse-specific plasticity, including LTP and long-term depression (LTD), that are dependent on group I mGluRs have been discovered at excitatory synapses of cortical interneurons. In a population of O/A interneurons, a form of Hebbian LTP induced by pairing of theta-burst synaptic stimulation (TBS) with postsynaptic depolarization required activation of mGluR1α (Perez et al., 2001; Lapointe et al., 2003; Croce et al., 2010). In addition, this form of LTP was initiated via pharmacological activation of either mGluR1α or mGluR5, indicating the possible independent implication of the two receptors in the

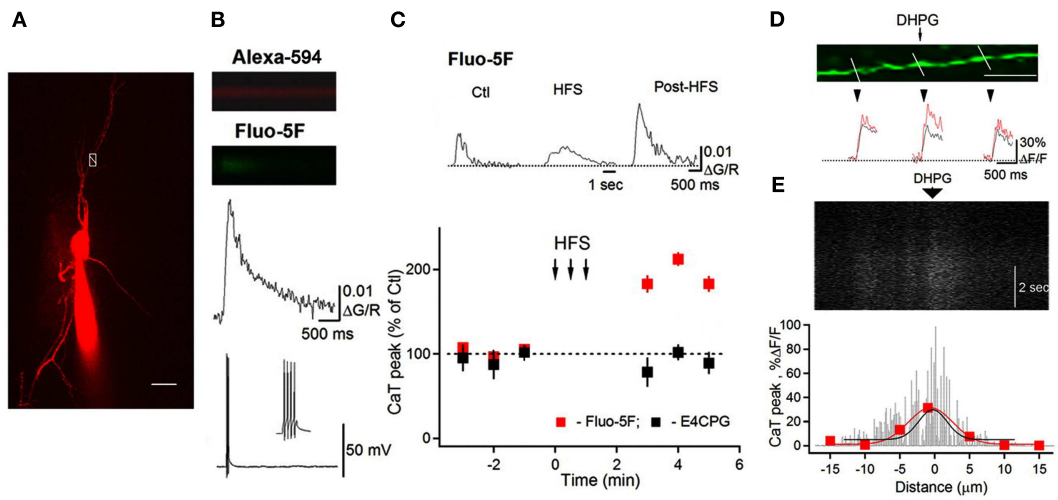

FIGURE 2 | Potentiation of bAP–CaTs in interneuron dendrites. (A) Two-photon image of an O/A interneuron filled with Alexa 594 and Fluo-5F. White box with a line across the dendrite indicate the position of the line scan to measure bAP–CaT shown in **(B)**. Scale bar, 20 μm. **(B)** Line scan images and associated bAP–CaT. **(C)** Representative bAP–CaTs evoked before (Ctl) during (middle traces; HFS) and after high-frequency synaptic stimulation (post-HFS) within the same dendritic region, and a summary plot, indicating a significant post-HFS potentiation of bAP–CaTs. HFS-induced AP–CaT potentiation was prevented by the mGluR1/mGluR5 antagonist E4CPG. **(D)** Magnified image of a dendrite with lines indicating locations for bAP–CaT measurements. Scale bar, 10 μm. Traces below show bAP–CaTs obtained from these locations in control (black) and after DHPG application (100 μM; red). **(E)** Line scan image collected along the middle part of the dendrite shown in **(D)** and demonstrating a slow DHPG Ca^{2+} response with corresponding spatial profile histogram (black fit). For comparison, the spatial profile of potentiated bAP–CaT (red) obtained from this region is shown superimposed. Modified from Topolnik et al. (2009) with permission.

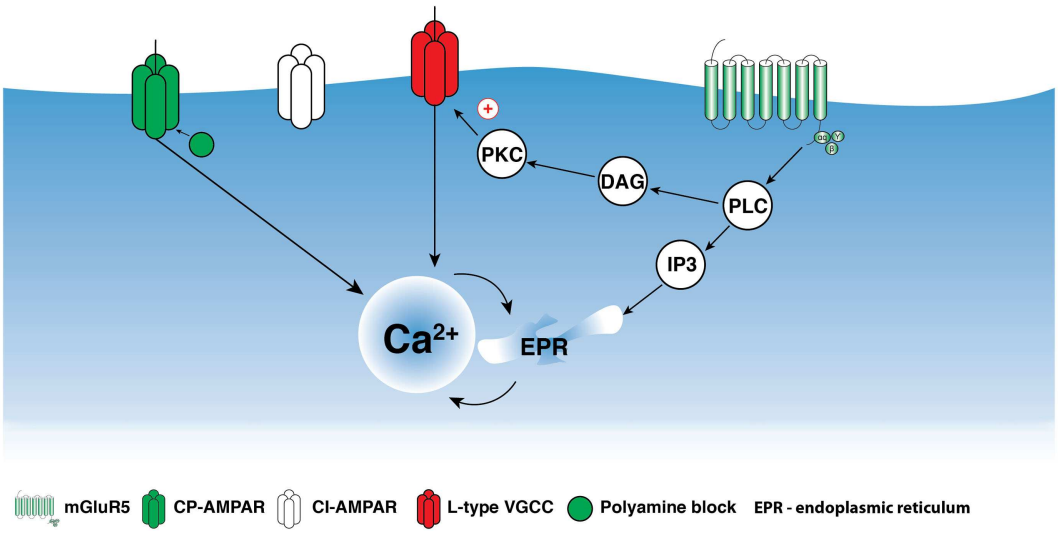

FIGURE 3 | Schematic representation of mGluR5 signaling in interneuron dendrites. Activation of mGluR5 may trigger phospholipase C (PLC) activation producing inositol-1,4,5-triphosphate (IP_3) and Ca^{2+} release from intracellular stores as well as diacylglycerol (DAG)/protein kinase C (PKC) activation. mGluR5-mediated Ca^{2+} release alone can be involved in LTD induction; however, together with Ca^{2+} entry through CP-AMPARs, mGluR5 appears to influence the induction of anti-Hebbian LTP. Moreover, mGluR5-dependent PKC activation produces persistent up-regulation of L-type VGCCs and may play a critical role in the regulation of Hebbian LTP.

induction of this form of plasticity (Le Vasseur et al., 2008). In these cells, mGluR1α activation led to an increase in intracellular Ca^{2+} via the activation of TRP channels and Ca^{2+}-induced Ca^{2+} release from ryanodine-sensitive stores (**Figure 1**), whereas mGluR5 activation was coupled solely to Ca^{2+} release (**Figure 3**; Woodhall et al., 1999; Topolnik et al., 2006). Interestingly, a similar Hebbian TBS protocol induced LTP in interneurons of the visual cortex, but this LTP was mediated by mGluR5 and not by mGluR1α (Sarihi et al., 2008). Furthermore, although these two examples of LTP required an increase in postsynaptic Ca^{2+}, the fact that potentiation was expressed post-synaptically in neocortical interneurons and both pre- and post-synaptically in hippocampal interneurons suggests that these two forms of Hebbian plasticity engage distinct mechanisms.

In addition to the Hebbian form of synaptic plasticity, an anti-Hebbian LTP involving group I mGluRs was reported in a population of hippocampal interneurons (Lamsa et al., 2007; Le Duigou and Kullmann, 2011; Szabo et al., 2012). This LTP was induced by synaptic or pharmacological stimulation at hyperpolarized levels of membrane potential. The anti-Hebbian LTP required the activation of Ca^{2+}-permeable α-amino-3-hydroxy-5-methyl-4-isoxazolepropionic acid receptors (CP-AMPARs) and of mGluR1α and mGluR5 (Oren et al., 2009; Le Duigou and Kullmann, 2011). The involvement of group I mGluRs in anti-Hebbian LTP is surprising, as this would require significant excitation of interneurons at hyperpolarized levels of membrane potential. Although such conditions can be met *in vivo*, for example during sharp-wave-associated ripples when O–LM interneurons are silenced but receive a strong excitatory drive from CA1 pyramidal neurons (Klausberger et al., 2003), it is clear that additional mechanisms that are activated at hyperpolarized potentials are likely to cooperate with group I mGluRs during LTP induction. For example, a possible functional interaction may exist between CP-AMPARs and group I mGluRs, as both are located within the same dendritic microdomain (Topolnik et al., 2005). CP-AMPAR Ca^{2+} influx increases slightly with membrane hyperpolarization (Goldberg et al., 2003b; Topolnik et al., 2005), as the CP-AMPAR channel is blocked by endogenous polyamines at depolarizing potentials. Accordingly, mGluR-induced Ca^{2+} release at hyperpolarized levels of membrane potential can lower the threshold for LTP induction (Kullmann and Lamsa, 2007) by increasing the magnitude and duration of dendritic Ca^{2+} elevations. Similar functional interactions exist between mGluRs and TRP channels or VGCCs (**Figures 1** and **3**; Topolnik et al., 2006, 2009) and are involved in the induction of Hebbian plasticity, suggesting that, regardless of the stimulation paradigm, different Ca^{2+} mechanisms may converge on a common Ca^{2+}-dependent signaling cascade, leading to LTP induction.

In addition to LTP, group I mGluRs play a role in the induction of LTD. In hippocampal stratum oriens and radiatum interneurons, application of the group I mGluR agonist (*S*)-DHPG at resting membrane potential resulted in synaptic depression, with mGluR1α inducing reversible depression and mGluR5 inducing long-lasting depression (Le Duigou et al., 2011). In stratum radiatum interneurons, group I mGluR-dependent LTD was also induced by high-frequency synaptic stimulation (Gibson et al., 2008). This type of LTD is likely to be common for synapses formed by Schaffer collaterals, as it was also demonstrated in CA1 pyramidal neurons (Fitzjohn et al., 2001; Huber et al., 2001; Mannaioni et al., 2001). Group I mGluRs also control the direction of plasticity in interneurons. At excitatory synapses of lacunosum-moleculare interneurons in hippocampal region *Cornu Ammonis* 3 (CA3), a protocol that induced Hebbian LTP also induced LTD

if mGluR1α was blocked (Galván et al., 2008). The two forms of plasticity required different levels of postsynaptic Ca^{2+} elevation. Whereas L-type VGCCs were involved in both LTP and LTD induction, mGluR1α-dependent Ca^{2+} release in conjunction with L-type VGCC activation was required for LTP. These data indicate that the polarity of plasticity in interneurons can be controlled by specific mGluR1α – L-type VGCC interaction.

Taken together, these findings indicate that the implication of group I mGluRs in the induction of different forms of plasticity in interneurons varies according to the type of interneuron, the stimulation paradigm, the level of membrane potential, the receptor subtype that is activated, and the expression of ionotropic receptors and ion channels that may be part of the mGluR and synaptic compartment. It is worth mentioning that most of the forms of plasticity discussed above were expressed in part presynaptically, implying the group I mGluR-dependent activation of retrograde signaling via yet unknown mechanisms.

CONCLUSION

There is growing evidence that group I mGluRs play a critical role in the regulation of dendritic excitability and synaptic plasticity in interneurons. The two receptor subtypes (mGluR1α and mGluR5) have cell type-specific distributions, can be activated by different patterns of synaptic activity, and, via coupling to distinct signaling cascades, can control specific cellular functions (**Figures 1** and **3**). In particular, mGluR1α can interact with TRP channels, whereas mGluR5 is involved in L-type VGCC modulation, and both receptor subtypes may signal the induction of several forms of synaptic plasticity in interneurons. However, the extent to which the mechanisms activated by the two receptor subtypes are specific to particular types of interneurons, whether these mechanisms reflect the local circuit interactions, and whether they operate under natural conditions *in vivo* remain to be determined.

ACKNOWLEDGMENTS

This work was supported by the Canadian Institutes of Health Research, Natural Sciences and Engineering Research Council of Canada (NSERC Discovery Grant), Canadian Foundation for Innovation, Fonds de recherche du Québec – Santé, and Savoy Foundation. Lisa Topolnik is recipient of the University Faculty Award from NSERC. Jean-Claude Lacaille holds the Canada Research Chair in Cellular and Molecular Neurophysiology.

REFERENCES

Aponte, Y., Bischofberger, J., and Jonas, P. (2008). Efficient Ca2+ buffering in fast-spiking basket cells of rat hippocampus. *J. Physiol. (Lond.)* 586, 2061–2075.

Aramori, I., and Nakanishi, S. (1992). Signal transduction and pharmacological characteristics of a metabotropic glutamate receptor, mGluR1, in transfected CHO cells. *Neuron* 8, 757–765.

Bartos, M., Vida, I., and Jonas, P. (2007). Synaptic mechanisms of synchronized gamma oscillations in inhibitory interneuron networks. *Nat. Rev. Neurosci.* 8, 45–56.

Baude, A., Nusser, Z., Roberts, J. D., Mulvihill, E., McIlhinney, R. A., and Somogyi, P. (1993). The metabotropic glutamate receptor (mGluR1 alpha) is concentrated at perisynaptic membrane of neuronal subpopulations as detected by immunogold reaction. *Neuron* 11, 771–787.

Brakeman, P. R., Lanahan, A. A., O'Brien, R., Roche, K., Barnes, C. A., Huganir, R. L., and Worley, P. F. (1997). Homer: a protein that selectively binds metabotropic glutamate receptors. *Nature* 386, 284–288.

Branco, T., and Häusser, M. (2010). The single dendritic branch as a fundamental functional unit in the nervous system. *Curr. Opin. Neurobiol.* 20, 494–502.

Carlier, E., Sourdet, V., Boudkkazi, S., Déglise, P., Ankri, N., Fronzaroli-Molinieres, L., and Debanne, D. (2006). Metabotropic glutamate receptor subtype 1 regulates sodium currents in rat neocortical pyramidal neurons. *J. Physiol. (Lond.)* 577, 141–154.

Chavis, P., Fagni, L., Lansman, J. B., and Bockaert, J. (1996). Functional coupling between ryanodine receptors and L-type calcium channels in neurons. *Nature* 382, 719–722.

Chuang, S. C., Bianchi, R., and Wong, R. K. (2000). Group I mGluR activation turns on a voltage-gated inward current in hippocampal pyramidal cells. *J. Neurophysiol.* 83, 2844–2853.

Congar, P., Leinekugel, X., Ben-Ari, Y., and Crépel, V. (1997). A long-lasting calcium-activated nonselective cationic current is generated by synaptic stimulation or exogenous activation of group I metabotropic glutamate receptors in CA1 pyramidal neurons. *J. Neurosci.* 17, 5366–5379.

Croce, A., Pelletier, J. G., Tartas, M., and Lacaille, J. C. (2010). Afferent-specific properties of interneuron synapses underlie selective long-term regulation of feedback inhibitory circuits in CA1 hippocampus. *J. Physiol. (Lond.)* 588, 2091–2107.

Egorov, A. V., Hamam, B. N., Fransén, E., Hasselmo, M. E., and Alonso, A. A. (2002). Graded persistent activity in entorhinal cortex neurons. *Nature* 420, 173–178.

Emri, Z., Antal, K., Gulyás, A. I., Megías, M., and Freund, T. F. (2001). Electrotonic profile and passive propagation of synaptic potentials in three subpopulations of hippocampal CA1 interneurons. *Neuroscience* 104, 1013–1026.

Evstratova, A., Chamberland, S., and Topolnik, L. (2011). Cell type-specific and activity-dependent dynamics of action potential-evoked Ca2+ signals in dendrites of hippocampal inhibitory interneurons. *J. Physiol. (Lond.)* 589, 1957–1977.

Ferraguti, F., Cobden, P., Pollard, M., Cope, D., Shigemoto, R., Watanabe, M., and Somogyi, P. (2004). Immunolocalization of metabotropic glutamate receptor 1alpha (mGluR1alpha) in distinct classes of interneuron in the CA1 region of the rat hippocampus. *Hippocampus* 14, 193–215.

Fitzjohn, S. M., Palmer, M. J., May, J. E., Neeson, A., Morris, S. A., and Collingridge, G. L. (2001). A characterisation of long-term depression induced by metabotropic glutamate receptor activation in the rat hippocampus in vitro. *J. Physiol. (Lond.)* 537, 421–430.

Frick, A., Magee, J., and Johnston, D. (2004). LTP is accompanied by an enhanced local excitability of pyramidal neuron dendrites. *Nat. Neurosci.* 7, 126–135.

Fricker, D., and Miles, R. (2000). EPSP amplification and the precision of spike timing in hippocampal neurons. *Neuron* 28, 559–569.

Galarreta, M., and Hestrin, S. (2001). Spike transmission and synchrony detection in networks of GABAergic interneurons. *Science* 292, 2295–2299.

Galván, E. J., Calixto, E., and Barrionuevo, G. (2008). Bidirectional Hebbian plasticity at hippocampal mossy fiber synapses on CA3 interneurons. *J. Neurosci.* 28, 14042–14055.

Gee, C. E., Benquet, P., and Gerber, U. (2003). Group I metabotropic glutamate receptors activate a calcium-sensitive transient receptor potential-like conductance in rat hippocampus. *J. Physiol. (Lond.)* 546, 655–664.

Gee, C. E., and Lacaille, J. C. (2004). Group I metabotropic glutamate receptor actions in oriens/alveus interneurons of rat hippocampal CA1 region. *Brain Res.* 1000, 92–101.

Geiger, J. R., Lübke, J., Roth, A., Frotscher, M., and Jonas, P. (1997). Submillisecond AMPA receptor-mediated signaling at a principal neuron-interneuron synapse. *Neuron* 18, 1009–1023.

Gibson, H. E., Edwards, J. G., Page, R. S., Van Hook, M. J., and Kauer, J. A. (2008). TRPV1 channels mediate long-term depression at synapses on hippocampal interneurons. *Neuron* 57, 746–759.

Goldberg, J. H., Tamas, G., and Yuste, R. (2003a). Ca2+ imaging of mouse neocortical interneurone dendrites: Ia-type K+ channels control action potential back-propagation. *J. Physiol. (Lond.)* 551, 49–65.

Goldberg, J. H., Yuste, R., and Tamas, G. (2003b). Calcium microdomains in aspiny dendrites. *Neuron* 13, 807–821.

Golding, N. L., Staff, N. P., and Spruston, N. (2002). Dendritic spikes as a mechanism for cooperative long-term potentiation. *Nature* 418, 326–331.

Goldstein, S. S., and Rall, W. (1974). Changes of action potential shape and velocity for changing core conductor geometry. *Biophys. J.* 14, 731–757.

Gulyás, A. I., Megías, M., Emri, Z., and Freund, T. F. (1999). Total number and ratio of excitatory and inhibitory synapses converging onto single interneurons of different types in the CA1 area of the rat hippocampus. *J. Neurosci.* 19, 10082–10097.

Hagenston, A. M., Fitzpatrick, J. S., and Yeckel, M. F. (2008). MGluR-mediated calcium waves that invade the soma regulate firing in layer V medial prefrontal cortical pyramidal neurons. *Cereb. Cortex* 18, 407–423.

Hartmann, J., Dragicevic, E., Adelsberger, H., Henning, H. A., Sumser, M., Abramowitz, J., Blum, R., Dietrich, A., Freichel, M., Flockerzi, V., Birnbaumer, L., and Konnerth, A. (2008). TRPC3 channels are required for synaptic transmission and motor coordination. *Neuron* 59, 392–398.

Hermans, E., and Challiss, R. A. (2001). Structural, signalling and regulatory properties of the group I metabotropic glutamate receptors: prototypic family C G-protein-coupled receptors. *Biochem. J.* 359, 465–484.

Heuss, C., Scanziani, M., Gähwiler, B. H., and Gerber, U. (1999). G-protein-independent signaling mediated by metabotropic glutamate receptors. *Nat. Neurosci.* 2, 1070–1077.

Hu, H., Martina, M., and Jonas, P. (2010). Dendritic mechanisms underlying rapid synaptic activation of fast-spiking hippocampal interneurons. *Science* 327, 52–58.

Huang, Y. H., Sinha, S. R., Tanaka, K., Rothstein, J. D., and Bergles, D. E. (2004). Astrocyte glutamate transporters regulate metabotropic glutamate receptor-mediated excitation of hippocampal interneurons. *J. Neurosci.* 24, 4551–4559.

Huber, K. M., Roder, J. C., and Bear, M. F. (2001). Chemical induction of mGluR5- and protein synthesis-dependent long-term depression in hippocampal area CA1. *J. Neurophysiol.* 86, 321–325.

Kaiser, K. M., Zilberter, Y., and Sakmann, B. (2001). Back-propagating action potentials mediate calcium signalling in dendrites of bitufted interneurons in layer 2/3 of rat somatosensory cortex. *J. Physiol. (Lond.)* 535, 17–31.

Klausberger, T., Magill, P. G., Marton, L. F., Roberts, J. D., Cobden, P. M., Buzsaki, G., and Somogyi, P. (2003). Brain state- and cell type-specific firing of hippocampal interneurons in vivo. *Nature* 421, 844–848.

Kullmann, D. M., and Lamsa, K. P. (2007). Long-term synaptic plasticity in hippocampal interneurons. *Nat. Rev. Neurosci.* 8, 687–699.

Kuwajima, M., Hall, R. A., Aiba, A., and Smith, Y. (2004). Subcellular and subsynaptic localization of group I metabotropic glutamate receptors in the monkey subthalamic nucleus. *J. Comp. Neurol.* 474, 589–602.

Lamsa, K. P., Heeroma, J. H., Somogyi, P., Rusakov, D. A., and Kullmann, D. M. (2007). Anti-Hebbian long-term potentiation in the hippocampal feedback inhibitory circuit. *Science* 315, 1262–1266.

Lapointe, V., Morin, F., Ratté, S., Croce, A., Conquet, F., and Lacaille, J. C. (2003). Synapse-specific mGluR1-dependent long-term potentiation in interneurones regulates mouse hippocampal inhibition. *J. Physiol. (Lond.)* 555, 125–135.

Larkum, M. E., Kaiser, K. M., and Sakmann, B. (1999). Calcium electrogenesis in distal apical dendrites of layer 5 pyramidal cells at a critical frequency of back-propagating action potentials. *Proc. Natl. Acad. Sci. U.S.A.* 96, 14600–14604.

Larkum, M. E., Watanabe, S., Nakamura, T., Lasser-Ross, N., and Ross, W. N. (2003). Synaptically activated Ca2+ waves in layer 2/3 and layer 5 rat neocortical pyramidal neurons. *J. Physiol. (Lond.)* 549, 471–488.

Le Duigou, C., Holden, T., and Kullmann, D. M. (2011). Short- and long-term depression at glutamatergic synapses on hippocampal interneurons by group I mGluR activation. *Neuropharmacology* 60, 748–756.

Le Duigou, C., and Kullmann, D. M. (2011). Group I mGluR agonist-evoked long-term potentiation in hippocampal oriens interneurons. *J. Neurosci.* 31, 5777–5781.

Le Vasseur, M., Ran, I., and Lacaille, J. C. (2008). Selective induction of metabotropic glutamate receptor 1- and metabotropic glutamate receptor 5-dependent chemical long-term potentiation at oriens/alveus interneuron synapses of mouse hippocampus. *Neuroscience* 151, 28–42.

Losonczy, A., and Magee, J. C. (2006). Integrative properties of radial oblique dendrites in hippocampal CA1 pyramidal neurons. *Neuron* 50, 291–307.

Lujan, R., Nusser, Z., Roberts, J. D., Shigemoto, R., and Somogyi, P. (1996). Perisynaptic location of metabotropic glutamate receptors mGluR1 and mGluR5 on dendrites and dendritic spines in the rat hippocampus. *Eur. J. Neurosci.* 8, 1488–1500.

Lüthi, A., Gähwiler, B. H., and Gerber, U. (1997). 1S, 3R-ACPD induces a region of negative slope conductance in the steady-state current-voltage relationship of hippocampal pyramidal cells. *J. Neurophysiol.* 77, 221–228.

Mannaioni, G., Marino, M. J., Valenti, O., Traynelis, S. F., and Conn, P. J. (2001). Metabotropic glutamate receptors 1 and 5 differentially regulate CA1 pyramidal cell function. *J. Neurosci.* 21, 5925–5934.

Martina, M., Vida, I., and Jonas, P. (2000). Distal initiation and active propagation of action potentials in interneuron dendrites. *Science* 287, 295–300.

Nakamura, T., Barbara, J. G., Nakamura, K., and Ross, W. N. (1999). Synergistic release of Ca2+ from IP3-sensitive stores evoked by synaptic activation of mGluRs paired with backpropagating action potentials. *Neuron* 24, 727–737.

Nakamura, T., Lasser-Ross, N., Nakamura, K., and Ross, W. N. (2002). Spatial segregation and interaction of calcium signalling mechanisms in rat hippocampal CA1 pyramidal neurons. *J. Physiol. (Lond.)* 543, 465–480.

Nistri, A., Ostroumov, K., Sharifullina, E., and Taccola, G. (2006). Tuning and playing a motor rhythm: how metabotropic glutamate receptors orchestrate generation of motor patterns in the mammalian central nervous system. *J. Physiol. (Lond.)* 572, 323–334.

Nörenberg, A., Hu, H., Vida, I., Bartos, M., and Jonas, P. (2010). Distinct nonuniform cable properties optimize rapid and efficient activation of fast-spiking GABAergic interneurons. *Proc. Natl. Acad. Sci. U.S.A.* 107, 894–899.

Nusser, Z., Mulvihill, E., Streit, P., and Somogyi, P. (1994). Subsynaptic segregation of metabotropic and ionotropic glutamate receptors as revealed by immunogold localization. *Neuroscience* 61, 421–427.

Oren, I., Nissen, W., Kullmann, D. M., Somogyi, P., and Lamsa, K. P. (2009). Role of ionotropic glutamate receptors in long-term potentiation in rat hippocampal CA1 oriens-lacunosum moleculare interneurons. *J. Neurosci.* 29, 939–950.

Perez, Y., Morin, F., and Lacaille, J. C. (2001). A Hebbian form of long-term potentiation dependent on mGluR1a in hippocampal inhibitory interneurons. *Proc. Natl. Acad. Sci. U.S.A.* 98, 9401–9406.

Pin, J. P., and Duvoisin, R. (1995). The metabotropic glutamate receptors: structure and functions. *Neuropharmacology* 34, 1–26.

Rae, M. G., and Irving, A. J. (2004). Both mGluR1 and mGluR5 mediate Ca2+ release and inward currents in hippocampal CA1 pyramidal neurons. *Neuropharmacology* 46, 1057–1069.

Rae, M. G., Martin, D. J., Collingridge, G. L., and Irving, A. J. (2000). Role of Ca2+ stores in metabotropic L-glutamate receptor-mediated supralinear Ca2+ signaling in rat hippocampal neurons. *J. Neurosci.* 20, 8628–8636.

Rall, W. (1964). "Theoretical significance of dendritic trees for neuronal input-output relations," in *Neural Theory and Modeling*, ed. R. F. Reiss (Stanford, CA: Stanford University Press), 73–97.

Ramón y Cajal, S. (1891). Sur la structure de l'ecorce cerebrale de quelques mamiferes. *Cellule* 7, 124–176.

Ramsey, I. S., Delling, M., and Clapham, D. E. (2006). An introduction to TRP channels. *Annu. Rev. Physiol.* 68, 619–647.

Ribeiro, F. M., Paquet, M., Cregan, S. P., and Ferguson, S. S. (2010). Group I metabotropic glutamate receptor signaling and its implication in neurological disease. *CNS Neurol. Disord. Drug Targets* 9, 574–595.

Sabatini, B. L., Oertner, T. G., and Svoboda, K. (2002). The life cycle of Ca(2+) ions in dendritic spines. *Neuron* 31, 439–452.

Sarihi, A., Jiang, B., Komaki, A., Sohya, K., Yanagawa, Y., and Tsumoto, T. (2008). Metabotropic glutamate receptor type 5-dependent long-term potentiation of excitatory synapses on fast-spiking GABAergic neurons in mouse visual cortex. *J. Neurosci.* 28, 1224–1235.

Schiller, J., Schiller, Y., Stuart, G., and Sakmann, B. (1997). Calcium action potentials restricted to distal apical dendrites of rat neocortical pyramidal neurons. *J. Physiol. (Lond.)* 505, 605–616.

Shigemoto, R., Kinoshita, A., Wada, E., Nomura, S., Ohishi, H., Takada, M., Flor, P. J., Neki, A., Abe, T., Nakanishi, S., and Mizuno, N. (1997). Differential presynaptic localization

of metabotropic glutamate receptor subtypes in the rat hippocampus. *J. Neurosci.* 17, 7503–7522.

Sjöström, P. J., and Häusser, M. (2006). A cooperative switch determines the sign of synaptic plasticity in distal dendrites of neocortical pyramidal neurons. *Neuron* 51, 227–238.

Spruston, N., Schiller, Y., Stuart, G., and Sakmann, B. (1995). Activity-dependent action potential invasion and calcium influx into hippocampal CA1 dendrites. *Science* 268, 297–300.

Stuart, G. J., and Sakmann, B. (1994). Active propagation of somatic action potentials into neocortical pyramidal cell dendrites. *Nature* 367, 69–72.

Sun, Q. Q., Zhang, Z., Jiao, Y., Zhang, C., Szabó, G., and Erdelyi, F. (2009). Differential metabotropic glutamate receptor expression and modulation in two neocortical inhibitory networks. *J. Neurophysiol.* 101, 2679–2692.

Szabo, A., Somogyi, J., Cauli, B., Lambolez, B., Somogyi, P., and Lamsa, K. P. (2012). Calcium-permeable AMPA receptors provide a common mechanism for LTP in glutamatergic synapses of distinct hippocampal interneuron types. *J. Neurosci.* 32, 6511–6516.

Topolnik, L., Azzi, M., Morin, F., Kougioumoutzakis, A., and Lacaille, J. C. (2006). mGluR1/5 subtype-specific calcium signalling and induction of long-term potentiation in rat hippocampal oriens/alveus interneurones. *J. Physiol. (Lond.)* 575, 115–131.

Topolnik, L., Chamberland, S., Pelletier, J. G., Ran, I., and Lacaille, J. C. (2009). Activity-dependent compartmentalized regulation of dendritic Ca2+ signaling in hippocampal interneurons. *J. Neurosci.* 29, 4658–4663.

Topolnik, L., Congar, P., and Lacaille, J. C. (2005). Differential regulation of metabotropic glutamate receptor- and AMPA receptor-mediated dendritic Ca2+ signals by presynaptic and postsynaptic activity in hippocampal interneurons. *J. Neurosci.* 25, 990–1001.

Topolnik, L., and Lacaille, J. C. (2009). "Functional reorganization of inhibitory circuits in epilepsy: mGluR1/5 signaling mechanisms and long-term plasticity," in *Encyclopedia of Basic Epilepsy Research*, ed. P. Schwartzkroin (Elsevier), 424–429.

van Hooft, J. A., Giuffrida, R., Blatow, M., and Monyer, H. (2000). Differential expression of group I metabotropic glutamate receptors in functionally distinct hippocampal interneurons. *J. Neurosci.* 20, 3544–3551.

Vetter, P., Roth, A., and Häusser, M. (2001). Propagation of action potentials in dendrites depends on dendritic morphology. *J. Neurophysiol.* 85, 926–937.

Vidnyánszky, Z., Hámori, J., Négyessy, L., Rüegg, D., Knöpfel, T., Kuhn, R., and Görcs, T. J. (1994). Cellular and subcellular localization of the mGluR5a metabotropic glutamate receptor in rat spinal cord. *Neuroreport* 6, 209–213.

Woodhall, G., Gee, C. E., Robitaille, R., and Lacaille, J. C. (1999). Membrane potential and intracellular Ca2+ oscillations activated by mGluRs in hippocampal stratum oriens/alveus interneurons. *J. Neurophysiol.* 81, 371–382.

Conflict of Interest Statement: The authors declare that the research was conducted in the absence of any commercial or financial relationships that could be construed as a potential conflict of interest.

Received: 01 April 2012; accepted: 21 June 2012; published online: 09 July 2012.
Citation: Camiré O, Lacaille J-C and Topolnik L (2012) Dendritic signaling in inhibitory interneurons: local tuning via group I metabotropic glutamate receptors. Front. Physio. ***3****:259. doi: 10.3389/fphys.2012.00259*
This article was submitted to Frontiers in Membrane Physiology and Biophysics, a specialty of Frontiers in Physiology.

frontiers in
PHYSIOLOGY

MINI REVIEW ARTICLE
published: 20 July 2012
doi: 10.3389/fphys.2012.00253

Tonic neuromodulation of the inspiratory rhythm generator

Fernando Peña-Ortega*

Departamento de Neurobiología del Desarrollo y Neurofisiología, Instituto de Neurobiología, UNAM-Campus Juriquilla, Querétaro, Mexico

Edited by:
Francisco Fernandez De-Miguel, Universidad Nacional Autónoma de México, Mexico

Reviewed by:
Francisco Fernandez De-Miguel, Universidad Nacional Autónoma de México, Mexico
Jaime Eugenin, Universidad de Santiago de Chile, Chile
Jan Marino Ramirez, University of Washington, USA

****Correspondence:***
Fernando Peña-Ortega, Departamento de Neurobiología del Desarrollo y Neurofisiología, Instituto de Neurobiología, Universidad Nacional Autónoma de México, Boulevard Juriquilla 3001, Querétaro 76230, México.
e-mail: jfpena@unam.mx

The generation of neural network dynamics relies on the interactions between the intrinsic and synaptic properties of their neural components. Moreover, neuromodulators allow networks to change these properties and adjust their activity to specific challenges. Endogenous continuous ("tonic") neuromodulation can regulate and sometimes be indispensible for networks to produce basal activity. This seems to be the case for the inspiratory rhythm generator located in the pre-Bötzinger complex (preBötC). This neural network is necessary and sufficient for generating inspiratory rhythms. The preBötC produces normal respiratory activity (eupnea) as well as sighs under normoxic conditions, and it generates gasping under hypoxic conditions after a reconfiguration process. The reconfiguration leading to gasping generation involves changes of synaptic and intrinsic properties that can be mediated by several neuromodulators. Over the past years, it has been shown that endogenous continuous neuromodulation of the preBötC may involve the continuous action of amines and peptides on extrasynaptic receptors. I will summarize the findings supporting the role of endogenous continuous neuromodulation in the generation and regulation of different inspiratory rhythms, exploring the possibility that these neuromodulatory actions involve extrasynaptic receptors along with evidence of glial modulation of preBötC activity.

Keywords: endogenous neuromodulation, glia, network activity, pacemaker neurons, reconfigu ation, extrasynaptic

INTRODUCTION

Neural network activity relies on the interactions between intrinsic and synaptic properties (Ramirez et al., 2004; Marder and Bucher, 2007; Peña, 2009). Here, I will consider "synaptic properties" as those provided by fast neurotransmission among neurons and "neuromodulation" as the slower changes in cellular and synaptic properties mediated by metabotropic receptors (Katz, 1998). Neuromodulators regulate the activity of networks, allowing their adaptation to different demands or even conditioning their basal activity (Katz, 1998; Tryba et al., 2006; Peña, 2009). This issue has been studied in the inspiratory rhythm generator, the pre-Bötzinger complex (preBötC), which generates the inspiratory commands that control the diaphragm (Smith et al., 1991; Feldman and Del Negro, 2006; Schwarzacher et al., 2011). Breathing is eliminated by lesioning or inactivating the preBötC (Ramirez et al., 1998; Wenninger et al., 2004), whereas the isolated preBötC is still able to generate the inspiratory rhythms in a brainstem slice preparation (Smith et al., 1991; Lieske et al., 2000; Peña et al., 2008; Armstrong et al., 2010) or even in preBötC islands (Ramírez-Jarquín et al., 2012).

In slices, the preBötC generates three distinct activity patterns that correspond to distinct forms of breathing: normal respiratory activity (eupnea), sighs, and gasps (Lieske et al., 2000). Gasping is generated during hypoxia as a "last-resort" respiratory effort to autoresuscitate (Gozal et al., 2002; Fewell et al., 2007; Zavala-Tecuapetla et al., 2008). Interestingly, babies that die from SIDS have a reduction in gasping generation and inefficient autoresuscitation (Poets et al., 1999; Sridhar et al., 2003). The preBötC contains several types of neurons, including expiratory, inspiratory, and postinspiratory neurons (Lieske et al., 2000) that interact through fast synaptic transmission (Greer et al., 1991; Funk et al., 1993; Shao and Feldman, 1997; Ren and Greer, 2006) to produce the inspiratory rhythms. Among the inspiratory preBötC neurons, a group of respiratory pacemaker neurons has been detected that plays a major role in rhythm generation (Thoby-Brisson and Ramirez, 2001; Peña et al., 2004; Del Negro et al., 2005; Peña and Aguileta, 2007). Characterization of these neurons revealed at least two types (Thoby-Brisson and Ramirez, 2001; Peña et al., 2004; Del Negro et al., 2005; Peña and Aguileta, 2007; Peña, 2008), one that generates bursts via a Ca^{2+}-activated cationic current (I_{CAN}) and the other that relies on the persistent Na^{+} current (I_{NaP}; Peña et al., 2004; Del Negro et al., 2005; Peña and Aguileta, 2007; Peña, 2008). Both types of pacemakers need to be inhibited to abolish rhythmogenesis under normoxia, both *in vitro* and *in vivo* (Peña et al., 2004; Peña and Ramirez, 2005; Tryba et al., 2006). In contrast, during hypoxic conditions, gasping generation critically relies on the activity of I_{NaP}-dependent (hypoxia-resistant) pacemaker neurons (Peña et al., 2004; Tryba et al., 2006; Peña and Aguileta, 2007). In addition to these mechanisms, the specific contribution of intrinsic and synaptic properties to rhythmogenesis depends on the neuromodulatory context. When applied exogenously, several neuromodulators modify the generation of the rhythmic activity by the preBötC (Doi and Ramirez, 2008). Moreover, several of these neuromodulators maintain a continuous endogenous modulation that, in some cases, is indispensable for rhythm generation (Peña and Ramirez, 2002, 2004; Tryba et al., 2006; Viemari et al., 2011; Ramírez-Jarquín et al., 2012). This continuous modulation, synonymous with "tonic neuromodulation,"

is maintained by continuous release of neuromodulators, mainly from tonic active neurons and glial cells (Hülsmann et al., 2000; Ptak et al., 2009).

CONTINUOUS ("TONIC") NEUROMODULATION OF THE preBötC

The actions of different neuromodulators on the inspiratory rhythm generator, including amines and peptides, were recently reviewed (Ballanyi, 2004; Peña and García, 2006; Doi and Ramirez, 2008; Peña, 2009). Therefore, I will focus on the evidence of endogenous continuous neuromodulations of the preBötC. In the CNS, several neuromodulators can be continuously released and act both at synaptic and extrasynaptic levels to regulate network function (Vizi et al., 2010). Extrasynaptic transmission was originally discovered for several monoamines that regulate the release of other neuromodulators and neurotransmitters despite the lack of synaptic contact between the two terminals (Vizi et al., 2010). In fact, the majority of monoaminergic and peptidergic neurons fail to make synaptic contacts and instead, they act on extrasynaptic receptors (Descarries and Mechawar, 2000; Vizi et al., 2010). Such neuromodulators are preferentially, but not exclusively, accumulated in large, dense-core vesicles, and they require a strong depolarization or high frequency stimulation to be released (Torrealba and Carrasco, 2004; De-Miguel and Trueta, 2005; Vizi et al., 2010). The fact that several neuromodulators, such as serotonin and adenosine, have been detected in the extracellular space of the preBötC by means of microdialysis (Richter et al., 1999), which detects neurotransmitters and neuromodulators that escaped the synaptic cleft (Peña and Tapia, 1999, 2000), suggests that they can reach extrasynaptic receptors and continuously modulate the preBötC. The extracellular concentration of these neuromodulators changes depending on the state of the network (i.e., hypoxia; Richter et al., 1999; Hehre et al., 2008) indicating that such continuous modulation adjusts the preBötC activity to fit particular demands. Next, I will present a catalog of neuromodulators that maintain a continuous neuromodulation of the preBötC, and discuss the possible involvement of extrasynaptic receptors or glial cells in this modulation. It is important to consider that respiratory rhythmogenesis is studied in a variety of experimental conditions ranging from behaving animals to preBötC islands (Ramírez-Jarquín et al., 2012). Thus, in most cases, the pharmacological manipulations could affect different respiratory circuits besides the preBötC (Zavala-Tecuapetla et al., 2008; Ramírez-Jarquín et al., 2012).

ADENOSINE

Adenosine is an inhibitory neuromodulator of the preBötC (Schmidt et al., 1995; Herlenius and Lagercrantz, 1999; Wilken et al., 2000; Huxtable et al., 2009) that can be directly released from neurons and glia or that can be extracellularly produced by the degradation of released ATP (Martín et al., 2007; Cunha, 2008; Zwicker et al., 2011). Ambient adenosine can exert its effects by diffusing far away from the release sites (Cunha, 2008; Vizi et al., 2010). An adenosinergic continuous modulation of the preBötC of mice has been evidenced by blocking adenosine-receptors with the non-selective, adenosine-receptor antagonist aminophylline (Wilken et al., 2000), which increases the frequency and amplitude of inspiratory rhythm in slices. This effect is similar to blocking the type 1 (A1) adenosine-receptor in rats with the specific antagonist DPCPX (Huxtable et al., 2009) These increases have also been observed in the brainstem-spinal cord preparation (also called the "*en bloc*") of rats (Herlenius and Lagercrantz, 1999) and in cats *in vivo* (Schmidt et al., 1995), where levels of adenosine increase in hypoxia (Richter et al., 1999), contributing to the respiratory depression observed during this condition. In fact, blocking A1-receptors attenuates hypoxia-induced breathing in the *en bloc* of rats (Kawai et al., 1995). Thus, it has been suggested that adenosine antagonists can be useful for the treatment of several respiratory dysfunctions (Mathew, 2011).

ATP

ATP excites the preBötC *in vitro* in rats (Huxtable et al., 2009; Zwicker et al., 2011) through the activation of P2Y-receptors (Lorier et al., 2007; Huxtable et al., 2009). Interestingly, blockade of endogenous activation of P2-receptors with suramin reduced inspiratory frequency in the slice preparation, while Cu^{2+}, an allosteric modulator of purinergic receptors, produced the opposite effect (Lorier et al., 2007, 2008). ATP is released during hypoxia, and blocking its tonic action on P2-receptors increases the hypoxia-induced slowing of the respiratory rhythm, suggesting that ATP is involved in maintaining respiration in hypoxia in rats (Gourine et al., 2005). Interestingly, the excitatory effect of exogenous ATP on the preBötC is precluded when glial cells are inhibited (Huxtable et al., 2009).

ACETYLCHOLINE

Acetylcholine (ACh) is another neuromodulator that tonically regulates preBötC activity in rats and mice (Shao and Feldman, 2009). Application of the acetylcholinesterase inhibitor physostigmine increases the frequency of rhythmic respiratory activity in the slice preparation involving the type-3-muscarinic and α4β2-nicotinic receptors in rats and mice, respectively (Shao and Feldman, 2005; Shao et al., 2008). Similarly, blockade of muscarinic-receptors with atropine reduces the amplitude and frequency of the respiratory rhythm in the *en bloc* from mice (Coddou et al., 2009). In the lamprey *en bloc*, physostigmine increases the respiratory frequency, while the nicotinic antagonists D-tubocurarine or bungarotoxin reduces it (Mutolo et al., 2011).

NORADRENALINE

Pre-Bötzinger complex activity is modulated by endogenous noradrenaline released from the A5, A6, A1C1, and A2C2 nuclei in rats and mice (Hilaire et al., 2004; Viemari, 2008). This continuous modulation involves activation of α-2-adrenoreceptors, since its blockade with yohimbine, piperoxane, or phentolamine decreases respiratory frequency in the *en bloc* in rats and mice (Errchidi et al., 1990; Zanella et al., 2006; Fujii and Arata, 2010) and abolishes gasping generation in slices from mice (Viemari et al., 2011). Accordingly, decreasing the extracellular noradrenaline concentration with pargyline, desipramine, or tyrosine increases the frequency of the rhythm, while methyltyrosine, an inhibitor of noradrenaline biosynthesis, increases the *en bloc* respiratory frequency in rats and mice (Errchidi et al., 1990; Zanella et al., 2006). There is some evidence of a continuous modulation of the preBötC by histamine and dopamine. Thus, the histamine-type-1-receptor antagonist, pyrilamine, reduces the *en bloc* respiratory

frequency and attenuates respiratory depression in hypoxia in mice (Dutschmann et al., 2003), while the dopamine-type-1-receptor antagonist SCH-23390 slows the respiratory rhythm of cats *in vivo* (Lalley, 2004, 2005).

SEROTONIN

The preBötC is modulated by 5-hydroxytryptamine (5-HT), which produces an excitatory effect mediated by 5-HT2-receptors and an inhibitory effect mediated by 5-HT1-receptors (Schwarzacher et al., 2002). The main source of 5-HT is the raphe nuclei (Richerson, 2004), whose projections can or cannot make synaptic contacts with their targets throughout the brain (Kosofsky and Molliver, 1987). In the preBötC, increasing the extracellular concentration of 5-HT with 5-HT-uptake inhibitors leads to an increase of respiratory activity in the *en bloc* from rats (Di Pasquale et al., 1994). In contrast, blocking 5-HT-receptors with the non-specific antagonist methysergide abolishes rhythmogenesis in the *en bloc* and in slices from rats (Di Pasquale et al., 1994; Ptak et al., 2009). In these preparations, excitation of raphe neurons increases the frequency of the respiratory rhythm mediated by the activation of 5-HT2-receptors (Al-Zubaidy et al., 1996; Ptak et al., 2009). Accordingly, blocking either 5-HT2B-receptors (Günther et al., 2006), 5-HT2C-receptors (Ptak et al., 2009), or 5-HT2A receptors (Peña and Ramirez, 2002; Ptak et al., 2009) reduces the respiratory rhythm frequency and its regularity in slices from rats and mice. Such findings have been corroborated for 5-HT2A- and 5-HT2C-receptors *in situ* in rats (Ptak et al., 2009). Interestingly, low micromolar concentrations of 5-HT induce bursting activity in non-bursting preBötC neurons (Ptak et al., 2009), while blockade of 5-HT2A receptors abolishes the intrinsic bursting of the I_{NaP}-dependent (hypoxia-resistant) pacemaker neurons (Peña and Ramirez, 2002; Tryba et al., 2006). Consequently, blockade of 5-HT2A receptors inhibits gasping generation in slices from mice (Tryba et al., 2006) and *in situ* in rats (Bale and Solomon, 2010). These findings may have clinical relevance, since it has been hypothesized that a deficiency of the medullary 5-HT network is a potential cause of SIDS (Kinney et al., 2001).

PEPTIDES

Several neuropeptides may exert a continuous regulation of the preBötC. Neuropeptides are typical non-synaptic transmitters, which are released extrasynaptically (Torrealba and Carrasco, 2004; Wotjak et al., 2008). Blocking the endogenous activation of the opioid-receptors with naloxone increases the respiratory output in cats (Lawson et al., 1979) and reduces hypoxia-induced respiratory depression in rats (Schlenker and Inamdar, 1995). In mice, blocking endogenous activation of somatostatin-receptors increases the respiratory rhythm frequency and reduces its regularity, both in slices and *in vivo* (Ramírez-Jarquín et al., 2012). Moreover, blockade of somatostatin-receptors, specifically subtype 2, prevents the reconfiguration of the preBötC during hypoxia *in vitro* and reduces gasping generation and autoresuscitation *in vivo* (Ramírez-Jarquín et al., 2012). In contrast, substance-P maintains an excitatory continuous modulation on the preBötC in rats and mice (Ptak et al., 2009; Doi and Ramirez, 2010). Blockade of the substance-P receptor (NK1) with SR 140333 or spantide inhibits rhythmogenesis *in vitro* and *in situ* in mice and rats, respectively (Telgkamp et al., 2002; Ptak et al., 2009). Interestingly, in mice, inhibition of respiratory activity with NK1 antagonists has no significant respiratory effect when the levels of 5-HT or noradrenaline are increased by stimulating the raphe magnus or locus coeruleus, respectively (Doi and Ramirez, 2010), indicating that the action of substance-P might be influenced by the neuromodulatory state of the network (Doi and Ramirez, 2010).

POSSIBLE REGULATION OF THE preBötC BY GABA AND GLUTAMATE ACTING ON EXTRASYNAPTIC RECEPTORS

Glutamatergic and GABAergic neurons were thought to release their transmitters exclusively at synapses, where they mediate the classical "fast synaptic transmission" (Vizi et al., 2010). However, it has been shown that ambient GABA and glutamate can also tonically activate high-affinity, extrasynaptic receptors, suggesting their spill-over from synaptic boutons, mediating a slower synaptic transmission (Semyanov et al., 2004; Farrant and Nusser, 2005; Aghajanian, 2009). Extrasynaptic $GABA_A$ inhibition can modulate the generation of hippocampal fast rhythms (Scanziani, 2000; Towers et al., 2004; Mann and Mody, 2010; Papatheodoropoulos and Koniaris, 2011), and it is likely that such modulation also occurs in the preBötC, where increasing the extracellular concentration of GABA, by inhibiting its uptake with nipecotic acid, decreases the respiratory frequency (Ren and Greer, 2006). The presence of delta-subunit-containing-$GABA_A$-receptors, which are mainly extrasynaptic (Nusser et al., 1998; Adkins et al., 2001; Brown et al., 2002) suggests a tonic GABAergic control of the preBötC. For instance, the application of the $GABA_A$-receptor agonist THIP, which preferentially activates extrasynaptic $GABA_A$-receptors containing delta-subunits (Nusser et al., 1998; Adkins et al., 2001; Brown et al., 2002), hyperpolarizes respiratory neurons and reduces the frequency of the respiratory rhythm (Shao and Feldman, 1997). Neurosteroids, which also target delta-containing, extrasynaptic $GABA_A$-receptors (Stell et al., 2003; Belelli and Lambert, 2005; Scimemi et al., 2006), modulate $GABA_A$-receptor-mediated hyperpolarization of respiratory neurons and the inhibition of rhythmogenesis in slices (Ren and Greer, 2006).

Ambient glutamate can also activate extrasynaptic, NR2B-subunit-containing, NMDA-receptors and modulate neural network activity (Lambe and Aghajanian, 2006, 2007; Aghajanian, 2009). It is likely that extrasynaptic, NMDA-receptor-mediated excitation is also present in the preBötC, where inhibition of glutamate uptake with dihydrokainate increases rhythmogenesis (Greer et al., 1991; Funk et al., 1993). Dihydrokainate can also restore rhythmogenesis in substance-P-depleted slices, in which capsaicin abolishes rhythm generation (Morgado-Valle and Feldman, 2004). Similarly, releasing NMDA-receptors from their Mg^{2+}-blockade restores rhythmogenesis in slices where the rhythm is abolished by AMPA-receptor blockade (Morgado-Valle and Feldman, 2007). This evidence supports the notion that a tone of extracellular glutamate can participate in rhythmogenesis. Furthermore, the presence of the NR2B-receptor has been extensively documented in the preBötC (Watanabe et al., 1994; Paarmann et al., 2000, 2005; Liu and Wong-Riley, 2010).

GLIAL MODULATION OF THE preBötC

Glial cells are integral functional elements of neural networks, since it is argued that they can respond to and regulate neuronal activity (Araque and Navarrete, 2010). The respiratory network is not an exception (Gourine et al., 2010). Glial cells can sense preBötC activity, and a portion of them display a phase-locked rhythmic activity (Schnell et al., 2011). Moreover, glial cells are essential for rhythmogenesis, since both fluoroacetate, which selectively blocks the glial Krebs cycle, and methionine-sulfoximine, which blocks glutamine synthetase (Hülsmann et al., 2000; Young et al., 2005; Huxtable et al., 2010), inhibit rhythmic respiratory burst activity in slices. In these conditions, addition of isocitrate or glutamine restores the rhythmic network activity (Hülsmann et al., 2000). Accordingly, methionine-sulfoximine-treated pups displayed a reduced breathing frequency and a reduced responsiveness to hypercapnia (Young et al., 2005). Moreover, glial cells are required not only for maintaining rhythm generation but also for the response of the preBötC to neuromodulators or to metabolic demands (Gourine et al., 2010). For instance, fluoroacetate and methionine-sulfoximine reduce preBötC responsiveness to ATP (Huxtable et al., 2010), and preBötC glial cells can respond to preBötC neuromodulators including 5-HT and substance-P (Härtel et al., 2009).

I conclude that continuous neuromodulation exerts a powerful influence on the preBötC; to the extent that, in some cases, it is necessary for rhythm generation. Continuous neuromodulation tunes the excitability of the preBötC to respond to different demands and also determines the weight of specific neuronal types or specific synaptic interactions in the generation of network dynamics. This property could allow the preBötC to adopt an infinite number of conformations based on the same circuit (neural units and connections). Moreover, the evidence that one neuromodulation is determined by tonic control exerted by other neuromodulators, supports the notion that the intrinsic and synaptic properties of the preBötC are not fixed, but can change in a state-dependent manner. The levels of modulation in the preBötC would determine the availability of neural properties (intrinsic, synaptic, or both) that can participate in network dynamics or are susceptible to subsequent neuromodulation.

ACKNOWLEDGMENTS

I would like to thank Dorothy Pless for reviewing the English version of this paper. I also thank José Rodolfo Fernandez and Arturo Franco for technical assistance. The research in my group is sponsored by grants (to F P-O) from DGAPA IB200212, CONACyT 151261, 181323 and from the Alzheimer's Association NIRG-11-205443.

REFERENCES

Adkins, C. E., Pillai, G. V., Kerby, J., Bonnert, T. P., Haldon, C., McKernan, R. M., Gonzalez, J. E., Oades, K., Whiting, P. J., and Simpson, P. B. (2001). Alpha4beta3delta GABAA receptors characterized by fluorescence resonance energy transfer-derived measurements of membrane potential. *J. Biol. Chem.* 276, 38934–38939.

Aghajanian, G. K. (2009). Modeling "psychosis" in vitro by inducing disordered neuronal network activity in cortical brain slices. *Psychopharmacology (Berl.)* 206, 575–585.

Al-Zubaidy, Z. A., Erickson, R. L., and Greer, J. J. (1996). Serotonergic and noradrenergic effects on respiratory neural discharge in the medullary slice preparation of neonatal rats. *Pflugers Arch.* 431, 942–949.

Araque, A., and Navarrete, M. (2010). Glial cells in neuronal network function. *Philos. Trans. R. Soc. Lond. B. Biol. Sci.* 365, 2375–2381.

Armstrong, G. A., López-Guerrero, J. J., Dawson-Scully, K., Peña, F., and Robertson, R. M. (2010). Inhibition of protein kinase G activity protects neonatal mouse respiratory network from hyperthermic and hypoxic stress. *Brain Res.* 1311, 64–72.

Bale, T. A., and Solomon, I. C. (2010). Influence of 5-HT2A receptor blockade on phrenic nerve discharge at three levels of extracellular K+ in arterially-perfused adult rat. *Adv. Exp. Med. Biol.* 669, 139–142.

Ballanyi, K. (2004). Neuromodulation of the perinatal respiratory network. *Curr. Neuropharmacol.* 2, 221–243.

Belelli, D., and Lambert, J. J. (2005). Neurosteroids, endogenous regulators of the GABAA receptor. *Nat. Rev. Neurosci.* 7, 565–575.

Brown, N., Kerby, J., Bonnert, T. P., Whiting, P. J., and Wafford, K. A. (2002). Pharmacological characterization of a novel cell line expressing human alpha 4beta 3delta GABAA. receptors. *Br. J. Pharmacol.* 136, 965–974.

Coddou, C., Bravo, E., and Eugenín, J. (2009). Alterations in cholinergic sensitivity of respiratory neurons induced by pre-natal nicotine, a mechanism for respiratory dysfunction in neonatal mice. *Philos. Trans. R. Soc. Lond. B. Biol. Sci.* 364, 2527–2535.

Cunha, R. A. (2008). Different cellular sources and different roles of adenosine, A1 receptor-mediated inhibition through astrocytic-driven volume transmission and synapse-restricted A2A receptor-mediated facilitation of plasticity. *Neurochem. Int.* 52, 65–72.

Del Negro, C. A., Morgado-Valle, C., Hayes, J. A., Mackay, D. D., Pace, R. W., Crowder, E. A., and Feldman, J. L. (2005). Sodium and calcium current-mediated pacemaker neurons and rhythmogenesis. *J. Neurosci.* 25, 446–453.

De-Miguel, F. F., and Trueta, C. (2005). Synaptic and extrasynaptic secretion of serotonin. *Cell. Mol. Neurobiol.* 25, 297–312.

Descarries, L., and Mechawar, N. (2000). Ultrastructural evidence for diffuse transmission by monoamine and acetylcholine neurons of the central nervous system. *Prog. Brain Res.* 125, 27–47.

Di Pasquale, E., Monteau, R., and Hilaire, G. (1994). Endogenous serotonin modulates the fetal respiratory rhythm, an in vitro study in the rat. *Brain Res. Dev. Brain Res.* 80, 222–232.

Doi, A., and Ramirez, J. M. (2008). Neuromodulation and the orchestration of the respiratory rhythm. *Respir. Physiol. Neurobiol.* 164, 96–104.

Doi, A., and Ramirez, J. M. (2010). State-dependent interactions between excitatory neuromodulators in the neuronal control of breathing. *J. Neurosci.* 30, 8251–8262.

Dutschmann, M., Bischoff, A. M., Büsselberg, D., and Richter, D. W. (2003). Histaminergic modulation of the intact respiratory network of adult mice. *Pflugers Arch.* 445, 570–576.

Errchidi, S., Hilaire, G., and Monteau, R. (1990). Permanent release of noradrenaline modulates respiratory frequency in the newborn rat, an in vitro study. *J. Physiol. (Lond.)* 429, 497–510.

Farrant, M., and Nusser, Z. (2005). Variations on an inhibitory theme, phasic and tonic activation of GABA A). receptors. *Nat. Rev. Neurosci.* 6, 215–229.

Feldman, J. L., and Del Negro, C. A. (2006). Looking for inspiration, new perspectives on respiratory rhythm. *Nat. Rev. Neurosci.* 7, 232–242.

Fewell, J. E., Zhang, C., and Gillis, A. M. (2007). Influence of adenosine A1-receptor blockade and vagotomy on the gasping and heart rate response to hypoxia in rats during early postnatal maturation. *J. Appl. Physiol.* 103, 1234–1241.

Fujii, M., and Arata, A. (2010). Adrenaline modulates on the respiratory network development. *Adv. Exp. Med. Biol.* 669, 25–28.

Funk, G. D., Smith, J. C., and Feldman, J. L. (1993). Generation and transmission of respiratory oscillations in medullary slices, role of excitatory amino acids. *J. Neurophysiol.* 70, 1497–1515.

Gourine, A. V., Kasymov, V., Marina, N., Tang, F., Figueiredo, M. F., Lane, S., Teschemacher, A. G., Spyer, K. M., Deisseroth, K., and Kasparov, S. (2010). Astrocytes control breathing through pH-dependent release of ATP. *Science* 329, 571–575.

Gourine, A. V., Llaudet, E., Dale, N., and Spyer, K. M. (2005). Release of ATP in the ventral medulla during hypoxia in rats, role in hypoxic ventilatory response. *J. Neurosci.* 25, 1211–1218.

Gozal, D., Gozal, E., Reeves, S. R., and Lipton, A. J. (2002). Gasping and autoresuscitation in the developing rat, effect of antecedent intermittent hypoxia. *J. Appl. Physiol.* 92, 1141–1144.

Greer, J. J., Smith, J. C., and Feldman, J. L. (1991). Role of excitatory amino acids in the generation and transmission of respiratory drive in neonatal rat. *J. Physiol. (Lond.)* 437, 727–749.

Günther, S., Maroteaux, L., and Schwarzacher, S. W. (2006). Endogenous 5-HT2B receptor activation regulates neonatal respiratory activity in vitro. *J. Neurobiol.* 66, 949–961.

Härtel, K., Schnell, C., and Hülsmann, S. (2009). Astrocytic calcium signals induced by neuromodulators via functional metabotropic receptors in the ventral respiratory group of neonatal mice. *Glia* 57, 815–827.

Hehre, D. A., Devia, C. J., Bancalari, E., and Suguihara, C. (2008). Brainstem amino acid neurotransmitters and ventilatory response to hypoxia in piglets. *Pediatr. Res.* 63, 46–50.

Herlenius, E., and Lagercrantz, H. (1999). Adenosinergic modulation of respiratory neurons in the neonatal rat brainstem in vitro. *J. Physiol. (Lond.)* 518, 159–172.

Hilaire, G., Viemari, J. C., Coulon, P., Simonneau, M., and Bévengut, M. (2004). Modulation of the respiratory rhythm generator by the pontine noradrenergic A5 and A6 groups in rodents. *Respir. Physiol. Neurobiol.* 143, 187–197.

Hülsmann, S., Oku, Y., Zhang, W., and Richter, D. W. (2000). Metabolic coupling between glia and neurons is necessary for maintaining respiratory activity in transverse medullary slices of neonatal mouse. *Eur. J. Neurosci.* 12, 856–862.

Huxtable, A. G., Zwicker, J. D., Alvares, T. S., Ruangkittisakul, A., Fang, X., Hahn, L. B., Posse de Chaves, E., Baker, G. B., Ballanyi, K., and Funk, G. D. (2010). Glia contribute to the purinergic modulation of inspiratory rhythm-generating networks. *J. Neurosci.* 30, 3947–3958.

Huxtable, A. G., Zwicker, J. D., Poon, B. Y., Pagliardini, S., Vrouwe, S. Q., Greer, J. J., and Funk, G. D. (2009). Tripartite purinergic modulation of central respiratory networks during perinatal development, the influence of ATP., ectonucleotidases, and ATP metabolites. *J. Neurosci.* 29, 14713–14725.

Katz, P. S. (1998). Comparison of extrinsic and intrinsic neuromodulation in two central pattern generator circuits in invertebrates. *Exp. Physiol.* 83, 281–292.

Kawai, A., Okada, Y., Mückenhoff, K., and Scheid, P. (1995). Theophylline and hypoxic ventilator response in the rat isolated brainstem-spinal cord. *Respir. Physiol.* 100, 25–32.

Kinney, H. C., Filiano, J. J., and White, W. F. (2001). Medullary serotonergic network deficiency in the sudden infant death syndrome, review of a 15-year study of a single dataset. *J. Neuropathol. Exp. Neurol.* 60, 228–247.

Kosofsky, B. E., and Molliver, M. E. (1987). The serotoninergic innervation of cerebral cortex, different classes of axon terminals arise from dorsal and median raphe nuclei. *Synapse* 2, 153–168.

Lalley, P. M. (2004). Dopamine1 receptor agonists reverse opioid respiratory network depression, increase CO2 reactivity. *Respir. Physiol. Neurobiol.* 139, 247–262.

Lalley, P. M. (2005). D1-dopamine receptor blockade slows respiratory rhythm and enhances opioid-mediated depression. *Respir. Physiol. Neurobiol.* 145, 13–22.

Lambe, E. K., and Aghajanian, G. K. (2006). Hallucinogen-induced UP states in the brain slice of rat prefrontal cortex, role of glutamate spillover and NR2B-NMDA receptors. *Neuropsychopharmacology* 31, 1682–1689.

Lambe, E. K., and Aghajanian, G. K. (2007). Prefrontal cortical network activity, opposite effects of psychedelic hallucinogens and D1/D5 dopamine receptor activation. *Neuroscience* 145, 900–910.

Lawson, E. E., Waldrop, T. G., and Eldridge, F. L. (1979). Naloxone enhances respiratory output in cats. *J. Appl. Physiol.* 47, 1105–1111.

Lieske, S. P., Thoby-Brisson, M., Telgkamp, P., and Ramirez, J. M. (2000). Reconfiguration of the neural network controlling multiple breathing patterns, eupnea, sighs and gasps. *Nat. Neurosci.* 3, 600–607.

Liu, Q., and Wong-Riley, M. T. (2010). Postnatal development of N-methyl-D-aspartate receptor subunits 2A, 2B, 2C, 2D, and 3B immunoreactivity in brain stem respiratory nuclei of the rat. *Neuroscience* 171, 637–654.

Lorier, A. R., Huxtable, A. G., Robinson, D. M., Lipski, J., Housley, G. D., and Funk, G. D. (2007). P2Y1 receptor modulation of the pre-Bötzinger complex inspiratory rhythm generating network in vitro. *J. Neurosci.* 27, 993–1005.

Lorier, A. R., Lipski, J., Housley, G. D., Greer, J. J., and Funk, G. D. (2008). ATP sensitivity of preBötzinger complex neurones in neonatal rat in vitro, mechanism underlying a P2 receptor-mediated increase in inspiratory frequency. *J. Physiol. (Lond.)* 586, 1429–1446.

Mann, E. O., and Mody, I. (2010). Control of hippocampal gamma oscillation frequency by tonic inhibition and excitation of interneurons. *Nat. Neurosci.* 13, 205–212.

Marder, E., and Bucher, D. (2007). Understanding circuit dynamics using the stomatogastric nervous system of lobsters and crabs. *Annu. Rev. Physiol.* 69, 291–316.

Martín, E. D., Fernández, M., Perea, G., Pascual, O., Haydon, P. G., Araque, A., and Ceña, V. (2007). Adenosine released by astrocytes contributes to hypoxia-induced modulation of synaptic transmission. *Glia* 55, 36–45.

Mathew, O. P. (2011). Apnea of prematurity, pathogenesis, and management strategies. *J. Perinatol.* 31, 302–310.

Morgado-Valle, C., and Feldman, J. L. (2004). Depletion of substance P and glutamate by capsaicin blocks respiratory rhythm in neonatal rat in vitro. *J. Physiol. (Lond.)* 555, 783–792.

Morgado-Valle, C., and Feldman, J. L. (2007). NMDA receptors in pre-Botzinger complex neurons can drive respiratory rhythm independent of AMPA receptors. *J. Physiol. (Lond.)* 582, 359–368.

Mutolo, D., Cinelli, E., Bongianni, F., and Pantaleo, T. (2011). Identification of a cholinergic modulatory and rhythmogenic mechanism within the lamprey respiratory network. *J. Neurosci.* 31, 13323–13332.

Nusser, Z., Sieghart, W., and Somogyi, P. (1998). Segregation of different GABAA receptors to synaptic, and extrasynaptic membranes of cerebellar granule cells. *J. Neurosci.* 18, 1693–1703.

Paarmann, I., Frermann, D., Keller, B. U., and Hollmann, M. (2000). Expression of 15 glutamate receptor subunits and various splice variants in tissue slices and single neurons of brainstem nuclei and potential functional implications. *J. Neurochem.* 74, 1335–1345.

Paarmann, I., Frermann, D., Keller, B. U., Villmann, C., Breitinger, H. G., and Hollmann, M. (2005). Kinetics and subunit composition of NMDA receptors in respiratory-related neurons. *J. Neurochem.* 93, 812–824.

Papatheodoropoulos, C., and Koniaris, E. (2011). α5GABAA receptors regulate hippocampal sharp wave-ripple activity in vitro. *Neuropharmacology* 60, 662–673.

Peña, F. (2008). Contribution of pacemaker neurons to respiratory rhythms generation in vitro. *Adv. Exp. Med. Biol.* 605, 114–118.

Peña, F. (2009). Neuronal network properties underlying the generation of gasping. *Clin. Exp. Pharmacol. Physiol.* 36, 1218–1228.

Peña, F., and Aguileta, M. A. (2007). Effects of riluzole, and flufenamic acid on eupnea, and gasping of neonatal mice in vivo. *Neurosci. Lett.* 415, 288–293.

Peña, F., and García, O. (2006). Breathing generation and potential pharmacotherapeutic approaches to central respiratory disorders. *Curr. Med. Chem.* 13, 2681–2693.

Peña, F., Meza-Andrade, R., Páez-Zayas, V., and González-Marín, M. C. (2008). Gasping generation in developing Swiss-Webster mice in vitro and in vivo. *Neurochem. Res.* 33, 1492–1500.

Peña, F., Parkis, M. A., Tryba, A. K., and Ramirez, J. M. (2004). Differential contribution of pacemaker properties to the generation of respiratory rhythms during normoxia, and hypoxia. *Neuron* 43, 105–117.

Peña, F., and Ramirez, J. M. (2002). Endogenous activation of serotonin-2A receptors is required for rhythmogenesis in vitro. *J. Neurosci.* 22, 11055–11064.

Peña, F., and Ramirez, J. M. (2004). Substance P-mediated modulation of pacemaker properties in the mammalian respiratory network. *J. Neurosci.* 24, 7549–7556.

Peña, F., and Ramirez, J. M. (2005). Hypoxia-induced changes in neuronal network properties. *Mol. Neurobiol.* 32, 251–283.

Peña, F., and Tapia, R. (1999). Relationships among seizures, extracellular amino acid changes, and neurodegeneration induced by 4-aminopyridine in rat hippocampus: a microdialysis and electrncephalographic study. *J. Neurochem.* 72, 2006–2014.

Peña, F., and Tapia, R. (2000). Seizures and neurodegeneration induced by 4-aminopyridine in rat hippocampus in vivo: role of glutamate- and GABA-mediated neurotransmission and of ion channels. *Neuroscience* 101, 547–561.

Poets, C. F., Meny, R. G., Chobanian, M. R., and Bonofiglo, R. E. (1999). Gasping and other

cardiorespiratory patterns during sudden infant deaths. *Pediatr. Res.* 45, 350–354.

Ptak, K., Yamanishi, T., Aungst, J., Milescu, L. S., Zhang, R., Richerson, G. B., and Smith, J. C. (2009). Raphé neurons stimulate respiratory circuit activity by multiple mechanisms via endogenously released serotonin and substance P. *J. Neurosci.* 29, 3720–3737.

Ramirez, J. M., Schwarzacher, S. W., Pierrefiche, O., Olivera, B. M., and Richter, D. W. (1998). Selective lesioning of the cat pre-Bötzinger complex in vivo eliminates breathing but not gasping. *J. Physiol. (Lond.)* 507, 895–907.

Ramirez, J. M., Tryba, A. K., and Peña, F. (2004). Pacemaker neurons and neuronal networks, an integrative view. *Curr. Opin. Neurobiol.* 14, 665–674.

Ramírez-Jarquín, J. O., Lara-Hernández, S., López-Guerrero, J. J., Aguileta, M. A., Rivera-Angulo, A. J., Sampieri, A., Vaca, L., Ordaz, B., and Peña-Ortega, F. (2012). Somatostatin modulates generation of inspiratory rhythms and determines asphyxia survival. *Peptides* 34, 360–372.

Ren, J., and Greer, J. J. (2006). Neurosteroid modulation of respiratory rhythm in rats during the perinatal period. *J. Physiol. (Lond.)* 574, 535–546.

Richerson, G. B. (2004). Serotonergic neurons as carbon dioxide sensors that maintain pH homeostasis. *Nat. Rev. Neurosci.* 5, 449–461.

Richter, D. W., Schmidt-Garcon, P., Pierrefiche, O., Bischoff, A. M., and Lalley, P. M. (1999). Neurotransmitters and neuromodulators controlling the hypoxic respiratory response in anaesthetized cats. *J. Physiol. (Lond.)* 514, 567–578.

Scanziani, M. (2000). GABA spillover activates postsynaptic GABA B) receptors to control rhythmic hippocampal activity. *Neuron* 25, 673–681.

Schlenker, E. H., and Inamdar, S. R. (1995). Effects of naloxone on oxygen consumption and ventilation in awake golden Syrian hamsters. *Physiol. Behav.* 57, 655–658.

Schmidt, C., Bellingham, M. C., and Richter, D. W. (1995). Adenosinergic modulation of respiratory neurones and hypoxic responses in the anaesthetized cat. *J. Physiol. (Lond.)* 483, 769–781.

Schnell, C., Fresemann, J., and Hülsmann, S. (2011). Determinants of functional coupling between astrocytes and respiratory neurons in the pre-Bötzinger complex. *PLoS ONE* 6, e26309. doi:10.1371/journal.pone.0026309

Schwarzacher, S. W., Pestean, A., Günther, S., and Ballanyi, K. (2002). Serotonergic modulation of respiratory motoneurons and interneurons in brainstem slices of perinatal rats. *Neuroscience* 115, 1247–1259.

Schwarzacher, S. W., Rüb, U., and Deller, T. (2011). Neuroanatomical characteristics of the human pre-Bötzinger complex and its involvement in neurodegenerative brainstem diseases. *Brain* 134, 24–35.

Scimemi, A., Andersson, A., Heeroma, J. H., Strandberg, J., Rydenhag, B., McEvoy, A. W., Thom, M., Asztely, F., and Walker, M. C. (2006). Tonic GABAA receptor-mediated currents in human brain. *Eur. J. Neurosci.* 24, 1157–1160.

Semyanov, A., Walker, M. C., Kullmann, D. M., and Silver, R. A. (2004). Tonically active GABA A receptors, modulating gain and maintaining the tone. *Trends Neurosci.* 27, 262–269.

Shao, X. M., and Feldman, J. L. (1997). Rhythmogenesis and synaptic inhibition of expiratory neurons in pre-Bötzinger complex, differential roles of glycinergic and GABAergic neural transmission. *J. Neurophysiol.* 77, 1853–1860.

Shao, X. M., and Feldman, J. L. (2005). Cholinergic neurotransmission in the preBötzinger Complex modulates excitability of inspiratory neurons and regulates respiratory rhythm. *Neuroscience* 130, 1069–1081.

Shao, X. M., and Feldman, J. L. (2009). Central cholinergic regulation of respiration, nicotinic receptors. *Acta Pharmacol. Sin.* 30, 761–770.

Shao, X. M., Tan, W., Xiu, J., Puskar, N., Fonck, C., Lester, H. A., and Feldman, J. L. (2008). Alpha4∗ nicotinic receptors in preBotzinger complex mediate cholinergic/nicotinic modulation of respiratory rhythm. *J. Neurosci.* 28, 519–528.

Smith, J. C., Ellenberger, H. H., Ballanyi, K., Richter, D. W., and Feldman, J. L. (1991). Pre-Bötzinger complex: a brainstem region that may generate respiratory rhythm in mammals. *Science* 254, 726–729.

Sridhar, R., Thach, B. T., Kelly, D. H., and Henslee, J. A. (2003). Characterization of successful and failed autoresuscitation in human infants, including those dying of SIDS. *Pediatr. Pulmonol.* 36, 113–122.

Stell, B. M., Brickley, S. G., Tang, C. Y., Farrant, M., and Mody, I. (2003). Neuroactive steroids reduce neuronal excitability by selectively enhancing tonic inhibition mediated by delta subunit-containing GABAA receptors. *Proc. Natl. Acad. Sci. U.S.A.* 100, 14439–14444.

Telgkamp, P., Cao, Y. Q., Basbaum, A. I., and Ramirez, J. M. (2002). Long-term deprivation of substance P in PPT-A mutant mice alters the anoxic response of the isolated respiratory network. *J. Neurophysiol.* 88, 206–213.

Thoby-Brisson, M., and Ramirez, J. M. (2001). Identification of two types of inspiratory pacemaker neurons in the isolated respiratory neural network of mice. *J. Neurophysiol.* 86, 104–112.

Torrealba, F., and Carrasco, M. A. (2004). A review on electron microscopy and neurotransmitter systems. *Brain Res. Brain Res. Rev.* 47, 5–17.

Towers, S. K., Gloveli, T., Traub, R. D., Driver, J. E., Engel, D., Fradley, R., Rosahl, T. W., Maubach, K., Buhl, E. H., and Whittington, M. A. (2004). Alpha 5 subunit-containing GABAA receptors affect the dynamic range of mouse hippocampal kainate-induced gamma frequency oscillations in vitro. *J. Physiol. (Lond.)* 559, 721–728.

Tryba, A. K., Peña, F., and Ramirez, J. M. (2006). Gasping activity in vitro, a rhythm dependent on 5-HT2A receptors. *J. Neurosci.* 26, 2623–2634.

Viemari, J. C. (2008). Noradrenergic modulation of the respiratory neural network. *Respir. Physiol. Neurobiol.* 164, 123–130.

Viemari, J. C., Garcia, A. J. III, Doi, A., and Ramirez, J. M. (2011). Activation of alpha-2 noradrenergic receptors is critical for the generation of fictive eupnea and fictive gasping inspiratory activities in mammals in vitro. *Eur. J. Neurosci.* 33, 2228–2237.

Vizi, E. S., Fekete, A., Karoly, R., and Mike, A. (2010). Non-synaptic receptors and transporters involved in brain functions and targets of drug treatment. *Br. J. Pharmacol.* 160, 785–809.

Watanabe, M., Mishina, M., and Inoue, Y. (1994). Distinct distributions of five NMDA receptor channel subunit mRNAs in the brainstem. *J. Comp. Neurol.* 343, 520–531.

Wenninger, J. M., Pan, L. G., Klum, L., Leekley, T., Bastastic, J., Hodges, M. R., Feroah, T. R., Davis, S., and Forster, H. V. (2004). Large lesions in the pre-Bötzinger complex area eliminate eupneic respiratory rhythm in awake goats. *J. Appl. Physiol.* 97, 1629–1636.

Wilken, B., Ramirez, J. M., Hanefeld, F., and Richter, D. W. (2000). Aminophylline modulation of the mouse respiratory network changes during postnatal maturation. *J. Appl. Physiol.* 89, 2015–2022.

Wotjak, C. T., Landgraf, R., and Engelmann, M. (2008). Listening to neuropeptides by microdialysis, echoes and new sounds? *Pharmacol. Biochem. Behav.* 90, 125–134.

Young, J. K., Dreshaj, I. A., Wilson, C. G., Martin, R. J., Zaidi, S. I., and Haxhiu, M. A. (2005). An astrocyte toxin influences the pattern of breathing and the ventilatory response to hypercapnia in neonatal rats. *Respir. Physiol. Neurobiol.* 147, 19–30.

Zanella, S., Roux, J. C., Viemari, J. C., and Hilaire, G. (2006). Possible modulation of the mouse respiratory rhythm generator by A1/C1 neurones. *Respir. Physiol. Neurobiol.* 153, 126–138.

Zavala-Tecuapetla, C., Aguileta, M. A., Lopez-Guerrero, J. J., González-Marín, M. C., and Peña, F. (2008). Calcium-activated potassium currents differentially modulate rhythmogenesis. *Eur. J. Neurosci.* 27, 2871–2884.

Zwicker, J. D., Rajani, V., Hahn, L. B., and Funk, G. D. (2011). Purinergic modulation of preBötzinger complex inspiratory rhythm in rodents: the interaction between ATP and adenosine. *J. Physiol. (Lond.)* 589, 4583–4600.

Conflict of Interest Statement: The author declares that the research was conducted in the absence of any commercial or financial relationships that could be construed as a potential conflict of interest.

Received: 22 March 2012; accepted: 19 June 2012; published online: 20 July 2012. Citation: Peña-Ortega F (2012) Tonic neuromodulation of the inspiratory rhythm generator. Front. Physio. ***3****:253. doi: 10.3389/fphys.2012.00253*

This article was submitted to Frontiers in Membrane Physiology and Biophysics, a specialty of Frontiers in Physiology.

frontiers in
PHYSIOLOGY

ORIGINAL RESEARCH ARTICLE
published: 06 November 2012
doi: 10.3389/fphys.2012.00414

The dynamics of somatic exocytosis in monoaminergic neurons

Bidyut Sarkar, Anand Kant Das, Senthil Arumugam†, Sanjeev Kumar Kaushalya†, Arkarup Bandyopadhyay†, Jayaprakash Balaji† and Sudipta Maiti*

Department of Chemical Sciences, Tata Institute of Fundamental Research, Mumbai, India

Edited by:
Francisco F. De-Miguel, Universidad Nacional Autonoma de Mexico, Mexico

Reviewed by:
Francisco F. De-Miguel, Universidad Nacional Autonoma de Mexico, Mexico
Citlali Trueta, Instituto Nacional de Psiquiatria Ramon de la Fuente Muñiz, Mexico

***Correspondence:**
Sudipta Maiti, Department of Chemical Sciences, Tata Institute of Fundamental Research, Mumbai 400005, India.
e-mail: maiti@tifr.res.in

†Present address:
Senthil Arumugam, Max Planck Institute of Molecular Cell Biology and Genetics and Biotechnology centre of the TU Dresden, Dresden 01307, Germany;
Sanjeev Kumar Kaushalya, Institute of Pharmacology, University of Heidelberg, Im Neuenheimer Feld 366, D-69120 Heidelberg, Germany;
Arkarup Bandyopadhyay, Watson School of Biological Sciences, Cold Spring Harbor Laboratory, Cold Spring Harbor, NY 11724, USA;
Jayaprakash Balaji, Centre for Neuroscience, Indian Institute of Science, Bangalore 560012, India.

Some monoaminergic neurons can release neurotransmitters by exocytosis from their cell bodies. The amount of monoamine released by somatic exocytosis can be comparable to that released by synaptic exocytosis, though neither the underlying mechanisms nor the functional significance of somatic exocytosis are well understood. A detailed examination of these characteristics may provide new routes for therapeutic intervention in mood disorders, substance addiction, and neurodegenerative diseases. The relatively large size of the cell body provides a unique opportunity to understand the mechanism of this mode of neuronal exocytosis in microscopic detail. Here we used three photon and total internal reflection fluorescence microscopy to focus on the dynamics of the pre-exocytotic events and explore the nature of somatic vesicle storage, transport, and docking at the membrane of serotonergic neurons from raphe nuclei of the rat brain. We find that the vesicles (or unresolved vesicular clusters) are quiescent (mean square displacement, MSD $\sim$0.04 μm^2/s) before depolarization, and they move minimally ($<$1 μm) from their locations over a timescale of minutes. However, within minutes of depolarization, the vesicles become more dynamic (MSD $\sim$0.3 μm^2/s), and display larger range (several μm) motions, though without any clear directionality. Docking and subsequent exocytosis at the membrane happen at a timescale ($\sim$25 ms) that is slower than most synaptic exocytosis processes, but faster than almost all somatic exocytosis processes observed in endocrine cells. We conclude that, (A) depolarization causes de-tethering of the neurotransmitter vesicles from their storage locations, and this constitutes a critical event in somatic exocytosis; (B) their subsequent transport kinetics can be described by a process of constrained diffusion, and (C) the pre-exocytosis kinetics at the membrane is faster than most other somatic exocytosis processes reported so far.

Keywords: confocal microscopy, depolarization, multiphoton imaging, neurotransmission, serotonin, total internal reflectio fluo escence microscopy, vesicle dynamics

INTRODUCTION

Monoaminergic neurotransmission is important for processes related to mood, memory, reward, and for neurodegenerative diseases such as Parkinson's and Alzheimer's (Carlsson, 1987; Nazarali and Reynolds, 1992; Kurian et al., 2011). Most monoaminergic neurotransmission is thought to occur through the synaptic exocytosis route. However, over the years, it has been shown that a substantial part of monoamine release may be extra synaptic (Descarries et al., 1975; Agnati et al., 1986; Bunin and Wightman, 1998; De-Miguel and Trueta, 2005; Fuxe et al., 2007; Kaushalya et al., 2008a; De-Miguel and Fuxe, 2012; Trueta and De-Miguel, 2012). Monoamine neurotransmitters in CNS neurons are contained in vesicles that are located not only at the synaptic terminals and in axonal processes, but also in the cell body (Coggeshall, 1972). Somatic release of neurotransmitters has been observed for more than three decades (Johnson and Pilar, 1980; Suetake et al., 1981; Agnati et al., 2010) and its quantal nature (suggesting vesicular release akin to synaptic exocytosis) was convincingly demonstrated in dopaminergic neurons of *Planorbis corneus* more than a decade ago (Chen et al., 1995). Subsequently, the phenomenon has been observed in multiple systems, including the dopaminergic neurons of rat and mice (Jaffe et al., 1998; Puopolo et al., 2001). This has also been observed in serotonergic neurons, such as the Retzius neurons of the leech (Bruns et al., 2000; Trueta et al., 2003, 2004; De-Miguel and Trueta, 2005), raphe neurons of the rat (Kaushalya and Maiti, 2008; Kaushalya et al., 2008a,c; Colgan et al., 2009), the mesencephalic trigeminal nucleus of the rat (Zhang et al., 2012), and in differentiated human embryonic stem cells (Kumar et al., 2009). De-Miguel and coworkers have identified the nature of the calcium channels which couple to the somatic exocytosis of serotonin (Trueta et al., 2003, 2004; De-Miguel and Trueta, 2005). However, not much is understood about the mechanism underlying this novel mode of exocytosis, and the role it may be playing in neurotransmission and neuromodulation.

In addition to its yet to be discovered role in normal neurotransmission, somatic exocytosis potentially offers a powerful handle to therapeutically control mood disorders, substance addiction, and neurodegenerative diseases in the human brain. Moreover, the sheer size of the soma compared to that of a typical presynaptic terminal offers a unique advantage for understanding this mode of neurotransmitter exocytosis, especially the pre-exocytosis events. However, this aspect is yet to be exploited fully.

One of the recurrent questions is how the characteristics of somatic exocytosis compare to the more common processes of synaptic exocytosis. Synaptic exocytosis is characterized by several defining aspects. For example, synapses contain different pools of readily releasable and reserve set of vesicles (Murthy and Stevens, 1999). These vesicles are relatively uniform in size (∼40 nm diameter) and neurotransmitter concentration (which is typically about a few 100 mM). The process is critically controlled by the increase of intracellular Ca^{++} levels which occurs rapidly after depolarization (Katz and Miledi, 1970; Llinas et al., 1981). Exocytosis occurs at special regions of the synapse which are known as "active zones." A number of proteins (such as CaM kinase II and synapsin I; Llinas et al., 1991) and networks of macromolecules, called "active zone materials," are involved in the release from the cytoskeleton, and subsequent transport and docking of the vesicles during exocytosis (Szule et al., 2012). The residence time of the vesicles at the membrane can be as low as 10 ms (He et al., 2006), or even a fraction of a ms (Wolfel and Schneggenburger, 2003). The whole cycle of vesicle filling, priming, exocytosis, and endocytosis typically takes less than 30 s (Ryan et al., 1993).

Some of these aspects have been studied for somatic exocytosis and clear similarities and differences with synaptic exocytosis have been found. Somatic vesicles, as observed in transmission electron microscopy (TEM) images, are usually larger than their synaptic counterparts, and range from ∼80 to a few 100 nm (Coggeshall, 1972; Bruns and Jahn, 1995; Chen et al., 1995; Bruns et al., 2000; Puopolo et al., 2001; Trueta et al., 2003). They appear to be of two types, large dense core vesicles, and smaller clear vesicles, the later being similar to those found at synapses (De-Miguel and Trueta, 2005). Some of the somatic (clear) vesicles can be organized in multi-vesicular bodies, which seem to get processed into dense core vesicles near the Golgi (Trueta et al., 2012). The process of exocytosis is known to be Ca^{++} dependent (Johnson and Pilar, 1980; Puopolo et al., 2001; Trueta et al., 2003, 2004; Patel et al., 2009). Also the neurotransmitter concentration of the vesicles is fairly similar, though dense core vesicles contain about an order of magnitude larger number of molecules compared to the synaptic vesicles (Bruns et al., 2000). It has been shown that three photon microscopy can directly visualize serotonin (Maiti et al., 1997). In our laboratory, we have employed this technique to uncover further aspects of somatic exocytosis in mammalian serotonergic neurons. We have shown that somatic vesicles can be imaged in live neurons and their contents can be estimated (Balaji et al., 2005). This is facilitated by changes in the serotonin emission spectrum under vesicular conditions (Kaushalya et al., 2008b; Nag et al., 2008). Quantitatively, somatic exocytosis forms a substantial fraction of the total serotonin release in a rat brain section under depolarization (Kaushalya et al., 2008c). Three photon microscopy of serotonergic neurons of the raphe nucleus of the rat brain has revealed serotonin fluorescent spots with an average diameter of ∼370 nm with an estimated serotonin concentration of ∼100's of mM (Kaushalya et al., 2008a; Nag et al., 2008). These individual spots could be large vesicles, or they can be unresolved clusters of multiple vesicles (Trueta et al., 2012). These serotonin fluorescent spots are distributed throughout the soma, but most seem to be arranged in a perinuclear fashion. These contents get exocytosed without any specific dependence on their storage locations, and they show no clear evidence of the presence of a reserve pool of vesicles. In low time resolution measurements (one frame per several minutes) the serotonin fluorescent spots appear fairly stationary at their "storage" locations until they stochastically disappear upon serotonin exocytosis. Later work using multiphoton microscopy has suggested that newly recycled serotonin vesicles release faster than a pre-existing reserve pool (Colgan et al., 2009). Also, a Total Internal Reflection Fluorescence (TIRF) study shows that exocytosis happens fairly uniformly throughout the basal cell membrane (through which the cell adheres to the cover glass), without any apparent active zone (Kaushalya et al., 2008a). However, the dynamics of vesicle release from the storage location, transport to the site of exocytosis, and docking events at the membrane have not been explored so far.

Here we employed faster imaging, using three photon and TIRF microscopy, to better resolve the events preceding exocytosis. We examined the vesicular dynamics associated with the process of exocytosis induced by depolarization with high K^+. A unique aspect of somatic exocytosis that distinguishes it from its synaptic counterpart is that somatic vesicles have to traverse a relatively long path (many μm) from the inside of the cell to the plasma membrane before exocytosis. This transport can in principle be diffusive or active. We analyzed individual tracks of serotonin fluorescent spots as they proceeded toward exocytosis to address this issue. We also measured the average residence time at the membrane with TIRF microscopy of FM 1-43 labeled vesicles. This gives an idea about the time it takes to assemble the exocytosis machinery at the site of exocytosis on the cell membrane and the time required for the pore to open. These are expected to be parameters which distinguish between synaptic exocytosis and somatic exocytosis observed in endocrine cells.

MATERIALS AND METHODS

PRIMARY CULTURE OF RAPHE NEURONS

The details of this procedure have been given earlier (Kaushalya et al., 2008a). All animal handling procedures were approved by the Animal Ethics Committee of the institute. In brief, female neonatal (P0–P2) Wistar rats were used for the cultures. The rostral brain stem containing a major portion of the raphe nuclei was dissected and put in ice-cold Thomson's buffer (146 mM NaCl, 5.4 mM KCl, 1.8 mM $CaCl_2$, 0.8 mM $MgSO_4$, 0.4 mM KH_2PO_4, 0.3 mM Na_2HPO_4, 5 mM dextrose, and 20 mM Na-HEPES, pH adjusted to 7.35).This was followed by Trypsin (0.025%) digestion for 30 min at 37°C, trituration, and plating on poly L-ornithine coated coverslip-bottomed Petri dishes. Cells were grown in glial conditioned medium [60% DMEM (containing 10% FBS) + 40% Neurobasal-A with B27 supplement and penicillin/streptomycin]. The medium was conditioned for 1 day with glial cultures. Basic fibroblast growth factor (b-FGF; 0.5 ng/ml) and fibroblast growth

factor 5 (FGF-5; 1 ng/ml) were also added to enhance the survival of cells. Medium was changed every 48 h. Images of the cells were recorded after 5 days using Thomson's solution as the buffer. The protocol led to serotonergic cultures mixed with other types of neurons and glia. A large majority of the neurons were of serotonergic type, which was easy to identify by serotonin auto-fluorescence (∼350 nm). The cell culture components were purchased from Sigma (FGF and FGF-5), Gibco (Neurobasal-A, B27), and Himedia (India; DMEM and FBS). Buffer salts were purchased from S. D. Fine-Chem, Ltd. (India).

BRAIN SLICES PREPARATION

Female neonatal Wistar rats (P2–P3) were used for obtaining brain slices. One hundred μm slices from the dorsal raphe region were cut with a microtome (Model 3000, Vibratome, St. Louis, USA). All dissections were performed in ice-cold oxygen bubbled Thomson's buffer. The brain slices were transferred to cover slip-bottomed Petri dishes and imaged in Thomson's solution.

KCl INDUCED DEPOLARIZATION OF NEURONS

Depolarization was induced by a modified Thomson's buffer (pH 7.35), where a part of the Na^+ ions was replaced with K^+ ions, and extra Ca^{++} was added, yielding a concentration of 100 mM K^+ and 16 mM Ca^{++} in the depolarizing solution. 500 μl of this solution was added to 500 μl of existing Thomson's buffer in the Petri dish, resulting in a final concentration of 50 mM K^+ and 8 mM Ca^{++}.

FM 1-43 STAINING OF VESICLES

Vesicle staining of cultured neurons was performed following published protocols for FM 1-43 dye staining, with some modifications (Betz et al., 1992; Brumback et al., 2004). The cultured primary serotonergic neurons were depolarized using depolarizing solution containing 5 μM FM 1-43. The exocytosis buffer was removed and replaced by normal Thomson's buffer after 10 min and the cells were left for 20 min in this buffer. This allowed the cells to repolarize and internalize the FM 1-43-loaded vesicles. FM 1-43 staining of the outer membrane of the cell was removed by washing three times with normal buffer. The cells were then depolarized again, resulting in exocytosis of vesicles loaded with FM 1-43, which were imaged using confocal or TIRF microscopy.

MULTIPHOTON IMAGING OF SEROTONIN

The multiphoton microscope set-up based on a modified MRC600 confocal microscope (BioRad, UK) has been described elsewhere (Balaji et al., 2005). Briefly, a Ti:Sapphire (MIRA, Coherent, Inc., USA) laser operating at 740 nm and producing ∼100 fs pulses (repetition rate, 76 MHz) caused three photon excitation of serotonin. The radiation was separated from the serotonin fluorescence by a dichroic mirror (670dcxruv, Chroma, USA), which was subsequently passed through a 1-cm thick liquid $CuSO_4$ emission filter. The filtered signal was detected externally by an analog photomultiplier tube (Model: P30A-01 Electron Tubes Limited, UK). For recording the movements of the vesicles, we performed three photon imaging of a single optical slice (taken at about the middle of a cell) continuously at the rate of 3 s/frame. This experiment is performed in primary cultures and also in brain tissue slices.

ANALYSIS OF TIME SERIES MOVIES

The analysis of the time series obtained by three photon microscopy of serotonergic neurons was performed using the Object Tracker wizard of the Huygen's Professional software (Scientific Volume Imaging, B.V Netherlands). By manually selecting the serotonin fluorescent spots and background regions, the Object Tracker was trained to differentiate between the objects and the background and to track the motion of the spots. Thresholding was performed on the brightness of the objects. Analysis was performed for the spots for which movement of the calculated center of mass of the objects (spots) were 2 μm or less per time frame. The data were analyzed, frame by frame, for the position and displacement, the x and y velocity of the tracked objects and the mean squared displacement (MSD) of the tracked objects. MSD was calculated by measuring the square of the distance traveled by a given spot from the origin and then dividing it by the time elapsed. Subsequently, this quantity is averaged over all the spots. The Huygens program does this automatically. Analysis was performed on a total of 149 fluorescent spots before and 137 spots after depolarization from six cells. We note that the upper bound for the movement is somewhat arbitrary, and it can allow two different spots to be counted as one in some cases. However, this should happen equally both before and after depolarization, unless the total movement before depolarization is small compared to that after depolarization. Therefore, any inference with respect to changes in vesicle dynamics should be robust with respect to such errors.

QUASI-SIMULTANEOUS IMAGING OF SEROTONIN AND FM 1-43

Femtosecond pulsed 740 nm light was used to excite serotonin (as described) and a continuous wave (CW) beam of 543 nm (from a He-Ne laser) was used for FM 1-43. Both were aligned along the same paths. The same cell (of primary cultured neurons) was imaged quasi-simultaneously by changing the dichroics for serotonin (detected using a external non-descanned detector) and FM 1-43 (detected using the internal detector, passed through a 605/75 emission filter), and switching the lasers. A 1-cm thick solution of Tetramine copper sulfate solution was used in front of serotonin detector to filter out any fluorescence coming from FM 1-43. For both serotonin and FM 1-43, Z-stacks with 1 μM separation were recorded before and after depolarization. The images were analyzed using the ImageJ software (open source, available from the website: http://rsbweb.nih.gov./ij/). Corresponding single Z-plane images for serotonin and FM 1-43 were analyzed for co-localization and reduction of brightness following depolarization.

TOTAL INTERNAL REFLECTION MICROSCOPY

The details of the objective-based TIRF microscope set-up have been described elsewhere (Kaushalya et al., 2008a). Briefly, a 532-nm laser excitation beam (Verdi V-10; Coherent, Inc.) was focused at the back focal plane (BFP) of the objective (Olympus Apo 3100 1.65 NA, oil objective) with a 30-cm focal length lens in an inverted microscope (Olympus IX-71). The beam was moved along the diameter of the BFP of the objective so that the beam emerged from the objective at high angles, undergoing total internal reflection at the coverslip – water interface. The emission was separated from the excitation by a 535 nm long-pass dichroic (Chroma, USA) and

filtered by a 605/75 nm emission filter (Chroma, USA). Images were captured using an Electron Gain Multiplier CCD (EM-CCD) camera (Andor, Ixon; model No. DV887ECS-UVB, Ireland). Special objective oil (refractive index: $\eta_{oil} = 1.78$; Cargille, USA) was used for imaging, and the cells (primary serotonergic neurons) were cultured on special coverslips ($\eta_{coverslip} = 1.65$; Olympus, Singapore). The penetration depth was ∼100 nm (estimated by the gradual withdrawal of a 20 nm fluorescent bead).

RESULTS

DYNAMICS OF VESICLES BEFORE AND AFTER DEPOLARIZATION

Figure 1 represents the analysis of the dynamics of the serotonin fluorescent spots obtained from a total of six serotonergic neurons recorded in three different experiments (once with primary cultured neurons and twice with raphe brain slices). A time series of a single focal plane was recorded from the neurons before depolarization (images were recorded every 3 s). Another time series was recorded from the same plane under depolarizing conditions starting 10 min after excess KCl addition. Individual spots were tracked as described in the Section "Materials and Methods." **Figure 1A** shows tracks obtained from a few representative spots before (**Figure 1A** top panel) and after (**Figure 1A**, bottom panel) depolarization with high K^+. The tracks in the upper panel show that the serotonin fluorescent spots perform very limited movement about their starting points. The tracks from the same fluorescent spots (in corresponding colors in the bottom panel) show that they move over a much larger range after depolarization. This is obvious also from the plot of average distance from the track origin of all identified tracks as plotted in **Figure 1B**. Before depolarization, the spots moved less than a μm (red) from their origin in ∼30 s (∼5 min in some cases), while after depolarization (blue) they moved considerably more within the same time. We also asked whether this movement is passive or active, and random or directed. **Figure 1C** analyzes the directionality of the motion by plotting *y* velocity vs. *x* velocity, with the velocities computed at each step. The plot displays a

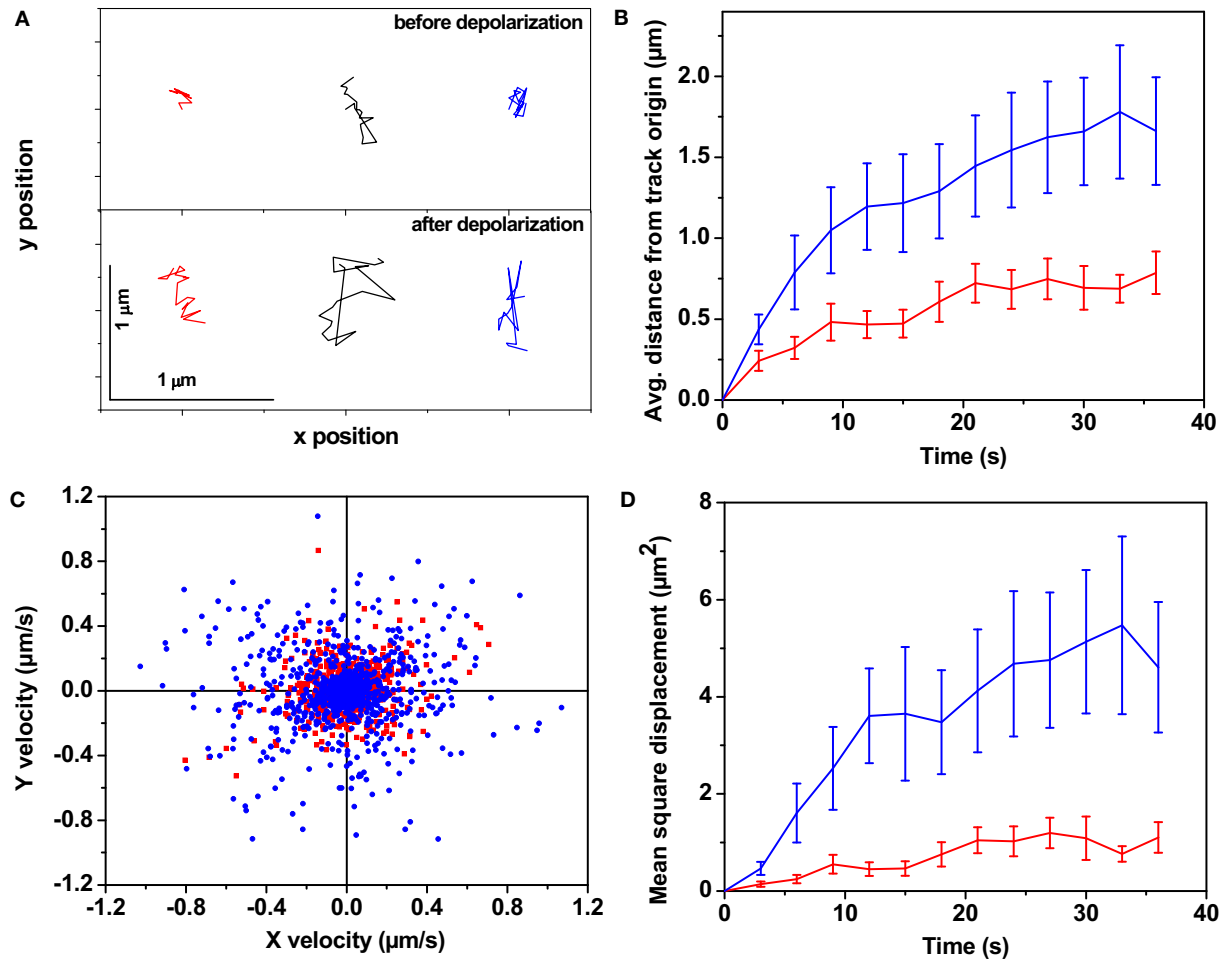

FIGURE 1 | The dynamics of somatic vesicles pre- and post-depolarization. Three photon excitation microscopy shows dynamics of somatic serotonergic vesicles (or unresolved vesicular clusters) in the cell body and in the processes before and after K^+-induced depolarization. **(A)** Individual tracks of a few serotonin fluorescent spots before (top) and after (bottom) depolarization. In the following, red and blue denote measurements performed before and after depolarization respectively. **(B)** Average displacement from the track origin vs. time, **(C)** Velocity distribution obtained from the tracks, **(D)** Mean squared displacement vs. time. (Error bars correspond to standard errors of the mean. $N = 149$ fluorescent spots before depolarization and $N = 137$ spots after depolarization from six cells).

nearly circular symmetry, which implies that there is no correlation between the x and the y velocities, indicating random movement. Finally, the MSD was calculated from the tracks (**Figure 1D**). The MSD was quasi-linear in the beginning, indicating a random diffusive motion (Berg, 1993) after depolarization. However, in about 15 s, the MSD values start to show a plateau. Such a plot indicates some degree of confinement (Daumas et al., 2003) within a spatial scale of several microns. This implies that at any instant, the particles are free to randomly move about within a short spatial range, but cannot go as far as a freely diffusing particle would reach at longer timescales. The MSD value per unit time calculated from the initial slope (first 12 s) was $\sim$0.04 μm^2/s before KCl addition (**Figure 1D**, red), while it increased to $\sim$0.3 μm^2/s after the addition (**Figure 1D**, blue).

The dynamics before and after the stimulation can be better observed through the Videos S1 and S2 in Supplementary Material, which are recorded from brain tissue before and 10 min after depolarization respectively. In Video S2 in Supplementary Material, the numbers of fluorescent spots are smaller, likely due to exocytosis in the intervening time. Of course, the disappearance of serotonin fluorescent spots from a single optical slice may also be due to the movement of the spots along the z (depth) direction. However, volume imaging of the cells before and after depolarization shows that the spots have indeed disappeared after depolarization (**Figure A1** in Appendix). We note that some of these data recorded at lower time resolution has been published elsewhere (Kaushalya et al., 2008a). Earlier work involving imaging of serotonergic cells in RN46A cell line as well as primary culture and Raphe tissue of rat brain at lower time resolution showed that the somatic exocytosis of serotonin upon KCl induced depolarization is rather slow and happens over a timescale of tens of minutes (Balaji et al., 2005; Kaushalya et al., 2008a).

CO-LOCALIZATION OF SEROTONIN AND FM 1-43

A co-localization study was performed to check whether the endosome labeling dye FM 1-43 used for the TIRF measurements did actually label the serotonin spots. Three photon imaging of serotonin and conventional confocal imaging of FM 1-43 was performed on the same cell (of cultured serotonergic neurons) quasi-simultaneously. **Figure 2A** shows a single Z-plane image of a cell. FM 1-43 labeled vesicles (or unresolved vesicular clusters, magenta) and serotonin fluorescent spots (5-HT, blue green) show good co-localization in the merged image (some of them are marked by white arrows). A few serotonin spots (marked by red arrows) do not co-localize with FM 1-43. These most likely mark the vesicles that did not undergo recycling. This can be better observed in the **Figure A2** in Appendix from a non-KCl treated cell where the red arrows show bright serotonin spots that are not observed in the FM 1-43 channel. Yellow arrows (**Figure A2** in Appendix) show spots bright in the FM 1-43 channel but not in the serotonin channel, ruling out the possibility of FM 1-43 leakage into the serotonin channel. There is a finite possibility that a spot in one channel is not seen in the other due to the movement of the spots within the intervening time. This possibility can be ruled out by imaging one channel both before and after the other channel. **Figure A2** in Appendix demonstrates this issue. Yellow arrows mark the same bright spots that were observed in the FM 1-43 channel (not co-localized with serotonin) recorded before (panel 1, 14 min) and after (panel 4, 35 min) serotonin imaging (panel 2, 21 min). These are possibly vesicles that have not been refilled with serotonin. Conversely, red arrows mark spots that are bright in the serotonin channel (panel 2, 21 min) but are absent in the FM 1-43 channel both before (panel 1, 14 min) and after (panel 4, 35 min) serotonin imaging. These are possibly non-recycled vesicles. The white arrows on the other hand show the spots with good co-localization. **Figure 2B** shows reduction of brightness in both serotonin (5-HT, false-colored according to green-fire-blue look up table or LUT) and FM 1-43 (in fire LUT) channels after high K^+ induced depolarization, while in the absence of depolarization the brightness does not reduce significantly over the same timescale (**Figure 2C**). This indicates that FM 1-43 indeed labeled the serotonin fluorescent spots, and the recycled vesicles can undergo exocytosis. Analysis of serotonin brightness shows a reduction of $\sim$36% over 20 min (**Figure 2B**, 5-HT 0 vs. 21 min) and $\sim$46% in 30 min (**Figure 2B**, 5-HT 0 vs. 28 min) following depolarization. These values are similar to those reported earlier by us (Balaji et al., 2005; Kaushalya et al., 2008a). Comparatively in the sham-treated control cells it is $\sim$10% in 30 min (**Figure 2C**, 5-HT 0 vs. 28 min). On the other hand, FM 1-43 brightness decreases by $\sim$47% from 7 to 14 min following depolarization and by $\sim$73% from 7 to 35 min (**Figure 2B**). This larger depletion is at least partly due to the higher level of background signal observed in the serotonin three photon images. However, this probably also indicates that the newly recycled vesicles are more readily exocytosed, which has been reported earlier (Colgan et al., 2009). For the sham-treated control cells (**Figure 2C**, FM 1-43 7, 14, and 35 min) the change in FM 1-43 brightness is negligible, indicating photobleaching is not a major issue. X-Z slice of a single cell imaged for serotonin before (**Figure A1A** in Appendix) and 20 min after depolarization (**Figure A1B** in Appendix) shows that the loss of fluorescent spots has no preferred location. This observation is also true for the recycled vesicles, as can be seen in a similar X-Z slice of another cell imaged with FM 1-43 (**Figures A3A–D** in Appendix). These results indicate that a considerable fraction of the spots observed in the FM1-43 channel likely represents serotonergic vesicles, although some other organelles may also get labeled. A separate larger area image is presented in **Figure A4** in Appendix to further ascertain the degree of co-localization. A large number of spots are observed in the serotonin channel and also in the FM1-43 channel. Vast majority of the spots observed in the FM1-43 channel appear to be nearly perfectly co-localized with those observed in the serotonin channel (though some cells observed in the serotonin channel hardly take up the FM 1-43 dye), suggesting that at least a large fraction of the vesicles/vesicular clusters stained by FM1-43 indeed contains serotonin.

TIRF MICROSCOPY OF VESICLE DYNAMICS AT THE MEMBRANE

FM-1-43 labeled vesicles (or vesicular clusters) of cultured serotonergic neurons were imaged with a home-built TIRF microscope. TIRF imaging was performed under depolarizing condition at a fast rate (down to 7 ms/frame) to resolve the time that the vesicles spend "docked" at the membrane on an average. The depth resolution of the microscope was about 100 nm, so that "docking" in this context merely refers to their being present within this distance from the membrane. Actual time spent at the membrane would be less than this. We observed that while some of the FM

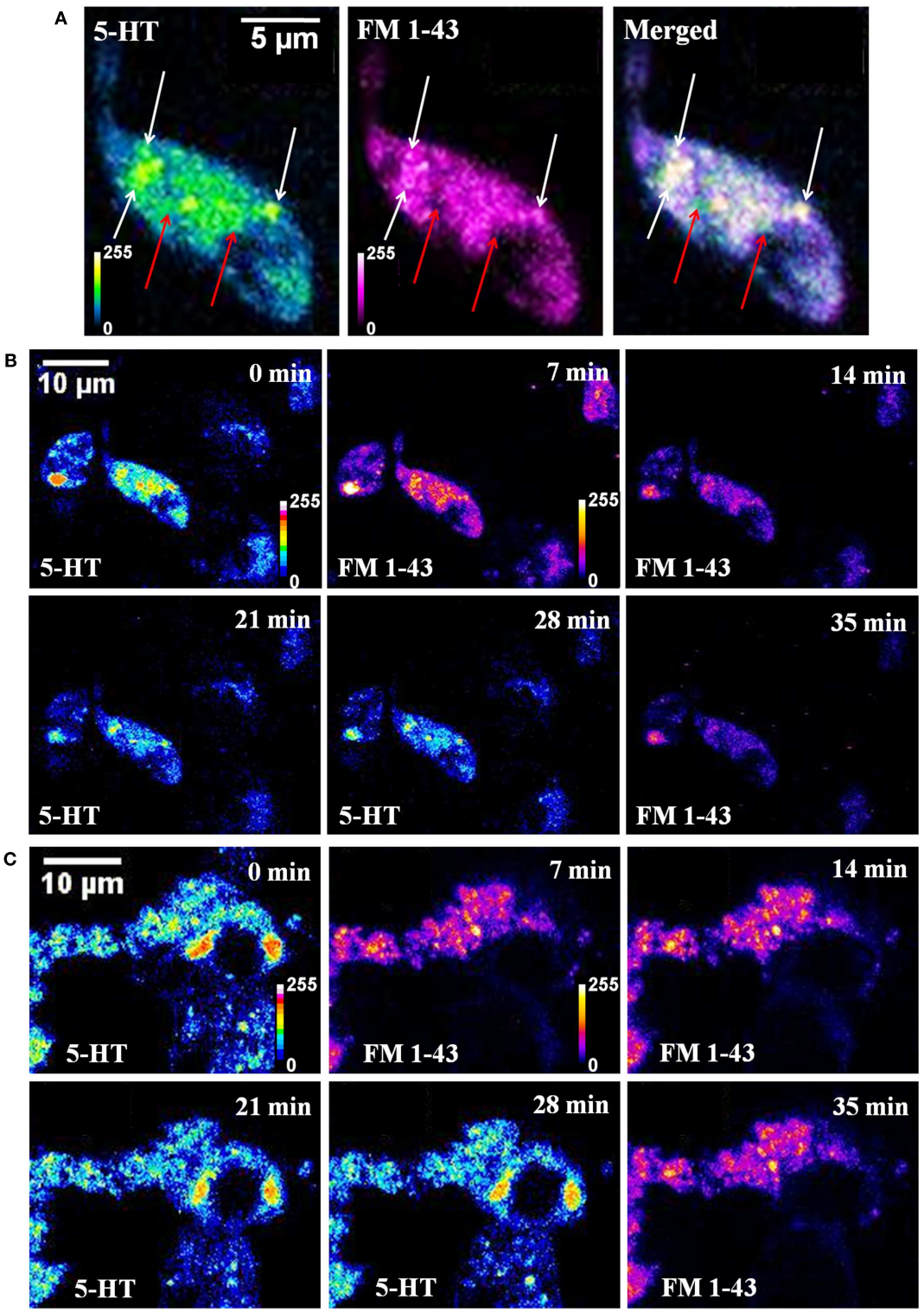

FIGURE 2 | Co-localization of serotonin and FM 1-43 labeled vesicles. (A) Serotonin (5-HT, blue green) and FM 1-43 (FM 1-43, magenta) images of a cultured serotonergic neuron. In the merged image, white arrows show co-localized vesicular structures, and red arrows mark spots visible in the serotonin channel only. **(B,C)** Time lapsed quasi-simultaneous imaging of serotonin (5-HT) and FM 1-43 in depolarized **(B)** and sham-treated control cells. **(C)** Top right corner of each image shows the starting time of image recording following treatment. All image intensities are false color coded.

1-43 labeled vesicles are present only in a single frame, most are present in more than one frame. For example **Figure 3A** shows a vesicle which is visible for one frame only (see frame t2; t1 and t3 recorded at the same place do not show the spot, where t1, t2, t3 are three consecutive frames separated by 7 ms each). **Figure 3B** shows another vesicle which is visible over four frames or about 28 ms (see t1–t6). We note that the vesicles were almost always observed to disappear completely at a single step (e.g., **Figure 3A**, t3; **Figure 3B**, t6), without any intermediate step where the vesicle appears dim. Since the vesicles on an average move about 100 nm/s (**Figure 1B**), it is unlikely that they will move out of the TIRF range of 100 nm within one frame (7 ms). Therefore the single step disappearance suggests that we are actually observing exocytosis of vesicles which are docked at the membrane. A histogram of the residence times at the membrane is plotted in **Figure 3C**. It shows a peak at 21 ms, and the average is about 25 ms (obtained from the analysis of 75

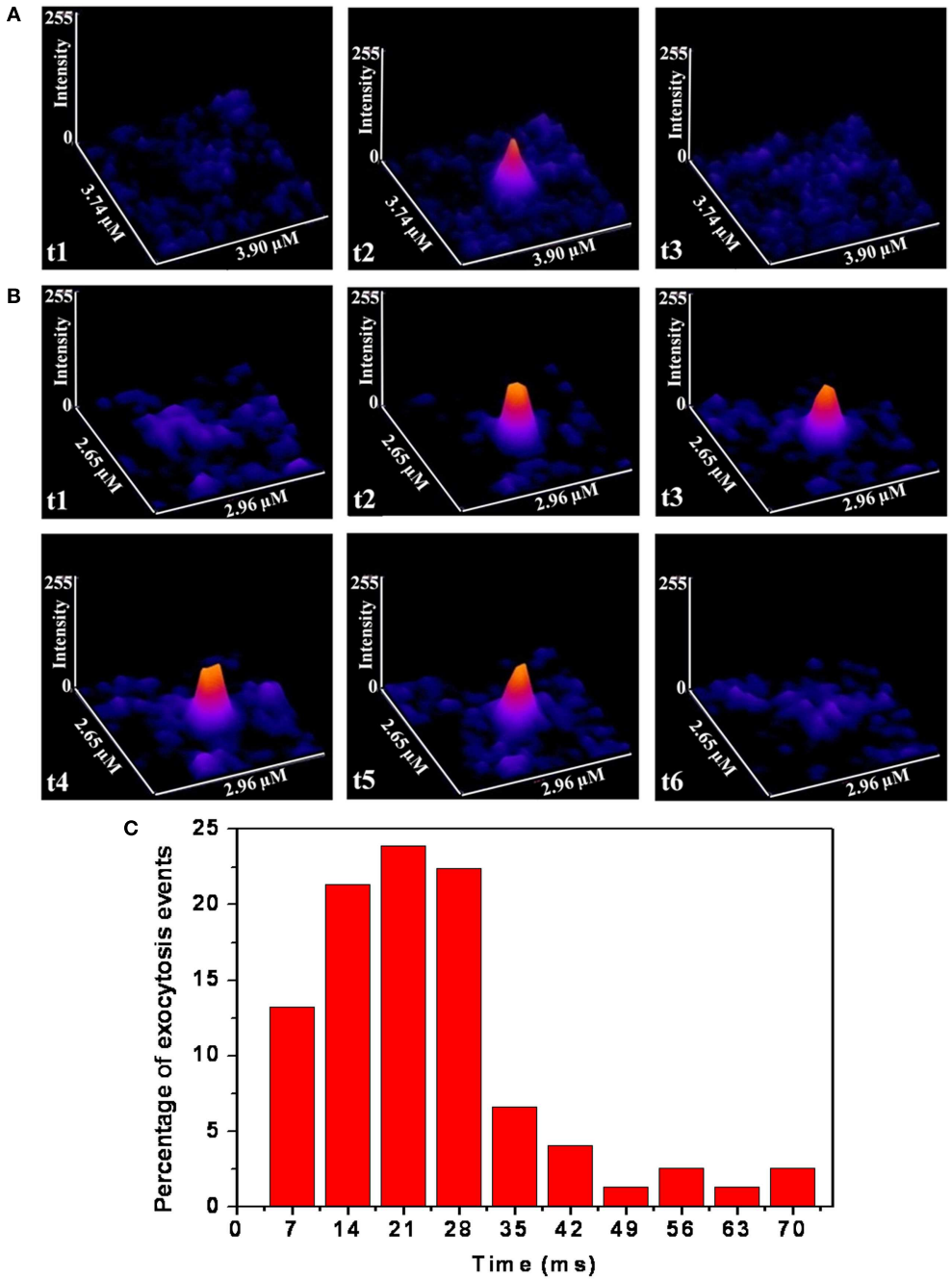

FIGURE 3 | TIRF images of somatic vesicles showing time spent at the membrane. (A,B) Montage of consecutive frames (each frame is 7 ms) showing individual release events following depolarization which last for 1 **(A)** and 4 **(B)** frames respectively. (Image intensities are false color coded) **(C)** Histogram of the percentage of events vs. docking times ($N = 75$ spots from three cultured serotonergic neurons).

spots from three cells). Since the peak of the distribution is well resolved in the histogram, we infer that the time resolution is adequate for a reliable estimate of the residence time. We note that in this analysis, any spot observed with reasonable intensity in a frame is assumed to have resided for the full length of time in that frame.

We note that what we observe in the serotonin channel are most likely vesicular clusters, but what we observe with TIRF is disappearance of individual vesicles. It is possible that during exocytosis, individual vesicles independently leave their host clusters. This should result in a step-wise reduction of the cluster brightness, and for clusters which are larger than the resolution limit, also their size. Indeed, for many of the cases we do observe that vesicle clusters lose their brightness post-depolarization, and at least in some cases it is evident that the clusters shrink in size in a step-wise fashion. This is highlighted in the **Figure A5** in Appendix which presents a zoomed up three photon image of an exocytosing cell (see vesicle clusters marked with arrows, before and after depolarization).

DISCUSSION

DYNAMICS OF VESICLES BEFORE AND AFTER DEPOLARIZATION

The ability to visualize neurotransmitter vesicles/vesicular clusters with their auto-fluorescence provides an unprecedented opportunity to track them in real time, anywhere in the cell and at any time, until their exocytosis. The technique of labeling vesicles by FM dyes, following the pioneering work by Betz et al. (1992), has made it possible to follow the dynamics of freshly recycled vesicles. However, this technique does not allow one to follow the vesicle content, or the movement of the non-recycled, stored original vesicles. Our observations using the three photon microscopy technique allows us to specifically look at all the neurotransmitter vesicles inside the cell. We observe that the predominant fraction of the somatic serotonin fluorescent spots are quiescent and appear to be attached to cellular structures which prevent substantial movement. They can remain so for rather long times (longer than 5 min). However, depolarization induces their release from captivity within minutes. These spots become much more dynamic, and they may move over several microns with randomly directed motion. We next ask if this random motion can be explained by passive diffusion. The hallmark of passive diffusion is a randomly directed movement with a mean square displacement that is proportional to time. The initial part of the mean square deviation plots are indeed reasonably linear (**Figure 1D**). However, it later tapers off to a plateau, indicating a process of constrained diffusion (Daumas et al., 2003). This implies that the vesicular motion is bounded by local cellular structures, as can be expected from a relatively large object of this size. We note that similar observations of undirected vesicle motion have been made with GFP-tagged neurotransmitters in drosophila neuromuscular junctions (Shakiryanova et al., 2005). It is pertinent to ask whether the observed numerical values are consistent with passive diffusion. The diameter of the serotonin fluorescent spots is about 370 nm (Kaushalya et al., 2008a), and their shape is expected to be spherical. In aqueous solutions this would translate to a diffusion constant (D) of 1.2 $\mu m^2/s$. If the cytosolic viscosity is about 3 times that of water (Swaminathan et al., 1997) then D would be about 0.4 $\mu m^2/s$. The calculated D in the cytosol from the initial slope after depolarization is 0.3 $\mu m^2/s$, which is similar. This value is somewhat larger than that reported for neurotransmitter vesicles in retina cells (0.11 $\mu m^2/s$; Rea et al., 2004), and much larger than that observed in frog neuromuscular junctions (Gaffield et al., 2006). However, the relative increase of mobility after excitation (about 7×) is similar to that reported by them (Gaffield et al., 2006). This suggests that a passive diffusion can explain the observed movements, though there are strong boundary effects that limit diffusion to spatial scales of a few μm. We note that our data do not exclude the possibility that the vesicles/clusters are tethered to the cytoskeleton in a way that allows them a range of relatively fast random movements, while they proceed slowly toward the plasma membrane (Trueta et al., 2012).

DOCKING TIMES

Exocytosis requires docking, priming, and pore opening at the membrane, and also requires the assembly of a large number of vesicular and plasma membrane protein molecules. The residence time at the membrane therefore reflects the total time required for these assembly processes. This process can take very different times in different types of cells. A comparison table between different experiments is given in the (**Table A1** in Appendix). Residence time at the membrane (referred to here as "docking time") can be a useful parameter to characterize the nature of vesicular exocytosis. Studies with various techniques such as capacitance measurement, amperometry, Ca^{++} uncaging, and fluorescence imaging yield a range of synaptic vesicle exocytosis timescales. Neuronal exocytosis processes range from about 0.6 ms in rat CNS neuron synapse (Wolfel and Schneggenburger, 2003) to about hundreds of milliseconds in the Calyx of Held neuron (He et al., 2006). This timescale is typically faster than what can be followed with three photon microscopy. We therefore follow this process by labeling the vesicles with FM 1-43, and using fast video microscopy in the TIRF mode to analyze the dynamics. Our co-localization studies prove that a large fraction of the structures that we observe with three photon microscopy are indeed labeled by FM 1-43. We have also shown earlier (from slower time-scale data) that the rate at which the FM 1-43 labeled vesicles appear goes up by an order of magnitude after KCl administration, clearly indicating that what we observe is a depolarization-driven exocytosis process (Kaushalya et al., 2008a). Our observation of docking timescale of 25 ms is amongst the slower category of exocytosis processes observed in the synapses. On the other hand, this timescale is much faster than those typically observed in endocrine cells (such as chromaffin cells; Albillos et al., 1997). The timescale is faster than even the very fast somatic exocytosis observed in melanotrophs (Thomas et al., 1993) and gonadotropes (Zhu et al., 2002), and is similar to the vesicle fusion timescale observed in artificial lipid bilayers (Liu et al., 2005). Thus it is amongst the fastest, if not the fastest, somatic exocytosis process observed so far.

CONCLUSION

We find that the kinetics of somatic exocytosis in serotonergic neurons has three main phases. Before depolarization, the vesicles/vesicular clusters appear confined. Post-depolarization, they are released from their storage locations and become much more dynamic, though their motion still appears to be constrained. The

vesicles subsequently reach their final destination at the membrane, possibly as individual vesicles which leave the host clusters. No preferred location for exocytosis was observed on the membrane. The final process of docking and exocytotic release of neurotransmitters takes place in ∼25 ms, which is much more rapid than somatic exocytosis in endocrine cells and as rapid as many types of synaptic exocytosis.

ACKNOWLEDGMENTS

This work was partially supported by grant no. BT/53/NE/TBP/2010 from the Department of Biotechnology, Government of India to Sudipta Maiti.

SUPPLEMENTARY MATERIAL

The Supplementary Material for this article can be found online at http://www.frontiersin.org/Membrane_Physiology_and_Biophysics/10.3389/fphys.2012.00414/abstract

Video S1 | Three photon excitation microscopy of a single optical slice shows false color intensity coded images of serotonin fluo escence spots in the cell body and in the processes of a serotonergic neuron in a cultured brain-slice containing the raphe, before depolarization. Twenty frames recorded at 3 s/frame.

Video S2 | Three photon excitation microscopy of the same plane 10 min post-depolarization. Thirteen frames recorded at 3 s/frame.

REFERENCES

Agnati, L. F., Fuxe, K., Zoli, M., Ozini, I., Toffano, G., and Ferraguti, F. (1986). A correlation analysis of the regional distribution of central enkephalin and beta-endorphin immunoreactive terminals and of opiate receptors in adult and old male rats. Evidence for the existence of two main types of communication in the central nervous system: the volume transmission and the wiring transmission. *Acta physiol. Scand.* 128, 201–207.

Agnati, L. F., Guidolin, D., Guescini, M., Genedani, S., and Fuxe, K. (2010). Understanding wiring and volume transmission. *Brain Res. Rev.* 64, 137–159.

Albillos, A., Dernick, G., Horstmann, H., Almers, W., Alvarez de Toledo, G., and Lindau, M. (1997). The exocytotic event in chromaffin cells revealed by patch amperometry. *Nature* 389, 509–512.

Balaji, J., Desai, R., Kaushalya, S. K., Eaton, M. J., and Maiti, S. (2005). Quantitative measurement of serotonin synthesis and sequestration in individual live neuronal cells. *J. Neurochem.* 95, 1217–1226.

Berg, H. C. (1993). *Random Walks in Biology*. New Jersey: Princeton University Press.

Betz, W. J., Bewick, G. S., and Ridge, R. M. (1992). Intracellular movements of fluorescently labeled synaptic vesicles in frog motor nerve terminals during nerve stimulation. *Neuron* 9, 805–813.

Beutner, D., Voets, T., Neher, E., and Moser, T. (2001). Calcium dependence of exocytosis and endocytosis at the cochlear inner hair cell afferent synapse. *Neuron* 29, 681–690.

Brumback, A. C., Lieber, J. L., Angleson, J. K., and Betz, W. J. (2004). Using FM1-43 to study neuropeptide granule dynamics and exocytosis. *Methods* 33, 287–294.

Bruns, D., and Jahn, R. (1995). Real-time measurement of transmitter release from single synaptic vesicles. *Nature* 377, 62–65.

Bruns, D., Riedel, D., Klingauf, J., and Jahn, R. (2000). Quantal release of serotonin. *Neuron* 28, 205–220.

Bunin, M. A., and Wightman, R. M. (1998). Quantitative evaluation of 5-hydroxytryptamine (serotonin) neuronal release and uptake: an investigation of extrasynaptic transmission. *J. Neurosci.* 18, 4854–4860.

Carlsson, A. (1987). Perspectives on the discovery of central monoaminergic neurotransmission. *Annu. Rev. Neurosci.* 10, 19–40.

Chen, G., Gavin, P. F., Luo, G., and Ewing, A. G. (1995). Observation and quantitation of exocytosis from the cell body of a fully developed neuron in *Planorbis corneus*. *J. Neurosci.* 15, 7747–7755.

Coggeshall, R. E. (1972). Autoradiographic and chemical localization of 5-hydroxytryptamine in identified neurons in the leech. *Anat. Rec.* 172, 489–498.

Colgan, L. A., Putzier, I., and Levitan, E. S. (2009). Activity-dependent vesicular monoamine transporter-mediated depletion of the nucleus supports somatic release by serotonin neurons. *J. Neurosci.* 29, 15878–15887.

Daumas, F., Destainville, N., Millot, C., Lopez, A., Dean, D., and Salome, L. (2003). Confined diffusion without fences of a g-protein-coupled receptor as revealed by single particle tracking. *Biophys. J.* 84, 356–366.

De-Miguel, F. F., and Fuxe, K. (2012). Extrasynaptic neurotransmission as a way of modulating neuronal functions. *Front. Physiol.* 3:16. doi:10.3389/fphys.2012.00016

De-Miguel, F. F., and Trueta, C. (2005). Synaptic and extrasynaptic secretion of serotonin. *Cell. Mol. Neurobiol.* 25, 297–312.

Descarries, L., Beaudet, A., and Watkins, K. C. (1975). Serotonin nerve terminals in adult rat neocortex. *Brain Res.* 100, 563–588.

Fuxe, K., Dahlstrom, A., Hoistad, M., Marcellino, D., Jansson, A., Rivera, A., et al. (2007). From the Golgi-cajal mapping to the transmitter-based characterization of the neuronal networks leading to two modes of brain communication: wiring and volume transmission. *Brain Res. Rev.* 55, 17–54.

Gaffield, M. A., Rizzoli, S. O., and Betz, W. J. (2006). Mobility of synaptic vesicles in different pools in resting and stimulated frog motor nerve terminals. *Neuron* 51, 317–325.

Gandhi, S. P., and Stevens, C. F. (2003). Three modes of synaptic vesicular recycling revealed by single-vesicle imaging. *Nature* 423, 607–613.

He, L., Wu, X. S., Mohan, R., and Wu, L. G. (2006). Two modes of fusion pore opening revealed by cell-attached recordings at a synapse. *Nature* 444, 102–105.

Jaffe, E. H., Marty, A., Schulte, A., and Chow, R. H. (1998). Extrasynaptic vesicular transmitter release from the somata of substantia nigra neurons in rat midbrain slices. *J. Neurosci.* 18, 3548–3553.

Johnson, D. A., and Pilar, G. (1980). The release of acetylcholine from postganglionic cell bodies in response to depolarization. *J. Physiol. (Lond.)* 299, 605–619.

Katz, B., and Miledi, R. (1970). Further study of the role of calcium in synaptic transmission. *J. Physiol. (Lond.)* 207, 789–801.

Kaushalya, S. K., Desai, R., Arumugam, S., Ghosh, H., Balaji, J., and Maiti, S. (2008a). Three-photon microscopy shows that somatic release can be a quantitatively significant component of serotonergic neurotransmission in the mammalian brain. *J. Neurosci. Res.* 86, 3469–3480.

Kaushalya, S. K., Nag, S., Balaji, J., and Maiti, S. (2008b). "Serotonin: multiphoton imaging and relevant spectral data," in *Proceedings of SPIE, Volume: 6860, Multiphoton Microscopy in the Biomedical Sciences VIII*, eds A. Periasamy and P. T. C. So. doi:10.1117/12.763020

Kaushalya, S. K., Nag, S., Ghosh, H., Arumugam, S., and Maiti, S. (2008c). A high-resolution large area serotonin map of a live rat brain section. *Neuroreport* 19, 717–721.

Kaushalya, S. K., and Maiti, S. (2008) "Quantitative imaging of serotonin autofluorescence with multiphoton microscopy," in *Serotonin Receptors in Neurobiology*, ed. Amitabha Chattopadhyay (Boca Raton: CRC Press), 1–18.

Kumar, M., Kaushalya, S. K., Gressens, P., Maiti, S., and Mani, S. (2009). Optimized derivation and functional characterization of 5-HT neurons from human embryonic stem cells. *Stem Cells Dev.* 18, 615–627.

Kurian, M. A., Gissen, P., Smith, M., Heales, S. Jr., and Clayton, P. T. (2011). The monoamine neurotransmitter disorders: an expanding range of neurological syndromes. *Lancet Neurol.* 10, 721–733.

Liu, T., Tucker, W. C., Bhalla, A., Chapman, E. R., and Weisshaar, J. C. (2005). SNARE-driven, 25-millisecond vesicle fusion in vitro. *Biophys. J.* 89, 2458–2472.

Llinas, R., Gruner, J. A., Sugimori, M., McGuinness, T. L., and Greengard, P. (1991). Regulation by synapsin I and Ca(2+)-calmodulin-dependent protein kinase II of the transmitter release in squid giant synapse. *J. Physiol. (Lond.)* 436, 257–282.

Llinas, R., Steinberg, I. Z., and Walton, K. (1981). Relationship between presynaptic calcium current and postsynaptic potential in squid giant synapse. *Biophys. J.* 33, 323–351.

Maiti, S., Shear, J. B., Williams, R. M., Zipfel, W. R., and Webb, W. W. (1997). Measuring serotonin distribution in live cells with three-photon excitation. *Science* 275, 530–532.

Murthy, V. N., and Stevens, C. F. (1999). Reversal of synaptic vesicle docking at central synapses. *Nat. Neurosci.* 2, 503–507.

Nag, S., Balaji, J., Madhu, P. K., and Maiti, S. (2008). Intermolecular association provides specific optical and NMR signatures for serotonin at intravesicular concentrations. *Biophys. J.* 94, 4145–4153.

Nazarali, A. J., and Reynolds, G. P. (1992). Monoamine neurotransmitters and their metabolites in brain regions in Alzheimer's disease: a postmortem study. *Cell. Mol. Neurobiol.* 12, 581–587.

Ninomiya, Y., Kishimoto, T., Yamazawa, T., Ikeda, H., Miyashita, Y., and Kasai, H. (1997). Kinetic diversity in the fusion of exocytotic vesicles. *EMBO J.* 16, 929–934.

Patel, J. C., Witkovsky, P., Avshalumov, M. V., and Rice, M. E. (2009). Mobilization of calcium from intracellular stores facilitates somatodendritic dopamine release. *J. Neurosci.* 29, 6568–6579.

Puopolo, M., Hochstetler, S. E., Gustincich, S., Wightman, R. M., and Raviola, E. (2001). Extrasynaptic release of dopamine in a retinal neuron: activity dependence and transmitter modulation. *Neuron* 30, 211–225.

Rea, R., Li, J., Dharia, A., Levitan, E. S., Sterling, P., and Kramer, R. H. (2004). Streamlined synaptic vesicle cycle in cone photoreceptor terminals. *Neuron* 41, 755–766.

Ryan, T. A., Reuter, H., Wendland, B., Schweizer, F. E., Tsien, R. W., and Smith, S. J. (1993). The kinetics of synaptic vesicle recycling measured at single presynaptic boutons. *Neuron* 11, 713–724.

Shakiryanova, D., Tully, A., Hewes, R. S., Deitcher, D. L., and Levitan, E. S. (2005). Activity-dependent liberation of synaptic neuropeptide vesicles. *Nat. Neurosci.* 8, 173–178.

Suetake, K., Kojima, H., Inanaga, K., and Koketsu, K. (1981). Catecholamine is released from non-synaptic cell-soma membrane: histochemical evidence in bullfrog sympathetic ganglion cells. *Brain Res.* 205, 436–440.

Swaminathan, R., Hoang, C. P., and Verkman, A. S. (1997). Photobleaching recovery and anisotropy decay of green fluorescent protein GFP-S65T in solution and cells: cytoplasmic viscosity probed by green fluorescent protein translational and rotational diffusion. *Biophys. J.* 72, 1900–1907.

Szule, J. A., Harlow, M. L., Jung, J. H., De-Miguel, F. F., Marshall, R. M., and McMahan, U. J. (2012). Regulation of synaptic vesicle docking by different classes of macromolecules in active zone material. *PLoS ONE* 7, e33333. doi:10.1371/journal.pone.0033333

Takahashi, N., Kadowaki, T., Yazaki, Y., Miyashita, Y., and Kasai, H. (1997). Multiple exocytotic pathways in pancreatic beta cells. *J. Cell Biol.* 138, 55–64.

Thomas, P., Wong, J. G., Lee, A. K., and Almers, W. (1993). A low affinity Ca2+ receptor controls the final steps in peptide secretion from pituitary melanotrophs. *Neuron* 11, 93–104.

Trueta, C., and De-Miguel, F. F. (2012). Extrasynaptic exocytosis and its mechanisms: a source of molecules mediating volume transmission in the nervous system. *Front. Physiol.* 3, 319. doi:10.3389/fphys.2012.00319

Trueta, C., Kuffler, D. P., and De-Miguel, F. F. (2012). Cycling of dense core vesicles involved in somatic exocytosis of serotonin by leech neurons. *Front. Physiol.* 3:175. doi:10.3389/fphys.2012.00175

Trueta, C., Mendez, B., and De-Miguel, F. F. (2003). Somatic exocytosis of serotonin mediated by L-type calcium channels in cultured leech neurones. *J. Physiol. (Lond.)* 547, 405–416.

Trueta, C., Sanchez-Armass, S., Morales, M. A., and De-Miguel, F. F. (2004). Calcium-induced calcium release contributes to somatic secretion of serotonin in leech Retzius neurons. *J. Neurobiol.* 61, 309–316.

Wolfel, M., and Schneggenburger, R. (2003). Presynaptic capacitance measurements and Ca2+ uncaging reveal submillisecond exocytosis kinetics and characterize the Ca2+ sensitivity of vesicle pool depletion at a fast CNS synapse. *J. Neurosci.* 23, 7059–7068.

Zenisek, D., Steyer, J. A., and Almers, W. (2000). Transport, capture and exocytosis of single synaptic vesicles at active zones. *Nature* 406, 849–854.

Zhang, B., Zhang, X. Y., Luo, P. F., Huang, W., Zhu, F. P., Liu, T., et al. (2012). Action potential-triggered somatic exocytosis in mesencephalic trigeminal nucleus neurons in rat brain slices. *J. Physiol. (Lond.)* 590, 753–762.

Zhu, H., Hille, B., and Xu, T. (2002). Sensitization of regulated exocytosis by protein kinase C. *Proc. Natl. Acad. Sci. U.S.A.* 99, 17055–17059.

Conflict of Interest Statement: The authors declare that the research was conducted in the absence of any commercial or financial relationships that could be construed as a potential conflict of interest.

Received: 15 April 2012; accepted: 08 October 2012; published online: 06 November 2012.

*Citation: Sarkar B, Das AK, Arumugam S, Kaushalya SK, Bandyopadhyay A, Balaji J and Maiti S (2012) The dynamics of somatic exocytosis in monoaminergic neurons. Front. Physio. **3**:414. doi: 10.3389/fphys.2012.00414*

This article was submitted to Frontiers in Membrane Physiology and Biophysics, a specialty of Frontiers in Physiology.

APPENDIX

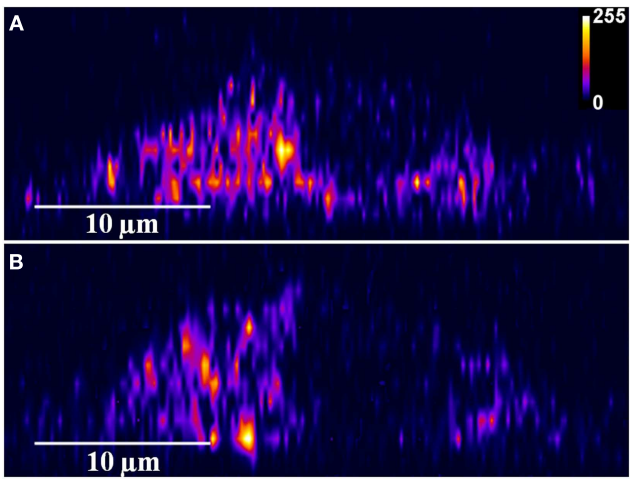

FIGURE A1 | Depolarization induces serotonin exocytosis. *X-Z* slices of three photon serotonin images of a single cell (of cultured serotonergic neurons) **(A)** before and **(B)** 20 min after depolarization (Intensities are false color coded).

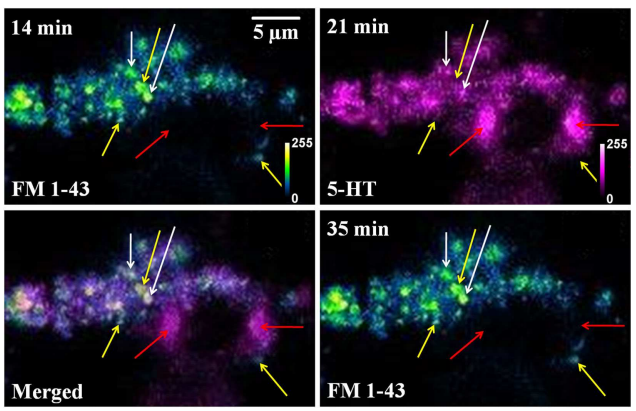

FIGURE A2 | FM 1-43 and serotonin co-localization is not caused by cross-talk between fluo escence channels. FM 1-43 (blue green) and Serotonin (5-HT, magenta) images of the same cultured serotonergic neuron. In the merged image (FM 1-43, 14min and 5-HT, 21 min) white arrows show co-localized vesicular structures (recycled vesicles), yellow arrows mark spots visible only in the FM 1-43 channel, and red arrows mark spots visible only in the serotonin channel. FM 1-43 images recorded before (14 min) and after (35 min) serotonin imaging shows the same bright spots (by yellow arrows), but these are absent in the serotonin channel (5-HT, 21 min). Top left corner of each image shows the starting time of image recording following sham treatment (Intensities false are color coded).

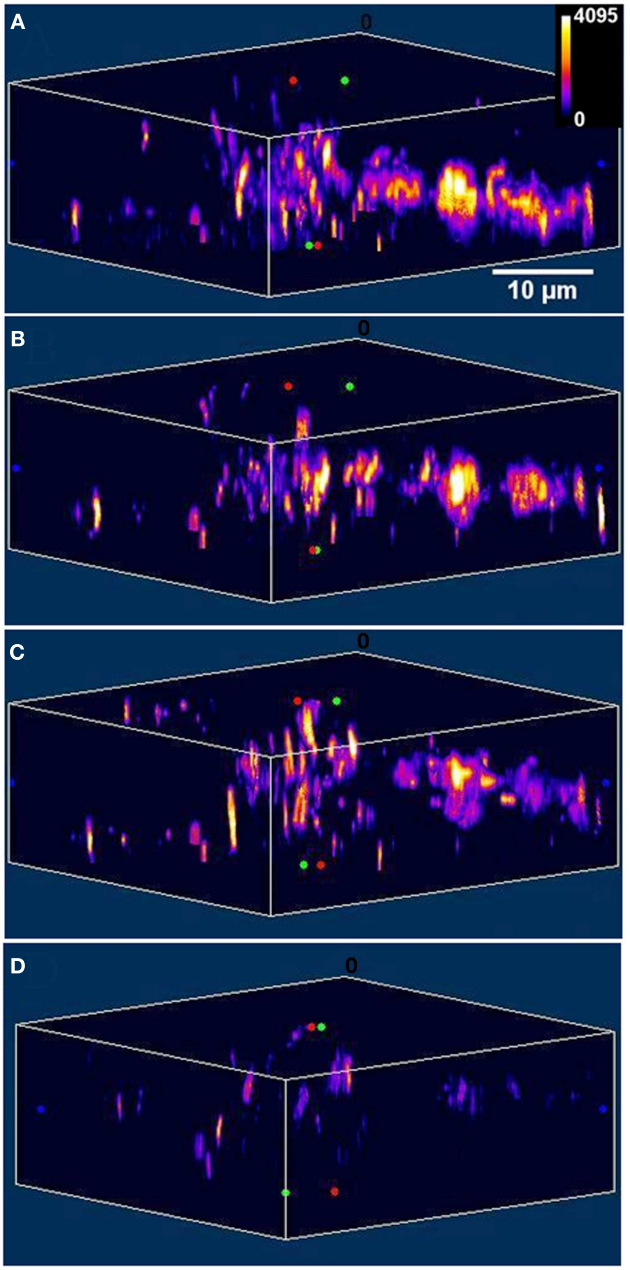

FIGURE A3 | Depolarization induces exocytosis of FM 1-43 labeled vesicles. *X-Z* slices of the images of FM 1-43 labeled vesicles in a cultured serotonergic neuron **(A)** before, and **(B–D)** 5, 15, and 30 min after depolarization respectively (Intensities are false color coded).

Table A1 | Timescales of exocytosis.

Cell type	Vesicle size (or type)	Release time	Technique
Melanotrophs (Thomas et al., 1993)	Dense core vesicle	40 ms	Capacitance
Leech motor neuron (Bruns and Jahn, 1995)	Small clear vesicle Large dense core vesicle	260 μs 1.3 ms	Amperometry
Chromaffin (Albillos et al., 1997)	420 nm	190 ± 20 ms	Patch amperometry
Pancreatic β cells (Takahashi et al., 1997)	70–1000 nm	85–2000 ms	Capacitance measurement
PC 12 cells (Ninomiya et al., 1997)	Small vesicle	30 ms	EPSC measurement
Goldfish retinal bipolar neuron ribbon synapse (Zenisek et al., 2000)	30 nm	210 ± 30 ms	TIRF, FM 1-43
Inner hair cell (Beutner et al., 2001)	Small vesicle	1 ms	Capacitance
Gonadotrope (Zhu et al., 2002)	Dense core vesicle	30 ms	Capacitance
Rat CNS neuron synapse (Wolfel and Schneggenburger, 2003)	–	0.6 ms	Capacitance measurement, Ca^{2+} uncaging
Hippocampal pyramidal cell/vesicle recycling (Gandhi and Stevens, 2003)	–	Three modes: Fast: 400–860 ms	SyPHluorin, WF fluorescence
	Slow: 8–21 s		
Stranded: >45 s			
In vitro lipid bilayer (Liu et al., 2005)	50 nm	25 ms	TIRF, TMR
Calyx of held neuron synapse (He et al., 2006)	30–80 nm	10 ms – 1 s, 273 ± 22 ms	Capacitance measurement

Comparison showing the size (or type) of the vesicles and the time of exocytosis in different types of cells.

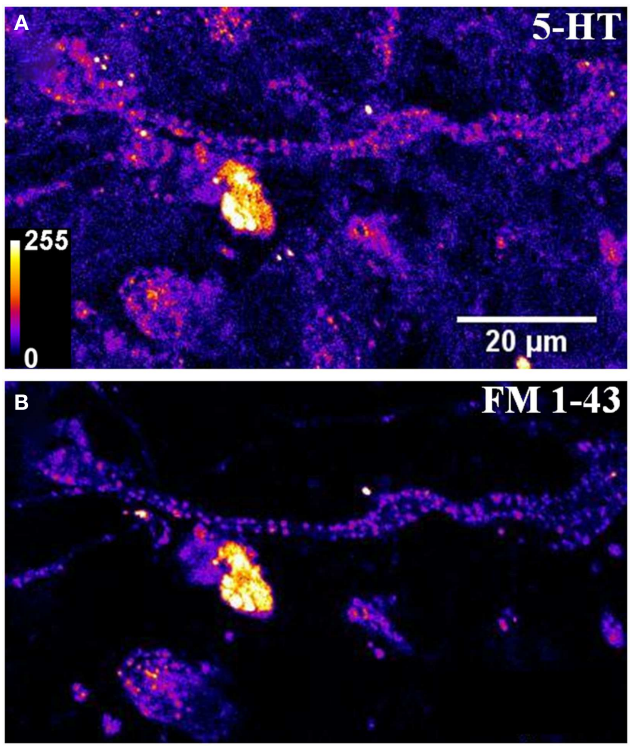

FIGURE A4 | A large area image of serotonergic cells shows a high degree of co-localization between (A) three photon image of serotonergic vesicular clusters and (B) confocal image of FM1-43 labeled spots. Most spots observed in the FM1-43 channel co-localize with bright spots observed in the serotonin channel, though there are entire cells in the serotonergic channel which do not appear to take up the dye FM 1-43 (Intensities false are color coded).

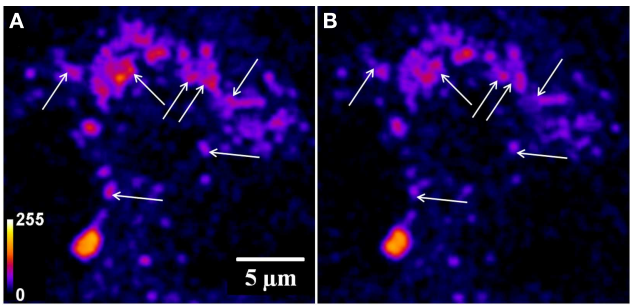

FIGURE A5 | Evidence for individual vesicles leaving a cluster during exocytosis. A three photon serotonin image of a cell at high zoom recorded **(A)** before and **(B)** 21 min after depolarization. The arrows mark vesicular clusters which appear to lose a fraction of the constituents during exocytosis (Intensities false are color coded).

frontiers in
PHYSIOLOGY

ORIGINAL RESEARCH ARTICLE
published: 06 June 2012
doi: 10.3389/fphys.2012.00175

Cycling of dense core vesicles involved in somatic exocytosis of serotonin by leech neurons

Citlali Trueta[1], Damien P. Kuffler[2] and Francisco F. De-Miguel[3]*

[1] *Instituto Nacional de Psiquiatría "Ramón de la Fuente Muñiz," México D. F., México*
[2] *Institute of Neurobiology, University of Puerto Rico, San Juan, Puerto Rico*
[3] *Instituto de Fisiología Celular-Neurociencias, Universidad Nacional Autónoma de México, México D. F., México*

Edited by:
Kjell Fuxe, Karolinska Institutet, Sweden

Reviewed by:
Kjell Fuxe, Karolinska Institutet, Sweden
Diego Guidolin, University of Padova, Italy

***Correspondence:**
Francisco F. De-Miguel, Instituto de Fisiología Celular-Neurociencias, Universidad Nacional Autónoma de México, Circuito Exterior, Ciudad Universitaria, 04510 México D. F., Mexico.
e-mail: ffernand@ifc.unam.mx

We studied the cycling of dense core vesicles producing somatic exocytosis of serotonin. Our experiments were made using electron microscopy and vesicle staining with fluorescent dye FM1-43 in Retzius neurons of the leech, which secrete serotonin from clusters of dense core vesicles in a frequency-dependent manner. Electron micrographs of neurons at rest or after 1 Hz stimulation showed two pools of dense core vesicles. A perinuclear pool near Golgi apparatuses, from which vesicles apparently form, and a peripheral pool with vesicle clusters at a distance from the plasma membrane. By contrast, after 20 Hz electrical stimulation 47% of the vesicle clusters were apposed to the plasma membrane, with some omega exocytosis structures. Dense core and small clear vesicles apparently originating from endocytosis were incorporated in multivesicular bodies. In another series of experiments, neurons were stimulated at 20 Hz while bathed in a solution containing peroxidase. Electron micrographs of these neurons contained gold particles coupled to anti-peroxidase antibodies in dense core vesicles and multivesicular bodies located near the plasma membrane. Cultured neurons depolarized with high potassium in the presence of FM1-43 displayed superficial fluorescent spots, each reflecting a vesicle cluster. A partial bleaching of the spots followed by another depolarization in the presence of FM1-43 produced restaining of some spots, other spots disappeared, some remained without restaining and new spots were formed. Several hours after electrical stimulation the FM1-43 spots accumulated at the center of the somata. This correlated with electron micrographs of multivesicular bodies releasing their contents near Golgi apparatuses. Our results suggest that dense core vesicle cycling related to somatic serotonin release involves two steps: the production of clear vesicles and multivesicular bodies after exocytosis, and the formation of new dense core vesicles in the perinuclear region.

Keywords: serotonin, somatic exocytosis, extrasynaptic exocytosis, dense core vesicle, vesicle cycle, volume transmission, endocytosis, leech

INTRODUCTION

Depolarization of the soma of serotonergic neurons induces serotonin secretion via the mobilization of serotonin-containing vesicles from central neuronal regions to the plasma membrane (Trueta et al., 2003; De-Miguel and Trueta, 2005; Kaushalya et al., 2008; Colgan et al., 2009). Serotonin in the soma of leech Retzius neurons, a classic preparation in the study of serotonin release (for Review, see Nicholls and Kuffler, 1990; Fernández-de-Miguel and Drapeau, 1995), is packed in clusters of dense core vesicles that, in response to brief trains of electrical impulses at high frequency are transported toward the plasma membrane (Trueta et al., 2004), with which they fuse during the following minutes. Vertebrate serotonergic neurons, including those in mammalians also pack serotonin into extrasynaptic clear and dense core vesicles (Chazal and Ralston, 1987; Descarries and Mechawar, 2000), and something similar happens in neurons containing dopamine, adrenaline, and peptides (see review by Trueta and De-Miguel in this issue). This mode of exocytosis may be responsible for volume transmission within the nervous system (for review, see Fuxe and Agnati, 1991; Agnati et al., 2006).

Although the mechanism of somatic secretion described for Retzius neurons seems to be part of a more general principle of somatic and extrasynaptic exocytosis in vertebrates and invertebrates (see review by Trueta and De-Miguel in this issue), the cycling of serotonin-containing vesicles has still not been elucidated. While clear vesicles at synapses may be reloaded and reused rapidly, within seconds after their fusion with the plasma membrane (Betz and Bewick, 1992, 1993; Betz et al., 1992; Cochilla et al., 1999; Richards et al., 2000), dense core vesicles undergo a longer cycle before their reuse (Herzog and Farquhar, 1977; Herzog and Miller, 1979; Patzak et al., 1987; Ceridono et al., 2011). Multiple studies have discussed the molecular mechanisms that contribute to the vesicle cycle in different types of cells (for review, see Piper and Katzmann, 2007; Park et al., 2009; Von Bartheld and Altick, 2011). However, since serotonin is reloaded into clear vesicles by vesicular transporters (Iversen, 1971), one question is whether somatic dense core vesicles are rapidly reused after exocytosis or do they enter the long cycle typically characterized for dense core vesicles. The focus in this study was to provide a descriptive overview of the basic steps of the vesicle cycling that leads to the formation,

transport, fusion, retrieval, and recycling of serotonin-containing dense core vesicles.

We addressed this question by taking advantage of the large size of serotonergic leech Retzius neurons, which have the largest somata in the ganglia and are the major serotonin-producing neurons in the leech nervous system. Because of their large (60–80 μm) soma diameters and the possibility of studying them within intact ganglia as well as in isolation in tissue culture, they are an excellent preparation on which to study the events underlying somatic exocytosis of serotonin.

Retzius neurons in the intact animal and in culture synthesize and pack serotonin in clear small (40 nm) synaptic vesicles and in large (100 nm) dense core vesicles that are distributed in the soma, extended processes, and perisynaptic regions (Henderson, 1983; Kuffler et al., 1987; Bruns and Jahn, 1995). The soma contains "astronomic" (Coggeshall, 1972) numbers of serotonin-containing dense core vesicles that at rest are clustered away from the plasma membrane (Trueta et al., 2004). Previous studies using staining of vesicles that undergo exocytosis followed by endocytosis in the presence of the fluorescent dye FM1-43 and electron microscopy have shown that electrical stimulation of Retzius neurons with trains of pulses at 10 or 20 Hz, but not 1 Hz, evoke calcium-dependent vesicle cluster mobilization followed by the fusion of vesicles with specific areas of the plasma membrane (Trueta et al., 2003, 2004).

To study the cycling of dense core vesicles from their perinuclear location at rest and for several hours after they had undergone exo- and endocytosis we used electron microscopy of neurons in the ganglion and the staining of vesicles by fluorescent FM1-43 dye as they fuse with the plasma membrane of cultured neurons. Electron microscopy was used to follow the sites of vesicle formation, their mobilization and fusion in response to depolarization, and their process of recycling after endocytosis.

MATERIALS AND METHODS

ISOLATION AND CULTURE OF NEURONS

Retzius neurons were isolated from the central nervous system of adult leeches *Hirudo* sp. The procedure has been described elsewhere (Dietzel et al., 1986). In brief, leeches were anesthetized by immersion in 8% ethanol. Nerve cords were dissected out and ganglion capsules opened to expose the cell somata. Ganglia were kept in Leibovitz L-15 culture medium, supplemented with 6 mg ml^{-1} glucose, 0.1 mg ml^{-1} gentamicin and 2% heat-inactivated fetal calf serum, and they were incubated for 1 h in 2 mg ml^{-1} collagenase/dispase solution (Boehringer-Mannheim, Mannheim, Germany). After enzyme treatment, Retzius neurons were sucked out one by one, rinsed several times in L-15, and then plated on glass bottomed culture dishes precoated with concanavalin-A. Experiments were performed after the neurons were 1–8 days in culture.

STIMULATION OF EXOCYTOSIS

Single trains of electrical stimulation were used for FM1-43 staining experiments, while series of 10 trains were used for studies to be evaluated in the electron microscope. One stimulation protocol involved the application of trains of 10 action potentials produced by intracellular injection of 20-ms current pulses at 1, or 20 Hz, using borosilicate microelectrodes with resistances of 18–25 MΩ when filled with 3 M KCl. Electrical recordings were acquired by an analog-to-digital board Digidata 1200 (Axon Instruments) at a sampling frequency of 20 kHz, using pCLAMP8 software (Axon Instruments) and the data was stored in a computer. Before withdrawing the microelectrode, the dye was washed out of the bathing solution for 2 min with physiological saline solution (mM: NaCl 120; KCl 4; $CaCl_2$ 2; Tris-maleate 10; *N*-methyl-D-glucamine 66) in the absence of Ca^{2+}, which was replaced by magnesium (2 mM) to reduce vesicle fusion induced by these manipulations. To test the Ca^{2+} dependence of serotonin secretion, neurons were maintained in an external bathing solution containing 2 mM Mg^{2+} instead of Ca^{2+}. *N*-methyl-D-glucamine was added to the bathing solution to adjust it's osmolarity to 330 mosmol l^{-1}. After the electrode was withdrawn, the cells were washed for 8 min with normal Ringer's solution.

ELECTRON MICROSCOPY

Neurons in the ganglion were stimulated with 10 trains of 10 impulses each at 1 or 20 Hz frequencies separated by 1 min intervals to evoke exocytosis from the external and internal vesicle pools. Some neurons were also stimulated using external solutions containing magnesium instead of calcium. Ganglia were then perfused with 0.08 M cacodylate buffer (pH 7.4; Sigma, St. Louis, MO, USA), and fixed for 60 min with 0.6% glutaraldehyde and 0.4% paraformaldehyde, followed by postfixation for 60 min in 1.0% osmium tetroxide (Kuffler et al., 1987). Thin 70–100 nM sections usually containing the nucleus were observed in a JEOL 1010 electron microscope (JEOL USA Inc., Peabody, MA, USA). For illustration, electron micrographs were digitized at 1200 dpi.

PEROXIDASE IMMUNODETECTION IN ELECTRON MICROSCOPY

Ganglia were opened with forceps to expose the Retzius neurons. After a 1-h incubation in 10 mg/ml peroxidase (Sigma) in the extracellular fluid, one of the neurons in the ganglion was electrically stimulated. Some ganglia were fixed during neuronal stimulation, while others were fixed 10 min after electrical stimulation had stopped. After fixation, ganglia were washed in PBS and fixed as described above. Ultrathin sections were obtained with a Reichert–Jung ultramicrotome calibrated to produce 50–70 nm thick sections, according to their interference silver color. Once mounted on nickel grids, sections were incubated with Tris-BSA supplemented with 1% Triton for 15 min, followed by the addition of 10% goat serum for 15 min. A primary anti-peroxidase rabbit antibody (Sigma) was added at a dilution of 1:50 for a final concentration of 0.2 mg/ml. After a 12-h incubation at room temperature, sections were washed with Tris-BSA medium and then incubated for 1 h with a secondary goat polyclonal anti-rabbit antibody coupled to 10 nm gold spheres (Sigma) at a 1:50 dilution. Control sections were incubated with goat serum. The sections were washed and contrast stained using lead citrate and uranyl acetate.

FM1-43 VESICLE STAINING

Exocytosis from living neurons was analyzed as described by Trueta et al. (2003), following the incorporation into vesicles of the fluorescent dye FM1-43 (Molecular Probes; Betz and Bewick, 1992;

Betz et al., 1992). FM1-43 (2 μm) was added to the bathing solution after the neurons had been impaled with a microelectrode and hyperpolarized to −60 mV to prevent spontaneous electrical activity. The rest of the stimulation protocol was described above.

In FM1-43 destaining and restaining experiments, sequential images of fluorescently labeled spots within the neuron soma were captured while the solution bathing the cultured neurons was changed to one containing 40 mM K^+. For this, FM1-43 was added to the tissue culture plates containing 1 ml of normal Ringer's solution, followed by the addition of 1 ml of modified Ringer's solution in which 76 mM NaCl was replaced by KCl by equimolar substitution, to reach a final concentration of 40 mM potassium. After 5 min, the dye was washed out. Some neurons were stimulated in Mg^{2+} solution. Other neurons were incubated with FM1-43 in normal (1.8 mM) Ca^{2+} Ringer without stimulation, or with 40 mM K^+ solution in the absence of FM1-43. The recording chamber was perfused by gravity feed and complete solution changes took 30 s.

FLUORESCENCE IMAGING

Individual neurons were viewed with a Nikon Eclipse TE 200 microscope through a Nikon ×100 oil immersion objective (NA 1.25). Neutral density filters reduced the illumination intensity by 90% to reduce photobleaching of the dye and neuronal damage. Fluorescence imaging of FM1-43-stained cells was performed with band-pass filters for excitation (peak 480 nM) and emission (peak 535 nM). Images were acquired by a CCD camera (Hamamatsu Photonics, Japan) coupled to an Argus 10 integrator (Hamamatsu Photonics) programmed to integrate from 128 to 256 images. In destaining/restaining experiments, the number of fluorescent FM1-43 labeled spots, which correspond to clusters of vesicles that underwent exo/endocytosis (Trueta et al., 2003), were manually counted using stereological criteria (Coggeshall and Lekan, 1996).

TIME LAPSE IMAGING OF FM1-43 FLUORESCENCE

Neurons were stimulated with 20 Hz trains in the presence of FM1-43, and 10 min after stimulation the extracellular dye was washed out as described and were imaged at different *Z* planes as described every 12 h over 48 h.

RESULTS

GENERAL ULTRASTRUCTURE OF THE SOMA OF RETZIUS NEURONS

Ultra thin sections from five somata that had been stimulated in the ganglion with trains at 1 Hz, a frequency that does not evoke somatic exocytosis, contained dense core vesicle clusters distributed in two main areas (**Figures 1** and **2**). A perinuclear region contained vesicles together with Golgi apparatuses, mitochondria, and endoplasmic reticulum. Small clear vesicles were located next to Golgi apparatuses and some small vesicles displayed dense cores. At larger distances from Golgi, vesicles were large and had dense cores. Multivesicular bodies were mainly located adjacent to the perinuclear vesicle clusters and were characterized by their bag shapes and membrane multilayers filled with dense core and clear vesicles (**Figure 1**, see also below).

A more peripheral pool of dense core vesicles consisted of clusters located between the perinuclear vesicle layer and the plasma membrane (**Figures 1** and **2**). Vesicles in these clusters appeared at different distances from the plasma membrane and were associated with microtubule fibers characterized by individual diameters of 20–25 nm (**Figure 1C**). These vesicle clusters were also associated with mitochondria and endoplasmic reticulum. The space between the vesicle clusters and the plasma membrane had only sporadic dense core vesicles and was occupied by smooth endoplasmic reticulum. In some sections microtubule bundles associated with the vesicle clusters appeared anchored to hemidesmosomes arriving at the plasma membrane in places where it usually formed invaginations (**Figure 1C**). The whole extracellular periphery of Retzius neurons was surrounded by layers of processes of giant segmental glia (Coggeshall and Fawcett, 1964), which were assembled in fingers that filled the invaginations of the Retzius cells. Similar structures were found in non-stimulated neurons, neurons stimulated at 1 Hz (**Figures 1A,C**), or neurons stimulated at 20 Hz in the presence of magnesium substituting for calcium in the external solution (**Figure 2A**).

In six neurons fixed after 20 Hz stimulation, 47% of the vesicle clusters were apposed to the plasma membrane (**Figure 1E**), vs. the 9% of vesicle clusters in neurons stimulated at 1 Hz (**Figure 1E**). The perinuclear clusters remained in the same region. In the plasma membrane, some vesicles had omega-like appearances indicative of vesicles that had fused with the plasma membrane in response to the electrical stimulation (**Figure 4**). Multivesicular bodies were commonly located within peripheral vesicle clusters and were surrounded by radial arrays of dense core vesicles (**Figure 1D**), suggesting that multivesicular bodies had been formed by endocytosis following exocytosis.

FLUORESCENT FM1-43 LABELING OF VESICLES UPON EXO- AND ENDOCYTOSIS

Electrical stimulation of cultured Retzius neurons with a 20-Hz train in the presence of FM1-43 in the external fluid produces a spotted fluorescent pattern, in which each fluorescent spot is due to exocytosis followed by endocytosis from a dense core vesicle cluster (Trueta et al., 2003). The fact that the FM1-43 fluorescence in Retzius neurons is diminished as a result of prolonged depolarization by high extracellular potassium solution has suggested that vesicles in the clusters may undergo a second round of vesicle fusion (Trueta et al., 2003). However, a plausible alternative is that the fluorescence is reduced as vesicles become transported back to more central parts of the neuronal soma. In addition, the finding that electrical stimulation at increasing frequencies increases the number of fluorescent spots suggests that new clusters of vesicles are transported to and fuse at different release sites (Trueta et al., 2003). These possibilities were explored in four neurons in which the fluorescent FM1-43 spots formed upon high potassium depolarization were partially bleached by continuous light exposure followed by additional high potassium depolarization in the presence of fresh FM1-43. When counting the number of fluorescent spots in the equatorial plane of the soma in the same focal plane of the neurons before and after the second depolarization, we found four complementary effects (**Figure 3**): (1) 41% of the spots became restained, suggesting either, the arrival of a second vesicle cluster, maybe from the perinuclear region of the cell, or a second round of fusion of the same vesicles. However the presence

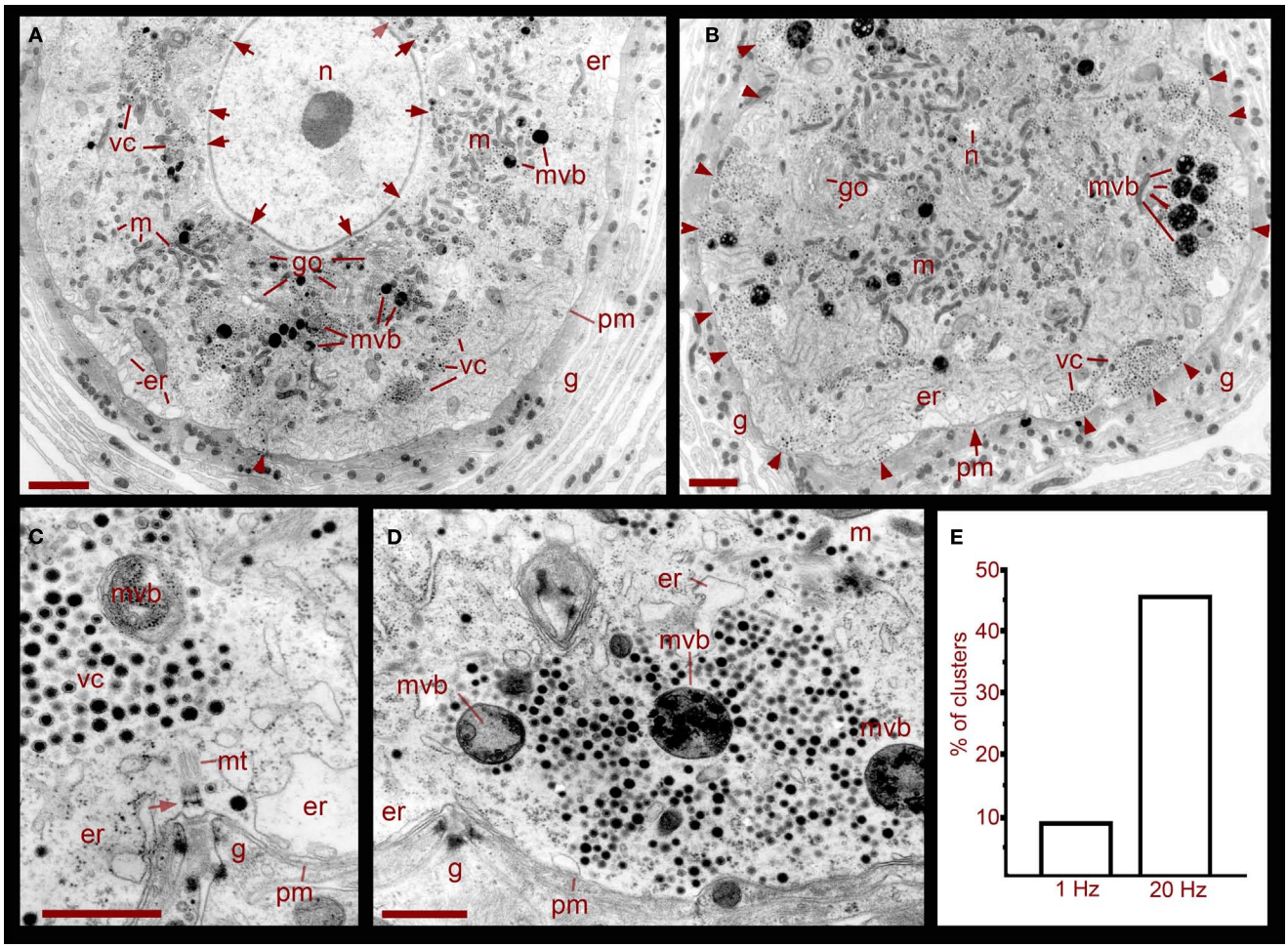

FIGURE 1 | Ultrastructure of the soma of Retzius neurons in relation to somatic exocytosis. (A) Low magnification electron micrograph of a neuron that had been stimulated at 1 Hz, a frequency that fails to evoke somatic serotonin exocytosis. Vesicle clusters located around the nucleus (n) are indicated with arrows. Clusters in the region midway between the nucleus and the plasma membrane are indicated as vc. Vesicle clusters and multivesicular bodies (mvb) are absent in the peripheral cytoplasmic area next to the plasma membrane. Some multivesicular bodies are interspersed within the vesicle clusters. Golgi apparatuses (go) are also more concentrated around the nucleus. Mitochondria (m) are near vesicles and endoplasmic reticulum (er) are located near the plasma membrane (pm). The arrowhead points to microtubule bundle arriving at the plasma membrane. The neuron is surrounded by layers of the giant glial cell (g). Scale = 2 μm. **(B)** Electron micrograph of a neuron stimulated at 20 Hz. A majority of the vesicle clusters are apposed to the plasma membrane (arrowheads). Multivesicular bodies lie within peripheral vesicle clusters and mitochondria can be seen around them (small arrows). Note that even after stimulation, vesicle clusters remained near the nucleus (n). Scale = 2 μm. **(C)** Magnified electron micrograph of a peripherally located vesicle cluster in a neuron that had been stimulated at 1 Hz. Vesicle clusters are located away from the plasma membrane and the intermediate space contains endoplasmic reticulum. A bundle of microtubules (mt) extends from the vesicle cluster vesicles to a hemi-desmosome (arrow) apposed to an invagination of the plasma membrane (arrowheads). Glial cell fingers characteristic of these structures penetrate into the somatic invagination. Scale = 1 μm. **(D)** Magnified electron micrograph of a neuron stimulated at 20 Hz. A vesicle cluster is apposed to the plasma membrane near an invagination (arrowheads). Vesicle rows formed radial arrays with multivesicular bodies. Scale = 1 μm. **(E)** Graph of the percentage of vesicle clusters apposed to the plasma membrane in neurons stimulated at frequencies of 1 vs. 20 Hz. Individual clusters were identified and counted from digital images low magnification and scanned at high resolution such as those in **(A)** and **(B)**. As seen in **(C,D)**, this vesicle cluster counting could be done easily since the clusters are self-delimited and they only contain vesicles and multivesicular bodies.

of two pools of vesicle clusters and their correlation with the double sigmoidal kinetics of the FM1-43 fluorescence (P. Noguez, C. Bustos, and F. F. De-Miguel, in preparation) support the idea of the arrival and fusion of a second vesicle cluster over the reuse of the same dense core vesicles. The following three evidences provide further support to this possibility. (2) 19% of the spots that were bleached were not restained in response to the second depolarization, although they stayed at the same position. (3) 22% percent of the prestained spots disappeared, suggesting their intracellular transport out of the focal plane. (4) New spots were formed in places that were previously not stained, accounting for 18% of the total final spots. This was consistent with the recruitment of new vesicle clusters that were fused at new release sites, as it happens with increases in the frequency of stimulation (see Figure 4 in Trueta et al., 2003) and suggest the slow vesicle recycling and the transport of fused vesicles back to internal cell sites.

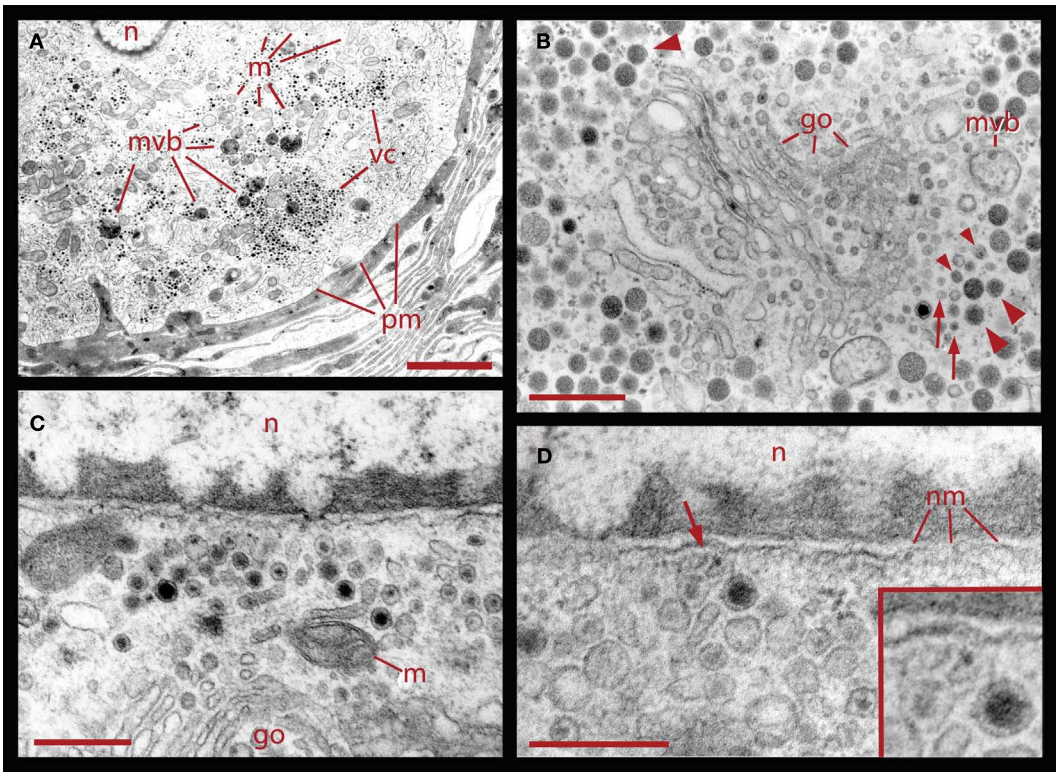

FIGURE 2 | Ultrastructural relationships of perinuclear vesicles with the nucleus (n), Golgi (go), and vesicle clusters (vc). (A) Low magnification image of the soma of a neuron that had been stimulated with 20 Hz trains in a bathing solution in which magnesium was substituted for calcium. Under these conditions, electrical activity fails to evoke somatic exocytosis and vesicle mobilization, and as can be seen, the areas immediate to the plasma membrane (pm) are devoid of vesicle clusters. Scale = 2.0 μm. **(B)** Golgi apparatus in the perinuclear area surrounded by clear and dense core vesicles. On the right, there are rows of small vesicles (arrows), some of which are clear while others have electron dense material (small arrowheads). More distantly there are small vesicles with dense cores continued by vesicles with large dense cores (large arrowheads). A fragment of a multivesicular body (mvb) can also be seen. On the top left electron dense vesicles align with the layers of the Golgi apparatus (large arrowhead). **(C)** Higher magnification image of vesicles adjacent to the nucleus, in the vicinity of mitochondria (m) and Golgi. **(D)** Clear and dense core vesicles are adjacent to the nuclear membrane (nm). A filament projecting from the vesicle toward the nuclear membrane is marked by the arrow and amplified in the inset. Scale bars for **(B–D)** = 500 nm.

ENDOCYTOSIS FOLLOWING EXOCYTOSIS

As shown in **Figure 4**, neurons fixed during 20 Hz stimulation had some dense core vesicles with omega-shaped structures, suggesting exo/endocytosis. In addition, adjacent to the release sites we found clear vesicles and cisternae, thus suggesting that these structures were formed also as result of endocytosis. To explore if dense core vesicles also underwent endocytosis, the extracellular fluid was added with peroxidase before stimulation and peroxidase was detected by colloidal gold-coupled antibodies. As shown in **Figure 5**, multiple dense core vesicles became labeled, confirming endocytosis of full dense core vesicles and also supporting that large numbers of vesicles in the cluster become fused upon electrical stimulation.

The relative restriction of colloidal gold electron dense spheres to dense core vesicles and multivesicular bodies (**Figures 5A,B**) indicates that the staining was highly specific. In addition we also detected some gold labeling in the membrane of endoplasmic reticulum but not free within the cytoplasm (**Figure 5A**). That gold label was also present inside multivesicular bodies (**Figures 5C,D**) suggests that they contained vesicles that had undergone exo-and endocytosis, and that vesicle degradation upon endocytosis plays a major role in dense core vesicle cycling associated to somatic serotonin secretion by Retzius neurons.

FORMATION OF MULTIVESICULAR BODIES

The formation of multivesicular bodies has been studied in a variety of cell types (for review, see Piper and Katzmann, 2007). Our electron micrographs fit with the general scheme by indicating that multivesicular bodies form when membranous structures, including vesicles, are surrounded by microtubules and endoplasmic reticulum. In **Figure 1** it was shown that after 20 Hz stimulation multivesicular bodies appear within the vesicle clusters near the plasma membrane. **Figure 6** shows several examples of multivesicular bodies in the periphery of vesicle clusters from neurons fixed 10 min after electrical stimulation at 20 Hz. Individual or aligned dense core vesicles are associated to multivesicular bodies (see also **Figure 1**), at parts in which they still seem to be opened. Some multivesicular bodies contain dense core and clear vesicles (**Figure 6A**). As shown above (**Figure 5**), multivesicular bodies formed by neurons stimulated in the presence of external

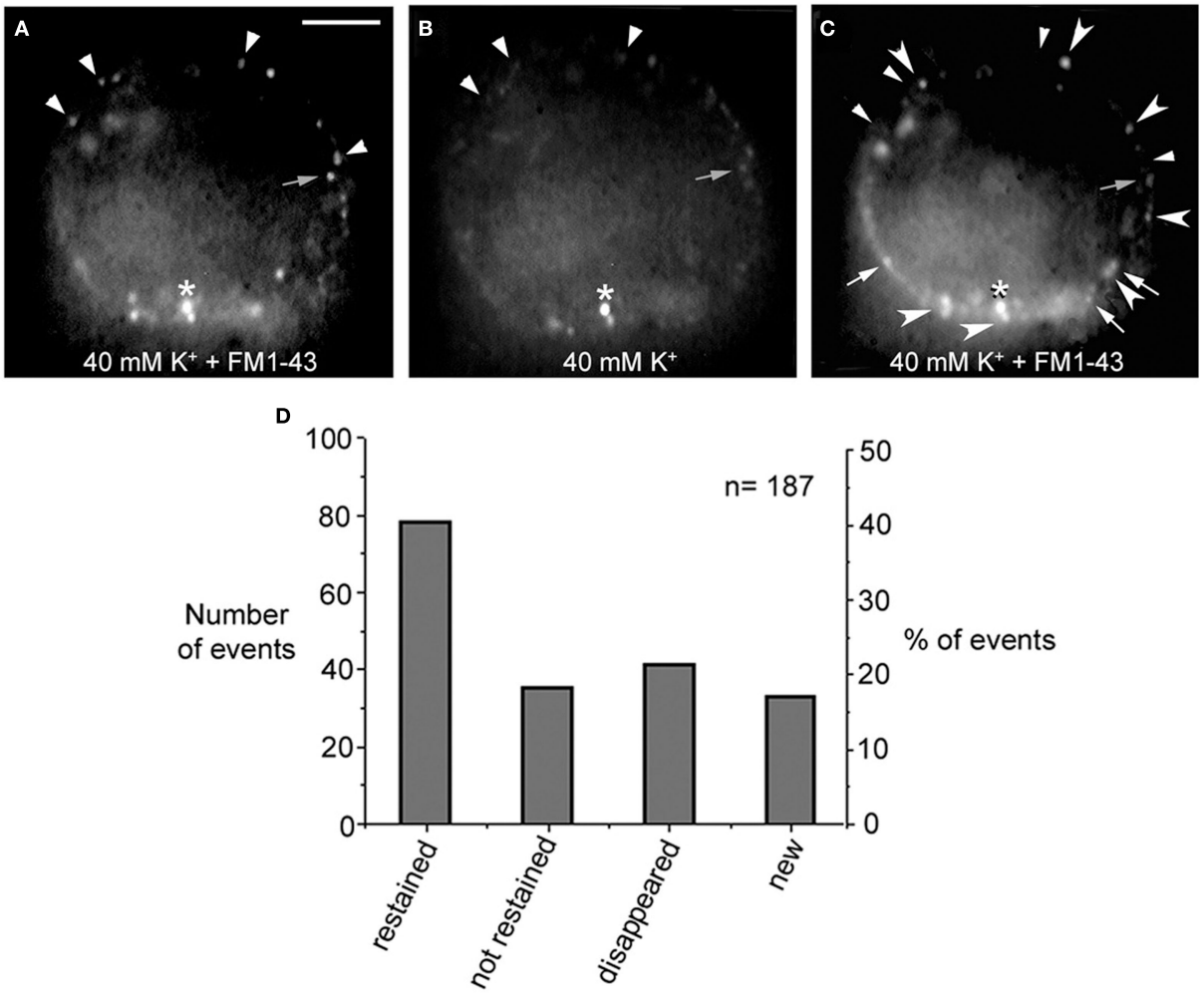

FIGURE 3 | FM1-43 staining upon subsequent depolarizations. **(A)** Equatorial image of the soma of a cultured neuron that had been depolarized with 40 mM potassium in the presence of FM1-43 in the external solution. Ten minutes after depolarization the dye was washed out from the fluid and neurons displayed their characteristic spotted pattern. Labeled spots are marked with the small arrowheads and small gray arrow. The asterisk marks an unspecific spot that was used as a reference for the following images in the series. **(B)** The FM1-43 fluorescence was partially photobleached to allow the testing of whether spots that were originally stained became restained. **(C)** After a second depolarization in the presence of fresh external FM1-43, some of the spots were restained (large arrowheads), some were not restained but could still be detected in their previous position (gray small arrows), others disappeared completely (small arrowheads), and others were newly formed (white arrows). Scale bar = 20 μm. **(D)** Graph of the distribution of the total number and percentage of fluorescent spots in each category described above.

peroxidase and their surrounding vesicles also displayed electron dense gold particles. This also occurred in multivesicular bodies in the apparent process of formation shown in **Figures 6C,D** and is consistent with the early observations that multivesicular bodies are capable to accumulate peroxidase (Rosenbluth and Wissig, 1964; Holtzman and Peterson, 1969; Birks et al., 1972; Weldon, 1975).

INTRACELLULAR MOBILIZATION OF FM1-43 FLUORESCENCE AFTER STIMULATION

The destiny of the material contained inside multivesicular bodies remains a matter of debate (for review, see Von Bartheld and Altick, 2011), however, that multivesicular bodies in our electromicrographs appear in the perinuclear region suggest they have been transported after their peripheral formation. To explore if after electrical stimulation vesicles and or multivesicular bodies become transported toward the plasma region, FM1-43 fluorescent spots of four neurons that had been stimulated at 20 Hz were imaged in the same focal planes 12, 36, and 48 h after stimulation (**Figure 7**). At the end of the experiments the neurons were known to be healthy because they had good resting potentials and the capacity to produce normal action potentials. As shown in **Figure 7**, at all times tested, fluorescence remained restricted to small spots, and the label gradually appeared in more central parts of the soma, while there was a decrease in the number of peripheral spots. The transport pathway (as exemplified by the sequence of images made at a depth of 20 μm from the plane of contact of the cell with the culture dish), produced a large concentration of

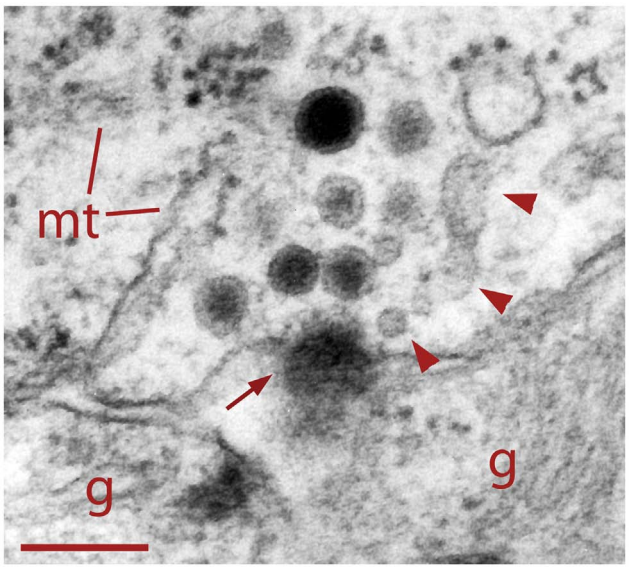

FIGURE 4 | Dense core vesicle fusion after electrical stimulation (arrow). To the right of the fusing vesicle are small clear vesicles and cisternae (arrowheads) atypical of somatic clusters before electrical stimulation. This suggests vesicle formation as part of the endocytic pathway. Glial cell fingers (g) can be seen outside the Retzius cell. Scale bar = 250 nm.

spots at the center of the soma. This suggests that the mobilization of the spots did not occur randomly but followed well-organized patterns.

ASSOCIATIONS BETWEEN MULTIVESICULAR BODIES, THE GOLGI APPARATUS, AND THE NUCLEUS

Correlating with the previous result, in neurons fixed 10 min after electrical stimulation had ended, multivesicular bodies were abundant deep in the perinuclear region, near Golgi apparatuses, vesicles, and mitochondria (**Figure 8**, see also **Figure 1**), right in the regions in which vesicles seem to be forming, as described above. The multivesicular bodies in some of the sections established links with Golgi elements, endoplasmic reticulum, and mitochondria. Their vesicle contents and degradation products with irregular shapes were apparently extruded from the multivesicular bodies and became a continuous with the vesicle accumulations aligned with the Golgi apparatus (**Figure 8A**). Multivesicular body fragments also appeared in the perinuclear region, making contacts with the nuclear membrane (**Figure 8B**). These structural associations suggest that the multivesicular body contents were recycled in the Golgi apparatus and also that some of their content contributed to communication between the nucleus and the extracellular space.

DISCUSSION

We studied the cycling of dense core vesicles associated with serotonin release through exocytosis by serotonergic leech neurons. Dense core vesicles are distributed in a perinuclear pool where they seem to be formed and also in a pool of peripheral clusters. Electrical stimulation induces the transport of dense core vesicle clusters toward the plasma membrane, with which vesicles fuse. Endocytosis generates dense core and clear vesicles, which are later incorporated into multivesicular bodies. In turn, multivesicular bodies are transported back to the perinuclear region, where their contents seem to be recycled by the Golgi apparatus.

Somatic exocytosis of serotonin is a highly regulated process in neurons of vertebrates and invertebrates, in which serotonin-containing vesicles are mobilized centrifugally in response to electrical stimulation and then fused (De-Miguel and Trueta, 2005; Kaushalya et al., 2008; see review by Trueta and De-Miguel in this issue). In Retzius neurons, stimulation with series of 20 Hz trains at 2 min intervals produces two sigmoidal exocytosis kinetics with a duration of hundreds of seconds, with each sigmoidal expressing the arrival of one vesicle cluster (P. Noguez, C. Bustos, and F. F. De Miguel, in preparation).

These kinetics seem to reflect the subsequent arrival of two vesicle clusters at the same release site, upon their mobilization and fusion in response to electrical stimulation. This also provides a good explanation for the second staining experiment (**Figure 3**), in which clusters of vesicles stained with FM1-43 and then bleached became restained again upon a second depolarization in the presence of the fluorescent dye. Since the vesicle pool surrounding the nucleus remains after electrical stimulation, it is possible that the clusters arriving at the plasma membrane in response to electrical stimulation belong to the peripheral pool. However, that some of the fluorescent FM1-43 spots remain peripheral after so many hours following electrical stimulation also suggest that some multivesicular bodies are not transported retrogradely or that not all the dense core vesicles are incorporated into multivesicular bodies after exocytosis. Therefore, some may be degraded locally or free vesicles remain and are reused later, while multivesicular bodies traveling back to the perinuclear region are destroyed there or their material is reused for new vesicle synthesis.

Since about 100 vesicle clusters become fused upon a single 20 Hz train (Trueta et al., 2003) and each cluster contains 100-1000 vesicles (P. Noguez, I. Santamaría-Holek, M. Rubí, and F. F. De Miguel, in preparation), we estimate that tens of thousands of vesicles fuse in response to a 20-Hz train, with each vesicle containing 67,000 molecules of serotonin (Bruns and Jahn, 1995). This adds to the serotonin secreted from other extrasynaptic sites including the axons and dendrite varicosities. An equivalent amount of serotonin is secreted by the other Retzius neuron in the ganglion, since both respond in parallel upon the activation of common synaptic inputs (Velázquez-Ulloa et al., 2003). Therefore it is not surprising that a neuron pair is capable of producing the multiple modulatory effects of serotonin seen in the leech (Willard, 1981; Kristan and Nusbaum, 1982; Burrell et al., 2002; Crisp and Mesce, 2006; Calviño and Szczupak, 2008; Bisson and Torre, 2011).

Serotonergic neurons fail to fire at high frequencies and have developed mechanisms of autoinhibition that are triggered by serotonin release (Aghajanian and Lakoski, 1984; Heinrich et al., 1999; Rose et al., 2006; Gocht and Heinrich, 2007; Cercós et al., 2009). This, in addition to the depletion of releasable vesicle pools, shows that serotonin exocytosis from extrasynaptic sites operates with a high degree of autoregulatory mechanisms. In this regard, that dense core vesicles do not re-enter immediately the

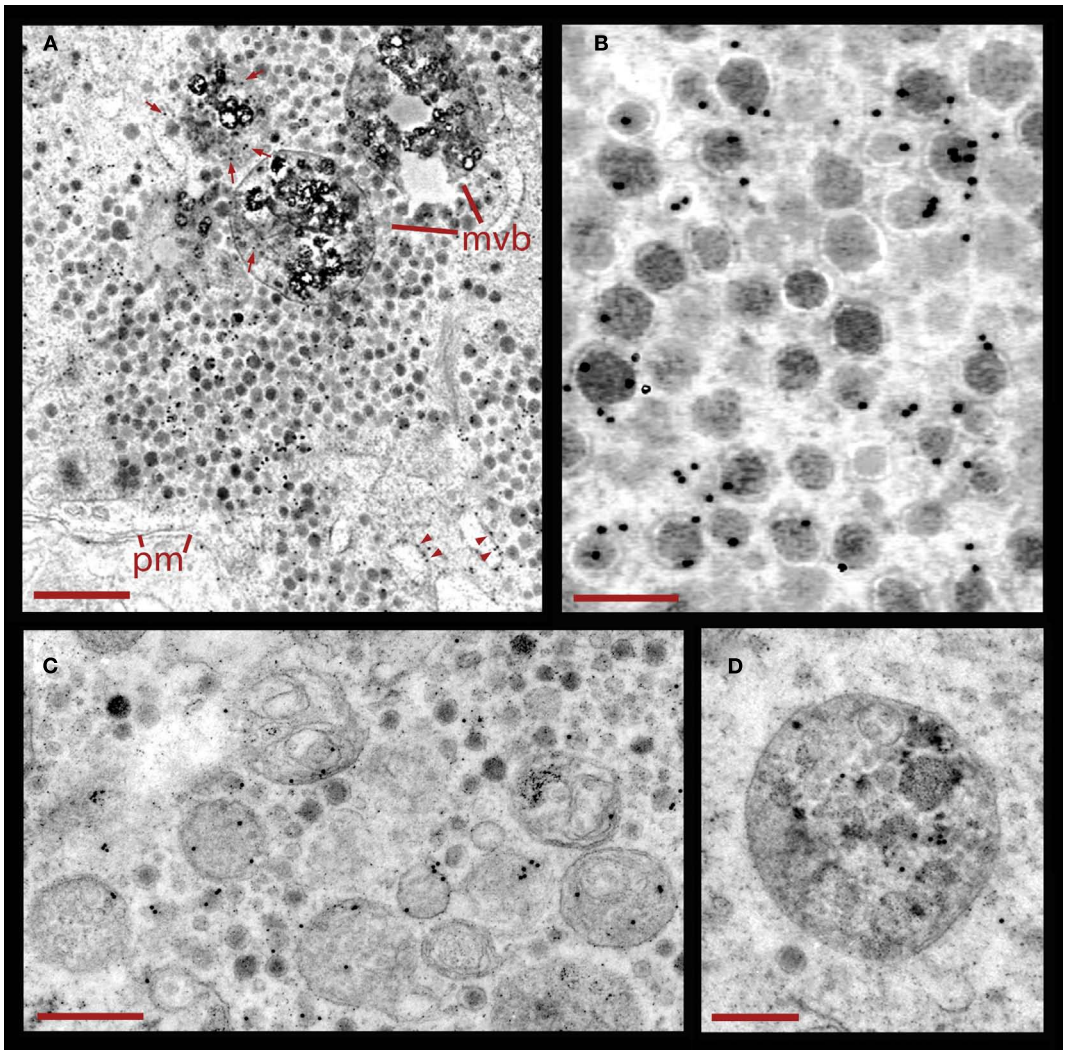

FIGURE 5 | Endocytosis of peroxidase following electrical stimulation. (A) Vesicle cluster in a neuron fixed during stimulation in the presence of external peroxidase. Large multivesicular bodies (mvb) are also present. Peroxidase was detected by a polyclonal antibody coupled to 10 nm gold particles. The black electron dense spots are associated with vesicles in the clusters located near the plasma membrane (pm), and labeling was considerably lower outside of the cluster. However, multivesicular bodies (arrows) and membranes of endoplasmic reticulum (arrowheads) also displayed gold particles. Scale = 1.0 μm. **(B)** Higher magnification of a vesicle cluster with electron dense spots accumulated over the vesicles. Scale = 200 nm. **(C)** Cluster with dense core vesicles and multivesicular bodies bearing gold particles. Scale = 1 μm. **(D)** Higher magnification of a multivesicular body that accumulated gold particles. Scale = 500 nm.

releasable pool but are packed, degraded, and transported towards the nucleus, contributes to this scheme by increasing the latency of vesicle replenish upon subsequent trains of electrical activity, when compared to the fast recycling occurring in synaptic vesicles (Betz and Bewick, 1992, 1993; Betz et al., 1992; Cochilla et al., 1999; Richards et al., 2000).

The clustering of dense core vesicle offers several advantages over having the same number of individual vesicles scattered, since their transport becomes more efficient and the plasma membrane specializations for vesicle fusion are concentrated at specific locations instead of being randomly distributed, thus increasing the efficiency of vesicle docking. Moreover, a localized release renders higher serotonin concentrations at particular release sites. Since serotonin is released onto surrounding glia, it may be proposed that glial cells regulate the diffusion of serotonin released from the soma, at least to the rest of the neurons wrapped within the same glial processes. This may also contribute to enlarge the timing of the serotonin effects on the central nervous system. Extrasynaptic communication or volume transmission between neurons and glia have been demonstrated already for different transmitter systems (Bjelke et al., 1996; Agnati et al., 2007, 2010; Pérez de la Mora et al., 2008; Araque and Navarrete, 2010; Fuxe et al., 2010, 2012).

The distance that vesicle clusters must move to reach the plasma membrane adds a lag to exocytosis, desynchronizes it from electrical activity and makes it slow compared to that from serotonergic

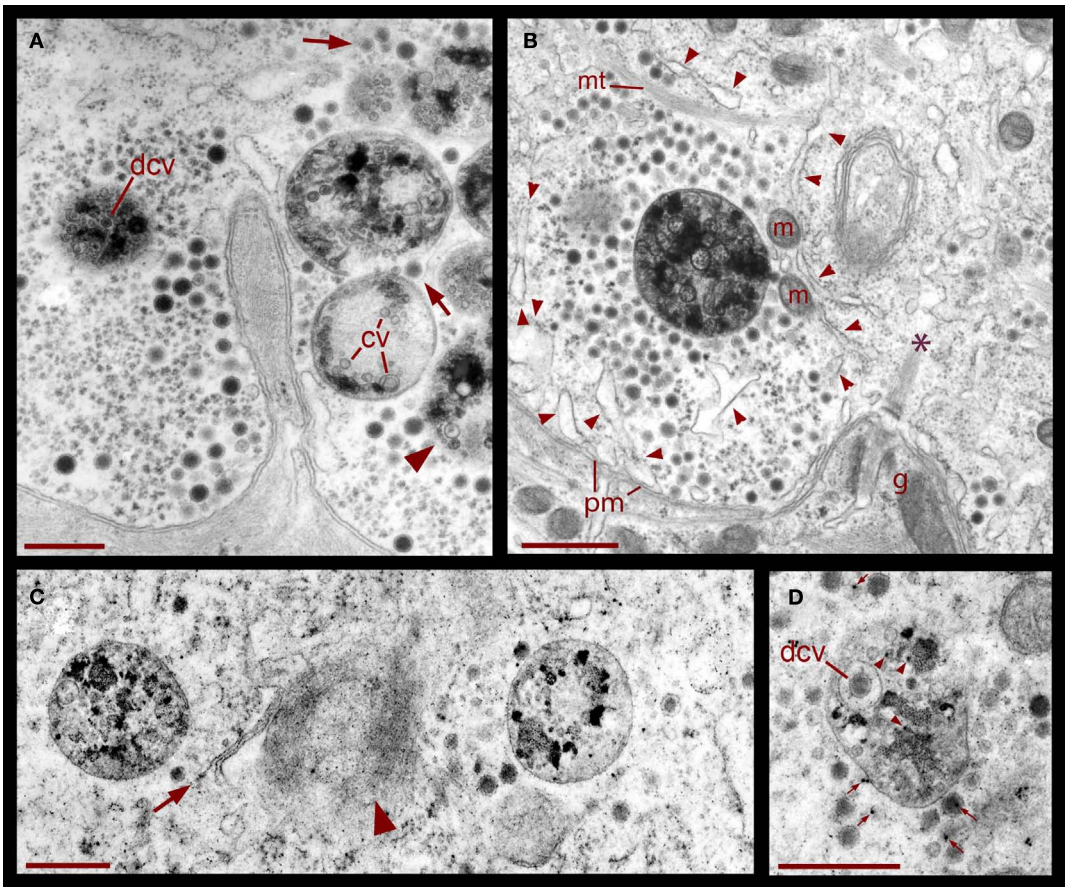

FIGURE 6 | Formation of multivesicular bodies after electrical stimulation. (A) Several multivesicular bodies near the plasma membrane with dense core vesicles around. The neuron was stimulated at 20 Hz and fixed 10 min later. Arrows point to vesicles associated with different multivesicular bodies, as they seem to be forming through the wrapping of endoplasmic reticulum. The arrowhead points to a multivesicular body containing different types of vesicles without a noticeable external layer of membranes. Clear vesicles (cv) and dense core vesicles (dcv) inside the multivesicular bodies can also be seen. **(B)** Multivesicular body surrounded by a radial array of dense core vesicles, endoplasmic reticulum (arrowheads), microtubules (mt), and mitochondria (m). Asterisk marks a bundle of microtubules attached to the plasma membrane through a hemi-desmosome. Stimulation was as in **(A)**. **(C)** Formation of a multivesicular body (arrow) with microtubule coiling (arrowhead). **(D)** A multivesicular body after the neuron was stimulated in the presence of extracellular peroxidase, displaying gold marks, and containing clear and dense core vesicles (dcv). Arrowheads point to gold particles inside multivesicular bodies and small arrows point to gold particles on top of vesicles and membrane corpses, maybe produced upon endocytosis. Scale bar = 1 μm.

synapses, in which events occur within the characteristic millisecond time scale (Fuchs et al., 1982; Henderson et al., 1983; Dietzel et al., 1986). This distance may determine at least in part the slow time course of secretion, which is similar to that of somatic exocytosis in other types of neurons (Zhang et al., 2007; Kaushalya et al., 2008; Colgan et al., 2009; Patel et al., 2009), and also by excitable endocrine cells (Penner and Neher, 1988; Heinemann et al., 1993; Chow et al., 1996; Rosé et al., 2002). This apparent type of microtubule-coupled transport suggests its dependence on kinesin motors. Therefore, somatic secretion has high energy requirements. On the way back to the perinuclear region, multivesicular bodies may also use microtubule backward transport, in this case coupled to dynein motors (van den Berg and Hoogenraad, 2012), thus increasing the energy expenses of exocytosis. That multivesicular bodies release their contents to the cytoplasm has been a provoking hypothesis since early studies (Palay, 1960). Our data are in agreement with this possibility and also suggest that multivesicular bodies in perinuclear regions may release their contents, which in turn are used for new vesicle synthesis and also for providing the nucleus with information from the extracellular space. However, we do not have any evidence that multivesicular bodies may serve as releasible pools, as has been proposed for other cell types (for review, see Von Bartheld and Altick, 2011; Fuxe et al., 2012), since we have never seen multivesicular bound to the plasma membrane after electrical stimulation and on the contrary, multivesicular bodies seem to be formed as result of vesicle endocytosis and moving toward the perinuclear regions of the neuron.

The formation of new vesicles in the perinuclear region also contributes to the regulated secretion of serotonin by imposing the large migratory distances of the vesicle clusters to reach their fusion sites. One of the several questions yet to be answered is

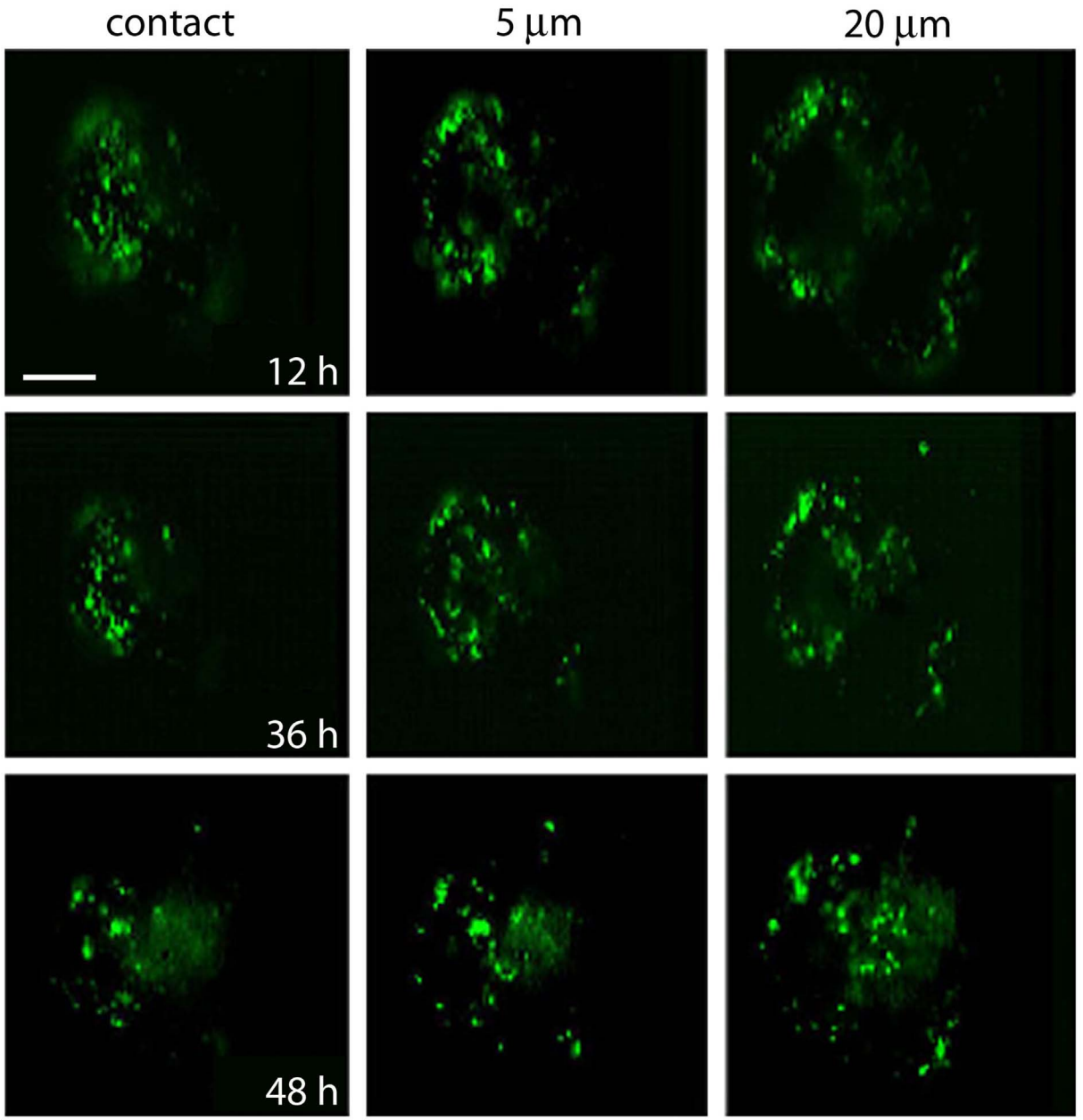

FIGURE 7 | Migration of fluo escent FM1-43 spots. Images taken from the site of contact with the dish bottom (left) and at 5 and 20 µm depth. Each area was imaged at 12, 36, and 48 h after depolarization of cultured neurons in bathing solution containing 40 mM potassium and FM1-43. Note the accumulation of spots to more internal regions of the soma at the 20-µm focal plane. Scale bar = 20 µm.

whether electrical activity induces the formation of new vesicles. This is a feasible possibility since electrical stimulation at high frequency evokes calcium-induced calcium release (Trueta et al., 2004) and calcium waves that reach the nucleus of Retzius neurons (Beck et al., 2001; C. Leon and F. F. De-Miguel, in preparation). Calcium in the nucleus activates gene expression (Bito et al., 1997; Wiegert and Bading, 2011), and therefore its role in vesicle cycling may include the activation of the vesicle formation, followed by their transport, exo- and endocytosis. Additional signals activating new vesicle synthesis may arrive with multivesicular bodies after vesicle endocytosis.

GENERAL SIGNIFICANCE

Somatic exocytosis is now recognized as a more general form of neuronal communication of central and peripheral neurons of vertebrates and invertebrates (see review by Trueta and De-Miguel in this issue). Since neuronal somatic secretion of transmitters and peptides occurs from dense core vesicles in different cells types (Huang and Neher, 1996; Zaidi and Matthews, 1997, 1999; Puopolo et al., 2001; Huang et al., 2007), the data presented here provides an example as to how the complexity of dense core vesicle cycling contributes to the regulation a fundamental mode of neuronal exocytosis and communication.

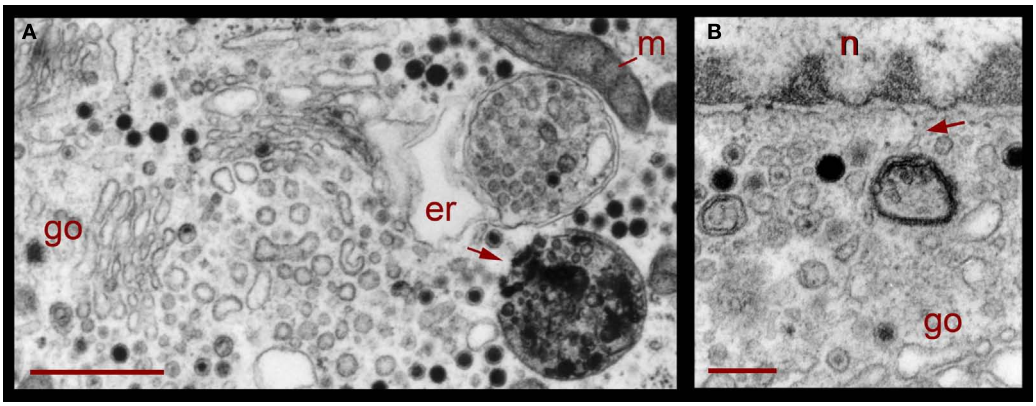

FIGURE 8 | Perinuclear multivesicular bodies. (A) Multivesicular bodies (mvb) coexisting with Golgi apparatus (go). The multivesicular body on the right top contains mostly clear vesicles and is in association with endoplasmic reticulum (er) and mitochondria (m). The one in the right bottom has a membrane discontinuity (arrowhead). On the left side of the image, small vesicles near the Golgi endings (asterisks) display electrodense material inside. **(B)** Contents of the multivesicular bodies are in association with the nuclear membrane and near Golgi apparatus (n = nucleus). The arrowhead points to structures possibly binding the multivesicular body fragment with the nuclear membrane. Scale bars = 500 nm.

ACKNOWLEDGMENTS

We wish to express our gratitude to Mr. Bruno Mendez for his invaluable technical assistance during the whole project and to the electron microscopy and computer units of IFC-UNAM, in particular to Rodolfo Paredes and Francisco Perez, for their outstanding technical support to this project. This work was founded by DGAPA-UNAM grant IN211511 and CONACYT GRANT 130031 to Francisco F. De-Miguel.

REFERENCES

Aghajanian, G. K., and Lakoski, J. M. (1984). Hyperpolarization of serotonergic neurons by serotonin and LSD: studies in brain slices showing increased K+ conductance. *Brain Res.* 305, 181–185.

Agnati, L. F., Genedani, S., Leo, G., Forni, A., Woods, A. S., Filaferro, M., Franco, R., and Fuxe, K. (2007). Abeta peptides as one of the crucial volume transmission signals in the trophic units and their interactions with homocysteine. Physiological implications and relevance for Alzheimer's disease. *J. Neural Transm.* 114, 21–31.

Agnati, L. F., Guidolin, D., Guescini, M., Genedani, S., and Fuxe, K. (2010). Understanding wiring and volume transmission. *Brain Res. Rev.* 64, 37–59.

Agnati, L. F., Leo, G., Zanardi, A., Genedani, S., Rivera, A., Fuxe, K., and Guidolin, D. (2006). Volume transmission and wiring transmission from cellular to molecular networks: history and perspectives. *Acta Physiol. (Oxf.)* 187, 329–344.

Araque, A., and Navarrete, M. (2010). Glial cells in neuronal network function. *Philos. Trans. R. Soc. Lond. B Biol. Sci.* 365, 2375–2381.

Beck, A., Lohr, C., and Deitmer, J. W. (2001). Calcium transients in subcompartments of the leech Retzius neuron as induced by single action potentials. *J. Neurobiol.* 48, 1–18.

Betz, W. J., and Bewick, G. S. (1992). Optical analysis of synaptic vesicle recycling at the frog neuromuscular junction. *Science* 255, 200–203.

Betz, W. J., and Bewick, G. S. (1993). Optical monitoring of transmitter release and synaptic vesicle recycling at the frog neuromuscular junction. *J. Physiol.* 460, 287–309.

Betz, W. J., Bewick, G. S., and Ridge, R. M. (1992). Intracellular movements of fluorescently labeled synaptic vesicles in frog motor nerve terminals during nerve stimulation. *Neuron* 9, 805–813.

Birks, R. I., MacKey, M. C., and Weldon, P. R. (1972). Organelle formation from pinocytotic elements in neurites of cultured sympathetic ganglia. *J. Neurocytol.* 1, 311–340.

Bisson, G., and Torre, V. (2011). Statistical characterization of social interactions and collective behavior in medicinal leeches. *J. Neurophysiol.* 106, 78–90.

Bito, H., Deisseroth, K., and Tsien, R. W. (1997). $Ca2^{+}$-dependent regulation in neuronal gene expression. *Curr. Opin. Neurobiol.* 7, 419–429.

Bjelke, B., Goldstein, M., Tinner, B., Andersson, C., Sesack, S. R., Steinbusch, H. W., Lew, J. Y., He, X., Watson, S., Tengroth, B., and Fuxe, K. (1996). Dopaminergic transmission in the rat retina: evidence for volume transmission. *J. Chem. Neuroanat.* 12, 37–50.

Bruns, D., and Jahn, R. (1995). Real-time measurement of transmitter release from single synaptic vesicles. *Nature* 377, 62–65.

Burrell, B. D., Sahley, C. L., and Muller, K. J. (2002). Differential effects of serotonin enhance activity of an electrically coupled neural network. *J. Neurophysiol.* 87, 2889–2895.

Calviño, M. A., and Szczupak, L. (2008). Spatial-specific action of serotonin within the leech midbody ganglion. *J. Comp. Physiol. A Neuroethol. Sens. Neural Behav. Physiol.* 194, 523–531.

Cercós, M. G., De-Miguel, F. F., and Trueta, C. (2009). Real-time measurements of synaptic autoinhibition produced by serotonin release in cultured leech neurons. *J. Neurophysiol.* 102, 1075–1085.

Ceridono, M., Ory, S., Momboisse, F., Chasserot-Golaz, S., Houy, S., Calco, V., Haeberlé, A.-M., Demais, V., Bailly, Y., Bader, M. F., and Gasman, S. (2011). Selective recapture of secretory granule components after full collapse exocytosis in neuroendocrine chromaffin cells. *Traffic* 12, 72–88.

Chazal, G. and Ralston, H. J. III. (1987). Serotonin-containing structures in the nucleus raphe dorsalis of the cat: an ultrastructural analysis of dendrites, presynaptic dendrites, and axon terminals. *J. Comp. Neurol.* 259, 317–329.

Chow, R. H., Klingauf, J., Heinemann, C., Zucker, R. S., and Neher, E. (1996). Mechanisms determining the time course of secretion in neuroendocrine cells. *Neuron* 16, 369–376.

Cochilla, A. J., Angleson, J. K., and Betz, W. J. (1999). Monitoring secretory membrane with FM1-43 fluorescence. *Annu. Rev. Neurosci.* 22, 1–10.

Coggeshall, R. E. (1972). Autoradiographic and chemical localization of 5-hydroxytryptamine in identified neurons in the leech. *Anat. Rec.* 172, 489–498.

Coggeshall, R. E., and Fawcett, D. W. (1964). The fine structure of the central nervous system of the leech, *Hirodu medicinalis. J. Neurophysiol.* 27, 229–289.

Coggeshall, R. E., and Lekan, H. A. (1996). Methods for determining numbers of cells and synapses: a case for more uniform standards of review. *J. Comp. Neurol.* 364, 6–15.

Colgan, L. A., Putzier, I., and Levitan, E. S. (2009). Activity-dependent vesicular monoamine transporter-mediated depletion of the nucleus supports somatic release by serotonin neurons. *J. Neurosci.* 29, 15878–15887.

Crisp, K. M., and Mesce, K. A. (2006). Beyond the central pattern generator: amine modulation of decision-making neural pathways descending from the brain of the medicinal leech. *J. Exp. Biol.* 209(Pt 9), 1746–1756.

De-Miguel, F. F., and Trueta, C. (2005). Synaptic and extrasynaptic secretion of serotonin. *Cell. Mol. Neurobiol.* 25, 297–312.

Descarries, L., and Mechawar, N. (2000). Ultrastructural evidence for diffuse transmission by monoamine and acetylcholine neurons of the central nervous system. *Prog. Brain Res.* 125, 27–47.

Dietzel, I. D., Drapeau, P., and Nicholls, J. G. (1986). Voltage dependence of 5-hydroxytryptamine release at a synapse between identified leech neurones in culture. *J. Physiol.* 372, 191–205.

Fernández-de-Miguel, F., and Drapeau, P. (1995). Synapse formation and function: insights from identified leech neurons in culture. *J. Neurobiol.* 27, 367–379.

Fuchs, P. A., Henderson, L. P., and Nicholls, J. G. (1982). Chemical transmission between individual Retzius and sensory neurones of the leech in culture. *J. Physiol.* 323, 195–210.

Fuxe, K., and Agnati, L. F. (eds). (1991). *Volume Transmission in the Brain: Novel Mechanisms of Neuronal Transmission*. New York: Raven Press.

Fuxe, K., Borroto-Escuela, D. O., Romero-Fernandez, W., Ciruela, F., Manger, P., Leo, G., Díaz-Cabiale, Z., and Agnati, L. F. (2012). *On the Role of Volume Transmission and Receptor-Receptor Interactions in Social Behaviour: Focus on Central Catecholamine and Oxytocin Neurons. Brain Research*. Available at: http://www.ncbi.nlm.nih.gov/pubmed/22373652 [accessed April 12, 2012].

Fuxe, K., Dahlström, A. B., Jonsson, G., Marcellino, D., Guescini, M., Dam, M., Manger, P., and Agnati, L. (2010). The discovery of central monoamine neurons gave volume transmission to the wired brain. *Prog. Neurobiol.* 90, 82–100.

Gocht, D., and Heinrich, R. (2007). Postactivation inhibition of spontaneously active neurosecretory neurons in the medicinal leech. *J. Comp. Physiol. A Neuroethol. Sens. Neural Behav. Physiol.* 193, 347–361.

Heinemann, C., Rüden, L., Chow, R. H., and Neher, E. (1993). A two-step model of secretion control in neuroendocrine cells. *Pflugers Archiv.* 424, 105–112.

Heinrich, R., Cromarty, S. I., Hörner, M., Edwards, D. H., and Kravitz, E. A. (1999). Autoinhibition of serotonin cells: an intrinsic regulatory mechanism sensitive to the pattern of usage of the cells. *Proc. Natl. Acad. Sci. U.S.A.* 96, 2473–2478.

Henderson, L. P. (1983). The role of 5-hydroxytryptamine as a transmitter between identified leech neurones in culture. *J. Physiol.* 339, 309–324.

Henderson, L. P., Kuffler, D. P., Nicholls, J., and Zhang, R. (1983). Structural and functional analysis of synaptic transmission between identified leech neurones in culture. *J. Physiol.* 340, 347–358.

Herzog, V., and Farquhar, M. G. (1977). Luminal membrane retrieved after exocytosis reaches most golgi cisternae in secretory cells. *Proc. Natl. Acad. Sci. U.S.A.* 74, 5073–5077.

Herzog, V., and Miller, F. (1979). Membrane retrieval in epithelial cells of isolated thyroid follicles. *Eur. J. Cell Biol.* 19, 203–215.

Holtzman, E., and Peterson, E. R. (1969). Uptake of protein by mammalian neurons. *J. Cell Biol.* 40, 863–869.

Huang, H.-P., Wang, S.-R., Yao, W., Zhang, C., Zhou, Y., Chen, X.-W., Zhang, B., Xiong, W., Wang, L. Y., Zheng, L. H., Landry, M., Hökfelt, T., Xu, Z. Q., and Zhou, Z. (2007). Long latency of evoked quantal transmitter release from somata of locus coeruleus neurons in rat pontine slices. *Proc. Natl. Acad. Sci. U.S.A.* 104, 1401–1406.

Huang, L. Y., and Neher, E. (1996). Ca(2+)-dependent exocytosis in the somata of dorsal root ganglion neurons. *Neuron* 17, 135–145.

Iversen, L. L. (1971). Role of transmitter uptake mechanisms in synaptic neurotransmission. *Br. J. Pharmacol.* 41, 571–591.

Kaushalya, S. K., Desai, R., Arumugam, S., Ghosh, H., Balaji, J., and Maiti, S. (2008). Three-photon microscopy shows that somatic release can be a quantitatively significant component of serotonergic neurotransmission in the mammalian brain. *J. Neurosci. Res.* 86, 3469–3480.

Kristan, W. B. Jr., and Nusbaum, M. P. (1982). The dual role of serotonin in leech swimming. *J. Physiol. (Paris)* 78, 743–747.

Kuffler, D. P., Nicholls, J., and Drapeau, P. (1987). Transmitter localization and vesicle turnover at a serotoninergic synapse between identified leech neurons in culture. *J. Comp. Neurol.* 256, 516–526.

Nicholls, J. G., and Kuffler, D. P. (1990). Quantal release of serotonin from presynaptic nerve terminals. *Neurochem. Int.* 17, 157–163.

Palay, S. L. (1960). The fine structure of secretory neurons in the preoptic nucleus of the goldish (*Carassius auratus*). *Anat. Rec.* 138, 417–443.

Park, J. J., Koshimizu, H., and Loh, Y. P. (2009). Biogenesis and transport of secretory granules to release site in neuroendocrine cells. *J. Mol. Neurosci.* 37, 151–159.

Patel, J. C., Witkovsky, P., Avshalumov, M. V., and Rice, M. E. (2009). Mobilization of calcium from intracellular stores facilitates somatodendritic dopamine release. *J. Neurosci.* 29, 6568–6579.

Patzak, A., Aunis, D., and Langley, K. (1987). Membrane recycling after exocytosis: an ultrastructural study of cultured chromaffin cells. *Exp. Cell Res.* 171, 346–356.

Penner, R., and Neher, E. (1988). The role of calcium in stimulus-secretion coupling in excitable and non-excitable cells. *J. Exp. Biol.* 139, 329–345.

Pérez de la Mora, M., Jacobsen, K. X., Crespo-Ramírez, M., Flores-Gracia, C., and Fuxe, K. (2008). Wiring and volume transmission in rat amygdala. Implications for fear and anxiety. *Neurochem. Res.* 33, 1618–1633.

Piper, R. C., and Katzmann, D. J. (2007). Biogenesis and function of multivesicular bodies. *Annu. Rev. Cell Dev. Biol.* 23, 519–547.

Puopolo, M., Hochstetler, S. E., Gustincich, S., Wightman, R. M., and Raviola, E. (2001). Extrasynaptic release of dopamine in a retinal neuron: activity dependence and transmitter modulation. *Neuron* 30, 211–225.

Richards, D. A., Guatimosim, C., and Betz, W. J. (2000). Two endocytic recycling routes selectively fill two vesicle pools in frog motor nerve terminals. *Neuron* 27, 551–559.

Rosé, S. D., Lejen, T., Casaletti, L., Larson, R. E., Pene, T. D., and Trifaró, J.-M. (2002). Molecular motors involved in chromaffin cell secretion. *Ann. N. Y. Acad. Sci.* 971, 222–231.

Rose, T., Gras, H., and Hörner, M. (2006). Activity-dependent suppression of spontaneous spike generation in the Retzius neurons of the leech *Hirudo medicinalis* L. *Invert. Neurosci.* 6, 169–176.

Rosenbluth, J., and Wissig, S. L. (1964). The distribution of exogenous ferritin in toad spinal ganglia and the mechanism of its uptake by neurons. *J. Cell Biol.* 23, 307–325.

Trueta, C., Méndez, B., and De-Miguel, F. F. (2003). Somatic exocytosis of serotonin mediated by L-type calcium channels in cultured leech neurones. *J. Physiol.* 547(Pt 2), 405–416.

Trueta, C., Sánchez-Armass, S., Morales, M. A., and De-Miguel, F. F. (2004). Calcium-induced calcium release contributes to somatic secretion of serotonin in leech Retzius neurons. *J. Neurobiol.* 61, 309–316.

van den Berg, R., and Hoogenraad, C. C. (2012). Molecular motors in cargo trafficking and synapse assembly. *Adv. Exp. Med. Biol.* 970, 173–196.

Velázquez-Ulloa, N., Blackshaw, S. E., Szczupak, L., Trueta, C., García, E., and De-Miguel, F. F. (2003). Convergence of mechanosensory inputs onto neuromodulatory serotonergic neurons in the leech. *J. Neurobiol.* 54, 604–617.

Von Bartheld, C. S., and Altick, A. L. (2011). Multivesicular bodies in neurons: distribution, protein content, and trafficking functions. *Prog. Neurobiol.* 93, 313–340.

Weldon, P. R. (1975). Pinocytotic uptake and intracellular distribution of colloidal thorium dioxide by cultured sensory neurites. *J. Neurocytol.* 4, 341–356.

Wiegert, J. S., and Bading, H. (2011). Activity-dependent calcium signaling and ERK-MAP kinases in neurons: a link to structural plasticity of the nucleus and gene transcription regulation. *Cell Calcium* 49, 296–305.

Willard, A. L. (1981). Effects of serotonin on the generation of the motor program for swimming by the medicinal leech. *J. Neurosci.* 1, 936–944.

Zaidi, Z. F., and Matthews, M. R. (1997). Exocytotic release from neuronal cell bodies, dendrites and nerve terminals in sympathetic ganglia of the rat, and its differential regulation. *Neuroscience* 80, 861–891.

Zaidi, Z. F., and Matthews, M. R. (1999). Stimulant-induced exocytosis from neuronal somata, dendrites, and newly formed synaptic nerve terminals in chronically decentralized sympathetic ganglia of the rat. *J. Comp. Neurol.* 415, 121–143.

Zhang, X., Chen, Y., Wang, C., and Huang, L.-Y. M. (2007). Neuronal

somatic ATP release triggers neuron-satellite glial cell communication in dorsal root ganglia. *Proc. Natl. Acad. Sci. U.S.A.* 104, 9864–9869.

Conflict of Interest Statement: The authors declare that the research was conducted in the absence of any commercial or financial relationships that could be construed as a potential conflict of interest.

Received: 13 April 2012; paper pending published: 26 April 2012; accepted: 14 May 2012; published online: 06 June 2012.

Citation: Trueta C, Kuffler DP and De-Miguel FF (2012) Cycling of dense core vesicles involved in somatic exocytosis of serotonin by leech neurons. Front. Physio. ***3****:175. doi: 10.3389/fphys.2012.00175*
This article was submitted to Frontiers in Membrane Physiology and Biophysics, a specialty of Frontiers in Physiology.

frontiers in
PHYSIOLOGY

ORIGINAL RESEARCH ARTICLE
published: 24 August 2012
doi: 10.3389/fphys.2012.00334

Extrasynaptic glutamate receptor activation as cellular bases for dynamic range compression in pyramidal neurons

Katerina D. Oikonomou†, Shaina M. Short†, Matthew T. Rich and Srdjan D. Antic*

Department of Neuroscience, University of Connecticut Health Center, Farmington, CT, USA

Edited by:
Francisco Fernandez De-Miguel, Universidad Nacional Autonoma de Mexico, Mexico

Reviewed by:
Mala Shah, University of London, UK
Francisco Fernandez De-Miguel, Universidad Nacional Autonoma de Mexico, Mexico

Correspondence:
Srdjan D. Antic, Department of Neuroscience, University of Connecticut Health Center, Farmington, CT 06030-3401, USA.
e-mail: antic@neuron.uchc.edu

†Katerina D. Oikonomou and Shaina M. Short have contributed equally to this work.

Repetitive synaptic stimulation overcomes the ability of astrocytic processes to clear glutamate from the extracellular space, allowing some dendritic segments to become submerged in a pool of glutamate, for a brief period of time. This dynamic arrangement activates extrasynaptic NMDA receptors located on dendritic shafts. We used voltage-sensitive and calcium-sensitive dyes to probe dendritic function in this glutamate-rich location. An excess of glutamate in the extrasynaptic space was achieved either by repetitive synaptic stimulation or by glutamate iontophoresis onto the dendrites of pyramidal neurons. Two successive activations of synaptic inputs produced a typical NMDA spike, whereas five successive synaptic inputs produced characteristic plateau potentials, reminiscent of cortical UP states. While NMDA spikes were coupled with brief calcium transients highly restricted to the glutamate input site, the dendritic plateau potentials were accompanied by calcium influx along the entire dendritic branch. Once initiated, the glutamate-mediated dendritic plateau potentials could not be interrupted by negative voltage pulses. Activation of extrasynaptic NMDA receptors in cellular compartments void of spines is sufficient to initiate and support plateau potentials. The only requirement for sustained depolarizing events is a surplus of free glutamate near a group of extrasynaptic receptors. Highly nonlinear dendritic spikes (plateau potentials) are summed in a highly sublinear fashion at the soma, revealing the cellular bases of signal compression in cortical circuits. Extrasynaptic NMDA receptors provide pyramidal neurons with a function analogous to a dynamic range compression in audio engineering. They limit or reduce the volume of "loud sounds" (i.e., strong glutamatergic inputs) and amplify "quiet sounds" (i.e., glutamatergic inputs that barely cross the dendritic threshold for local spike initiation). Our data also explain why consecutive cortical UP states have uniform amplitudes in a given neuron.

Keywords: prefrontal cortex, pyramidal neuron, synaptic integration, dendritic spike, voltage-sensitive dye

INTRODUCTION

Each pyramidal neuron in the mammalian cerebral cortex receives several thousands of glutamatergic synapses (Elston, 2003), over 2/3 of which impinge on basal and oblique dendrites (Larkman, 1991). Being directly connected to the cell body, the basal dendrites are in a prime location for delivering large amounts of depolarizing current to the cell body (Oakley et al., 2001; Benucci et al., 2004; Enoki et al., 2004; Milojkovic et al., 2004). In principle, one can identify two parts of the depolarizing current in basal dendrites. One part of this current is of synaptic origin; mediated by the opening of ion channels in dendritic spines (Yasuda et al., 2003; Nimchinsky et al., 2004). The second portion of this current is mediated by the opening of voltage-gated and ligand-gated membrane conductances located on the dendritic shafts of basal dendrites (Schiller et al., 1995; Enoki et al., 2004; Milojkovic et al., 2005b; Kampa and Stuart, 2006; Acker and Antic, 2009; Chalifoux and Carter, 2011). The contributions from these two sources of depolarizing current (synaptic and extrasynaptic) vary with the amount of glutamatergic input. The total glutamatergic input in one dendritic region is determined by the frequency of afferent activity (temporal summation of glutamate) or convergence of afferent axon terminals into the same region (spatial summation of glutamate). When glutamatergic inputs are sparse and scattered (Swadlow and Hicks, 1997), tiny amounts of glutamate that spill out from synaptic clefts are quickly removed from the extracellular space by astrocytic processes (**Figure 1A**); this mechanism is especially effective at physiological temperatures (Asztely et al., 1997; Kullmann et al., 1999). Clustered synaptic activity (**Figure 1B**), on the other hand, overcomes the astrocytic ability to remove glutamate, allowing the excitatory neurotransmitter to freely exit loose synaptic clefts (Herman et al., 2011) and reach areas of the neuronal membrane between dendritic spines (Chalifoux and Carter, 2011). To a first approximation, an astrocytic process can handle glutamate from one active spine (**Figure 1A**), but it fails to completely remove glutamate from the extrasynaptic space when many neighboring spines are active at the same moment of time (**Figure 1B**). The residual glutamate then becomes available to activate extrasynaptic NMDA receptors (Tovar and Westbrook,

1999). Upon just two consecutive activations of synaptic inputs the conditions are met to trigger a local dendritic spike (Polsky et al., 2004), fully mediated by NMDA receptor channels (Schiller et al., 2000; Major et al., 2008).

Initially, the NMDA spike was thought to be a pure voltage spike (Schiller et al., 2000; Rhodes, 2006), just like the axonal action potential (AP; Hodgkin and Huxley, 1952). This was based on the fact that both Na^+ channels and NMDA receptor channels exhibit a region of negative slope conductance, which is the biophysical substrate of regenerative property (Mayer et al., 1984; Nowak et al., 1984). We now think that NMDA spikes are not solely based on the summation of voltage (Gasparini et al., 2004; Rhodes, 2006), but rather on the summation of glutamate contributed by many individual boutons that converge in a small space (**Figure 1B**). In support of this view, it has recently been shown that glutamatergic synapses are functionally clustered on developing dendrites. Synapses that are located near each other on the same dendritic branch exhibit a higher degree of temporal correlation than synaptic pairs on different dendrites (Kleindienst et al., 2011). Spatio-temporal clustering of synaptic inputs (Larkum and Nevian, 2008) and activation of extrasynaptic receptors due to this clustering (Suzuki et al., 2008; Chalifoux and Carter, 2011) are broadening the realm in which we view information processing in the central nervous system (Poirazi et al., 2003; Antic et al., 2007; Magee, 2011; De-Miguel and Fuxe, 2012).

In the present paper, we will compare NMDA spikes with glutamate-evoked plateau potentials (Antic et al., 2010), and argue that both events are mediated by the extrasynaptic NMDA receptors (Schiller et al., 2000; Polsky et al., 2009; Chalifoux and Carter, 2011). In spite of many similarities, these two events show some important differences. Compared to NMDA spikes, the glutamate-mediated dendritic plateau potentials are larger in amplitude and duration. Unlike the NMDA spike, the dendritic plateau potential depolarizes the cell body beyond the AP threshold and lasts for more than 100 ms (Oakley et al., 2001; Wei et al., 2001; Cai et al., 2004; Milojkovic et al., 2004, 2005a; Major et al., 2008). During an intense outburst of cortical activity, glutamate released from multiple axon terminals completely overcomes the ability of astrocytic processes to clear extrasynaptic glutamate (Parpura et al., 1994). Not only does the uptake of glutamate in astrocytic processes begin to significantly slow down, but also, in response to repetitive afferent activity, the astrocytes begin to actively release glutamate back into the extracellular matrix (Parpura et al., 1994; Jourdain et al., 2007; Min and Nevian, 2012). For a brief period of time, the dendritic shaft, and accompanying dendritic spines are submerged in a pool of glutamate (**Figure 1C**). This temporary arrangement triggers a qualitatively different signal compared to a classical NMDA spike. The glutamate-evoked plateau potential is unique in two physiological aspects: (1) somatic membrane potential and (2) dendritic calcium dynamics. Dendritic plateau potentials initially start as NMDA spikes (Milojkovic et al., 2004, 2005a; Major et al., 2008). Upon conversion from NMDA spike to dendritic plateau potential, the somatic voltage waveform is no longer like a large, pointy EPSP (Polsky et al., 2004); it becomes a more sustained depolarization event, reminiscent of a cortical UP state (Milojkovic et al., 2004, 2005a; Antic et al., 2007). After this transition, the dendritic calcium signal switches from a highly localized calcium transient characteristic of NMDA spikes (Schiller et al., 2000; Holthoff et al., 2004; Chalifoux and Carter, 2011; Katona et al., 2011) to a robust calcium flux that engulfs the entire dendritic branch (Milojkovic et al., 2007; Major et al., 2008; **Figure 1C**, black contour). During intense cortical activity, it is highly probable that two plateau potentials may coincide in the dendritic tree of a pyramidal neuron. Here, we studied how two dendritic plateau potentials occurring simultaneously in two basal dendrites summate in the cell body.

MATERIALS AND METHODS

BRAIN SLICE AND ELECTROPHYSIOLOGY

Sprague Dawley rats (P21–42) were anesthetized with isoflurane inhalation, decapitated, and the brains were extracted with the head immersed in ice-cold, artificial cerebrospinal fluid (ACSF), according to an animal protocol approved by the Center for Laboratory Animal Care, University of Connecticut. ACSF contained (in mM) 125 NaCl, 26 $NaHCO_3$, 10 glucose, 2.3 KCl, 1.26 KH_2PO_4, 2 $CaCl_2$, and 1 $MgSO_4$, pH 7.4. Coronal slices (300 μm) were cut from frontal lobes. All experimental measurements were performed at 32–34°C. Whole-cell recordings were made from visually identified layer 5 pyramidal neurons within the ventral medial PFC, including prelimbic and infralimbic cortex. Intracellular solution contained (in mM) 135 *K*-gluconate, 2 $MgCl_2$, 3 Na_2-ATP, 10 Na_2-phosphocreatine, 0.3 Na_2-GTP, and 10 HEPES (pH 7.3). Electrical signals were amplified with Multiclamp 700B and digitized with two input boards: (1) Digidata Series 1322A (Molecular Devices, Union City, CA, USA) and (2) Neuroplex (RedShirtImaging, Decatur, GA, USA). Only cells with a membrane potential more negative than −50 mV (not corrected for junction potential), and AP amplitudes exceeding 70 mV (measured from the baseline) were included in this study. APs were evoked with depolarizing current steps injected into the cell body (intensity 150–300 pA, duration 250 ms). Sodium channel blocker Tetrodotoxin (TTX) and NMDA receptor blocker DL-2-Amino-5-phosphonopentanoic acid (APV) were purchased from Sigma (St. Louis, MO, USA) and used at final concentrations of 1 and 50 μM, respectively.

DYE INJECTION

Voltage-sensitive dye (JPW-3028, synthesized by Dr. Leslie Loew, University of Connecticut Health Center), and calcium-sensitive dyes (Ca-Green-1, Oregon Green BAPTA-1, and bis-fura-2; purchased from Invitrogen, Carlsbad, CA, USA) were dissolved in intracellular solution. The protocol for voltage-sensitive dye injection has been previously described (Antic, 2003). Briefly, neurons were filled through whole-cell patching pipettes with JPW-3028 for 45 min. Dye-free solution was at the tip of the pipette, while the back of the pipette lumen was loaded with dye-rich solution (400–800 μM). After 45 min of loading with voltage-sensitive dye, the filling pipette was pulled out (outside-out patch) and brain slices were left to incubate for 1–3 h at room temperature, allowing the dye to diffuse into dendritic tree. Right before optical recordings the cells were re-patched with a dye-free pipette. In calcium imaging experiments, Alexa Fluor 594 (50 μM) was included in the intracellular solution to aid the visually guided positioning of glutamate electrodes onto dendrites.

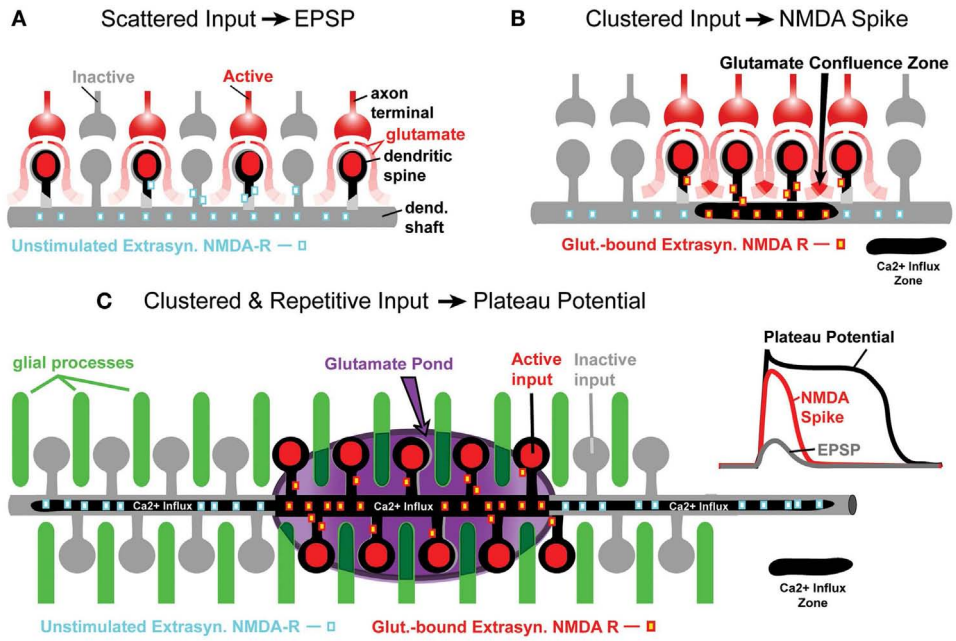

FIGURE 1 | Glutamate processing in spiny neurons. (A) Sparse glutamatergic inputs fail to activate extrasynaptic NMDA receptors located on dendritic shafts and spine necks. Ca^{2+} influx zone (black contour) restricted to spine heads only. **(B)** Clustered synaptic activity is an effective stimulus for extrasynaptic NMDA receptors, because glutamate spilled from several neighboring synapses summates between active dendritic spines (glutamate confluence zone). Ca^{2+} influx zone now contains the input receiving spines and a short segment of the dendritic shaft (black contour). **(C)** The gray contour represents a segment of a spiny dendrite. Glial processes (green cylinders) are interposed between dendritic spines. Darker green indicates less glutamate uptake in glial process, or release of glutamate from the glial process. For a period of time, an entire segment of the spiny dendrite is surrounded by extracellular matrix rich in glutamate ("glutamate pond") – marked by purple ellipsoid. The Ca^{2+} influx zone now includes spines and dendritic shaft below spines. The Ca^{2+} influx occurring proximally and distally to the clustered synaptic input site is due to bi-directional propagation of dendritic plateau potential, which initiated inside the glutamate pond. Inset traces: schematic representation of dendritic voltage waveforms associated with EPSPs, NMDA spikes, and plateau potentials.

The calcium-sensitive dyes (100–200 μM) were injected for 30–45 min before optical recordings.

DENDRITIC VOLTAGE AND CALCIUM IMAGING

Multi-site dendritic imaging was performed on either Olympus BX51WI or Zeiss, Axioskop FS microscope, equipped with UV-compatible 40× objective, two camera ports, and a low-ripple Xenon arc lamp (OptiQuip, Highland Mills, NY, USA) for epi-illumination. Functional dendritic imaging was performed with a NeuroCCD camera (80 × 80 pixels, RedShirtImaging, LLC, Decatur, GA, USA). Voltage-sensitive dye signals were sampled at 1,000 and 500 Hz frame rates. At these sampling rates the AP voltage waveforms riding on top of dendritic plateau potentials were severely under sampled. However, in this project we were focused on the slow component of dendritic depolarizations, which was accurately represented at these sampling rates (**Figure 3B**, ROI). Calcium-dye signals were sampled at 500 Hz full frame rate. Neutral density filters were used to reduce the intensity of epi-illumination light during positioning and focusing. Duration of illumination epochs were kept to minimum: Ca^{2+} imaging 2,500–5,000 ms; voltage imaging 500–2,500 ms. In spite of all precautions, after ∼16 optical recording sweeps, on average, neurons began to show an increase in AP half-width due to phototoxicity (Antic et al., 1999). At that point experiments were stopped. Optical filters were purchased from Chroma Technology (Rockingham, VT, USA) and Omega Optical (Brattleboro, VT, USA). Filters for Alexa Fluor 594 were a Chroma exciter HQ580/20× (570–590 nm bandpass), dichroic Q595LP, and emitter HQ630/60 m (600–660 nm bandpass). The filter cube for Ca-Green-1 and Oregon Green BAPTA-1 contained an Omega exciter 500AF25, dichroic 525DRLP, and emitter 530ALP. The filter set for voltage imaging (JPW-3028) consisted of a Chroma exciter D510/60 (480–540 nm bandpass), dichroic 570dcxru, and emitter E600lp (600 nm longpass). The filter cube for bis-fura-2 contained a Chroma exciter D380/30× (365–395 nm bandpass), dichroic 400dclp, and emitter E470lp (470 nm longpass).

STIMULATIONS

Stimulation electrodes were pulled from borosilicate glass with filament (1.5 mm outer diameter). Synaptic stimulation pipettes (7 MΩ) were filled with regular ACSF and glutamate stimulation pipettes (40–50 MΩ) were filled with 200 mM Na-glutamate (pH = 9). A programmable stimulator, Master-8, and a stimulus isolation unit, IsoFlex (A.M.P.I., Jerusalem, Israel), were used to generate current pulses for both synaptic stimulation and glutamate iontophoresis. Following the spread of fluorescent dyes into the dendrites, the stimulation pipettes were positioned in mid-regions of basal branches; between 65 and 130 μm from the

cell body. Navigation of the flexible glass pipettes through the slice tissue was achieved with the aid of a "fourth axis" (concomitant engagement of both *X* and *Z* axis), available on Sutter Instruments M-285 motorized micromanipulator. The intensities of current pulses for synaptic stimulation (two to five pulses, 50 Hz, 100 μs, 50–90 μA), or of single glutamate microiontophoresis puffs (5 ms, 0.9–2.5 μA), were adjusted to produce a long-lasting somatic depolarization (half-width 200–500 ms) crowned by two to six APs (UP-state-like depolarization). The reported stimulation current intensities are nominal values obtained from the IsoFlex settings.

DATA ANALYSIS

Analysis of optical data, including spatial averaging, high pass, and low pass filtering, was conducted with Neuroplex 8.0.0 (RedShirtImaging). To process off-line calcium imaging data, we applied a Butterworth high pass filter at 0.1 Hz cut-off and a Gaussian low pass filter at 30 Hz cut-off; for voltage imaging data, the high and low pass filters were set at Butterworth 0.1 Hz and Gaussian 150 Hz, unless otherwise specified. Electrical recordings were analyzed in Clampfit 9 (Molecular Devices, Sunnyvale, CA, USA). Plateau amplitude, also termed "amplitude of the slow component of the somatic depolarization," was measured from base line (resting membrane potential) to the shoulder following AP burst (**Figure 3D**, plateau amplitude). If the depolarization "shoulder" was masked by APs, plateau amplitude was measured from base line to the trough between the last two APs in the burst. Plateau amplitude in TTX-treated neurons was measured in the last 1/4 of the plateau phase, to avoid the broad peaks that were often prominent in the first half of the plateau phase (**Figure 2B**, Inset, red trace). Plateau duration was measured at half amplitude of the slow component of somatic depolarization (**Figure 3D**, plateau amplitude). The success rate of plateau initiation was systematically studied in five pyramidal neurons by delivering synaptic shocks on multiple basal dendrites. Synaptically evoked plateau depolarizations with amplitude less than 8 mV, or duration less than 100 ms, were considered failures. In experiments with TTX, the neurons were stimulated with three glutamate pulses (1 Hz). In the paired *t*-test analysis of the TTX data the first glutamate pulse in control condition (before TTX) was compared with the first glutamate pulse in the test condition (after TTX). The same was done for the second and third glutamate pulses, respectively. Experimental data on the summation of subthreshold plateau potentials (**Figure 10**) was divided in three groups. In the first group termed "*Two Small Resulting in no AP*" (**Figure 10A**), each summand in the summation experiment was less than 10.2 mV before summation (the full range of peak amplitudes in this group was from 4.2 to 10.2 mV). The critical criteria for sorting data into this group were that both summands in each pair of summands were in the lower part of the amplitude range (less than 10.2 mV), and that somatic APs were not generated upon summation. This strategy resulted in the formation of a group in which the average arithmetic sum of summand pairs was only 14.8 ± 0.74 mV ($n = 13$ experiments). The entire group, consisting of all plateau amplitudes before summation, is plotted in **Figure 10D**, *Small no AP*. In the second group termed "*Two Large Resulting in no AP*," all individual summands had a peak amplitude greater than 8.4 mV before summation, and somatic APs were not generated (**Figure 10B**). This strategy resulted in the formation of the second data group in which the average arithmetic sum of summand pairs was 21.7 ± 0.67 mV ($n = 16$ experiments). The full range of peak amplitudes in the second group was from 8.4 to 18.2 mV (**Figure 10D**, *Large no AP*). In the third group termed "*Two Large Resulting in 1 or 2 AP*," all individual summands had a peak amplitude greater than 7 mV (range 7.1–18.8 mV). The average arithmetic sum of summand pairs in the third group was 22.6 ± 0.96 mV ($n = 25$ experiments). The critical criterion for sorting data into the third group was that one or two APs accompanied the physiological sum (**Figure 10C**). The entire group 3, including all plateau amplitudes before summation, is plotted in **Figure 10D**, *Large Resulting in APs*. Statistical tests were performed using SigmaPlot 8.02 (Systat Software, San Jose, CA, USA). All statistics were done on raw data points before normalization unless otherwise specified. Paired Student's *t*-tests were used for comparing data obtained from the same neuron (in two different conditions). Unpaired Student's *t*-test was used for data obtained from different neurons. Significance was set at $p < 0.05$ (one asterisk), and high significance at $p < 0.01$ (two asterisks). Values are presented as mean ± SEM.

RESULTS

COMPARISONS BETWEEN NMDA SPIKES AND PLATEAU POTENTIALS

We studied glutamate-mediated dendritic spikes in layer 5 pyramidal neurons using a combination of whole-cell recordings, synaptic stimulation, glutamate microiontophoresis, calcium imaging, and voltage-sensitive dye imaging. Dendritic NMDA spikes were triggered by two synaptic shocks (50 Hz) delivered in the vicinity of basal dendrites (**Figure 2A**, Drawing). Synaptically evoked dendritic NMDA spikes had an average amplitude of 9.3 ± 0.4 mV ($n = 12$ neurons, $N = 27$ trials), when measured with patch electrodes in the soma (**Figure 2A**, patch). Increasing the number of synaptic shocks from two to five caused a dramatic qualitative change in the voltage waveform. A train of five synaptic shocks (50 Hz) triggered plateau potentials, characterized with a rapid onset, somatic amplitude of (15.7 ± 0.9 mV), and plateau phase which lasted 260 ± 27 ms ($n = 35$ trials in 15 neurons), followed by a rapid collapse back to the resting membrane potential (**Figure 2B**). Success rates of NMDA spike and plateau potential initiations were systematically studied in five pyramidal neurons by delivering synaptic shocks on multiple basal dendrites. While the NMDA spike initiation was successful in ∼100% of dendrites tested (19 out of 20 dendrites), the success rate of synaptically evoked plateau potentials was notably lower, ∼37% (7 out of 19 dendrites). Nevertheless, the successful recordings of plateau potentials (**Figure 2B**) show that synaptic terminals activated by a single electrode can release a sufficient amount of glutamate to depolarize pyramidal neurons for hundreds of milliseconds and generate bursts of AP firing. An equivalent depolarization plateau, characterized by 15–20 mV amplitude (slow component) and ∼300 ms duration was triggered by a single 5-ms iontophoretic pulse of glutamate delivered in the middle segment of a basal dendrite (65–130 μm from the soma) in all neurons tested in this way ($n = 20$, success rate = ∼100%; **Figure 2B**, Inset, blue trace).

Besides differences in voltage waveforms (**Figures 2A,B**, black traces), dendritic NMDA spikes, and dendritic plateau potentials may also differ in respect to the dendritic calcium transients

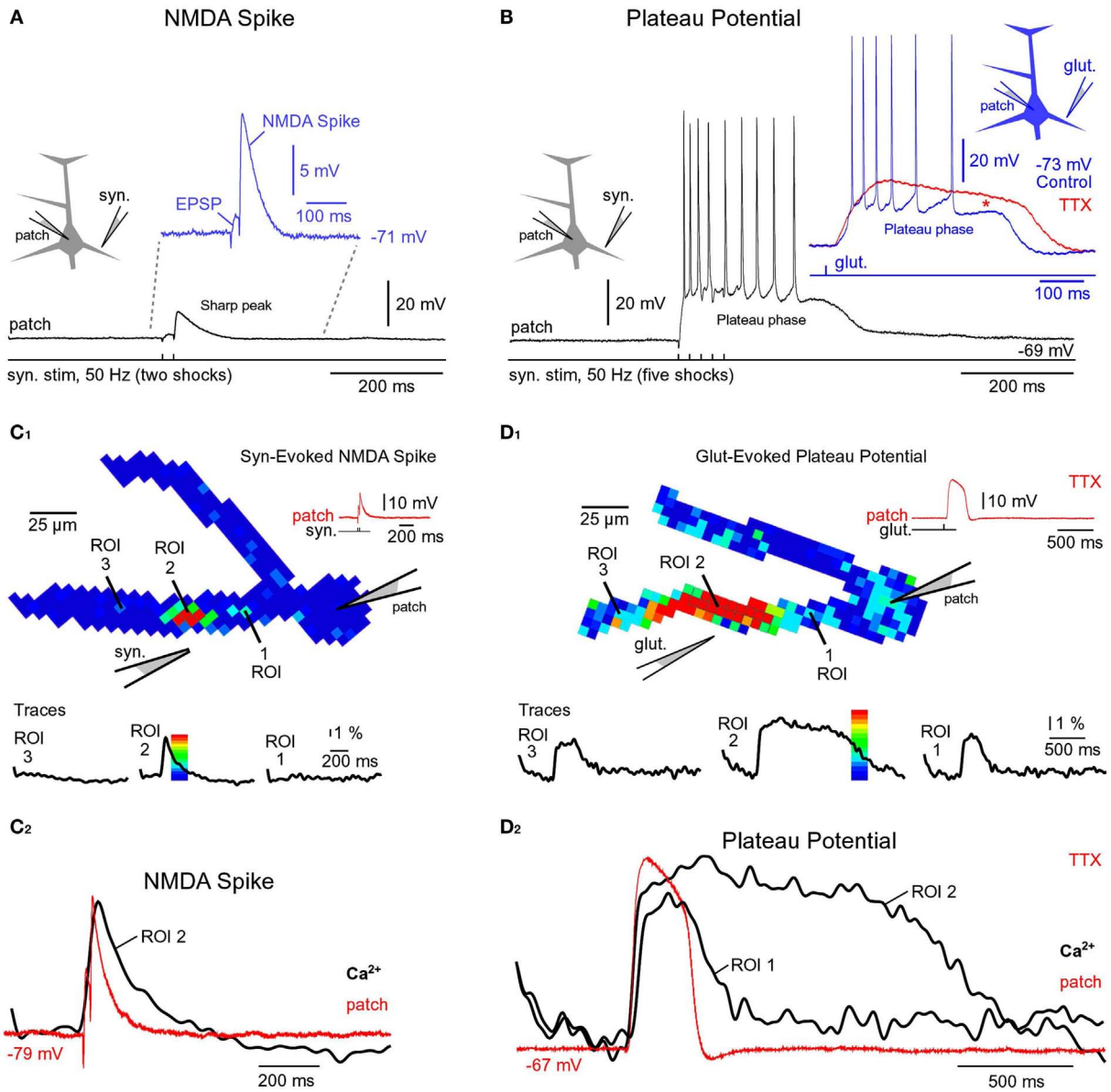

FIGURE 2 | Comparisons of NMDA spike and plateau potential. (A) Schematic drawing of the experimental outline. "Patch" marks somatic whole-cell recordings. Two synaptic shocks produce an EPSP followed by the NMDA spike. Inset: blowup of the same event. In this and all of the following figures the resting membrane potential is displayed next to the trace. **(B)** Five synaptic shocks (50 Hz) produce a dendritic plateau potential ~300 ms in duration and ~20 mV in amplitude. Same voltage and time scales in **(A,B)**, black traces. Inset: glutamate iontophoresis (duration 5 ms) in mid segment of a basal dendrite produces a glutamate-evoked plateau potential (blue trace). Block of sodium channels by bath application of TTX revealed the underlying slow component (red trace). Red asterisk marks a TTX-induced increase in plateau amplitude. **(C_1)** Multi-site optical imaging reveals spatial distribution of calcium transients in two basal dendrites at the peak of the synaptically evoked NMDA spike. Ca^{2+} signal amplitude is color-coded according to the scale shown superimposed on the trace. Traces: three ROIs (5–8 pixels spatially averaged) were selected for display. Note that Ca^{2+} transient is absent from dendritic segments proximal (ROI 1) and distal (ROI 3) to the synaptic input site (ROI 2). **(C_2)** Somatic whole-cell recording (red) and dendritic calcium signal (black) are copied from **(C_1)** and superimposed. **(D_1)** Same as in **(C_1)**, except glutamate iontophoresis (5 ms) was used to trigger dendritic plateau potential (duration ~300 ms). Robust Ca^{2+} transients are present proximally and distally to the glutamate input site (ROI 2). Note that Ca^{2+} transients in ROI 1 and ROI 3 have different temporal dynamics than the transient obtained at the glutamate input site (ROI 2). **(D_2)** Same as in **(C_2)** except signals copied from **(D_1)**.

that accompany them. To test this hypothesis, in the next series of experiments pyramidal neurons were injected with calcium-sensitive dyes and calcium signals were sampled simultaneously from the entire length of a basal branch. Multi-site recordings provide a more complete account of the spatial aspect of dendritic physiology than laser scanning methods, which explore one dendritic spine at a time (Yasuda et al., 2003), or one spine and one spot on the dendritic shaft in the immediate vicinity of that

spine (Chalifoux and Carter, 2011). Wide-field calcium imaging revealed that during a synaptically evoked NMDA spike, dendritic segments proximal to the synaptic input site (**Figure 2C$_1$**, ROI 1), or distal to the input site (**Figure 2C$_1$**, ROI 3), did not experience any detectable changes in the internal calcium ion concentration ($n = 11$ out of 11 basal dendrites tested). The dendritic calcium influx was restricted to a very short dendritic segment, directly opposed to the synaptic stimulation electrode (**Figure 2C$_1$**, ROI 2). In these cells, the length of the dendritic segment experiencing an NMDA spike-associated calcium influx was on average $22.7 \pm 2\,\mu m$ ($n = 11$ basal dendrites in 11 neurons), consistent with glutamate-evoked NMDA spikes (Schiller et al., 2000; their Figure 1D). Durations of dendritic calcium transients and corresponding somatic depolarizations were very similar (**Figure 2C$_2$**). The ratio between dendritic calcium signal half-width and somatic voltage signal half-width was 1.38 ± 0.23 ($n = 127$ sweeps obtained in 11 cells), consistent with two-photon imaging data (Chalifoux and Carter, 2011).

The same wide-field optical imaging method used for NMDA spikes (**Figure 2C**) was next used to characterize dendritic calcium influx during glutamate-evoked plateau potentials in basal dendrites. Brain slices were bathed in 1 μM TTX to remove the calcium influx due to backpropagating APs. Plateau potentials were triggered by iontophoretically ejecting glutamate (duration = 5 ms) in the middle segment of a basal dendrite. The temporal and spatial profiles of dendritic calcium transients during plateau potentials (**Figure 2D**) were very different from those observed during NMDA spikes (**Figure 2C**). The half-widths of dendritic calcium signals at the glutamate input site (**Figure 2D$_2$**, ROI 2, black trace) were on average 5.19 ± 0.4-fold ($n = 8$) greater than the half-widths of somatic voltage signals recorded by the patch pipette (red trace). In all neurons tested in this way (eight out of eight), dendritic segments proximal (**Figure 2D$_1$**, ROI 1), and distal (**Figure 2D$_1$**, ROI 3) to the glutamate input site experienced robust calcium transients. The durations of dendritic calcium transients outside the glutamate input site were similar to the duration of the voltage waveform obtained in the cell body (**Figure 2D$_2$**, compare ROI 1 and patch). More specifically, the ratio of the dendritic calcium signal half-width to the somatic voltage signal half-width was 1.63 ± 0.12 ($n = 8$) for dendritic segments 60 μm more distal to the glutamate input site and 1.37 ± 0.10 ($n = 8$) for dendritic segments 60 μm more proximal to the glutamate input site. These results show that dendritic NMDA spikes and dendritic plateau potentials can be distinguished based on three principle differences: (1) voltage waveforms in the cell body; (2) calcium dynamics at the glutamate input site; and (3) spatial distribution of calcium transients along the input receiving branch.

DENDRITIC UP STATES DRIVE SOMATIC DEPOLARIZED STATES

A step-wise increase in the amount of iontophoretically applied glutamate was used to model glutamatergic inputs that may be received by basal dendrites of PFC pyramidal neurons at different levels of afferent presynaptic activity (**Figure 3A**). Glutamate iontophoretic current was increased gradually in fixed increments (0.1 or 0.2 μA), while glutamate-evoked potentials were recorded simultaneously in cell body (patch) and in dendrites using voltage-sensitive dye (**Figure 3A**, ROI). A transition from subthreshold to suprathreshold dendritic potential (dendritic spike) was invariably accompanied by somatic transition from subthreshold EPSP-like depolarization to plateau potential (**Figure 3A**, brown trace). A further increase in glutamate stimulation intensity yielded very small increases in dendritic potential amplitude (**Figure 3A**, voltage imaging), resembling an all-or-none mechanism (spike). Unlike axonal APs, which have precisely uniform durations (half-widths) determined by activation and inactivation kinetics of Na^+ and K^+ currents (Hodgkin and Huxley, 1952), the durations (half-widths) of glutamate-evoked dendritic plateau potentials are not fixed by intrinsic membrane properties. The durations of dendritic plateau potentials are variable and increase as the intensity of the glutamatergic input increases (Milojkovic et al., 2005a; Major et al., 2008). When basal dendrites transitioned from resting to a depolarized state (**Figure 3A**, ROI, UP State), the cell bodies invariably responded to this transition by entering the sustained depolarized state (**Figure 3A**, patch, UP State). Simultaneous dendritic (voltage-sensitive dye) and somatic (whole-cell) recordings revealed that durations of dendritic plateau potentials (half-widths) were in strict correlation with durations of the corresponding somatic depolarizations (**Figure 3B**). The ratio of dendritic/somatic duration was 1.009 ± 0.006 ($n = 184$ sweeps in 33 neurons, correlation coefficient = 0.9876). In this data set we included 4 types of experiments: (1) glutamate-evoked plateau potentials with bursts of APs (**Figure 3A**) $n = 79$ sweeps obtained in 18 pyramidal neurons; (2) glutamate-evoked plateau potentials without APs ($n = 28$ sweeps in 7 cells); (3) synaptically evoked plateau potentials (**Figure 2B**), $n = 15$ sweeps in nine cells; and (4) glutamate-evoked plateau potentials in TTX (**Figure 2B**, Inset, red trace), $n = 62$ sweeps in 11 cells. In each of these four groups, the correlation coefficient between dendritic and somatic voltage waveforms (half-width) was greater than 0.97. These data indicate that sustained depolarizations, observed in the cell body during glutamatergic or repetitive synaptic stimulation of basal dendrites, are nothing more than passive reflections of dendritic plateau potentials. What can be potentially interpreted as a neuronal UP state (**Figure 3A**, patch, UP State) is actually a dendritic UP state (**Figure 3A**, ROI, UP State) observed from the somatic recording site (Milojkovic et al., 2005a).

Voltage-sensitive dyes are toxic and can influence the membrane currents of cortical pyramidal neurons (Antic et al., 1999). In order to determine whether the toxic effect of voltage-sensitive dyes caused or contributed to the physiological responses described in **Figures 3A,B**, neurons were injected with the fluorescent marker rhodamine to guide the positioning of glutamate electrodes onto basal dendrites (**Figure 3C**, image). Glutamate iontophoretic current was increased gradually in fixed increments (0.1 or 0.2 μA), while glutamate-evoked potentials were recorded in the cell body (**Figure 3C**, patch). Similar input-output functions, including the transitions from subthreshold to suprathreshold depolarizations, were obtained in all rhodamine-filled neurons (five out of five). Plateau amplitude was quantified by measuring the depolarization amplitude after the last AP in the burst, while the plateau duration was measured at half amplitude (**Figure 3D**). The plot of somatic plateau amplitude versus intensity of dendritic glutamate stimulus showed that plateau

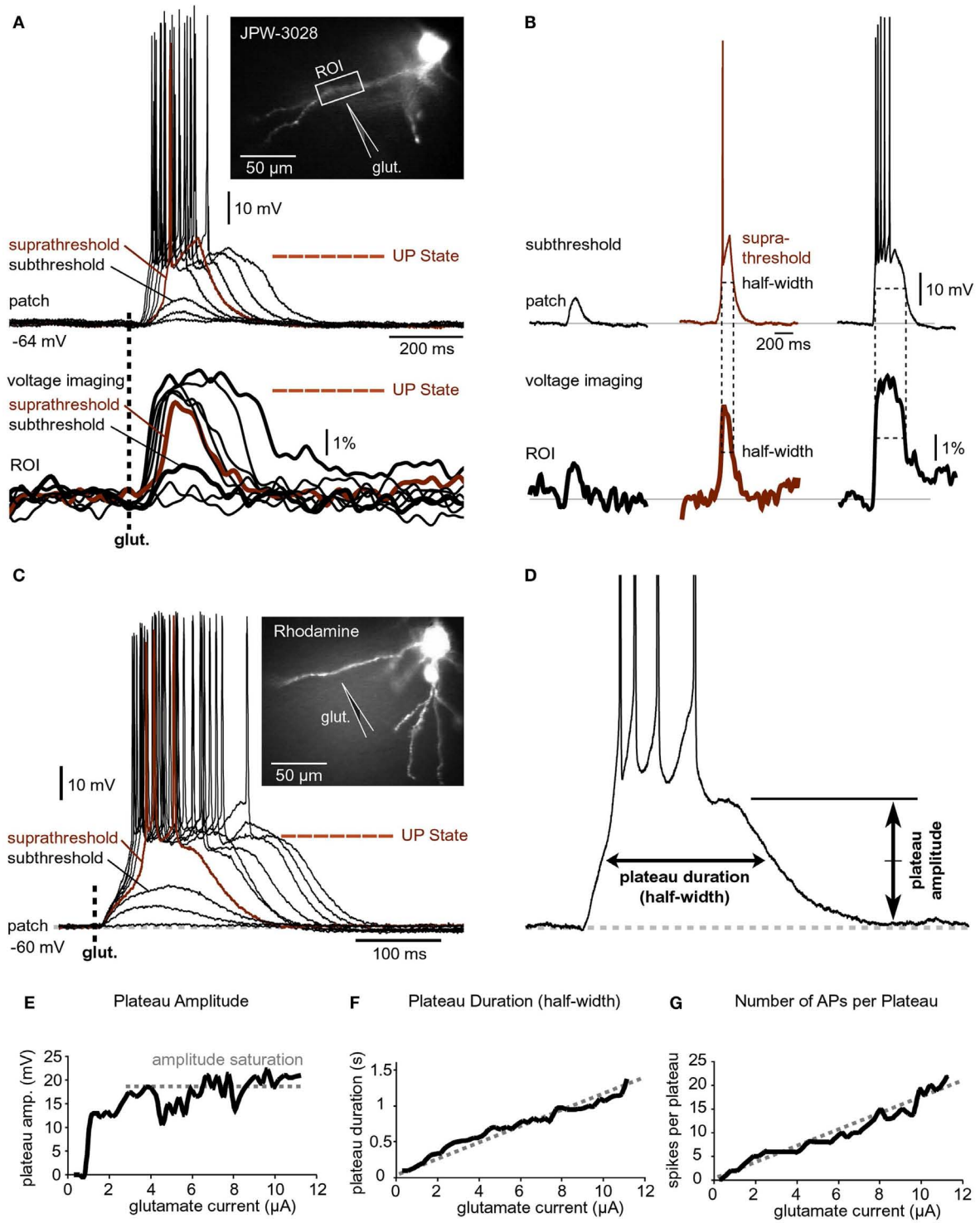

FIGURE 3 | Input-output functions. (A) A pyramidal neuron was injected with the voltage-sensitive dye (JPW-3028) and stimulated by glutamate microiontophoresis (inset). Intensity of glutamate iontophoretic current was gradually increased (fixed increment), while dendritic depolarizations were recorded optically in dendrite (ROI) and electrically in the soma (patch). Brown color marks a sudden jump – spike. **(B)** Three experimental sweeps selected from **(A)** are aligned individually for comparisons between signal half-widths in dendrite (ROI) and in soma (patch). **(C)** Same as in **(A)** except rhodamine was injected to trace dendrites. **(D)** Plateau amplitude and plateau duration were measured from the slow component of the somatic electrical signal. Different cell than in **(C)**. **(E–G)** Plateau amplitude, plateau duration, and number of APs per plateau are plotted against the intensity of glutamate stimulus. Different cell than in **(D)**.

amplitudes saturated at low glutamate intensities (**Figure 3E**). Although the plateau amplitudes were fairly constant throughout a wide range of glutamate intensities (**Figure 3E**, amplitude saturation), the plateau durations grew linearly with intensity of the dendritic glutamate stimulus (**Figure 3F**). A linear relationship was also detected between the intensity of glutamate stimulus and the number of APs that accompanied each plateau depolarization (**Figure 3G**). These data indicate that basal dendrites of PFC pyramidal neurons employ two strategies for coding the intensity of glutamatergic input received in a unit of time: (1) by the amplitude of the slow component of depolarization (**Figure 3E**); and (2) by duration of the slow component of depolarization (**Figure 3F**).

IONIC BASIS OF THE DENDRITIC PLATEAU POTENTIAL

Application of the NMDA receptor blocker APV (50 μM) resulted in the loss of amplitude and shape of the glutamate-evoked plateau potential (**Figure 4A**, compare black and red trace). In the presence of APV the amplitude of the slow somatic depolarization was reduced to $57.5 \pm 6\%$ ($n = 7$) compared to control measurements obtained in the same neuron (**Figure 4A**, black trace). A paired t-test performed on raw data prior to normalization, determined a statistically significant difference in depolarization amplitudes obtained before and after application of NMDA receptor antagonists ($p < 0.01$, $n = 7$). The excitability of the cell body was not affected by application of APV, as determined by somatic current injections performed during each experimental trial (**Figure 4A**, c.i.). These data indicate that glutamate-evoked plateau potentials are mediated by NMDA receptor channels.

Sodium channels in basal dendrites of cortical pyramidal neurons support the generation of fast dendritic spikes (Ariav et al., 2003; Milojkovic et al., 2005b). To determine the contribution of Na^+ channels to the voltage waveforms of glutamate-evoked plateau potentials we stimulated basal dendrites with glutamate pulses (5 ms) before (**Figure 4B**, black trace) and after bath application of the Na^+ channel antagonist TTX (1 μM; **Figure 4B**, red trace). TTX application caused an increase in plateau amplitude (mean amplitude ratio TTX/CTRL $= 1.1 \pm 0.03$, $n = 27$ plateaus from nine cells). A paired t-test performed on raw data before normalization determined a statistically significant difference between plateau amplitudes measured in the same neuron before and after application of TTX ($p < 0.01$, $n = 27$). TTX application caused on average a ∼21% increase in plateau half-width (average half-width ratio TTX/CTRL $= 1.21 \pm 0.04$, $n = 27$ plateaus from nine cells). Paired t-test performed on raw data before normalization determined a statistically significant difference between plateau durations measured in the same neuron before and after application of TTX ($p < 0.001$, $n = 27$). The paradoxical increase in amplitude and duration (**Figure 4B**, compare black and red trace at the time point marked by "glut.") can be attributed to the loss of AP-induced K^+ currents (Bekkers, 2000; Korngreen and Sakmann, 2000; Schaefer et al., 2007).

In the next series of experiments we tested whether the block of Na^+ current affects the dendritic input-output function. Glutamate iontophoretic current was increased gradually in fixed increments (0.1 or 0.2 μA), while glutamate-evoked potentials were recorded in the cell body before (**Figure 4C$_1$**) and after application of TTX (1 μM; **Figure 4C$_2$**). The amplitudes of the slow component were normalized against the first suprathreshold amplitude in the control sequence (**Figure 4C$_1$**, blue trace, corresponding to 100%) and plotted versus the intensity of the glutamate stimulus (**Figure 4D**). For each dendrite tested before and after TTX, the transition from subthreshold to suprathreshold dendritic potential ("dendritic spike") occurred at the same glutamate intensity in both conditions ($n = 4$ dendrites in four neurons), marked by "0 μA" on the graph (**Figure 4D**). The "control" and "TTX" dendritic input-output functions both exhibited a sigmoidal shape characterized by a clear saturation of the amplitude (**Figure 4D**), except the peak amplitudes in TTX (red) were consistently greater than in control (black). In both conditions (control and TTX), there was a certain stimulus intensity at which generation of dendritic spike occurred (**Figures 4C$_1$,C$_2$**, blue traces). A further increase in glutamate stimulation intensity above the intensity required for generation of dendritic spike yielded very small increases in the amplitude of the somatic slow component (**Figures 4C$_1$,C$_2$**). In the absence of Na^+ currents, the durations of somatic plateau potentials increased as the intensity of the glutamatergic input increased (**Figure 4C$_2$**). These data indicate that voltage-gated Na^+ current is not necessary for the transition of dendritic and somatic potentials from Down to UP states.

DENDRITIC FUNCTION IN THE ABUNDANCE OF GLUTAMATE

It has been postulated that local regenerative membrane potentials underlie both phenomena; dendritic NMDA spikes (Schiller et al., 2000; Rhodes, 2006) and dendritic plateau potentials (Milojkovic et al., 2004). The binding of two glutamate molecules converts the ligand-gated NMDA receptor channels into functional voltage-gated channels (Mayer et al., 1984; Nowak et al., 1984). Hyperpolarization, if employed for a sufficient period of time (hundreds of milliseconds) may affect the onset, amplitude, or duration of the NMDA current. Any alterations in dendritic plateau potential would be reflected in somatic voltage waveforms, as determined by voltage imaging (**Figures 3A,B**). To test if negative voltages can interrupt or in some other way affect plateau potentials, a series of hyperpolarizing current pulses of variable intensities were injected in the middle of a glutamate-evoked plateau potential. Pulse durations were set at >100 ms to allow time for proper charging of the neuronal membrane. The somatic amplitude of hyperpolarization was set to exceed −100 mV. In four out of four neurons tested in this way (**Figure 5A**), the plateau potentials were not affected by strong hyperpolarization pulses that reached ∼50 mV more negative than the resting potential (**Figure 5B**). After cessation of large negative pulses the somatic membrane potentials swiftly returned to the plateau level, as if hyperpolarizing pulses never occurred (**Figure 5B**, Inset, black trace). Glutamate-evoked plateau potentials were completely insensitive to hyperpolarizing pulses even when glutamate pipettes were re-positioned to dendritic locations closer to the soma, the source of hyperpolarizing current (**Figure 5C**). We also applied hyperpolarizing pulses in different phases of the plateau potential (not shown) and found that neither amplitude nor duration of glutamate-evoked dendritic potential could be affected by somatic hyperpolarization to −100 mV ($n = 4$), consistent with Major et al. (2008).

To investigate if hyperpolarizing pulses injected in the soma affect the membrane potential in basal dendrites, we filled

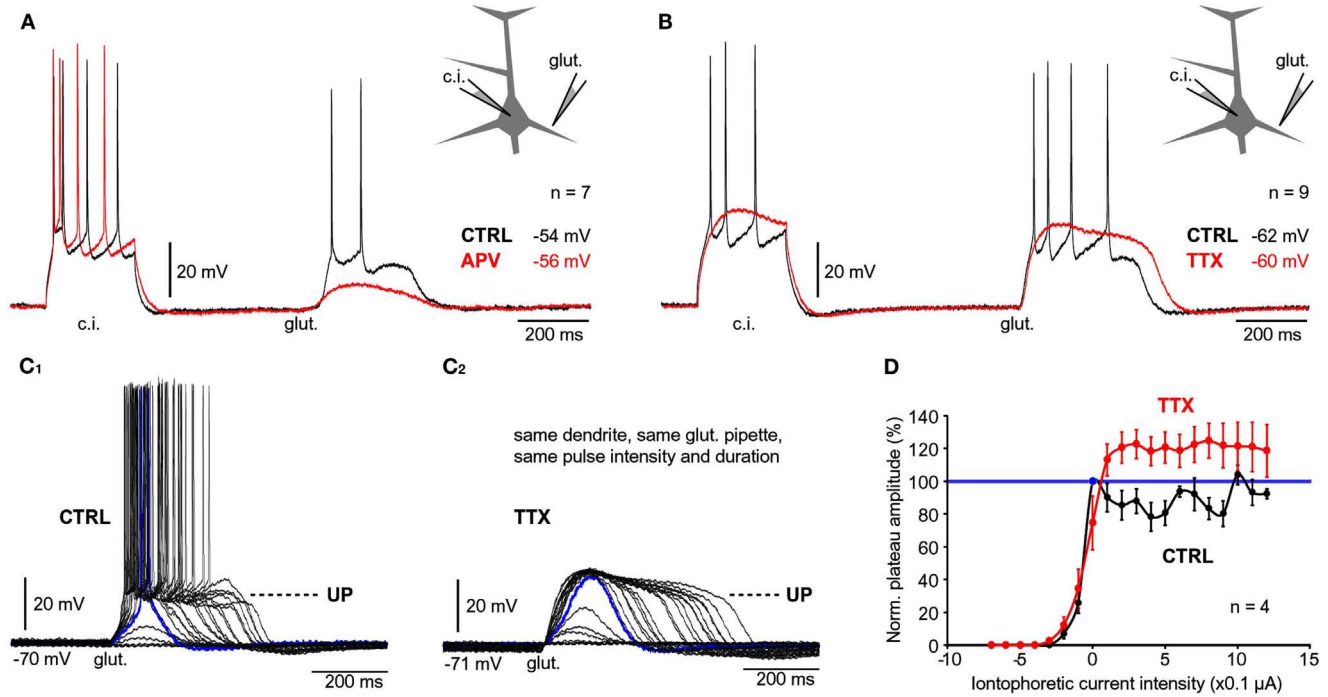

FIGURE 4 | Contribution of NMDA receptors and sodium channels. (A) Whole-cell recordings of APs evoked by current injection (c.i.) followed by a plateau potential evoked by glutamate iontophoresis (glut.). Recordings were made before (CTRL, black trace) and after application of NMDA receptor antagonist, APV (50 μM, red trace). **(B)** Same as in **(A)** except TTX was used to block VGSC. **(C_1)** Glutamate electrode was positioned in the middle segment of one basal branch. Intensity of glutamate iontophoretic current was gradually increased (fixed increments), while somatic depolarizations were recorded via whole-cell electrode. **(C_2)** Same measurements in **(C_1)**, were repeated in the presence of TTX. **(D)** Amplitude of depolarization is plotted against the intensity of glutamate stimulus before (CTRL, black) and after introduction of TTX (red). All values are normalized against the amplitude of the first plateau in the sequence (blue data point), corresponding to the blue trace in **(C_1)**.

pyramidal neurons with voltage-sensitive dyes (**Figure 5D**) and recorded hyperpolarizing dendritic potentials at multiple sites along basal branches (**Figure 5E**). Despite low sensitivity of voltage-sensitive dye recordings (∼4% for 100 mV change), we were able to detect hyperpolarizing voltage pulses (−25 to −35 mV amplitude at soma) in dendritic segments 140–200 μm away from the soma (**Figure 5F**, 202 μm), in four out of four pyramidal neurons tested in this way. These data suggest that somatic injections of hyperpolarizing current affect the membrane potential in basal dendrites. The failure of hyperpolarizing somatic pulses to change the amplitude or the duration of dendritic plateau potentials is consistent with the model presented in **Figure 1C**. Dendritic plateau potentials occur only if dendritic shafts and associated extrasynaptic NMDA receptors are surrounded by a surplus of glutamate ions (**Figure 1C**, glutamate pond). During an intense glutamatergic drive, with both AMPA and NMDA receptors saturated in synaptic and extrasynaptic surfaces, the input receiving dendritic segment is clamped to the glutamate reversal potential (∼0 mV). Upon cessation of the hyperpolarizing pulse the dendritic membrane potential promptly returns to 0 mV, which restores the supply of depolarizing current to the soma (**Figure 5B**, Inset, black trace). These data also suggest that chemical summation of glutamate in a confined space (**Figure 1C**) may not only be responsible for the initiation (Major et al., 2008), but also for the maintenance of the plateau phase during glutamate-mediated plateau potentials. That is, the neuron remains in a sustained depolarized state (UP state) as long as one of its basal dendrites is surrounded by a group of glial processes that have stopped absorbing glutamate (**Figure 1C**, dark green glia).

PLATEAU DEPOLARIZATIONS IN NEURONAL COMPARTMENTS WITHOUT SPINES

The somatic and perisomatic membranes of cortical pyramidal neurons contain functional NMDA receptors (Dodt et al., 1998). Because there are no synaptic contacts or postsynaptic densities on the cell bodies and in the proximal 30 μm of basal dendrites (Larkman, 1991), all somatic and perisomatic NMDA receptors can be considered extrasynaptic. To test if activation of extrasynaptic NMDA receptors is sufficient for the initiation of glutamate-mediated plateau potentials, glutamate-filled micropipettes were positioned ∼10 μm from the lateral edge of the cell body (**Figure $6A_1$**), also depicted in (Moore et al., 2011), their **Figure 1**. In all neurons treated this way (three out of three) glutamate pulses (5 ms duration) triggered plateau potentials lasting several hundred milliseconds (**Figure $6A_2$**). In order to compare the glutamate excitability of cell body and basal dendrites, in the next series of experiments plateau potentials were first evoked by glutamate microiontophoresis on basal dendrites (**Figure $6B_1$**, loc. 1). The same glutamate electrode was then positioned ∼10 μm near the soma (**Figure $6B_1$**, loc. 2). In four neurons we kept the

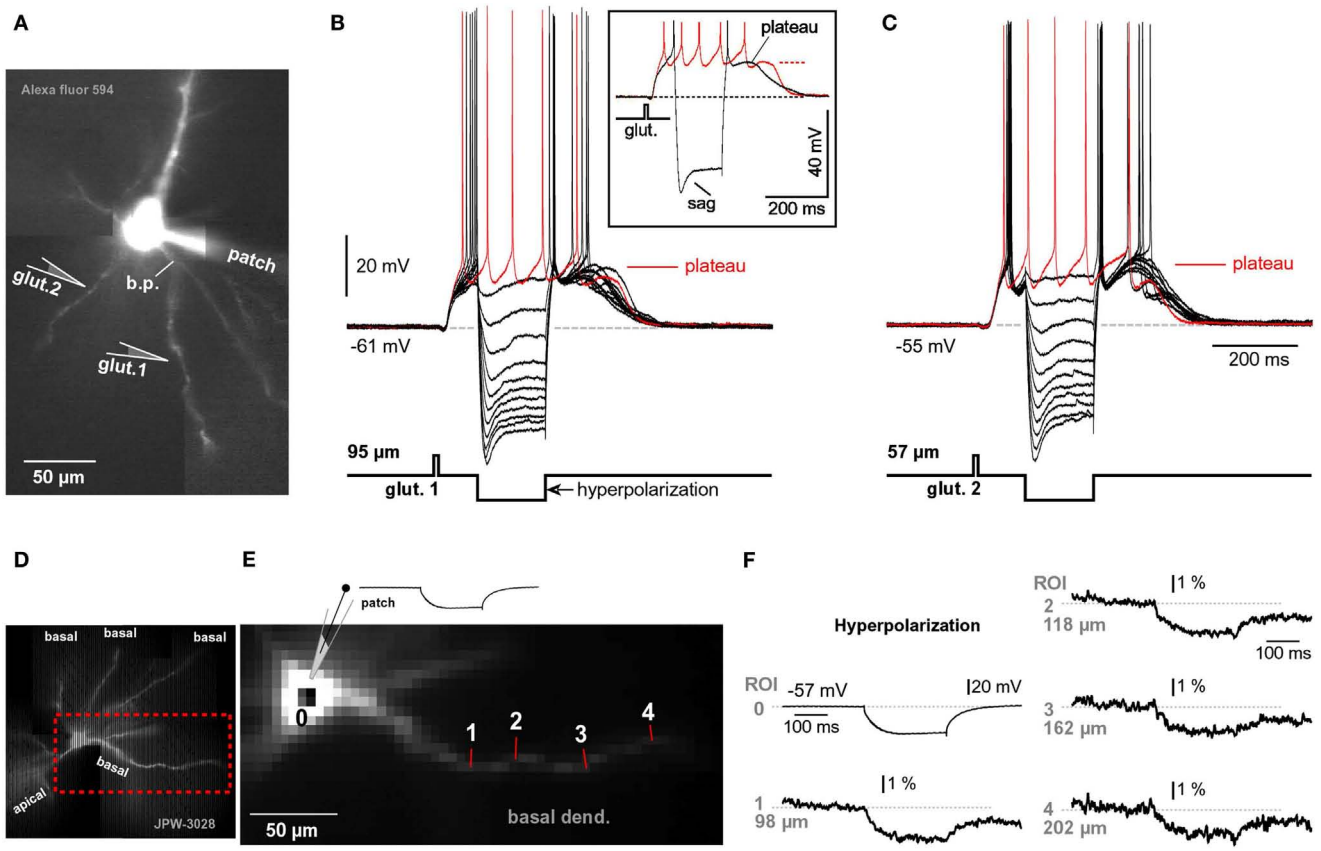

FIGURE 5 | Hyperpolarization cannot interrupt glutamate-evoked plateau potentials. (A) Pyramidal neuron filled with Alexa Fluor 594. b.p., Branch point. **(B)** A 5-ms glutamate pulse, applied 95 µm from the center of the cell body (glut. 1), triggered a glutamate-evoked plateau potential (red sweep). Next, the glutamatergic stimulation (*glut. 1*) was paired with negative current injections into the soma (black sweeps). Inset: maximal negative current sweep (black) is superimposed with glutamate alone sweep (red). AP, truncated. Characteristic sag is caused by "*h*" current. Gray dashed line – resting potential. Red dashed line – UP state (plateau). **(C)** Same experimental paradigm as in **(B)**, except glutamate application micropipette was positioned closer to the cell body, at location marked by "*glut. 2*," 57 µm from the soma. **(D)** Microphotograph of a pyramidal cell filled with voltage-sensitive dye JPW-3028. **(E)** Fast camera capture of the region marked by rectangle in **(D)**. Six to nine individual pixels were used for spatial averaging in each region of interest (ROI 1–4). **(F)** Patch clamp recording (ROI 0) is aligned with simultaneous voltage-sensitive dye recordings from four ROIs during somatic hyperpolarization (−36 mV peak amplitude measured in the soma). Each optical trace is a temporal average of four trials.

duration and intensity of glutamate iontophoretic pulse fixed at both locations, which allowed us to make quantitative comparisons. For the same glutamatergic stimulus, the ratio between somatic, and dendritic plateau was 0.91 ± 0.06 for amplitude and 0.106 ± 0.08 for duration (half-width), $n = 17$ measurements in four cells. In other words, 5-ms glutamate pulses were successful at maintaining the cell in a sustained depolarized state when applied on the cell body, as they were on spiny segments of basal dendrites (**Figures 6B$_2$,B$_3$**). A major concern in these experiments was a potential spill of glutamate from the somatic stimulation site onto the neighboring dendrites. To determine how far glutamate can diffuse from the ejection site, the tips of glutamate iontophoretic electrodes were first positioned 5–10 µm from the shafts of visually identified basal dendrites (**Figure 6C$_1$**), and the glutamate pipette was gradually retracted from the dendrite. Before the beginning of the pipette withdrawal procedure, the intensity of the glutamate iontophoretic current was adjusted so that a single 5-ms-long glutamate pulse triggered a somatic plateau potential (half-width, ∼100 ms). With the iontophoretic current fixed at this value, the glutamate pipette was retracted in micrometer steps (**Figure 6C$_2$**). At each stop, a glutamate pulse was re-applied and somatic response was recorded (**Figure 6C$_3$**). At an average distance of 22.6 ± 2.5 µm ($n = 13$) the plateau potential was less than 50% of the initial value (at 0 µm). Since the initial 30 µm of basal dendrites are virtually spineless (Larkman, 1991; Ballesteros-Yanez et al., 2006), these data indicate that during somatic stimulations (**Figures 6A,B**) the dendritic spines were not involved in the initiation of plateau potentials. That is, the NMDA receptors located on the cell body and on the shafts of proximal dendritic segments (extrasynaptic NMDA receptors) can support glutamate plateau potentials.

PERSISTENT ACTIVITY MADE FROM PLATEAU POTENTIALS

To investigate how temporal summation of glutamate-evoked plateau potentials may contribute to the neuronal AP output, glutamate-filled micropipettes were positioned in middle

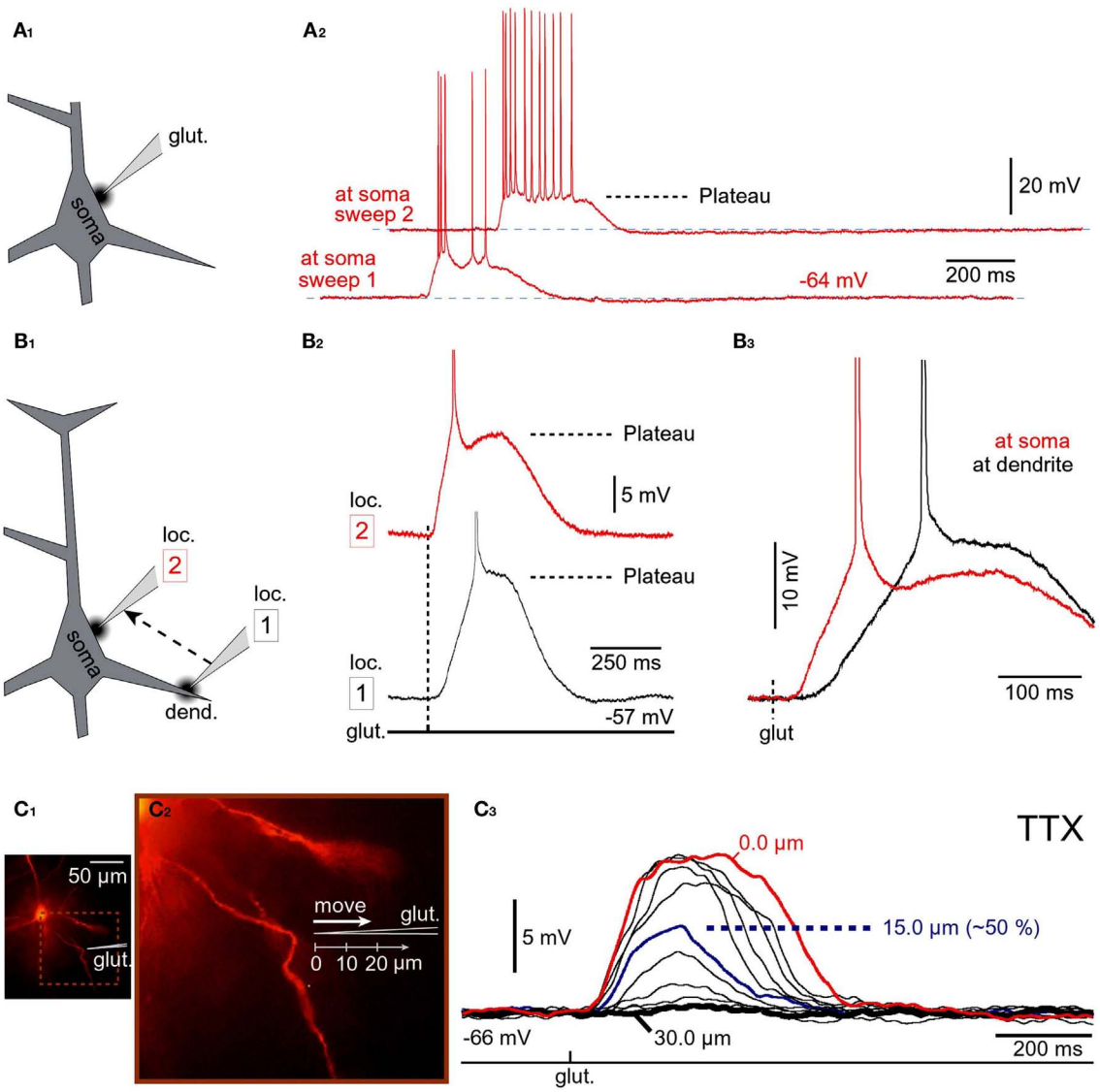

FIGURE 6 | Stimulation of NMDA receptors on the cell body. (A_1) Schematic representation of the experimental outline. The tip of the glutamate pipette is 10 µm from the soma. **(A_2)** Neuronal response to somatic application of glutamate was tested using two intensities of iontophoretic glutamate current; pulse duration was fixed at 5 ms. **(B_1)** Schematic representation of the experimental outline. The same glutamate-filled micropipette was alternated between dendritic (loc. 1) and somatic (loc. 2) stimulation sites. **(B_2)** Glutamate-evoked plateau potentials at dendritic and somatic locations of the same cell; glutamate pulse unchanged. **(B_3)** Same traces as in **(B_2)** except superimposed on fast time scale. **(C_1)** Microphotograph of a rhodamine-filled neuron. **(C_2)** Schematic representation of the experimental outline. The tip of the glutamate application electrode (glut.) was gradually retracted in equal increments (3 µm). **(C_3)** At each stop an identical glutamate pulse was applied in the presence of TTX (1 µM). At 15 µm away from the initial stimulation site, the amplitude of the glutamate-evoked depolarization is ∼50% of its value at the initial stimulation site (0 µm). At 30 µm, glutamate is not detected by the dendrite.

segments of basilar branches and glutamate was iontophoretically released for 5 ms, every second (eight glutamate pulses per train). In some experiments, the train of eight glutamate pulses was preceded by simple current injection into the soma (duration = 250 ms) to monitor neuronal integrity (**Figure 7A$_1$**, c.i.). In these experiments, the starting intensity of glutamate stimulus was adjusted to trigger an event that was suprathreshold for both the dendrite (dendritic plateau potential) and the soma (somatic APs, **Figures 3A,C**, UP state). At lower glutamate stimulation intensities, each glutamate pulse produced an isolated event consisting of a sustained somatic depolarization accompanied by a burst of APs riding on top of the plateau depolarization (**Figure 7A$_1$**). Between glutamate pulses the membrane potential promptly returned to the resting level (**Figures 7A$_1$–A$_3$**). The rapid rise of the glutamate-evoked plateau potential and the rapid collapse at the end of its plateau phase, together with uniform amplitudes and durations of individual depolarizing events, are reminiscent of UP states that occur in cortical pyramidal neurons

during slow wave sleep (Cowan and Wilson, 1994; Branchereau et al., 1996; Lewis and O'Donnell, 2000). Closer inspection of whole-cell recordings (**Figure 7B$_1$**) as well as quantification of these data (**Figure 7B$_2$**), revealed a tendency for the duration (but not the amplitude) to increase with the sequential order of the glutamate pulse. On average, each subsequent plateau was longer than the previous (**Figure 7B$_2$**). Paired *t*-tests performed on the raw measurements before normalization detected significant differences between the first plateau (**Figure 7B$_1$**, red) and each subsequent plateau in the train (**Figure 7B$_1$**, black 2–8). The progressive increase in plateau half-width (**Figure 7B$_2$**), especially prominent at higher glutamate stimulation intensities (**Figures 7A$_2$,A$_3$**), suggests that residual glutamate was slowly increasing with repetitive glutamatergic input. The ability of glia to eliminate the focally released glutamate was diminished immediately following the first plateau (note the statistically significant difference between the *first* and the *second* plateau; **Figure 7B$_2$**). Glutamate slowly accumulates in the extrasynaptic space on each following stimulus 2–8, resulting in a statistically significant difference between the first event and all subsequent events in a train (**Figure 7B$_2$**, asterisks). These data suggested that the glutamate uptake and glutamate diffusion mechanisms failed to completely eliminate the residual glutamate.

RESIDUAL GLUTAMATE

We next asked if stronger glutamatergic stimuli impose a greater burden on glutamate elimination than weaker stimuli. For this purpose, two trains consisting of eight glutamate pulses were delivered on the same dendrite. Following the first train (**Figure 7C$_1$**, red trace), the intensity of iontophoretic current was decreased in order to reduce plateau duration by ∼50% (**Figure 7C$_1$**, black trace). The relative increases in plateau duration for traces with "long" plateaus (**Figure 7C$_1$**, *red trace*) were significantly greater than for the traces with "brief" plateaus (**Figure 7C$_1$**, *black trace*). Statistically significant differences were detected on the fifth, sixth, seventh, and eighth event in the train (**Figure 7C$_2$**, *asterisks*). These data suggested that glutamate uptake and glutamate diffusion mechanisms are less effective in eliminating the residual glutamate for stronger glutamate stimulation intensities.

The previous experiments showed that the duration of glutamate-evoked plateau increases with subsequent applications of glutamate on basal dendrites. Does this phenomenon occur if the plateau was not accompanied by bursts of APs? To answer this question we applied glutamate trains (1 Hz) at distal dendritic segments (range 90–125 μm path distance from the soma, $n = 14$). At these stimulation sites, the dendritic plateau potentials often fail to trigger the somatic APs (Milojkovic et al., 2004; Major et al., 2008). In all neurons tested in this way ($n = 14$) we found a progressive increase in plateau duration (**Figure 7D$_1$**). For example, the duration of plateau #8 (the eighth event in the sequence) was on average $130 \pm 2.2\%$ of the initial plateau (plateau #1, $n = 14$; **Figure 7D$_2$**). This relative increase was very similar to the one obtained for plateaus accompanied by bursts of APs, $129 \pm 4.1\%$; $n = 23$ (**Figures 7B$_1$,B$_2$**). These data indicate that intrinsic membrane currents activated during AP burst firing are not responsible for the observed increase in plateau duration with subsequent glutamate applications.

FUSION OF PLATEAU POTENTIALS

In the previous experiments we varied the intensity of the glutamate stimulus while keeping the frequency of glutamate pulses fixed between trials (**Figure 7A$_1$**). In the next series of experiments, we varied the interval between glutamate pulses in order to mimic increasing levels of cortical afferent activity arriving at the basilar dendritic tree. Decreasing the interval between glutamate pulses caused the duration of plateau potentials to increase with the sequential order of glutamate pulse in the train (**Figure 8A**), suggesting that residual glutamate slowly accumulates in the extracellular matrix surrounding NMDA receptors. Decreasing the interval between glutamate pulses caused plateau depolarizations to fuse into a continuous UP state (**Figure 8B**). In three out of three neurons tested in this way, the gradual fusion of glutamate plateau potentials (slow component) did not immediately result in a continuous train of APs. Instead, we observed apparent interruptions in AP firing in between individual glutamate pulses (**Figure 8B**, arrows), suggesting that pyramidal neurons can distinguish between bursts of electrical activity associated with individual glutamate-evoked dendritic plateau potentials even when their slow components are completely fused. However, this information became lost at higher stimulation frequencies, as further reduction in inter-pulse interval produced an uninterrupted train of APs (**Figure 8C**), reminiscent of persistent neuronal activity in the awake cortex (Timofeev et al., 2001).

SPATIAL SUMMATION OF PLATEAU POTENTIALS

Layer 5 pyramidal neurons in the rat PFC typically contain three to eight primary basal dendrites and many more secondary and tertiary basal branches (Zhou et al., 2008, their **Figure 10**). With thousands of synaptic contacts distributed on the basilar dendritic tree (Larkman, 1991; Benavides-Piccione et al., 2006), it is likely that two or more basal dendrites can experience glutamate-dependent plateau potentials at the same moment of time. To study integration of dendritic plateau potentials, neurons were filled with fluorescent dyes (**Figure 9A**) and two glutamate-filled micropipettes were positioned in middle segments of two basal branches (**Figure 9B**). Glutamate was released for 5 ms from either micropipette (**Figure 9C**, *1* or *2*) and from both micropipettes at the same time ("*1* + *2*"). In order to determine the specificity of glutamate input onto one dendritic branch, experiments were initially performed in combination with simultaneous multi-site calcium imaging at 200 Hz frame rate (Antic, 2003). Every time an individual glutamate pulse resulted in somatic plateau depolarization, as detected in whole-cell recording (patch), there was an associated long-lasting calcium plateau at the glutamate input site; depicted in **Figures 2D$_1$,D$_2$**. The duration of the dendritic calcium plateau was not determined by the duration of the corresponding voltage plateau, as calcium plateaus always persisted after the collapse of somatic plateau potential (**Figure 9D$_1$**, vertical dashed line). Regardless of the stimulating electrode used (1 or 2), in each experimental trial the calcium plateau was restricted to one basal branch (**Figures 9D$_1$,D$_2$**, plat.), indicating that focally applied glutamate did not diffuse from one dendrite to another. Unstimulated basal branches also experienced some calcium influx during plateau potentials; however,

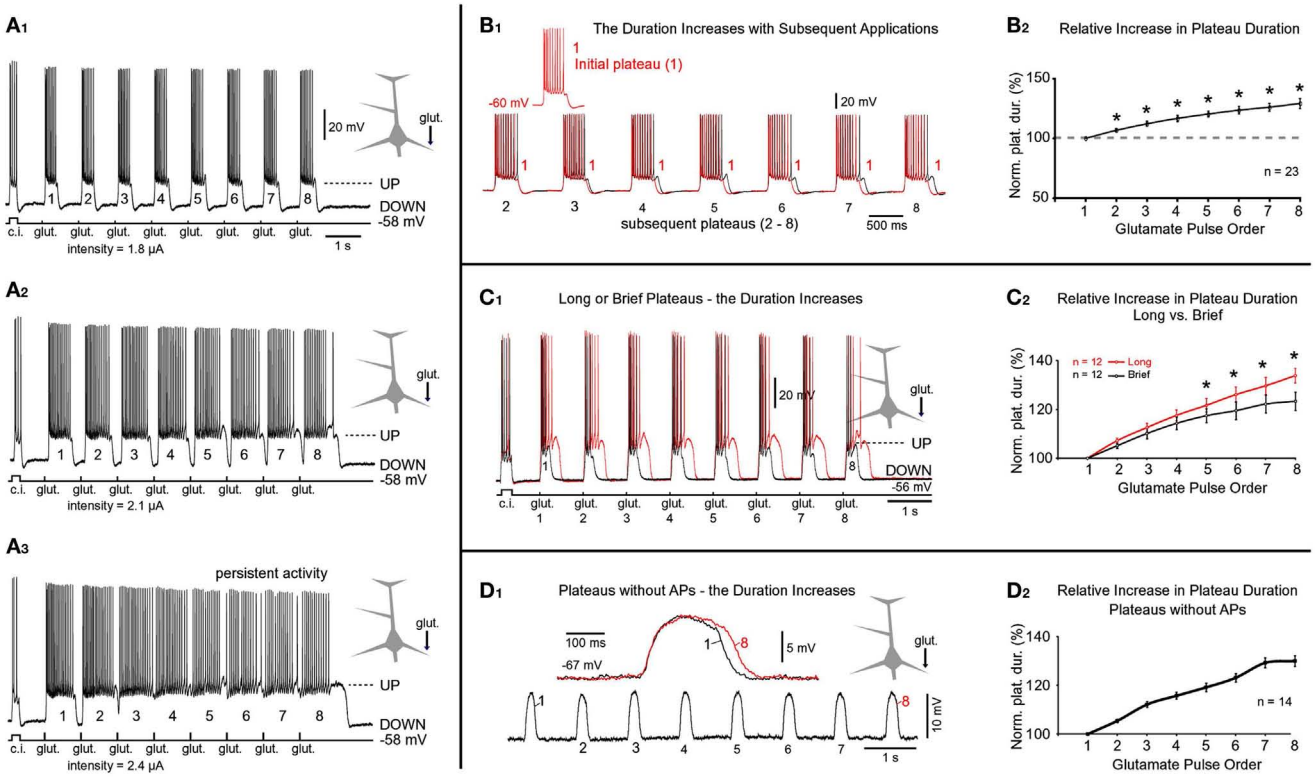

FIGURE 7 | Progressive increases in plateau durations during repetitive glutamatergic stimulations. (A$_1$) Glutamate pulses (duration = 5 ms) were delivered on the basal dendrite and evoked potentials were recorded in the soma. Prior to a train of eight glutamate pulses, the cell body was injected with depolarizing current to monitor neuronal intrinsic membrane excitability (current injection, c.i.). In subsequent sweeps **(A$_2$,A$_3$)**, the intensity of glutamate current was gradually increased, as indicated below the trace. **(B$_1$)** The first plateau (*1*) is superimposed with each subsequent plateau in the train (2–8). **(B$_2$)** Plateau half-widths (durations) were normalized against the first plateau in the train (*1*), averaged across 23 trains obtained in nine neurons, and plotted versus the chronological order of the glutamate pulse. *Paired *t*-test, $p < 0.01$, compared to the initial plateau *1*. [**(C$_1$)** *Red trace*: eight glutamate pulses; duration = 5 ms each] were delivered on one basal dendrite and evoked potentials were recorded in the soma. The stimulus intensity was then reduced to shorten the duration of plateaus by ∼50% (black trace). **(C$_2$)** *Red graph*: plateau durations were normalized against the first plateau in the sequence and averaged across 12 cells using traces with long plateaus (∼500 ms). *Black graph*: traces with brief plateaus (∼250 ms) from the same 12 cells were normalized and averaged. *$p < 0.05$, the corresponding plateaus were compared using paired *t*-test. **(D$_1$)** Same experimental setting as in **(A$_1$)** except plateau depolarizations did not trigger somatic action potentials. Inset: the first and the eighth plateaus are superimposed on a faster time scale. **(D$_2$)** Plateau durations were normalized against the first plateau in the sequence and averaged across 14 cells using traces with 8 spikeless plateaus.

these calcium transients were smaller in amplitude and drastically shorter in duration (**Figures 9D,E**, AP). The peaks of smaller transients coincided with somatic APs in every sweep of every neuron tested in this way ($n = 16$ sweeps in three neurons). These calcium imaging data provide evidence that during paired (*1* + *2*) glutamate stimulations, the glutamate-evoked dendritic plateau potentials (**Figure 2B**) originate in two distinct branches (and no more) and summate in the cell body (**Figure 9D$_3$**).

In the remainder of this paper we will quantify the summation of subthreshold and suprathreshold glutamate-evoked potentials arriving from two basal branches. All of the summands were active dendritic spikes – plateau potentials (suprathreshold in dendrite). The terms *sub-* and *supra-threshold* hereafter refer to the ability of an individual dendritic plateau potential to trigger somatic APs on its own; before the summation. An example of a subthreshold plateau is shown in **Figure 7D$_1$**. An example of a suprathreshold plateau is shown in **Figure 7B$_1$**.

SPATIAL SUMMATION OF SUBTHRESHOLD PLATEAU POTENTIALS

To study the integration of subthreshold plateau potentials, neurons were filled with fluorescent dyes and two glutamate-filled micropipettes were positioned in middle segments of two basal branches (**Figure 9B**). Glutamate was released for 5 ms from either micropipette (*1* or *2*) and from both micropipettes at the same time ("*1* + *2*"), as depicted schematically by three drawings on the top of **Figure 10**. Based on the amplitudes of individual plateau potentials before summation ("Summand *1*" or "Summand *2*"), the experimental data was divided into 3 groups: "*Two Small Resulting in no AP*"; "*Two Large Resulting in no AP*;" and "*Two Large Resulting in 1 or 2 APs*."

When both summands ("*1*" or "*2*") were small (as defined in Materials and Methods), their physiological sum in the cell body was similar in amplitude to their arithmetic sum (**Figure 10A**); the summation was linear. Thirteen such experiments carried out in four neurons were quantified, normalized against their corresponding arithmetic sums, averaged, and displayed in the

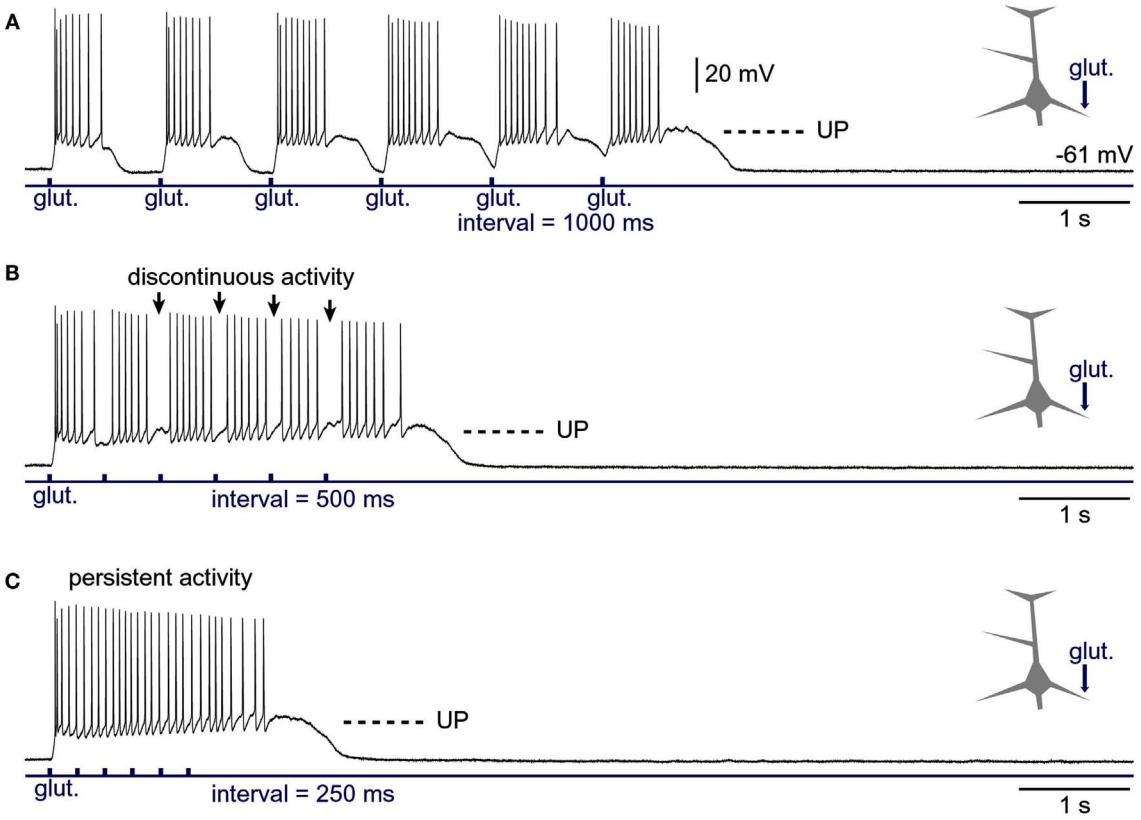

FIGURE 8 | Generation of persistent activity from consecutive plateau potentials. (A) Six glutamate pulses (duration = 5 ms each) were delivered on the basal dendrite and evoked potentials were recorded in the soma. In subsequent sweeps **(B,C)**, the inter-pulse interval was gradually decreased, as indicated below the trace. Arrows in **(B)** mark pauses in AP firing.

bar diagram (**Figure 10E$_1$**). The average summand amplitude in the "Small no AP" group was 7.4 ± 0.35 mV ($n = 26$ summands in 13 pairs). The distribution of the plateau amplitudes before summation is plotted in (**Figure 10D**, *Small no AP*).

When both summands were large (as defined in the Materials and Methods), their physiological sum in the cell body was less than their arithmetic sum (**Figure 10B**). Sixteen experiments from three neurons were quantified and displayed in the bar diagram (**Figure 10E$_2$**). Because the actual sum was considerably less than the arithmetic sum (**Figure 10E$_2$**), the summation process was characterized as "sublinear." The summation process in group "Large no AP" was inherently different from the summation process in group "Small no AP"; confirmed by a comparison of the relative amplitudes after normalization (**Figure 10E**, asterisk, unpaired, $p < 0.01$). The average amplitude of all summands in the "Large no AP" group was 10.8 ± 0.39 mV ($n = 32$ summands). The distribution of the summand amplitudes in this group is plotted in (**Figure 10D**, *Large no AP*).

If both summands were sufficiently large so that their summation resulted in the somatic plateau depolarization accompanied by 1 or 2 APs, again the amplitude of the actual slow component in the cell body was less than the arithmetic sum of two individual dendritic plateaus (sublinear summation; **Figure 10C**). Twenty-five such experiments from seven neurons were quantified and displayed in the bar diagram (**Figure 10E$_3$**). The average summand amplitude in this group was 11.3 ± 0.44 mV ($n = 50$ summands, **Figure 10D**, *Large Resulting in APs*).

In summary, these data show that "small" plateau potentials (both small, see Materials and Methods) summate linearly in the cell body (**Figure 10E$_1$**). Larger plateaus, on the other hand, summate sublinearly – their physiological sum is always less than expected from a simple arithmetic summation (**Figure 10E$_2$**). The presence of somatic AP firing did not change the outcome of summation, as determined by unpaired t-test (**Figure 10E$_3$**, "#," $p > 0.05$).

SPATIAL SUMMATION OF SUPRATHRESHOLD PLATEAU POTENTIALS

The parameters of glutamatergic inputs (dendritic location, iontophoretic current intensity, pulse duration) were adjusted so that each dendritic potential by itself brings the cell body into an UP state crowned with AP firing (e.g., **Figure 7B$_1$**). When two such dendritic UP states collide in the cell body (**Figure 11B**, black trace), the amplitude of somatic plateau depolarization (plateau amplitude as defined in the Materials and Methods) is not greater than the individual components, glut. 1 or glut. 2 (**Figure 11B**, blue and red trace). When two dendritic UP states collide in the cell body, the duration of the resulting somatic plateau depolarization (plateau duration) is not greater than the

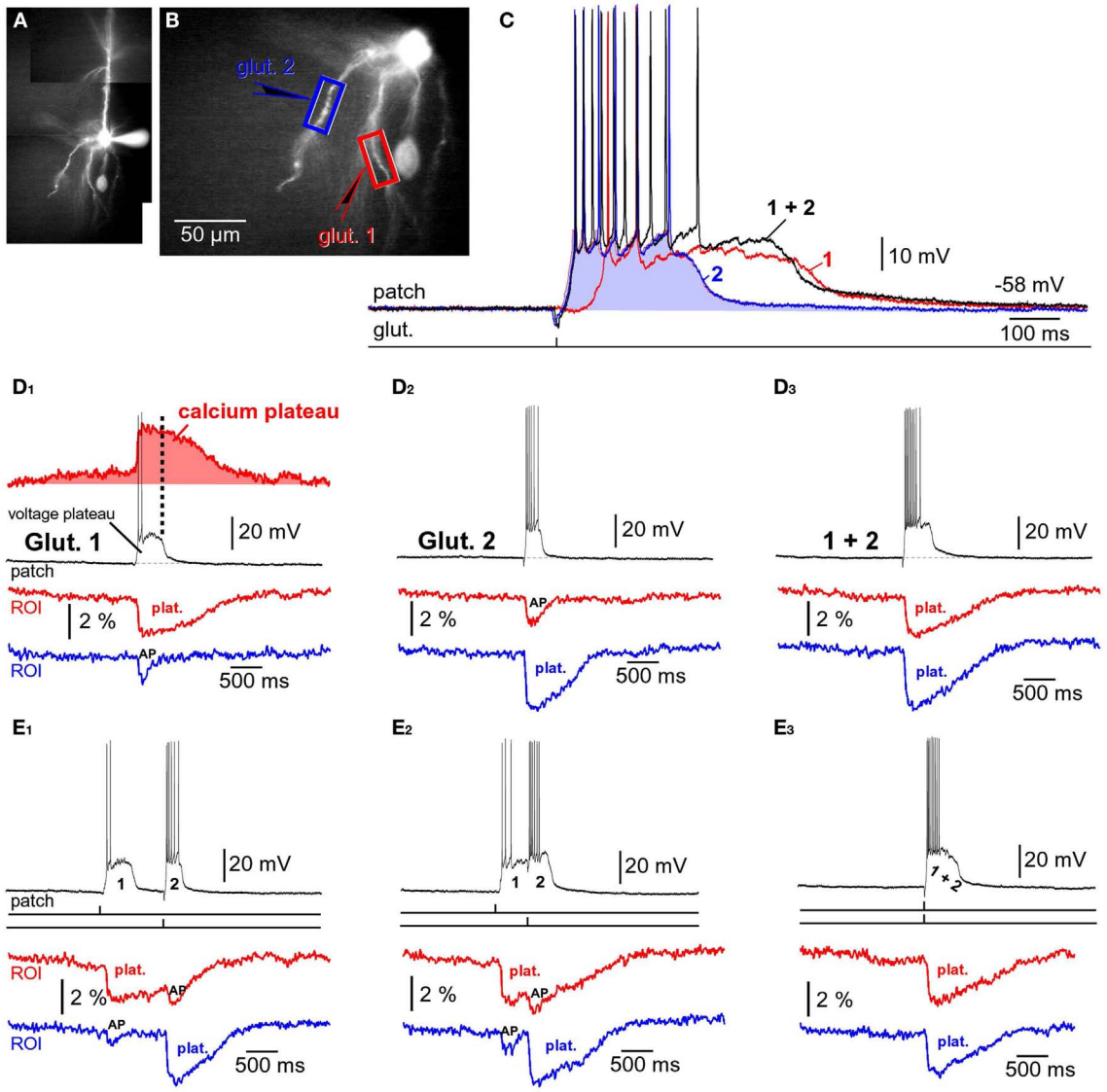

FIGURE 9 | Summation of glutamate-evoked plateau potentials. (A,B) Pyramidal neuron filled with bis-fura-2 and Alexa Fluor 594. **(C)** Somatic membrane potential transients (patch) in response to one glutamate pulse (5 ms) delivered at location "*glut. 1*" (red trace), or one glutamate pulse delivered at location "*glut. 2*" (blue trace). Black trace (1 + 2) is the neuronal response to glut. 1 and glut. 2 pulses applied together. **(D_1)** Simultaneous recordings of dendritic calcium transients at two regions of interest (ROIs) marked by boxes in **(B)**, and recording of somatic membrane potential (patch) during glutamate microiontophoresis at location "glut. 1." "*Plat.*" marks Ca^{2+} plateau. "AP" marks dendritic calcium influx induced by backpropagating action potentials. Ca^{2+} signal from the red ROI was inverted, arbitrarily scaled, and the area underneath the trace shaded red. Vertical dashed line marks the end of the neuronal plateau depolarization. **(D_2)** Same as in **(D_1)**, except glutamate pulse was applied at location glut. 2. **(D_3)** Same as in **(D_1)**, except two pulses (1 and 2) were co-applied at the same moment. **(E_1)** Ca^{2+} transients (ROIs) and somatic membrane potential (patch) during glutamate iontophoresis on two basal dendrites. Precise timings of glut. 1 and glut. 2 pulses are marked by vertical ticks beneath the patch recording. Time interval between glut. 1 and glut. 2 was 1000 ms. **(E_2)** Same as in **(E_1)**, except time interval between 1 and 2 was 500 ms. **(E_3)** Same as in **(E_1)**, except 1 and 2 were applied simultaneously (interval = 0 ms).

duration of the longer individual component. Compare the durations of somatic plateaus in red (glut. 2 only) and black (paired) traces in three experiments shown in **Figures 11B–D**. The only somatic parameter that seemed to reflect the co-occurrence of two suprathreshold dendritic plateau potentials in the basilar dendritic tree was the frequency of AP firing. The cell bodies of layer 5 pyramidal neurons fired a greater number of APs during the simultaneous occurrence of two plateaus than during each dendritic plateau potential alone (**Figure 11D**). However, the summation of spike numbers was still sublinear. For example, a five-spike potential (in response to glut. 1) and six-spike potential (glut. 2), when triggered together generated eight spikes (**Figure 11D**, black trace), which is only 75% of what should be expected if spike numbers were additive biophysical parameters

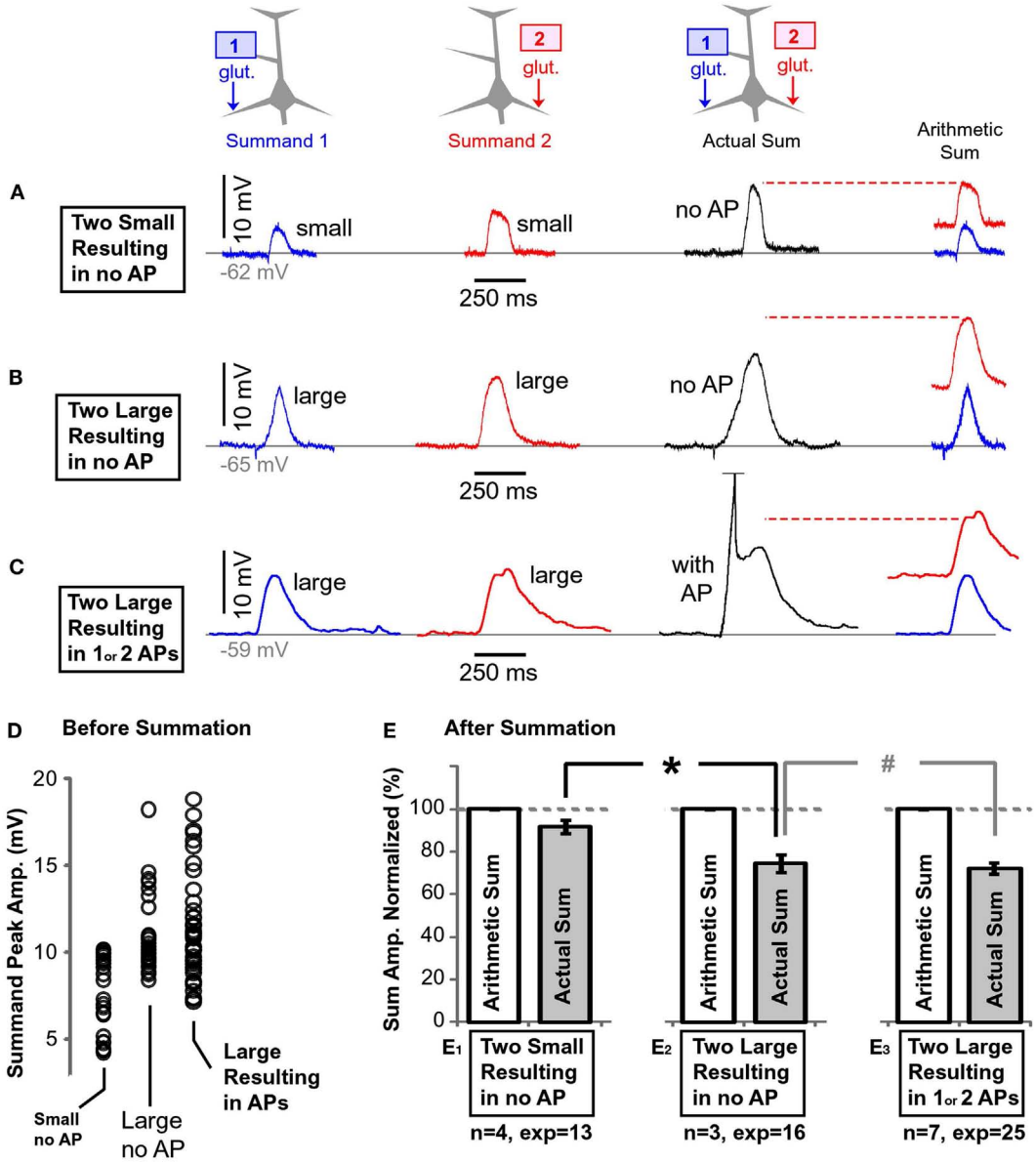

FIGURE 10 | Summation of plateau potentials in the absence of somatic AP fi ing. (A) *Blue trace*: somatic recording of a plateau potential evoked by a 5-ms application of glutamate on the left basal branch, as schematically depicted by the drawing above the blue trace. *Red trace*: somatic recording of a plateau potential evoked by a 5-ms application of glutamate on the right basal branch, as schematically depicted in the drawing above the red trace. Note that each summand is "small," as defined in Section "Materials and Methods." *Black trace*: somatic depolarization resulting from glutamatergic stimulation of both dendrites at the same time, as depicted in the drawing above the black trace. *Arithmetic sum*: the dashed horizontal red line indicates the arithmetic sum of blue and red trace. **(B)** Same as in **(A)** except both summands (blue and red) are "large," as defined in Section "Materials and Methods." **(C)** Same as in **(B)** except summation resulted in AP firing (truncated). **(D)** Peak amplitudes of each summand (before summation) separated in three groups using criteria explained in Section "Materials and Methods." **(E)** The amplitude of the actual depolarization (black trace) was divided by the corresponding arithmetic sum, and averaged across all experiments within one group. The name of the data group, number of cells (*n*) and the number of experiments (exp) are shown below each pair of bars. The dashed horizontal gray line marks the expected value if summation of two dendritic plateau potentials were perfectly linear. $^*p < 0.05$ (unpaired *t*-test). $\#p > 0.05$.

$(5 + 6 = 11)$. Two individual plateau potentials coming from two basal branches at the same moment of time integrate in such a manner that the number of APs generated per plateau is greater than the number generated from either individual component on its own (**Figure 11E**, #APs). Quantification of data obtained in nine pyramidal neurons (**Figure 11E**) was performed by normalizing plateau amplitudes, plateau durations, and spike numbers per plateau (*glut. 1* or *glut. 2*) against values obtained when *1* and *2* were paired. The numbers were arranged so that smaller amplitudes, shorter durations, and fewer APs per plateau were

always named *glut. 1* (**Figure 11E**, blue columns), and larger ones were always named *glut. 2* (**Figure 11E**, red columns). This was done to emphasize that smaller and shorter plateau potentials (**Figure 11D**, Inset, blue trace) are eclipsed by larger and longer plateaus (red trace), when paired together (black trace). In other words, from the point of the somatic voltage change (i.e., slow component), a smaller or shorter plateau potential is completely invisible if co-occurring with a larger and longer plateau potential. It must be noted that this conclusion applies only if two dendritic plateaus are perfectly aligned in time. If one plateau begins sooner or ends later than the plateau arriving from the other basal dendrite, these timing discrepancies will be detected in the somatic voltage waveform. The average duration of paired stimulations, "1 + 2" (**Figure 11E**, duration, white column) was slightly greater than the duration of the individual (longer) plateau in the pair ("2," red column). This is because in some experiments the rise of the shorter plateau (blue column) was faster than the rise of the longer plateau (red column), as shown in **Figure 9C** (the rise of the blue trace precedes the rise of the red trace). When two individual plateau potentials coming from two basal branches are not perfectly synchronized, then they integrate in such a way that the cell body is maintained in a depolarized UP state for a longer period of time than either individual component would do on its own (**Figure 9E$_2$**). Although it may appear from the graph in **Figure 11E** that both plateau duration and the AP count increase by summation, these gains are made for different reasons. The gains in duration (**Figure 11E**, duration) only occur if the summating plateau potentials are not perfectly synchronous. The gains in the number of APs (**Figure 11E**, #APs) occur regardless of whether or not the two summating plateaus are perfectly synchronous in rise and decline.

DISCUSSION

The experiments based on two-photon imaging of a spine and its adjacent dendritic shaft unequivocally showed that extrasynaptic NMDA receptors are activated during synaptically evoked NMDA spikes (Chalifoux and Carter, 2011). If two synaptic inputs at 50 Hz (**Figure 2A**) activated extrasynaptic receptors via glutamate spillover (Chalifoux and Carter, 2011), then five of such synaptic inputs would cause even stronger activation of extrasynaptic NMDA receptors, as the amount of glutamate released by five shocks exceeds that released by two synaptic shocks. Five synaptic stimulations produced dendritic plateau potentials (**Figure 2B**). Therefore, dendritic NMDA spikes (Polsky et al., 2004; Chalifoux and Carter, 2011) and dendritic plateau potentials (Milojkovic et al., 2004, 2005a) represent two characteristic physiological states involving the activation of extrasynaptic NMDA receptors. Although their cellular mechanisms are essentially the same: (1) clustered glutamatergic inputs in space and time (Larkum and Nevian, 2008; Magee, 2011), (2) failure of glial processes to clear the surplus of glutamate (Suzuki et al., 2008; Chalifoux and Carter, 2011), and (3) activation of extrasynaptic NMDA receptors (Tovar and Westbrook, 1999; Harris and Pettit, 2007), these two signals (NMDA spike and plateau potential) still represent two qualitatively different events in dendritic integration (**Figures 2A,B**).

Our emphasis on physiological differences between NMDA spikes (Polsky et al., 2004; Chalifoux and Carter, 2011) and plateau potentials (Wei et al., 2001; Milojkovic et al., 2004, 2005a; Suzuki et al., 2008) are based on side-by-side comparison of these two potentials in the basal dendrites of L5 pyramidal neurons in the rat PFC. We have shown that dendritic NMDA spikes and dendritic plateau potentials differ by two fundamental physiological properties: (1) voltage waveform and (2) calcium influx. The NMDA spikes are predominantly subthreshold events at the cell body that resemble pointy EPSPs (**Figure 2A**, Inset). Synaptically evoked dendritic plateau potentials are endowed with much larger depolarization amplitudes that reach the threshold for AP firing (**Figure 2B**). Furthermore, plateau potentials last much longer than NMDA spikes, providing stable depolarizations of the cell body for several hundred milliseconds. The calcium influx associated with an NMDA spike is restricted to a very narrow dendritic segment; ∼20 μm in length (**Figure 2C**). A dendritic plateau potential, in contrast, triggers a massive calcium influx at the glutamate input site and very substantial calcium signals in the remainder of the dendrite (**Figure 2D**). The massive calcium plateau at the input site is mediated by NMDA receptor channels (Milojkovic et al., 2007; Major et al., 2008), while calcium signals in the remainder of the input receiving dendrite are mediated by bi-directional propagation of the dendritic plateau potential (Milojkovic et al., 2004, 2005a, 2007). Overall, dendritic NMDA spikes and dendritic plateau potentials are two distinct outcomes of dendritic processing of glutamatergic inputs in thin dendrites of cortical pyramidal neurons, potentially having distinct functional roles in dendritic plasticity, synaptic plasticity, and information processing (Antic et al., 2010). For example, slow dendritic dynamics are necessary for the stabilization of network activity bumps in noisy networks (Morita, 2008; Kurashige and Cateau, 2011). "Slow dendritic dynamics" is embodied in the plateau phase of the glutamate-mediated plateau potential, while the voltage waveform of the NMDA spike clearly lacks this plateau phase (**Figure 2A**, blue trace).

GLUTAMATE POND

Dendritic NMDA spikes were thought to be regenerative membrane potentials (spikes) carried by the negative slope conductance of the NMDA receptor current (Mayer et al., 1984; Nowak et al., 1984). The experimental proof of dendritic regenerative properties was based on somatic recordings (Schiller et al., 2000; Major et al., 2008). We have shown that the dendritic membrane potential actually exhibits the characteristic transition from subthreshold potential to spike in the presence of TTX (Milojkovic et al., 2005a), their **Figure 8**) and in drug-free saline (**Figure 3A**, ROI). At the same instant of time when a basal dendrite jumps from a subthreshold to a plateau potential, the somatic membrane potential invariably jumps from subthreshold to plateau potential (**Figure 3A**, brown trace). The slow component of the somatic voltage waveform of cortical pyramidal neurons is nothing more than a reflection of the glutamatergic integration event occurring somewhere in the dendritic tree (Milojkovic et al., 2005a; Antic et al., 2007). Simply, the cell body is in DOWN state if the dendrite is in DOWN state. When the dendrite transitions from DOWN to UP state, the cell body passively follows, by transitioning from

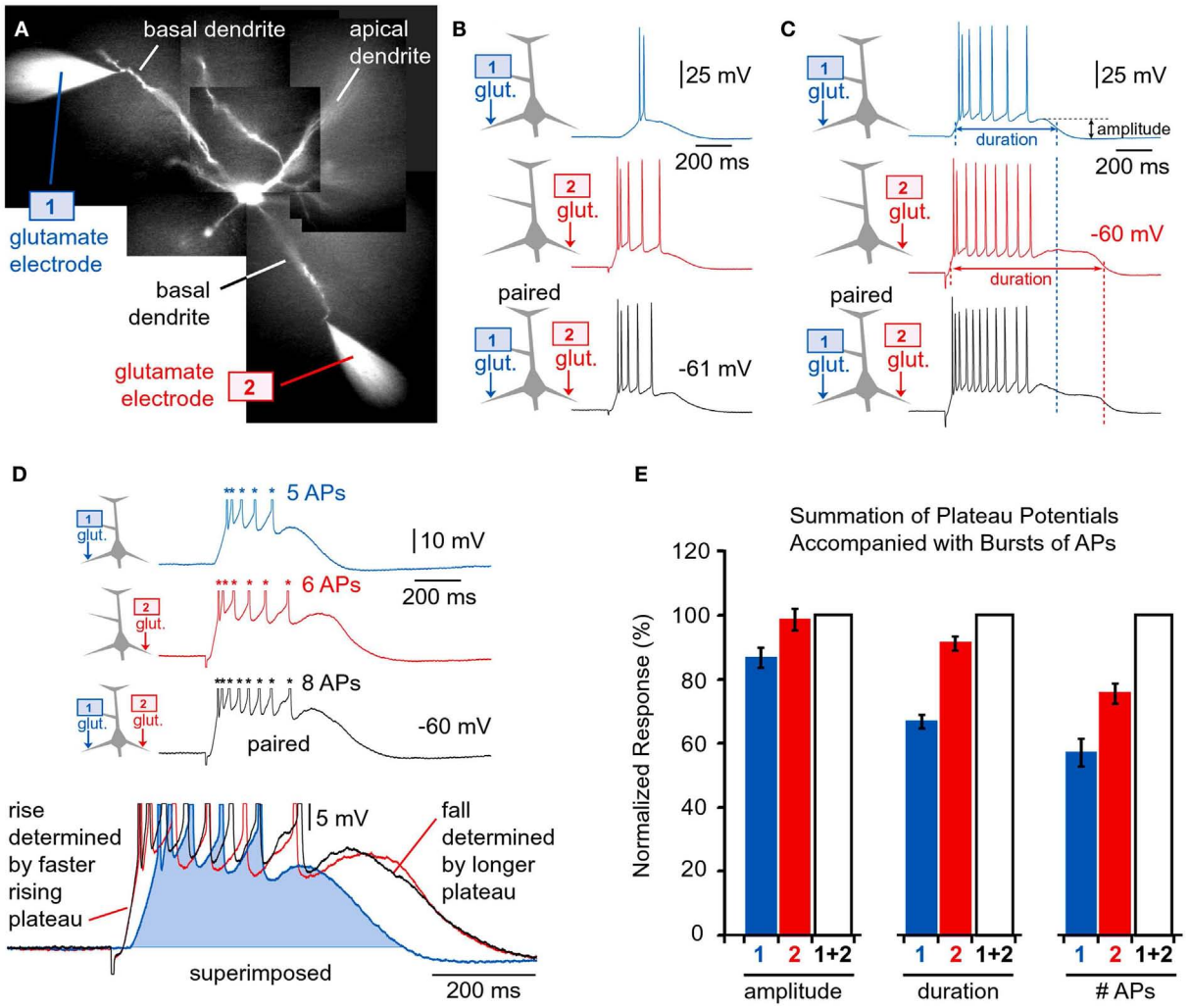

FIGURE 11 | Quenching of dendritic plateau potentials at the soma. (A) Two rhodamine-filled glutamate electrodes positioned next to two rhodamine-filled basal dendrites. **(B–D)** Drawing of an experimental outline precedes each whole-cell recording. Whole-cell recordings are colored to match the glutamate pipette used. Black traces indicate simultaneous release from both glutamate electrodes (paired). Vertical dashed line marks the end of the corresponding plateau. **(D)** Inset: glutamate-evoked plateau potentials in response to *1*, *2*, and *1 + 2* stimulation are superimposed to show that the shorter plateau potential (blue, *glut. 1*) is totally eclipsed by the longer plateau potential (red, *glut. 2*) during co-activation (black, *1 + 2*, paired). **(E)** Amplitude of the glutamate-evoked depolarization [slow component amplitude marked in **(C)**] is divided by the plateau amplitude obtained during co-activation (*1 + 2*), and averaged across nine neurons; 21 triplets of sweeps. Duration of the plateau depolarization was measured at half amplitude [as indicated in **(C)**], normalized against *1 + 2* and averaged across 21 triplets of sweeps obtained in nine neurons. The number of action potentials (#AP) was normalized against trace "*1 + 2*" and averaged across seven neurons. Plateau potentials of smaller amplitude and shorter duration (blue traces) are completely eclipsed by larger and longer plateaus (red traces), when paired (black traces).

DOWN to UP state (**Figures 3A,B**). The ability of thin dendritic branches to deliver sustained depolarizing current to the soma was firmly established in experiments that combined somatic recordings with dendritic imaging (Oakley et al., 2001; Wei et al., 2001; Cai et al., 2004; Milojkovic et al., 2004; Major et al., 2008). This mechanism may be involved in the cellular manifestation of cortical UP states during slow wave sleep (Milojkovic et al., 2004, 2005a; Antic et al., 2007). Dendritic plateau potentials are not causing cortical UP states – they are just reporting network UP states to the neuronal cell body (Antic et al., 2010). Initial efforts to detect dendritic plateau potentials *in vivo* have failed (Waters and Helmchen, 2004; Jia et al., 2010), but recently some experimental data has begun to suggest that clustered synaptic activity and highly localized calcium influxes potentially associated with local dendritic spikes may occur spontaneously in cortical networks (Katona et al., 2011; Kleindienst et al., 2011; Varga et al., 2011).

Although dendritic NMDA spikes have been shown to exhibit a voltage threshold (Schiller et al., 2000; Milojkovic et al., 2004; Rhodes, 2006), recent experimental evidence of combined glutamate-voltage sensitivity (Major et al., 2008; Polsky et al., 2009) sheds new light on this biophysical phenomenon. The spike mechanism is complex because the presence of glutamate molecules is

not simply a permissive factor, but it may also represent the primary mechanism of the observed voltage jump from subthreshold to spike (Schiller et al., 2000; Milojkovic et al., 2004, 2005a; Cha-Min Tang, personal communication). Several lines of evidence indicate that glutamate plays a more important role than voltage. For example, the experimental finding that spike-mediated calcium influx is severely restricted to a narrow, ∼20 μm segment of the basal branch (**Figure 2C$_1$**) emphasizes an overriding importance of reaching the NMDA conductance threshold locally within a dendritic branch, as opposed to simply reaching a local voltage threshold (Polsky et al., 2009). In the two-pulse stimulation paradigm (**Figure 2A**), the carryover of depolarization from the first pulse in a pair had surprisingly little impact on the stimulus threshold at which an NMDA spike could be generated by a second pulse (Polsky et al., 2009). That is, dendritic voltage plays a relatively minor role in setting a better-or-worse initial condition for NMDA spike generation (Polsky et al., 2009). Here we postulate that the glutamate threshold (Milojkovic et al., 2005b; Major et al., 2008; Polsky et al., 2009) is reached when glia can no longer cope with repetitive glutamatergic inputs arriving in a confined space (**Figure 1B**). For a brief period of time the dendritic segment is surrounded by a surplus of glutamate (**Figure 1C**, "glutamate pond"). During such an overwhelming glutamatergic stimulus, the dendritic spike cannot be perturbed by voltage (**Figures 5B,C**; Major et al., 2008). The finding that NMDA receptors on the cell body and on the most proximal dendritic segments (extrasynaptic receptors by definition) can readily support plateau potentials (**Figure 6**) is consistent with the idea that extrasynaptic NMDA receptors are the major carriers of the plateau current during dendritic plateau potentials (Suzuki et al., 2008), and also that the dendritic shaft is surrounded by an abundance of glutamate during that period of time (**Figure 1C**). The NMDA spike initiation is sensitive to the frequency of synaptic activation (Polsky et al., 2004, 2009) not exclusively because of the temporal summation of voltage, but primarily due to a chemical summation of the glutamate originating from two sources: (1) synaptic spillover and (2) release from astrocytic processes (Parpura et al., 1994; Jourdain et al., 2007; Min and Nevian, 2012).

The well-established requirement for the initiation of NMDA spikes is to shock synaptic terminals more than once (Polsky et al., 2004; Chalifoux and Carter, 2011; **Figure 2A**). These recent publications suggest that repetitive input is not needed to depolarize the dendrite to some voltage threshold for spike initiation, but instead multiple shocks are necessary to reverse glial function from glutamate uptake to glutamate release (**Figure 1C**, dark green glia). In glutamate uncaging experiments, the NMDA spike is initiated only when experimenters select neighboring dendritic spines (Losonczy et al., 2008; Remy et al., 2009; Branco and Hausser, 2011). The new evidence (Major et al., 2008; Polsky et al., 2009, present data) suggests that dendritic spikes in glutamate uncaging experiments do not arise from summation of voltage alone, but rather from summation of three glutamate sources: (1) uncaged glutamate; (2) synaptically released glutamate triggered by the presence of uncaged glutamate; and (3) glutamate released from glia (Min and Nevian, 2012) stimulated by uncaged glutamate.

TEMPORAL SUMMATION OF SUPRATHRESHOLD PLATEAU POTENTIALS

Early experiments employed temporal summation of *subthreshold* depolarizations (Milojkovic et al., 2004, 2007; Polsky et al., 2004, 2009). In the present project we investigated neuronal responses to temporal summation of *suprathreshold* dendritic plateau potentials. We sought to investigate the somatic voltage response during a period of time when a narrow segment of a basal dendrite is bombarded with suprathreshold glutamatergic inputs; suprathreshold both in the dendrite (dendritic spike) and in the soma (AP; **Figure 3A**). Instead of going into depolarization blocks from overwhelming excitatory input (Campbell and Hablitz, 2005), PFC L5 pyramidal neurons alternated from a resting (DOWN) to a depolarized (UP) state, with each given pulse, thus faithfully reporting each glutamatergic salvo at low frequency (∼1 Hz, **Figure 7A$_1$**). These data indicate that basal dendrites of PFC L5 pyramidal neurons are endowed with a robust membrane mechanism, capable of decoding large amounts of excitatory neurotransmitter into sustained depolarizations and then quickly recovering from the activation of ligand-gated and voltage-gated dendritic conductances. Suprathreshold salvoes of glutamate, arriving at frequencies higher than 1 Hz, also showed no signs of a depolarization block. Instead, individual plateaus gradually merged into one continuous depolarized state (**Figure 8C**). Sustained depolarizations with persistent AP firing that are occasionally interrupted by a DOWN state (**Figure 7A$_3$**), are reminiscent of intracellular recordings obtained in animal cortices during transitions from sleep to awake state (Timofeev et al., 2001). According to our working model, the interruptions in persistent activity (transient DOWN states, Timofeev et al., 2001) indicate brief periods of time in which the instantaneous count of plateau potentials across the entire basilar dendritic tree was equal to zero.

SPATIAL SUMMATION OF SUPRATHRESHOLD PLATEAU POTENTIALS

In the elaborate dendritic tree of one cortical pyramidal neuron, substantial glutamatergic inputs impinge simultaneously on two or more dendritic branches (Varga et al., 2011), providing the necessary conditions for spatial summation of dendritic voltages in the cell body. Summation of subthreshold synaptic inputs has been initially studied in multicompartmental biophysical models (London and Segev, 2001; Poirazi et al., 2003; Polsky et al., 2009). In brain slice experiments the summation of subthreshold potentials was explored using two glutamate iontophoresis electrodes (Cash and Yuste, 1999), or dual pipette synaptic stimulation (Polsky et al., 2004; Larkum et al., 2009). The traditional view of signal integration in the cerebral cortex is based on the idea that the neuronal computational task is to summate thousands of subthreshold synaptic inputs (Cash and Yuste, 1999; London and Segev, 2001). Departing from the traditional, in the present study we asked what the neuronal response would be if two dendritic plateau potentials, each capable of bringing the cell body into firing a burst of APs on its own, occurred at two dendritic locations simultaneously. We studied the summation of glutamatergic inputs that were pre-integrated into robust local spikes at their respective dendritic integration sites, consistent with a two-stage model of pyramidal neuron, where the first stage of signal integration takes place in the dendrite (Poirazi et al., 2003).

In our experimental design, the individual elements of summation were not only suprathreshold for the dendrite (dendritic plateau-spike) but also for the cell body (plateau depolarization crowned by bursts of APs, **Figures 9D$_1$,D$_2$**). Surprisingly, robust glutamate-evoked plateau potentials arriving from two basal branches into the cell body, each contributing ∼20 mV of depolarization on its own, did not contribute to the amplitude of the slow component of somatic depolarization when co-applied at the same moment of time (**Figure 11E**, *amplitude*). Additionally, two robust plateau potentials, each lasting hundreds of milliseconds on its own, did not contribute to the duration of somatic plateau depolarization when arriving at the same instance of time. A longer plateau regularly eclipsed the shorter plateau (**Figure 11D**, inset). The only way for shorter plateaus to affect the somatic voltage was to start before, or end after the longer plateau (**Figure 9C**). These results (**Figures 9–11**) may explain why the summation of dendritic plateau potentials was never suspected from intracellular recordings (Timofeev et al., 2001). The "quenching" of robust suprathreshold events in the same unit of time (**Figure 11E**, *amplitude*) explains why, in a given neuron, all cortical UP states have uniform amplitudes (Cowan and Wilson, 1994; Branchereau et al., 1996; Lewis and O'Donnell, 2000; Timofeev et al., 2001). Two or more suprathreshold dendritic plateau potentials, arriving from two basal dendrites at the same moment of time, produce similar amplitude of sustained depolarization as either plateau alone (**Figure 11E**, amplitude).

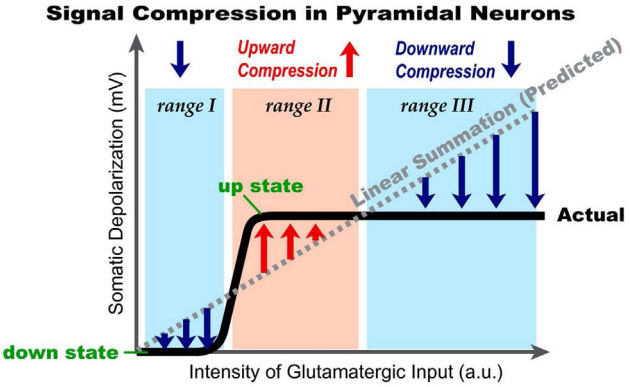

FIGURE 12 | Cellular bases of signal compression in the basilar dendritic tree of cortical pyramidal neurons. Schematic representation of data obtained by summation of glutamatergic inputs in the basilar dendritic tree. Thick black line (*Actual*) represents a sigmoidal shape of somatic depolarization obtained experimentally by gradually increasing the intensity of glutamatergic stimulation delivered on one basal dendrite or by summation of inputs from two basal branches. The dashed gray line represents an expected depolarization in the cell body, based on the arithmetic (linear) summation of plateau potentials occurring in one or two basal dendrites simultaneously. Pink rectangle marks the range of glutamatergic input intensities (*range II*), in which cellular (dendritic) mechanisms boost the amplitude of the somatic depolarization. Blue rectangle marks the range of glutamatergic input intensities (*range III*), in which cellular mechanisms (dendritic and somatic) suppress the amount of somatic depolarization. As a result of active boosting (red arrows) or active suppression (blue arrows) the neuronal output (somatic depolarization) is compressed in a narrow range of amplitudes, marked by "*up state*."

SIGNAL COMPPRESSION IN CORTICAL PYRAMIDAL NEURONS

The extrasynaptic NMDA receptors and voltage-gated K^+ currents together provide pyramidal neurons with the ability to respond to a wide range of input intensities (**Figure 12**, *ranges II and III*) with a very narrow range of somatic depolarizations (**Figure 12**, UP state). This function is analogous to a dynamic range compression in audio engineering. Audio compressors amplify quiet sounds (*upward compression*) and limit or reduce the volume of loud sounds (*downward compression*). In our working model (**Figure 12**), the quiet sounds are equivalent to weak glutamatergic inputs; and the loud sounds are equivalent to suprathreshold glutamatergic inputs. If a pyramidal neuron were a simple integrator, the somatic depolarization would be proportional to the intensity of glutamatergic input received by dendrites (**Figure 12**, dashed gray line). However, our experimental measurements (**Figures 3E** and **4D**) indicate that the amplitude of the somatic depolarization remains in a very narrow range of values despite the increasing intensity of glutamatergic drive (**Figure 12**, abscissa). In one particular range of glutamatergic intensities (**Figure 12**, *range II*) the cellular mechanisms boost the amplitude of the somatic depolarization (**Figure 12**, *Upward compression*, red arrows). In another range of glutamatergic intensities (**Figure 12**, *range III*) the cellular mechanisms work together to suppress the amplitude of the somatic depolarization (**Figure 12**, *Downward compression*, blue arrows). *UPWARD COMPRESSION*: excitatory inputs that reach the local threshold are amplified by regenerative properties of NMDA currents in basal dendrites (Schiller et al., 2000; Milojkovic et al., 2004, 2005a; Rhodes, 2006; Major et al., 2008) to a small degree, and by local summation of released glutamate in a confined extracellular space to a larger degree (**Figure 1C**). Glutamate required for reaching the glutamate threshold (Major et al., 2008; Polsky et al., 2009) is not only released from the active synaptic afferents (**Figure 1C**), but also from synaptically activated astrocytic processes (Parpura et al., 1994; Jourdain et al., 2007; Min and Nevian, 2012). Both the dendritic membrane currents and the accumulation of glutamate in the extracellular space effectively boost near-threshold afferent inputs, causing the neuronal output function to shift upward (**Figure 12**, red arrows). *DOWNWARD COMPRESSION*: glutamatergic inputs that greatly exceed the threshold for the creation of a local glutamate pond cannot depolarize the dendritic membrane above the glutamate reversal potential (∼0 mV). In addition to this hard limit, the dendritic K^+ currents activated by the voltage waveform of dendritic plateau potentials (Milojkovic et al., 2004, 2005a) and by a massive calcium influx (Milojkovic et al., 2007; Major et al., 2008) limit the amount of dendritic depolarization (Wilson and Kawaguchi, 1996; Contreras et al., 1997; Cai et al., 2004). These dendritic plateau potentials are then attenuated by dendritic cable properties en route to the soma (Milojkovic et al., 2004; their **Figures 4** and **7**) and finally compressed by AP-activated K^+ current in the somatic membrane (Bekkers, 2000; Korngreen and Sakmann, 2000; Schaefer et al., 2007). Note that plateau amplitudes increased upon blocking APs with TTX (**Figure 4B**). Because of these biophysical properties, the maximal amount of depolarizing current that basal dendrites can generate and deliver to the cell body is strictly limited. Once

the dendritic plateau potential has been initiated, an entire range of suprathreshold glutamatergic inputs (**Figure 12**, *ranges II and III*) actually produces only one current amplitude (**Figure 12**, *UP state*). That is, during a dendritic UP state (**Figures 2B**, **3A**, **4C$_2$**, and **7A**) mediated by extrasynaptic NMDA receptors (Suzuki et al., 2008; Chalifoux and Carter, 2011), the neuronal output is strongly compressed in a narrow range, fluctuating around a single value (**Figure 12**, *UP state*). Dynamic range compression manifested by a steep sigmoidal input-output function (**Figure 12**, *Actual*) has been implicated as one of the crucial components of signal processing in the central nervous system (Geisler and Albrecht, 1995; Clatworthy et al., 2003; Nizami, 2005; Persi et al., 2011).

AUTHOR CONTRIBUTIONS

The work was done in Srdjan D. Antic laboratory. Srdjan D. Antic designed the experiments. Katerina D. Oikonomou, Shaina M. Short, Matthew T. Rich, and Srdjan D. Antic performed the experiments and analyzed the data. Manuscript was drafted by Srdjan D. Antic. Comments on drafts and approval of the final version: all authors.

ACKNOWLEDGMENTS

Srdjan D. Antic would like to thank Guy Major for insightful discussions on glutamate-mediated dendritic potentials. This work was supported by National Institutes of Health grant (MH063503), and a NARSAD Young Investigator Award 2009.

REFERENCES

Acker, C. D., and Antic, S. D. (2009). Quantitative assessment of the distributions of membrane conductances involved in action potential backpropagation along Basal dendrites. *J. Neurophysiol.* 101, 1524–1541.

Antic, S., Major, G., and Zecevic, D. (1999). Fast optical recordings of membrane potential changes from dendrites of pyramidal neurons. *J. Neurophysiol.* 82, 1615–1621.

Antic, S. D. (2003). Action potentials in basal and oblique dendrites of rat neocortical pyramidal neurons. *J. Physiol. (Lond.)* 550, 35–50.

Antic, S. D., Acker, C. D., Zhou, W. L., Moore, A. R., and Milojkovic, B. A. (2007). "The role of dendrites in the maintenance of the UP state," in *Mechanisms of Spontaneous Active States in the Neocortex*, ed. I. Timofeev (Kerala: Research Signpost), 45–72.

Antic, S. D., Zhou, W. L., Moore, A. R., Short, S. M., and Ikonomu, K. D. (2010). The decade of the dendritic NMDA spike. *J. Neurosci. Res.* 88, 2991–3001.

Ariav, G., Polsky, A., and Schiller, J. (2003). Submillisecond precision of the input-output transformation function mediated by fast sodium dendritic spikes in basal dendrites of CA1 pyramidal neurons. *J. Neurosci.* 23, 7750–7758.

Asztely, F., Erdemli, G., and Kullmann, D. M. (1997). Extrasynaptic glutamate spillover in the hippocampus: dependence on temperature and the role of active glutamate uptake. *Neuron* 18, 281–293.

Ballesteros-Yanez, I., Benavides-Piccione, R., Elston, G. N., Yuste, R., and DeFelipe, J. (2006). Density and morphology of dendritic spines in mouse neocortex. *Neuroscience* 138, 403–409.

Bekkers, J. M. (2000). Properties of voltage-gated potassium currents in nucleated patches from large layer 5 cortical pyramidal neurons of the rat. *J. Physiol.* 3, 593–609.

Benavides-Piccione, R., Hamzei-Sichani, F., Ballesteros-Yanez, I., DeFelipe, J., and Yuste, R. (2006). Dendritic size of pyramidal neurons differs among mouse cortical regions. *Cereb. Cortex* 16, 990–1001.

Benucci, A., Verschure, P. F., and Konig, P. (2004). Two-state membrane potential fluctuations driven by weak pairwise correlations. *Neural Comput.* 16, 2351–2378.

Branchereau, P., Van Bockstaele, E. J., Chan, J., and Pickel, V. M. (1996). Pyramidal neurons in rat prefrontal cortex show a complex synaptic response to single electrical stimulation of the locus coeruleus region: evidence for antidromic activation and GABAergic inhibition using in vivo intracellular recording and electron microscopy. *Synapse* 22, 313–331.

Branco, T., and Hausser, M. (2011). Synaptic integration gradients in single cortical pyramidal cell dendrites. *Neuron* 69, 885–892.

Cai, X., Liang, C. W., Muralidharan, S., Kao, J. P., Tang, C. M., and Thompson, S. M. (2004). Unique roles of SK and Kv4.2 potassium channels in dendritic integration. *Neuron* 44, 351–364.

Campbell, S., and Hablitz, J. J. (2005). Modification of epileptiform discharges in neocortical neurons following glutamate uptake inhibition. *Epilepsia* 46(Suppl. 5), 129–133.

Cash, S., and Yuste, R. (1999). Linear summation of excitatory inputs by CA1 pyramidal neurons. *Neuron* 22, 383–394.

Chalifoux, J. R., and Carter, A. G. (2011). Glutamate spillover promotes the generation of NMDA spikes. *J. Neurosci.* 31, 16435–16446.

Clatworthy, P. L., Chirimuuta, M., Lauritzen, J. S., and Tolhurst, D. J. (2003). Coding of the contrasts in natural images by populations of neurons in primary visual cortex (V1). *Vision Res.* 43, 1983–2001.

Contreras, D., Durmuller, N., and Steriade, M. (1997). Plateau potentials in cat neocortical association cells in vivo: synaptic control of dendritic excitability. *Eur. J. Neurosci.* 9, 2588–2595.

Cowan, R. L., and Wilson, C. J. (1994). Spontaneous firing patterns and axonal projections of single corticostriatal neurons in the rat medial agranular cortex. *J. Neurophysiol.* 71, 17–32.

De-Miguel, F. F., and Fuxe, K. (2012). Extrasynaptic neurotransmission as a way of modulating neuronal functions. *Front. Physiol.* 3:16. doi:10.3389/fphys.2012.00016

Dodt, H. U., Frick, A., Kampe, K., and Zieglgansberger, W. (1998). NMDA and AMPA receptors on neocortical neurons are differentially distributed. *Eur. J. Neurosci.* 10, 3351–3357.

Elston, G. N. (2003). Cortex, cognition and the cell: new insights into the pyramidal neuron and prefrontal function. *Cereb. Cortex* 13, 1124–1138.

Enoki, R., Kiuchi, T., Koizumi, A., Sasaki, G., Kudo, Y., and Miyakawa, H. (2004). NMDA receptor-mediated depolarizing after-potentials in the basal dendrites of CA1 pyramidal neurons. *Neurosci. Res.* 48, 325–333.

Gasparini, S., Migliore, M., and Magee, J. C. (2004). On the initiation and propagation of dendritic spikes in CA1 pyramidal neurons. *J. Neurosci.* 24, 11046–11056.

Geisler, W. S., and Albrecht, D. G. (1995). Bayesian analysis of identification performance in monkey visual cortex: nonlinear mechanisms and stimulus certainty. *Vision Res.* 35, 2723–2730.

Harris, A. Z., and Pettit, D. L. (2007). Extrasynaptic and synaptic NMDA receptors form stable and uniform pools in rat hippocampal slices. *J. Physiol. (Lond.)* 584, 509–519.

Herman, M. A., Nahir, B., and Jahr, C. E. (2011). Distribution of extracellular glutamate in the neuropil of hippocampus. *PLoS ONE* 6, e26501. doi:10.1371/journal.pone.0026501

Hodgkin, A. L., and Huxley, A. F. (1952). A quantitative description of membrane current and its application to conduction and excitation in nerve. *J. Physiol. (Lond.)* 117, 500–544.

Holthoff, K., Kovalchuk, Y., Yuste, R., and Konnerth, A. (2004). Single-shock LTD by local dendritic spikes in pyramidal neurons of mouse visual cortex. *J. Physiol. (Lond.)* 560, 27–36.

Jia, H., Rochefort, N. L., Chen, X., and Konnerth, A. (2010). Dendritic organization of sensory input to cortical neurons in vivo. *Nature* 464, 1307–1312.

Jourdain, P., Bergersen, L. H., Bhaukaurally, K., Bezzi, P., Santello, M., Domercq, M., Matute, C., Tonello, F., Gundersen, V., and Volterra, A. (2007). Glutamate exocytosis from astrocytes controls synaptic strength. *Nat. Neurosci.* 10, 331–339.

Kampa, B. M., and Stuart, G. J. (2006). Calcium spikes in basal dendrites of layer 5 pyramidal neurons during action potential bursts. *J. Neurosci.* 26, 7424–7432.

Katona, G., Kaszas, A., Turi, G. F., Hajos, N., Tamas, G., Vizi, E. S., and Rozsa, B. (2011). Roller Coaster Scanning reveals spontaneous triggering of dendritic spikes in CA1 interneurons. *Proc. Natl. Acad. Sci. U.S.A.* 108, 2148–2153.

Kleindienst, T., Winnubst, J., Roth-Alpermann, C., Bonhoeffer, T., and Lohmann, C. (2011). Activity-dependent clustering of functional synaptic inputs on developing hippocampal dendrites. *Neuron* 72, 1012–1024.

Korngreen, A., and Sakmann, B. (2000). Voltage-gated K+ channels in layer 5 neocortical pyramidal neurones from young rats: subtypes and gradients. *J. Physiol.* 3, 621–639.

Kullmann, D. M., Min, M. Y., Asztely, F., and Rusakov, D. A. (1999). Extracellular glutamate diffusion determines the occupancy of glutamate receptors at CA1 synapses in the hippocampus. *Philos. Trans. R. Soc. Lond. B Biol. Sci.* 354, 395–402.

Kurashige, H., and Cateau, H. (2011). Dendritic slow dynamics enables localized cortical activity to switch between mobile and immobile modes with noisy background input. *PLoS ONE* 6, e24007. doi:10.1371/journal.pone.0024007

Larkman, A. U. (1991). Dendritic morphology of pyramidal neurones of the visual cortex of the rat: III. Spine distributions. *J. Comp. Neurol.* 306, 332–343.

Larkum, M. E., and Nevian, T. (2008). Synaptic clustering by dendritic signalling mechanisms. *Curr. Opin. Neurobiol.* 18, 321–331.

Larkum, M. E., Nevian, T., Sandler, M., Polsky, A., and Schiller, J. (2009). Synaptic integration in tuft dendrites of layer 5 pyramidal neurons: a new unifying principle. *Science* 325, 756–760.

Lewis, B. L., and O'Donnell, P. (2000). Ventral tegmental area afferents to the prefrontal cortex maintain membrane potential 'up' states in pyramidal neurons via D(1) dopamine receptors. *Cereb. Cortex* 10, 1168–1175.

London, M., and Segev, I. (2001). Synaptic scaling in vitro and in vivo. *Nat. Neurosci.* 4, 853–855.

Losonczy, A., Makara, J. K., and Magee, J. C. (2008). Compartmentalized dendritic plasticity and input feature storage in neurons. *Nature* 452, 436–441.

Magee, J. C. (2011). Observations on clustered synaptic plasticity and highly structured input patterns. *Neuron* 72, 887–888.

Major, G., Polsky, A., Denk, W., Schiller, J., and Tank, D. W. (2008). Spatiotemporally graded NMDA spike/plateau potentials in basal dendrites of neocortical pyramidal neurons. *J. Neurophysiol.* 99, 2584–2601.

Mayer, M. L., Westbrook, G. L., and Guthrie, P. B. (1984). Voltage-dependent block by Mg2+ of NMDA responses in spinal cord neurones. *Nature* 309, 261–263.

Milojkovic, B. A., Radojicic, M. S., and Antic, S. D. (2005a). A strict correlation between dendritic and somatic plateau depolarizations in the rat prefrontal cortex pyramidal neurons. *J. Neurosci.* 25, 3940–3951.

Milojkovic, B. A., Wuskell, J. P., Loew, L. M., and Antic, S. D. (2005b). Initiation of sodium spikelets in basal dendrites of neocortical pyramidal neurons. *J. Membr. Biol.* 208, 155–169.

Milojkovic, B. A., Radojicic, M. S., Goldman-Rakic, P. S., and Antic, S. D. (2004). Burst generation in rat pyramidal neurones by regenerative potentials elicited in a restricted part of the basilar dendritic tree. *J. Physiol. (Lond.)* 558, 193–211.

Milojkovic, B. A., Zhou, W. L., and Antic, S. D. (2007). Voltage and calcium transients in basal dendrites of the rat prefrontal cortex. *J. Physiol. (Lond.)* 585, 447–468.

Min, R., and Nevian, T. (2012). Astrocyte signaling controls spike timing-dependent depression at neocortical synapses. *Nat. Neurosci.* 15, 746–753.

Moore, A. R., Zhou, W. L., Potapenko, E. S., Kim, E. J., and Antic, S. D. (2011). Brief dopaminergic stimulations produce transient physiological changes in prefrontal pyramidal neurons. *Brain Res.* 1370, 1–15.

Morita, K. (2008). Possible role of dendritic compartmentalization in the spatial working memory circuit. *J. Neurosci.* 28, 7699–7724.

Nimchinsky, E. A., Yasuda, R., Oertner, T. G., and Svoboda, K. (2004). The number of glutamate receptors opened by synaptic stimulation in single hippocampal spines. *J. Neurosci.* 24, 2054–2064.

Nizami, L. (2005). Dynamic range relations for auditory primary afferents. *Hear. Res.* 208, 26–46.

Nowak, L., Bregestovski, P., Ascher, P., Herbet, A., and Prochiantz, A. (1984). Magnesium gates glutamate-activated channels in mouse central neurones. *Nature* 307, 462–465.

Oakley, J. C., Schwindt, P. C., and Crill, W. E. (2001). Dendritic calcium spikes in layer 5 pyramidal neurons amplify and limit transmission of ligand-gated dendritic current to soma. *J. Neurophysiol.* 86, 514–527.

Parpura, V., Basarsky, T. A., Liu, F., Jeftinija, K., Jeftinija, S., and Haydon, P. G. (1994). Glutamate-mediated astrocyte-neuron signalling. *Nature* 369, 744–747.

Persi, E., Hansel, D., Nowak, L., Barone, P., and van Vreeswijk, C. (2011). Power-law input-output transfer functions explain the contrast-response and tuning properties of neurons in visual cortex. *PLoS Comput. Biol.* 7, e1001078. doi:10.1371/journal.pcbi.1001078

Poirazi, P., Brannon, T., and Mel, B. W. (2003). Pyramidal neuron as two-layer neural network. *Neuron* 37, 989–999.

Polsky, A., Mel, B., and Schiller, J. (2009). Encoding and decoding bursts by NMDA spikes in basal dendrites of layer 5 pyramidal neurons. *J. Neurosci.* 29, 11891–11903.

Polsky, A., Mel, B. W., and Schiller, J. (2004). Computational subunits in thin dendrites of pyramidal cells. *Nat. Neurosci.* 7, 621–627.

Remy, S., Csicsvari, J., and Beck, H. (2009). Activity-dependent control of neuronal output by local and global dendritic spike attenuation. *Neuron* 61, 906–916.

Rhodes, P. (2006). The properties and implications of NMDA spikes in neocortical pyramidal cells. *J. Neurosci.* 26, 6704–6715.

Schaefer, A. T., Helmstaedter, M., Schmitt, A. C., Bar-Yehuda, D., Almog, M., Ben-Porat, H., Sakmann, B., and Korngreen, A. (2007). Dendritic voltage-gated K+ conductance gradient in pyramidal neurones of neocortical layer 5B from rats. *J. Physiol. (Lond.)* 579, 737–752.

Schiller, J., Helmchen, F., and Sakmann, B. (1995). Spatial profile of dendritic calcium transients evoked by action potentials in rat neocortical pyramidal neurones. *J. Physiol.* 487, 583–600.

Schiller, J., Major, G., Koester, H. J., and Schiller, Y. (2000). NMDA spikes in basal dendrites of cortical pyramidal neurons. *Nature* 404, 285–289.

Suzuki, T., Kodama, S., Hoshino, C., Izumi, T., and Miyakawa, H. (2008). A plateau potential mediated by the activation of extrasynaptic NMDA receptors in rat hippocampal CA1 pyramidal neurons. *Eur. J. Neurosci.* 28, 521–534.

Swadlow, H. A., and Hicks, T. P. (1997). Subthreshold receptive fields and baseline excitability of "silent" S1 callosal neurons in awake rabbits: contributions of AMPA/kainate and NMDA receptors. *Exp. Brain Res.* 115, 403–409.

Timofeev, I., Grenier, F., and Steriade, M. (2001). Disfacilitation and active inhibition in the neocortex during the natural sleep-wake cycle: an intracellular study. *Proc. Natl. Acad. Sci. U.S.A.* 98, 1924–1929.

Tovar, K. R., and Westbrook, G. L. (1999). The incorporation of NMDA receptors with a distinct subunit composition at nascent hippocampal synapses in vitro. *J. Neurosci.* 19, 4180–4188.

Varga, Z., Jia, H., Sakmann, B., and Konnerth, A. (2011). Dendritic coding of multiple sensory inputs in single cortical neurons in vivo. *Proc. Natl. Acad. Sci. U.S.A.* 108, 15420–15425.

Waters, J., and Helmchen, F. (2004). Boosting of action potential backpropagation by neocortical network activity in vivo. *J. Neurosci.* 24, 11127–11136.

Wei, D. S., Mei, Y. A., Bagal, A., Kao, J. P., Thompson, S. M., and Tang, C. M. (2001). Compartmentalized and binary behavior of terminal dendrites in hippocampal pyramidal neurons. *Science* 293, 2272–2275.

Wilson, C. J., and Kawaguchi, Y. (1996). The origins of two-state spontaneous membrane potential fluctuations of neostriatal spiny neurons. *J. Neurosci.* 16, 2397–2410.

Yasuda, R., Sabatini, B. L., and Svoboda, K. (2003). Plasticity of calcium channels in dendritic spines. *Nat. Neurosci.* 6, 948–955.

Zhou, W. L., Yan, P., Wuskell, J. P., Loew, L. M., and Antic, S. D. (2008). Dynamics of action potential backpropagation in basal dendrites of prefrontal cortical pyramidal neurons. *Eur. J. Neurosci.* 27, 1–14.

Conflict of Interest Statement: The authors declare that the research was conducted in the absence of any commercial or financial relationships that could be construed as a potential conflict of interest.

Received: 15 May 2012; paper pending published: 10 June 2012; accepted: 30 July 2012; published online: 24 August 2012.
*Citation: Oikonomou KD, Short SM, Rich MT and Antic SD (2012) Extrasynaptic glutamate receptor activation as cellular bases for dynamic range compression in pyramidal neurons. Front. Physio. **3**:334. doi: 10.3389/fphys.2012.00334*
This article was submitted to Frontiers in Membrane Physiology and Biophysics, a specialty of Frontiers in Physiology.

frontiers in
PHYSIOLOGY

REVIEW ARTICLE
published: 25 September 2012
doi: 10.3389/fphys.2012.00372

Investigations into potential extrasynaptic communication between the dopaminergic and nitrergic systems

M. Mitkovski*[1], *F. E. Padovan-Neto*[2,3], *R. Raisman-Vozari*[4,5,6], *L. Ginestet*[4,5], *C. A. da-Silva*[2] and *E. A. Del-Bel*[2,3]

[1] *Light Microscopy Facility, Max-Planck-Institute of Experimental Medicine, Göttingen, Germany*
[2] *Department MEF-Physiology, Dental School of Ribeirão Preto, University of São Paulo, Ribeirão Preto, Brazil*
[3] *Neurology-Neurociences, Medical School, University of São Paulo, Ribeirão Preto, Brazil*
[4] *INSERM, UMR 975, CRICM, Thérapeutique Expérimentale de la Neurodégénérescence, Paris, France*
[5] *Faculté de Médecine, Université Pierre-et-Marie-Curie, Paris, France*
[6] *CNRS, UMR 7225, Paris, France*

Edited by:
Francisco F. De-Miguel, Universidad Nacional Autónoma de Mexico, Mexico

Reviewed by:
Francisco F. De-Miguel, Universidad Nacional Autónoma de Mexico, Mexico
Tatiana Fiordelisio, Universidad Nacional Autónoma de México, Mexico

****Correspondence:***
E. A. Del-Bel, Department of MEF-Physiology, Dental School of Ribeirão Preto, Campus University of São Paulo, Avenue Café S/N, 14040-904 Ribeirão Preto, São Paulo, Brazil.
e-mail: eadelbel@forp.usp.br

Nitric oxide is unconstrained by cell membranes and can therefore act along a broad distance as a *volume transmitter*. Spillover of nitric oxide between neurons may have a major impact on central nervous system diseases and particularly on neurodegeneration. There is evidence whereby communication between nitrergic and dopaminergic systems plays an essential role in the control of the nigrostriatal pathway. However, there is sparse information for either the coexistence or overlap of nitric oxide and dopaminergic structures. The dual localization of immunoreactivity for nitric oxide synthase (NOS) and tyrosine hydroxylase, enzymes responsible for the synthesis of nitric oxide and dopamine, respectively, was examined in neurons of the nigrostriatal pathway in the rat brain by means of a double-immunohistochemical method and confocal laser scanning microscopy, acquired at the resolution limit. After perfusional fixation, the brains were cut and double-immunostained. A proximity analysis of tyrosine hydroxylase and NOS structures was done using binary masks generated from the respective maximum projections, using confocal laser microscopy. Unrevealed regions were determined somatodendritic positive for both NOS and tyrosine hydroxylase, within an image limit resolution at 2 μm-wide margin. The described interconnected localization of nNOS(+) and TH(+) containing neuronal fibers and cells bodies in the nigrostriatal pathway propose a close anatomical link between the two neurotransmitters.

Keywords: dopamine, nitric oxide synthase, Parkinson disease, volume transmission, neurotransmitter spillover, synapse, plasticity, tyrosine hydroxylase

INTRODUCTION

The mammalian basal ganglia (also referred to as caudate–putamen or neostriatum) are a group of subcortical nuclei implicated in a multiplicity of functions including motor, cognitive, and mnemonic behaviors (Bolam et al., 2000; Graybiel, 2000; Gerfen and Surmeier, 2011). The response of the basal ganglia circuitry to cortical stimuli is modulated by the neurotransmitter dopamine (Shen et al., 2008). Dopamine is crucial to motor, motivational, and reward-related functions of the central nervous system (Bolam et al., 2000; Graybiel, 2000). Degeneration of the dopamine system causes neurological disorders such as Parkinson's disease and is involved in multisystem atrophy (Haavik and Toska, 1998; Nagatsu and Ichinose, 1999; Benavides-Piccione and DeFelipe, 2003).

In addition to releasing dopamine from nerve terminals in striatum, nigrostriatal dopamine neurons synthesize and release dopamine from the soma and dendrites Geffen et al., 1976; Paden et al., 1976; Nieoullon et al., 1977; Wilson et al., 1977; Heeringa and Abercrombie, 1995). The molecular mechanisms underlying the modulatory role of dopamine on striatal and consequently on cortical transmission occur mostly by somatodendritic release (Gonon, 1997; Cragg and Rice, 2004; Rice and Cragg, 2004; see **Figure 1**). Geffen et al. (1976) suggested that the process of somatodendritic dopaminergic release is vesicular and exocytotic, like axonal release (see **Figure 1**). The release of a single vesicle of dopamine could modulate the excitability of tens to thousands of synapses within a few micrometers of a release site, in both substantia nigra compacta and striatum (Cragg et al., 2001; Rice and Cragg, 2008). It has been proposed that the sphere-of-influence of dopamine spillover in a concentration sufficient to stimulate dopamine receptors, has a radius of 2–8 μm (Rice and Cragg, 2008; see also Gonon, 1997; Cragg and Rice, 2004; Arbuthnott and Wickens, 2007). In addition, there is evidence for a lack of post-synaptic specialization at 60–70% of suggested dopamine release sites in the striatum (Descarries et al., 1996) and limited evidence for either

Abbreviations: 6-OHDA, 6-hydroxy-dopamine; CLSM, confocal laser scanning microscopy; CY3, cyanine-3; DA, dopamine; FITC, fluorescein isothiocyanate; GABA, gamma-aminobutyric acid; L-NAME, N^G-nitro- L-arginine methyl ester; NADPH, nicotinamide adenine dinucleotide phosphate; NMDA, *N*-Methyl-D-aspartate acid; nNOS, neuronal nitric oxide synthase; NOS, nitric oxide synthase; TH, tyrosine hydroxylase.

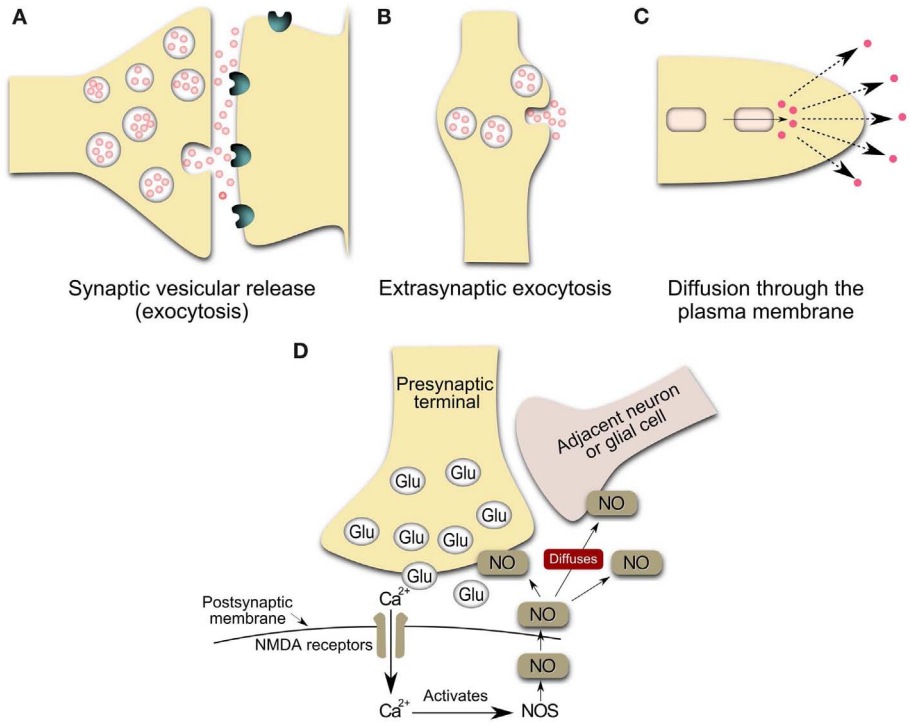

FIGURE 1 | Schematic representation of the main sources of volume transmission involving dopamine and nitric oxide signals in the central nervous system (Inspired by Zoli et al., 1999; Syková, 2004). (A) Synaptic transmission: Synaptic vesicular release followed by the diffusion of the transmitter outside the synaptic cleft at an effective concentration. Neurotransmitters can escape from the synaptic cleft (especially during repetitive stimulation and/or the massive release of a transmitter) and affect extrasynaptic receptors on glia or neurons or reach a neighboring synapse. These phenomena have been called "transmitter spillover" and "synaptic crosstalk." This loss of synaptic independence means that transmitter release at one synapse can lead to the activation of receptors in nearby synapses. **(B)** Volume transmission: vesicular release from non-junctional varicosities, i.e. varicosities lacking pre-synaptic specializations and post-synaptic densities. Axons both in the central nervous system and in the autonomic nervous system form varicose (*boutons-en-passant*) branches that may release and uptake neurotransmitters. The transmitter release from varicosity without synaptic contact diffuses far away from the release site and activates remote receptors of high affinity. **(C,D)** Release of gaseous transmitters, e.g. nitric oxide release from neurons. The inside cell squares are representative of a local synthesis of the neurotransmitter, frequently by enzymatic regulated activity. Nitric oxide presumably operates within a 3-dimensional volume of tissue rather than, more conventionally, between immediately adjacent cellular partners (Kiss and Vizi, 2001). Glu, glutamate vesicles; NOS, nitric oxide synthase; NO, nitric oxide; NMDA, *N*-Methyl-d-Aspartate.

pre- or post-synaptic specializations to delineate somatodendritic dopamine release sites in midbrain dopaminergic neurons (Wilson et al., 1977). Spillover is required for signaling by dopamine since its receptors are largely extrasynaptic (Cragg et al., 2004). This extrasynaptic interaction would be a communication intermediary between classic neurotransmission and the relatively non-specific neuroendocrine secretion (Agnati et al., 1986, 1995, 2010; Descarries et al., 1996; Descarries and Mechawar, 2000; Cragg and Rice, 2004; Bullock et al., 2005; Fuxe et al., 2007, 2010; De-Miguel and Fuxe, 2012).

Neurochemical and morphological evidence indicate that many other neurotransmitters may be released from both synaptic and extrasynaptic sites for diffusion to target cells (Agnati et al., 1986, 1995, 2010; Descarries et al., 1996; Descarries and Mechawar, 2000; Cragg and Rice, 2004; Bullock et al., 2005; De-Miguel and Trueta, 2005; Fuxe et al., 2007, 2010; De-Miguel and Fuxe, 2012). Dopaminergic signals can be inhibited or enhanced by a variety of identified factors that regulate axonal and somatodendritic dopamine release. Specific factors include dopamine autoreceptors, Ca^{2+}, glutamate, GABA, acethilcholine, opioids, cannabinoids, and the diffusible messengers hydrogen peroxide and nitric oxide (Wightman, 2006; Rice et al., 2011). Recent findings indicate that nitric oxide may be involved in the extrasynaptic interactions (**Figure 1**; Kiss and Vizi, 2001; Kiss et al., 2004; Steinert et al., 2008). Volume signaling by nitric oxide is supported by studies modeling the spread of nitric oxide in space and time (Philippides et al., 2000). The function of nitric oxide as a "volume" transmitter has been proposed in systems where the source and target of nitric oxide are anatomically segregated (Gally et al., 1990; Wood and Garthwaite, 1994; Philippides et al., 2005; Steinert et al., 2008). Artinian et al. (2010) support the notion that cellular nitric oxide release can modulate neuronal firing properties in synaptically unconnected neurons, in direct support of nitric oxide functioning as a volume messenger.

Nitric oxide is a gaseous neurotransmitter and an unstable free radical highly diffusible in aqueous and lipid environments. Nitric oxide is produced from L-Arginine by nitric oxide synthase (NOS) after *N*-Methyl D-Aspartate (NMDA) receptor activation and calcium influx (Snyder and Ferris, 2000; Garthwaite, 2008). Once inside target cells, nitric oxide binds the iron in the heme group

contained within the active site of soluble guanylyl cyclase, thereby activating the enzyme to form cyclic guanosine monophosphate and other effector enzymes located in pre-synaptic and post-synaptic elements (Garthwaite and Boulton, 1995; Garthwaite, 2008). Also, nitric oxide can serve as a link between monoaminergic and glutamatergic synaptic extrasynaptic transmission (Kiss and Vizi, 2001; Vizi et al., 2004).

Given that nitric oxide is freely diffusible and thus can readily enter adjacent neuronal cells or other cells, NOS enzymatic activity is exceptionally regulated (Snyder and Ferris, 2000). There are at least three different forms of this enzyme (Griffith and Stuehr, 1995): the endothelial that is responsible essentially for cardiovascular actions, the inducible form found originally in macrophages and involved mainly in immune processes and the neuronal NOS (nNOS), present mostly in neurons but also in mitochondria and chondrocytes. All NOS contain multiple regulation sites (Griffith and Stuehr, 1995; see also Garthwaite, 2008; Steinert et al., 2008 for review). Even though nearly all oxidative enzymes employ one electron donor, NOS is further complexed (Snyder and Ferris, 2000) since it possesses a tightly bound flavin adenine mononucleotide and dinucleotide, in addition to NADPH. It further utilizes heme and tetrahydrobiopterin as electron donors. NOS possesses sites for phosphorylation by the major phosphorylating enzymes, including cyclic AMP-dependent protein kinase, protein kinase C, calcium-calmodulin-dependent protein kinase, and cyclic guanosine monophosphate-dependent protein kinase (see Garthwaite, 2008; Steinert et al., 2008 for review). Hence, NOS must be activated every time a neuron releases nitric oxide, which is then released as soon as it is synthesized.

Neuronal NOS is a cytoplasmic enzyme (Garthwaite, 2008) that is expressed by discreet populations of neurons in the central nervous system (Vincent and Kimura, 1992). All nNOS interneurons express also nicotinamide adenine dinucleotide phosphate diaphorase (NADPH-d; Sancesario et al., 2004; see also Rushlow et al., 1995; Figueredo-Cardenas et al., 1996). Within the striatum, interneurons expressing nNOS are well characterized by cytochemical and physiological criteria (Kawaguchi, 1993; Kawaguchi et al., 1995, 1997). nNOS-containing interneurons represent only about 1% of neuronal cells in the brain (Sancesario et al., 2004; see also Rushlow et al., 1995; Figueredo-Cardenas et al., 1996). Because nNOS is not necessarily confined to pre- or post-synaptic specializations, nitric oxide can potentially be released from extensive extrasynaptic regions of nitrergic neurons (Philippides et al., 2005). Therefore, the somata and dendrites of nNOS cells represent potentially large sources of nitric oxide (see **Figure 1**).

Nitric oxide is an activity-dependent volume modulator, adapting intrinsic excitability and synaptic efficacy and modulating both active and inactive neuronal populations to the same physiological input (Gally et al., 1990; Philippides et al., 2005; Steinert et al., 2008). The proximity of the target cells is one factor that will determine the strength of the nitric oxide signal they receive. Even if the signal from a single small nitric oxide source is very local, multiple active sources can cooperate to cover large tissue volumes with nitric oxide concentrations that exceed those generated at the surface of a singly active source (Philippides et al., 2005). The proximity of the nitrergic inputs to dopaminergic inputs on medium spiny neurons in the striatum (Hidaka and Totterdell, 2001) suggests an important role for nitric oxide transmission in modulating the responsiveness of medium spiny neurons to afferent drive (for review see West et al., 2002). This consideration raises the possibility that the topography of nNOS-containing cells and the degree of their overlap with dopaminergic neurons may be of functional significance.

Dopamine neurons are easily identified by the presence of TH(+), a rate-limiting enzyme for catecholamine synthesis that catalyzes the conversion of tyrosine to L-DOPA, the first step in catecholamine neurotransmitter production (Hökfelt et al., 1976, 1977). TH(+) immunoreactive fibers and neurons are generally regarded as dopaminergic (Bouyer et al., 1984). In the brain, the synthetic enzyme for nitric oxide in neurons, the nNOS, is easily identified (Kawaguchi, 1993; Rushlow et al., 1995; Figueredo-Cardenas et al., 1996). Abundant evidence indicates interaction between nitrergic and dopaminergic systems playing an important role in the control of motor function and in the context of neurodegenerative diseases, such as Parkinson's (Galati et al., 2008; Gomes et al., 2008) and L-DOPA-induced dyskinesia (Padovan-Neto et al., 2009, 2011; Novaretti et al., 2010; Yuste et al., 2011; Takuma et al., 2012; for review see Jenner, 2008; Del Bel et al., 2011; Iravani and Jenner, 2011; Pierucci et al., 2011; West and Tseng, 2011; Iravani et al., 2012). A similar localization/interaction in either neuronal compartment would reinforce the suggestion, whereby nitric oxide influences the outcome of a movement, perhaps, opening new strategies for novel therapeutic regimes.

Our aim is to explore the hypothesis that the spatial relationships between either axons or somata of the nitric oxide and dopaminergic cells may represent selective associations between the nitrergic and dopaminergic systems. For this purpose, the dual localization of immunoreactivity for NOS and tyrosine hydroxylase in neurons of the nigrostriatal pathway in the rat brain was examined by means of a double-immunohistochemical method and confocal laser scanning microscopy (CLSM).

MATERIALS AND METHODS

ANIMALS

Adult male *Wistar* rats (200–250 g) were housed in groups of five per cage in a temperature-controlled room (23°C), under 12 h light-dark cycles with free access to food and water. Experiments were conducted according to the principles and procedures described by the Guidelines for the Care and Use of Mammals in Neuroscience and Behavioral Research (ILAR, USA) and Guidelines from the School of Medicine (USP, Brazil). The institutions housing conditions and experimental procedures were previously approved by the local Animal Ethics Committee.

TISSUE PROCESSING

Rats were deeply anesthetized with urethane (25 mg/kg) and then rapidly perfused transcardially with 250 ml of cold saline and 400 ml of 4% paraformaldehyde (PFA) in 0.1 M phosphate buffer (pH 7.4). Brains were immediately removed and fixed in 4% PFA for 24 h and cryoprotected in 30% sucrose solution. Brains were snap frozen in isopenthane (−40°C, Sigma) and stored at −70°C till use. The tissues were cut at 40 μm on a cryostat. Sections through the brain regions were collected in 0.01 M PBS solution containing 0.02% sodium azide and stored at 4°C until use.

IMMUNOHISTOCHEMISTRY REACTION

Herbison et al. (1996) reported the production and specificity of the K205 sheep anti-rat nNOS antibody and, in particular, noted that it detects one main protein with a molecular mass of 155 kDa in the rat brain. To assess antibody specificity within the rat brainstem, liquid phase adsorption experiments were undertaken in the present study by incubating the K205 at working dilution (1:5000) with recombinant rat nNOS (1 mM) overnight at 4°C and then carrying out immunocytochemistry on brainstem sections using the adsorbed antiserum in parallel with the normal K205 (Simonian and Herbison, 1996). These experiments showed that all immunoreactivity was abolished by adsorption of the K205 antiserum.

Immunohistochemistry was performed using a standard peroxidase-based method (Gomes et al., 2008). The sections were incubated with the TH-specific primary antibody (1:2000, Pel Freez, Rogers, AR, USA) overnight at 4°C, followed by biotinylated secondary antibody (Vectastain ABC kit, Vector Laboratories) and HRP-conjugated streptavidin (Vectastain ABC kit, Vector laboratories) incubation. The sections were developed using diaminobenzidine as the chromogen, mounted on slides and cover slipped for subsequent microscopic observation. Structure localization was determined with the help of the Paxinos and Watson (1999). Images containing TH immunostaining were captured with a digital Olympus DP70 camera mounted on a wide field microscope. Immunoreactive cells in a field of 1.02 mm × 0.78 mm were then counted using the image processing and analysis software package Image J.

Double-immunolabeling was carried out in the same brain region to characterize nNOS and TH expression. The sections were incubated overnight at 4°C with an anti-TH antibody (1:1000, Pel Freez, Rogers, AR, USA) followed by a 2 h incubation at room temperature with a secondary donkey anti-mouse IgG (H + L) antibody coupled to Alexa Fluor 488 (1:250; Invitrogen, Scotland, UK). After TH labeling, the tissue was washed three times with PBS and incubated overnight with a polyclonal antibody specific for rat nNOS (1:1000; sheep anti-nNOS, K205, gift of P. Emson, Cambridge, UK). The primary nNOS antibody was then revealed with a Cy3-coupled donkey anti-sheep IgG (H + L; 1:250; Jackson Immuno Research, USA). The primary antibodies were diluted in PBS (0.1 M; pH 7.4) containing 0.02% thimerosal, 5% normal goat serum (NGS, Jackson Immuno Research, USA), 0.2% Triton X-100, while the secondary antibodies were diluted only in PBS (0.1 M; pH 7.4).

Controls for the fluorescent double-labeling experiments involved the omission of one of the primary antibodies in the presence of the other and both secondary antibodies. In these experiments, neither Cy3 nor Alexa Fluor 488 staining was apparent on cells when either the TH or the nNOS antiserum was omitted. Double-stained sections were analyzed using a fluorescence microscopy setup (Nikon, Japan) equipped with a 60x objective (numerical aperture 1.4) and connected to an image analysis system (Mercator, Explora Nova, La Rochelle, France). A total of six sections of each selected brain region, encompassing rostral, middle, and caudal levels of the striatum, subthalamic nuclei, substantia nigra *pars* compacta and reticulate, ventral tegmental

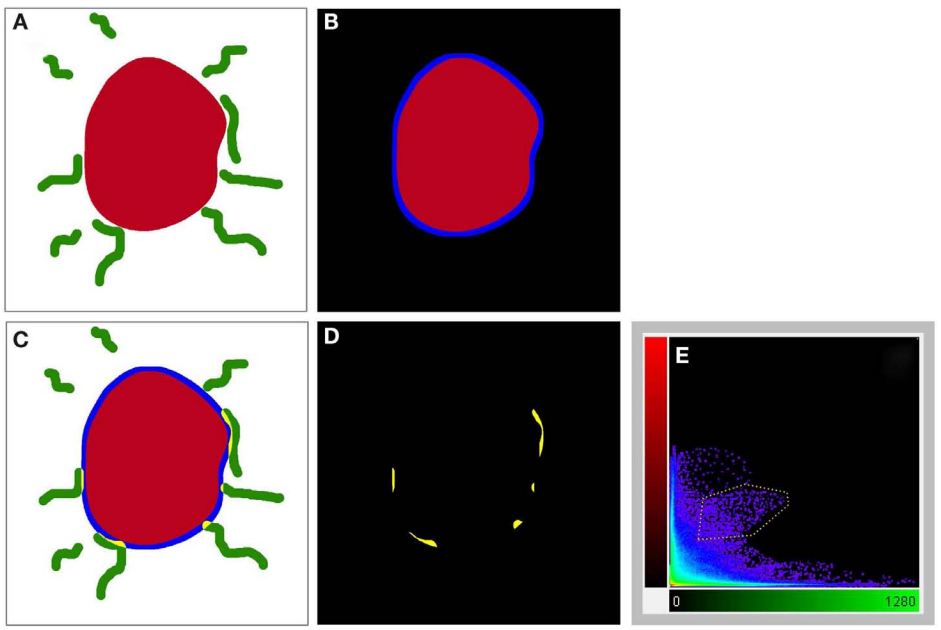

FIGURE 2 | A schematic illustrating the method used to visualize processes present in the cell periphery. The cell body (red) was thresholded **(A)** to generate a binary mask and then enlarged [blue line in **(B,C)**] to occupy an additional 2 μm around its periphery. Areas occupied within the blue periphery by the green processes are shown in [**(C,D)**; yellow areas]. In **(D)**, only the pixels where processes are within the 2 μm proximity of the cell body are shown. A 2D scatter plot **(E)** was generated using Imaris 7.5 (Bitplane) revealing a pixel population (outlined with yellow line) with correlating intensities (Pearson ∼0.7), out of which a new channel was generated.

area, and pedunculopontine nuclei were examined, as previously described (Debeir et al., 2005).

CELL NUCLEI LABELING

A fluorescent stain that labels DNA and allows for easy visualization of the nucleus in interphase cells and chromosomes in mitotic cells is 4′,6-diamidino-2-phenylindole (DAPI, Chazotte, 2011). DAPI (10 mg/mL in H_2O stock solution; Invitrogen D1306) was diluted 1:5000 with PBS (DAPI labeling solution). The slides were incubated for 1–5 min at room temperature in DAPI labeling solution. The slides were rinsed three times in PBS^+ and the coverslips mounted (Chazotte, 2011).

CONFOCAL LASER SCANNING MICROSCOPY

Sections double-stained for nNOS and TH were inspected using a Leica SP2 and Leica SP5 confocal laser scanning microscopes (both Leica Microsystems, Wetzlar, Germany). Z-stacks of the frontal cortex were acquired with a 40× oil objective (1.25NA, HCX PL APO CS), while regions from the striatum and substantia nigra were acquired at the optical resolution limit (43 nm × 43 nm × 130 nm) with a 63× (HCX PL APO) oil objective and subsequently deconvolved with AutoQuant®X (Ver. X2.2.1, Media Cybernetics, MD, USA) to obtain an improved signal-to-noise ratio. The Alexa Fluor 488 fluorophore (Abs = 495 nm, Em = 519 nm) was excited with the 488 nm laser line of an Ar-laser, while the *Cy*3 fluorophore (Abs = 550 nm, Em = 570 nm) was excited at 561 nm, with emission being collected in a line-by-line fashion at 500–530 and 570–650 nm, respectively.

TYROSINE HYDROXYLASE AND NITRIC OXIDE SYNTHASE-POSITIVE STRUCTURES PROXIMITY ANALYSIS

For the ensuing analysis, cells were chosen whose the major, longitudinal axis is orthogonal with respect to the *z*-axis of the stack. A maximum intensity projection was then generated with Fiji software package (Walter et al., 2010) from the nNOS(+) and TH(+) channels, respectively, based on a 5 μm-thick optical section centered at the widest *z*-position of the cell body. Binary masks were then generated from both maximum projection types (schematic representation in **Figure 2A**). Fiji was then used to grow the binary mask of the cell body such that the resulting area covered an additional 2 μm-wide margin at the periphery of the nNOS(+) immunoreactive cell body (blue margin in **Figure 2B**). The expanded binary mask depicting the cell body was added to the mask representing the fibrous structures (**Figure 2C**). In a final step, pixels within this newly generated margin that were positive for both, nNOS(+) and TH(+) immunoreactivity were identified (yellow pixels in **Figures 2C,D**). Imaris 7.4.2 (Bitplane) was used to generate 3D representations of the respective z-stacks and for colocalization analysis (**Figure 2E**).

RESULTS

Both hemispheres of all animals showed a similar distribution pattern of the TH(+) and nNOS(+) immunoreactive cells and fibers within the striatum-nigra pathway. Using CLSM optical sections acquired at the resolution limit, colocalized regions (Pearson correlation coefficient ≥0.7) were identified (yellow). The yellow pseudo-color for these structures visible in CLSM images could represent the superimposition of TH(+) immunoreactivity (green) on nNOS(+) immunoreactivity (red) neurons/fibers and *vice versa*. Assessment of sections double-stained for nNOS(+) and TH(+) immunoreactivity revealed a considerable overlap of their topographies. The distribution of nNOS(+) immunoreactivity is generally in agreement with the data published by others using either an immunocytochemical (Bredt et al., 1990; Schmidt et al., 1992; Egberongbe et al., 1994; DeVente et al., 1998) or a histochemical approach (Vincent and Kimura, 1992; Southam and Garthwaite, 1993).

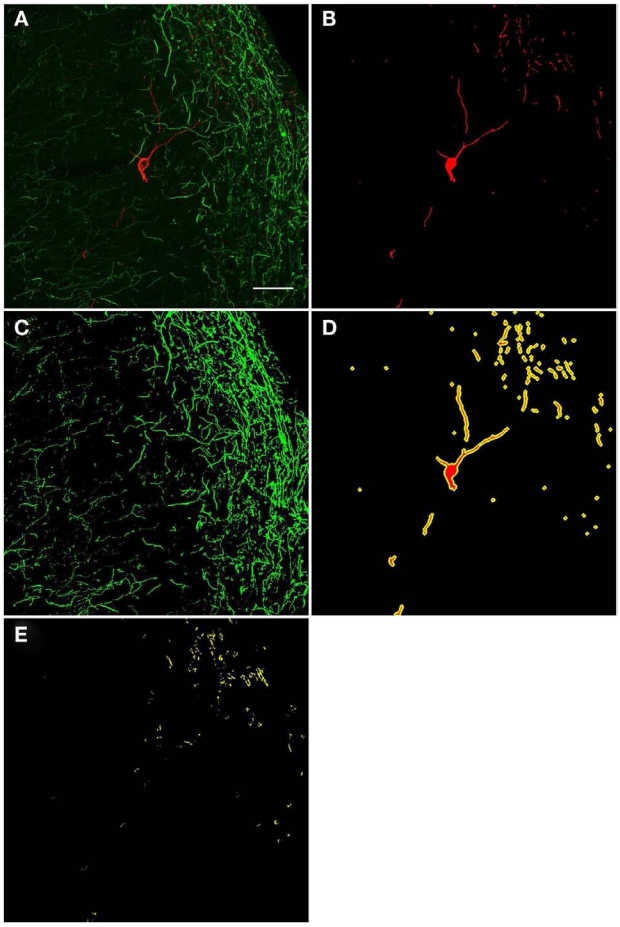

FIGURE 3 | Confocal laser scanning microscopy of TH(+) and nNOS(+) double-immunostained sections from the rat cingulate cortex. The TH(+) immunoreactivity **(A,C)** is shown in green, whereas the nNOS(+) immunoreactivity **(A,B)** is red, in the same double-stained section. In **(B,C)**, the binary masks of the nNOS(+) and TH(+) signals are shown, respectively, while **(D)** additionally shows the 2 μm-wide periphery (yellow) of the nNOS(+) cell body and processes (red). The yellow areas in **(E)** indicate the location of TH(+) processes within the 2 μm periphery of the nNOS(+) cell. There is absence of complete colocalization between nNOS(+) and TH(+) immunoreactivity in the rat cortex but a large number of fibers are present within the 2 μm nNOS(+) cell periphery. Scale bar is 50 μm.

CORTEX

The prefrontal, anterior cingulate, insular, piriform, perirhinal, entorhinal, motor, premotor, parietal, temporal, and posterior

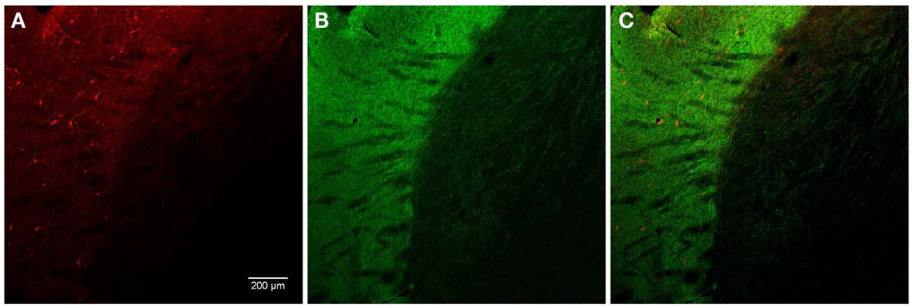

FIGURE 4 | Photomicrographs of nNOS(+) immunoreactive neurons (A) and TH(+) nerve fiber (B) in sections from the caudate–putamen/globus pallidus [merge in (C)]. nNOS(+) immunoreactive neurons appear polygonal or fusiform in shape with long smooth dendrites and a plexus of nerve fibers in the neuropil. The low-power photomicrograph shows the intense staining of the TH(+) immunoreactivity and the large number of nNOS(+) cell body in the caudal striatum. Scale bar = 200 µm.

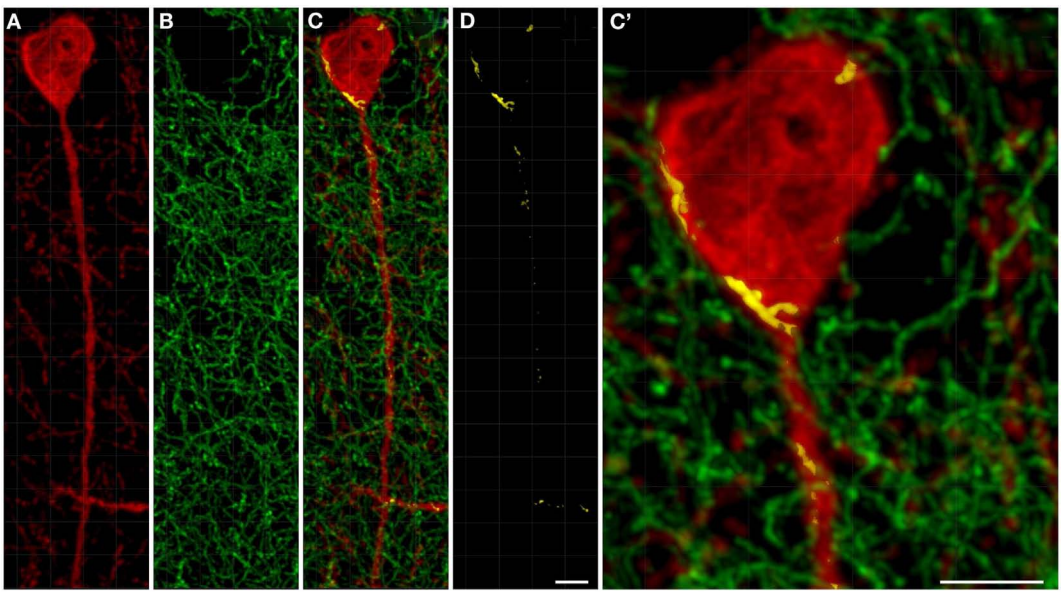

FIGURE 5 | Confocal laser scanning microscopy of TH(+) and nNOS(+) immunoreactive double-immunostained sections from the rat striatum. Fibers immunoreactive for TH(+; green) are presented in **(B,C,C')**. A neuron immunoreactive for nNOS(+)(red) is presented in **(A,C,C')**. Using CLSM optical sections acquired at the resolution limit, colocalized regions (Pearson correlation coefficient of ≥0.7) were identified (yellow). The yellow areas in **(C,D,C')** also indicate the location of TH(+) processes within the 2 µm periphery of the nNOS(+) cell. Detail of the cell body is presented in **(C')**. In the rat striatum a large number of TH(+) fibers are present within the 2 µm nNOS(+) cell body. Scale bar in **(D,C')** = 5 µm.

cingulate cortices had a dense distribution of TH(+) immunoreactive fibers. A small population of medium-large, intensely nNOS(+) immunoreactive multipolar neurons was found scattered throughout layers 2–4 of all examined cortices. The reaction product for nNOS(+) immunohistochemistry in the cortical neurons formed dense, conspicuous masses with no nuclei labeling.

A qualitative analysis of the area 2 µm proximal to the nNOS(+) cell body was carried out (**Figure 3**) in the anterior cingulate cortex (Bregma 0.797–0.251, Paxinos and Watson, 2009). The TH(+) immunoreactivity (**Figures 3A,C**) is shown in green, whereas the nNOS(+) immunoreactivity (**Figures 3A,B**) is red, in the same double-stained section. In **Figures 3B,C**, the binary masks of the nNOS(+) and TH(+) signals are shown, respectively. The yellow area in **Figure 3D** represents the 2 µm periphery of the nNOS(+) cell. **Figure 3E** shows only areas where the TH(+) immunoreactive cell body or processes are located within the 2 µm proximity of the nNOS(+) immunoreactive cell body or processes thereof.

STRIATUM

In general, nNOS(+) immunolabeling was detected in the cytoplasmic domains of the cell body and dendrites. The nucleus was unstained and the reaction product was evenly distributed in the cytoplasm. A dense network of NOS(+) varicose fibers was observed in the striatal complex. TH(+) immunohistochemistry

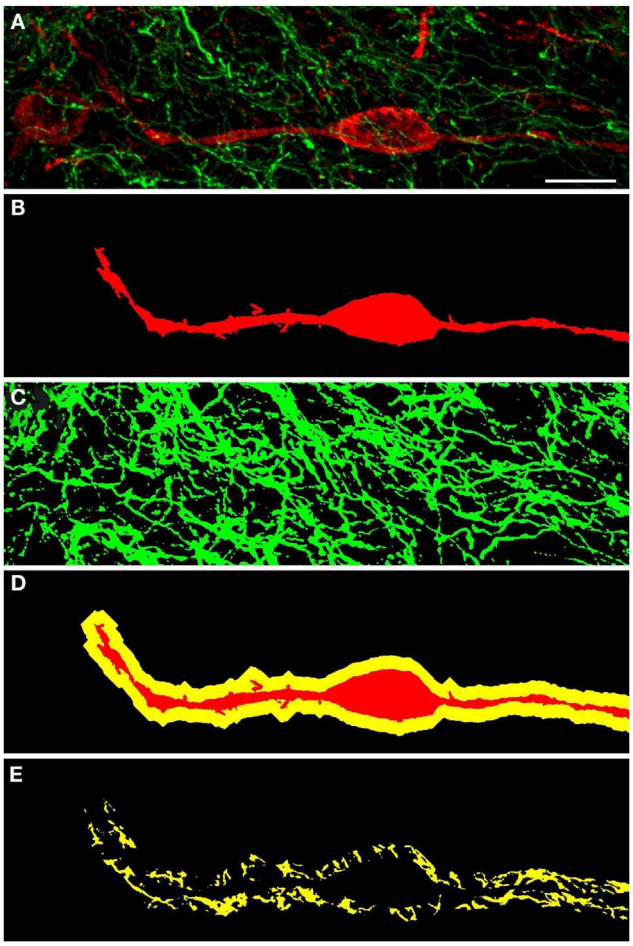

FIGURE 6 | Confocal laser scanning microscopy of TH(+) and nNOS(+) immunoreactive double-immunostained sections from the rat striatum: a proximity analysis study. Distribution pattern of immunoreactivity for TH(+) and a nNOS(+) in double-stained sections of the striatum. Both, nNOS (red) and TH (green) fluorescent signals are shown in **(A)**, while **(B,C)** show the corresponding binary masks. The 2 μm periphery (yellow) is shown in **(D)** and the area occupied by TH(+) immunoreactive fibers around the nNOS(+) immunoreactive cell body is shown in **(E)**. The yellow areas in E indicate the location of TH(+) and nNOS(+) possible interaction. Scale bar in **(A)** is 10 μm.

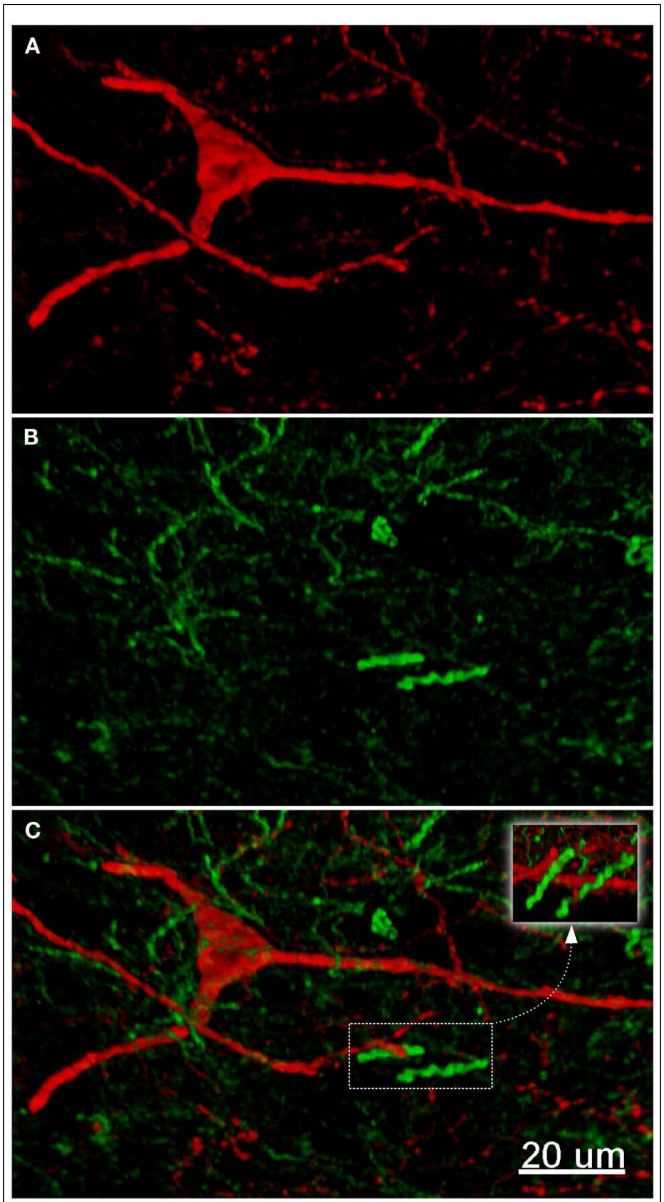

FIGURE 7 | The fluo escence pattern in a double-stained section of the nucleus accumbens, showing nNOS(+) [(A,C) – cell body) and TH(+) [(B,C) axons] immunoreactivities. Immunoreactivity for TH(+) and a nNOS(+) in double-stained sections of the nucleus accumbens. Both, nNOS (red) and TH (green) fluorescent signals are shown in **(C)**. Whereas the TH(+) fiber immunoreactivity appears homogeneously distributed throughout the whole nuclei, the nNOS(+) immunoreactive neurons and fibers are stained much more sparsely. Scale bar in **(A)** = 10 μm, it applies to **(B,C)** also.

demonstrated TH(+) immunoreactive terminals or varicose fibers in the neuropil of the striatum (**Figures 4**, **6C**, and **8D**).

TH(+) immunolabeling in the striatum appeared as a dense, inhomogeneous plexus of fibers with an absence of cell bodies at any level (see Moss and Bolam, 2008). Several punctate structures (**Figures 5C,C′,D** and **6D,E**; yellow dots) showing TH(+) immunoreactivity and nNOS(+) were in close contact. They were surrounding either the cell bodies or the cell processes (see **Figures 5** and **6**). The yellow areas in **Figures 5C,D,C′** also indicate the location of TH(+) processes within the 2 μm periphery of the nNOS(+) cell. Detail of the cell body is presented in **Figure 5C′**.

The nucleus accumbens (ventral striatum) displayed TH(+) immunoreactivity and nNOS(+) immunoreactivity similar to that of the dorsal striatum (**Figure 7**). There was a range of nNOS(+) cell body shapes, from which two to four smooth and extensive, poorly branching dendrites emanated, similar to those described by Hussain et al. (1996). The nNOS(+) immunoreactive cells were of medium size, fusiform and spiny interneurons with long, poorly branched dendrites that comprise only a small percentage of the striatal neuronal population.

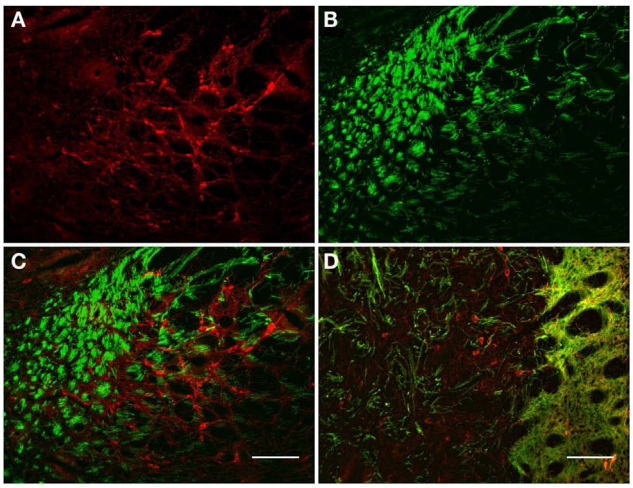

FIGURE 8 | Internal globus pallidus [entopeduncular nucleus-(A,B), merge in (C)] and external globus pallidus (D) photomicrographs of nNOS(+) immunoreactive neurons and TH(+) nerve fibers (A–C) TH(+) and nNOS(+) immunoreactive fiber staining representative of the typical honeycomb-like pattern in the entopeduncular nucleus [merge in **(C)**]. TH(+) immunoreactivity corresponds to the medial forebrain bundle. **(D)** Photomicrography of nNOS(+) immunoreactive neurons and TH(+) nerve fibers (merge) from a section of the external globus pallidus/caudal striatum. Note the nNOS(+) immunoreactive cells (red), the dark staining surrounds areas of lighter immunoreactivity (external globus pallidus) and the dense TH(+) fibers in the striatum. nNOS(+) immunoreactive neurons appear polygonal in shape with long smooth dendrites and a plexus of nerve fibers in the neuropil. Scale bars, 100 μm.

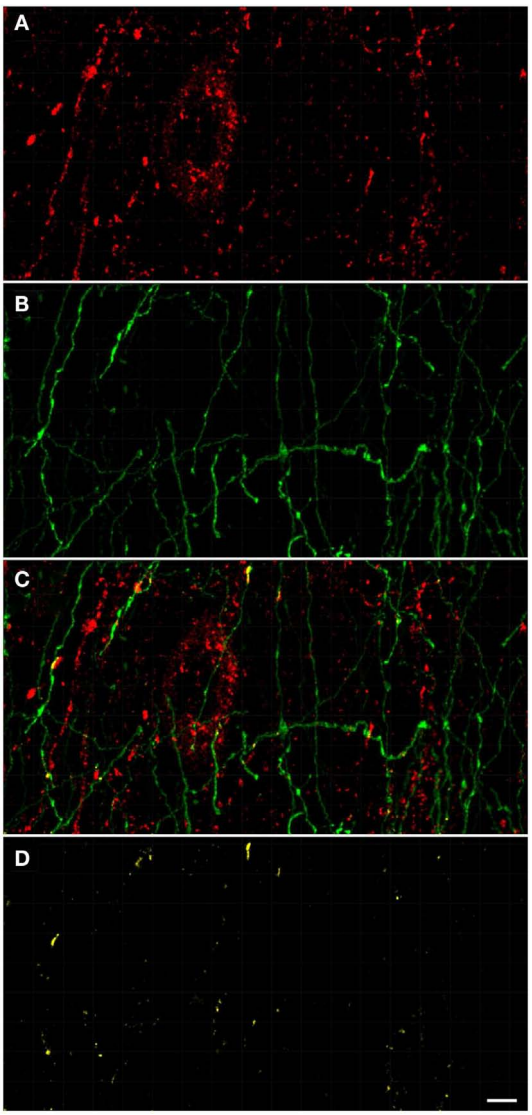

FIGURE 9 | Confocal laser scanning microscopy of the external globus pallidus in TH(+) and nNOS(+) immunoreactive double-immunostained sections. The axons are immunoreactive for TH(+) [green, **(B,C)**] and the neurons/axons immunoreactive for NOS(+) [**(A,C)**, red] in double-stained sections of the external globus pallidus. Both, TH(+) and nNOS(+) immunoreactivities are presented in **(C)**. Observe the lower fluorescence of nNOS(+) immunoreactive cells surrounded by areas of lighter immunoreactivity of the TH(+)fibers. The nNOS(+) immunoreactivity delineating a neuronal cell body structure is covered by dots of TH(+) immunolabeling in yellow **(C,D)**. Using CLSM, zones of cellular colocalization were ascertained [yellow, **(C,D)**]. Scale bar is 25 μm.

GLOBUS PALLIDUS EXTERNAL AND INTERNAL (ENTOPEDUNCULAR NUCLEI)

The TH(+) and nNOS(+) immunoreactivity double-labeling in the pallidus external and internal (entopeduncular nucleus in the rat) is presented in **Figures 8** and **9**. In the internal globus pallidus we observed clusters of numerous NOS(+) cell bodies. TH(+) and nNOS(+) immunoreactivity in the fiber staining represent a typical honeycomb-like pattern (**Figure 8**). TH(+) immunoreactivity corresponds to the medial forebrain bundle. In **Figure 8D**, note the nNOS(+) immunoreactive cells (red) in the external globus pallidus and the less intense staining surrounding areas of lighter immunoreactivity. nNOS(+) immunoreactive neurons appear polygonal in shape with long smooth dendrites and a plexus of nerve fibers in the neuropil.

In the external globus pallidus (**Figures 8D** and **9**), there is a distinct punctuate pericellular nNOS(+) labeling of the whole neuronal soma and dendritic/axonal processes (**Figure 9**). TH(+) fibers make multiple contacts onto the nNOS(+) immunoreactive delineated structure. Using CLSM, zones of cellular colocalization were ascertained (yellow, **Figures 9C,D**).

SUBSTANTIA NIGRA/VENTRAL TEGMENTAL AREA

Most TH(+) immunoreactivity is grouped in the substantia nigra *pars* compacta, where it is spread forming a dense band that lies dorsally from the ventral tegmental area (see **Figure 10**). In the substantia nigra *pars* reticulata particularly in its medial two-thirds, a few TH(+) immunoreactive cells are present, some of them arranged in linear bridges which cross the substantia nigra *pars* reticulata perpendicularly to the substantia nigra *pars* compacta (see **Figure 10B**). nNOS(+) immunoreactive neurons appear occasionally in the substantia nigra *pars* compacta, stained much more sparsely, with long smooth dendrites (**Figures 10A,B**). In the substantia nigra *pars* compacta we found a dense pattern of TH(+) immunoreactive cells and fibers next to a small

number of fibers and cell somata with strong NOS(+) immunoreactivity (**Figures 10A,B**). A double-labeled cell is visualized in **Figure 10C** but cell colocalization between nNOS(+) and TH (+) immunoreactivity is almost absent.

TH(+) immunoreactive and NOS(+) immunoreactive cells could be observed adjacent to each other, with areas of perfect match (**Figure 11**). Fibers and cell bodies are in close proximity (**Figure 11**). **Figure 11** presents in further detail a nNOS(+) immunoreactive neuron surrounded by TH(+) immunoreactive fibers. The yellow area in **Figure 11D** represents the 2 μm periphery of the nNOS(+) neuron. In a further step, the area within this 2 μm periphery is visualized, where TH(+) processes are present (**Figure 11E**). Zones of colocalization were demonstrated in a single optical section of the substantia nigra compacta acquired at the resolution limit. Actual colocalization between the two markers was rarely observed. In **Figure 11E** the area occupied by the TH(+) processes within the 2 μm proximity is visualized.

SUBTHALAMIC NUCLEUS

Functional importance of the subthalamic nucleus neurons is reflected by its anatomical connections to the main output nuclei of the basal ganglia, including both segments of the globus pallidus and the substantia nigra. In the subthalamic nucleus we observed numerous NOS(+) immunoreactive cell bodies and an intense pattern in the TH(+) immunoreactive fiber staining (**Figure 12**), corresponding to the medial forebrain bundle. nNOS(+) immunoreactive neurons appear massively at the subthalamic nuclei with long smooth dendrites. A very small proportion of subthalamic nucleus neuronal somata were apposed by immunoreactive axons (**Figure 12**-insect). The cell nuclei are labeled with DAPI. Colocalization between the two markers was almost absent.

PEDUNCULOPONTINE TEGMENTAL NUCLEUS

The pedunculopontine tegmental nuclei are a loosely defined aggregate of cholinergic and non-cholinergic neurons in the midbrain which neurons project to substantia nigra compacta dopaminergic neurons. Our observations revealed clusters of intensely labeled NOS(+) immunoreactive neurons (**Figures 13A,C**) and TH(+)immunoreactive fibers (**Figures 13B,D**) in the pedunculopontine tegmental nucleus (**Figure 13**). Double-labeling experiments indicate that the majority of TH(+) immunoreactive neurons in the pedunculopontine tegmental nucleus did not express NOS(+) immunoreactivity. However, fibers and cell bodies are in close proximity (**Figure 13D**).

DISCUSSION

We compared the spatial relationship between dopaminergic and nitrergic nigrostriatal fibers/cell body through the dual localization of the immunoreactivity for nNOS(+) and TH(+). The approach was based on double-immunohistochemical staining method using CLSM optical sections acquired at the resolution limit. A proximity analysis of TH(+) and nNOS(+) structures was done using binary masks generated from the respective maximum projections and revealed regions positive for both, nNOS(+)

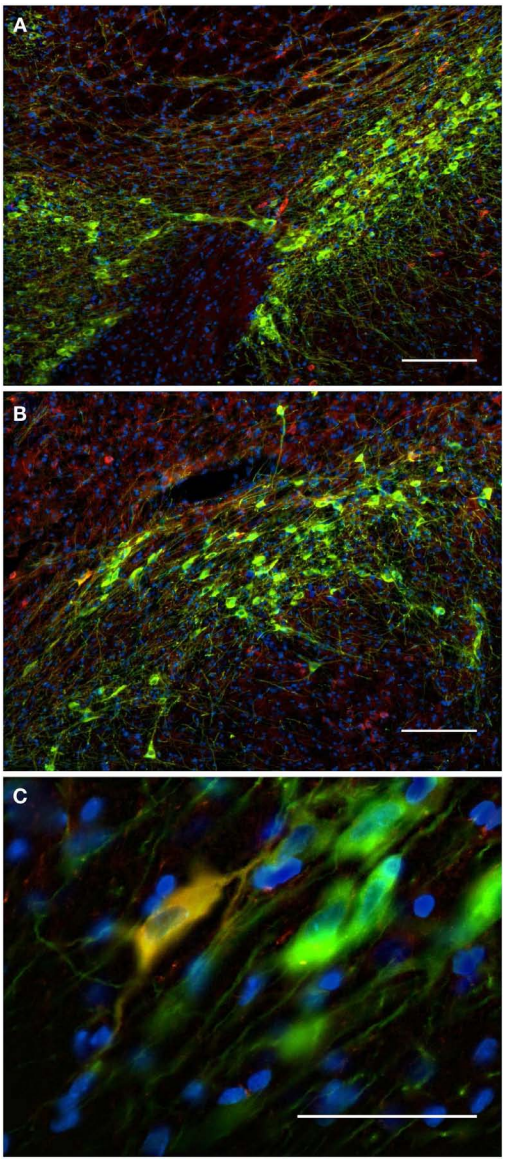

FIGURE 10 | The substantia nigra compacta and ventral tegmental area nNOS(+) and TH(+) immunoreactive neurons and fibers Distribution pattern of axons/cells immunoreactive for nNOS(+) **(A)** and TH(+) **(B)** in double-stained sections of the substantia nigra [**(C)**, merge]. Cell nuclei are labeled in blue with DAPI. Using CLSM **(A–C)**, zones of cellular colocalization were demonstrated in a single optical section of the substantia nigra compacta [**(C)**, scale bar is = 5 μm]. Observe the dense staining of the TH(+) immunoreactive cells and fibers homogeneously distributed throughout the substantia nigra compacta and the ventral tegmental area **(A)**. In the substantia nigra, dopaminergic cells are arranged in two bands (Fallon and Loughlin, 1995). The substantia nigra reticulate caudoventral emits cell bridges that make contact with the substantia nigra compacta rostrodorsal [González-Hernández and Rodríguez, 2000; **(A,B)**]. The substantia nigra compacta is characterized by a high density of dopaminergic somata as well as a dense network of overlapping dopaminergic dendrites. Scattered neurons in both substantia nigra compacta and reticulata display immunoreactivity to nNOS [Rodrigo et al., 1994; **(A,B)**]. Cell colocalization between nNOS(+) and TH (+) immunoreactivity is almost absent but a double-labeled cell is visualized in **(C)**. Scale bars, 50 μm **(A–C)**.

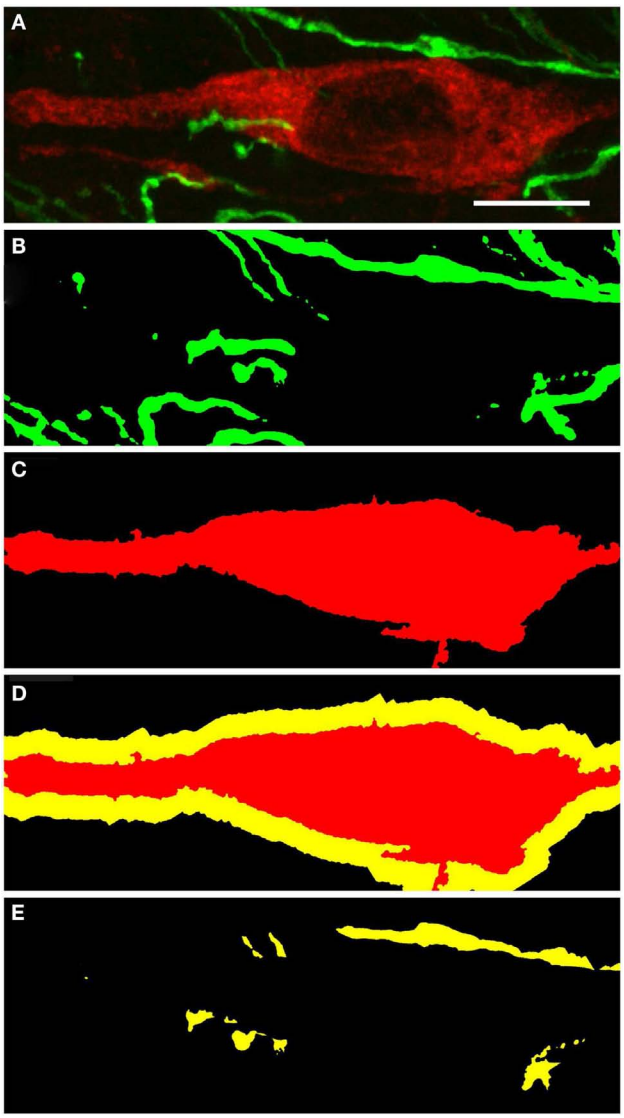

FIGURE 11 | Substantia nigra compacta nNOS(+) immunoreactive neuron and TH(+) fibers CLSM analysis of a double-immunostained section. **(A)** Show in detail a nNOS(+)immunoreactive neuron (red) surrounded by TH(+) immunoreactive fibers (green). **(B,C)** Show the binary masks of the TH(+) and nNOS(+) stains, respectively. In **(D)**, the 2 μm proximity of the nNOS(+) cell is shown, while in **(E)** the area occupied by the TH(+) processes within the 2 μm proximity is visualized. Zones of colocalization were demonstrated in a single optical section of the substantia nigra compacta acquired at the resolution limit. Scale bar 10 μm.

and TH(+) immunoreactivity, within a 2 μm-wide margin. Colocalized regions were identified with a Pearson correlation coefficient ≥0.7. A large proportion of nNOS(+) immunoreactive soma/axon/dendrite themselves were directly apposed by TH(+) immunoreactive ones, within a radius of 1 and 2 μm.

In the dopaminergic synapses, dopamine is released from presynaptic structures by exocytose, binds post-synaptic receptors and generates pre- and post-synaptic cascades of events (Bertorello et al., 1990; Beckstead et al., 2004; Jorgensen, 2004; Yao et al., 2008).

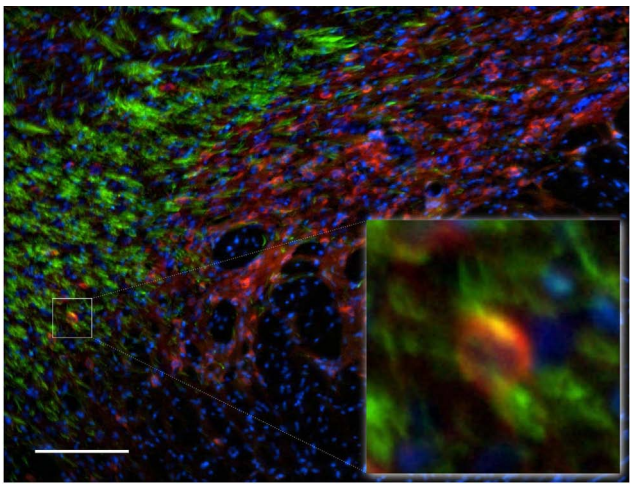

FIGURE 12 | Subthalamic nuclei of a control rat brain: distribution pattern of axons/cells immunoreactive for TH(+; green) and NOS(+; red) in double-stained sections. The cell nuclei are labeled with DAPI. Observe the dense staining of the TH(+) immunoreactive fibers of the medial forebrain bundle (green fibers). nNOS(+) immunoreactive neurons appear massively at the subthalamic nuclei with long smooth dendrites. The area occupied by TH(+) immunoreactive fibers around the nNOS(+) immunoreactive cell body is shown in the inset. Cell colocalization between nNOS(+) and TH (+) immunoreactivity is absent. Scale bar is 100 μm.

The discovery that dopamine is located not only in the terminals but also in perikarya and dendrites of nigrostriatal neurons led to the suggestion that dopamine may be released from dendrites in the substantia nigra (Bjorklund and Lindvall, 1975; more information in the review from Trueta and De-Miguel, 2012). Subsequent immunohistochemical investigations have confirmed that the synthesizing enzymes (Tyrosine hydroxylase), for this catecholamine are also present in the dendrites of these neurons, some of which extend ventrally into the substantia nigra pars reticulata (Hökfelt et al., 1984; Jaeger et al., 1984). Release of dopamine from cell bodies and dendrites is typically referred to as somatodendritic release. Somatodendritic release of dopamine in the substantia nigra compacta and axonal dopamine release in the dorsal striatum are both necessary for the expression of basal ganglia-mediated motor behaviors and various cognitive functions. Dendritically released dopamine may modulate striatal outflow and thereby play an important role in basal ganglia function (Robertson and Robertson, 1987). Nigral dopamine neurons do not only release their transmitter into the striatum, but also interact with each other through release of dopamine from their somata and dendrites (Centonze et al., 2003; Rice and Cragg, 2004, 2008; complementary information in the review from Trueta and De-Miguel, 2012).

As described by Cragg and Rice (2004), the sphere-of-influence of dopamine spillover in a concentration adequate to stimulate dopamine receptor has a radius of 2–8 μm (see also Gonon, 1997; Arbuthnott and Wickens, 2007; Moss and Bolam, 2008; Rice and Cragg, 2008). Dopaminergic boutons correspond to almost 10% of all striatal synapses (Groves et al., 1994; Kreitzer, 2009), and the nearest-neighbor space among dopaminergic boutons is only 1.18 μm (Arbuthnott and Wickens, 2007; Kreitzer, 2009).

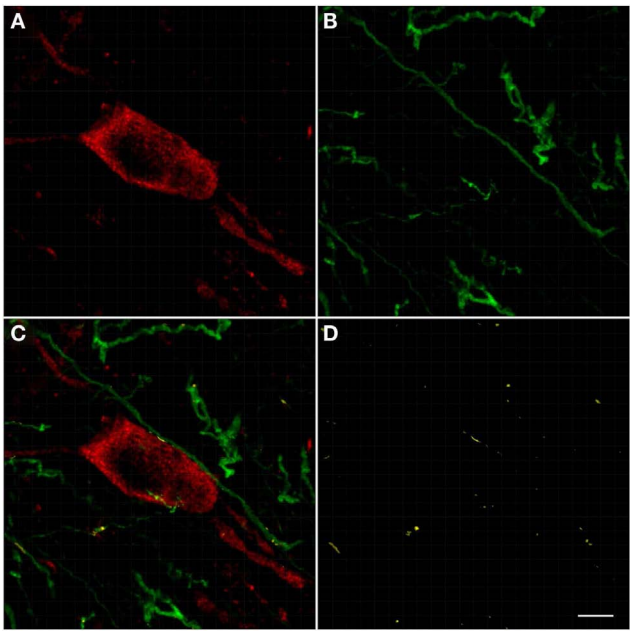

FIGURE 13 | Confocal laser scanning microscopy of the pedunculopontine nuclei in a TH(+) and nNOS(+) double-immunostained section. Distribution pattern of axons/cells immunoreactive for TH(+) [green in **(B,C)**] and NOS(+) [red in **(A,C)**] is presented in this double-stained section. Observe the nNOS(+) immunoreactive neurons surrounded by sparse TH(+) fibers. TH(+) immunoreactive fibers appear scattered all around the cell soma. Scale bar 50 μm. Scale bar in **(D)** is 5 μm.

Nitric oxide at high concentrations can be used to mediate physiological responses in a restricted area over short periods (Kiss and Vizi, 2001; Kiss et al., 2004). It is predicted that the physiological volume of influence of a single source of nitric oxide that emits for 1–10 s has a diameter (in theory) of about 20 mm, corresponding to a volume of brain enclosing two million synapses (Wood and Garthwaite, 1994). Tornieri and Rehder (2007) demonstrated that nitric oxide has physiological effects at distances of up to 100 μm (Tornieri and Rehder, 2007). It was described by Ignarro (2010) that nNOS(+) immunoreactive neurons in the microenvironment could accomplish nitric oxide levels 100 times higher than required to stimulate for example, vasorelaxation of vascular smooth muscle cells. As described by Garthwaite and Boulton (1995), nitric oxide generated at a single point source should be able to influence function within a sphere with a diameter of 300–350 μm, even with a half-life of a few seconds, which is very large compared with the dimensions of a synapse. Taking into account some of the known radical scavenging properties of the tissues, Beckman and Koppenol (1996) reported the approximate ranges of diffusion for nitric oxide to be approximately 130 μm (Bidmon et al., 2001). Since medium-sized neurons are usually 10–25 μm in diameter, it becomes obvious that nitric oxide may diffuse into many cells

Therefore, our findings demonstrated that every nitric oxide molecule will be within overlapping spheres-of-influence of synaptically released dopamine in all the analyzed brain regions. Nitric oxide structures are likely to be within reach of a concentration of dopamine that is high enough to stimulate both high and low affinity receptors (Rice and Cragg, 2008). The topography of nNOS(+) and TH(+) immunoreactive cells and the degree of their overlap may be of functional significance.

Our observations are in agreement with Fujiyama and Masuko (1996); Simonian and Herbison (1996); DeVente et al. (2000); Hidaka and Totterdell (2001); Benavides-Piccione and DeFelipe (2003). In many cases, nitrergic terminals are closely apposed to TH(+) immunoreactive neuronal endings and both converge onto dendrites of spiny neurons (Hidaka and Totterdell, 2001). Alternatively, TH(+) immunoreactive neurons form direct synaptic contacts with nNOS(+) immunoreactive neurons (Hidaka and Totterdell, 2001). Fujiyama and Masuko (1996) simultaneously demonstrated NADPH-d reactivity and TH(+) immunoreactivity within the same section of the rat striatum using electron microscopy. Symmetrical and asymmetrical synaptic contacts were found on cell bodies and proximal dendrites. Other extrasynaptic TH(+) immunoreactive boutons were occasionally associated with unlabeled terminals adjacent to the NADPH-d positive dendrites (Fujiyama and Masuko, 1996). Double-labeling techniques showed that a small population of NOS(+) neurons in the medulla also contained immunoreactivity to the aminergic neuron marker TH (Dun et al., 1994). Also, occasionally double-labeling for nNOS(+) and TH(+) could be observed in some neurons in rat primary mesencephalic cultures (Salum et al., 2008). In contrast, Klejbor et al. (2004) found numerous TH(+) and NOS(+) immunoreactive neurons in the ventral tegmental area. The presence of nNOS(+) immunoreactive cell staining in the rat entopeduncular nucleus, with typical honeycomb-like pattern in the nucleus was hardly ever described before (Del Bel et al., 2011). Most frequently, in the external globus pallidus, the presence of nNOS(+) neurons was described as almost absent. However, in the external globus pallidus, we observed nNOS(+) immunoreactivity, with a distinct punctuate pericellular labeling which seems to correspond to the neuronal soma and/or dendritic/axonal processes. TH(+) fibers make multiple contacts onto the nNOS(+) immunoreactive delineated structure. It is curious that Arellano et al. (2004) and Castro et al. (2011) have shown similar pericellular pattern of parvalbumin-positive labeling cells in the hippocampus of epileptic patients.

These anatomical arrangements facilitate nitric oxide-mediated modulation of pre- and post-synaptic events such as dopamine release (Hanbauer et al., 1992; Sancesario et al., 2000; West and Grace, 2000; DiGiovanni et al., 2003; DiMatteo et al., 2009; Park and West, 2009). Studies showing that nNOS(+) immunoreactive interneurons facilitate the concurrent release of dopamine and glutamate by a nitric oxide-dependent process (West and Galloway, 1997; West and Grace, 2000; Park and West, 2009), suggest that nitric oxide might contribute in the integration of convergent motor information in striatal networks (West and Grace, 2000). As gap junction permeability between medium-sized, densely spiny neurons can be modulated by dopamine in the nucleus accumbens (O'Donnell and Grace, 1993), and by nitric oxide in the dorsal striatum (O'Donnell and Grace, 1997), these inputs may act together to modulate activities of individual projection neurons by means of conventional chemical synapses, or may influence

electrotonic transmission between networks of neurons connected by gap junctions.

Consequently, even though we generally did not find soma colocalization in the analyzed regions, the implications of this finding are far-reaching. The ultimate distribution of dopaminergic and nitrergic structures in the nigro-striatal pathway is unlikely to be a targeted phenomenon, suggesting that the populations of TH(+) and NOS(+) immunoreactive neurons interact with each other in all analyzed regions. Together, our observations corroborate evidence of dopamine and nitric oxide being intertwined in the anatomy in addition to physiology and pathology of the nigrostriatal pathway (Del Bel et al., 2005, 2011; Jenner, 2008; Pierucci et al., 2011; West and Tseng, 2011; Iravani et al., 2012).

Nitric oxide (Calabresi et al., 1999) and dopamine (Calabresi et al., 2000) are essential for the expression of synaptic plasticity, although the effects of nitric oxide may not be restricted to synaptic release sites. nNOS(+) interneurons, via nitric oxide release, have a strong impact on corticostriatal information processing since they exert a modulatory influence on medium spiny neurons (Sardo et al., 2002; West and Grace, 2004) and control the induction of long term depression in medium spiny neurons (Calabresi et al., 1999; Sergeeva et al., 2007). Moreover, nitric oxide acts as a volume transmitter regulating post-synaptic excitability at glutamatergic synapses (Steinert et al., 2008). Nevertheless, the molecular mechanisms of the interactions between the nitric oxide and dopaminergic systems have not been precisely clarified.

Neuromodulators including, nitric oxide play important roles in the physiology of striatal neurons. However, what is the role of the interaction between nitric oxide and dopamine? In the striatum, nitric oxide production has been linked to increased oxidative damage and to both, necrotic and apoptotic neuronal death (Brown and Borutaite, 2002; Kim and Koh, 2002; Ischiropoulos and Beckman, 2003; Przedborski et al., 2003; for a recent review see Brown, 2010). Since dopamine like nitric oxide is redox active (Przedborski et al., 2003), the production of nitric oxide within a TH(+) immunoreactive neuron may provide a unique vulnerability of this cellular subtype compared to other TH(+) immunoreactive neurons that also do not express nNOS(+). On the other hand, cellular nitric oxide demonstrated neuroprotective effects (Wink et al., 1998; Mohanakumar et al., 2002; Sancesario et al., 2004).

The interrelated localization of nNOS(+) and TH(+) containing fibers and cells bodies in the nigrostriatal pathway propose an anatomical link between the two neurotransmitters. Nitric oxide in combination with dopamine may represent suitable targets for therapeutic intervention in neurodegenerative diseases as for example Parkinson's (for review see Przedborski et al., 2003; Del Bel et al., 2005, 2011; Pierucci et al., 2011; West and Tseng, 2011). The success of this type of strategy is well documented in Padovan-Neto et al. (2009, 2011), Novaretti et al. (2010), Brzozowski et al. (2011), Takuma et al. (2012), and in the recent reviews (Del Bel et al., 2005, 2011; Jenner, 2008; Pierucci et al., 2011; West and Tseng, 2011; Iravani et al., 2012). Future studies will be required to understand how these two factors interact to regulate basal ganglia circuit function.

ACKNOWLEDGMENTS

The author is most grateful to the past and current students in the group who made this research possible. We also acknowledge grants from FAPESP, FAPESP-INSERM, CAPES-COFECUB, CAPES-DAAD, and CNPQ. The FAPESP also supported collaborators in this research with a PhD fellowship (Fernando E. Padovan-Neto). This research would never be possible without the help of Prof. Walter Stühmer and Dr. Luis Pardo from the Max-Planck-Institute of Experimental Medicine (Göttingen, Germany) and Prof. Francisco S. Guimarães (University of São Paulo, Medical School of Ribeirao Preto).

REFERENCES

Agnati, L. F., Fuxe, K., Zoli, M., Ozini, I., Toffano, G., and Ferraguti, F. (1986). A correlation analysis of the regional distribution of central enkephalin and beta-endorphin immunoreactive terminals and of opiate receptors in adult and old male rats. Evidence for the existence of two main types of communication in the central nervous system: the volume transmission and the wiring transmission. *Acta Physiol. Scand.* 128, 201–207.

Agnati, L. F., Guidolin, D., Guescini, M., Genedani, S., and Fuxe, K. (2010). Understanding wiring and volume transmission. *Brain Res. Rev.* 64, 137–159.

Agnati, L. F., Zoli, M., Strömberg, I., and Fuxe, K. (1995). Intercellular communication in the brain: wiring versus volume transmission. *Neuroscience* 69, 711–726.

Arbuthnott, G. W., and Wickens, J. (2007). Space, time and dopamine. *Trends Neurosci.* 30, 62–69.

Arellano, J. I., Muñoz, A., Ballesteros-Yañez, I., Sola, R. G., and DeFelipe, J. (2004). Histopathology and reorganization of chandelier cells in the human epileptic sclerotic hippocampus. *Brain* 127, 45–64.

Artinian, L., Tornieri, K., Zhong, L., Baro, D., and Rehder, V. (2010). Nitric oxide acts as a volume transmitter to modulate electrical properties of spontaneously firing neurons via apamin-sensitive potassium channels. *J. Neurosci.* 30, 1699–1711.

Beckman, J. S., and Koppenol, W. H. (1996). Nitric oxide, superoxide, and peroxynitrite: the good, the bad, and ugly. *Am. J. Physiol.* 271, C1424–C1437.

Beckstead, M. J., Grandy, D. K., Wickman, K., and Williams, J. T. (2004). Vesicular dopamine release elicits an inhibitory postsynaptic current in midbrain dopamine neurons. *Neuron* 42, 939–946.

Benavides-Piccione, R., and DeFelipe, J. (2003). Different populations of tyrosine-hydroxylase-immuno reactive neurons defined by differential expression of nitric oxide synthase in the human temporal cortex. *Cereb. Cortex* 13, 297–307.

Bertorello, A. M., Hopfield, J. F., Aperia, A., and Greengard, P. (1990). Inhibition by dopamine of (Na(+)+K+)ATPase activity in neostriatal neurons through D1 and D2 dopamine receptor synergism. *Nature* 347, 386–388.

Bidmon, H. J., Emde, B., Kowalski, T., Schmitt, M., Mayer, B., Kato, K., Asayama, K., Witte, O. W., and Zilles, K. (2001). Nitric oxide synthase-I containing cortical interneurons co-express antioxidative enzymes and anti-apoptotic Bcl-2 following focal ischemia: evidence for direct and indirect mechanisms towards their resistance to neuropathology. *J. Chem. Neuroanat.* 22, 167–184.

Bjorklund, A., and Lindvall, O. (1975). Dopamine in dendrites of substantia nigra neurons: suggestions for a role in dendritic terminals. *Brain Res.* 83, 531–537.

Bolam, J. P., Hanley, J. J., Booth, P. A., and Bevan, M. D. (2000). Synaptic organisation of the basal ganglia. *J. Anat.* 196(Pt 4), 527–542.

Bouyer, J. J., Joh, T. H., and Pickel, V. M. (1984). Ultrastructural localization of tyrosine hydroxylase in rat nucleus accumbens. *J. Comp. Neurol.* 227, 92-103

Bredt, D. S., Hwang, P. M., and Snyder, S. H. (1990). Localization of nitric oxide synthase indicating a neural role for nitric oxide. *Nature* 347, 768–770.

Brown, G. C. (2010). Nitric oxide and neuronal death. *Nitric Oxide* 23, 153–165.

Brown, G. C., and Borutaite, V. (2002). Nitric oxide inhibition of mitochondrial respiration and its role in cell death. *Free Radic. Biol. Med.* 33, 1440–1450.

Brzozowski, M. J., Alcantara, S. L., Iravani, M. M., Rose, S., and Jenner, P. (2011). The effect of nNOS inhibitors on toxin-induced cell death in dopaminergic cell lines depends on the extent of enzyme expression. *Brain Res.* 1404, 21–30.

Bullock, T. H., Bennett, M. V., Johnston, D., Josephson, R., Marder, E., and Fields, R. D. (2005). Neuroscience. The neuron doctrine, redux. *Science* 310, 791–793.

Calabresi, P., Centonze, D., Gubellini, P., Marfia, G. A., Pisani, A., Sancesario, G., and Bernardi, G. (2000). Synaptic transmission in the striatum: from plasticity to neurodegeneration. *Prog. Neurobiol.* 61, 231–265.

Calabresi, P., Gubellini, P., Centonze, D., Sancesario, G., Morello, M., Giorgi, M., Pisani, A., and Bernardi, G. (1999). A critical role of the nitric oxide/cGMP pathway in corticostriatal long-term depression. *J. Neurosci.* 19, 2489–2499.

Castro, O. W., Furtado, M. A., Tilelli, C. Q., Fernandes, A., Pajolla, G. P., and Garcia-Cairasco, N. (2011). Comparative neuroanatomical and temporal characterization of FluoroJade-positive neurodegeneration after status epilepticus induced by systemic and intrahippocampal pilocarpine in Wistar rats. *Brain Res.* 16, 43–55.

Centonze, D., Gubellini, P., Pisani, A., Bernardi, G., and Calabresi, P. (2003). Dopamine, acetylcholine and nitric oxide systems interact to induce corticostriatal synaptic plasticity. *Rev. Neurosc.* 14, 207–216.

Chazotte, B. (2011). Labeling nuclear DNA using DAPI. *Cold Spring Harb. Protoc.* 1, pdb.prot 5556.

Cragg, S. J., Baufreton, J., Xue, Y., Bolam, J. P., and Bevan, M. D. (2004). Synaptic release of dopamine in the subthalamic nucleus. *Eur. J. Neurosci.* 20, 1788–1802.

Cragg, S. J., Nicholson, C., Kume-Kick, J., Tao, L., and Rice, M. E. (2001). Dopamine-mediated volume transmission in midbrain is regulated by distinct extracellular geometry and uptake. *J. Neurophysiol.* 85, 1761–1771.

Cragg, S. J., and Rice, M. E. (2004). DAncing past the DAT at a DA synapse. *Trends Neurosci.* 27, 270–277.

Debeir, T., Ginestet, L., François, C., Laurens, S., Martel, J. C., Chopin, P., Marien, M., Colpaert, F., and Raisman-Vozari, R. (2005). Effect of intrastriatal 6-OHDA lesion on DA innervation of the rat cortex and globus pallidus. *Exp. Neurol.* 193, 444–454.

Del Bel, E., Padovan-Neto, F. E., Raisman-Vozari, R., and Lazzarini, M. (2011). Role of nitric oxide in motor control: implications for Parkinson's disease pathophysiology and treatment. *Curr. Pharm. Des.* 17, 471–488.

Del Bel, E. A., Guimarães, F. S., Bermúdez-Echeverry, M., Gomes, M. Z., Schiaveto-de-Souza, A., Padovan-Neto, F. E., Tumas, V., Barion-Cavalcanti, A. P., Lazzarini, M., Nucci-da-Silva, L. P., and de Paula-Souza, D. (2005). Role of nitric oxide on motor behavior. *Cell. Mol. Neurobiol.* 25, 371–392.

De-Miguel, F. F., and Fuxe, K. (2012). Extrasynaptic neurotransmission as a way of modulating neuronal functions. *Front. Physiol.* 3:16. doi:10.3389/fphys.2012.00016

De-Miguel, F. F., and Trueta, C. (2005). Synaptic and extrasynaptic secretion of serotonin. *Cell. Mol. Neurobiol.* 25, 297–312.

Descarries, L., and Mechawar, N. (2000). Ultrastructural evidence for diffuse transmission by monoamine and acetylcholine neurons of the central nervous system. *Prog. Brain Res.*125, 27–47.

Descarries, L., Watkins, K. C., Garcia, S., Bosler, O., and Doucet, G. (1996). Dual character, asynaptic and synaptic, of the dopamine innervation in adult rat neostriatum: A quantitative autoradiographic and immunocytochemical analysis. *J. Comp. Neurol.* 375, 167–186.

DeVente, J., Hopkins, D. A., Markerink-van Ittersum, M., Emson, P. C., Schmidt, H. H. H. W., and Steinbusch, H. W. M. (1998). Distribution of nitric oxide synthase and nitric oxide-receptive, cGMP-producing structures in the rat brain. *Neuroscience* 87, 207–241.

DeVente, J., Markerink-van Ittersum, M., vanAbeelen, J., Emson, P. C., Axer, H., and Steinbusch, H. W. (2000). NO-mediated cGMP synthesis in cholinergic neurons in the rat forebrain: effects of lesioning dopaminergic or serotonergic pathways on nNOS and cGMP synthesis. *Eur. J. Neurosci.* 12, 507–519.

DiGiovanni, G., Ferraro, G., Sardo, P., Galati, S., Esposito, E., and La Grutta, V. (2003). Nitric oxide modulates striatal neuronal activity via soluble guanylyl cyclase: an in vivo microiontophoretic study in rats. *Synapse* 48, 100–107.

DiMatteo, V., Pierucci, M., Benigno, A., Crescimanno, G., Esposito, E., and Di Giovanni, G. (2009). Involvement of nitric oxide in nigrostriatal dopaminergic system degeneration: a neurochemical study. *Ann. N. Y. Acad. Sci.* 1155, 309–315.

Dun, N. J., Dun, S. L., and Förstermann, U. (1994). Nitric oxide synthase immunoreactivity in rat pontine medullary neurons. *Neuroscience* 59, 429–445.

Egberongbe, Y. I., Gentleman, S. M., Falkai, P., Bogerts, B., Polak, J. M., and Roberts, G. W. (1994). The distribution of nitric oxide synthase immunoreactivity in the human brain. *Neuroscience* 59, 561–578.

Fallon, J. H., and Loughlin, S. E. (1995). "Substantia nigra," in *The Rat Nervous System*, 2nd Edn, ed. G. Paxinos (New York: Academic Press), 215–237.

Figueredo-Cardenas, G., Morello, M., Sancesario, G., Bernardi, G., and Reiner, A. (1996). Colocalization of somatostatin, neuropeptide Y, neuronal nitric oxide synthase and NADPH-diaphorase in striatal interneurons in rats. *Brain Res.* 735, 317–324.

Fujiyama, F., and Masuko, S. (1996). Association of dopaminergic terminals and neurons releasing nitric oxide in the rat striatum: an electron microscopic study using NADPH-diaphorase histochemistry and tyrosine hydroxylase immunohistochemistry. *Brain Res. Bull.* 40, 121–127.

Fuxe, K., Dahlstrom, A., Hoistad, M., Marcellino, D., Jansson, A., Rivera, A., Diaz-Cabiale, Z., Jacobsen, K., Tinner-Staines, B., Hagman, B., Leo, G., Staines, W., Guidolin, D., Kehr, J., Genedani, S., Belluardo, N., and Agnati, L. F. (2007). From the Golgi–Cajal mapping to the transmitter-based characterization of the neuronal networks leading to two modes of brain communication: wiring and volume transmission. *Brain Res. Rev.* 55, 17–54.

Fuxe, K., Dahlström, A. B., Jonsson, G., Marcellino, D., Guescini, M., Dam, M., Manger, P., and Agnati, L. (2010). The discovery of central monoamine neurons gave volume transmission to the wired brain. *Prog. Neurobiol.* 90, 82–100.

Galati, S., D'angelo, V., Scarnati, E., Stanzione, P., Martorana, A., Procopio, T., Sancesario, G., and Stefani, A. (2008). In vivo electrophysiology of dopamine-denervated striatum: focus on the nitric oxide/cGMP signaling pathway. *Synapse.* 62, 409–420.

Gally, J. A., Montague, P. R., and Reeke, G. N. Jr., and Edelman, G. M. (1990). The NO hypothesis: possible effects of a short-lived, rapidly diffusible signal in the development and function of the nervous system. *Proc. Natl. Acad. Sci. U.S.A.* 87, 3547–3551.

Garthwaite, J. (2008). Concepts of neural nitric oxide-mediated transmission. *Eur. J. Neurosci.* 27, 2783–2802.

Garthwaite, J., and Boulton, C. L. (1995). Nitric oxide signaling in the central nervous system. *Annu. Rev. Physiol.* 57, 683–706.

Geffen, L. B., Jessell, T. M., Cuello, A. C., and Iversen, L. L. (1976). Release of dopamine from dendrites in rat substantia nigra. *Nature* 260, 258–260.

Gerfen, C. R., and Surmeier, D. J. (2011). Modulation of striatal projection systems by dopamine. *Annu. Rev. Neurosci.* 34, 441–466.

Gomes, M. Z., Raisman-Vozari, R., and Del Bel, E. A. (2008). A nitric oxide synthase inhibitor decreases 6-hydroxydopamine effects on tyrosine hydroxylase and neuronal nitric oxide synthase in the rat nigrostriatal pathway. *Brain Res.* 8, 160–169.

Gonon, F. (1997). Prolonged and extrasynaptic excitatory action of dopamine mediated by D1 receptors in the rat striatum in vivo. *J. Neurosci.* 17, 5972–5978.

González-Hernández, T., and Rodríguez, M. (2000). Compartmental organization and chemical profile of dopaminergic and GABAergic neurons in the substantia nigra of the rat. *J. Comp. Neurol.* 421, 107–135.

Graybiel, A. M. (2000). The basal ganglia. *Curr. Biol.* 10, R509–R511.

Griffith, O. W., and Stuehr, D. J. (1995). Nitric oxide synthases: properties and catalytic mechanism. *Annu. Rev. Physiol.* 57, 707–736.

Groves, P. M., Linder, J. C., and Young, S. J. (1994). 5-hydroxydopamine-labeled dopaminergic axons: three-dimensional reconstructions of axons, synapses and postsynaptic targets in rat neostriatum. *Neuroscience* 58, 593–604.

Haavik, J., and Toska, K. (1998). Tyrosine hydroxylase and Parkinson's disease. *Mol. Neurobiol.* 16, 285–309.

Hanbauer, I., Wink, D., Osawa, Y., Edelman, G. M., and Gally, J. A. (1992). Role of nitric oxide in NMDA-evoked release of (3H)-dopamine from striatal slices. *Neuroreport* 3, 409–440.

Heeringa, M. J., and Abercrombie, E. D. (1995). Biochemistry of somatodendritic dopamine release in substantia nigra: an in vivo comparison with striatal dopamine release. *J. Neurochem.* 65, 192–200.

Herbison, A. E., Simonian, S. X., Norris, P. J., and Emson, P. C. (1996). Relationship of neuronal nitric oxide synthase immunoreactivity to GnRH neurons in the ovariectomized and intact female rat. *J. Neuroendocrinol.* 8, 73–82.

Hidaka, S., and Totterdell, S. (2001). Ultrastructural features of the nitric oxide synthase-containing interneurons in the nucleus accumbens and their relationship with tyrosine hydroxylase-containing terminals. *J. Comp. Neurol.* 431, 139–154.

Hökfelt, T., Johansson, O., Fuxe, K., Goldstein, M., and Park, D. (1976). Immunohistochemical studies on the localization and distribution of monoamine neuron systems in the rat brain. I. Tyrosine hydroxylase in the mes- and diencephalon. *Med. Biol.* 54, 427–453.

Hökfelt, T., Johansson, O., Fuxe, K., Goldstein, M., and Park, D. (1977). Immunohistochemical studies on the localization and distribution of monoamine neuron systems in the rat brain. *Med. Biol.* 55, 21–40.

Hökfelt, T., Johansson, O., and Goldstein, M. (1984). Chemical anatomy of the brain. *Science* 225, 1326–1334.

Hussain, S., and Slikker, W. Jr., and Ali, S. F. (1996). Role of metallothionein and other antioxidants in scavenging superoxide radicals and their possible role in neuroprotection. *Neurochem. Int.* 29, 145–152.

Ignarro, L. L. (2010). No stupid questions. Interview by Ruth Williams. *Circ. Res.* 106, 420–422.

Iravani, M. M., and Jenner, P. (2011). Mechanisms underlying the onset and expression of levodopa-induced dyskinesia and their pharmacological manipulation. *J. Neural Transm.* 118, 1661–1690.

Iravani, M. M., McCreary, A. C., and Jenner, P. (2012). Striatal plasticity in Parkinson's disease and L-DOPA induced dyskinesia. *Parkinsonism Relat. Disord.* (Suppl. 1), S123–S125.

Ischiropoulos, H., and Beckman, J. S. (2003). Oxidative stress and nitration in neurodegeneration: cause, effect, or association? *J. Clin. Invest.* 111, 163–169.

Jaeger, C. B., Ruggiero, D. A., Albert, V. R., Park, D. H., Joh, T. H., and Reis, D. J. (1984). Aromatic L-amino acid decarboxylase in the rat brain: immunocytochemical localization in neurons of the brain stem. *Neuroscience* 11, 691–713.

Jenner, P. (2008). Molecular mechanisms of L-DOPA-induced dyskinesia. *Nat. Rev. Neurosci.* 9, 665–677.

Jorgensen, E. M. (2004). Dopamine: should I stay or should I go now? *Nat. Neurosci.* 7, 1019–1021.

Kawaguchi, Y. (1993). Physiological, morphological, and histochemical characterization of three classes of interneurons in rat neostriatum. *J. Neurosci.* 13, 4908–4923.

Kawaguchi, Y., Wilson, C. J., Augood, S. J., and Emson, P. C. (1997). Striatal interneurones: chemical, physiological and morphological characterization. *Trends Neurosci.* 12, 527–535.

Kawaguchi, Y., Wilson, C. J. Augood, S. J., and Emson, P. C. (1995). Striatal interneurones: chemical, physiological and morphological characterization. *Trends Neurosci.* 18, 527–535.

Kim, Y. H., and Koh, J. Y. (2002). The role of NADPH oxidase and neuronal nitric oxide synthase in zinc-induced poly(ADP-ribose) polymerase activation and cell death in cortical culture. *Exp. Neurol.* 177, 407–418.

Kiss, J. P., and Vizi, E. S. (2001). Nitric oxide: a novel link between synaptic and nonsynaptic transmission. *Trends Neurosci.* 24, 211–215.

Kiss, J. P., Zsilla, G., and Vizi, E. S. (2004). Inhibitory effect of nitric oxide on dopamine transporters: interneuronal communication without receptors. *Neurochem. Int.* 45, 485–489.

Klejbor, I., Domaradzka-Pytel, B., Ludkiewicz, B., Wójcik, S., and Morys, J. (2004). The relationships between neurons containing dopamine and nitric oxide synthase in the ventral tegmental area. *Folia Histochem. Cytobiol.* 42, 83–87.

Kreitzer, A. C. (2009). Physiology and pharmacology of striatal neurons. *Annu. Rev. Neurosci.* 32, 127–147.

Mohanakumar, K. P. B., Thomas, S. M., Sharma, D., Muralikrishnan, R., Chowdhury, C., and Chiueh, C. (2002). Nitric oxide: an antioxidant and neuroprotector. *Ann. N. Y. Acad. Sci.* 962, 389–401.

Moss, J., and Bolam, J. P. (2008). A dopaminergic axon lattice in the striatum and its relationship with cortical and thalamic terminals. *J. Neurosci.* 28, 11221–11230.

Nagatsu, T., and Ichinose, H. (1999). Molecular biology of catecholamine-related enzymes in relation to Parkinson's disease. *Cell. Mol. Neurobiol.* 19, 57–66.

Nieoullon, A., Cheramy, A., and Glowinski, J. (1977). Release of dopamine in vivo from cat substantia nigra. *Nature* 266, 375–377.

Novaretti, N., Padovan-Neto, F. E., Tumas, V., da-Silva, C. A., and Del Bel, E. A. (2010). Lack of tolerance for the anti-dyskinetic effects of 7-nitroindazole, a neuronal nitric oxide synthase inhibitor in rats. *Braz. J. Med. Biol. Res.* 43, 1047–1053.

O'Donnell, P., and Grace, A. A. (1993). Dopaminergic modulation of dye coupling between neurons in the core and shell regions of the nucleus accumbens. *J. Neurosci.* 13, 3456–3471.

O'Donnell, P., and Grace, A. A. (1997). Cortical afferents modulate striatal gap junction permeability via nitric oxide. *Neuroscience* 76, 1–5.

Paden, C., Wilson, C. J., and Groves, P. M. (1976). Amphetamine-induced release of dopamine from the substantia nigra in vitro. *Life Sci.* 19, 1499–1506.

Padovan-Neto, F. E., Echeverry, M. B., Chiavegatto, S., and Del-Bel, E. (2011). Nitric oxide synthase inhibitor improves de novo and long-term L-DOPA-induced dyskinesia in hemiparkinsonian Rats. *Front. Syst. Neurosci.* 5:40. doi:10.3389/fnsys.2011.00040

Padovan-Neto, F. E., Echeverry, M. B., Tumas, V., and Del-Bel, E. A. (2009). Nitric oxide synthase inhibition attenuates L-DOPA-induced dyskinesias in a rodent model of Parkinson's disease. *Neuroscience* 159, 927–935.

Park, D. J., and West, A. R. (2009). Regulation of striatal nitric oxide synthesis by local dopamine and glutamate interactions. *J. Neurochem.* 111, 1457–1465.

Paxinos, G., and Watson, C. (1999). *The Rat Brain in Stereotaxic Coordinates.* San Diego: Academic Press.

Paxinos, G., and Watson, C. (2009). *Chemoarchitectonic Atlas of the Rat Brain.* San Diego: Academic Press.

Philippides, A., Husbands, P., and O'Shea, M. (2000). Four-dimensional neuronal signaling by nitric oxide: a computational analysis. *J. Neurosci.* 20, 1199–1207.

Philippides, A., Ott, S. R., Husbands, P., Lovick, T. A., and O'Shea, M. (2005). Modeling cooperative volume signaling in a plexus of nitric-oxide-synthase expressing neurons. *J. Neurosci.* 25, 6520–6532.

Pierucci, M., Galati, S., Valentino, M., Di Matteo, V., Benigno, A., Pitruzzella, A., Muscat, R., and Di Giovanni, G. (2011). Nitric oxide modulation of the Basal Ganglia circuitry: therapeutic implication for Parkinson's disease and other motor disorders. *CNS Neurol. Disord. Drug Targets* 10, 777–791.

Przedborski, S., Jackson-Lewis, V., Vila, M., Wudu, C., Teismann, P., Tieu, K., Choi, D. K., and Cohen, O. (2003). Free radical and nitric oxide toxicity in Parkinson's disease. *Adv. Neurol.* 91, 83–94.

Rice, M. E., and Cragg, S. J. (2004). Nicotine amplifies reward-related dopamine signals instriatum. *Nat. Neurosci.* 7, 583–584.

Rice, M. E., and Cragg, S. J. (2008). Dopamine spillover after quantal release: rethinking dopamine transmission in the nigrostriatal pathway. *Brain Res. Rev.* 58, 303–313.

Rice, M. E., Patel, J. C., and Cragg, S. J. (2011). Dopamine release in the basal ganglia. *Neuroscience* 198, 112–137.

Robertson, H. A., and Robertson, G. S. (1987). Combined L-dopa and bromocriptine therapy for Parkinson's disease: a proposed mechanism of action. *Clin. Neuropharmacol.* 10, 384–387.

Rodrigo, J., Springall, D. R., Uttenthal, O., Bentura, M. L., Abadia-Molina, F., Riveros-Moreno, V., Martinez-Murillo, R., Polak, J. M., and Moncada, S. (1994). Localization of NOS in the adult rat brain. *Philos. Trans. R. Soc. Lond. Biol. Sci.* 345, 175–221.

Rushlow, W., Flumerfelt, B. A., and Naus, C. C. (1995). Colocalization of somatostatin, neuropeptide Y, and NADPH-diaphorase in the caudate-putamen of the rat. *J. Comp. Neurol.* 351, 499–508.

Salum, C., Raisman-Vozari, R., Michel, P. P., Gomes, M. Z., Mitkovski, M., Ferrario, J. E., Ginestet, L., and Del Bel, E. A. (2008). Modulation of dopamine uptake by nitric oxide in cultured mesencephalic neurons. *Brain Res.* 1198, 27–33.

Sancesario, G., Giorgi, M., D'Angelo, V., Modica, A., Martorana, A., Morello, M., Bengtson, C. P., and Bernardi, G. (2004). Down-regulation of nitrergic transmission in the rat striatum after chronic nigrostriatal deafferentation. *Eur. J. Neurosci.* 20, 989–1000.

Sancesario, G., Morello, M., Reiner, A., Giacomini, P., Massa, R., Schoen, S., and Bernardi, G. (2000). Nitrergic neurons make synapses on dual-input dendritic spines of neurons in the cerebral cortex and the striatum of the rat: implication for a postsynaptic action of nitric oxide. *Neuroscience* 99, 627–642.

Sardo, P., Ferraro, G., Di Giovanni, G., Galati, S., and La Grutta, V. (2002). Inhibition of nitric oxide synthase influences the activity of striatal neurons in the rat. *Neurosci. Lett.* 325, 179–182.

Schmidt, H. H. H. W., Gagne, G. D., Nakane, M., Pollock, J. S., Miller, M. F., and Murad, F. (1992). Mapping of neural nitric oxide synthase in the rat suggests frequent co-localization with NADPH-diaphorase but not with soluble guanylyl cyclase, and novel paraneural functions for nitrinergic signal transduction. *J. Histochem. Cytochem.* 40, 1439–1456.

Sergeeva, O. A., Doreulee, N., Chepkova, A. N., Kazmierczak, T., and Haas, H. L. (2007). Long-term depression of cortico-striatal synaptic transmission by DHPG depends on endocannabinoid release and nitric oxide synthesis. *Eur. J. Neurosci.* 26, 1889–1894.

Shen, W., Flajolet, M., Greengard, P., and Surmeier, D. J. (2008). Dichotomous dopaminergic control of striatal synaptic plasticity. *Science* 321, 848–851.

Simonian, S. X., and Herbison, A. E. (1996). Localization of neuronal nitric oxide synthase-immunoreactivity within sub-populations of noradrenergic A1 and A2 neurons in the rat. *Brain Res.* 732, 247–252.

Snyder, S. H., and Ferris, C. D. (2000). Novel neurotransmitters and their neuropsychiatric relevance. *Am. J. Psychiatry* 157, 1738–1751.

Southam, E., and Garthwaite, J. (1993). The nitric oxide–cyclic GMP signalling pathway in rat brain. *Neuropharmacology* 32, 1267–1277.

Steinert, J. R., Kopp-Scheinpflug, C., Baker, C., Challiss, R. A., Mistry, R., Haustein, M. D., Griffin, S. J., Tong, H., Graham, B. P., and Forsythe, I. D. (2008). Nitric oxide is a volume transmitter regulating postsynaptic excitability at a glutamatergic synapse. *Neuron* 60, 642–656.

Syková, E. (2004). Extrasynaptic volume transmission and diffusion parameters of the extracellular space. *Neuroscience* 129, 861–876.

Takuma, K., Tanaka, T., Takahashi, T., Hiramatsu, N., Ota, Y., Ago, Y., and Matsuda, T. (2012). Neuronal nitric oxide synthase inhibition attenuates the development of L-DOPA-induced dyskinesia in hemi-Parkinsonian rats. *Eur. J. Pharmacol.* 683,166–173.

Tornieri, K., and Rehder, V. (2007). Nitric oxide release from a single cell affects filopodial motility on growth cones of neighboring neurons. *Dev. Neurobiol.* 67, 1932–1943.

Trueta, C., and De-Miguel, F. F. (2012). Extrasynaptic exocytosis and its mechanisms: a source of molecules mediating volume transmission in the nervous system. *Front. Physiol.* 3:319. doi:10.3389/fphys.2012.00319

Vincent, S. R., and Kimura, H. (1992). Histochemical mapping of nitric oxide synthase in the rat brain. *Neuroscience* 46, 755–784.

Vizi, E. S., Kiss, J. P., and Lendvai, B. (2004). Nonsynaptic communication in the central nervous system. *Neurochem. Int.* 45, 443–451.

Walter, T., Shattuck, D. W., Baldock, R., Bastin, M. E., Carpenter, A. E., Duce, S., Ellenberg, J., Fraser, A., Hamilton, N., Pieper, S., Ragan, M. A., Schneider, J. E., Tomancak, P., and Heriche, J.-K. (2010). Visualization of image data from cells to organisms. *Nat. Methods* 7(Suppl. 3), S26–S24.

West, A. R., and Galloway, M. P. (1997). Endogenous nitric oxide facilitates striatal dopamine and glutamate efflux in vivo: role of ionotropic glutamate receptor-dependent mechanisms. *Neuropharmacology* 36, 1571–1581.

West, A. R., Galloway, M. P., and Grace, A. A. (2002). Regulation of striatal dopamine neurotransmission by nitric oxide: effector pathways and signaling mechanisms. *Synapse* 44, 227–245.

West, A. R., and Grace, A. A. (2000). Striatal nitric oxide signaling regulates the neuronal activity of midbrain dopamine neurons in vivo. *J. Neurophysiol.* 83, 1796–1808.

West, A. R., and Tseng, K. Y. (2011). Nitric oxide-soluble guanylyl cyclase-cyclic GMP signaling in the striatum: new targets for the treatment of Parkinson's Disease? *Front. Syst. Neurosci.* 5:55. doi:10.3389/fnsys.2011.00055

West, A. R., and Grace, A. A. (2004). The nitric oxide-guanylyl cyclase signaling pathway modulates membrane activity states and electrophysiological properties of striatal medium spiny neurons recorded in vivo. *J. Neurosci.* 24, 1924–1935.

Wightman, R. M. (2006). Detection technologies. Probing cellular chemistry in biological systems with microelectrodes. *Science* 311, 1570–1574.

Wilson, C. J., Groves, P. M., and Fifkova, E. (1977). Monoaminergic synapses, including dendrodendritic synapses in the rat substantia nigra. *Exp. Brain Res.* 30, 161–174.

Wink, D., Feelisch, A. M., Fukuto, J., Chistodoulou, D., Jourd'heuil, D., Grisham, M. B., Vodovotz, Y., Cook, J. A., Krishna, M., DeGraff, W. G., Kim, S., Gamson, J., and Mitchell, J. B. (1998). The cytotoxicity of nitroxyl: possible implications for the pathophysiological role of NO. *Arch. Biochem. Biophys.* 351, 66–74.

Wood, J., and Garthwaite, J. (1994). Models of the diffusional spread of nitric oxide: implications for neural nitric oxide signaling and its pharmacological properties. *Neuropharmacology* 33, 1235–1244.

Yao, W. D., Spealman, R. D., and Zhang, J. (2008). Dopaminergic signaling in dendritic spines. *Biochem. Pharmacol.* 75, 2055–2069.

Yuste, J. E., Bermúdez, M., Bernal, F. R., Barcia, C., Martin, J., Del Bel, E., Villalba, E. F., and Herrero, M. T. (2011). NOS inhibitors improve L-DOPA-induced dyskinesias in experimental models of Parkinsonism. *Mov. Disord.* 26(Suppl. 2), S257–S258.

Zoli, M., Jansson, A., Syková, E., Agnati, L. F., and Fuxe, K. (1999). Intercellular communication in the central nervous system: the emergence of the volume transmission concept and its relevance for neuropsychopharmacology. *Trends Pharmacol. Sci.* 20, 142–150.

Conflict of Interest Statement: The authors declare that the research was conducted in the absence of any commercial or financial relationships that could be construed as a potential conflict of interest.

Received: 20 April 2012; accepted: 29 August 2012; published online: 25 September 2012.

*Citation: Mitkovski M, Padovan-Neto FE, Raisman-Vozari R, Ginestet L, da-Silva CA and Del-Bel EA (2012) Investigations into potential extrasynaptic communication between the dopaminergic and nitrergic systems. Front. Physio. **3**:372. doi: 10.3389/fphys.2012.00372*

This article was submitted to Frontiers in Membrane Physiology and Biophysics, a specialty of Frontiers in Physiology.

frontiers in PHYSIOLOGY

ORIGINAL RESEARCH ARTICLE
published: 02 October 2012
doi: 10.3389/fphys.2012.00391

Development of inflammation-induced hyperalgesia and allodynia is associated with the upregulation of extrasynaptic AMPA receptors in tonically firing lamina II dorsal horn neurons

Olga Kopach, Viacheslav Viatchenko-Karpinski, Pavel Belan and Nana Voitenko*

State Key Laboratory of Molecular and Cellular Biology, Bogomoletz Institute of Physiology, Kiev, Ukraine

Edited by:
Francisco F. De-Miguel, Universidad Nacional Autonoma de Mexico, Mexico

Reviewed by:
Alberto Lopez-Avila, Instituto Nacional de Psiquiatría Ramón de la Fuente Muñiz, Mexico
Leonardo Rodriguez-Sosa, UNAM, Mexico

***Correspondence:**
Nana Voitenko, Department of General Physiology of Nervous System, Bogomoletz Institute of Physiology, Bogomoletz Str. 4, Kiev 01024, Ukraine.
e-mail: nana@biph.kiev.ua

Persistent peripheral inflammation changes AMPA receptor (AMPAR) trafficking in dorsal horn neurons by promoting internalization of GluR2-containing, Ca^{2+}-impermeable AMPARs from the synapses and by increasing insertion of GluR1-containing, Ca^{2+}-permeable AMPARs in extrasynaptic plasma membrane. These changes contribute to the maintenance of persistent inflammatory pain. However, much less is known about AMPAR trafficking during development of persistent inflammatory pain and direct studies of extrasynaptic AMPARs functioning during this period are still lacking. Using Complete Freund's adjuvant (CFA)-induced model of long-lasting peripheral inflammation, we showed that remarkable hyperalgesia and allodynia developes in 1–3 h after intraplantar CFA injection. By utilizing patch-clamp recording combined with Ca^{2+} imaging, we found a significant upregulation of extrasynaptic AMPARs in substantia gelatinosa (SG) neurons of the rat spinal cord 2–3 h after CFA injection. This upregulation was manifested as a robust increase in the amplitude of AMPAR-mediated currents 2–3 h post-CFA. These changes were observed specifically in SG neurons characterized by intrinsic tonic firing properties, but not in those that exhibited strong adaptation. Our results indicate that CFA-induced inflammation increases functional expression of extrasynaptic AMPARs in tonically firing SG neurons during development of pain hypersensitivity and that this increase may contribute to the development of peripheral persistent pain.

Keywords: extrasynaptic AMPA receptors, development of infl mmatory pain, substantia gelatinosa neurons, hyperalgesia, allodynia

INTRODUCTION

Persistent or chronic pain is a public health problem worldwide and may result from infection, inflammation, peripheral injury to tissue or nerve. Understanding the molecular mechanisms underlying development and maintenance of chronic pain ensures success of its treatment by developing alternative strategies, which target specific molecules precisely, and would therefore be of potential benefit in treatment or even prevention of persistent pain. Cumulative evidence demonstrates that altered AMPAR trafficking in dorsal horn neurons is required for the persistent inflammatory pain maintenance. However, a role of AMPARs in persistent inflammatory pain development is not completely understood. Besides, current studies in this field are predominantly concentrated on synaptic AMPARs, leaving functioning of extrasynaptic AMPARs population out of direct investigation.

α-amino-3-hydroxy-5-methyl-4-isoxazolepropionic acid receptors (AMPARs) expression level at extrasynaptic sites of neuronal plasma membrane is high throughout the central nervous system (CNS). Extrasynaptic AMPARs are localized within spines, dendrites, and somata (Malinow and Malenka, 2002; Bredt and Nicoll, 2003). They are mobile and rapidly move between the plasma membrane and intracellular compartments by exocytosis and endocytosis, and can migrate laterally to and from synaptic sites adjusting synaptic strength (Borgdorff and Choquet, 2002; Choquet and Triller, 2003; Adesnik et al., 2005; Cognet et al., 2006). Extrasynaptic AMPARs may also contribute to glutamatergic signaling at nonsynaptic locations. Glutamate, released from the presynaptic neurons and from astrocytes, can bath the extrasynaptic plasma membrane by the glutamate spillover and activates extrasynaptic AMPARs, thus strengthening glutamatergic transmission. During neuropathological conditions, when a primary afferent input is strong, glutamate spillover is excessive (Allan and Rothwell, 2001) and results in increased excitotoxic vulnerability and neurons injury (Kullmann, 2000; Allan and Rothwell, 2001; Weng et al., 2006).

The changes in AMPAR subunit trafficking, subunit composition, phosphorylation of AMPAR subunits or their interaction with partner proteins may contribute to spinal nociceptive transmission (Santos et al., 2009; Wang et al., 2010; He et al., 2011). In a spinal cord, AMPAR trafficking has been suggested as one of key mechanisms for central sensitization, a specific form of plasticity underlying induction and maintenance of pain (Hartmann et al., 2004; Park et al., 2008, 2009; Latremoliere and Woolf, 2009; Tao, 2010; Kopach et al., 2011).

Recent studies demonstrated that altered AMPAR trafficking in dorsal horn neurons is causally linked to peripheral inflammatory pain maintenance (Hartmann et al., 2004; Katano et al., 2008; Park et al., 2009). Persistent peripheral inflammation promotes internalization of GluR2-containing, Ca^{2+}-impermeable AMPARs from the synapses (Park et al., 2009) and insertion of GluR1-containing, Ca^{2+}-permeable AMPARs at extrasynaptic membrane of lamina II dorsal horn neurons (Kopach et al., 2011) during inflammatory pain maintenance. However, much less is known about extrasynaptic AMPAR trafficking in dorsal horn neurons during development of inflammatory pain. So far as inflammation-induced peripheral hypersensitivity develops rapidly (2–3 h) after intraplantar complete Freund's adjuvant (CFA) injection and is comparable to one observed during the period of inflammatory pain maintenance (Zhang et al., 2003; Park et al., 2009), the same peripheral inflammatory insult may also potentially alter AMPAR trafficking in dorsal horn neurons when hypersensitivity is being developed. The altered AMPAR trafficking may in turn contribute to the observed hypersensitivity and strength pain development and maintenance.

In this work, we used electrophysiology combined with $[Ca^{2+}]_i$ imaging to study extrasynaptic AMPAR functioning in dorsal horn substantia gelatinosa (SG) neurons during the development period of peripheral inflammatory pain. We show that development of inflammation-induced hyperalgesia and allodynia is associated with the upregulation of extrasynaptic AMPA receptors (AMPARs) in specific subtype of lamina II dorsal horn neuron.

MATERIALS AND METHODS

ANIMAL PREPARATION

Male rats were housed in cages on a standard 12:12 h light/dark cycle. Water and food were available ad libitum until rats were transported to the laboratory for experiments. The animals were used in accordance with protocols that were approved by the Animal Care and Use Committee at the Bogomoletz Institute of Physiology and were consistent with the ethical guidelines of the National Institutes of Health and the International Association for the Study of Pain. All efforts were made to minimize animal suffering and to reduce the number of animals used.

EXPERIMENTAL DRUGS

CFA was purchased from Sigma Chemical Co. (St. Louis, MO). Fura-2 was obtained from Invitrogen (Carlsbad, CA, USA). Tetrodotoxin (TTX) was obtained from Alomone Labs Ltd. (Jerusalem, Israel). NBQX, APV, AMPA, cyclothiazide (CTZ), bicuculline, and strychnine were purchased from Tocris Bioscience (Ellisville, MO).

INDUCTION OF PERIPHERAL INFLAMMATION

To produce unilateral peripheral inflammation and nociceptive hypersensitivity, 100 μl of CFA (*Mycobacterium tuberculosis*) suspended in an oil-saline (1:1) emulsion was injected subcutaneously into the plantar side of one hind paw of the rats. Saline injection (0.9%; 100 μl) was used as a control.

BEHAVIORAL TESTING

Animals were acclimatized to the experimental setup before the testing. The experimenters were blinded to the treatment groups during behavioral testing.

Paw withdrawal responses to thermal stimuli were measured in rats by using the Hargreaves technique (Hargreaves et al., 1988). For measurement of paw withdrawal responses to noxious heat stimuli, the animal was placed in a Plexiglas chamber on a glass plate located above a light box (Bioseb, Italy). Radiant heat was applied by focused infrared beam through a hole in the light box through the glass plate to the middle of the plantar surface of each hind paw. When the animal lifted its foot, the light beam was automatically turned off. The length of time between the start of the beam and the foot lift was defined as the paw withdrawal latency. Each trial was repeated five times at 5-min intervals for each paw. A cut-off time of 30 s was used to avoid tissue damage. Behavioral tests were performed before and after CFA injection.

To measure paw withdrawal responses to repeated mechanical stimuli, we used von Frey method. A rat was placed in a Plexiglas chamber on an elevated mesh screen and each von Frey monofilament (Bioseb, Italy) was applied to the hind paw for approximately 1–2 s. Trials of each hind paw were repeated 10 times at 1-min intervals. The occurrence of paw withdrawal in each of these trials was expressed as a percentage response frequency.

SPINAL CORD SLICE PREPARATION

Spinal cord slices were prepared from 18–21-day-old male rats subjected to saline or CFA injection as described previously (Voitenko et al., 2004; Kopach et al., 2011). Briefly, after rats were deeply anesthetized with an overdose of isoflurane, the L_{4-5} spinal segments were removed. Transverse slices (300 μm thick) were cut on a vibratome (Campden Instrument, UK) in an ice-cold solution that was continuously bubbled with 95% O_2 and 5% CO_2 and contained (in mM) 250 sucrose, 2 KCl, 1.2 NaH_2PO_4, 0.5 $CaCl_2$, 7 $MgCl_2$, 26 $NaHCO_3$, and 11 glucose (pH 7.4). Slices were maintained at room temperature in a physiologic Krebs bicarbonate solution that contained (in mM) 125 NaCl, 2.5 KCl, 1.25 NaH_2PO_4, 2 $CaCl_2$, 1 $MgCl_2$, 26 $NaHCO_3$, and 10 glucose (pH 7.4, osmolarity 310–320 mOsM) and was equilibrated with 95% O_2 and 5% CO_2.

SIMULTANEOUS CA^{2+} IMAGING AND PATCH-CLAMP RECORDING

Simultaneous Ca^{2+} imaging and whole-cell electrophysiologic recordings were obtained from SG neurons of the spinal L_{4-5} dorsal horn as described previously (Voitenko et al., 2004; Kopach et al., 2011). Briefly, the neurons were visually identified with a video microscope (Olympus, Japan). The patch pipettes with resistance of 6–10 MΩ were filled with an internal solution containing (in mM) 133 K-gluconate, 5 NaCl, 0.5 $MgCl_2$, 10 HEPES-Na, 2 MgATP, 0.1 GTP-Na, and 0.2 fura-2 pentapotassium salt (pH 7.2, osmolarity 290 mOsM). The membrane potential of SG neurons was held at –60 mV by a patch-clamp amplifier PC-505B (Warner Instruments, Hamden, CT) and Digidata board 1320A (Molecular Devices, Union City, CA) controlled by pCLAMP 8.2 software (Axon Instruments, USA) in current or voltage-clamp

mode. Only data from neurons that exhibited a resting membrane potential negative to –60 mV were included in the analysis.

Neurons were randomly chosen in the SG, but were mainly localized in its media-lateral part (**Figure 3A**). All SG neurons were categorized according to their discharge pattern in response to the series of 1-s current pulses, as described previously (Kopach et al., 2011).

To isolate AMPAR-mediated membrane current and associated increase in free calcium concentration in cytosol ($[Ca^{2+}]_i$), we performed recordings in the continuous presence of D-APV (50 μM), bicuculline (5 μM), and strychnine (2 μM) to block NMDA, $GABA_A$, and glycine receptors, respectively. In addition, TTX (0.5 μM) and cadmium chloride (100 μM) were added to Krebs bicarbonate solution to block corresponding voltage-activated sodium and calcium channels. To prevent a desensitization of AMPARs during bath application of the agonist, we applied AMPA to the slices in the continuous presence of CTZ (20 μM). Typically, one neuron was studied per slice.

Fura-2 fluorescence from SG neurons, located between 50 and 100 μm below the surface of the slice, was measured by using a 60×, NA 0.9 water-immersion objective (Olympus, Japan) and a 12-bit cooled CCD camera and capturing board (Sensicam, PCO, Germany). Fluorescence intensity was measured at wavelengths >510 nm when excited at 380 and 340 nm by a PolyChrome IV monochromator (Till Photonics, Germany) using Imaging Workbench software (INDEC System, USA). Fura-2 fluorescence were measured in soma and dendrites of SG neurons and expressed as changes in the ratio of fluorescence at 340–380 nm. The background area closest to the areas of interest was subtracted for each wavelength. The amplitude of the AMPA-induced $[Ca^{2+}]_i$ transient was calculated as the difference between the fura-2 fluorescence ratio before AMPA application and the ratio at the maximum $[Ca^{2+}]_i$ rise during AMPARs activation.

STATISTICAL ANALYSIS

All data are presented as mean ± SEM with n referring to the number of cells analyzed. Student's *t*-tests (two-tailed unpaired) were used to determine statistically significant differences. A *p*-value of less than 0.05 was considered statistically significant.

RESULTS

DEVELOPMENT OF CFA-INDUCED PERIPHERAL HYPERSENSITIVITY

Our previous studies (Park et al., 2009) and those of others (Zhang et al., 2003; Park et al., 2008) show that subcutaneous injection of CFA into a hind paw led to development of robust hypersensitivity on the ipsilateral side. This inflammation-induced hypersensitivity reached a peak around 24 h after the injection of CFA and maintained for a few days, representing the maintenance period of persistent pain. Here, we examined how persistent pain develops. For this, we thoroughly measured paw withdrawal responses to both thermal and mechanical stimuli. before CFA injection, and then at 0.5, 1, 2, 3, 4, 5, 6, 7, and 8 h after CFA injection. Consistent with previous reports (Zhang et al., 2003), CFA injection produced a rapid development of thermal hypersensitivity, as evidenced by a decrease in ipsilateral paw withdrawal latency (**Figure 1**). This hypersensitivity was observed even at 0.5 h after CFA injection and further progressed in following 2–4 h ($n = 6$; $p < 0.01$; **Figure 1**). After 4–8 h, this hypersensitivity was maintained at the similar level for a few days after CFA injection, representing maintenance period of CFA-induced inflammatory pain (**Figure 1**).

CFA (but not saline) injection led also to development of mechanical hypersensitivity that manifested as a marked increase in paw withdrawal frequencies in response to von Frey filaments applied to the injected hind paw (**Figure 2**). As with the paw withdrawal latency, a significant increase in paw withdrawal frequency started at 0.5 h after CFA injection and further progressed

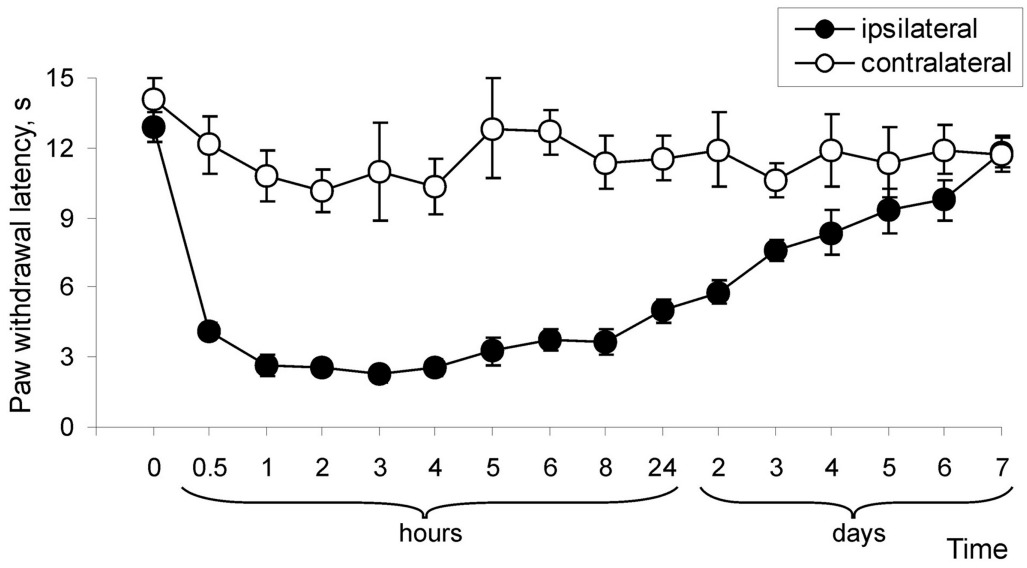

FIGURE 1 | Development of CFA-induced peripheral thermal hypersensitivity in rats. CFA injection induced a decrease in paw withdrawal latency in response to thermal stimulation ($n = 6$/time point).

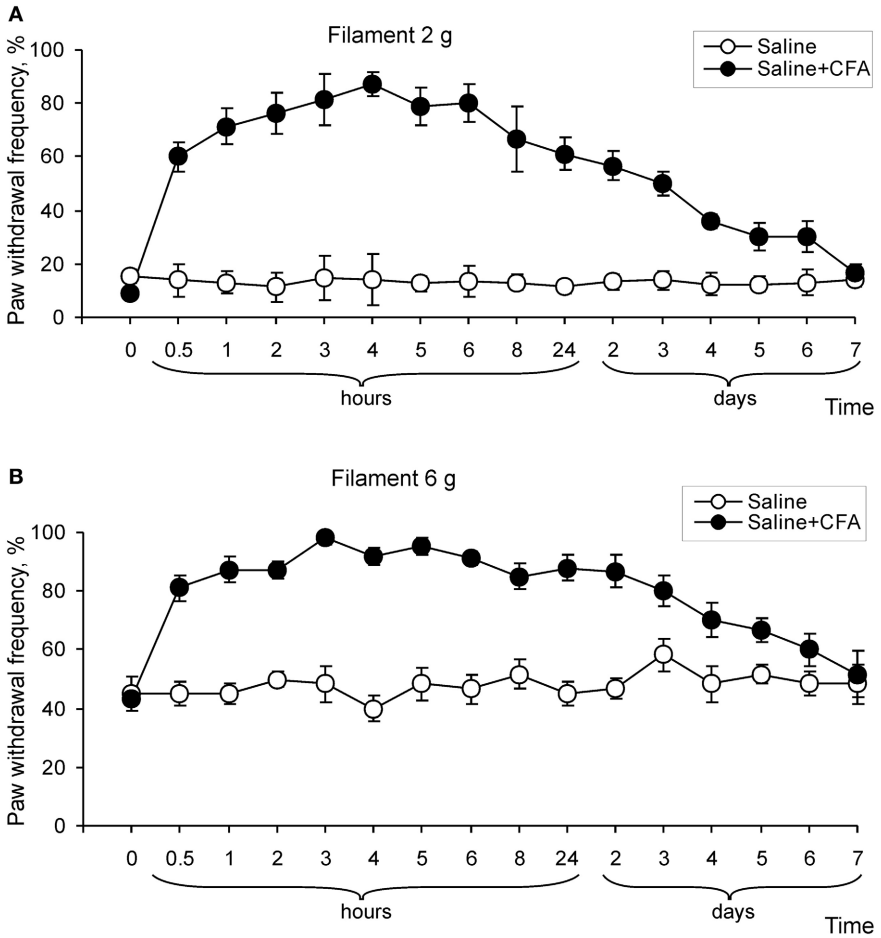

FIGURE 2 | Development of mechanical hypersensitivity after CFA injection. (A,B) Paw withdrawal frequency in response to 2 g **(A)** and 6 g **(B)** von Frey filaments changed over time on the ipsilateral side after CFA, but not after saline injection into a hind paw ($n > 6$/time point for saline and CFA).

over 2–4 h ($n = 8$; $p < 0.01$), then was maintained for a few days (**Figure 2**). In addition, CFA injection significantly increased the paw withdrawal frequencies in response to innoxious (2 and 4 g) and noxious (6 and 8 g) von Frey filaments, indicating development of mechanical allodynia and hyperalgesia, respectively ($n = 6$; $p < 0.01$; **Figures 2A,B**; data for 4 and 8 g are not shown). These results indicate that remarkable thermal and mechanical hypersensitivities develop in a time interval of 1–6 h after CFA injection and these changes of peripheral sensitivity are comparable to the changes observed during the maintenance period of chronic inflammatory pain (1–7 days after CFA injection).

CFA-INDUCED INFLAMMATION UPREGULATES EXTRASYNAPTIC AMPARs IN TONICALLY FIRING SG NEURONS RATHER THAN IN TRANSIENT NEURONS

Previously we showed that CFA-induced peripheral inflammation substantially increases functional expression of Ca^{2+}-permeable AMPARs in the extrasynaptic plasma membrane of lamina II dorsal horn neurons during the maintenance period of persistent inflammatory pain (Kopach et al., 2011) and altered AMPAR trafficking is necessary for the maintenance of inflammatory pain (Park et al., 2009). In this work, we studied whether CFA-induced peripheral inflammation affects extrasynaptic AMPARs functioning in these neurons during the development phase of persistent inflammatory pain. Because of our behavioral results and those of others (Zhang et al., 2003) have shown that CFA-induced robust thermal and mechanical hypersensitivities develop over 2–4 h after CFA injection, we chose the time point of 3 h after CFA injection to represent the development phase of CFA-induced persistent inflammatory pain. To directly evaluate CFA-induced changes in functional expression of extrasynaptic AMPARs during inflammatory pain development, we performed simultaneous recordings of membrane current and associated $[Ca^{2+}]_i$ transients produced by a selective agonist of AMPARs, AMPA, 3 h after saline or CFA injection (**Figures 3A,B**). We recorded AMPA-induced $[Ca^{2+}]_i$ transients in both the soma and dendrites of SG neurons.

Consistent with our previous reports (Voitenko et al., 2004; Kopach et al., 2011), bath application of AMPA (5 μM, 60 s) to the spinal cord slices evoked an inward current in all SG neurons at a holding potential of –60 mV. This current was characterized

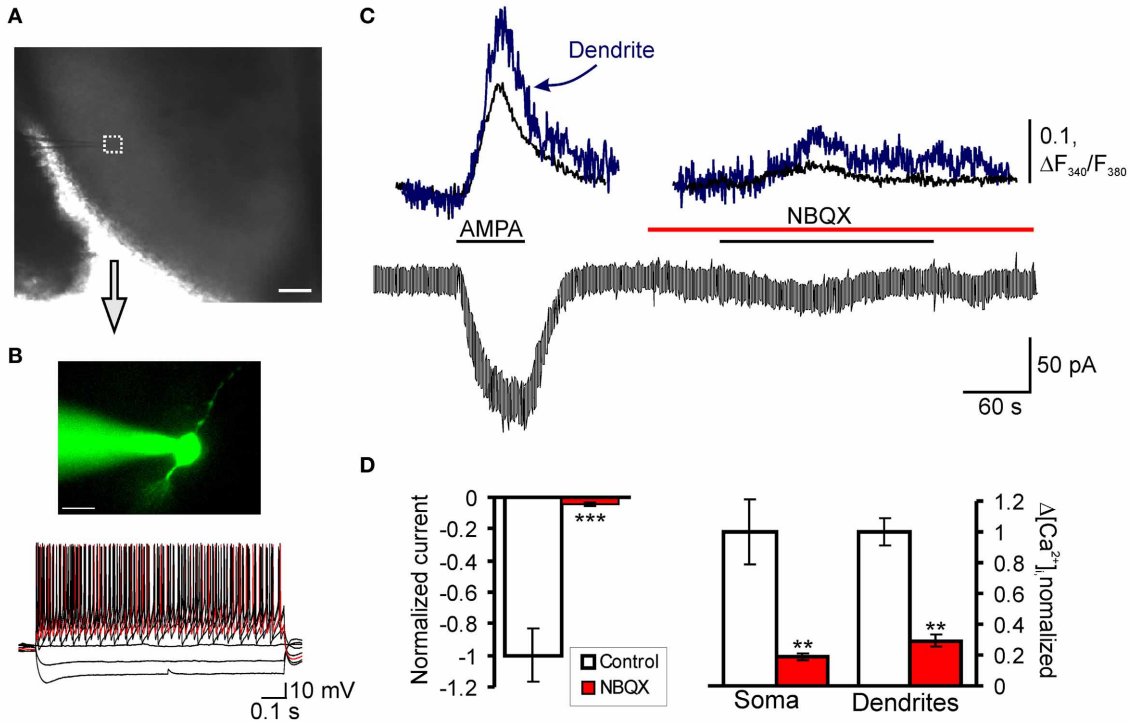

FIGURE 3 | AMPAR-mediated currents and associated $[Ca^{2+}]_i$ transients in SG neurons of spinal cord slices. (A) Transmitted light image of patch electrode position (square) in the SG of a transverse spinal cord slice; scale bar = 200 μm. **(B)** A fluorescent image of SG neuron loaded with fura-2 (200 μM) and current-clamp recording of typical firing pattern for tonic neurons; scale bar = 20 μm. **(C)** Representative trace of a membrane current recorded from the soma in tonic neurons during AMPA bath application (5 μM) before and after pre-application of AMPAR antagonist NBQX (30 μM). **(D)** A statistical summary of the AMPA-induced current amplitudes (left graph) and $[Ca^{2+}]_i$ transients (right graph) in soma and dendrites of SG neurons before and after pre-application of AMPAR antagonists NBQX. $^{**}p < 0.01$, $^{***}p < 0.001$ versus control.

by a slow rising phase and subsequent plateau, reached within 20–60 seconds (**Figure 3C**). Although bath applied AMPA activates a total pool of plasma membrane AMPARs, the extrasynaptic receptors are the predominant contributor to AMPA-induced current because they are relatively more abundant in neuronal plasma membrane and have weaker desensitization than synaptic AMPARs (Guire et al., 2008; Arendt et al., 2010; Vizi et al., 2010). In addition, substantial differences in a rectification index and a sensitivity to polyamine blockers between AMPA-induced currents (Kopach et al., 2011) and AMPAR-mediated excitatory postsynaptic currents evoked by dorsal root stimulation in SG neurons (Katano et al., 2008; Vikman et al., 2008; Park et al., 2009) further confirm a major contribution of extrasynaptic receptors to AMPA-induced currents.

The AMPA-induced current was associated with a synchronous rise in $[Ca^{2+}]_i$ observed in both soma and dendrites of examined neurons (**Figure 3C**). The observed current and associated $[Ca^{2+}]_i$ transients were mediated by an activation of AMPARs, as a potent AMPAR antagonist NBQX (30 μM) almost completely inhibited both the current and $[Ca^{2+}]_i$ transients (**Figures 3C,D**). Other selective AMPAR antagonist, GYKI 52466, also inhibited both the current and associated $[Ca^{2+}]_i$ transients similar to NBQX (Kopach et al., 2011), further indicating an activation of AMPARs.

Taking into account that the population of SG neurons is not homogeneous and displays distinct immunohistochemical (Engelman et al., 1999), electrophysiological (Grudt and Perl, 2002) and functional properties (Graham et al., 2004), we divided all neurons accordingly to their firing pattern in a response to sustained depolarizing current. Furthermore, our previous results have shown that persistent peripheral inflammation changes extrasynaptic AMPAR trafficking specifically in subpopulation of SG neurons characterized by intrinsic tonic firing properties, but not in those that exhibited strong adaptation (Kopach et al., 2011). Therefore, we divided all SG neurons tested into two main groups: "tonic" and "transient." Tonic neurons were those that supported continued discharge of action potentials during 1-s depolarizing inward current with increased frequency of discharge in a response to increased current intensity (**Figure 3B**). Transient neurons were those that exhibited a strong adaptation by generating short bursts of spikes or just a single spike regardless of depolarizing current intensity (**Figure 5A**).

In tonically firing SG neurons, the average amplitude of AMPA-induced currents comprised 236 ± 39 pA ($n = 23$) in the saline-treated group; the amplitude of associated $[Ca^{2+}]_i$ transients, expressed as an increase in the ratio of fura-2 fluorescence at 340–380 nm, ΔR (see "Materials and Methods"), were

0.47 ± 0.10 ($n = 21$) for soma and 0.60 ± 0.12 ($n = 14$) for dendrites (**Figures 4A,B**). CFA-induced inflammation significantly increased the amplitude of AMPA-induced current in the tonic SG neurons 3 h after CFA injection (**Figure 5C**). In particular, the average amplitude of AMPA-induced current was -236 ± 39 pA ($n = 23$) in 3 h post-saline group, but -437 ± 41 pA ($n = 23$; $p < 0.001$) in 3 h post-CFA group (**Figure 4B**). CFA-induced inflammation led to a tendency toward an increase in the amplitude of associated $[Ca^{2+}]_i$ transients in soma and dendrites of tonic SG neurons 3 h after injection (**Figures 4A,B**). In soma, the average amplitudes of AMPA-induced $[Ca^{2+}]_i$ transients were 0.47 ± 0.10 ($n = 21$) vs 0.54 ± 0.10 ($n = 20$) in the post-saline and post-CFA groups, respectively (**Figure 4B**). In dendrites, the average amplitudes of $[Ca^{2+}]_i$ transients were 0.60 ± 0.12 ($n = 14$) 3 h after saline vs 0.84 ± 0.23 ($n = 15$) 3 h after CFA (**Figure 4B**). However, these changes were not significant ($p > 0.05$).

These findings indicate that CFA-induced peripheral inflammation significantly upregulates functional expression of extrasynaptic AMPARs in tonically firing SG neurons during the development period of inflammatory pain.

CFA-induced inflammation did not significantly change the AMPA-induced current and associated $[Ca^{2+}]_i$ transients in the transient subtype of SG neurons during the development period of inflammatory pain. In the saline-treated group, average amplitude of AMPA-induced current was -177 ± 22 pA ($n = 24$) in the transient SG neurons that was not significantly different from that in the tonic neurons ($p > 0.05$). In the transient SG neurons from the CFA-treated group, the current amplitude was -259 ± 35 pA at 3 h after CFA injection ($n = 34$; $p > 0.05$ compared to the saline-treated group; **Figures 5A–C**). No significant differences were observed also in the average amplitudes of AMPA-induced $[Ca^{2+}]_i$ transients in soma and dendrites of transient SG neurons between the saline- and CFA-treated groups 3 h after injection. In soma, average amplitudes of $[Ca^{2+}]_i$ transients were: 0.48 ± 0.09 ($n = 22$) and 0.39 ± 0.04 ($n = 31$) for the saline- and CFA-treated groups, respectively ($p > 0.05$; **Figure 5B**). In dendrites, average amplitudes of $[Ca^{2+}]_i$ transients were 0.52 ± 0.09 ($n = 18$) for the saline-treated and 0.54 ± 0.09 ($n = 18$) for the CFA-treated groups 3 h after injection ($p > 0.05$; **Figure 5B**). These results demonstrate that in the transient type of SG neurons extrasynaptic AMPARs functioning is not significantly altered during development of CFA-induced inflammatory pain.

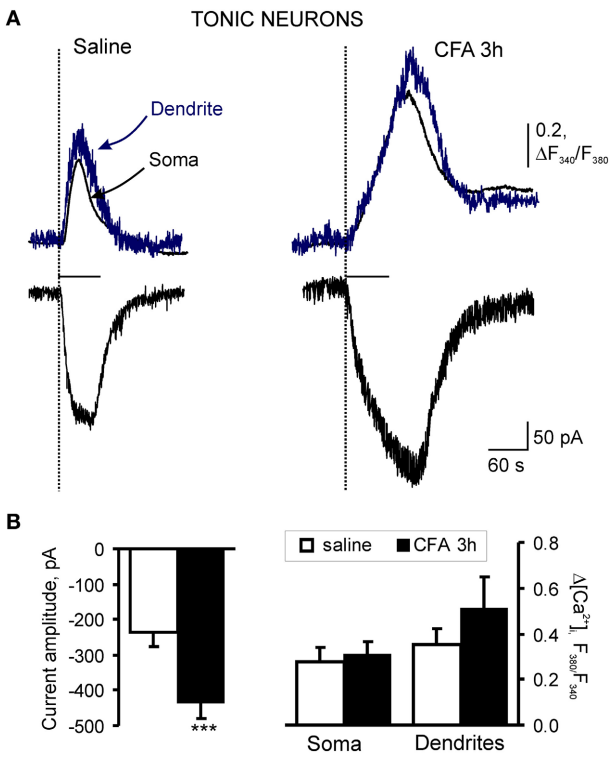

FIGURE 4 | Extrasynaptic AMPARs are markedly upregulated in tonic SG neurons during development of CFA-induced infl mmatory pain. **(A)** Representative examples of AMPA-induced membrane current (bottom traces) and associated $[Ca^{2+}]_i$ transients in soma (upper black traces) and dendrites (upper blue traces) in tonic neurons 3 h after saline (left traces) or CFA injection (right traces). **(B)** A statistical summary of current amplitudes (left graph) and $[Ca^{2+}]_i$ transients (right graph) in soma and dendrites of tonic SG neurons 3 h after saline or CFA injection. AMPA-induced currents were significantly increased during chronic pain development. Despite the tendency toward an increase in $[Ca^{2+}]_i$ transients in SG neurons 3 h after CFA injection, no significant change in their amplitudes was observed. ***$p < 0.001$ versus the saline-treated group.

DISCUSSION

In this work, we have demonstrated that extrasynaptic AMPARs are significantly upregulated in tonically firing dorsal horn SG neurons during the development of persistent inflammatory pain. This upregulation of AMPARs in dorsal horn neurons is associated with inflammation-induced hyperalgesia and allodynia and might contribute to the development and maintenance of persistent inflammatory pain.

Our findings and those of others (Zhang et al., 2003; Park et al., 2009) show that CFA-induced peripheral inflammation produces rapid development of peripheral hyperalgesia and allodynia (2–3 h after CFA injection) that represents developmental period of persistent inflammatory pain, whereas pain hypersensitivities observed during 1–7 d post-CFA reflects the maintenance phase of inflammatory pain (**Figures 1** and **2**). Spinal cord dorsal horn sensitization is considered to be a central mechanism that underlies the induction and maintenance of pain hypersensitivities (Woolf and Salter, 2000; Latremoliere and Woolf, 2009; Wang et al., 2010). Central sensitization produces a substantial prolongation and enhancement of responses to both noxious and innocuous stimuli (hyperalgesia and allodynia) and is a specific form of synaptic plasticity in spinal cord, which depends crucially on recruitment of glutamate receptors (Woolf and Salter, 2000; Latremoliere and Woolf, 2009; Wang et al., 2010). Activation of particularly NMDA receptors and AMPARs in dorsal horn neurons is required for the development and maintenance of spinal sensitization and hyperalgesia (Woolf and Salter, 2000; Hartmann et al., 2004; Katano et al., 2008; Vikman et al., 2008; Latremoliere and Woolf, 2009; Park et al., 2009).

Previously we and others showed that persistent inflammation produces a switch of Ca^{2+}-impermeable to Ca^{2+}-permeable AMPAR-mediated neurotransmission at synapses in dorsal horn

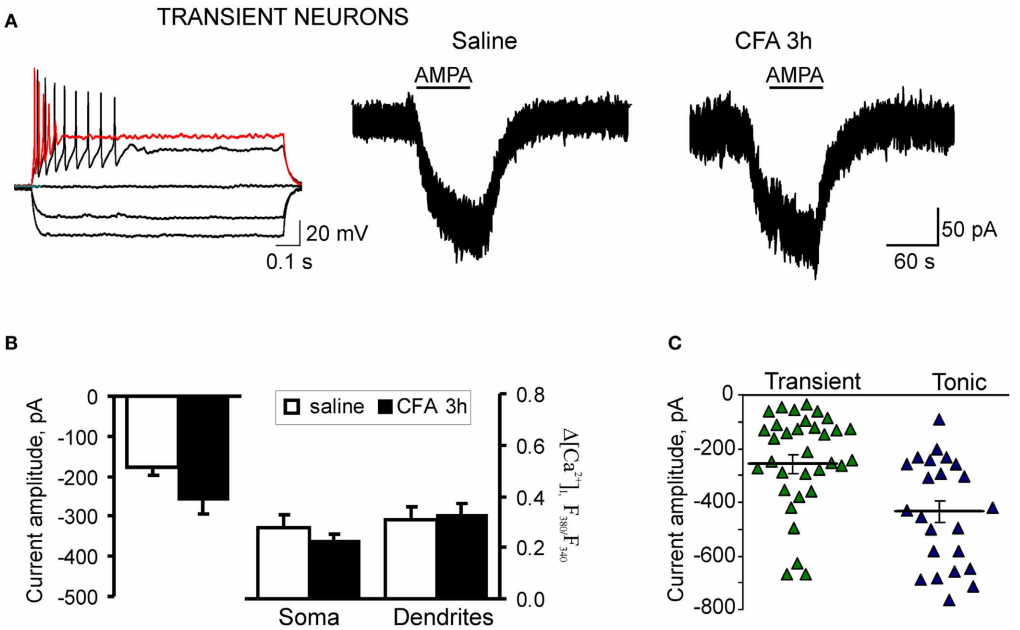

FIGURE 5 | Extrasynaptic AMPARs functioning is not altered in the transient SG neurons during development of CFA-induced inflammatory pain. (A) Typical firing pattern (left traces) and representative examples of AMPA-induced somatic currents (right traces) in the transient SG neurons 3 h after saline (control) or CFA injection. **(B)** A statistical summary of the current amplitudes (left graphs) and $[Ca^{2+}]_i$ transients (right graphs) in soma and dendrites of transient SG neurons 3 h after injection of saline or CFA. No significant difference was found in all measured parameters. **(C)** The scatter plot illustrates a spread in AMPA-induced currents in the tonic (blue) and transient (green) neurons 3 h after CFA injection. Difference in the amplitudes of AMPA-induced currents between the transient and tonic SG neurons was significant in the CFA-inflamed group ($p < 0.01$), but not significant 3 h post-saline ($p > 0.05$).

during the maintenance of inflammatory pain (Katano et al., 2008; Vikman et al., 2008; Park et al., 2009) and these changes are necessary for the peripheral inflammatory pain maintenance (Park et al., 2009). Peripheral inflammatory insult also increases functional expression of extrasynaptic Ca^{2+}-permeable AMPARs in the tonically firing SG neurons during the maintenance period of inflammatory pain, as we reported recently (Kopach et al., 2011). Our current work illustrates that CFA-induced inflammation substantially upregulates extrasynaptic AMPARs in tonically firing SG neurons during the inflammatory pain development (3 h after CFA injection). Our electrophysiological results suggest that the number of extrasynaptic AMPARs is substantially increased in the SG neurons during development of CFA-induced peripheral hyperalgesia and allodynia. This upregulation of AMPARs may contribute to the observed hypersensitivities during pain development, as altered AMPAR trafficking is necessary for the persistent pain maintenance (Park et al., 2009). In contrast to the maintenance of inflammatory pain, AMPAR-mediated Ca^{2+} signaling in the tonic firing SG neurons was not significantly changed during the inflammatory pain development. We suggest that the upregulation of extrasynaptic AMPARs during pain development may be mediated mainly by an increase in GluR2-containing, Ca^{2+}-impermeable AMPARs followed by a subsequent upregulation of GluR2-lacking, Ca^{2+}-permeable extrasynaptic AMPARs, which was observed during the maintenance period of persistent inflammation (Kopach et al., 2011). Phosphorylation of AMPAR subunits may underlie the observed CFA-induced upregulation of extrasynaptic AMPARs in dorsal horn SG neurons during inflammatory pain development. As we have demonstrated previously, CFA injection significantly changes the level of GluR2 phosphorylation 2 h after CFA injection (Park et al., 2009), supporting our current electrophysiological results. However, the precise mechanisms of AMPARs regulation are not completely clear because of their complexity (Santos et al., 2009; Wang et al., 2010; He et al., 2011).

Other important finding of this study is the fact that extrasynaptic AMPAR upregulation during development of persistent inflammatory pain was observed specifically in a subpopulation of SG neurons that exhibit intrinsic tonic firing properties, with no significant changes in the neurons that exhibit strong adaptation (transient neurons). This indicates that CFA alters extrasynaptic AMPARs in tonic firing SG neurons, whereas the pool of extrasynaptic AMPAR in the transient neurons is stable during the development of inflammatory pain and even during the persistent pain maintenance (Kopach et al., 2011). Taking into account similar patterns of extrasynaptic AMPAR expression in tonic and transient SG neurons under normal conditions (Kopach et al., 2011), these findings suggest different contribution of neuronal subtypes to the detection and/or transmission of nociceptive stimuli, resulting in different involvement in persistent inflammatory pain development and maintenance.

In conclusion, our study shows that CFA-induced peripheral inflammation upregulates extrasynaptic AMPARs specifically in tonic firing SG neurons during the development of inflammatory pain. These neurons may represent a specific population of neurons that carry out nociceptive inputs and

contribute to spinal central sensitization during development and maintenance of persistent inflammatory pain. The upregulated extrasynaptic AMPARs in dorsal horn neurons during the inflammatory pain development might contribute to persistent pain hypersensitivities.

ACKNOWLEDGMENTS

This work was supported by DFFD F46.2/001, NASU Biotechnology Grants (Nana Voitenko), by STCU/NASU Project #5510 (Pavel Belan), and by NASU Grant for Young Scientists (Olga Kopach).

REFERENCES

Adesnik, H., Nicoll, R. A., and England, P. M. (2005). Photoinactivation of native AMPA receptors reveals their real-time trafficking. *Neuron* 48, 977–985.

Allan, S. M., and Rothwell, N. J. (2001). Cytokines and acute neurodegeneration. *Nat. Rev. Neurosci.* 2, 734–744.

Arendt, K. L., Royo, M., Fernandez-Monreal, M., Knafo, S., Petrok, C. N., Martens, J. R., et al. (2010). PIP3 controls synaptic function by maintaining AMPA receptor clustering at the postsynaptic membrane. *Nat. Neurosci.* 13, 36–44.

Borgdorff, A. J., and Choquet, D. (2002). Regulation of AMPA receptor lateral movements. *Nature* 417, 649–653.

Bredt, D. S., and Nicoll, R. A. (2003). AMPA receptor trafficking at excitatory synapses. *Neuron* 40, 361–379.

Choquet, D., and Triller, A. (2003). The role of receptor diffusion in the organization of the postsynaptic membrane. *Nat. Rev. Neurosci.* 4, 251–265.

Cognet, L., Groc, L., Lounis, B., and Choquet, D. (2006). Multiple routes for glutamate receptor trafficking: surface diffusion and membrane traffic cooperate to bring receptors to synapses. *Sci. STKE* 2006, e13.

Engelman, H. S., Allen, T. B. and MacDermott, A. B. (1999). The distribution of neurons expressing calcium-permeable AMPA receptors in the superficial laminae of the spinal cord dorsal horn. *J. Neurosci.* 19, 2081–2089.

Graham, B. A., Brichta, A. M., and Callister, R. J. (2004). *In vivo* responses of mouse superficial dorsal horn neurones to both current injection and peripheral cutaneous stimulation. *J. Physiol.* 561, 749–763.

Grudt, T. J., and Perl, E. R. (2002). Correlations between neuronal morphology and electrophysiological features in the rodent superficial dorsal horn. *J. Physiol.* 540, 189–207.

Guire, E. S., Oh, M. C., Soderling, T. R., and Derkach, V. A. (2008). Recruitment of calcium-permeable AMPA receptors during synaptic potentiation is regulated by CaM-kinase I. *J. Neurosci.* 28, 6000–6009.

Hargreaves, K., Dubner, R., Brown, F., Flores, C., and Joris, J. (1988). A new and sensitive method for measuring thermal nociception in cutaneous hyperalgesia. *Pain* 32, 77–88.

Hartmann, B., Ahmadi, S., Heppenstall, P. A., Lewin, G. R., Schott, C., Borchardt, T., et al. (2004). The AMPA receptor subunits GluR-A and GluR-B reciprocally modulate spinal synaptic plasticity and inflammatory pain. *Neuron* 44, 637–650.

He, K., Goel, A., Ciarkowski, C. E., Song, L., and Lee, H. K. (2011). Brain area specific regulation of synaptic AMPA receptors by phosphorylation. *Commun. Integr. Biol.* 4, 569–572.

Katano, T., Furue, H., Okuda-Ashitaka, E., Tagaya, M., Watanabe, M., Yoshimura, M., et al. (2008). N-ethylmaleimide-sensitive fusion protein (NSF) is involved in central sensitization in the spinal cord through GluR2 subunit composition switch after inflammation. *Eur. J. Neurosci.* 27, 3161–3170.

Kopach, O., Kao, S. C., Petralia, R. S., Belan, P., Tao, Y. X., and Voitenko, N. (2011). Inflammation alters trafficking of extrasynaptic AMPA receptors in tonically firing lamina II neurons of the rat spinal dorsal horn. *Pain* 152, 912–923.

Kullmann, D. M. (2000). Spillover and synaptic cross talk mediated by glutamate and GABA in the mammalian brain. *Prog. Brain Res.* 125, 339–351.

Latremoliere, A., and Woolf, C. J. (2009). Central sensitization: a generator of pain hypersensitivity by central neural plasticity. *J. Pain* 10, 895–926.

Malinow, R., and Malenka, R. C. (2002). AMPA receptor trafficking and synaptic plasticity. *Annu. Rev. Neurosci.* 25, 103–126.

Park, J. S., Voitenko, N., Petralia, R. S., Guan, X., Xu, J. T., Steinberg, J. P., et al. (2009). Persistent inflammation induces GluR2 internalization via NMDA receptor-triggered PKC activation in dorsal horn neurons. *J. Neurosci.* 29, 3206–3219.

Park, J. S., Yaster, M., Guan, X., Xu, J. T., Shih, M. H., Guan, Y., et al. (2008). Role of spinal cord alpha-amino-3-hydroxy-5-methyl-4-isoxazolepropionic acid receptors in complete Freund's adjuvant-induced inflammatory pain. *Mol. Pain* 4, 67.

Santos, S. D., Carvalho, A. L., Caldeira, M. V., and Duarte, C. B. (2009). Regulation of AMPA receptors and synaptic plasticity. *Neuroscience* 58, 105–125.

Tao, Y. X. (2010). Dorsal horn alpha-amino-3-hydroxy-5-methyl-4-isoxazolepropionic acid receptor trafficking in inflammatory pain. *Anesthesiology* 112, 1259–1265.

Vikman, K. S., Rycroft, B. K., and Christie, M. J. (2008). Switch to Ca^{2+}-permeable AMPA and reduced NR2B NMDA receptor-mediated neurotransmission at dorsal horn nociceptive synapses during inflammatory pain in the rat. *J. Physiol.* 586, 515–527.

Vizi, E. S., Fekete, A., Karoly, R., and Mike, A. (2010). Non-synaptic receptors and transporters involved in brain functions and targets of drug treatment. *Br. J. Pharmacol.* 160, 785–809.

Voitenko, N., Gerber, G., Youn, D., and Randic, M. (2004). Peripheral inflamation-induced increase of AMPA-mediated currents and Ca^{2+} transients in the presence of cyclothiazide in the rat substantia gelatinosa neurons. *Cell Calcium* 35, 461–469.

Wang, Y., Wu, J., Wu, Z., Lin, Q., Yue, Y., and Fang, L. (2010). Regulation of AMPA receptors in spinal nociception. *Mol. Pain* 6, 5.

Weng, H. R., Chen, J. H., and Cata, J. P. (2006). Inhibition of glutamate uptake in the spinal cord induces hyperalgesia and increased responses of spinal dorsal horn neurons to peripheral afferent stimulation. *Neuroscience* 138, 1351–1360.

Woolf, C. J., and Salter, M. W. (2000). Neuronal plasticity: increasing the gain in pain. *Science* 288, 1765–1769.

Zhang, B., Tao, F., Liaw, W. J., Bredt, D. S., Johns, R. A., and Tao, Y. X. (2003). Effect of knock down of spinal cord PSD-93/chapsin-110 on persistent pain induced by complete Freund's adjuvant and peripheral nerve injury. *Pain* 106, 187–196.

Conflict of Interest Statement: The authors declare that the research was conducted in the absence of any commercial or financial relationships that could be construed as a potential conflict of interest.

Received: 15 April 2012; accepted: 13 September 2012; published online: 02 October 2012.

Citation: Kopach O, Viatchenko-Karpinski V, Belan P and Voitenko N (2012) Development of inflammation-induced hyperalgesia and allodynia is associated with the upregulation of extrasynaptic AMPA receptors in tonically firing lamina II dorsal horn neurons. Front. Physio. ***3****:391. doi: 10.3389/fphys.2012.00391*

This article was submitted to Frontiers in Membrane Physiology and Biophysics, a specialty of Frontiers in Physiology.

frontiers in
PHYSIOLOGY

GENERAL COMMENTARY
published: 28 May 2012
doi: 10.3389/fphys.2012.00158

Extrasynaptic release of serotonin affects the social dynamics of leeches

Enrique Hernández-Lemus*

Computational Genomics Department, National Institute of Genomic Medicine, México City, Mexico
**Correspondence: ehernandez@inmegen.gob.mx*

A commentary on

The dynamics of group formation among leeches

by Bisson, G., Bianconi, G., and Torre, V. (2012). Front. Physiol. 3:133. doi: 10.3389/fphys.2012.00133

In order to attain significative advance in almost any area in modern-day scientific research, it is often necessary to *think out-of-the-box*. That is, if we want to catch something fresh and new, we need to abandon traditional paradigms and preconceived ways of reasoning. In this sense, the paper by Bisson et al. (2012) in this special issue results quite enlightening, for it seems that, their way of *thinking out of the box* is based on their ability to *think inside many boxes at a time*. In this paper, the authors discuss about group formation in leeches, and the way that extrasynaptic neuromodulation affects this phenomenon. Group formation is shown to be facilitated by body injection of serotonin (5-HT). It is also mentioned how the level of endogenous 5-HT is elevated in leeches belonging to a large group. To test the role of 5-HT neuromodulation in group formation, leeches were injected with 5-HT antagonists that prevented them from joining a large group. Sensilla ablation and supraesophageal ganglion disconnection also prevented group formation. It is discussed the role that neurochemicals may have on social decision making in leeches, resembling the case in human interactions. Interesting parallels were thus sketched between social group formation in leeches and in humans. For instance, the authors revealed the presence of social reinforcement dynamics as a feature of group formation. Social reinforcement is known to play an important role in human social interactions (Cattuto et al., 2009; Stehlé et al., 2010). It is also shown that before socializing on a *permanent basis*, leeches first "*get acquainted with each other*" as the authors argue in the beginning of the subsection *Properties of group formation*, recalling that groups formed in the first hour are *not stable*.

The findings and conclusions of this paper are thus very appealing and intriguing. However, no less riveting result the methods used to reach such conclusions. Apart from the obvious display of ability in the methods of experimental neurobiology; the group, headed by Professor Vincent Torre, embarked upon a research project that combines ethology (by studying leech behavior), social network dynamics (e.g., reinforcement dynamics), imaging and image processing (image acquisition, discretization techniques), computational geometry (contour-tracing and polygon-filling algorithms), mathematical optimization (constrained quadratic programming), and an overall view from the standpoint of complex systems science; all of this, without abandoning their neurobiological foundations.

The scope of studies of this kind, as well as their outreach possibilities, is large. Such disparate areas of research as social network epidemiology (Christakis and Fowler, 2008, 2012), flocking and swarming (Miramontes and De Souza, 2008; Aldana et al., 2009; Nagy et al., 2010), collective neural computation (Hopfield, 1982; Colorni et al., 1992), and of course, physiology and neuroscience, may be influenced by the ideas and methods combined in this study. Last but not least we may mention another feature of this paper that, while it should be a rule on scientific inquiry, it results somehow dismissed in many instances nowadays, likely due to publication pressure. We refer to the role that *alternative hypothesis testing* should have in research. In order to prove their point about the role that 5-HT may have in the dynamics of group formation in leeches, the authors injected leeches with both, the neurotransmitter and its antagonists, tested the medium for chemotaxis, ablated the Sensilla and disconnected the supraesophageal ganglion to physically block the effects of 5-HT. They also probed about the influence of illumination and seasonal variability for the possible impact on their results. Overall: a gripping, novel – yet somehow risky-analysis, on a quite outstanding series of experimental results that seem to suggest a non-trivial relation between extrasynaptic signaling and social behavior.

REFERENCES

Aldana, M., Larralde, H., and Vázquez, B. (2009). On the emergence of collective order in swarming systems: a recent debate. *Int. J. Mod. Phys. B* 23, 3661–3685.

Bisson, G., Bianconi, G., and Torre, V. (2012). The dynamics of group formation among leeches. *Front. Physiol.* 3:133. doi: 10.3389/fphys.2012.00133

Cattuto, C., Barrat, A., Baldassarri, A., Schehr, G., and Loreto, V. (2009). Collective dynamics of social annotation. *Proc. Natl. Acad. Sci. U.S.A.* 106, 10511–10515.

Christakis, N. A., and Fowler, J. H. (2008). The collective dynamics of smoking in a large social network. *N. Engl. J. Med.* 358, 2249–2258.

Christakis, N. A., and Fowler, J. H. (2012). Social network sensors for early detection of contagious outbreaks. *PLoS ONE* 5, e12948. doi: 10.1371/journal.pone.0012948

Colorni, A., Dorigo, M., and Maniezzo, V. (1992). "Distributed optimization by ant colonies," in *Toward a Practice of Autonomous Systems: Proceedings of the First European Conference on Artificial Life*, F. eds J. Varela and P. Bourgine (Cambridge, MA: MIT Press/Bradford Books), 1341–42.

Hopfield, J. J. (1982). Neural networks and physical systems with emergent collective computational abilities. *Proc. Natl. Acad. Sci. U.S.A.* 79, 2554–2558.

Miramontes, O., and De Souza, O. (2008). Individual basis for collective behaviour in the termite, *Cornitermes cumulans*. *J. Insect Sci.* 8, 1–22.

Nagy, M., Ákos, Z., Biro, D., and Vicsek, T. (2010). Hierarchical group dynamics in pigeon flocks. *Nature* 464, 890–893.

Stehlé, J., Barrat, A., and Bianconi, G. (2010). Dynamical and bursty interactions in social networks. *Phys. Rev. E* 81, 035101.

Received: 02 May 2012; accepted: 06 May 2012; published online: 28 May 2012.
*Citation: Hernández-Lemus E (2012) Extrasynaptic release of serotonin affects the social dynamics of leeches. Front. Physio. **3**:158. doi: 10.3389/fphys.2012.00158*
This article was submitted to Frontiers in Membrane Physiology and Biophysics, a specialty of Frontiers in Physiology.

frontiers in
PHYSIOLOGY

ORIGINAL RESEARCH ARTICLE
published: 17 May 2012
doi: 10.3389/fphys.2012.00133

The dynamics of group formation among leeches

Giacomo Bisson[1], Ginestra Bianconi[2] and Vincent Torre[1]*

[1] *Neurobiology Sector, Scuola Internazionale Superiore di Studi Avanzati, Trieste, Italy*
[2] *Department of Physics, Northeastern University, Boston, MA, USA*

Edited by:
Francisco Fernandez De-Miguel, Universidad Nacional Autonoma de Mexico, Mexico

Reviewed by:
Hai Huang, Oregon Health and Science University, USA
Enrique Hernandez-Lemus, National Institute of Genomic Medicine, Mexico

***Correspondence:**
Vincent Torre, Neurobiology Sector, Scuola Internazionale Superiore di Studi Avanzati, Via Bonomea 265, 34136 Trieste, Italy.
e-mail: torre@sissa.it

Leeches exploring a new environment continuously meet each other and merge in temporary groups. After 2–3 h, leeches become attracted to each other eventually forming a large and stable group. When their number is reduced, leeches remain solitary, behaving independently. Group formation is facilitated by body injection of serotonin (5-HT) and the level of endogenous 5-HT is elevated in leeches forming a large group. In contrast, intravenous injection of 5-HT antagonists prevented injected leeches from joining a large group of conspecifics. When sensilla near the head were ablated or the supraesophageal ganglion disconnected, leeches remained solitary, but explored the environment swimming and crawling. These results suggest that group formation is initiated by a release of 5-HT triggered by sensilla stimulation and its dynamics can be explained by the establishment of a reinforcement dynamics, as observed during human group formation. As 5-HT affects social interactions also in humans, group formation in leeches and humans share a similar dynamics and hormonal control.

Keywords: serotonin, leech nervous system, social behavior, extrasynaptic release

INTRODUCTION

Animals from simple invertebrates to mammals and humans, not only interact with the environment but establish social interactions with their conspecifics (Anstey et al., 2009; Makris et al., 2009; Nagy et al., 2010; Sokolowski, 2010; Zhao et al., 2011). In lower invertebrates these interactions lead to a swarming behavior with the formation of groups of several tens and even thousands of conspecifics adopting the same behavior. Locusts can switch from a solitary to a social behavior, advantageous when competing for limited resources or during migration (Buhl et al., 2006; Bazazi et al., 2008; Anstey et al., 2009). Several species of fish form large shoals (Blaxter and Hunter, 1982; Hoare et al., 2000) often before migration (Makris et al., 2009). Birds form flocks able to fly collectively (Ballerini et al., 2008; Nagy et al., 2010). We have studied the emergence of group formation in leeches for two reasons: firstly, because it is possible to quantify their behavior easily and precisely (Garcia-Perez et al., 2005; Mazzoni et al., 2005; Bisson and Torre, 2011). Secondly, the nervous system of the leech *Hirudo medicinalis* has been extensively studied (Macagno, 1980; Muller et al., 1981) so that it is possible to relate its behavior to underlying neuronal networks (Kristan et al., 2005) and specific neuromodulators, such as serotonin (5-HT), dopamine (DA), and octopamine (Willard, 1981; Puhl and Mesce, 2008). In the present manuscript, we quantify the dynamics of formation of leech groups. When the density of conspecifics is low (less than five conspecifics in 700 cm^2) leeches move independently, but when their density is doubled the formation of stable groups is observed. The critical density for group formation is lowered by elevating the level of intracellular 5-HT inside the leech bodies. Ablation experiments show that a neurobiological signal modulating group formation is initiated by sensory receptors located near the leech's head and processed in the supraesophageal ganglion. We have detected an elevation of the level of endogenous 5-HT in leeches forming a large group and this observation raises the possibility that a somatic, i.e., an extrasynaptic release of 5-HT is involved in group formation. Indeed extrasynaptic release of 5-HT able to diffuse to remote receptor sites has been detected and characterized in several preparations where is associated to functional roles (Bunin et al., 1998; Bunin and Wightman, 1999; De-Miguel and Trueta, 2005; Kaushalya et al., 2008). At a formal level, the formation of stable groups can be explained by the establishment of a reinforcement dynamics (Cattuto et al., 2009; Stehlé et al., 2010) depending on the leech density and the intracellular level of 5-HT, which can be modeled in a mathematical way, very similar to that used to describe human aggregation (Stehlé et al., 2010; Zhao et al., 2011).

MATERIALS AND METHODS

ANIMALS AND PREPARATIONS

Adult leeches (*Hirudo verbana*) obtained from Ricarimpex (Eysines, France) were housed in groups of about 30 animals in 20-l tanks of artificial pond water [Instant Ocean salts (Aquarium Systems) diluted with deionized water to 1/1000 of ocean strength]. Leeches were kept in a circular tank (diameter: 30 cm, height: 6 cm), filled with artificial pond water kept at about 16°C, under daily illumination, and used within few months after shipping. Since Ricarimpex breeds leeches outdoors, we assume that they retain the seasonal rhythm established during development. Observation tanks were illuminated with a circular array of white light LEDs which provided dim, diffuse illumination with no abrupt spatial and/or temporal gradients. No additional sensory stimuli, such as chemical, mechanical, or visual inputs were intentionally applied. A transparent, plastic disk was used to keep leeches inside the tank.

DETERMINATION OF THE LEVEL OF 5-HT BY HPLC

Serotonin (5-hydroxytryptamine, 5-HT) was quantified in extracts of chains of leech ganglia by reverse-phase high performance liquid chromatography (HPLC). Leeches were positioned in the usual observation tank and after 3–5 h leeches which formed a group of at least eight conspecifics (gregarious leeches) and those who remained solitary were selected for the determination of their body level of 5-HT. Solitary and gregarious leeches were immediately submerged in liquid nitrogen for approximately 1 or 2 min and frozen leeches were placed on an ice cooled block. Chains of ganglia from the tail to the head ganglion – usually composed by around 20 individual ganglia – were dissected out and placed in a 100-μl microhomogenizer containing 50 μl of ice-cold 0.15 M perchloric acid and homogenized for 3 min on ice. The homogenate was transferred to 1.5 ml Eppendorf tubes using a Hamilton syringe and centrifuged at 17500 *g* for 20 min at room temperature. The supernatant was transferred to a second Eppendorf tube and stored at −80°C until HPLC analysis. A sample of 100–200 μl of their blood was also extracted and treated as treated as chains of ganglia. 5-HT was quantified by reference to external standards.

DELIVERY OF NEUROMODULATORS

Some leeches were injected with specific amounts of 5-HT, ketanserin, or mianserin (Sigma-Aldrich). All neuromodulator stock solutions (5-HT: 1 mM, mianserin: 10 mM, ketanserin: 5 mM) were prepared using distilled water (except ketanserin, which was dissolved in 0.1 M HCl solution), stored at −20°C in 500 μl aliquots and defrosted in 15 min at room temperature. The final concentration was reached by dilution in our normal leech saline solution (in mM: 116 NaCl, 1.8 $CaCl_2$, 4 KCl, 1.5 $MgCl_2$, 10 glucose, 10 Tris maleate buffered to pH 7.4) immediately before use and delivery. We injected 300 μl of 200 μM 5-HT solution using 1 ml insulin syringes with 29 GA and 15 mm long needles. Injection of 150 μl containing 1 mM ketanserin or 2 mM mianserin solutions were followed by another injection of 150 μl containing 400 μM 5-HT solution. Each leech was gently held in one hand and the needle was inserted under the skin of the dorsal side, along its dorsal axis at a depth of about 10% of the body thickness. We calculated that the injected solution was diluted into the extracellular space roughly 25–30% of the leech volume, usually 3–4 ml. Therefore, the final drug concentration injected in the leeches is approximately one-fourth of the injected drug concentration. The body volume of an adult leech is 3–4 ml, while the overall blood volume is about 8–9% of the body mass, corresponding to 240–360 μl (Wenning and Meyer, 2007). Changes of body volume are well tolerated by leeches because they can increase their initial weight by 8–11 times during feeding (Dickinson and Lent, 1984), it is likely that an increase of the body volume (about 10% of its body mass) caused by the injection did not impair the animal's movements.

ABLATION STUDIES

Leeches were anesthetized with 8% ethanol in leech Ringer's solution and iridectomy scissors were used to cut away the band of dorsal lip organs visible in the light microscope, with 1 or 2 mm of skin on either side including the rows of smaller lip organs detected with the scanning electron microscope (Elliott, 1986) but not visible in the light microscope. Sham operations were performed in the same way, except that a band of skin dorsally adjacent to the lip organs (along the dorsal surface of the head) was removed and the lip organs themselves were left intact. Leeches were allowed to recover for 1 day in water. The day after surgery, ablated leeches, injected with 300 μl of 200 μM 5-HT and sham-ablated leeches, were tested, along with normal controls, for social interactions.

IMAGING

We used a color CCD camera (640 × 480 pixels of image size; model DFK 21BF04; The Imaging Source Europe) to image leeches from above and to monitor their movements (**Figure 1A**). The camera was connected via the FireWire-output to a frame grabber (PCI-1394; Texas Instruments) installed on a personal computer, able to process images in real-time. Leeches' bodies were tracked at 7.5 Hz in RGB mode using a software program developed in Matlab language (MathWorks, Natick, MA, USA). The tracking algorithm is composed of two subroutines. The first subroutine is executed in real-time and extracts the borders of all the groups of leeches. Its purpose is to detect and store leech shapes. Each frame was converted into grayscale by means of the *average method* (i.e., by taking the average of the Red, Green, and Blue signals; Pratt, 1991). The resulting 8 bit grayscale image has values ranging between 0 (corresponding to white) and 255 (corresponding to black). A threshold equal to 50 is then applied to the grayscale image: all the pixels that have values major or equal to this threshold are set to value 255, 0 otherwise. We refer to this resulting image as the binary version of the frame (in which its pixels can assume only two possible values) and each leech – or group of leeches – appears as a black shape or blob. The extraction of the closed contours of each blob was achieved by applying a *Radial Sweep algorithm* (a contour tracing algorithm; Pavlidis, 1995) to the image, implemented in the Matlab function *bwboundaries* (Image Processing Toolbox, MathWorks, Natick, MA, USA). Each closed contour defines a blob representing a single leech or a group of leeches (**Figures 1E,F**, green lines). Blobs with an area below a threshold of 20 pixels^2 (usually caused by leech shadows) were discarded, as the average area of a single, small leech, is major than 30 pixels^2. The subroutine stores only the pixels belonging to the contour of the detected blobs so that it was possible to monitor leeches behavior for several hours, minimizing the storage size of the recording file.

The second subroutine is performed off-line and processes the previously extracted contours. Its purpose is to determine the number of leeches belonging to the blobs identified by their contour. In the generic frame k, each blob B^k can be labeled as the i-th blob (with i that ranges between 1 and N, where N is the total number of blobs in the k-th frame). If we overlap the frame k over the frame $k-1$ we will see that blobs representing a non-moving leech or groups of leeches will match almost perfectly (the small differences being caused by recording noise), whereas blobs representing moving leeches or groups of leeches will share just a portion of their area (usually minor than 80%). Moreover, two blobs observed in frame $k-1$, that merge (**Figure 1E**) between frames $k-1$ and k will partially overlap with the resulting blob observed in frame k. Finally, a single blob observed in frame $k-1$,

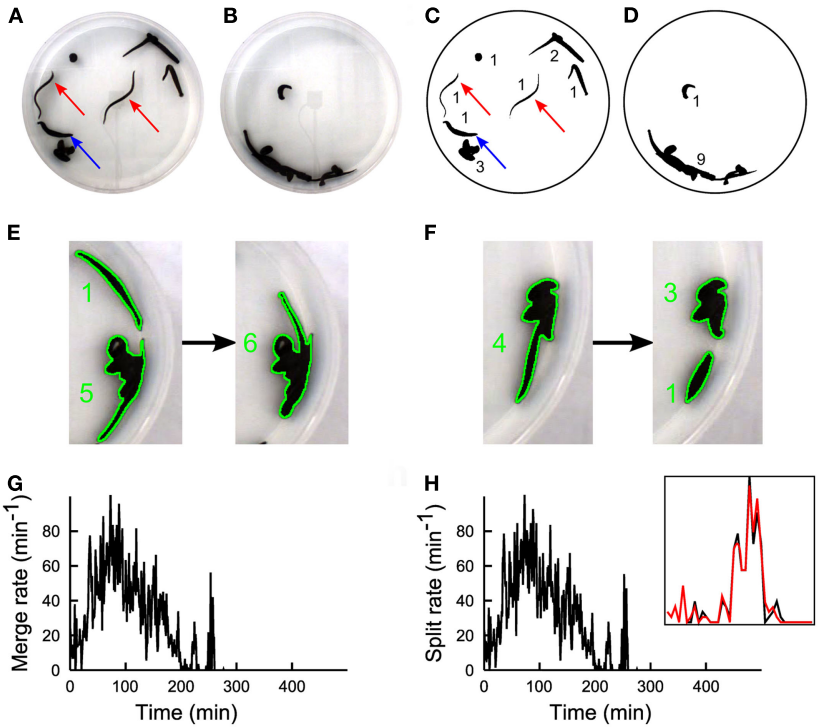

FIGURE 1 | The experimental set-up. A color CCD camera imaged from above the observation tank containing 10 leeches. **(A)** During the first 2 h, leeches inspected the environment. **(B)** Following the searching phase a stable large group of leeches in mutual contact was observed. **(C,D)** Images shown in **(A,B)**, after processing. Numbers in **(C,D)** indicate the number of conspecifics present in each group. A real-time algorithm extracted the borders of all leech groups (black blobs) and an off-line algorithm determined the number of leeches in each blob (black numbers). During the process of group formation, two kinds of events occurred: two groups could merge **(E)** forming a larger group, or a single group could split **(F)** forming two groups. During the searching phase, merge **(G)**, and split **(H)** rates have similar values, because leeches are highly active and no formation of stable groups can be observed. Inset in panel h shows a zoom of Merge (black) and Split(red) on an enlarged scale. Merge and split plots are very similar because they are evaluated on a sliding time window of size 5 min. Subtle differences between these two signals determine the group formation dynamics.

that splits (**Figure 1F**) between frames $k-1$ and k will partially overlap with the resulting blobs observed in frame k. The area of intersection between two blobs j and i (the first belonging to frame $k-1$, B_i^{k-1}, and the second to frame k, B_i^k) can be calculated by performing a multiplication between the binary image containing only B_j^{k-1} and the binary image containing only B_i^k. These two images can be obtained by filling the contours of the two blobs, using a *polygon fill* algorithm (Hearn and Baker, 1997) implemented in the Matlab function *poly2mask*. The multiplication is equivalent to performing a logical AND operation: the number of resulting pixels is the area of intersection between the two blobs. We can now define the overlap matrix Ω_{ij}^k as:

$$\Omega_{ij}^k = A\left(B_i^k \cap B_j^{k-1}\right)/A\left(B_j^{k-1}\right). \quad (1)$$

where A stands for "area" and the symbol $\cap$ indicates intersection between blobs: the element ω_{ij} of the overlap matrix represents the area of intersection between the blob i in frame k and the blob j in frame $k-1$ divided by the area of the latter blob. The overlap matrix has size NxM, where N is the number of blobs in frame k and M the number of blobs in frame $k-1$. If, for example, row number 3 has more than one non-zero entry, then blob number 3 in frame k is formed by a merge of two or more blobs in frame $k-1$ (**Figure 1E**). If, for example, column number 5 has more than one non-zero entry, then blob number 5 in frame $k-1$ splits in two or more blobs in frame k (**Figure 1F**). The central assumption of the algorithm is that the number of leeches belonging to blob B_j^{k-1} in frame $k-1$, multiplied by the non-zero entries ω_{ij} of the overlap matrix Ω_{ij}^k give a non-integer estimate of the number of leeches belonging to blobs B_i^k that have non-zero area of intersection with B_j^{k-1}. This assumption is supported by the experimental evidence that a leech, in a time interval of 130 ms, cannot vary its shape area in a substantial way and it can be viewed as a rigid body. Let $\boldsymbol{g}_0$ be the Mx1 vector containing the number of leeches belonging to each of the M blobs found in frame 0. The non-integer estimate of $\boldsymbol{g}_1$ (i.e., the Nx1 vector containing the number of leeches belonging to each of the N blobs found in frame 1) is given by:

$$\boldsymbol{g}_1 = \Omega^1 \cdot \boldsymbol{g}_0 \quad (2)$$

This estimate is also affected by additive noise μ:

$$\boldsymbol{g}_1 = \Omega^1 \cdot \boldsymbol{g}_0 + \boldsymbol{\mu} \quad (3)$$

Minimizing the effect of the additive noise μ on the estimate $\boldsymbol{g}_1$ corresponds to minimizing the quantity:

$$\left(\boldsymbol{g}_1 - \Omega^1 \cdot \boldsymbol{g}_0\right)^2 \tag{4}$$

This, in turn, corresponds to solving a quadratic programming problem

$$\boldsymbol{g}^* \left\lfloor argmin \left\{ \left(\boldsymbol{g}_1 - \Omega^1 \cdot \boldsymbol{g}_0\right)^T I \left(\boldsymbol{g}_1 - \Omega^1 \cdot \boldsymbol{g}_0\right) \right\} + 0.5 \right\rfloor \tag{5}$$

Where $\boldsymbol{g}^*$ is the integer estimate of $\boldsymbol{g}_1$ (obtained using the floor operator), i.e., the estimate of the number of leeches belonging to the blobs observed in frame 1. The design matrix I (identity matrix) is also positive-definite: this ensures that the problem has a global minimizer. However, the problem needs to be constrained: first, the size of two blobs in frame 1 that are the result of a split of a blob in frame 0 must be equal to the size of the single blob in frame 0. Moreover, the sum of all blob sizes in every frame must be equal to the number of leeches in the tank. A constraint on the merge was not necessary, since it is included in the latter constraint. These two constraints can be included in a single equation, where A_{eq} is a matrix whose entries are either 0 or 1, opportunely derived from Ω^1 (its last column having all entries equal to 1, in order to describe the second constraint) and the first column b_{eq} is $\boldsymbol{g}_0$ while all the entries of the second column are equal to the number of leeches in the tank. Finally, we also constrained the number of leeches belonging to a blob, to stay between two reasonable bounds that are dependent on the area of the blob itself: for example, a blob with area 60 pixels^2 is likely to contain one leech or at the most three leeches well in contact. We estimated the normal distributions of the areas of a group, given its size (for size ranging from 1 to 20). Then, each blob area was assigned to the closest area distribution, using the Mahalanobis metric.

$$d = \frac{(\alpha - \mu)^2}{\sigma} \tag{6}$$

Where μ and σ are the mean and the standard deviations of the area distribution under consideration: a distance is calculated for each of the 20 distributions, and the minimum one was retained. The closest area distribution (in terms of the Mahalanobis distance) determined the "most likely" size of the considered blob. Thus, the lowest bound $\boldsymbol{l}$ for its size was the size associated to the most likely area distribution to which it belongs, minus 2, while the upper bound $\boldsymbol{u}$ is the size associated to the most likely area distribution to which it belongs, plus 2.

$$\begin{cases} \boldsymbol{g}^* = \left\lfloor \text{argmin} \left\{ \left(\boldsymbol{g}_1 - \Omega^1 \cdot \boldsymbol{g}_0\right)^T I \left(\boldsymbol{g}_1 - \Omega^1 \cdot \boldsymbol{g}_0\right) \right\} + 0.5 \right\rfloor \\ A_{\text{eq}} \cdot \boldsymbol{g}^* = b_{\text{eq}} \\ \boldsymbol{l} \leq \boldsymbol{g}^* \leq \boldsymbol{u} \end{cases} \tag{7}$$

The quadratic programming problem is solved by using the Matlab function quadprog, starting from an initial condition: the sizes associated to each blob in frame 0, which are manually set by the operator, i.e., $\boldsymbol{g}_0$. The algorithm estimates the group sizes of the blobs in frame 1, then in frame 2 and so on. We applied this algorithm to 89 experiments lasting for a time that varied from 1 h to more than 8 h with a number of leeches varying from 5 to 20. The structure of the problem and the constraints imposed seem to guarantee a good performance of the algorithm, with an error of ± 1 leech per blob of size major than 1, at the most.

THE MODEL OF GROUP FORMATION

The model of group formation describes the dynamics of splits and merges of leech groups. The model is based on the reinforcement mechanism already used to model face-to-face human interaction (Stehlé et al., 2010; Zhao et al., 2011). The reinforcement mechanism implies that the longer is the lifetime of a group the less likely it is that its composition changes. This mechanism is responsible for the broad distribution of lifetime of social groups observed in the present experiments with leeches as well as in human face-to-face interactions (Cattuto et al., 2010). In addition to this mechanism we include a second reinforcement mechanism mediated by the role of 5-HT level in the blood, in agreement with the experimental observations reported in the present manuscript. We assume in particular that the level of 5-HT in the blood increases the leech sociality by increasing the probability of merges. Moreover we assume that, as the number of social interactions increases, the level of 5-HT in the blood of the animals increases.

We start from initial conditions in which leeches are connected in groups of size 2. Each group i is characterized by its size n_i and its duration $\Delta t_i = t - t_i$ where t_i is the last time in which group i was modified. At each time step first we update the following parameters determining the dynamics of group formations (splits and merges of social groups):

- The variable s, indicating the 5-HT level in the blood of the animals increases proportionally to the number of contacts $\langle n^2 \rangle$ (with multiplicative constant c_1) and is at the same time degraded with probability c_2. Therefore s is updated at each time according to

$$s \rightarrow (1 - c_2)\, s + c_1 \left\langle n^2 \right\rangle; \tag{8}$$

- The parameter λ modulates the probability that there is a merge in the dynamics of group formation. We assume that λ is activated by s, the 5-HT level in the blood of the animals, and therefore we take

$$\lambda = \frac{s}{s + K_{\text{met}}}; \tag{9}$$

The constant K_{met} sets the typical scale for the 5-HT level in the blood to activate the "social behavior" and enhances the probability of merges in the group formation dynamics.

At each time we run the dynamics of group formation:

- We choose one random group i;

One conspecific of group i splits from the group with probability

$$D_n(\Delta t) = \frac{a_n}{\Delta t + b_n}. \tag{10}$$

This probability encodes for a reinforcement dynamics responsible for the broad distribution of group lifetimes. The

longer leeches interact with each other the less likely they are to split from their own group. We adopt a minimal hypothesis, summarized by Eq. 10 previously used to model face-to-face social interactions in humans during scientific conferences (Stehlé et al., 2010; Zhao et al., 2011) The constants a_n and b_n are responsible for the shape of the lifetime distribution of a group of size n.

- If the split occurs, two options are allowed:
  - The animal merges with another group j of size n_j and duration Δt_j with probability proportional to λ

$$\prod_j = \lambda \frac{D_{n(j)}\left(\Delta t_j\right)}{\sum_r D_{n(r)}\left(\Delta t_r\right)}. \quad (11)$$

  - The animal remains isolated with probability $(1-\lambda)$.
- Finally we update the time of this system according to the expression

$$t \rightarrow t + \frac{1}{\text{Number of groups}} \quad (12)$$

RESULTS

We positioned up to 20 leeches *H. medicinalis* in an observation tank filled with artificial pond water. The tank had a diameter of 30 cm with a height of 6 cm, where leeches could swim, crawl, and search around. A CCD camera viewing the observation tank from above allowed a precise quantification of leech motion and behavior (Garcia-Perez et al., 2005; Mazzoni et al., 2005; Bisson and Torre, 2011). When 10 leeches were in the tank, they inspected the environment (**Figure 1A**). During this phase, leeches swam (red arrows) or explored the new environment with their head, keeping the tail sucker attached to the bottom of the tank (blue arrow). After 2–3 h leeches appeared to the viewing CCD camera aggregated in a compact silhouette (**Figure 1B**) formed by almost all the conspecifics. When the number of leeches was less or equal to 5, after an initial transient exploration, leeches stopped moving and rested in isolation. Therefore leeches, as several other species (Buhl et al., 2006; Ballerini et al., 2008; Bazazi et al., 2008; Anstey et al., 2009; Makris et al., 2009; Nagy et al., 2010) exhibit a transition from solitary to social behavior when their density is above a critical threshold.

In order to quantify the dynamics of group formation, we developed a suitable software: Images (640 × 480 pixels) were acquired at 7.5 Hz and binarized (**Figures 1C,D**) and an algorithm determined in each image I_i ($i = 1,\ldots, K$) the number of distinct groups $N_n(i)$ formed by n conspecifics (see numbers near black shapes in **Figures 1C,D**). The algorithm was also able to determine merges, i.e., when two groups of leeches unified in a single group (**Figure 1E**) and split, i.e., when a group of leeches broke in two subgroups (**Figure 1F**). From these data we determined:

- $M(i\Delta t)$ and $S(i\Delta t)$ the number of *merges*(M) and *splits*(S) in the time widow $[i\Delta t, (i+1)\Delta t]$ (**Figures 1G,H**).
- $N^*(i\Delta t)$ the *mean number of groups* in the time widow $[i\Delta t, (i+1)\Delta t]$ (**Figure 2B**).
- $<N_n>(i\Delta t)$ the *mean size of groups* in the time widow $[i\Delta t, (i+1)\Delta t]$ (**Figure 2C**).
- $f_{n,m}(i\Delta t)$ the *frequency* that a group of i conspecifics becomes composed of n conspecifics in the time widow $[i\Delta t, (i+1)\Delta t]$ (**Figure 3**). If $m < n$ a split occurs and if $m > n$ we have a merge.
- $<N_{mov}>(i\Delta t)$ the *mean number of moving conspecifics* in the time window $[i\Delta t, (i+1)\Delta t]$ (**Figure 4A**).

A key feature triggering the transition from solitary to social behavior is the number and duration of encounters among conspecifics. Given the shallow geometry of the tank used for our experiments, we can assume that leeches that belong to a group are also in contact with the majority of them. Therefore, the number of contacts established in the group n of size N_n is at the most N_n^2. The sum of the number of contacts established in all groups at the time $k\Delta T$ (where ΔT is the capture interval of the frames, i.e., about 130 ms), is $\Sigma_n\, N_n(k\Delta t)^2$. We quantified the encounters between leeches, by computing the cumulative sum over time of the number of reciprocal *contacts per second* (**Figure 4C**), normalized by $N_{\text{conspecifics}}$ (the overall number of leeches in the tank), as

$$-<C(i\Delta t)> = \sum_{k=0\ldots i} \sum_n N_n(k\Delta t)^2 / N_{\text{conspecifics}} / \Delta t \quad (13)$$

PROPERTIES OF GROUP FORMATION

Groups of conspecifics formed within the first 60 min are not stable. Indeed, during the first 2 h, in the presence of 5 and 10 leeches, the rate of splits and merges could be as high as 20 (**Figure 2A**) and 80/min (**Figure 2E**) respectively. In the presence of five leeches the mean number of groups $N^*(i\Delta t)$ varied between 1 and 5 (**Figure 2B**) and the mean size of these groups $<N_n>(i\Delta t)$ varied similarly between 1 and 5 (**Figure 2C**).

Leeches continued to explore the tank for 2–4 h forming transient groups and then slowed down and eventually stopped remaining in isolation (**Figures 2D–F**). Only rarely (4/53) a group of more than three conspecifics was formed (**Figure 2E**) and a stable group formed by all five leeches was never observed. In the presence of 10 leeches, a different dynamics was observed: leeches continued to merge and split with a rate often up to 80/min (**Figure 2E**), but, after 2–3 h, they formed stable large groups of 5–10 conspecifics (**Figures 2G–L**). In the great majority of experiments performed in spring or summer (see **Figure 8**, which considers 62 experiments performed over a 2-year period) leeches aggregated in a single group, where they remained in physical contact, possibly moving their heads or tails in an exploratory or a pseudo-swimming behavior. These large groups persisted for additional 3–6 h, i.e., the usual duration of an experiment. We investigated in detail the dynamics when 5 (7 experiments), 6 (3 experiments), and 10 (10 experiments) leeches were in the observation tank. The group size distribution under the assumption of independent behavior (i.e., constant merge and split rates, regardless group size) is expected to be proportional to $\exp(-\lambda n)$, where λ is a constant and n is the group size(Gueron and Levin, 1995). When less than five leeches are in the observation tank, the frequency $f(n)$ of finding a group of n leeches is proportional to $\exp(-\lambda n$; blue bars in **Figure 2M**, theoretical fit in red line) in agreement with the notion of an independent behavior when the leech density is below a given threshold (Bisson and Torre, 2011). When the number of conspecifics in the tank is increased to more than five, $f(n)$ is not proportional anymore to $\exp(-\lambda n$;

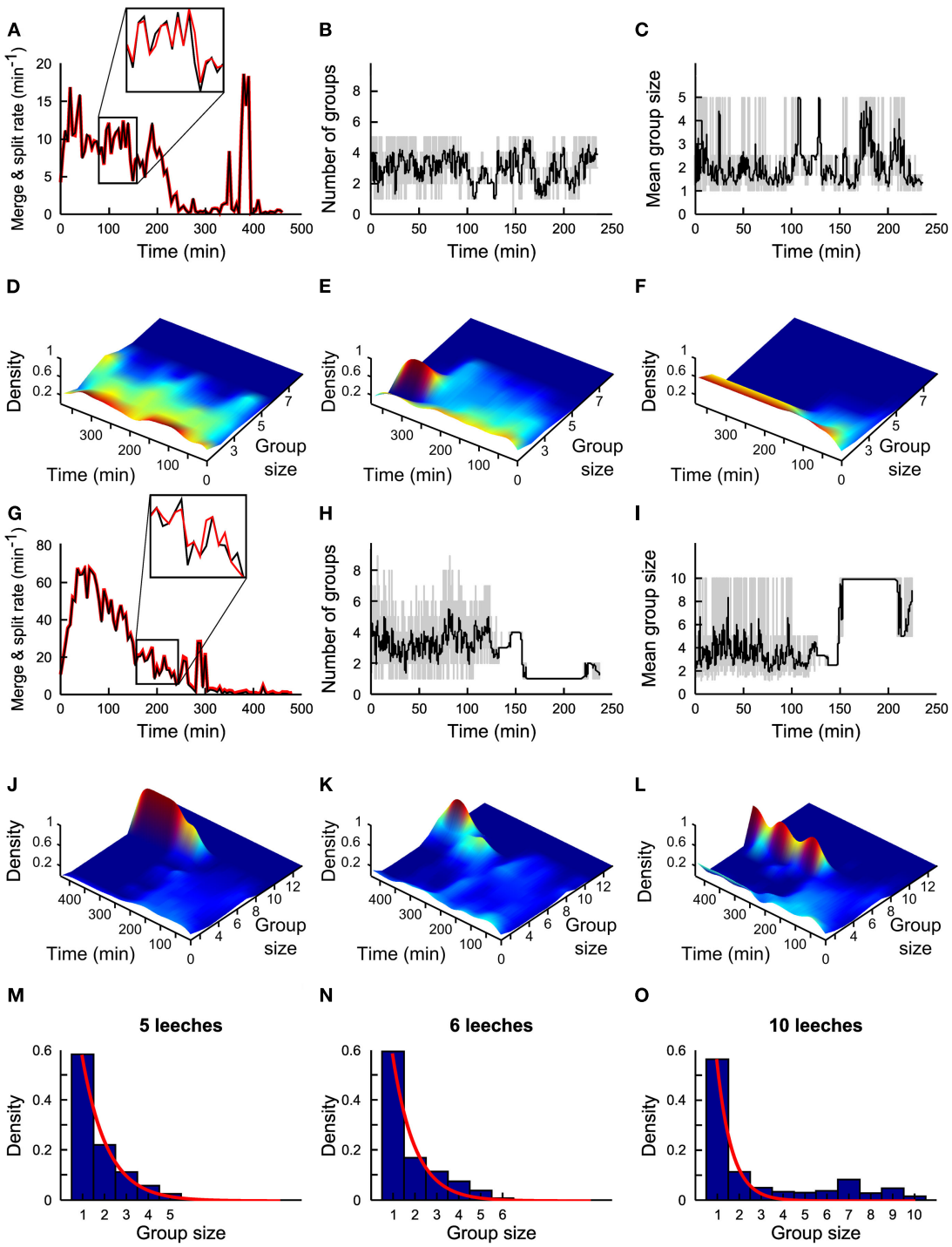

FIGURE 2 | Statistics of group formation. (A) Time evolution of merges (black line) and of splits (red line) in a time window of 5 min. **(B)** Time evolution of number of groups in a time window of 1 min (gray line) and in 5 min (black line). **(C)** Time evolution of average group size in a time window of 1 min (gray line) and in 5 min (black line). **(A–C)** Refer to experiments with five leeches. **(D–F)** Time evolution of density of groups over 4 h for three different experiments. Color coded scale from dark blue (0 groups) to deep red (5 groups). **(G–L)** As in **(A–F)** but with 10 leeches. Inset in panel g shows a zoom of Merge (black) and Split(red) on an enlarged scale. Merge and split plots are very similar but not identical and small differences determine group formation. **(M–O)** Probability density of group size in the presence of 5, 6, and 10 conspecifics respectively. Plots in **(A,G)** are averages from 7 and 10 experiments, respectively. Continuous red lines in panels **(M–O)** are obtained by fitting the experimental data with an exponential distribution[21]. **(B–F)** and **(H–L)** Are based on a single experiment. Plots in **(M–O)** are averages from 7, 3, and 10 experiments, respectively.

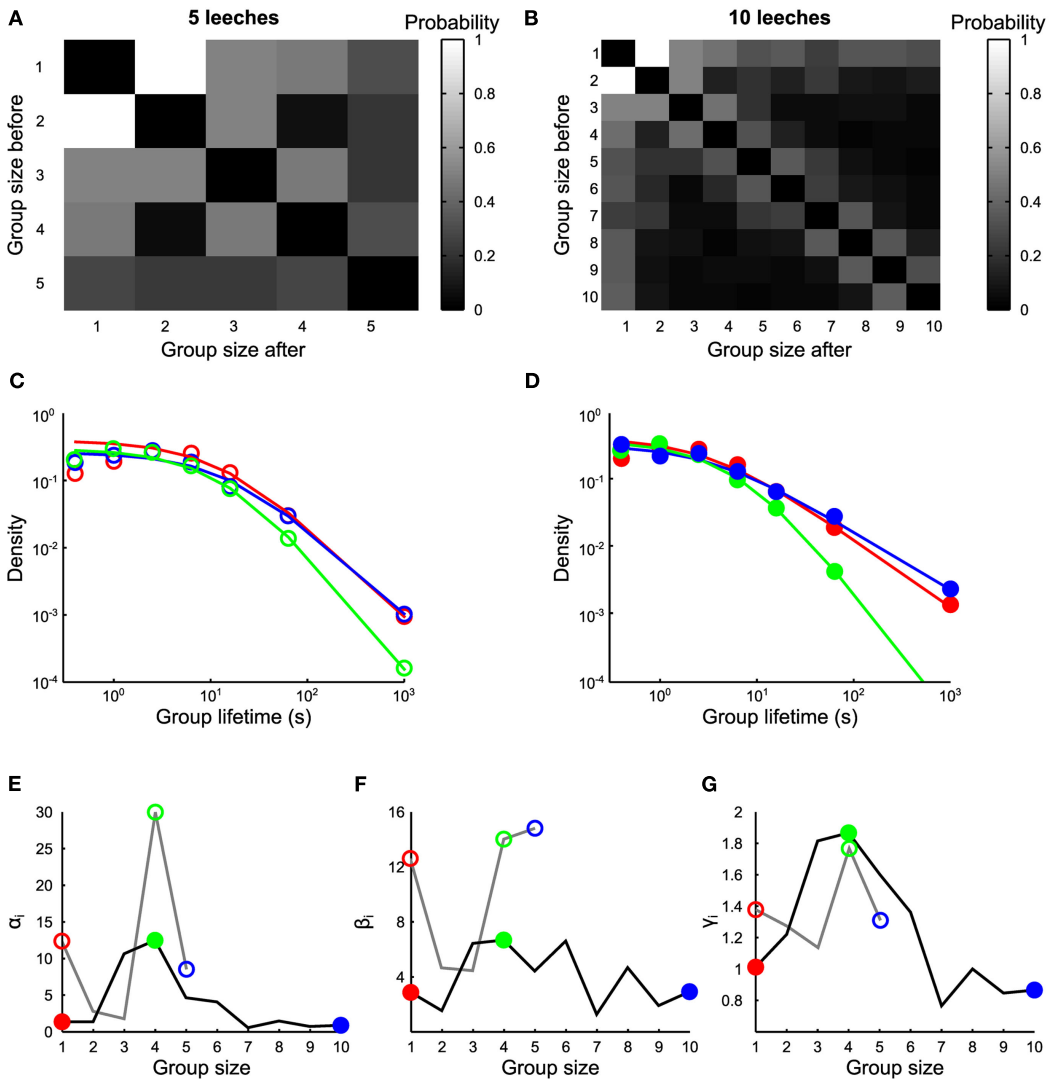

FIGURE 3 | Transitions between groups. (A,B) Transition rates from groups of size *n* to groups of size m, in the presence of 5 and 10 leeches respectively (average values estimated from 7 and 10 experiments, respectively). **(C)** Life time density of groups of one (red empty circles), four (green empty circles), and five (blue empty circles) leeches, and associated fit (continuous lines) with Eq. 1 for experiments with five leeches. **(D)** Life time density of groups of 1 (red filled circles), 4 (green filled circles), and 10 (blue filled circles) leeches, and associated fit (continuous lines) with Eq. 1 for experiments with 10 leeches. **(E–G)** Values of α_n, β_n, and γ_n as a function of *n*, with 5 leeches (gray continuous lines) and 10 leeches (black continuous lines). Empty and filled colored circles highlight the parameter values of fits reported in **(C,D)** respectively.

Figures 2N,O, theoretical fit in red line), indicating the onset of a cooperative behavior in which individual leeches do not remain solitary for long. In order to identify the neurobiological basis of this behavior, we asked whether this transition was mediated by the accumulation in the tank of molecules/pheromones secreted by the leeches. We positioned 20 leeches in the tank and after the formation of a large group of more than 13 conspecifics, leeches were removed from the tank and – leaving the same water – replaced by five naïve leeches. These naïve leeches did not form a group, even though they were sensing the same local chemical medium where previously a large group of conspecifics was formed. Therefore, we posit that group formation is not likely triggered by chemicals secreted into the bath.

STATISTICS OF TRANSITIONS BETWEEN DIFFERENT GROUPS

We have also analyzed the frequency of transitions p_{ij} between groups of different sizes. The most frequent transitions were those from groups of n conspecifics to groups of $n+1$ or $n-1$ conspecifics, i.e., merges and splits usually involved one animal leaving or joining a group. This pattern was clearly observed in the presence of 10 (**Figure 3B**, estimates over 10 experiments) and – to a lesser extent – of five conspecifics (**Figure 3A**, estimates over 7 experiments). The lifetimes distribution of groups of size n when 5 (**Figure 3C**) and 10 leeches (**Figure 3D**) were in the observation tank could be fitted by the equation

$$\alpha_n / (\beta_n + \Delta t)\, \gamma_n \qquad (14)$$

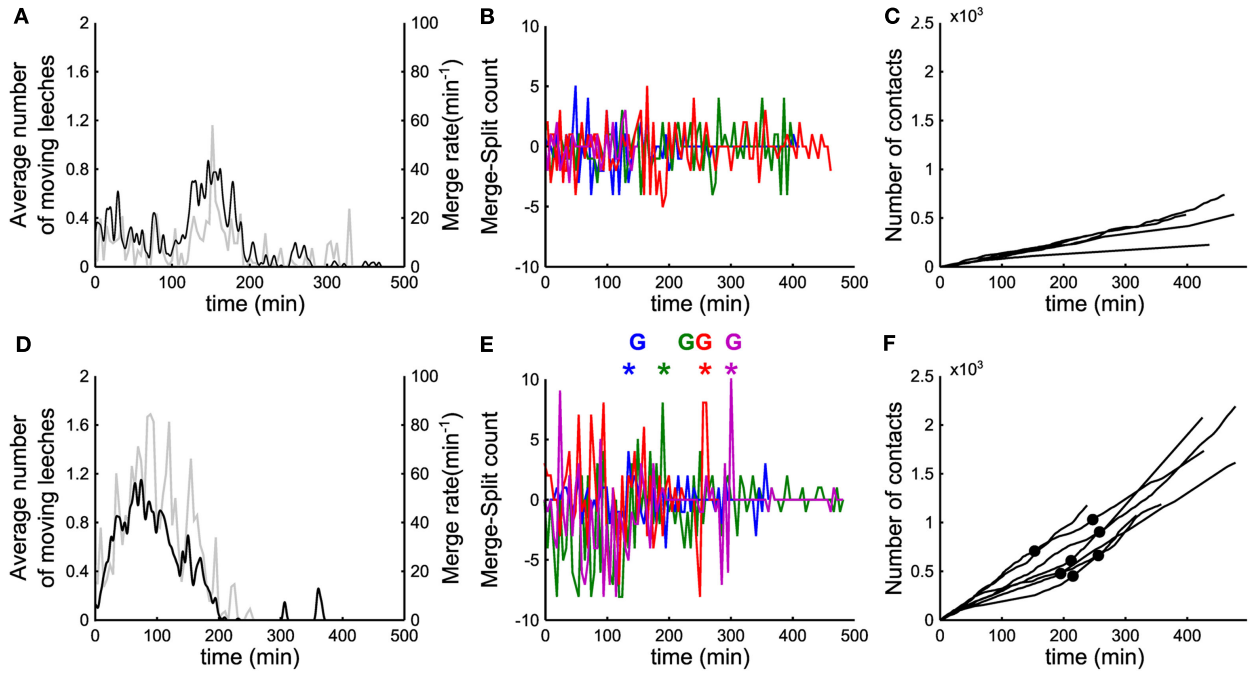

FIGURE 4 | Events leading to group formation. (A,D) Time evolution of the number of moving leeches $<N_{mov}>$ ($n\Delta$t; black line, left vertical axis) and of the merge rate M ($n\Delta$t; gray line, right vertical axis) in a window Δt of 5 min. **(B)** Time evolution of the difference between merges and splits [i.e., $M(i\Delta t) - S(i\Delta t)$] in a window Δt of 5 min. **(C)** Time evolution of number of contacts per minute (cumulative sum). **(A–C)** Data for five leeches. **(D–F)** As in **(A–C)** but for 10 leeches. In **(B,E)** data from 4 experiments in different colors. In **(E)**, colored asterisks mark the occurrence of a peak of merges preceding the formation of a stable group, marked with the letter G (same color). In **(F)**, filled black dots mark the time instant in which a stable group forms.

With α_n, β_n, and γ_n as free parameters. The value of β_n controls the average lifetime of a group of n conspecifics (**Figure 3F**): it has a high value for long lasting groups and varies from 2 to 16 s. The exponent γ_n in Eq. 14 determines how stable a group of n conspecifics (**Figure 3G**) is: when 10 leeches were in the tank, the value of γ_n was close to 1.8 for groups composed by three to five conspecifics, otherwise it was close to 1. Groups of three to four conspecifics had a shorter mean lifetime, indicating that these groups are unstable and either split in smaller groups or merged with other leeches. Groups of more than five leeches are more stable indicating that the presence of a positive feedback value of α_n (**Figure 3F**) influences the ratio α_n/β_n, which has values varying between 0.2 and 2 s and determines approximately the asymptotic value of short lifetimes. The experimentally observed distribution of lifetimes (**Figures 3C,D**) strongly deviates from an exponential distribution, expected from a uniform rate of merges and splits (Barrat et al., 2010). A similar deviation is observed also in human behavior (Cattuto et al., 2010), where a power–law distribution of face-to-face interactions is observed. This power–law distribution is explained by a reinforcement dynamics (Stehlé et al., 2010; Zhao et al., 2011) in which the longer a conspecific stays in a group the lesser is likely to leave the group. In humans, the exponent γ_n increases linearly with n, implying that larger groups are more unstable than smaller groups while the opposite behavior (γ_n decreasing with n) is observed in leeches. In humans the linear increase of γ_n with the group size n is explained by assuming that each individual acts independently of the group size. In this view, larger groups are more unstable because there is a larger possibility that individuals of the group decide to leave it or split it. In leeches, however, in order to explain the experimental data we need to suppose that the split probability depends on the group size.

In order to understand the mechanisms leading to the formation of a large group of conspecifics we analyzed in detail the events preceding it. The average number of moving leeches (m.l.) $<N_{\text{moving}}>$ decreased from an initial value around 0.7 and 1.4 m.l./s for groups of 5 and 10 leeches respectively (**Figures 4A,D**, average values over 15 and 17 experiments, respectively) to less than 0.2 m.l./s after 3 h. However, after 2–3 h, five leeches in the tank moved more often than 10 leeches (compare **Figures 4A,D**) and continued to merge and split (**Figures 4B,E**).

During the initial exploratory phase, encounters among 10 leeches are more frequent: indeed, the average number of contacts $<C(i\Delta t)>$ (**Figures 4C,F**) was consistently higher with 10 leeches than with 5, because encounters among conspecifics are easier in a more crowded environment. In the presence of 10 leeches, the number of merges–splits oscillated during the first hour, but had large positive peaks in a time window of 10–30 min (asterisks in **Figure 4E**) preceding the formation of a large group (G letters in **Figure 4E**). The results of **Figure 4** indicate two features of group formation: (1) – leeches explore for 2–3 h the new environment before coming to rest and (2) – if during the exploratory phase leeches encounter enough conspecifics a reinforcement dynamics is triggered and leeches stop and rest not in isolation but in groups.

THE ROLE OF 5-HT IN GROUP FORMATION

In order to understand the biological basis of group formation, we asked which neurotransmitters could be involved. An elevation of the body concentration of 5-HT shifts locusts from a solitary to a social behavior (Anstey et al., 2009). We isolated from solitary leeches their entire spinal cord from the tail to the head ganglion and we took a sample of 100–200 μl of their blood and we repeated the same dissection from gregarious leeches, which had formed a group of at least eight conspecifics. We measured the concentration of 5-HT with High Pressure Liquid Chromatography: the concentration of 5-HT in ganglia from the spinal cord of gregarious leeches increased by 37% (with a significance of 0.0493; one tail t-test. $N = 5$ solitary leeches, six gregarious leeches) over that measured in solitary leeches. Also the level of 5-HT in the blood of gregarious leeches was higher but at a lower extent: indeed the level of 5-HT in the blood of gregarious leeches was 25% higher than in solitary leeches (with a significance of 0.04; one tail t-test. $N = 4$ solitary leeches, 7 gregarious leeches). These experiments were performed from May to September when leeches are more gregarious (see **Figure 8**). We repeated the same experiments in winter when leeches are less gregarious and do not form easily groups (see **Figure 8**) and in this period of the year changes of level of 5-HT between gregarious and solitary leeches could not be determined with an adequate statistical significance.

Therefore we studied group formation when five leeches were injected with 300 μl of 200 μM 5-HT solution. In this case (**Figure 5A**, gray bars: 15 experiments involving five not injected leeches, black bars: 12 experiments involving five injected leeches), groups of three or four conspecifics occur more frequently than what is expected from an independent behavior (red bars). The difference between merges and splits, (**Figure 5B** and to be compared with **Figure 4**) approached values close to 0, with positive peaks (asterisks) preceding the formation of a group (G). The average number of contacts $<C(i\Delta t)>$ for five leeches injected with 5-HT was higher than for the case of five uninjected leeches (**Figure 5C**). When an isolated leech was injected with 300 μl of 200 μM 5-HT and was moved to a tank where a large group of conspecifics had formed, the injected leech quickly joined the large group (see red trajectory in **Figure 5D**). The results of these experiments did not have the seasonal variation of spontaneous group formation described in **Figure 8**.

There are many types of 5-HT receptors and several of them have been identified in the leech nervous system: in leeches, 5-HT can activate cationic channels (Sanchez-Armass et al., 1991; Catarsi and Drapeau, 1997; Burrell et al., 2001), anionic channels (Sanchez-Armass et al., 1991; Ali et al., 1998; Burrell et al., 2001), and affect its own reuptake (Bruns et al., 1993; Calviño et al., 2005; De-Miguel and Trueta, 2005). The role of these distinct

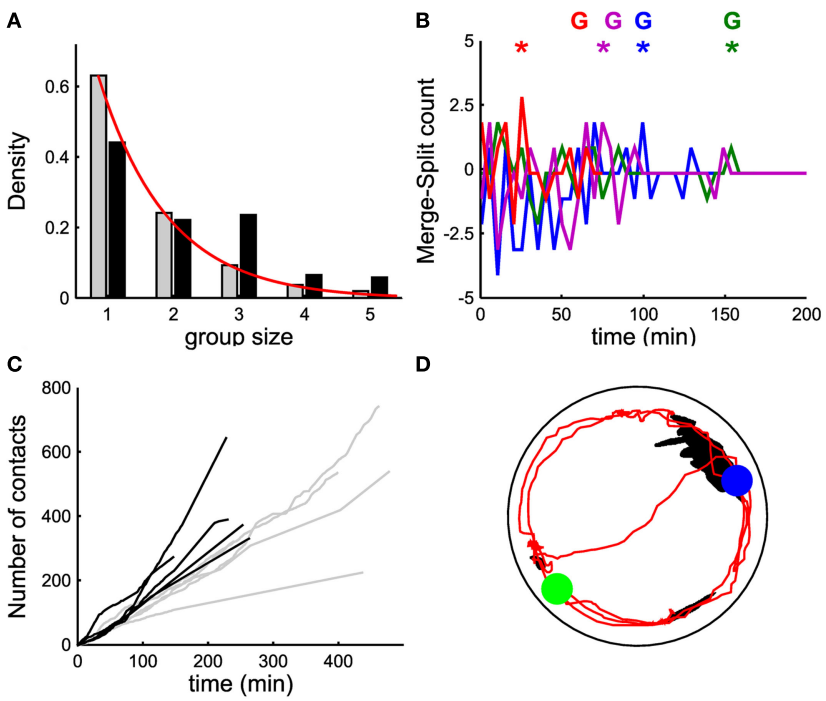

FIGURE 5 | The role of 5-HT. (A) Probability density of group size with five non-injected leeches (gray bars) and with five leeches injected with 300 μl of 200 μM 5-HT solution (black bars). **(B)** Time evolution of the difference between merges and splits [i.e., $M(i\Delta t) - S(i\Delta t)$] in a window Δt of 5 min for four experiments with five leeches injected with 5-HT; colored asterisks mark the occurrence of a peak of merges leading to the formation of a stable group, marked with the letter G (same color). **(C)** Time evolution of number of contacts per minute (cumulative sum) for five leeches injected with 5-HT (black lines) and for five non-injected leeches (gray lines). Continuous red line in panel a was obtained by fitting the experimental data with an exponential distribution[21]. **(D)** Trajectory (in red) of a leech injected with 5-HT in the presence of an already formed group of eight non-injected leeches (black blob). The blue (green) filled circle indicates the final (initial) position of the injected leech. Leeches injected with 5-HT joined the large leech group within some tens of minutes.

actions of 5-HT can be dissected by using antagonists such as ketanserin blocking cationic 5-HT gated ionic channels 5-HT_{2A} and 5-HT_{2C} (Sanchez-Armass et al., 1991; Mar and Drapeau, 1996) or mianserin blocking 5-HT gated ionic channels (Gaudry and Kristan, 2009).

In contrast to what observed when a leech is injected with 5-HT (**Figure 5D**), leeches injected with 150 μl of 1 mM ketanserin (**Figure 6A**) or of 150 μl of 2 mM mianserin (**Figure 6B**) and subsequently moved to a tank where a large group of conspecifics had formed, remained solitary and rarely joined the large group. This behavior was also observed when the injection of the antagonist was followed by a subsequent injection of 5-HT (**Figure 6C**, eight experiments under saline conditions, seven under ketanserin, six under mianserin, eight under 5-HT). Leeches injected with a 5-HT antagonist were picked from the water tank where either they were solitary or formed large groups of conspecifics. Their behavior following the injection of 5-HT antagonist was not dependent whether they were solitary or gregarious in the water tank. Leeches injected with a saline solution (cyan line in **Figure 6D**) remained solitary, as well as leeches injected with both 5-HT and mianserin or ketanserin (red and green lines, respectively), while those injected with 5-HT joined large groups (blue trajectory). Not injected leeches remained solitary, presumably because they could not encounter their conspecifics during the exploratory phase. The simultaneous injection of ketanserin and mianserin into leeches is expected to have a larger effect of the injection of a single 5-HT antagonist.

NEUROBIOLOGICAL MECHANISMS UNDERLYING GROUP FORMATION

Leeches are often observed exploring other conspecifics' bodies by flaring the mouth over their skin, chemoreception could be at basis of group formation. Chemoreception in leeches is mediated by sensilla, ciliated, button-like structures lining the edge of the dorsal lip (Dickinson and Lent, 1984; Elliott, 1984, 1986; Lent and Dickinson, 1984; Gaudry et al., 2010). There are two classes of sensilla: structures with a size of 25–30 μm readily detectable with a light microscope as unpigmented spots in the skin, and smaller structures with a size of 8–10 μm flanking the larger organs not easily detectable with a light microscope (**Figure 7A**, green dots). The chemical signals detected by sensilla are conveyed to the supraesophageal and subesophageal ganglion. These two ganglia form the head brain of the leech and are connected to the chain of 21 ganglia constituting the central nervous system of the leech (**Figure 7A**, blue structure).

Therefore we investigated the effect of the surgical removal of the dorsal lip sensilla visible in the light microscope (**Figure 7B**, red dashed line enclosing green dots). Sham ablations were done in the same way and a band of the dorsal skin adjacent to the lip organs was removed while leaving sensilla intact (**Figure 7B**, red dashed line not enclosing green dots). After ablation, leeches

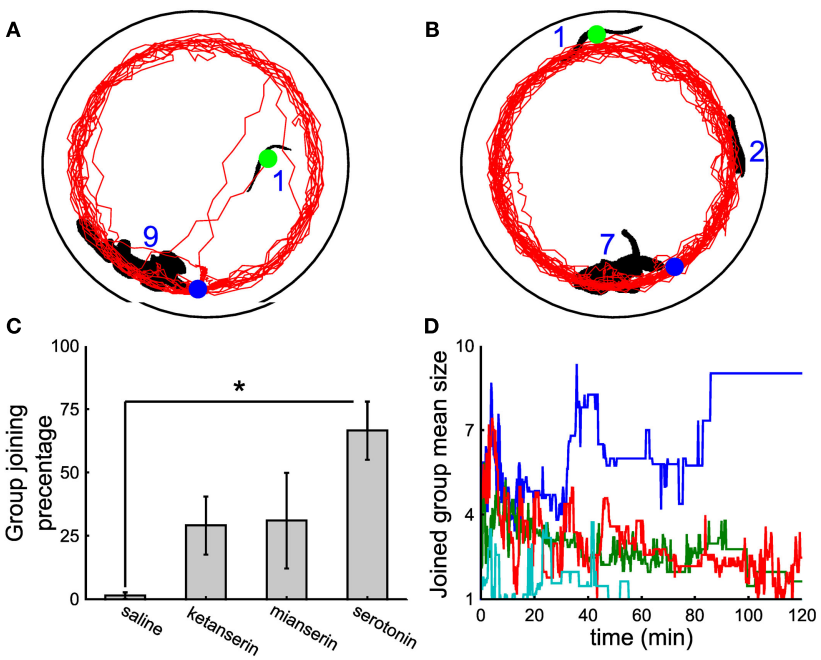

FIGURE 6 | The effect of 5-HT antagonists. (A,B) Black shapes indicate large groups of nine and seven leeches, respectively and the leeches profile (black blob with green circle) injected with 150 μl of 1 mM ketanserin **(A)** or 2 mM mianserin **(B)** solutions. Trajectories of injected leeches in red. In both panels, the initial and final positions of the injected leech are marked by the green and the blue dot respectively. Injection of 5-HT antagonists was followed by another injection of 150 μM 5-HT solution. **(C)** Percentage of time spent by injected leeches in contact with the large group of conspecifics, when leeches were injected with 300 μl of saline solution, with 150 μl of 1 mM ketanserin or 2 mM mianserin solutions, followed by another injection of 150 μl of 400 μM 5-HT solution, or 300 μl of 200 μM 5-HT solution. **(D)** Time evolution of the mean size of the group joined by the injected leech under the same treatments described in **(C)** cyan, blue, red, and green lines refer to leeches injected with a saline solution, 5-HT, mianserin, and ketanserin respectively. Student's *t*-test, $*p < 0.05$.

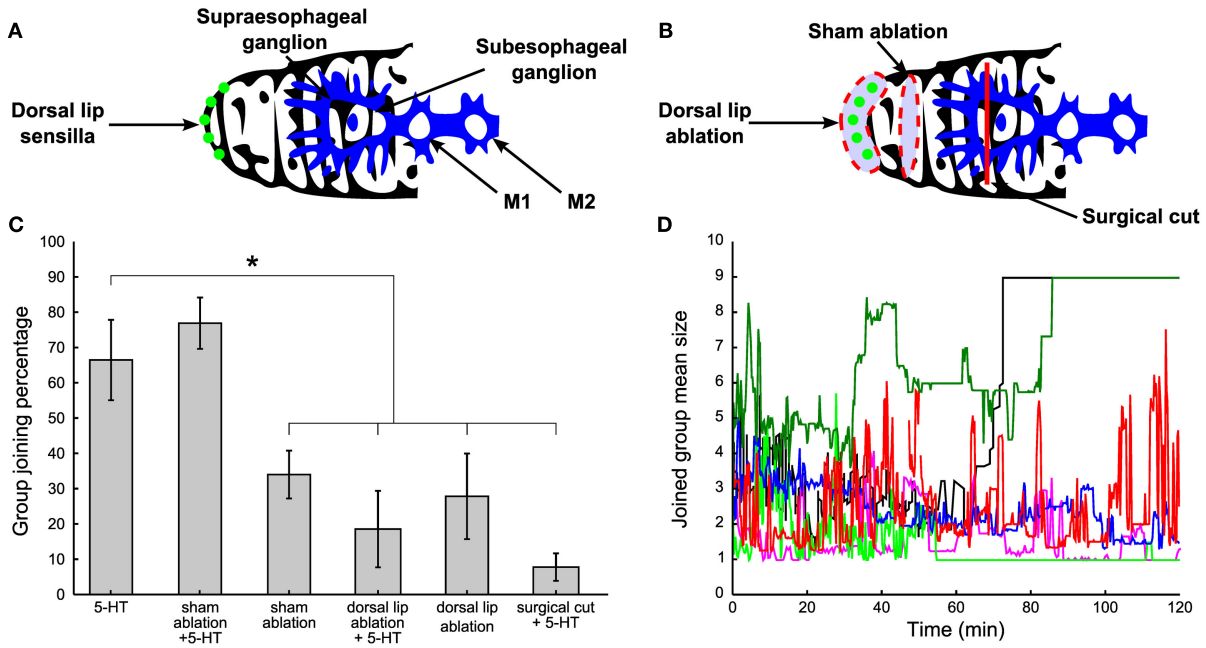

FIGURE 7 | The role of chemoreceptors. (A) Normal control: leeches with intact lips (green dots) and head brain (blue structure) were tested for social attitude previous the injection of 300 μl of 200 μM 5-HT solution. **(B)** Surgical treatment: the band of dorsal lip organs visible in the light microscope (a, green dots), was cut away in ablated experiments (red dashed line enclosing the green dots). Sham operations were done in the same way except that a band of skin dorsally adjacent to the lip organs (along the dorsal surface of the head) was removed and the lip organs themselves were left intact (red dashed line not enclosing the green dots). The supraesophageal ganglion was surgically disconnected by applying a deep and localized cut (red vertical line). **(C)** Percentage of time spent by leeches under the above explained surgical treatments in comparison with normal 5-HT injected leeches. Three-hundred microliter of 200 μM 5-HT were injected in both ablated and supraesophageal ganglion impaired leeches. **(D)** Time evolution of the mean size of the group joined by the injected leech under the same treatments described in **(A,B)**. Blue trajectories refer to 5-HT injected leeches and sham-ablated, 5-HT injected leeches respectively, red trajectories refer to sham-ablated leeches, dorsal lip ablated leeches, while light green trajectories refer to dorsal lip ablated and supraesophageal ganglion impaired leeches, all injected with μl of 200 μM 5-HT. Student's *t*-test, $^{*}p < 0.05$.

were allowed to recover for 1 day in water and exhibited a normal behavior with frequent episodes of swimming and crawling. After recovery from surgery, ablated, and sham-ablated leeches, injected with 300 μl of 200 μM 5-HT were tested. Ablated leeches, either 5-HT injected ($N = 5$) or not ($N = 7$), remained solitary (**Figures 7C,D**, see legend, Student's *t*-test, $^{*}p < 0.05$.), while not ablated ($N = 8$) and sham-ablated 5-HT injected leeches ($N = 6$) joined the other leeches (**Figures 7C,D**, see legend Student's *t*-test, $^{*}p < 0.05$.), indicating that group formation depended on the presence of intact sensilla.

It is possible to disconnect the supraesophageal ganglion from the leech central nervous system by cutting the neuronal projections from the supraesophageal to the subesophageal ganglion (**Figure 7B**, red vertical line). Leeches with a disconnected supraesophageal ganglion recovered from surgery and 1 day later they swam and crawled as intact leeches do. When these leeches were injected with 5-HT, they remained solitary and did not join and mixed with other leeches and behaved as intact leeches not injected with 5-HT (Student's *t*-test, $p < 0.05$, $N = 3$).

SEASONAL VARIABILITY

Deviations from an independent behavior and the formation of large groups of conspecifics were observed both in well-fed and hungry leeches. However, a careful examination of data collected over more than 2 years of experiments showed a seasonal variability: leeches received from the supplier (Ricarimpex, see Materials and Methods) in late spring or summer were more active and prone to social aggregation, while those received in winter did not move very much and appeared to be less " sociable" and more solitary. Leeches supplied by Ricarimpex were kept outside and therefore were exposed to seasonal changes. We measured several properties of group formation mediating data over a time window of 3 months. In all our experiments the water temperature did not change more than 2°C, from winter to summer, and its average value was about 16°C.

The tendency to group formation was quantified by computing the average group size (**Figure 8A**), the average number of contacts established within 4 h (**Figure 8B**), the average velocity during the initial exploratory phase (**Figure 8C**) and the average number of moving leeches per minute (**Figure 8D**) when 10 leeches were in the observation tank ($N = 62$ experiments uniformly performed over 2 years). By using all four criteria, we observed a recurrent dependence between group formation and the season. Leeches were more prone to form large groups between May and September, corresponding to warm weather in continental Europe. During European winter, leeches were less active and more solitary. These results show that the transition from solitary to social behavior is a complex process, likely to depend on the overall state

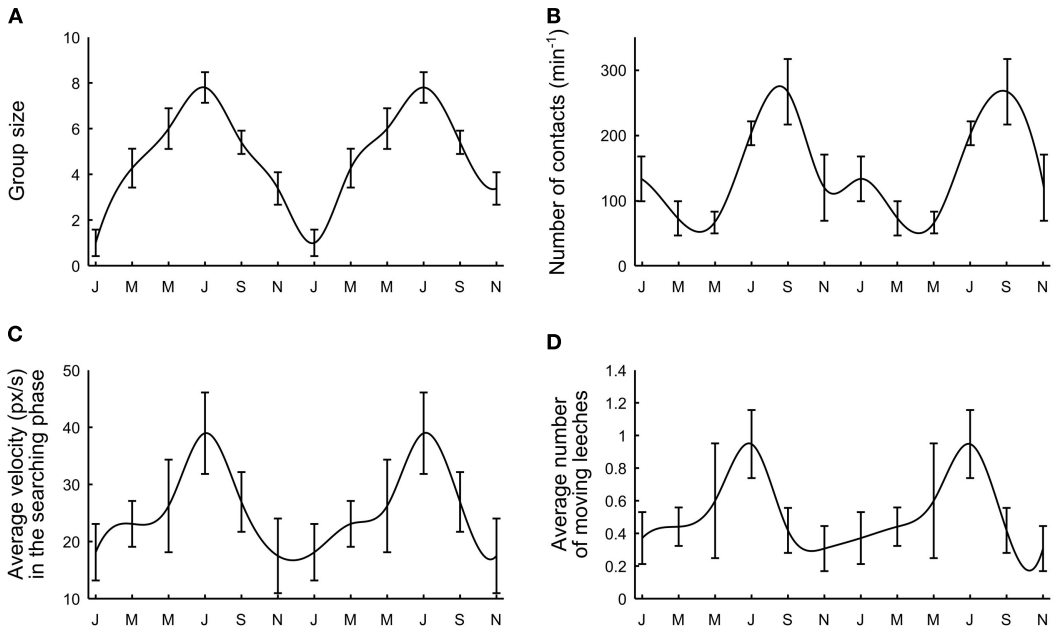

FIGURE 8 | Seasonal variability. (A) Average group size. **(B)** Maximal number of contacts per minute reached after 1 h. **(C)** Average leech velocity. **(D)** Average number of moving leeches. Data were collected over 2 years and were averaged over periods of 3 months. Letters on the time axis indicate months (January, March, May, July, September, November). Smooth curves through the data drawn by eye.

of the animals, also influenced by seasonal variations and possibly by the length of daylight.

DISCUSSION

Group formation is an important aspect of social interactions (Sokolowski, 2010), occurring when conspecifics make collective decisions and adopt a similar behavior. Group formation can happen for different ethological reasons, but its dynamics – as we show in this study – can be similar in distant species such as leeches and humans (Stehlé et al., 2010; Zhao et al., 2011), when the population of leeches exceeds a critical value, they aggregate in large groups. Similar conspecifics aggregation has been observed in simple model systems, such as the worm *C. elegans* the fruit fly *Drosophila* (Sokolowski, 2010), in fish shoals (Makris et al., 2009), in locust swarms (Anstey et al., 2009) but also in higher primates and humans (Goodson and Thompson, 2010). Group formation in several species is not primarily caused by a mutual attraction among conspecifics but is produced by aggregation around abiotic factors, – in worms, for instance – as a response to oxygen levels (De Bono and Bargmann, 1998). Leeches are negative phototactic (Elliott, 1973; Sawyer, 1986b) and they tend to move away from a light source, therefore the observed group formation could have been simply their way to escape from the light and find a shelter among other leeches. When five or less leeches were placed in the observation tank of a given area they hardly noticed each other and their motion and behavior followed the pattern indicating independence with a high statistical significance (Bisson and Torre, 2011). When a higher number of leeches were placed in the same tank, a different dynamics was observed, difficult to reconcile with *negative phototaxis*. Similarly, group formation observed in a smaller number of leeches injected with 5-HT strongly indicated the emergence of social interactions, i.e., reciprocal attraction among conspecifics.

Similarly to what observed in locusts (Anstey et al., 2009), the hormone 5-HT participates in the onset and control of group formation. 5-HT plays a role similar to oxytocin, arginin, and vasopressin. These non-apeptides mediate social interactions and behavior in several species from invertebrates (Donaldson and Young, 2008) to rodents (Insel, 2010) and possibly also in humans (Goodson and Thompson, 2010). In humans, 5-HT is involved in mood regulation and its disruption is at the basis of several kinds of mood disorders (Chiao, 2010). The segmental ganglia of the leech contain a network of 5-HT releasing neurons (Lent and Frazer, 1977; De-Miguel and Trueta, 2005) modulating the swimming motor program (Ort et al., 1974; Kristan and Nusbaum, 1982; Friesen, 1989). These neurons are one pair of large Retzius cells, one pair of dorso-lateral (DL) and ventro-lateral (VL) interneurons, and two pairs of medial interneurons (cells E and M; Lent et al., 1991). 5-HT is known to influence social behavior and in particular social ranking in lobsters (Kravitz, 1988) and in crayfish (Yeh et al., 1996).

NEUROBIOLOGICAL MECHANISMS FOR GROUP FORMATION

Sensilla play a strategic role in chemoreception and several associated behaviors such as feeding (Dickinson and Lent, 1984; Elliott, 1984, 1986; Lent and Dickinson, 1984; Gaudry et al., 2010). The presence of conspecifics is detected by chemoreceptors located in the sensilla present in the dorsal lip and the associated neurobiological signal is transmitted through the supraesophageal ganglion

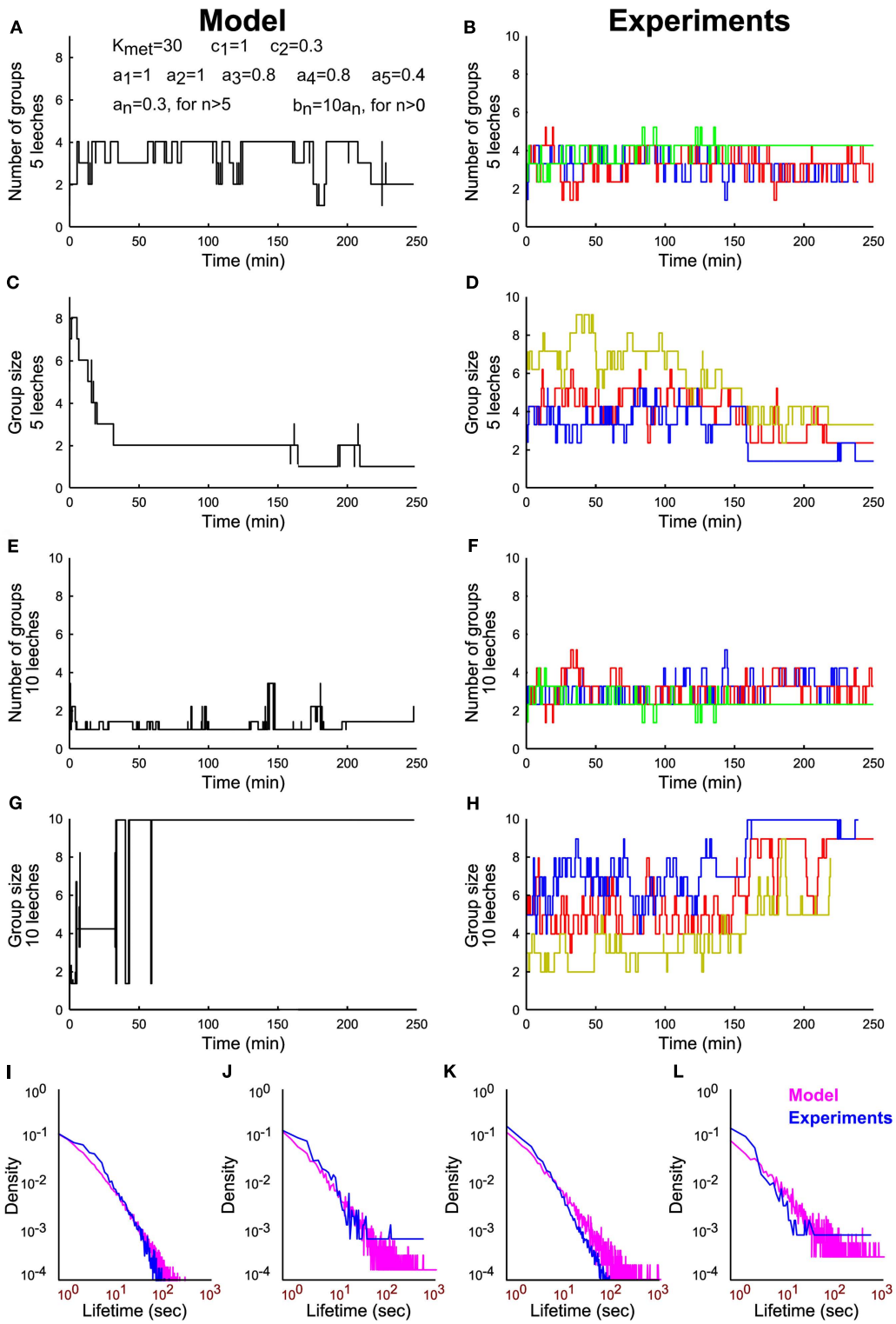

FIGURE 9 | Modeling group formation in leeches and comparison with experimental data. (A) Time evolution of number of groups from a simulation of Eqs 3–5 with five leeches and using the parameters $K_{met} = 30$; $c_1 = 1$; $c_2 = 0.3$; $a_1 = 1$, $a_2 = 1$, $a_3 = 0.8$, $a_4 = 0.8$, $a_5 = 0.4$, and all other $a_n = 0.3$, $b_n = 10^* a_n$. **(B)** Time evolution of number of groups in three different experiments with five leeches. **(C)** Time evolution of the average group size from a simulation of Eqs 3–5 with five leeches. **(D)** Time evolution of the average group size in three different experiments with five leeches. **(E–H)** As in **(A–D)**, but with 10 leeches. **(I,J)** Comparison of the lifetime distributions that result from experimental data (blue line) and simulated data (magenta line) for groups of size 1 **(I)** and 5 **(J)** in experiments with five leeches. **(K,L)** As in **I–J** but for groups of size 1 **(K)** and 10 **(L)** in experiments involving 10 leeches.

to the central nervous system of the leech, where it promotes the increase of the intracellular level of 5-HT. Ablation experiments indicate a specific neurobiological pathway mediating the establishment of social interactions. Impairment of the dorsal lip or of the supraesophageal ganglion compromises conspecifics detection, as in fake group experiments (Bisson and Torre, 2011) and abolishes social attitude. There are many types of 5-HT receptors and several of them have been identified in the leech nervous system, where 5-HT can activate cationic channels, anionic channels, and affect its own reuptake (Calviño et al., 2005). Ketanserin blocking cationic 5-HT gated ionic channels 5-HT_{2A} and 5-HT_{2C} and mianserin blocking 5-HT gated ionic channels make leeches more solitary (**Figure 6**) suggesting 5-HT could promote group formation by activating the whole population of 5-HT receptors. As the body concentration of 5-HT in ganglia of gregarious leeches is by 37% larger than in solitary leeches we propose that social interactions occur because of an elevation of the body level of 5-HT.

Supraesophageal leech ganglia, similarly to all leech ganglia, have two large Retzius cells able to secrete 5-HT both from the soma and synaptic terminals (Sawyer, 1986a). Retzius neurons are the major serotonergic neurons in the leech central nervous system and indeed contain approximately half of the total concentration of 5-HT (Coggeshall et al., 1972). We speculate, therefore, that 5-HT released extrasynaptically from the soma of Retzius cells in the supraesophageal ganglion diffuse into the leech body and is the source of the measured elevation of 5-HT. 5-HT diffusing out of the release site will have a variety of actions, such as autoinhibition of 5-HT releasing Retzius cells (Cercós et al., 2009) and may also produce slow electrical responses, as happens in dopaminergic neurons (Sombers, 2009) and ultimately triggers group formation. The time course of group formation occurs in 1 h or so and therefore acts on a time scale more compatible with an extrasynaptic release of 5-HT (Bunin et al., 1998; Bunin and Wightman, 1999; De-Miguel and Trueta, 2005; Kaushalya et al., 2008).

MODELING GROUP FORMATION

During the analysis of leech aggregation, we observed that the lifetimes distribution of leech groups (Eq. 14 and **Figures 3C,D**) were very similar to those seen among humans (Stehlé et al., 2010; Zhao et al., 2011). Therefore, we decided to model group formation among leeches, on the basis of the reinforcement dynamics used to describe human social interactions (Stehlé et al., 2010; Zhao et al., 2011). We assumed that leech aggregation (**Figure 3B**) is determined primarily by transitions of the type

$$\mathrm{n} \rightarrow \mathrm{n}+1 \left(\text{a merge}\right)$$
$$\mathrm{n} \rightarrow \mathrm{n}+1 \left(\text{a split}\right)$$

in which a single conspecific leaves or joins another group. As suggested by **Figures 3C,D**, the probability $D_{\mathrm{n}}(\Delta t)$ that an animal makes a transition and leaves a group of n conspecifics which has persisted for a time Δt is

$$D_n(\Delta t) = \frac{a_n}{\Delta t + b_n}. \tag{15}$$

This is the simplest and minimal hypothesis able to explain the distribution of lifetimes of Eq. 14. Eq. 14 indicates the existence of a reinforcement dynamics so that the longer a group lasts the less likely it is to split. The constants a_n and b_n set the temporal scale of this reinforcement dynamics and the limit of this probability for $\Delta t \rightarrow 0$.

This transition will be a merge with another random group with probability $D_n(\Delta t)\ \lambda$ or a split with probability $D_n(\Delta t)\ (1-\lambda)$. In agreement with the presumed role of 5-HT (**Figures 5** and **6**) merges are promoted by the intra body concentration of 5-HT s, as

$$\lambda = \frac{s}{s + \boldsymbol{K}_{\mathrm{met}}}. \tag{16}$$

This expression assumes that the probability to merge with another group is an activated process modulated by the parameter λ reminiscent of Michaelis–Menten kinetics. K_{met} sets the typical scale for s at which the activation process takes place. We assumed also that s increases when leeches encounter their conspecifics and that s is subsequently degraded. These assumptions are modeled as:

$$\begin{aligned} \frac{ds}{dt} &= c_1 N_{\mathrm{contacts}}(t) - c_2 s \\ \boldsymbol{N}_{\mathrm{contacts}} &= \sum_{i=1,G} n_1^2 \end{aligned} \tag{17}$$

Where c_1 is the rate at which 5-HT concentration increases for each group contact and c_2 is the degradation constant.

From Eqs 3–5 – and the parameter values reported in the legend – we simulated the time evolution of the number of groups in the presence of 5 (**Figure 9A**) and 10 leeches (**Figure 9C**): the formation of a large group of conspecifics is observed for 10 leeches and not for 5 as experimentally observed (**Figures 9B,D**). Also the simulated time course of group size (**Figures 9E,G**) formation is in agreement with what experimentally observed (**Figures 9F,H**). The simple model reproduces qualitatively also the lifetime distribution of groups of conspecifics (**Figures 9I–L**). The essence of the reinforcement dynamics, leading to the formation of a large group with 10 but not with 5 leeches is contained in Eqs 4–5: the asymptotic rate of merges λ increases with the number of conspecifics, because the number of contacts is higher with a larger number of conspecifics (**Figure 4**).

These results indicate that group formation is caused by a reinforcement dynamics that can be modeled by similar equations in different species, such as leeches and humans. The neuromodulator 5-HT promotes group formation in leeches and its involvement in interpersonal relationships among humans is well-established (Goodson and Thompson, 2010). Therefore group formation, important aspect of social interactions in leeches and in humans, share common dynamical properties and specific neuromodulators.

ACKNOWLEDGMENTS

We are grateful to W. B. Kristan and K. French for giving us many helpful suggestions.

REFERENCES

Ali, D. W., Catarsi, S., and Drapeau, P. (1998). Ionotropic and metabotropic activation of a neuronal chloride channel by serotonin and dopamine in the leech *Hirudo medicinalis*. *J. Physiol. (Lond.)* 509(Pt 1), 211–219.

Anstey, M. L., Rogers, S. M., Ott, S. R., Burrows, M., and Simpson, S. J. (2009). Serotonin mediates behavioral gregarization underlying swarm formation in desert locusts. *Science* 323, 627.

Ballerini, M., Cabibbo, N., Candelier, R., Cavagna, A., Cisbani, E., Giardina, I., Orlandi, A., Parisi, G., and Procaccini, A. (2008). Empirical investigation of starling flocks: a benchmark study in collective animal behaviour. *Anim. Behav.* 76, 201–215.

Barrat, A., Cattuto, C., Szomszor, M., Van den Broeck, W., and Alani, H. (2010). Social dynamics in conferences: analyses of data from the Live Social Semantics application. *Semant. Web* 2010, 17–33.

Bazazi, S., Buhl, J., Hale, J. J., Anstey, M. L., Sword, G. A., Simpson, S. J., and Couzin, I. D. (2008). Collective motion and cannibalism in locust migratory bands. *Curr. Biol.* 18, 735–739.

Bisson, G., and Torre, V. (2011). Statistical characterization of social interactions and collective behavior in medicinal leeches. *J. Neurophysiol.* 106, 78–90.

Blaxter, J. H. S., and Hunter, J. R. (1982). The biology of the clupeoid fishes. *Adv. Mar. Biol.* 20, 1–223.

Bruns, D., Engert, F., and Lux, H. D. (1993). A fast activating presynaptic reuptake current during serotonergic transmission in identified neurons of Hirudo. *Neuron* 10, 559–572.

Buhl, J., Sumpter, D. J. T., Couzin, I. D., Hale, J. J., Despland, E., Miller, E. R., and Simpson, S. J. (2006). From disorder to order in marching locusts. *Science* 312, 1402.

Bunin, M. A., Prioleau, C., Mailman, R. B., and Wightman, R. M. (1998). Release and uptake rates of 5-hydroxytryptamine in the dorsal raphe and substantia nigra reticulata of the rat brain. *J. Neurochem.* 70, 1077–1087.

Bunin, M. A., and Wightman, R. M. (1999). Paracrine neurotransmission in the CNS: involvement of 5-HT. *Trends Neurosci.* 22, 377–382.

Burrell, B. D., Sahley, C. L., and Muller, K. J. (2001). Non-associative learning and serotonin induce similar bi-directional changes in excitability of a neuron critical for learning in the medicinal leech. *J. Neurosci.* 21, 1401.

Calviño, M. A., Iscla, I. R., and Szczupak, L. (2005). Selective serotonin reuptake inhibitors induce spontaneous interneuronal activity in the leech nervous system. *J. Neurophysiol.* 93, 2644–2655.

Catarsi, S., and Drapeau, P. (1997). Requirement for tyrosine phosphatase during serotonergic neuromodulation by protein kinase C. *J. Neurosci.* 17, 5792–5797.

Cattuto, C., Barrat, A., Baldassarri, A., Schehr, G., and Loreto, V. (2009). Collective dynamics of social annotation. *Proc. Natl. Acad. Sci. U.S.A.* 106, 10511–10515.

Cattuto, C., Van den Broeck, W., Barrat, A., Colizza, V., Pinton, J. F., and Vespignani, A. (2010). Dynamics of person-to-person interactions from distributed RFID sensor networks. *PLoS ONE* 5, e11596. doi:10.1371/journal.pone.0011596

Cercós, M. G., De-Miguel, F. F., and Trueta, C. (2009). Real-time measurements of synaptic autoinhibition produced by serotonin release in cultured leech neurons. *J. Neurophysiol.* 102, 1075–1085.

Chiao, J. Y. (2010). Neural basis of social status hierarchy across species. *Curr. Opin. Neurobiol.* 20, 803–809.

Coggeshall, R. E., Dewhurst, S. A., Weinreich, D., and McCaman, R. E. (1972). Aromatic acid decarboxylase and choline acetylase activities in a single identified 5-HT containing cell of the leech. *J. Neurobiol.* 3, 259–265.

De Bono, M., and Bargmann, C. I. (1998). Natural variation in a neuropeptide Y receptor homolog modifies social behavior and food response in *C. elegans*. *Cell* 94, 679–689.

De-Miguel, F. F., and Trueta, C. (2005). Synaptic and extrasynaptic secretion of serotonin. *Cell. Mol. Neurobiol.* 25, 297–312.

Dickinson, M. H., and Lent, C. M. (1984). Feeding behavior of the medicinal leech, *Hirudo medicinalis* L. *J. Comp. Physiol. A Neuroethol. Sens. Neural Behav. Physiol.* 154, 449–455.

Donaldson, Z. R., and Young, L. J. (2008). Oxytocin, vasopressin, and the neurogenetics of sociality. *Science* 322, 900.

Elliott, E. J. (1984). Chemoreception in the leech. *Neurosci. Soc. Abst.* 10, 656.

Elliott, E. J. (1986). Chemosensory stimuli in feeding behavior of the leech *Hirudo medicinalis*. *J. Comp. Physiol.* 159, 391–401.

Elliott, J. M. (1973). The diel activity pattern, drifting and food of the leech *Erpobdella octoculata* (L.) (Hirudinea: Erpobdellidae) in a lake district stream. *J. Anim. Ecol.* 42, 449–459.

Friesen, W. O. (1989). Neuronal control of leech swimming movements. *J. Comp. Physiol. A Neuroethol. Sens. Neural Behav. Physiol.* 166, 205–215.

Garcia-Perez, E., Mazzoni, A., Zoccolan, D., Robinson, H. P., and Torre, V. (2005). Statistics of decision making in the leech. *J. Neurosci.* 25, 2597.

Gaudry, Q., and Kristan, W. B. (2009). Behavioral choice by presynaptic inhibition of tactile sensory terminals. *Nat. Neurosci.* 12, 1450–1457.

Gaudry, Q., Ruiz, N., Huang, T., Kristan, W. B., and Kristan, W. B. (2010). Behavioral choice across leech species: chacun à son goût. *J. Exp. Biol.* 213, 1356–1365.

Goodson, J. L., and Thompson, R. R. (2010). Nonapeptide mechanisms of social cognition, behavior and species-specific social systems. *Curr. Opin. Neurobiol.* 20, 784–794.

Gueron, S., and Levin, S. A. (1995). The dynamics of group formation. *Math. Biosci.* 128, 243–264.

Hearn, D., and Baker, M. P. (1997). *Computer Graphics C Version*, 2nd Edn. Upper Saddle River: Prentice Hall Press.

Hoare, D. J., Ruxton, G. D., Godin, J. G., and Krause, J. (2000). The social organization of free-ranging fish shoals. *Oikos* 89, 546–554.

Insel, T. R. (2010). The challenge of translation in social neuroscience: a review of oxytocin, vasopressin, and affiliative behavior. *Neuron* 65, 768–779.

Kaushalya, S., Desai, R., Arumugam, S., Ghosh, H., Balaji, J., and Maiti, S. (2008). Three-photon microscopy shows that somatic release can be a quantitatively significant component of serotonergic neurotransmission in the mammalian brain. *J. Neurosci. Res.* 86, 3469–3480.

Kravitz, E. A. (1988). Hormonal control of behavior: amines and the biasing of behavioral output in lobsters. *Science* 241, 1775.

Kristan, W. B., Calabreseb, R. L., and Friesen, W. O. (2005). Neuronal control of leech behavior. *Prog. Neurobiol.* 76, 279–327.

Kristan, W. B., and Nusbaum, M. P. (1982). The dual role of serotonin in leech swimming. *J. Physiol. (Paris)* 78, 743–747.

Lent, C., Zundel, D., Freedman, E., and Groome, J. (1991). Serotonin in the leech central nervous system: anatomical correlates and behavioral effects. *J. Comp. Physiol. A Neuroethol. Sens. Neural Behav. Physiol.* 168, 191–200.

Lent, C. M., and Dickinson, M. H. (1984). Serotonin integrates the feeding behavior of the medicinal leech. *J. Comp. Physiol. A Neuroethol. Sens. Neural Behav. Physiol.* 154, 457–471.

Lent, C. M., and Frazer, B. M. (1977). Connectivity of the monoamine-containing neurones in central nervous system of leech. *Nature* 266, 844–847.

Macagno, E. R. (1980). Number and distribution of neurons in leech segmental ganglia. *J. Comp. Neurol.* 190, 283–302.

Makris, N. C., Ratilal, P., Jagannathan, S., Gong, Z., Andrews, M., Bertsatos, I., Godo, O. R., Nero, R. W., and Jech, J. M. (2009). Critical population density triggers rapid formation of vast oceanic fish shoals. *Science* 323, 1734.

Mar, A., and Drapeau, P. (1996). Modulation of conduction block in leech mechanosensory neurons. *J. Neurosci.* 16, 4335.

Mazzoni, A., Garcia-Perez, E., Zoccolan, D., Graziosi, S., and Torre, V. (2005). Quantitative characterization and classification of leech behavior. *J. Neurophysiol.* 93, 580.

Muller, K. J., Nicholls, J. G., and Stent, G. S. (1981). *Neurobiology of the Leech*. Cold Spring Harbor, NY: Cold Spring Harbor Laboratory.

Nagy, M., Ákos, Z., Biro, D., and Vicsek, T. (2010). Hierarchical group dynamics in pigeon flocks. *Nature* 464, 890–893.

Ort, C. A., Kristan, W. B., and Stent, G. S. (1974). Neuronal control of swimming in the medicinal leech. *J. Comp. Physiol. A Neuroethol. Sens. Neural Behav. Physiol.* 94, 121–154.

Pavlidis, T. (1995). *Algorithms for Graphics and Image Processing*. Berlin: W H Freeman & Co (Sd).

Pratt, W. K. (1991). *Digital Image Processing*, 2nd Edn. New York: Wiley-Interscience.

Puhl, J. G., and Mesce, K. A. (2008). Dopamine activates the motor pattern for crawling in the medicinal leech. *J. Neurosci.* 28, 4192–4200.

Sanchez-Armass, S., Merz, D. C., and Drapeau, P. (1991). Distinct receptors, second messengers and conductances underlying the dual responses to serotonin in an identified leech neurone. *J. Exp. Biol.* 155, 531–547.

Sawyer, R. T. (1986a). *Leech Biology and Behaviour: Anatomy, Physiology and*

Behaviour, Vol. I. Oxford: Oxford University Press.

Sawyer, R. T. (1986b). *Leech Biology and Behaviour: Feeding Biology, Ecology, and Systematics*, Vol. II. Oxford: Oxford University Press.

Sokolowski, M. B. (2010). Social interactions in "simple" model systems. *Neuron* 65, 780–794.

Sombers, L. A., Beyene, M., Carelli, R. M., and Wightman, R. M. (2009). Synaptic overflow of dopamine in the nucleus accumbens arises from neuronal activity in the ventral tegmental area. *J. Neuroscicv.* 29, 1735-1742.

Stehlé, J., Barrat, A., and Bianconi, G. (2010). Dynamical and bursty interactions in social networks. *Phys. Rev. E* 81, 035101.

Wenning, A., and Meyer, E. P. (2007). Hemodynamics in the leech: blood flow in two hearts switching between two constriction patterns. *J. Exp. Biol.* 210, 2627–2636.

Willard, A. L. (1981). Effects of serotonin on the generation of the motor program for swimming by the medicinal leech. *J. Neurosci.* 1, 936–944.

Yeh, S. R., Fricke, R. A., and Edwards, D. H. (1996). The effect of social experience on serotonergic modulation of the escape circuit of crayfish. *Science* 271, 366.

Zhao, K., Stehlé, J., Bianconi, G., and Barrat, A. (2011). Social network dynamics of face-to-face interactions. *Phys. Rev. E* 83, 056109.

Conflict of Interest Statement: The authors declare that the research was conducted in the absence of any commercial or financial relationships that could be construed as a potential conflict of interest.

Received: 06 March 2012; paper pending published: 23 March 2012; accepted: 21 April 2012; published online: 17 May 2012.

Citation: Bisson G, Bianconi G and Torre V (2012) The dynamics of group formation among leeches. Front. Physio. ***3****:133. doi: 10.3389/fphys.2012.00133*

This article was submitted to Frontiers in Membrane Physiology and Biophysics, a specialty of Frontiers in Physiology.